

Technical and Economic Analysis of Connecting Nuclear Generation to the National Electricity Transmission System via HVDC Technology

Richard Poole

School of Engineering and Technology

This thesis is submitted to the University of Hertfordshire in partial fulfilment of the requirements of the degree of Doctor of Engineering (EngD)

25th April 2016

Abstract

High Voltage Direct Current (HVDC) technology has never before been used to connect a Nuclear Power Plant (NPP) directly to the National Electricity Transmission System (NETS). There are both technical and economic factors which need to be considered and understood before such a technology is adopted for an NPP connection.

In this thesis, both technical and economic factors surrounding the suitability of Current Source Converter (CSC) and Voltage Source Converter (VSC) HVDC technology for NPP connections are investigated. Power system models of both HVDC technologies, connected to an NPP, are studied in Power System Computer Aided Design (PSCAD) software.

The studies highlight the susceptibility of CSC-HVDC technology to commutation failure during a three-phase fault condition at the inverter, and simulations demonstrate some key benefits of adopting VSC-HVDC technology for NPP connections: provision of independent reactive power support to both the NPP and AC system; black-start capability; fast current reversal for dynamic conditions; and the ability to connect to a weak High Voltage Alternating Current (HVAC) system. The simulations show the vulnerability of VSC-HVDC vector current control when the short circuit ratio of the AC system is very low (<1); in such cases, the Phase Locked Loop (PLL) is affected and power transfer through the VSC-HVDC link may drop to 50% of nominal rating.

An economic analysis of HVDC technology development, cost and converter station size is presented. The size of a CSC-HVDC converter station can be much larger than an equivalent-rated VSC due to the additional filters required for reactive power compensation and harmonic mitigation. With the fast evolution of VSC-HVDC technology, the ratings required for an NPP connection are now available. The cost difference between the two technologies can vary from project to project and hence neither one can be ruled out for an NPP connection based only on price.

Acknowledgements

The author would like to thank National Grid for the opportunity to carry out this professional Engineering Doctorate (EngD) research project. Particular thanks go to my internal company supervisor Dr Paul Coventry for his continued supervision within National Grid.

The author would like to thank the University of Hertfordshire for the chance to study on the EngD programme. Particular thanks go to my academic supervisors Matthew Harrington, Georgios Pissanidis, and Maloud Denai for their continued supervision and guidance throughout the duration of this research programme.

Thanks go to my life partner Emma Alaball for her continued support and patience on a year-by-year basis while the author has been working and studying over the last four years.

Special thanks goes to ABB Ltd, Siemens, Alstom grid and the Institute of Electrical and Electronic Engineers (IEEE) for the technical reference sources used in the preparation and writing of this thesis.

A great deal of thanks goes to Hinkley Point B, Sizewell B, Heysham 2, Wylfa and Torness nuclear power stations for the guided tours and technical information provided to contribute to the nuclear elements of this thesis.

The author would like to thank Manitoba Hydro Ltd for providing the PSCAD HVDC models and technical support provided over the last 4 years.

Table of Contents

Abstract	i
Acknowledgements	ii
Table of Contents	iii
List of Tables	ix
List of Figures.....	x
Nomenclature.....	xvii
Chapter 1: Introduction	1
1.1 Motivation	1
1.1.1 Connecting nuclear power plants to the NETS.....	1
1.1.2 Connecting nuclear power plants by HVDC technology.....	2
1.2 Objective and main contributions of the thesis	3
1.3 Outline of the thesis	5
Chapter 2: Literature Review.....	8
2.1 NPPs connected by HVDC technology.....	8
2.2 HVDC technology.....	9
2.2.1 HVDC versus HVAC	9
2.2.2 Current source converter HVDC technology	11
2.2.3 VSC-HVDC technology	25
2.3 Nuclear power	43
2.3.1 Pressurised water reactor	44
2.3.2 Boiling water reactor	44
2.3.3 High temperature advanced gas cooled reactors	45
2.3.4 Layout of a modern NPP.....	45
2.3.5 Development of an NPP	48
2.3.6 Electric grid vulnerability	49
2.3.7 Interfacing NPPs with AC grids	50
2.3.8 Influence of grid disturbances on nuclear power plants.....	51
2.3.9 History of nuclear power plant disturbances	53
2.4 Chapter 2 summary	55

Chapter 3: Connecting NPPs by AC Technology	56
3.1 Introduction.....	56
3.2 Modelling of an NPP connected by AC technology	56
3.2.1 AC generator model.....	56
3.2.2 AC double-wound transformer model	58
3.2.3 Autotransformer model.....	61
3.2.4 On-load tap changer model.....	62
3.2.5 AC overhead transmission line model.....	63
3.2.6 AC induction motor model	66
3.2.7 AC circuit breaker model	67
3.2.8 Load model	67
3.3 Power system setup	68
3.3.1 NPP model	68
3.3.2 AC grid	69
3.4 Load flow analysis.....	72
3.4.1 PSCAD load flow results.....	72
3.4.2 Power World Simulator load flow results.....	73
3.4.3 Load flow analysis comparison.....	73
3.5 Transient analysis of an NPP connected by AC technology.....	75
3.5.1 General transient analysis	75
3.5.2 Detailed transient analysis	78
3.6 Chapter 3 summary	88
Chapter 4: Connecting NPPs by CSC-HVDC Technology.....	89
4.1 Introduction.....	89
4.2 Modelling of an NPP connected by CSC-HVDC technology	89
4.2.1 Six-pulse bridge	90
4.2.2 Firing and blocking control	90
4.2.3 Converter transformer tap changer	92
4.2.4 AC filters	93

4.2.5	Shunt capacitor.....	96
4.2.6	DC cable.....	97
4.2.7	Short circuit ratio.....	98
4.2.8	CSC-HVDC bipole model in PSCAD.....	101
4.2.9	CSC-HVDC controls.....	103
4.3	Impact of effective short circuit ratio on CSC-HVDC operation.....	106
4.3.1	Rectifier ESCR 1.8 and inverter ESCR 3.5.....	107
4.3.2	Rectifier ESCR 1.4 and inverter ESCR 3.5.....	108
4.3.3	Rectifier ESCR 1.0 and inverter ESCR 3.5.....	109
4.3.4	Rectifier ESCR 1.8 and inverter ESCR 2.4.....	111
4.3.5	Rectifier ESCR 1.8 and inverter ESCR 1.8.....	112
4.3.6	Rectifier ESCR 1.8 and inverter ESCR 1.4.....	114
4.3.7	Summary.....	116
4.4	Transient analysis of a CSC-HVDC NPP connection.....	117
4.4.1	General transient analysis.....	117
4.4.2	Detailed transient analysis.....	120
4.4.3	CSC-HVDC contingency analysis.....	135
4.5	Chapter 4 summary.....	146
Chapter 5: Connecting NPPs by VSC-HVDC Technology.....		148
5.1	Introduction.....	148
5.2	Modelling of an NPP connected by VSC-HVDC technology.....	148
5.2.1	VSC-HVDC converter bridge model.....	148
5.2.2	VSC-HVDC converter transformer model.....	150
5.2.3	High-pass filter model.....	150
5.2.4	DC cable model.....	151
5.2.5	PSCAD VSC-HVDC bipole model.....	152
5.2.6	Controls used in the PSCAD VSC-HVDC model.....	154
5.2.7	Comparison of PSCAD/MATLAB VSC-HVDC models.....	164
5.3	Impact of short circuit ratio on VSC-HVDC operation.....	170

5.3.1	Rectifier SCR 2.5 and inverter 4.1.....	171
5.3.2	Rectifier SCR 2.0 and inverter 4.1.....	173
5.3.3	Rectifier SCR 1.6 and inverter 4.1.....	176
5.3.4	Rectifier SCR 1.0 and inverter 4.1.....	179
5.3.5	Rectifier SCR 2.5 and inverter 3.0.....	182
5.3.6	Rectifier SCR 2.5 and inverter 2.5.....	183
5.3.7	Rectifier SCR 2.5 and inverter 2.0.....	185
5.3.8	Rectifier SCR 2.5 and inverter 1.6.....	188
5.3.9	Rectifier SCR 2.5 and inverter 1.0.....	191
5.3.10	Rectifier SCR 1.0 and inverter 1.0.....	193
5.3.11	VSC-HVDC SCR analysis summary.....	198
5.4	Transient analysis of a VSC-HVDC NPP connection.....	198
5.4.1	General transient analysis	199
5.4.2	Detailed transient analysis of a VSC-HVDC NPP connection	201
5.4.3	Contingency analysis	216
5.5	Chapter 5 summary and conclusions	223
Chapter 6: Design of Nuclear Power Plant Connections		225
6.1	Design of an NPP connection utilising AC technology.....	225
6.1.1	Design of a 4500 MW rated NPP	225
6.1.2	Design of a 400 kV NPP AC interface substation	227
6.1.3	Design of a 400 kV AC grid substation.....	235
6.1.4	Overall design of an NPP AC connection to the transmission grid.....	237
6.2	Design of an NPP connection utilising CSC-HVDC technology.....	239
6.2.1	CSC-HVDC bipole converter station design	239
6.2.2	Final design CSC-HVDC NPP connection.....	247
6.3	Design of an NPP connection utilising VSC-HVDC technology	250
6.3.1	VSC-HVDC bipole converter station design	250
6.4	Design of an control system for an HVDC NPP connection	254
6.4.1	Power system setup	254

6.4.2	HVDC control system design.....	259
6.4.3	Thermal contingency analysis for NPP HVDC connection	261
6.4.4	HVDC frequency controller design	263
6.5	Chapter 6 summary and conclusions	266
Chapter 7: Economic Analysis of NPP HVDC Connections		268
7.1	Costs of AC technology for NPP connections	268
7.1.1	AC technology cost review of Hinkley Point C NPP	268
7.1.2	AC technology cost review of Sizewell C NPP.....	272
7.2	Costs of CSC-HVDC technology for NPP connections	275
7.2.1	Cost of CSC-HVDC technology	275
7.3	Costs of VSC-HVDC technology for NPP connections.....	277
7.3.1	Cost comparison between AC and HVDC technology	279
7.4	AC technology footprint for NPP connections	286
7.4.1	AC technology footprint for Hinkley NPP connection	286
7.4.2	AC technology footprint for NPP connection in Cumbria.....	287
7.5	CSC-HVDC technology footprint for NPP connections	289
7.6	VSC-HVDC technology footprint for NPP connections	291
7.6.1	Comparison of technology footprints for NPP connection	295
7.7	Transmission technology development for NPP connections.....	297
7.7.1	Development of AC technology for NPP connections	297
7.7.2	Development of HVDC technology for NPP connections	301
7.7.3	Comparison of AC and DC technology for NPP connections	303
7.8	Chapter 7 review	303
Chapter 8: Conclusions and Future Work.....		305
8.1	Conclusions.....	305
8.2	Further work.....	306
8.2.1	Simulation using larger-rated HVDC models	306
8.2.1	Impact of HVDC frequency control on NPP operation	306
8.2.2	HVDC protection and control operating times.....	307

8.2.3	Further in-house study	307
8.2.4	Industry interaction	307
Appendix A	308
Appendix B	309
Appendix C	310
Appendix D	311
Appendix E	312
Appendix F	313
Appendix G	314
List of References	315
List of Publications	327

List of Tables

Table 1: The effects of changing PI parameters	39
Table 2: Grid disturbance effects on NPP 1993–2003 [20].....	54
Table 3: Grid conditions affecting NPP 1993–2003	54
Table 4: Initiating events for NPP actions	55
Table 5: Data for the transformer shown in Figure 34	59
Table 6: Table showing PSCAD component data for Figure 43.....	71
Table 7: PSCAD load flow analysis results.....	72
Table 8: Power World Simulator load flow analysis results.....	73
Table 9: Resultant outcomes of load flow analysis comparison.....	74
Table 10: General fault analysis results	76
Table 11: Parameters for CSC-HVDC link model used in PSCAD	100
Table 12: Summary of results for ESCR variation.....	116
Table 13: General fault analysis results	118
Table 14: Abbreviations for PI controller constants used in VSC-HVDC model.....	155
Table 15: Comparison between PSCAD and MATLAB VSC-HVDC models for AC faults	169
Table 16: Control parameter settings for fixed SCR values.....	171
Table 17: Optimised PI controller gains for different combination of SCRs	197
Table 18: Results for VSC-HVDC general transient analysis	200
Table 19: Circuit designation and thermal ratings for Figure 152	256
Table 20: Circuit designation and thermal ratings for Figure 152	258
Table 21: Circuit designation and control actions required for Figure 152	262
Table 22: Table showing commissioned CSC-HVDC projects around the world.....	276
Table 23: VSC-HVDC projects commissioned around the world	278
Table 24: Table showing connection options and circuit routes for Hinkley Point C NPP	280
Table 25: Table showing connection options and circuit routes for Cumbrian NPP	283
Table 26: Table of HVDC projects showing converter station footprint.....	292
Table 27: Power ratings of different AC technologies for connection of NPP in Cumbria.....	299

List of Figures

Figure 1: Map of proposed construction sites for new NPPs within the UK [3].....	2
Figure 2: CSC-HVDC twelve-pulse converter	11
Figure 3: Stages 1–6 of the twelve-pulse commutation sequence	13
Figure 4: Stages 7–12 of the twelve-pulse commutation sequence	14
Figure 5: Effect of firing angle on converter operation	15
Figure 6: Commutation failure at the inverter in a CSC-HVDC link	17
Figure 7: Monopolar with ground return	18
Figure 8: Monopole HVDC with metallic return	19
Figure 9: Bipolar HVDC system.....	19
Figure 10: Back-to-back HVDC system.....	20
Figure 11: Control characteristic of CSC-HVDC [41]	21
Figure 12: VSC-HVDC operating principles	25
Figure 13: Principles of reactive power control	27
Figure 14: Principles of active power control.....	28
Figure 15: VSC active and reactive power capability curve.....	29
Figure 16: Point-to-point VSC-HVDC link and corresponding components	30
Figure 17: Two-level VSC.....	30
Figure 18: Three-level VSC.....	31
Figure 19: Symmetrical monopole VSC-HVDC converter.....	31
Figure 20: Asymmetrical monopole with metallic return	32
Figure 21: Asymmetrical monopole with ground return	32
Figure 22: Bipolar configuration.....	33
Figure 23: Axis transformation for vector current control [19].....	35
Figure 24: Control strategies with reference time frames.....	36
Figure 25: Schematic of the VSC system	37
Figure 26: PID controller.....	38
Figure 27: Control system for VSC-HVDC technology	40

Figure 28: Pressurised water reactor.....	44
Figure 29: Boiling water reactor.....	45
Figure 30: Layout of an NPP and associated AC switchyard	46
Figure 31: Fundamental voltage source connected to an impedance source.	57
Figure 32: Short circuit level at the NPP	57
Figure 33: Short circuit level of the AC grid	58
Figure 34: AC transformer with circuit breakers.....	58
Figure 35: Autotransformer model used in PSCAD.....	61
Figure 36: On-load tap changer principle of operation	62
Figure 37: AC overhead transmission line model used in PSCAD	63
Figure 38: Voltages and currents in an N-conductor transmission line.....	64
Figure 39: EMTDC frequency-dependent (phase) model time-domain interface.....	65
Figure 40: AC induction motor model used in PSCAD	66
Figure 41: AC circuit breaker component used in PSCAD.....	67
Figure 42: Resistive load	68
<i>Figure 43: Overall power system setup in PSCAD.....</i>	<i>70</i>
Figure 44: General fault analysis for NPP connected by AC technology.....	77
Figure 45: AC system profiles for successive A–G faults on transmission line 1 circuits	79
Figure 46: AC system profiles for three-phase fault on busbar 21.....	81
Figure 47: AC system profiles for three-phase fault applied to busbar 1	83
Figure 48: AC system profiles for three-phase fault on TL1C1	85
Figure 49: AC system profiles for three-phase fault on busbar 2.....	87
Figure 50: Six-pulse bridge model used in PSCAD.....	90
Figure 51: Rectifier 150 Mvar C-type filter	94
Figure 52: Inverter 150 Mvar C-type filter	94
Figure 53: Rectifier 150 Mvar high-pass RLC filter	95
Figure 54: Inverter 150 Mvar high-pass RLC filter.....	95
Figure 55: Rectifier 301 Mvar shunt capacitor	96
Figure 56: Inverter 301 Mvar shunt capacitor.....	97

Figure 57: DC cable model used in PSCAD.....	97
Figure 58: Parameters for rectifier AC connection	100
Figure 59: Parameters for inverter AC connection	100
Figure 60: CSC-HVDC bipole model used in PSCAD	102
Figure 61: Rectifier controls used in the PSCAD CSC-HVDC model.....	103
Figure 62: Inverter gamma control.....	104
Figure 63: Inverter current control.....	105
Figure 64: Rectifier ESCR 1.8, inverter ESCR 3.5	107
Figure 65: Rectifier ESCR 1.4, inverter ESCR 3.5	109
Figure 66: Rectifier ESCR 1.0, inverter ESCR 3.5	110
Figure 67: Rectifier ESCR 1.8, inverter ESCR 2.4	112
Figure 68: Rectifier ESCR 1.8, inverter ESCR 1.8	113
Figure 69: Rectifier ESCR 1.8, inverter ESCR 1.4	115
Figure 70: General fault analysis for NPP connected by HVDC technology.....	119
Figure 71: DC profiles for three-phase fault on busbar 3	121
Figure 72: DC profiles for a three-phase fault on busbar 3.....	122
Figure 73: DC profiles for a three-phase fault on busbar 20.....	124
Figure 74: AC profiles for three-phase fault on busbar 20	125
Figure 75: DC profiles for three-phase fault on busbar 4	127
Figure 76: AC profiles for three-phase fault on busbar 4.....	128
Figure 77: DC profiles for permanent pole-to-ground fault.....	130
Figure 78: AC profiles for permanent pole-to-ground fault.....	131
Figure 79: DC profiles for a permanent DC pole-to-pole fault	133
Figure 80: AC profiles for a permanent DC pole-to-pole fault.....	134
Figure 81: DC profiles for contingency 1	136
Figure 82: AC profiles for contingency 1	138
Figure 83: DC profiles for CSC-HVDC contingency 2.....	140
Figure 84: AC profiles for CSC-HVDC contingency 2.....	141
Figure 85: Power system state for contingency 3.....	143

Figure 86: Measured frequency on busbar 20 reactor station 2 with no DC control action	144
Figure 87: DC profiles for contingency 3 with active power runback activated.....	145
Figure 88: Post-fault frequency profile in reactor 2 station.....	146
Figure 89: VSC-HVDC six-pulse Converter Bridge used in PSCAD	149
Figure 90: V-I characteristic for the GTO/IGBT model used in PSCAD	149
Figure 91: VSC-HVDC converter transformer model used in PSCAD	150
Figure 92: High-pass filter used in VSC-HVDC model.....	151
Figure 93: VSC DC cable model used in PSCAD	151
Figure 94: VSC-HVDC bipole model used in PSCAD.....	153
Figure 95: Detailed VSC-HVDC control model used in PSCAD.....	154
Figure 96: Optimal controller gains/constants for the VSC-HVDC rectifier	155
Figure 97: Optimal controller gains/constants for VSC-HVDC inverter.....	156
Figure 98: Rectifier controls used in VSC-HVDC PSCAD model.....	156
Figure 99: Firing pulse controls	157
Figure 100: VSC inner current control loops	158
Figure 101: PLL used for generating the synchronising angle (θ)	160
Figure 102: VSC frequency controller	160
Figure 103: VSC active power controller.....	161
Figure 104: VSC DC voltage controller	162
Figure 105: VSC AC voltage controller	163
Figure 106: VSC-HVDC bipole model developed in MATLAB/Simulink	165
Figure 107: VSC-HVDC control loops used in MATLAB/Simulink.....	166
Figure 108: Profiles for rectifier SCR 2.5 and inverter 4.1.....	172
Figure 109: Profiles for rectifier SCR 2.0 and inverter 4.1 with nominal control parameters	173
Figure 110: Profiles with rectifier SCR 2.0 and inverter 4.1 with adjusted control parameters	175
Figure 111: Profiles for rectifier SCR 2.0 and inverter 4.1 with nominal control parameters	176
Figure 112: Profiles for rectifier SCR 2.0 and inverter 4.1 with adjusted control parameters.....	178
Figure 113: Profiles for rectifier SCR 1.0 and inverter 4.1 with nominal control parameters	179
Figure 114: Profiles for rectifier SCR 1.0 and inverter 4.1 with adjusted control parameters.....	181

Figure 115: Profiles for rectifier SCR 2.5 and inverter 3.0 with nominal control parameters	182
Figure 116: Profiles for rectifier SCR 2.5 and inverter 2.5 with nominal control parameters	184
Figure 117: Profiles for rectifier SCR 2.5 and inverter 2.5 with adjusted control parameters	185
Figure 118: Profiles for rectifier SCR 2.5 and inverter 2.0 with nominal control parameters	186
Figure 119: Profiles for rectifier SCR 2.5 and inverter 2.0 with adjusted control parameters	187
Figure 120: Profiles for rectifier SCR 2.5 and inverter 1.6 with nominal control parameters	189
Figure 121: Profiles for rectifier SCR 2.5 and inverter 1.6 with adjusted control parameters	190
Figure 122: Profiles for rectifier SCR 2.0 and inverter 1.0 with nominal control parameters	191
Figure 123: Profiles for rectifier SCR 2.5 and inverter 1.6 with adjusted control parameters	193
Figure 124: Profiles for rectifier SCR 1.0 and inverter 1.0 with adjusted control parameters	194
Figure 125: Profiles for rectifier SCR 1.0 and inverter 1.0 with adjusted control parameters	196
Figure 126: VSC profiles for three-phase fault on busbar 3.....	202
Figure 127: AC/DC profiles for three-phase fault placed at busbar 3.....	203
Figure 128: VSC system profiles for three-phase fault at busbar 20.....	205
Figure 129: AC/DC profiles for three-phase fault at busbar 20	206
Figure 130: VSC profiles for three-phase fault applied on AC side of VSC2	208
Figure 131: AC/DC Profile for three-phase fault applied on AC side of VSC2.....	209
Figure 132: VSC system profiles for pole-to-ground fault	211
Figure 133: AC system profiles for DC pole-to-ground fault	212
Figure 134: VSC profiles for DC pole-to-pole fault	214
Figure 135: AC/DC profiles for DC pole-to-pole fault.....	215
Figure 136: VSC profiles for inverter AC pole breaker trip.....	217
Figure 137: AC system profiles after inverter AC pole breaker trip	218
Figure 138: NPP frequency after reactor generator trip.....	219
Figure 139: VSC profiles for single-phase-to-ground fault on busbar 20.....	220
Figure 140: VSC system profiles for reactor 2 generator trip and black start	222
Figure 141: Simplified single diagram of 4500 MW NPP.....	226
Figure 142: NPP 400 kV AC interface substation.....	228
Figure 143: Protection scheme design for NPP AC interface substation	230

Figure 144: Operation principle of unit protection.....	232
Figure 145: Operation principle of distance protection	233
Figure 146: Protection arrangement for 400/132 kV autotransformer	234
Figure 147: New 400 kV AC grid substation to connect NPP into the 400 kV transmission system	236
Figure 148: Design for connecting an NPP to the transmission grid by AC technology.....	238
Figure 149: Design of a bipole CSC-HVDC converter station	240
Figure 150: Protection system design for CSC-HVDC bipole converter station.....	243
Figure 151: Protection scheme for converter transformer.....	246
Figure 152: Final design of an NPP connected to the AC grid by CSC-HVDC technology	249
Figure 153: Design for a VSC-HVDC bipole converter station	251
Figure 154: Final design for connecting an NPP by VSC-HVDC technology to an AC grid	253
Figure 155: Power system setup for thermal case study.....	255
Figure 156: Design of an HVDC frequency controller for NPP operation	264
Figure 157: Hinkley Point C NPP AC technology connection option A	269
Figure 158: Hinkley Point C NPP AC technology connection option B	271
Figure 159: Connection option A for Sizewell C NPP	272
Figure 160: Connection option B for Sizewell C NPP	273
Figure 161: Graph showing the total AC cost versus connection option	274
Figure 162: Graph showing number of commissioned CSC-HVDC projects	277
Figure 163: Graph showing the total of commissioned VSC-HVDC projects.....	279
Figure 164: Graph comparing different technology costs for Hinkley Point C connection options	282
Figure 165: Graph comparing different technology costs for Hinkley Point C connection options	284
Figure 166: AC substation footprint for NPP connection	286
Figure 167: Example of the size of a 400 kV GIS substation for an NPP connection	288
Figure 168: Layout and footprint of a CSC-HVDC converter station for NPP connections.....	289
Figure 169: Layout design and dimensions for a ± 600 kV 2250 MW VSC-HVDC bipole converter station	294
Figure 170: Graph comparing the dimensions between AC and DC technology for a 4500 MW NPP connection.....	296

Figure 171: Overhead line power ratings versus distance	298
Figure 172: Single circuit power ratings of different AC technologies for NPP connection.....	300
Figure 173: Available HVDC technology ratings in industry	302
Figure 174: MATLAB/Simulink rectifier profiles for three-phase fault condition.....	311
Figure 175: MATLAB/Simulink inverter profiles for three-phase fault condition	312
Figure 176: PSCAD rectifier profiles for three-phase fault condition.....	313
Figure 177: PSCAD inverter profiles for three-phase fault condition.....	314

Nomenclature

Abbreviation	Translation
ABB	Asea, Brown and Boveri
AC	Alternating Current
Alpha	Rectifier Firing Angle °
Block	Blocking of firing pulses to valves
BWR	Boiling Water Reactor
CCGT	Combined Cycle Gas Turbine
CSC	Current Source Converter
DC	Direct Current
dq	Active/Reactive Current
EDF	Energie de France
EDG	Emergency Diesel Generator
ENWL	Electricity North-West Ltd
ESOF	Emergency Switch-Off Sequence
FACTS	Flexible AC Transmission
GAMMA	Inverter firing angle °
GW	Giga Watts
HTGCR	High Temperature Gas Cooled Reactors
HVAC	High Voltage Alternating Current
HVDC	High Voltage Direct Current
IGBT	Insulated Gate Bipolar Transistor
LOOP	Loss of Off-site Power
MMC	Modular Multilevel Converter
MW	Mega Watts
NETS	Network Electricity Transmission System

NPP	Nuclear Power Plant
POD	Power Oscillation Damping
PSCAD	Power Systems Analysis Software
PWR	Pressurised Water Reactor
SCRAM	Reactor trip and shutdown
SSR	Sub-synchronous resonance
STATCOM	Static Compensator
SVC	Static Var Compensator
SQSS	Security and Quality of Supply Standard
VCDOL	Voltage Dependent Current Order Limiter
VSC	Voltage Source Converter

Chapter 1: Introduction

This chapter describes the background of the thesis and motivation for the work undertaken. The objective and outline of the thesis is presented, followed by the main contributions to the work.

1.1 Motivation

1.1.1 Connecting nuclear power plants to the NETS

The National Electricity Transmission System (NETS) is continuously being stressed due to the increasing load demand encountered on a yearly basis. New generation in the form of renewables, such as tidal and nuclear power will require connection to the NETS within the next decade or so. New High Voltage Direct Current (HVDC) links and High Voltage Alternating Current (HVAC) circuits are being considered to facilitate the connection of this generation.

Nuclear Power Plants (NPPs) are set to play a vital role in supplying the energy demand of the United Kingdom (UK) for years to come. Some of the NPPs will be in excess of 3000 MW in power rating and will need connecting to the NETS by 2030 [1]. These large power ratings will trigger network reinforcements to the NETS to ensure a secure and reliable connection for the NPPs. Designing and building the necessary infrastructure to connect these to the NETS is going to pose a significant challenge for National Grid over the next decade or so [2].

Most of the nominated sites for the NPPs are located in coastal regions of the UK. This keeps them as far away as possible from heavily populated cities and offers a constant supply of sea water to provide an instant source of cooling for the nuclear reactors. Due to the geographical locations, the challenge of connecting some of the NPPs to the NETS is increased.

The distance of the nearest connection point into the NETS from the NPPs can be over 100 km. New 400 kV AC overhead lines are large in size and may cross public parks and areas of outstanding natural beauty. Such transmission lines are not usually welcomed by the general public and this requires other technologies to be assessed as part of the technology assessment for NPP connections. Other technologies such as AC cables, Gas Insulated Line (GIL) and HVDC technology have also been considered as part of the strategic optioneering process for NPP connections.

Figure 1 shows the existing NPPs scheduled for shutdown within the UK [3]. New sites for future nuclear units are proposed in the same coastal locations as the existing plants.



Figure 1: Map of proposed construction sites for new NPPs within the UK [3]

1.1.2 Connecting nuclear power plants by HVDC technology

HVDC technology has never before been used to connect an NPP to the NETS [2]. This presents a large and unproven technological risk to any transmission utility considering HVDC as an option for an NPP connection. There are both technical and economic factors which need to be considered and understood before such a technology is adopted for an NPP connection [2]. In order to provide a secure and reliable NPP connection, the following technical factors associated with HVDC technology need to be considered and understood:

- The speed and response of the HVDC controls to power system faults and system contingencies.

- The stability of the HVDC links when connected to weak AC networks.
- The benefits that HVDC technology could offer to the NPP and AC network to improve operation and increase system reliability.
- The interaction between the NPP and HVDC control systems.

The first three of the above technical factors are studied in this thesis.

Economic factors will also have an influence on whether HVDC technology is selected for an NPP connection [4]. Such factors include the following:

- Cost.
- Technology availability.
- Converter station footprint.

An HVDC solution may prove to be more expensive than an HVAC option. The land footprint required to accommodate the HVDC converter stations will be larger and this will result in increased costs [5]. For long-distance connections into the NETS (>60 km) HVDC may prove to be the best option. The fast development of VSC-HVDC technology and increased power ratings would make this a suitable option for an NPP connection.

Each of these areas need to be considered carefully for a large NPP connection project to ensure that the solution is fit for purpose and balances the economic and technical requirements.

1.2 Objective and main contributions of the thesis

The main objective of the thesis is to undertake a technical and economic analysis of connecting NPPs to the NETS via HVDC technology.

The main contributions of the thesis are as follows:

- Designing NPP and AC power system models within PSCAD to study the connection of both CSC- and VSC-HVDC links. A load flow analysis is carried out to determine the steady-state power system variables, such as voltage and active power, before transient simulations are undertaken.
- Analysing the effects of three-phase faults on both the power system and the NPP, in PSCAD, when AC overhead line technology is used as the sole connection option. In particular, the effect of voltage depressions in the vicinity of the NPP caused by three-phase faults is monitored. The effects that the faults have on the active power output of the nuclear reactor generator are also studied.

- Modelling and analysis of both strong and weak AC systems to determine their effects on the operation of CSC- and VSC-HVDC technology during steady-state conditions. For CSC-HVDC technology, this consists of the Effective Short Circuit Ratio (ESCR) where the contribution of the reactive filters is considered. For VSC-HVDC technology, the gains of the DC voltage, active power and AC voltage controllers are adjusted to ascertain their effects on the control system for a combination of different Short Circuit Ratios (SCR).
- Comparisons between the response to system faults of a VSC-HVDC PSCAD model and a similar one in MATLAB/Simulink is made. In the PSCAD model, AC voltage control is applied whereas in MATLAB/Simulink, reactive power control is adopted. Differences in simulation results are found, due to alternative control strategies employed in each model. AC voltage control provides the best reactive power response during transient fault conditions.
- The performance of the HVDC control systems during AC and DC fault conditions is investigated. In particular the speed of response, stability performance, and fault ride-through capability of both HVDC links is assessed via simulation.
- The performance of both the CSC- and VSC-HVDC links are analysed for different contingencies (circuit outages) within the power system. This includes an assessment of the frequency support and active power control responses for both HVDC technologies during different system configurations. For the VSC-HVDC link, the advantage of fast current reversal and black-start control functions is assessed for the complete loss of both on-site and off-site power supplies to the NPP.
- Single-line diagrams showing application and design of both AC and CSC/VSC-HVDC technology for connecting an NPP to the NETS in practice is produced. An NPP consisting of three reactors, 1500 MW each, connected to a 400 kV double busbar AC substation is designed. One design consists of two-bipole CSC-HVDC links with a combined connection capacity of 4500 MW (2 x 2250 MW). A similar design for two-bipole VSC-HVDC connections of the same rating is produced. Each design includes two 400 kV HVAC double busbar substations to provide the infrastructure required to connect the NPP into the transmission grid. Protection schemes are designed for the HVDC links; HVAC feeder circuits, transformers, and both 400 kV double busbar HVAC substations.
- A schematic design for a frequency controller to successfully interface an NPP with an HVDC link is produced in Microsoft Office Visio. The controller's main purpose is to manage the frequency within the AC power system or the NPP. Within the schematic design, an additional control loop is included to allow the HVDC link to take over the frequency control within the NPP during an islanded situation.

- A case study is undertaken analysing the required responses of two 2250 MW HVDC links when connecting a 4500 MW NPP to the NETS. The overall system was designed in Microsoft Office Visio for a real power flow condition obtained from National Grid. Here the majority of power is flowing south through the HVDC links from the NPP into the AC system. Following the protective tripping of different circuits within the system, a table is created showing the required actions from the HVDC links to prevent thermal overloading of circuits. This includes highlighting the protective tripping of nuclear generator circuit breakers to maintain power system stability if required.
- An economic analysis is carried out for both HVAC and HVDC technology. Technology cost data was obtained and is compared from different projects around the world. Information on the sizes of both HVAC substations and HVDC converter stations is compared. An assessment of the availability and ratings of HVAC and CSC/VSC-HVDC technologies is undertaken to determine the suitability of each for an NPP connection.
- Recommendations for further work surrounding the technical issues for HVDC NPP connections are made based upon the findings in this thesis.

1.3 Outline of the thesis

The EngD thesis is divided into eight separate chapters. The contents of each chapter are described as follows:

- **Chapter 1.** This has already been presented and describes the background of the thesis and motivation for the work undertaken. The objective and outline of the thesis is presented. Finally, the main contributions of the work undertaken are specified.
 - **Chapter 2.** This chapter presents a critical literature review of the key subject areas for the EngD thesis. Here, the fundamental principles of both CSC- and VSC-HVDC technology are presented, including the arrangements of each system, the features and strategy of the protection and control systems, as well as the advantages and disadvantages of each technology. The principles of nuclear power are also discussed, along with the different types of nuclear reactors, NPP design, and requirements for successful connection to an HVAC grid.
- Chapter 3.** In this chapter a technical assessment of HVAC technology for connecting NPPs to an AC system is performed and the model of the NPP and AC system developed in PSCAD is described. Each of the key components which make up the overall system are presented and load flow analysis is carried out to ascertain the steady-state values of the overall system. Finally, dynamic simulations, analysing three-phase faults and their effects on the NPP and AC network are carried out in PSCAD.

- Chapter 4.** In this chapter a technical assessment of CSC-HVDC technology for connecting NPPs to an AC system is performed, describing each of the key components and different control blocks of the CSC-HVDC model and including mathematical analysis where applicable. Simulations are carried out to analyse the response of the HVDC link during steady-state conditions for a combination of different ECSRs at both the rectifier and inverter. The speed of response and behaviour of the HVDC control system for both AC and DC fault conditions are analysed. Finally, the response of the HVDC link to different system contingencies is presented, with particular focus given to the effectiveness of the frequency and active power control functions.

Chapter 5. In this chapter a technical assessment of VSC-HVDC technology for connecting NPPs to an AC system is performed, describing each of the key components and different control blocks of the VSC-HVDC model and including mathematical analysis where applicable. Simulations are carried out to analyse the response of the VSC-HVDC link during steady-state conditions for a combination of different SCR at both the rectifier and inverter. The speed of response and behaviour of the HVDC control system for both AC and DC fault conditions are analysed. Finally, the response of the VSC-HVDC link to different system contingencies is presented, with particular focus on the effectiveness of the black start and past power reversal functions of the VSC-HVDC link control system.
- Chapter 6.** In this chapter single-line designs are produced to demonstrate the complexity involved in HVDC connection of an NPP. First, a 4500 MW NPP consisting of three reactors is designed, along with a 400 kV HVAC double busbar substation to allow power export from the NPP. Three separate technologies for connecting the NPP to the AC grid have been considered in separate designs. The first design presents two AC overhead lines at a transmission voltage of 400 kV. The second design utilises two 600 kV CSC-HVDC links, each rated at 2250 MW. The final design consists of two VSC-HVDC bipole links with the same power and voltage ratings as the CSC-HVDC converters. A schematic design for a controller to demonstrate how the frequency could be controlled by the HVDC link when the NPP is islanded from the AC grid has been designed in Microsoft Office Visio. Finally a case study analysing the responses required from HVDC links to prevent AC circuits from being overloaded is presented.
- Chapter 7.** In this chapter an economic analysis of both HVAC and HVDC technology is made, reviewing the sizes of different HVDC converter and HVAC stations and considering cost data collected from both HVAC and HVDC projects for different voltage and power ratings.

The development and current industry availability of both HVAC and HVDC technology power/voltage ratings is assessed and comparisons are drawn.

- **Chapter 8.** Finally, conclusions from the work undertaken are presented, with recommendations made for further work to address the key technical issues found during the research.

Chapter 2: Literature Review

In this chapter a literature survey pertaining to the connection of nuclear power stations by HVAC and HVDC technology is presented. The principles of both CSC- and VSC-HVDC technology are reviewed. Configurations and protection and control philosophies for both technologies are presented. Finally, the principles of nuclear power are covered, focusing on aspects such as NPP design, requirements for successful connection to an AC grid, and technical issues during transient disturbances.

2.1 NPPs connected by HVDC technology

From the literature review for previous cases of nuclear power connections connected to HVDC systems, it is apparent that this arrangement is extremely rare. The only references found are from the IEEE (Institution of Electronic and Electrical Engineers) Xplore website, and are all taken from Japan in the mid-1980s when, it seems, the Tokyo Electric Power Company was exploring the possibility of such a connection in [6], [7], [8].

In 1983, Sakurai [6] investigated the use of a co-operative control scheme for isolated Boiling Water Reactor (BWR) Nuclear Power Plants (NPPs) connected to HVDC systems. Digital fault simulations were carried out on a system comprising of two-bipole HVDC links between a BWR NPP and an AC transmission system. The authors concluded that the NPP was able to maintain normal operation in the case of a single-pole DC fault without the use of turbine speed controllers. Under a DC pole-pole fault or a three-phase-to-ground fault on the AC terminals, turbine speed controllers were needed to maintain normal operation. Due to the age of the paper it is assumed that CSC-HVDC technology was used, since VSC-HVDC technology appeared in 1997, and the world's first commercial installation, the Gotland HVDC light project did not enter service until 1999 [9].

In [8], the authors developed a “coordinated multivariable control system” for the same arrangement as described in [7]. The control scheme allows the NPP to be operated safely while connected by the HVDC circuits.

In the mid-1980s, the Tokyo Electric Power Company was investigating the feasibility of connecting a BWR NPP some 800 km from the major load demand centre via HVDC links. Ishikawa et al. [7] proposed a control scheme for such an application. The authors carried out a series of simulations on a laboratory test rig representing a BWR NPP connected to the transmission grid via both HVDC and Ultra High Voltage Alternating Current (UHVAC) circuits.

The control algorithm ensures secure operation of the simulated NPP during both hybrid operation (AC and DC circuits in parallel) and pure DC transmission (AC circuit out of service).

The cases investigated in [6], [7], and [8] clearly demonstrate that the feasibility of NPP HVDC links have been considered. From additional literature information in [10], and [11], it seems that no further work has been carried out in this area. It also appears that the proposed control schemes were never put into practice, and with no further mention of these schemes in the literature, it can be assumed that they were not.

2.2 HVDC technology

HVDC power transmission systems used to be constructed using mercury arc valves to perform the conversion from AC to DC [12]. Over time, as larger power ratings were required due to the increasing demand for power, a new era of power thyristor technology began, with the first thyristors being put into operation in the late 1970s [13].

As thyristor technology has developed over the past decades, current and voltage rating has also progressed. This has resulted in less series-connected thyristors are required per valve. As a direct result of this, the cost has reduced. As the technology has been developing at a fast rate both technical and economic benefits have been gained by utilities all around the world [14].

AC transmission is still the most dominant and extensively used means of power transmission, generation and distribution worldwide [15]. With UHVAC transmission systems being developed in large countries like China and India, the use of HVAC for long-distance power transmission is becoming ever more popular [16].

2.2.1 HVDC versus HVAC

Within the power transmission industry, the demand for power is increasing. With cutbacks on fossil fuel power stations and the introduction of clean, emission-free power such as wind, hydro, solar, nuclear and tidal comes the challenge of long-distance power transmission [16].

In countries with large populations and vast land area, the generation sources could be hundreds of miles away from large cities. AC power transmission may not be favourable over such vast distances [17].

An AC transmission line contains parameters such as resistance, inductance and shunt capacitance. These different parameters affect how much power can be transferred through a circuit from the sending end to the receiving end [17]. At light loads on long circuits, reactive power is generated and the voltage profile increases. System instability can occur when the voltage profiles become severely high and drop outside of the required limits [17].

For heavy inductive loads where reactive power is being absorbed from the line, the voltage profile will drop the real power being utilised is decreased [17]. As a direct consequence of this, system voltage instability can be encountered.

AC cable circuits are predominantly capacitive in nature and generate reactive power and possess high capacitive charging currents. A phenomenon known as the “skin effect”, where the AC current becomes distributed within a conductor and reduces the effective cross-sectional area is another issue. Both of these issues reduce the power transmitted through the length of the cable. If shunt reactors are applied to reduce the capacitive effect the distance is still limited to a value of approximately 50–80 km [18].

If two asynchronous systems (e.g. 50 and 60 Hz) are to be interconnected to each other, then AC transmission is not viable. With each of the generators rotating at different speeds, corresponding to the required frequency, there is great difficulty in maintaining synchronism between the two. When an HVDC link is adopted, the two systems are de-coupled and any disturbance that occurs at one end of the AC system will not propagate to the other due to this “firewall” function [19].

In some networks additional AC feeder circuits are required to allow additional transfer of power from new generation sources to load demand centres. The fault level of the AC system can be greatly enhanced due to the addition of extra circuits providing an additional source of fault infeed. This can cause the maximum current rating of switchgear on the affected system to be exceeded [20]. If an HVDC connection is used, then the contribution to the fault level will be minimal due to the current being limited by the control system [19]. This can provide an alternative solution compared to a new AC circuit where the maximum system fault level approaches the full rating of the switchgear.

The fast control of HVDC links can be used to divert power flows around the AC grid, helping to relieve bottlenecks within the transmission system and increase operational flexibility.

2.2.2 Current source converter HVDC technology

Current source converter HVDC technology is widely used in industry today. Thyristors are used to achieve the necessary voltage rating by connecting several of these in series [21]. A synchronous voltage source is required for them to successfully operate. The main component used for HVDC conversion is the three-phase, full-wave bridge. This is often referred to as a six-pulse converter or Graetz bridge. According to [21], two six-pulse converters can be connected in series to form a twelve-pulse bridge; such an arrangement is shown in

Figure 2 and is standard practice for HVDC thyristor links.

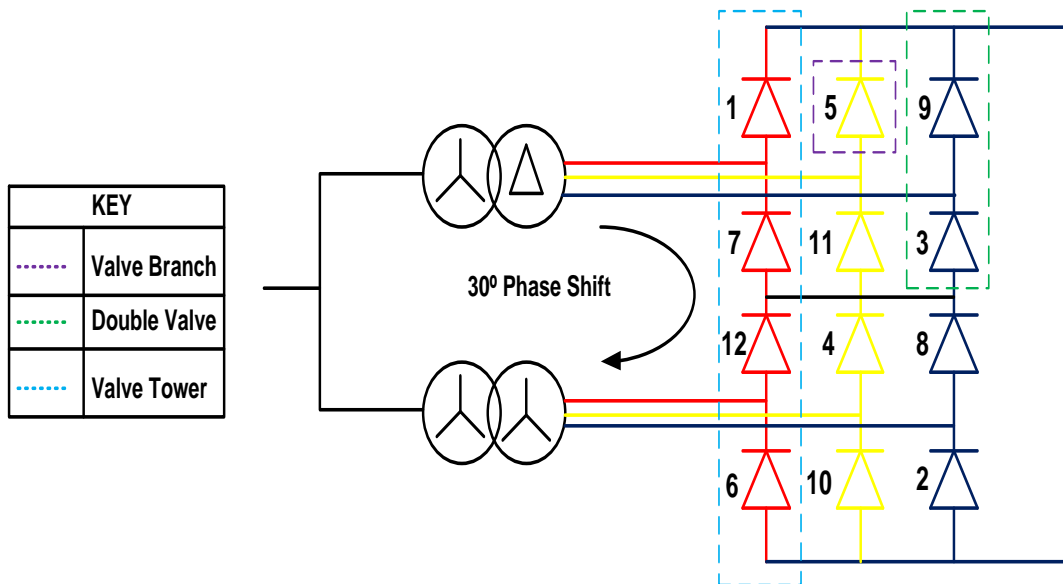


Figure 2: CSC-HVDC twelve-pulse converter

The term six-pulse relates to six commutations or switching operations per period. The output obtained is a characteristic ripple of six times the fundamental frequency in the DC output voltage [22]. Each six-pulse bridge comprises of six thyristor valves. Each contains a number of series-connected thyristors, which helps to achieve the desired DC voltage rating. According to [22], the DC terminals of two six-pulse bridges with AC voltage sources displaced by 30 degrees can be connected in series to help increase the voltage and help eliminate some of these characteristic harmonics [22]. The author is aware that this feature has been applied extensively on many CSC-HVDC projects in practice and operation in this configuration is often referred to as twelve-pulse operation.

2.2.2.1 Requirements for successful converter operation

In [23] it is stated that CSC-HVDC converters require a relatively strong synchronous voltage source in order to commute.

Commutation is the transfer of current from one phase to another in a synchronised firing sequence of the thyristor valves. The requirement for a strong voltage source is very real and there have been many instances in practice where valve commutation has failed due to the AC system being weak.

In a six-pulse converter the valves are fired every 60 degrees. However, this can result in the production of more harmonics, which may cause voltage distortions within the AC network. Alternatively, by adopting the twelve-pulse converter, the valves are fired every 30 degrees. By doing this it is claimed in [23] that “the production of further harmonics is reduced”. As described in [24], this is a proven method in industry to mitigate the harmonic effects through appropriate changing of firing angle control that is sometimes known as equidistant firing control. In most literature, the commutation sequence of a six-pulse bridge is described, for purposes of simplicity, but a detailed understanding of twelve-pulse operation is important as this is the most common configuration employed in practice [25]. The full twelve-pulse commutation sequence is shown in Figures 3 and 4 and a description of each of the twelve stages of commutation is described as follows:

Stage 1

Diode 1 starts to conduct when the red phase becomes positive. Diode 6 turns on when the yellow phase voltage (green) enters the zero crossing with the blue phase voltage on the negative cycle.

Stage 2

The blue phase becomes positive on the negative cycle and diode 2 turns on. The yellow phase enters the zero crossing with the red phase and diode 6 turns off.

Stage 3

The red phase enters the zero crossing with the blue phase and diode 1 turns off. The yellow phase becomes positive and diode 3 turns on.

Stage 4

The blue phase enters the zero crossing with the yellow phase and diode 2 turns off. The red phase become positive on the negative cycle and diode 4 is turned on.

Stage 5

The red phase enters the zero crossing with the yellow phase and diode 3 turns off. The blue phase becomes positive and diode 5 turns on.

Stage 6

The red phase enters the zero crossing with the blue phase and diode 4 turns off. The yellow phase becomes positive on the negative cycle and diode 6 turns on.

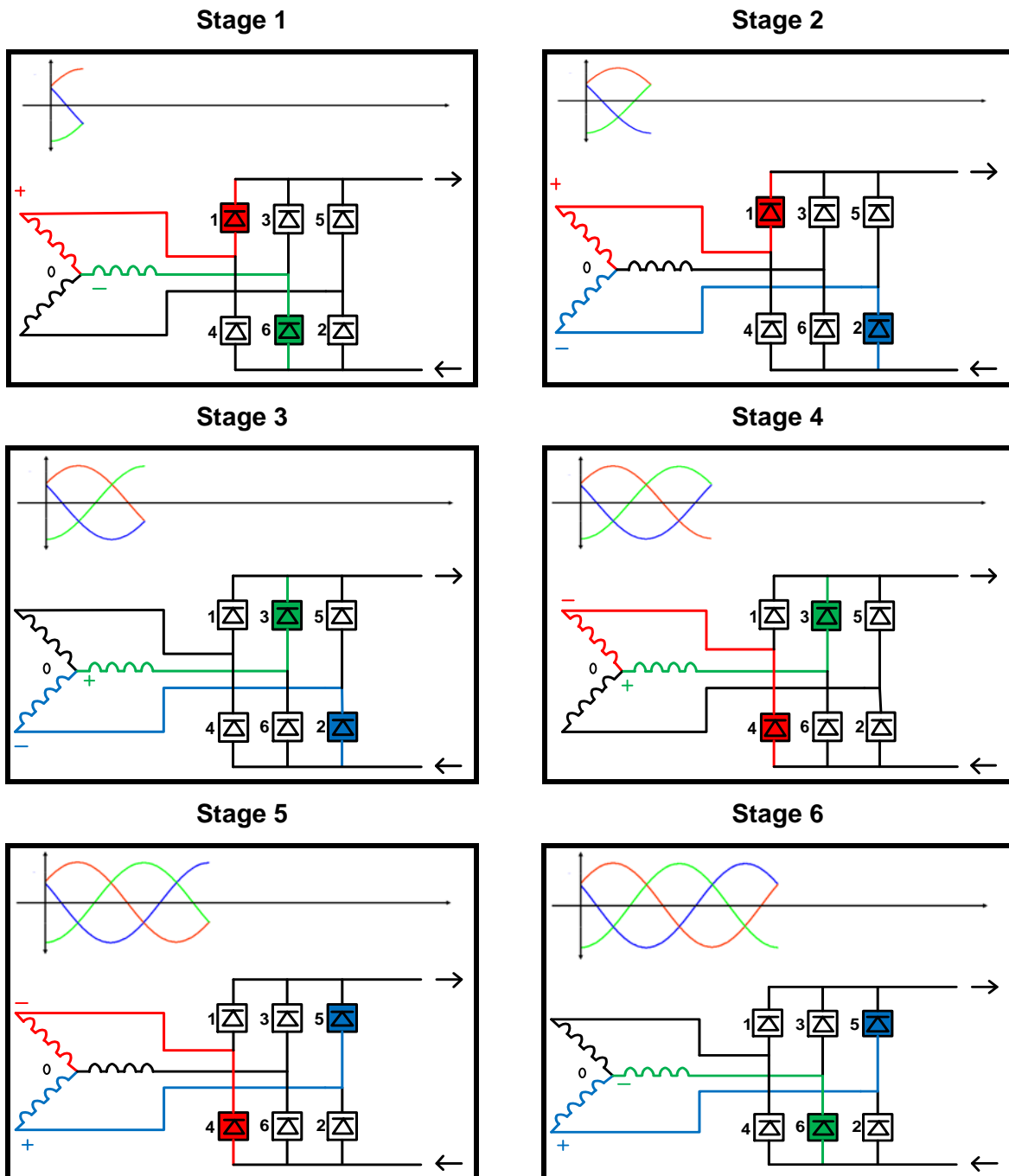


Figure 3: Stages 1–6 of the twelve-pulse commutation sequence

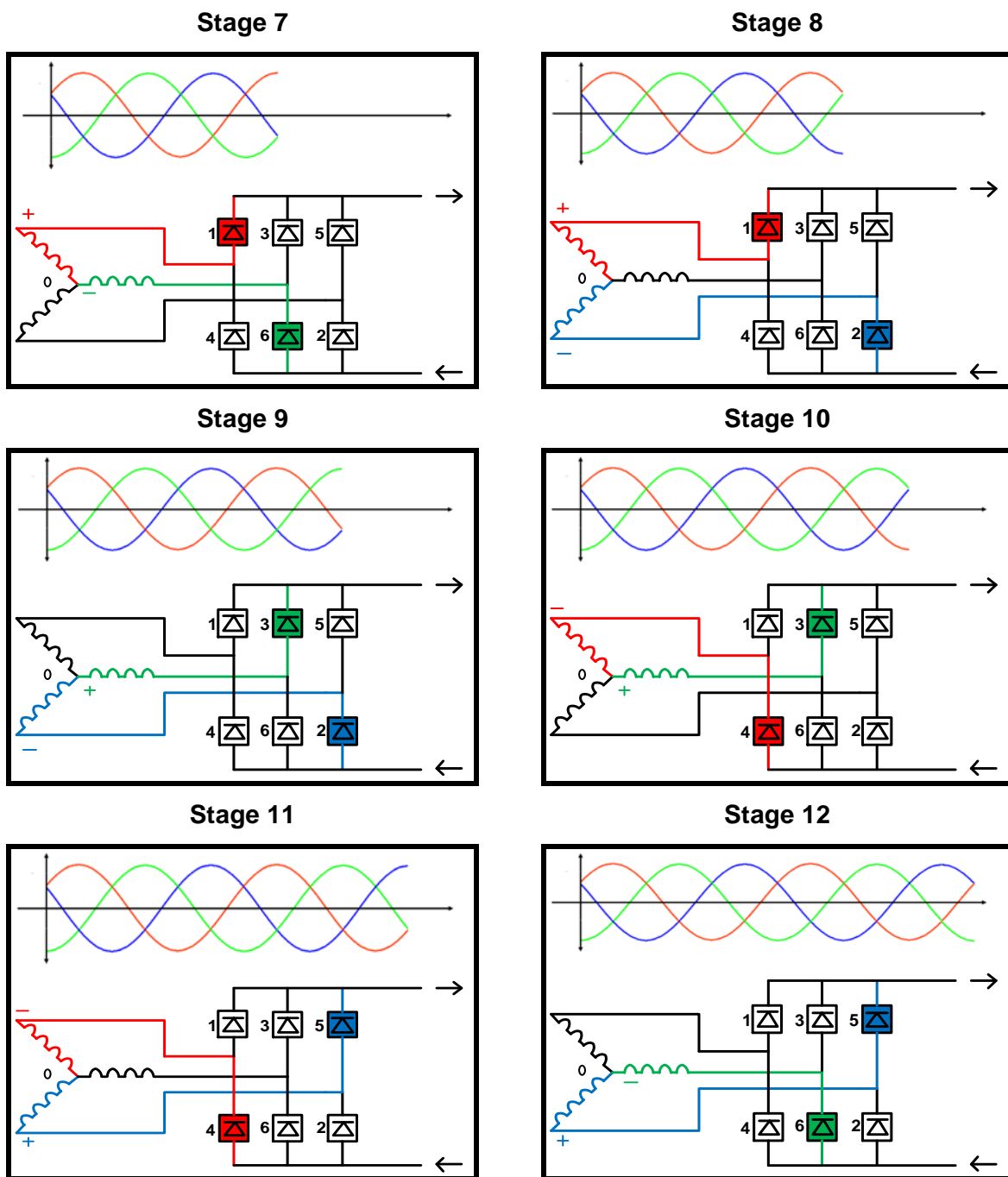


Figure 4: Stages 7–12 of the twelve-pulse commutation sequence

Stage 7

The blue phase enters the zero crossing with the yellow phase and diode 5 turns off. The red phase becomes positive and diode 1 turns on.

Stage 8

The yellow phase enters the zero crossing with the red phase and diode 6 turns off. The blue phase becomes positive on the negative cycle and diode 2 turns on.

Stage 9

The red phase enters the zero crossing with the blue phase and diode 1 turns off. The yellow phase becomes positive and diode 3 turns on.

Stage 10

The blue phase enters the zero crossing with the yellow phase and diode 2 turns off. The red phase becomes positive on the negative cycle and diode 4 turns on.

Stage 11

The yellow phase enters the zero crossing with the red phase and diode 3 turns off. The blue phase becomes positive and diode 5 turns on.

Stage 12

The red phase enters the zero crossing with the blue phase and diode 4 turns off. The yellow phase becomes positive on the negative cycle and diode 6 turns on.

Current will flow down the positive pole and return along the negative pole. The power flow is in one direction only and will be split between the two poles. When the diodes above are replaced with thyristors, the devices can be switched on by applying a firing pulse to the gate terminal. Once the anode current has exceeded the latching current, the device stays on. A thyristor can be switched off if the anode becomes negatively biased; this is otherwise known as line commutation.

In [26] the firing angle alpha (α) is defined as the angle between the phase voltage crossing of the valve winding voltage and the instant when the thyristor is fired. This is seen to be the case in

Figure 5, which shows the effect that the firing angle has on converter operation.

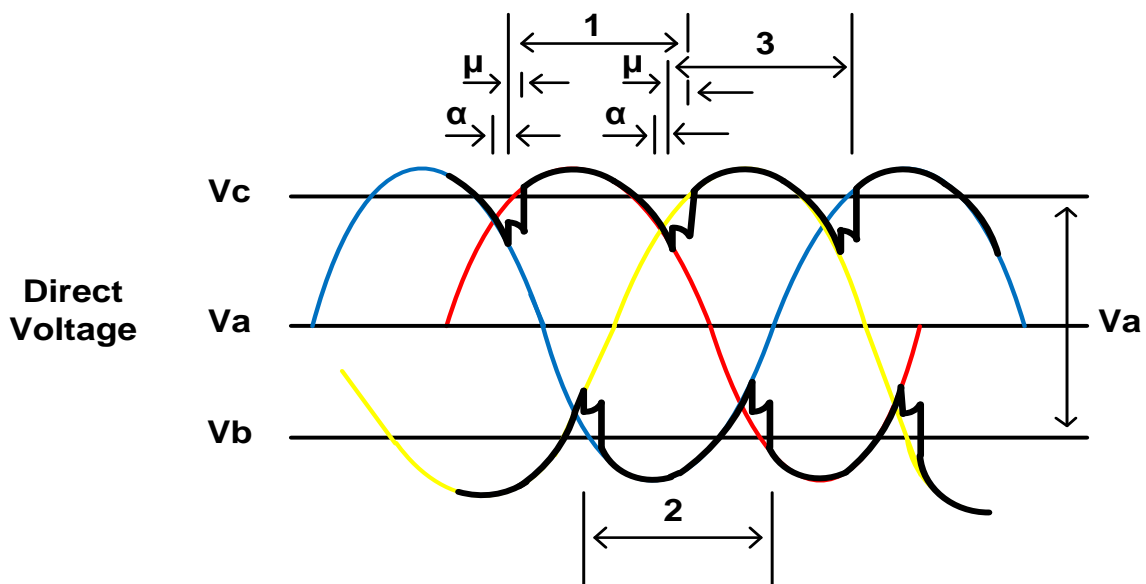


Figure 5: Effect of firing angle on converter operation

In [27] the delay angle is shown to control when the commutation process commences where the greater the delay angle (μ), the smaller the mean direct voltage. If the firing angle α is increased beyond 90° , the area of the phase-to-phase voltage connected to the DC terminals will be negative. This paragraph is accurate as beyond 90° the firing angle of the converter becomes large and is often called the “extinction angle” or “gamma” γ . This angle represents the time between the end of the overlap period and the time when the phase voltage associated with the outgoing valve becomes more positive/negative than that of the next valve [28].

It is also described in [29] how notches appearing in the waveforms are caused when commutation takes place and how commutation is a momentary line-to-line short circuit imposed by the converter valves. Apparently this does not produce serious fault currents due the valve reaching equality with the DC voltage, the current turns off and the circulating path is interrupted. This is true as the three-phase symmetrical short circuit capacity available from the network at the converter station connection point should be at least twice the converter rating to ensure successful operation [30].

CSC-HVDC technology operates with the AC current lagging the voltage. This creates a demand for reactive power, which unless provided locally can drain the reserves of the AC system and cause severe voltage dips, potentially resulting in system instability [30].

It is described in [31] how Flexible AC Transmission devices (FACTS), such as Static Compensators (STATCOMs), Synchronous Condensers or Static Var Compensators (SVCs) can be used to provide reactive power support to maintain the necessary voltage for successful valve commutation. Such devices have been employed on numerous projects for this reason [32] and hence these are important options when the AC system strength is weak.

Pre-established AC voltages within distinct operational ranges are among the pre-requisites for a CSC-HVDC converter station to start operation. In [33] it is described that AC system disturbances may cause CSC-HVDC links to suffer from commutation failures that can lead to system disturbances. There have been many incidents of this happening in practice and several control methods in [34], [35], and [36] have been investigated to deal with this issue. The principles of commutation failure are described in the next section.

2.2.2.2 Commutation failure in CSC-HVDC technology

Rectification or inversion for HVDC systems is achieved through the process known as line or natural commutation.

Commutation is the process of the transfer of current between any two converter valves that are both carrying current simultaneously during the process. The voltage at the rectifier and inverter is supplied by the AC networks to which each end connects [36]. As each valve switches on, conduction will commence while the current begins to fall to zero in the next valve to turn off. The principle of commutation failure is shown in Figure 6.

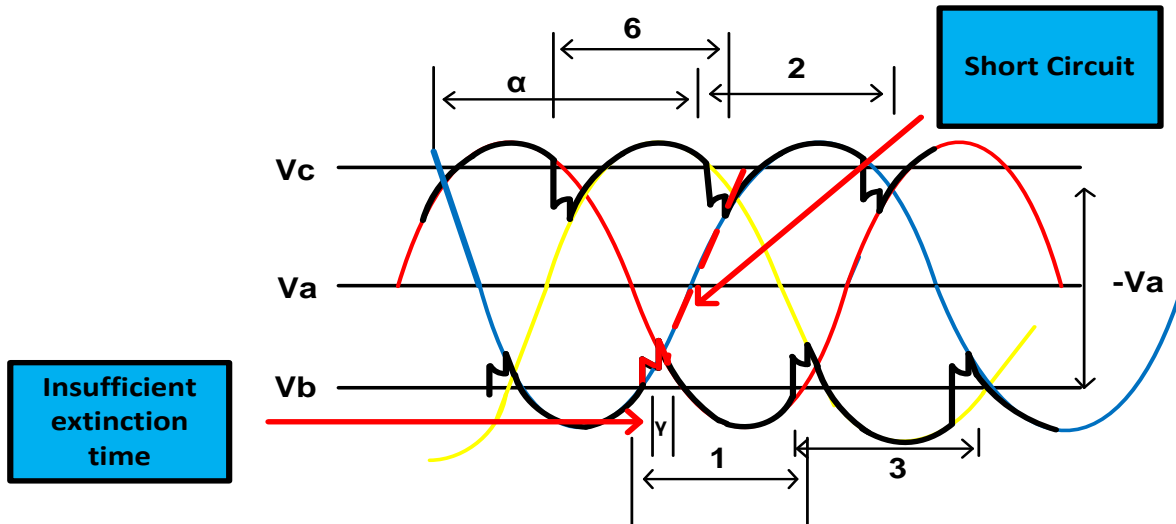


Figure 6: Commutation failure at the inverter in a CSC-HVDC link

The inverter valve can only turn on and conduct when the positive voltage from the DC line is greater than the back negative voltage derived from the commutation voltage of the AC system. In [37] and [38] it is described that “a minimum extinction time is required in order for the valve in conduction to fully turn off before its terminal voltage becomes positive again”. If the voltage depression is high during the fault and the extinction angle is too small, then the valve does not turn off and re-conduction is encountered. This prevents the commutation of the current to the next valve from occurring 60° later. When the other valve connected to the same phase in the six-pulse bridge conducts, a short circuit occurs and a temporary cessation of power transfer will be encountered until the protection and control system has successfully removed the short circuit. From Figure 6 it can be seen that a short circuit will occur if the above requirements are not satisfied.

In [39] and [40] it is described how “the commutation prevention function” within the DC control system can help prevent continuous failure by increasing the extinction angle at the inverter. This is true but if the extinction angle is increased too much, then additional harmonics, losses and reactive power absorption may occur [41]. If the HVDC link is connected to a weak AC system, then further voltage depressions can be experienced due to the increase in extinction angle [41]. Therefore, it appears that additional controls are required to achieve an optimum solution.

In [42] it is described that an extinction angle safety margin can be incorporated into the control system to help overcome this. If the commutation condition persists, then the DC protection and control system will remove the link from service. From further reading and investigation in [43] and [44], this control strategy has been employed in practice and has proven effective at minimising instability to the HVDC link and AC system caused by the commutation failure.

2.2.2.3 CSC-HVDC configurations

Thyristor valves and converter transformers can be developed into many different configurations. Some of the more important of these configurations are described in this section.

Monopolar HVDC systems. These normally contain either a ground return or metallic return. In the event of a pole outage, 100% power transmission is lost. One or more six-pulse converter units are connected in either series or parallel and a single conductor connects the positive pole at one end to the positive pole at the other [45].

In [45] it is described how “a ground return is installed either through the earth or sea and is constructed to allow continuous operation”. In the event of either a pole outage or permanent DC cable fault, 100% of active power transmission through the link will be lost. From the monopolar configuration shown in Figure 7, it can be seen that this is the case.

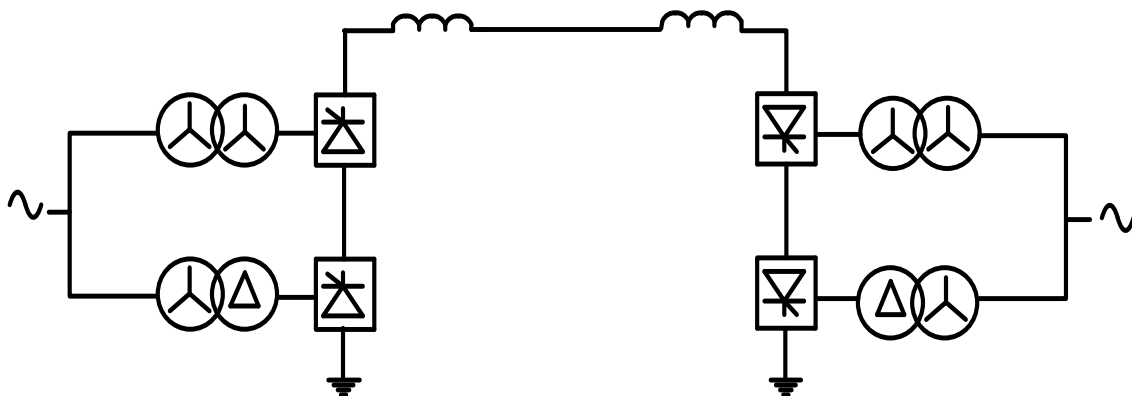


Figure 7: Monopolar with ground return

The above configuration can be a cost-effective solution for HVDC cable transmission or can form the first part of a potential bipolar upgrade [45].

A modification can be made to the configuration in Figure 7 to include a metallic return option. This option can be used as the first stage of a bipolar scheme, which will help to avoid ground currents [45]. This configuration consists of one high and one medium voltage conductor. A monopolar HVDC system with metallic return is shown in Figure 8.

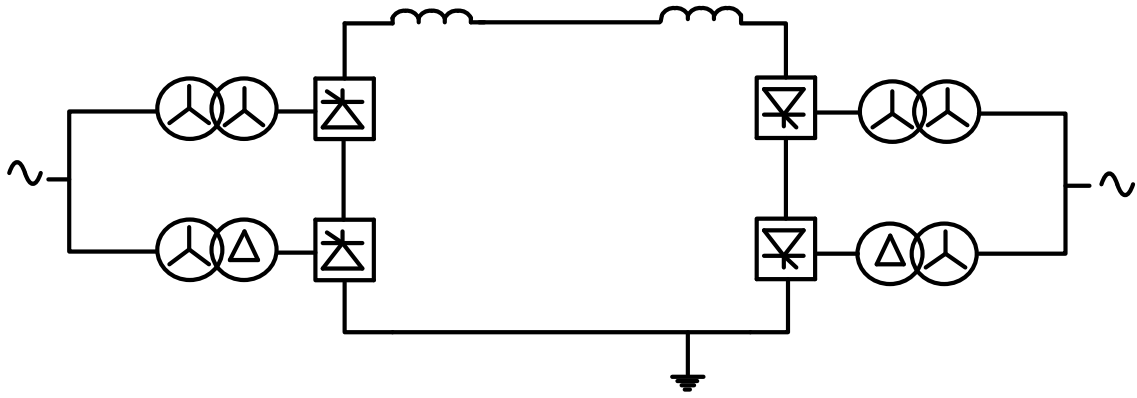


Figure 8: Monopole HVDC with metallic return

If the connection distance between the two ends is very short, then this option may be preferred to that of the line and ground electrode option [45].

Bipolar HVDC systems. These consist of two poles, each of which includes one or more twelve-pulse converters connected in series or parallel. One pole is positive and the other has negative polarity to ground for power flow in one direction only [45]. A bipole is a combination of two monopolar schemes. An example of this is shown in Figure 9.

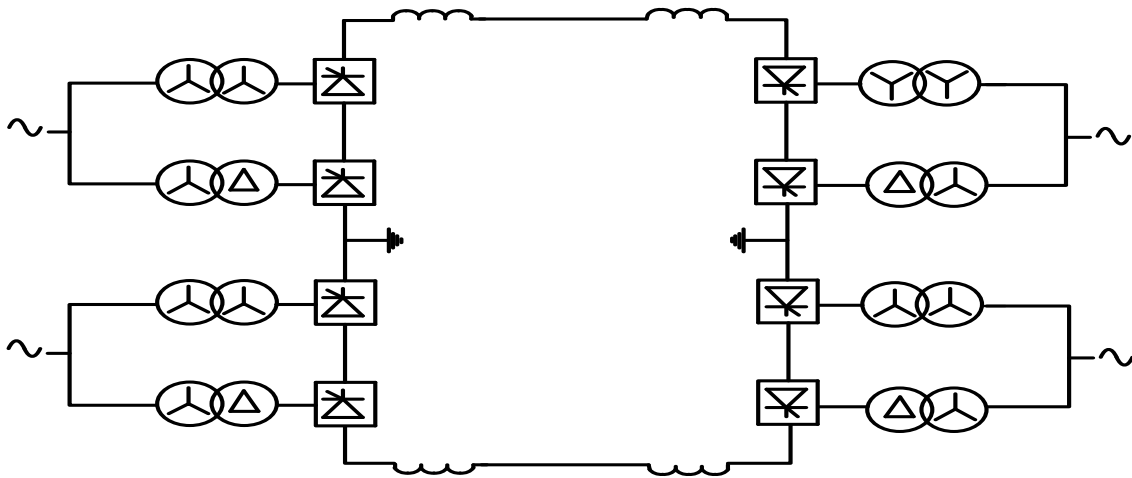


Figure 9: Bipolar HVDC system

The addition of a ground return offers good operational flexibility. During an outage of one pole, the other can operate continuously with ground return [41]. If a pole outage is required over a long period, then the system can be operated in monopolar return mode, providing proper switching arrangements are provided. When one pole cannot be operated at full load current, then the two poles of the bipolar scheme can be operated with different currents, as long as both ground electrodes are connected [41].

Back-to-back HVDC systems. These are special cases of monopole HVDC connections where there is no transmission line or cable present and both converters are located in the same substation. An example of such a system is shown in Figure 10 [41].

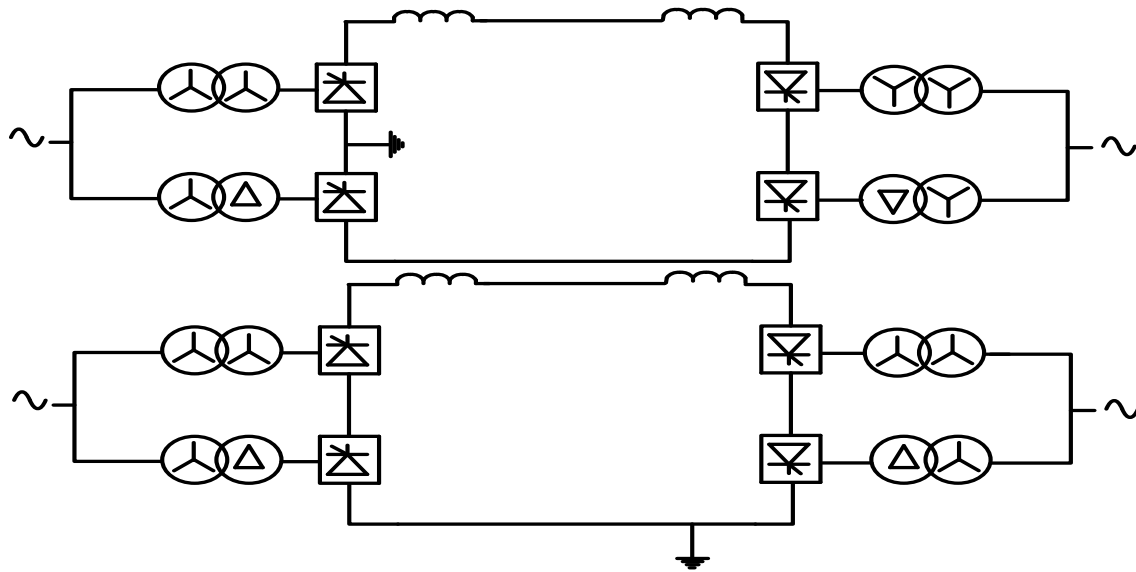


Figure 10: Back-to-back HVDC system

For back-to-back converters, the DC voltage is low and the current is high due to a much shorter interconnection between the two ends. These particular systems may be required for interconnecting two asynchronous networks, with the whole installation sited in one location [46].

2.2.2.4 Power reversal in CSC-HVDC technology

CSC-HVDC technology utilises thyristor based converter stations. The DC current direction is fixed, since the thyristors can carry the current in one direction only. To change the power direction, the DC voltage polarity has to be changed, which can be achieved through the firing control of the valves. In [47] there is a description of how “The time taken to perform a full change in power direction may be a few minutes or more”.

If fast high speed switches are used, then this may be reduced. If a cable is installed however, then a sufficient amount of de-ionisation time is required [41]. In [41] a time of 200–300 ms is needed to discharge the DC cable before re-energisation takes place. If this is not completed, then a large overvoltage may occur when power transfer recommences and the DC cable is still charged. From the literature sources, the time of voltage polarity reversal and DC cable discharge will vary, but are important factors in CSC-HVDC operation.

During a DC fault condition, a “forced inversion” action at the rectifier is activated to discharge the cable, where the firing angle at the rectifier is forced passed 90 degrees and the converter becomes an inverter. This is followed by blocking of the DC valves and opening of the converter AC circuit breakers to clear the fault. High speed switches are then opened to isolate the DC cable from the converter and the cable is subsequently discharged so that the damage can be located and repaired.

2.2.2.5 Protection and control of CSC-HVDC systems

In [48] and [49], based upon real HVDC projects, the protection and control for a CSC-HVDC system is vital for the successful operation and protection of the link during steady-state and transient conditions. Many high-level functions reside within the control system and can be used to enhance the operation of the link, as well as to provide additional benefits to the AC system as compared to AC technologies.

Within a CSC-HVDC system, the DC voltage and current are precisely controlled to achieve the desired power transfer [41]. Continuous and accurate measurement quantities such as the DC current and firing angles for both the rectifier (α) and the inverter (γ) are required. Under steady-state conditions, the inverter is assigned the task of controlling DC voltage, which can be done by maintaining a constant extinction angle (γ), which in turn causes the DC voltage to droop with increasing current [41] as shown by the **A–B–C–D** characteristic in Figure 11.

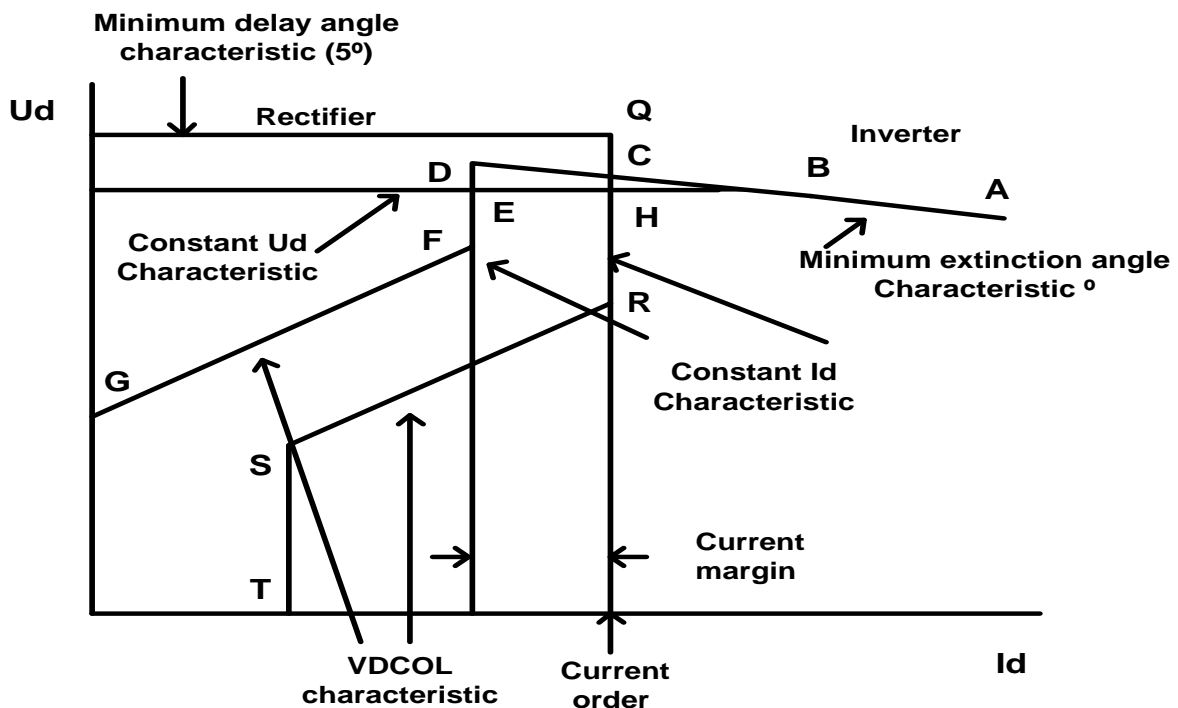


Figure 11: Control characteristic of CSC-HVDC [41]

The weaker the AC system connection that the inverter is connected to the steeper the droop U_d . The inverter can operate in DC voltage controlling mode that is constant to the characteristic B–H–E [41]. This will result in the extinction angle increasing beyond its minimum limit. While the inverter is operating in any of the above control modes, the rectifier controls the DC current (I_d). When the rectifier is operating in current control during steady state, its characteristic takes the form of the vertical section Q–C–H–R [41]. The operating point of the HVDC system is where the rectifier and inverter characteristics intersect, either at points C or H; this particular operating point can be reached by utilising the on-line tap changers on the converter transformers. The inverter must establish the DC voltage control (U_d) by adjusting its own tap changer to attain the desired operating level if it is in constant minimum (γ) control [50].

If the inverter is in constant DC voltage control, the tap changer will control U_d with an extinction angle equal or slightly larger than its minimum setting [51]. If the inverter is operating in constant DC voltage control at the operating point of H and the current order I , is increased, the operating point H moves towards and beyond point B. As a direct result the inverter will change to constant extinction angle control and operate on the characteristic A–B [51].

The DC current order is sent to both the rectifier and inverter. A small value of the current order may be subtracted from the current order sent to the inverter; this is otherwise known as the current margin (I margin). Despite the inverter also possessing a current controller, the rectifier will override this to maintain the DC current at the required order. The current control at the inverter becomes active only when the current control at the rectifier ceases, when its delay angle is held against its minimum delay angle limit, which can be readily seen in Figure 11, where the minimum angle delay limit at the rectifier is the horizontal characteristic Q.

If the AC commutation voltage at the rectifier end is low and the Q characteristic falls below point E, then the operating point will shift from point H to somewhere on the vertical characteristic D–E–F [51]. The inverter then changes to current control mode, controlling the current I_d . The rectifier controls the DC voltage as long as it is operating along the minimum delay angle characteristic Q. The controls can be designed to enable transition from the rectifier controlling the current [51].

If a CSC-HVDC link is connected to a weak AC system, then a disturbance has the potential to depress the AC voltage at either the rectifier or inverter.

In an attempt to compensate for this, the HVDC control system will try and maintain full load current. A drop in voltage at each end will result in a lowered DC voltage; the DC current order is normally reduced if the DC voltage is lowered. This can be observed in the rectifier R–S–T and inverter F–G characteristic shown in Figure 11.

Work has been carried out in [52] and [53] analysing this Voltage Dependent Current Order Limiter (VDCOL) control function. If an AC system disturbance is created, then the VDCOL control will keep the DC current (I_d) to the lowered limit during recovery, which aids the revival of the DC system and only when the voltage has recovered sufficiently will the DC current return to its original value. This work has shown the importance of the VDCOL function within the HVDC control system during transient conditions.

In addition to the standard control functions that are performed by the HVDC control system; there are some special-purpose controls which can enhance the performance of the AC system. These special-purpose controls have been investigated and described in [54] and [55] and a summary of these control functions is provided:

- **AC system frequency control.** The frequency of the AC system can be regulated via a slow-responding controller to either increase (run-up) or decrease (run back) the active power order. Power can be drawn from one system to the other to assist in stabilisation.
- **AC system damping controls.** AC systems can be subject to power swings due to electromechanical oscillations through the power system. Either the DC power or current order can be modulated by a special controller to provide the necessary damping margin. The frequency or voltage phase angle of the AC system is measured at both ends and based on these values the controller will provide the required adjustment in modulation quantity [54].
- **Sub-synchronous oscillation damping.** Steam turbines and electric generators can experience mechanical oscillation modes between different stages of operation. If a generator is feeding into a rectifier of the DC link, then supplementary control may be required to ensure any sub-synchronous oscillation modes are positively damped out to reduce torsional stresses on the turbine shafts [55].
- **Step change power adjustment.** A defined step change in power adjustment can be implemented to rapidly increase or reduce the active power. If a generator or transmission line is ready to be tripped by AC protection, a signal can be sent to the DC control system to adjust the power or current order to compensate the actual loss [55].

- **AC undervoltage compensation.** In areas of an AC power system that are prone to voltage collapse, the HVDC controls can be used to perform a fast power or current order reduction to help alleviate the situation [55]. This reduction in either active or reactive power can remove the undervoltage stress on the system and aid with system recovery.

During fault conditions a sequence of protective actions is initiated to clear the fault, prevent system instability, and remove the affected section from the power system as soon as possible. The sequence of protective actions for CSC-HVDC technology will depend on the manufacturer concerned but in [56] and [57] some fundamental actions are considered. The following fundamental control actions are encountered in the protection sequences for CSC-HVDC technology:

- **Temporary block.** If excessive current is present on the system for a very short time, then a temporary “blocking action” may be sent to the valves until the current and voltage have recovered.
- **Permanent block.** Permanent faults require the complete removal and isolation of the faulted section from the HVDC system. Depending on the location of the fault then following converter blocking the AC pole circuit breakers are opened to ensure full clearance is achieved.
- **Forced inversion.** To minimise stress on equipment and ensure a fast discharge of the DC cable/line, the rectifier firing angle (α) is increased past 90° to enable forced inversion during fault clearance. For a minimum time period, 200–300 ms, this function is enabled during the protection sequence prior to the blocking command being issued to the valve firing control. A range of different blocking sequences can be initiated depending on the type and location of the fault.
- **Emergency switch-off.** As part of the protective sequence involving the clearance of a permanent fault, an emergency “switch-off” command may be issued to the DC control system. The switch-off will prevent the DC pole control from initiating any further unwanted control actions which could aggravate the system during fault clearance.
- **Emergency shutdown.** If, during a reconfiguration sequence, an error occurs somewhere in the process, then an emergency shutdown will be issued to remove the DC link from service. This action helps to limit any potential damage from occurring to the DC equipment.

2.2.3 VSC-HVDC technology

Due to the progress of power electronic devices with fast “turn-on” and “turn-off” capability; VSC-HVDC technology has become extensively adopted for the connection of energy to transmission systems [58]. Their capability to change current direction, as well as yielding fast active and reactive power modulation provides significant operating advantages [58].

In [59] it is shown that VSC-HVDC technology has been in use since the 1980s and applied to motor drives. Their “soft-start” switching capabilities combined with Pulse Width Modulation (PWM) control allows smooth switching and exact control of motor starting and stalling. A detailed literature review of VSC-HVDC technology is presented in the following sections.

2.2.3.1 Operating principles of VSC-HVDC technology

In [60], a description is provided of how VSC-HVDC technology can be used to inject power into the AC network (capacitive mode) or absorb it from the AC network (inductive mode). These functionalities can be carried out independently at the rectifier or inverter. The term VSC originates relates to the connection of a voltage source on the DC side of the converter [60].

Based upon the description in [60], a diagram showing a VSC-HVDC link is shown in Figure 12. A DC voltage source (U_s) has a DC resistor (R_d) which represents the circuit resistance. The DC shunt capacitor stabilises the DC voltage (U_d). VSC-HVDC technology can appear in different topologies, hence the DC storage capacitor can be connected between both poles or as multiple storage capacitors dispersed throughout the converter phase units [60].

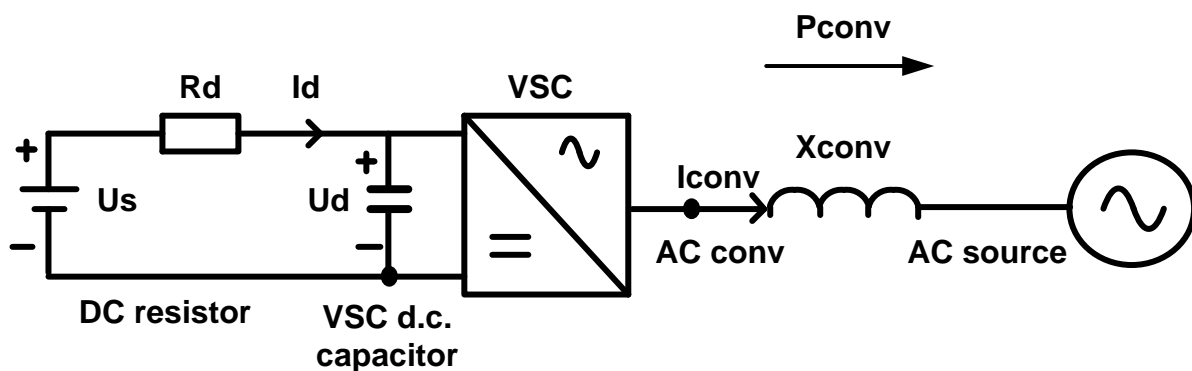


Figure 12: VSC-HVDC operating principles

The active and reactive power flow through the link can be controlled in a simple manner via the control method known as power angle control.

By changing the phase angle across the reactor in the figure above, the active power can be adjusted and the voltage amplitude enables the reactive power to be controlled. The following formulae show this relationship [60].

$$P = U_{conv} \times UL \times \sin \theta \quad (2.1)$$

$$Q = U_{conv} \times (U_{conv} - UL) \times \cos \theta \quad (2.2)$$

Where:

- θ = The phase angle between the converter bus voltage U_{conv} and AC system UL
- L = The inductance of the HVDC converter

In [60], on the AC side, the inductance (X_{conv}) stabilises the AC current and controls the active and reactive power of the the VSC. This inductance can be implemented either as leakage inductances in transformers, in reactors, or as a combination of both.

In [61] a VSC can be used to connect a passive or strong AC network to the AC side. When connected to a passive network, the power flow is from the DC input side towards the passive load on the AC side. In the opposite scenario when connected to an active network, the power can be in both directions by controlling the AC voltage U_{conv} of the VSC. These unique capabilities have resulted in the extensive deployment of VSC-HVDC technology [62].

Like all power electronic converters, VSCs can generate harmonic voltages in the AC and DC systems. In a simplified manner, a VSC can be considered as a harmonic current source connected in parallel with the storage capacitor. This behaviour is opposite to that of conventional current source converters [62].

VSCs can generate or absorb reactive power. Both real and reactive power can be controlled independently. The direction of power flow can be reversed without changing the polarity of the DC voltage [62]. VSCs do not require a synchronous AC voltage for their operation. The above characteristics have resulted in its selection for many projects around the world [63], [64], [65].

In [66] the self-commutation of VSCs permits black-start capability, where the converter operates like a synchronous generator. The dynamic support of the AC voltage at each converter terminal improves the stability and increases the transfer capability of the both the rectifier and inverter. The startup procedure for a VSC-HVDC black start procedure is described in detail in [67] and was used on the Cross Sound project during the August 2003 blackout in the north-eastern United States to provide emergency power to the AC grid [68]. The independent reactive power and active control ensured a smooth startup of the AC network.

A VSC-HVDC link can be considered as the equivalent of an asynchronous generator without inertia, but with the capability to control both reactive and active power. The principle of reactive power control is shown in Figure 13.

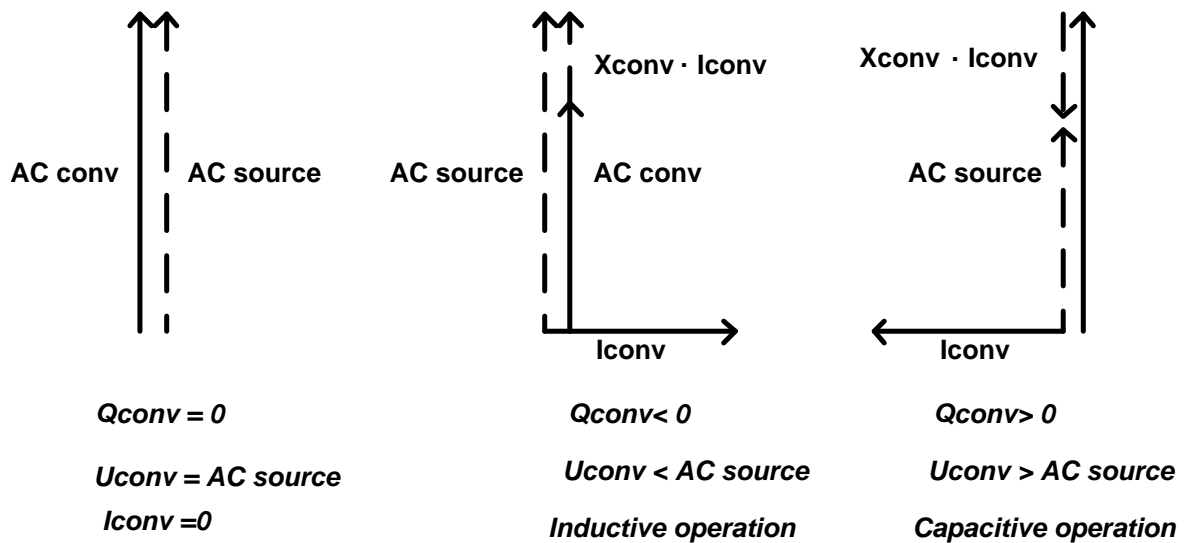


Figure 13: Principles of reactive power control

In [60] the active power is controlled by adjusting the amplitude of the VSC AC output voltage. If the amplitude of the VSC output voltage U_{conv} is higher than the AC grid voltage U_L , then the VSC will inject reactive power into the AC grid (capacitive mode). In the opposite situation, the VSC will absorb reactive power from the AC grid (inductive mode) [60].

The principles of active power control are shown in Figure 14, where regulation of the VSC voltage angle determined the direction of flow through the interface inductance. If the angle of the VSC output lags the AC grid voltage, active power will be injected into the AC grid, acting as an inverter [60].

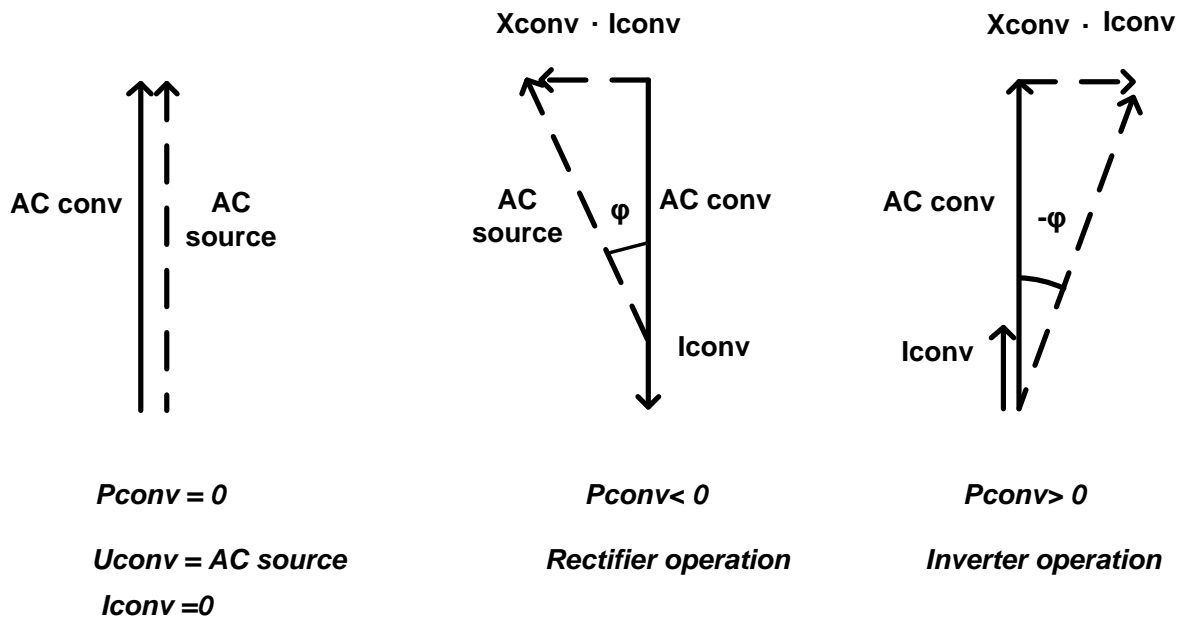


Figure 14: Principles of active power control

On the DC side a current will be drawn from the DC source and the voltage U_d will reduce in accordance with Ohm's law [60]. If the VSC output voltage lags the AC grid voltage, active power will be absorbed from the AC grid. In rectifier operation, on the DC side an equivalent current will be injected into the DC source and the voltage U_d will increase in accordance with Ohm's law [60].

If the VSC is connected to a passive load, an AC output current will be drawn from the VSC determined by Ohm's law [60]. An equivalent DC current will be drawn from the source and the voltage U_d on the DC capacitor will drop. No power is transferred from the passive network otherwise voltage instability could result on the network in question [60].

An active/reactive power capability (PQ) chart for a VSC-HVDC link is shown in Figure 15. In the inductive region the AC current is the restraining factor. There will be a voltage drop across the inductive components (converter transformer and reactor) such that the AC voltage applied to the converter valves will be lower than the AC system voltage. In order to achieve a constant MVA with a reducing AC voltage, the AC current would need to be significantly increased to provide adequate compensation. This in turn would increase the overall rating of the converter which adds to size and cost. The AC current is therefore constrained so that the overall rating of the converter is not exceeded [69], [70].

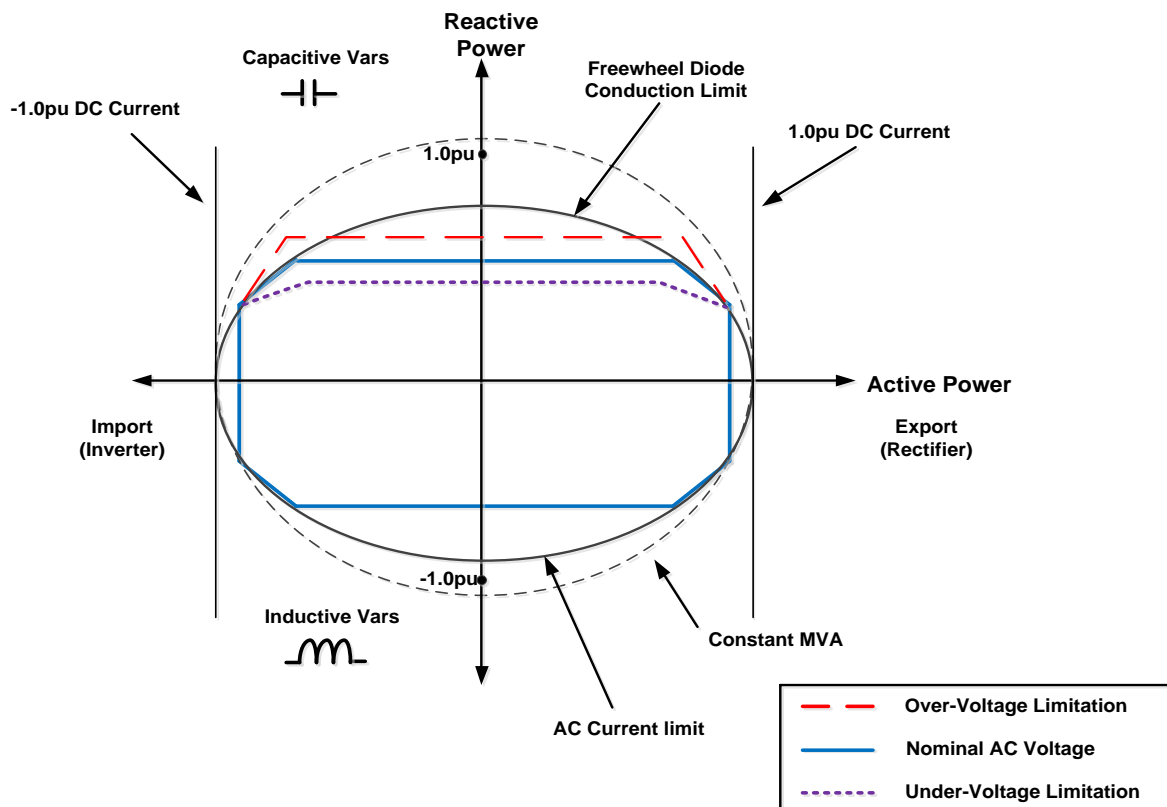


Figure 15: VSC active and reactive power capability curve

In the capacitive region, capacitive current through the circuit inductances leads to a voltage rise, where the voltage applied to the converter is greater than the AC system voltage. In half-bridge configurations, the applied DC voltage must always be higher than the AC valve winding voltage in order to keep the free-wheeling diodes reverse biased; this helps to avoid the converter becoming an uncontrolled diode bridge rectifier. The capacitive current is therefore constrained [22].

2.2.3.2 VSC-HVDC configurations

Like CSC-HVDC technology, VSC systems can appear in many different configurations. An example of a point-to-point scheme is shown in Figure 16, where two VSCs are connected on the DC side [22]. The DC voltage polarity depends on the direction of power transfer. The direction of the power flow is determined by the DC current direction. The current and power flows from VSC1 (the rectifier) to VSC2 (the inverter). The DC current direction is always from a higher DC voltage to a lower level. The voltage at the sending end of will be high compared to that at the inverter end. The above principles are described in [22] and [21].

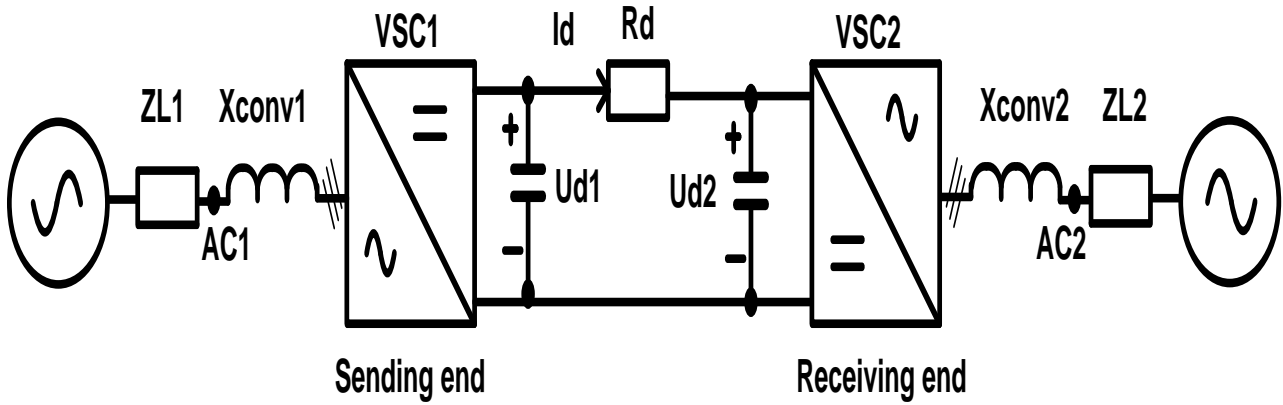


Figure 16: Point-to-point VSC-HVDC link and corresponding components

The power flow can be controlled by keeping the DC voltage at one end fixed. The opposite end controls the DC current.

There are two types of configurations that have been used in VSC-HVDC transmission applications in the past and present. The first was the two-level VSC described in [71] and [72], which is otherwise known as a three-phase, two-level six-pulse converter bridge, which is shown in Figure 17.

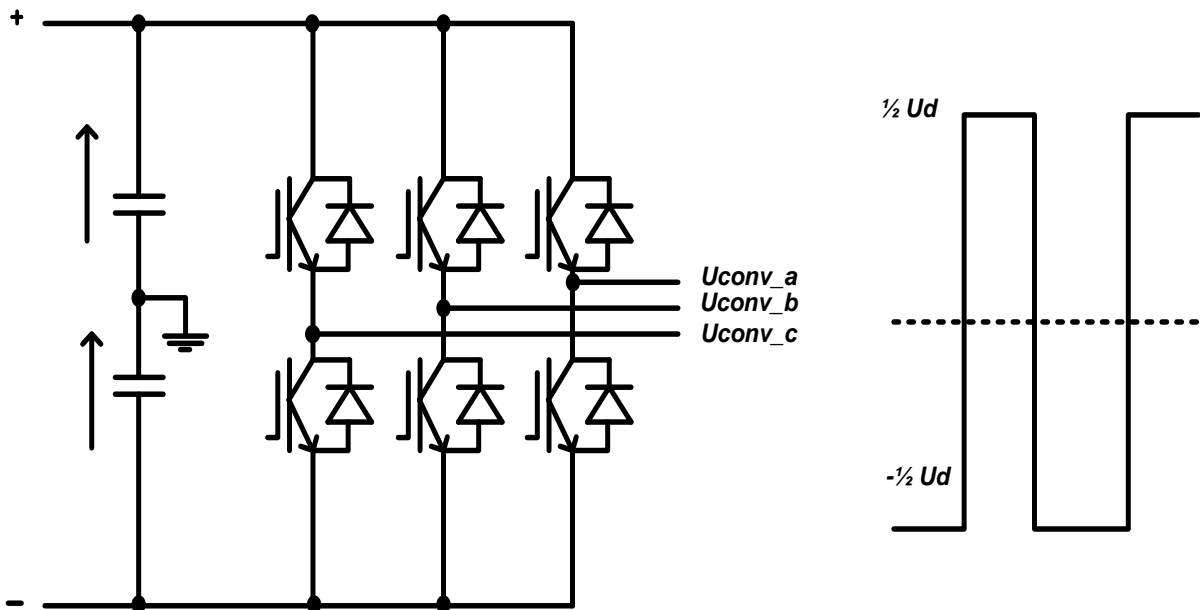


Figure 17: Two-level VSC

Six valves are present and each valve consists of Insulated Gate Bipolar Transistors (IGBTs), together with an anti-parallel diode, hence a \pm voltage level is generated.

A three-level VSC or twelve-pulse converter consists of 12 valves, meaning a high power level can be achieved. In this configuration one arm of the converter consists of four valves. Such a configuration is shown in Figure 18.

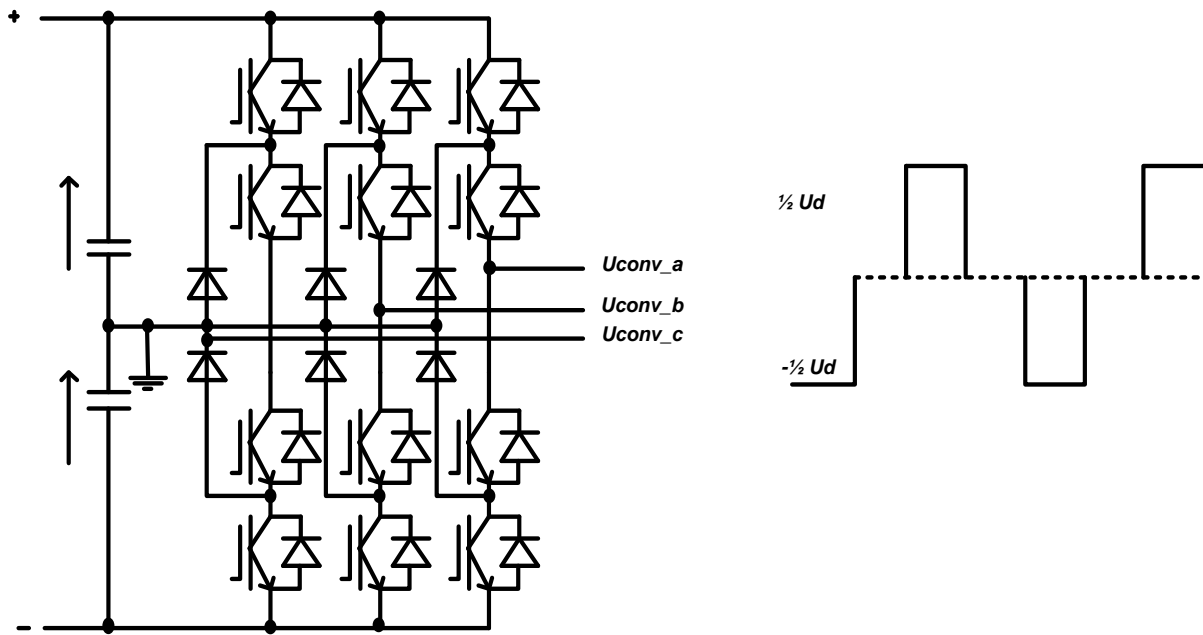


Figure 18: Three-level VSC

More recently, Modular Multilevel Converters (MMCs) have been employed due to their reduced losses compared to the two- and three-level options.

In [19], [22] and [59], different operating configurations of VSC-HVDC systems are briefly mentioned. Each has advantages and disadvantages and is selected according to the requirements of a given project. A summary of such configurations is provided:

Symmetrical monopole. In the symmetrical monopole configuration shown in Figure 19, the AC interface transformers are not exposed to the levels of DC stresses associated with other arrangements such as asymmetrical converters [19].

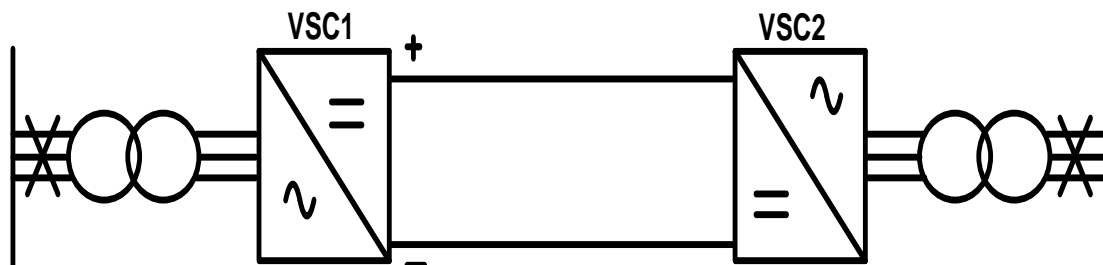


Figure 19: Symmetrical monopole VSC-HVDC converter

Under DC pole-to-ground faults there is no infeed of fault current from the AC side and no DC ground current is encountered during operation [19]. Both cables are required to be fully rated for the maximum voltage levels encountered, which adds cost. A permanent cable fault results in the loss of 100% of power transmission.

Asymmetrical monopole with metallic return. An asymmetrical monopole VSC-HVDC converter is shown in Figure 20.

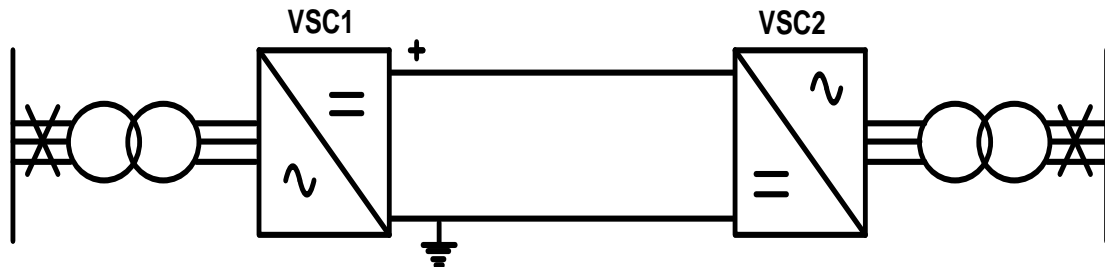


Figure 20: Asymmetrical monopole with metallic return

With this particular formation only one cable needs to be fully rated for the voltage levels encountered. The metallic return cable does not need to be fully rated and hence this configuration can help save on project cost [22]. This can also form the first stage of a later bipolar configuration, where the power rating can be increased by the addition of extra poles when required. No DC ground current is encountered during operation, but the transformers must be fully rated to tolerate the maximum DC stresses encountered [22]. Just like the symmetrical monopole, a permanent cable fault or pole outage will result in 100% loss of power transmission.

Asymmetrical monopole with ground return. The Asymmetric converter with ground return is shown in Figure 21.

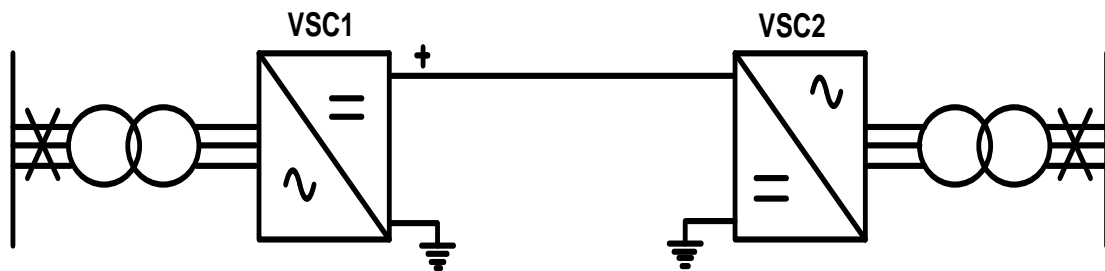


Figure 21: Asymmetrical monopole with ground return

For phase-to-ground faults between the AC transformer and converter, there will be an infeed of fault current from the AC side to the DC side if a half-bridge design is used [22].

The current will flow back through the diode bridge to the AC side and completes the fault current loop. A DC component superimposed onto the AC current can reduce the natural current zero crossing encountered on the AC pole circuit breaker, requiring special precautions [73]. In the case of a permanent cable fault or pole outage, 100% of power transmission is lost. The transformers must be designed for the maximum DC stresses encountered and permission is required for continuous operation with ground current, requiring consents for the electrodes in the first instance [73]. The system can be expanded to form a bipolar configuration later on and, due to requiring only one fully rated conductor, this configuration can help save on cost.

Bipolar configuration. An alternative solution to the ones previously discussed is a bipolar configuration as shown in Figure 22.

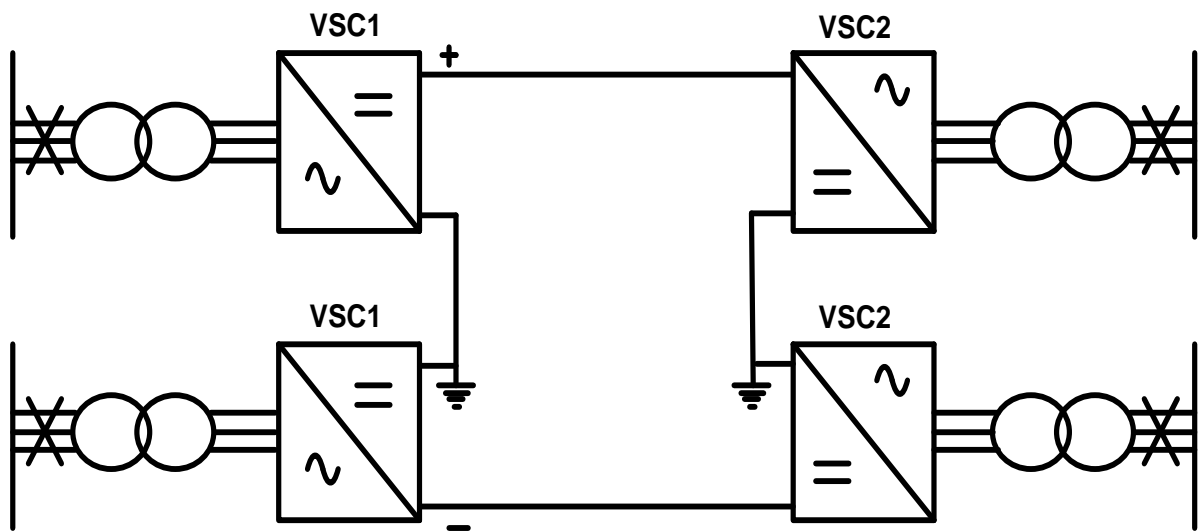


Figure 22: Bipolar configuration

The main advantage of a bipolar configuration is that in the event of a pole outage, 50% power transfer is still possible by utilising appropriate switching mechanisms. If a ground or metallic return is installed, then this can also enable 50% power rating to be maintained under a permanent DC cable fault scenario [73]. Bipolar configuration allows much higher voltage and power ratings to be achieved, though the IGBTs are the limiting factor in terms of the maximum current rating that can be continuously handled [73]. The AC transformers must be designed for maximum DC stresses and if electrodes are utilised, these will be subject to the same considerations mentioned previously [22]. The AC transformers are now classed as converter transformers due to the extra insulation and design requirements necessary to cope with the DC voltage stresses [73]. The applications of VSC-HVDC technology are described briefly in the next section.

2.2.3.3 Applications of VSC-HVDC technology

Normally, HVDC transmission systems are used for long-distance bulk power transmission and connecting together asynchronous networks. Due to the fast control of IGBTs, and their ability to control both active and reactive power, VSC-HVDC technology can be used for many other applications where CSC-HVDC technology might not be suitable.

Some of these include [73]:

- VSC-HVDC can provide voltage and frequency control of the AC system where weak connections may be present and can be used to supply passive networks.
- VSC-HVDC technology does not suffer from commutation failures and can be connected to systems with zero short circuit power.
- Due to self-commutation, VSC-HVDC technology can permit “black starting” of a de-energised AC network.
- VSC-HVDC technology is suitable for connecting offshore wind farms where the AC voltage needs to be kept constant while importing active power to the onshore network.
- Stable power supplies to offshore oil rigs can be provided over long distances.

2.2.3.4 Power reversal in VSC-HVDC technology

In [74] and [75], VSC transmission systems transmit active power in either direction with the same control setup. Active power can be reversed quickly without any change of control mode, and without any filter switching or blocking. This is achieved by changing the DC current direction compared to voltage polarity reversal associated with CSC-HVDC technology. This is theoretically true and observed in real examples, but the speed of reversal is determined by the AC network, where the strength of the connecting AC network, together with the inductance of the DC network determines the speed of reversal, which is limited to a ramp rate that can ensure stability during the process [76].

2.2.3.5 Protection and control of VSC-HVDC systems

Just like CSC-HVDC technology, VSC systems possess controls for both normal operation and high-level controls for special system conditions. The purpose of the protection system is to ensure the prompt removal of any element of the electrical system during a fault condition. Both vector current control [77] and power synchronisation control [78] have been studied and some publications ([78], [79]), seem to favour power synchronisation control due to its capability of operating in very weak AC grids, where the full active power transfer of the VSC-HVDC link can be maintained.

Other publications in [80] and [81] have highlighted potential weaknesses with vector current control and difficulties for the Phase Locked Loop (PLL) when connected to a weak AC system. In the following section, the basic principles of vector current control are described as this has been employed extensively in practice and form the main control strategy employed in this thesis.

2.2.3.6 Vector current control for VSC-HVDC systems

Vector current control utilises the modelling of three-phase AC systems and can be used to obtain separate control of active and reactive power orders. One major advantage of this control principle is that vectors of AC currents and voltages occur as normal vectors in steady state, and hence by using Proportional Integral (PI) controllers, static errors in the control system can be avoided [19]. The principles of this process are shown in Figure 23.

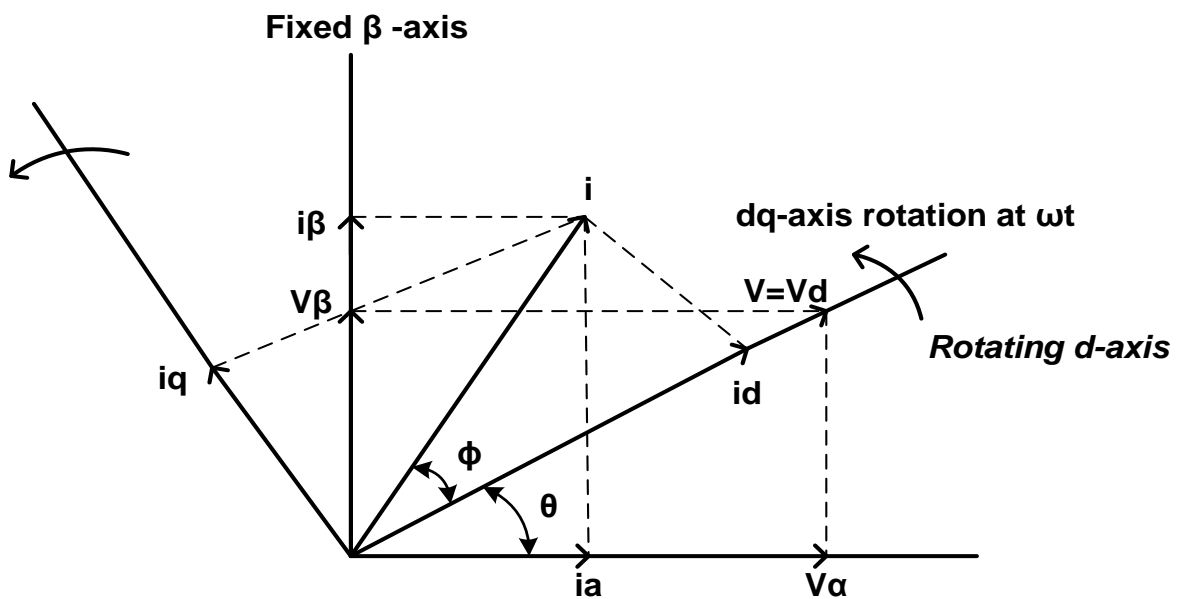


Figure 23: Axis transformation for vector current control [19].

Coordinates from the three-phase stationary coordinate system are changed to the dq rotating system in the process known as the dq transformation.

This process consists of two steps [19]:

- Converting the three-phase stationary coordinate system to the two phase α - β stationary coordinate system.
- Transformation from the α - β stationary coordinate system to the dq rotating coordinate system.

Clark and inverse-Clark transformations can be used to convert the phase values of voltages and currents into a stationary α - β reference frame and vice-versa [19].

In [19] Park and inverse-Park transformations convert the values from the stationary α - β reference frame to the synchronously rotating dq reference frame and vice-versa. The stationary α axis is aligned with the three-phase a-axis for easier analysis [19]. The dq reference frame is rotating at synchronous speed (ω) with respect to the stationary α - β frame. In [19] it describes how using the a-b-c to dq transformations, the converter three-phase currents and voltages can be expressed in the 2-axis dq reference frame. The grid voltage vector is defined to be along the d axis direction and then a virtual grid flux vector can be assumed to be acting along the q axis [19]. With this alignment, the instantaneous active and reactive power injected into or absorbed from the AC system is given by Equations (2.3) and (2.4) [83].

$$P = \frac{3}{2} \cdot V_d \cdot I_d \quad (2.3)$$

$$q = -\frac{3}{2} \cdot V_d \cdot I_q \quad (2.4)$$

The angle between the α axis of the α - β frame and the d axis of the dq frame is used for transformation between the α - β frame and dq frame [83]. The information on this instantaneous phase angle of the grid voltage is necessary for independent control of active and reactive power [19]. The value of the angle θ is calculated by a synchronisation technique known as the PLL. The process is shown in Figure 24.

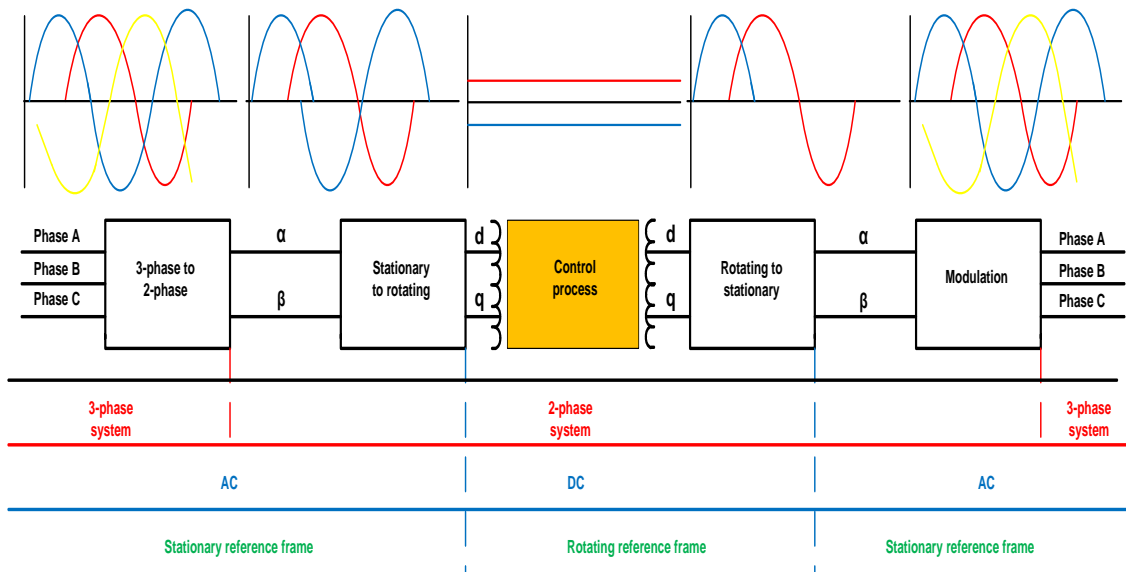


Figure 24: Control strategies with reference time frames

The information from here is used to synchronise the turning on and off of the IGBTs and to calculate and control the flow of active/reactive power by transforming the feedback variables to a reference frame suitable for control purposes [83].

For the analysis of vector current control, three-phase currents and vectors are usually described as vectors in a complex reference frame. When analysing the system shown in Figure 25, some equations are used to describe the behaviour of the detailed analysis already carried out in [84] and [85].

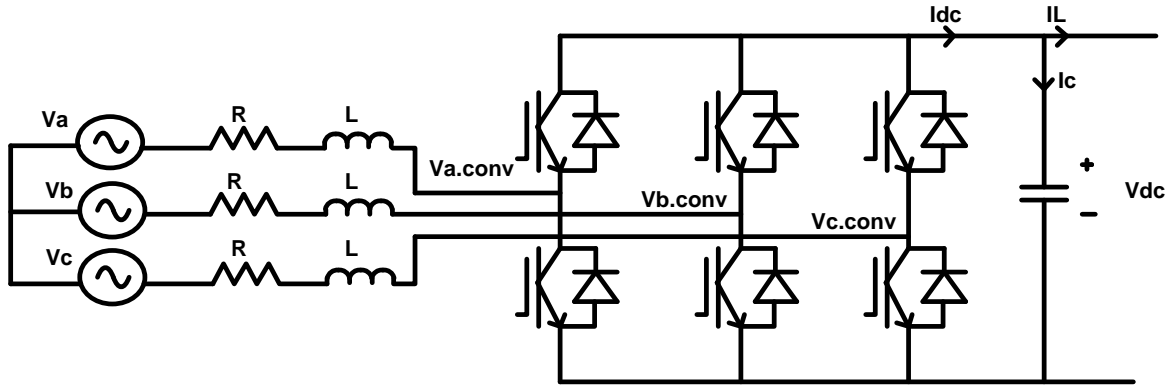


Figure 25: Schematic of the VSC system

The grid voltages can be defined as V_{abc} , the currents i_{abc} , the converter input voltages $V_{abc,conv}$, and inductance (L) and resistance (R) between the converter and the AC grid.

Hence the voltage at the grid side of the converter can be expressed by Equation (2.5) [84]:

$$V_{abc} = R \cdot i_{abc} + L \frac{d}{dt} i_{abc} + V_{abc,conv} \quad (2.5)$$

Using the a–b–c to dq transformations, the converter three-phase currents and voltages are expressed in 2-axis dq reference frame, synchronously rotating at the given AC frequency ω [84].

$$L \frac{Did}{dt} = -Rid + \omega Liq - vd_{conv} + vd \quad (2.6)$$

$$L \frac{Diq}{dt} = -Riq - \omega Lid - vq_{conv} + vq \quad (2.7)$$

The power balance relationship between AC input and DC output is given by Equation (2.8) [85], where V_{dc} and I_{dc} are the DC output voltage and current respectively.

$$P = \frac{3}{2} (vd \cdot id + vq \cdot iq) = V_{dc} \cdot idc \quad (2.8)$$

The grid voltage vector is defined along the d axis direction, and then a virtual grid flux vector acts along the q axis. Following this alignment, the instantaneous real and reactive power injected or absorbed from the AC system is given by Equations (2.9) and (2.10) [85].

$$P = \frac{3}{2} \cdot v_d \cdot i_d \quad (2.9)$$

$$Q = \frac{3}{2} \cdot v_d \cdot i_q \quad (2.10)$$

The transformation into the rotating dq coordinate system, oriented with respect to the grid voltage vector, leads to a split of the current into two parts.

One important aspect of VSC-HVDC technology operation is the Proportional Integral Derivative (PID) controller. The principles and importance of this controller are described briefly in the next section.

2.2.3.7 Proportional integral control

A PID controller is a control loop feedback mechanism which is widely used in industrial control systems, an example of which is shown in Figure 26.

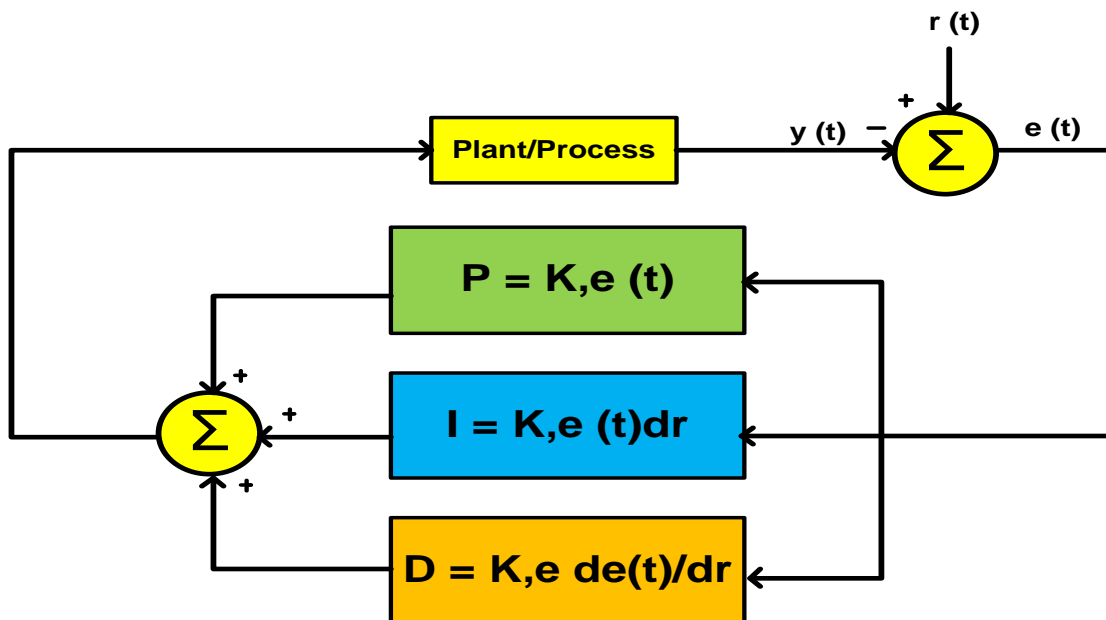


Figure 26: PID controller

An error value is calculated as the difference between a measured variable and a desired setpoint. The controller will attempt to minimise the error by adjusting the process through the use of a manipulated variable.

In [86] a controller algorithm is described that involves three separate parameters, known as the integral, the proportional, and the derivative values denoted as I, P and D. The present error (P), accumulation of past errors (I) and the prediction of future errors (D) are based on current rate of change. The controller can be tuned to change its behaviour according to the process it is involved in. Manual tuning can be applied by changing the K variables shown in Figure 26.

In [87] too much increase or decrease of the gain is shown to be a potential cause of system instability, overshoot and large oscillations. For HVDC control systems, the controller must be pre-tuned for the AC system before detailed simulations are undertaken. Once the controller demonstrates a stable output response, then the individual gains can be re-adjusted to try and improve the overall performance of the system. If this is attempted before the system has been preliminary tuned, then the undesired effects detailed previously may be encountered.

Table 3 demonstrates the effects of changing the parameters in Figure 26 [86].

Table 1: The effects of changing PI parameters

Parameter	Rise time	Overshoot	Settling time	Steady-state error	Stability
Kp	Decrease	Increase	Small change	Decrease	Degrade
Ki	Decrease	Increase	Increase	Eliminate	Degrade
Kd	Minor change	Decrease	Decrease	No effect	Improve if Kp is small

It can be seen that changing each parameter can vary the overall impact on the PID controller. For the present error (Kp), changing the value will decrease the steady-state error but could degrade system stability. For any past errors (Ki), the stability of the system can also be degraded but the steady-state error can be eliminated. Any changes made to future errors can improve the system stability and decrease the settling time, making the control response faster.

From the above data in Table 3 and that described in [86] and [87] it is apparent that the tuning of PID controllers is a vital component in the successful operation of a VSC-HVDC converter.

2.2.3.8 Standard VSC-HVDC controls

The basics of vector current control have already been described. The standard control for VSC-HVDC and how the vector current control is applied is shown in Figure 27.

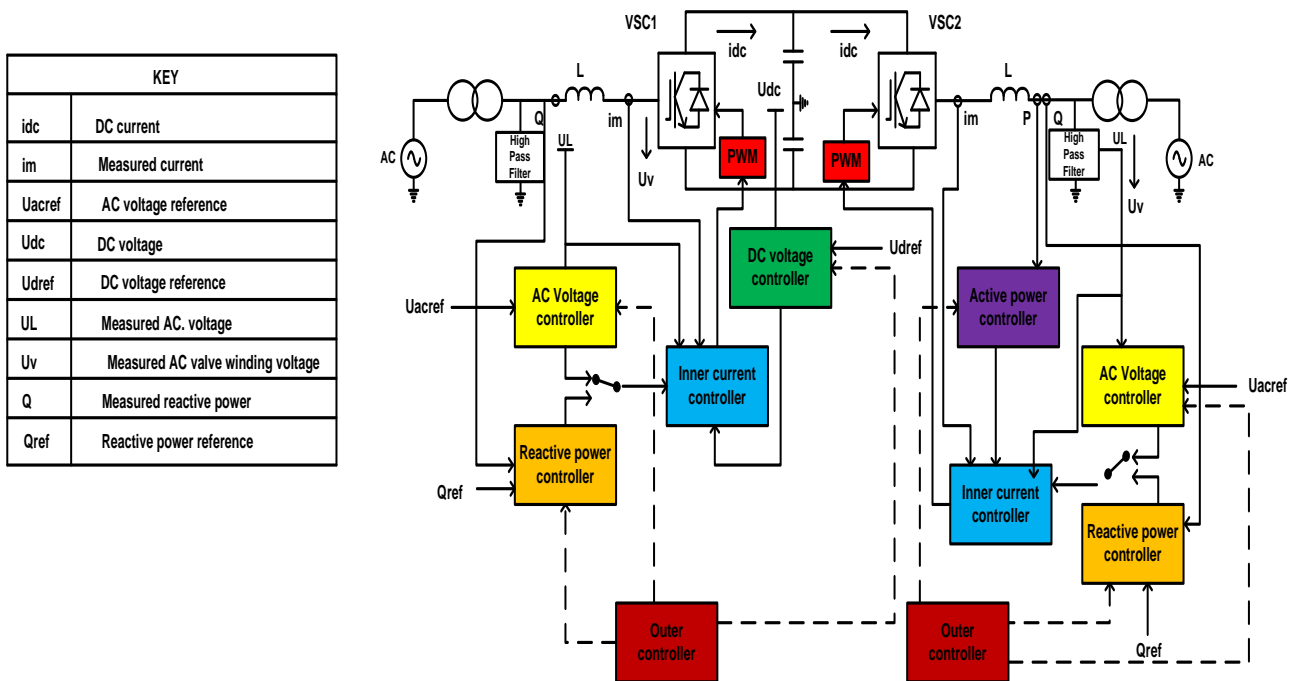


Figure 27: Control system for VSC-HVDC technology

The active power loop can be set to control either the DC side voltage or the active power. The reactive power loop can be used to control either the reactive power or the AC voltage. For AC voltage control, the measurement is made at the valve winding side of the converter transformer [88]. The measured value is subtracted from the reference value and provides the voltage error, which is fed to the internal control loop to generate the necessary firing pulses to the valve-based electronics. The phase locked loop is used to synchronise the converter control with the line voltage [88]. The converter bus voltage is measured and a time dependent phase angle is generated. The switching pulse generator uses this angle and PWM to generate the switching order according to the AC current reference from the AC current control. The reactive power control loop follows a similar process to that of the AC voltage control function [89].

In [88] and [89], some of the standard controls within a VSC-HVDC converter are mentioned and are briefly explained here:

DC voltage control. The highest DC voltage value is used to follow the reference setting via feedback control this in turn produces an active current order [88].

Active power control. Active power control generates a contribution to the DC voltage reference depending on the active power reference [88]. The voltage difference between the converter stations causes the flow of DC current. A while feedback control loop keeps the power at the desired value. The power can be increased to a new value is ramped if desired. To keep the system balanced, one station is in DC voltage control while the other is in active power control mode [88].

Reactive power control. VSC technology can generate or consume reactive power independently of each station. A reactive power reference value generated by the operator and this is tracked by the control system. The reactive power at the network side of the transformer maintained via feedback control to meet the reference value [88]. If the AC voltage cannot be controlled to the reference value a change in control modes is applied. The converter will temporarily switch over to AC voltage control to keep the AC voltage within operational limits [88].

AC voltage control. If the converter is set to AC voltage control, the control system will control the AC voltage by through the injection or absorption of reactive power. The reactive power value will be adjusted to within the full PQ capability of the converter. The AC voltage setting and ramp speed is selectable by the operator [88].

AC current control. Two regulators are employed for AC current control. One regulator controls the active current component and the other controls the reactive component. This particular control function is also accessible to the operator [89].

Tap changer control. The purpose of the tap changer is to keep the converter bus voltage and the relationship between the AC and DC voltage (modulation index) within specified ranges [88].

Islanded network control. If the converter station is connected to an islanded network, then both the reactive and active power are determined by the difference between the total load and total generation within the islanded network [89].

2.2.3.9 High-level VSC-HVDC controls

Apart from the standard controls that were mentioned previously, some high-level controls are available that can improve AC system performance [90].

Some of these are described below.

Damping Control: Similar to CSC-HVDC, fast controller action can be used to mitigate low frequency oscillations. As well as active power modulation, the VSC utilises reactive power control to achieve similar results [90]. For Inter-area oscillations traditional power system stabilisers maybe less effective and can be replaced by a well-designed modulation scheme.

Emergency Power Control: The fast control of both active and reactive power can enhance the dynamic performance of the AC grid during system disturbances. Fast active power runbacks, run-ups or an instant power reversal can be used to maintain synchronised grid operation. The functions can either be activated by the operator or signals from the control system [90].

Overvoltage Functionality: The control system can be configured to react to AC voltage rises above predefined limits. The converter will be ordered to consume as much reactive power as possible to get the DC voltage back within the required operating range.

Frequency Control: Just like CSC-HVDC technology, the VSC can feed or reduce active power into a disturbed system and obtain a much faster control of the frequency than a system generator. Energy can be drawn from the remote system and control the local frequency [90].

Black start: The VSC control system can be used to black start a local network during a power outage. This can help restore sections of a system very quickly, which can then be used to start up large ac networks.

2.2.3.10 High-level VSC-HVDC controls

The purpose of the HVDC protection system is to successfully detect and clear system faults. For DC side faults the protection must clear these as quickly as possible otherwise system instability could occur in the local AC networks and equipment within the converter station can become damaged [90]. A range of different protection actions are initiated and are dependent on the manufacturer concerned. As part of these protective actions, the AC/DC current can be clamped by the control system to prevent it from increasing beyond the ratings of equipment during a fault condition [91].

Alternatively, the current can be rapidly reduced (ramped down) to help prevent damage to equipment and aid system recovery post fault. A combination of both may be applied to each end of the VSC-HVDC link if one particular AC connection is weak [92], [93].

Some of the actions associated with the VSC protection system are briefly described:

Alarms. Alarms are sometimes generated prior to protection operation to notify the operator in advance that something is wrong. This allows the operator to take some early action to address the issue without the DC link being taken out of service by the protection system [90].

Temporary blocking. If the converter cells experience a high voltage or current, then a temporary turn-off pulse is sent to all IGBTs. If and when the voltages and currents return to a safe level, then normal operation will be resumed [90].

Permanent blocking. In the event of an enduring fault occurring, a permanent blocking signal is sent to the IGBTs and will always precede the tripping of the AC circuit breaker to achieve successful fault clearance [90].

AC circuit breaker trip. Tripping of the AC circuit breaker is required to disconnect the converter from the AC network. Two trip coils are energised when tripping signals are sent to ensure a successful operation even if one coil was to fail. The tripping of the AC circuit breaker is required for half-bridge converters due to the free-wheeling diode rectification encountered under a DC side fault scenario [90].

Set lockout of the AC circuit breaker. When an AC circuit breaker has been tripped, an order to lock out the breaker may also be executed, preventing the breaker from being reclosed before the operator has investigated the case for the trip [92].

Pole isolation. This particular sequence disconnects the DC side (positive and negative poles) from the DC cable. This is done either manually during shutdown, or automatically by the system protections.

2.3 Nuclear power

In [94] and [95] a nuclear reactor is a system that contains and controls sustained nuclear chain reactions. Fuel made up of heavy atoms split when they absorb neutrons and are positioned in the reactor vessel with a small neutron source. The neutrons start a chain reaction where each atom splits and releases more neutrons which cause other atoms to split [95].

Each time an atom splits large amounts of energy are released and these in turn generate heat. The heat is carried out of the reactor via a coolant, which consists of plain water most of the time. The coolant heats up and produces steam which is transferred to a turbine to spin a generator [95]. This nuclear fission process has been in use for decades and is well proven in industry [95]. A review of nuclear reactor design is presented in the next section.

2.3.1 Pressurised water reactor

One of the most common types of nuclear reactors in industry is the Pressurised Water Reactor (PWR), which uses regular water as coolant. This type of reactor is shown in Figure 28.

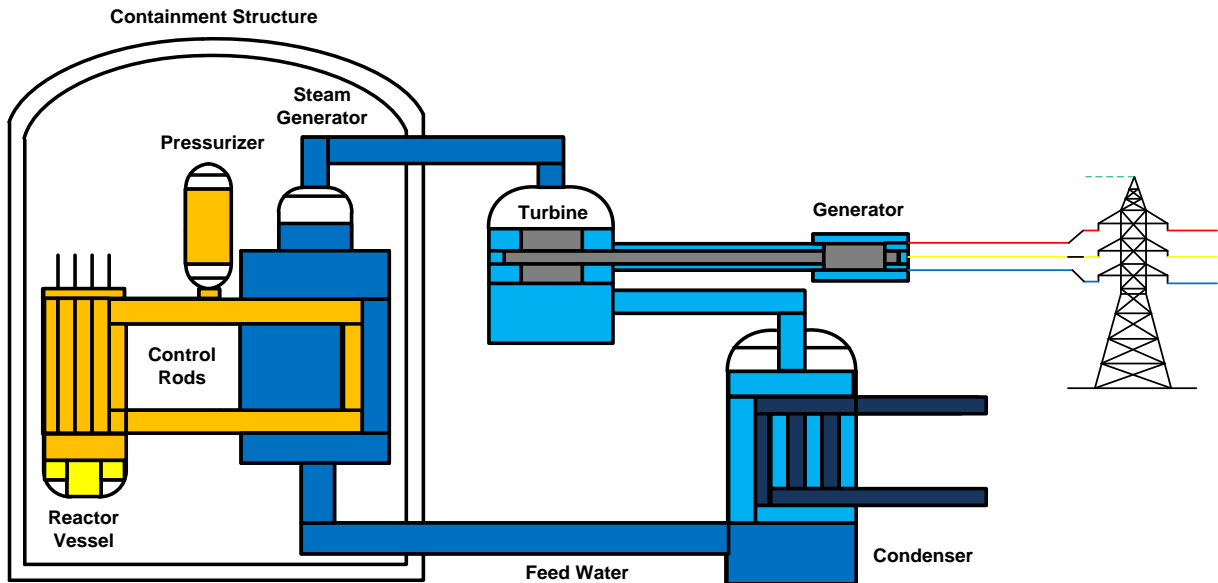


Figure 28: Pressurised water reactor

The primary cooling water is kept at very high pressure so it does not boil. It transfers through a heat exchanger where the heat is transferred to a secondary coolant loop. The secondary coolant loop spins the turbine [96].

2.3.2 Boiling water reactor

The BWR is similar to the PWR although they possess a single coolant loop. The nuclear fuel boils the water on its way out of the reactor where the steam is transferred to the turbine [96].

An example of a BWR is shown in Figure 29.

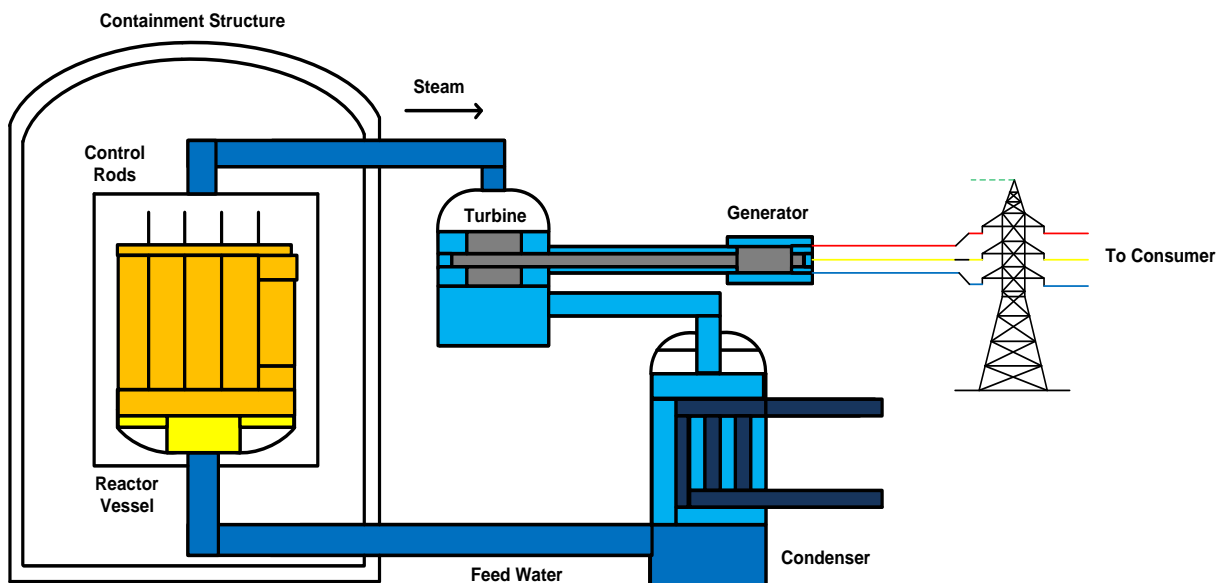


Figure 29: Boiling water reactor

In [97] these types of reactors were originally designed by Allis-Chalmers and General Electric (GE). The General Electric design has survived, whereas all Allis-Chalmers units are now shut down [97].

2.3.3 High temperature advanced gas cooled reactors

High Temperature Advanced Gas Cooled Reactors (HTAGCRs) use small pellets of fuel packed into hexagonal compacts [97]. Gas, such as helium or carbon dioxide, is passed through the reactor rapidly to cool it. Due to their low pressure density, these reactors are seen as promising for using nuclear energy outside of electricity: such as transportation, industry and in residential regimes [97].

From the literature sources [95], [96] and [97] the use of HTAGCRs is not as common as the PWR and BWR reactor types. For future NPP designs Advanced Boiling Water Reactors (ABWRs) are being planned. The layout of an NPP can be affected by the type of reactor design employed. The layout of NPPs is discussed in the next section.

2.3.4 Layout of a modern NPP

The design and layout of an NPP can vary and this can influence the way in which the plant is connected to the NETS [98]. In [99] and [100], most NPPs have segregated and independent AC power circuits for security reasons. An example layout is shown in Figure 30.

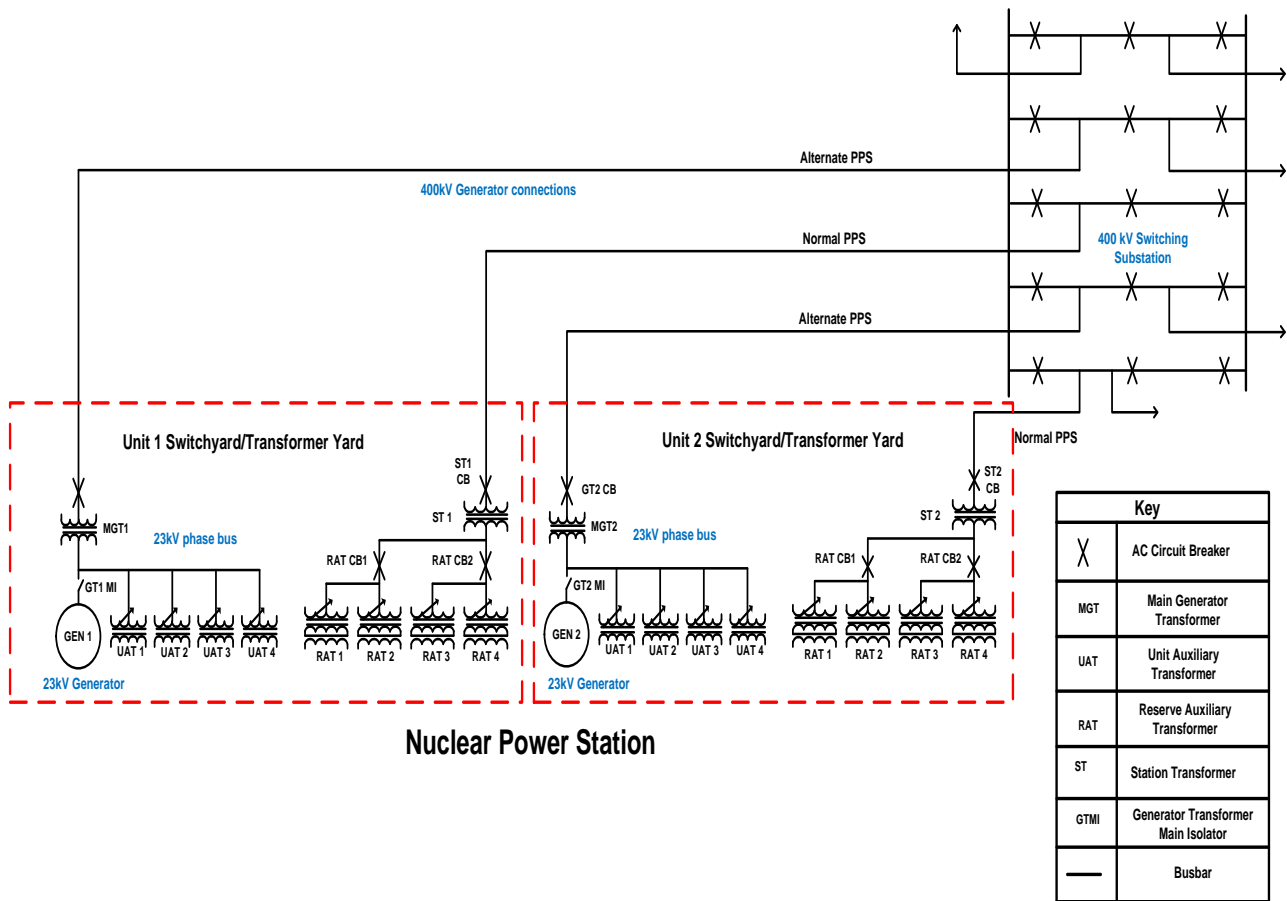


Figure 30: Layout of an NPP and associated AC switchyard

Four 400 kV AC overhead line circuits provide the connection interface to the transmission system. They consist of two circuits per tower, with two towers in total. The preferred power export (supply) to the AC system is referred to as the “alternate preferred power supply” with two independent circuits on two different towers. This ensures security of supply if one connection to a tower is lost, and another circuit is available to export power to the grid. The “preferred power supply” is also formed of two physically separated circuits, but in this instance provides supplies to the safety systems of the NPP itself. If both supplies to the NPP safety systems are lost, then power can be supplied via the “alternate preferred power supplies” via the main transformer circuit breakers.

The above example is just one design for providing reliable off-site power supplies to the NPP and, depending on cost and power levels, the design could be simpler and involve fewer transmission circuits. Some of the key components inside the NPP are described in the next section.

2.3.4.1 Key components inside the NPP

In [101] the content of an NPP includes equipment such as the turbine and generator, the spent fuel pond, backup diesel generators and dry waste storage. The local environment must also be considered, as a potential radiation leak could be disastrous to anyone within the vicinity of the NPP. Within the NPP there are some key components which are vital to the operation as well as to the security of the site during normal operation. Some of these are described below [101]:

Steam generator. The Steam Generator converts the steam turbines' rotation into electricity. It consists of a rotor and a stator. The rotor is a set of electromagnets connected to the turbines by a shaft. When the turbines spin, the rotor spins. The stator is a series of wire coils surrounding the rotor. When the rotor spins, an electric current is generated within the stator's wire coils [101].

Reactor cooling pumps. The reactor coolant circulates water around the reactor, transferring heat from the fuel in the reactor vessel to the steam generator. The water is kept at roughly 155 times atmospheric pressure at around 300 degrees Celsius, so the pump has to be robust [102]. Modern NPPs typically have four reactor coolant pumps, each of which circulates around 20,000 cubic metres (m³) of water per hour. A series of seals keeps each pump completely water tight and sensors inform staff of any particular issues [101].

Backup generators. Many of the NPP's essential systems need electricity to function. Essential systems are those that need to keep functioning under any circumstances; reactor vessel cooling is an example. Normally, these systems are powered either by the electricity that the plant generates itself, or via the NETS. The backup systems are independent electrical generators powered by diesel engines. Their function is to keep essential safety systems operating in situations when the National Grid cannot provide the necessary power [102].

Gas turbines. Some NPPs may also have gas turbines that can be instantly started in case the off-site supplies (NETS) and on-site supplies (diesel generators etc.) are lost.

Passive safety systems. Future NPPs will also have passive safety systems that do not rely on secure electrical supplies being available for successful operation. Pressure valves are one example of such a system; these operate to relieve pressure within the reactor once it exceeds a predetermined limit. Some of the new breeds of reactors are being designed to cater for up to 100% load rejection. The International Atomic Energy Agency (IAEA) recommends that at least two independent connections to the transmission network are required to power the reactor safety systems during a shutdown [103].

According to Westinghouse, the manufacturer of the new AP1000 nuclear reactor, no electricity supplies are needed due to its passive safety systems [104]. During a station blackout with a loss of all electrical supplies, the AP1000 will shut down automatically with no need for human intervention for up to 72 hours [104].

2.3.5 Development of an NPP

According to [105] the introduction and development of NPP is a major undertaking within any country. In order to accommodate such large power stations as these, the country concerned has to build and develop the necessary infrastructure so it can construct and operate an NPP securely, safely and in a technically sound manner [105].

In [106], depending on the chosen location of the NPP there may already be a suitable amount of electricity infrastructure to connect to; otherwise a large and major investment may be required. The NETS must also be efficient, safe, and operate reliably in the case of a nuclear power station connection.

In [107] the NETS is the electrical highway through which all electricity passes as energy is moved from the very start of the chain (generation) through transmission to distribution and eventually to the customer (load). The Main Interconnected Transmission System (MITS) is formed by interconnected grids. They can consist of thousands of kilometres of transmission and distribution lines, together with millions of different loads.

In [107] NPPs are described as unique and powerful generators compared with other types of plants such as coal-fired or Combined Cycle Gas Turbine (CCGT). Large quantities of energy can be supplied to the NETS in bulk supply. NPPs equally rely on the NETS to provide a secure and reliable source of power for crucial safety operations, especially during emergency conditions [107]. The safe startup and shutdown of such plants requires a stable and secure power supply from the NETS, this is often referred to as “off-site power” [107].

In [107] the NETS' principal function is to transport electricity from the generating plants to the load centres (customers). A reliable and secure transmission system is essential for bringing NPPs online as well as operating them effectively. The cooling arrangement of the NPP is a vital safety system which is responsible for keeping the nuclear fuel cool after a reactor has been shut down [107]. On-site backup supplies in the form of batteries, diesel generators or gas turbines are also present. The fewer instabilities and interruptions there are in the NETS the better the NPP can perform at supplying maximum power to customers consistently [107].

2.3.6 Electric grid vulnerability

In [108] and [109] the transmission system must maintain a precise frequency of AC current, where only a small imprecision can cause issues. A balanced system can be subject to events that have the potential to cause large-scale disturbances as well as the possibility of system collapse. [109]. It seems that the above actions can trigger a chain reaction of failures which could have disastrous consequences for the power system and NPP.

According to [110], in developed countries the transmission systems are normally designed and operated with a contingency margin. Operation is planned so that no single fault on the system can lead to problems such as abnormal frequency, disconnection of demand or abnormal voltage. If this margin is not maintained or if multiple faults happen close together in time, then major failures can still occur [110]. An example of this was on August 2003 where much of the north-eastern United States of America and part of Canada were plunged into darkness when a disruption in the transmission system's intricate balance caused a massive blackout with substantial economic consequences [111]. This was an example of cascading events resulting in a complete shutdown of the grid, such a blackout as this one affected 10 million people in Ontario and 40 million in eight different US states. This grid collapse was caused by a combination of human errors and technical challenges such as: overextended controllers; transmission line failures; power plant outages; amongst others [111].

In [111].the North American blackout was only one of seven blackouts in a six-week period in 2003 that affected more than 120 million people in eight different countries: Canada; Denmark; Finland; Italy; Malaysia; Sweden; UK and USA [110]. In [112], within Sweden an NPP tripped (i.e. rapidly shut down), resulting in the loss of 1200 MW to the transmission system. Five minutes after this a system failure caused the shutdown of two units at another NPP with a further loss of 1800 MW. To respond to this combined loss of 3000 MW (about 20% of Sweden's electricity consumption) the system operators isolated the southern Sweden to eastern Denmark section of this system, but the voltage eventually collapsed due to the insufficient power supply [112]. At the time of the original reactor trip, two high voltage transmission lines and three links to neighbouring countries were out of service for normal maintenance work and four nuclear units were offline for annual overloads [112]. From the above details, the unavailability of certain power supplies severely limited the options of the system operators. This highlights the importance of stable power sources.

2.3.7 Interfacing NPPs with AC grids

In [113] electric transmission systems and NPPs are described as fascinating engineering achievements in their own right. However, when they come together in a highly controlled and distributed network, further complexity is created. This complexity is down to several factors such as: the sheer size and connectivity of the transmission systems; the safety requirements imposed on NPPs; the need to balance electricity supply and consumption throughout the system at all times; the nature of electricity [113]. This demands continual surveillance and adjustment to ensure supply always matches demand [114].

NPPs are normally operated in base load (i.e. steady-state operation at full power) and less frequently in load following mode [114]. The integration onto a transmission system brings nuclear safety requirements to the design, operation and stability. When not generating electricity, NPPs still need electricity from the NETS to support maintenance work, operate other equipment, keep the plant ready to start, and, very importantly, operate critical safety systems [114].

In NPPs the nuclear chain reaction can be turned off in a few secs. However, significant heat is still generated from the long term decay of highly radio-active fission products [114]. This residual heat has to be removed from the reactor core indefinitely to prevent overheating of the fuel.

In [115], as part of nuclear safety, the reactor cooling systems are powered by stable sources of electricity. To prevent fuel rod damage, sufficient and reliable power is needed to maintain conditions in the coolant systems and containment and to run vital safety related instrumentation, control, monitoring and surveillance systems [115]. Electric power is needed for the heating, ventilation and air conditioning systems used to assure that there is an operable environment for both equipment and personnel [115].

In [115] the reliability of off-site power is secured by two or more physically independent circuits to the NPP in order to minimise the likelihood of their simultaneous failure. The reliability of on-site power is improved by segregated power sources such as batteries, diesel generators, gas turbines and on-site electric distribution systems [115]. Due to the importance of reliable off-site power the transmission system is an important factor in NPP site selection [115].

This selection must consider the NPPs position within the AC grid as well as its proximity to centres of electricity demand [116]. Any unexpected sudden disconnection of the NPP from an otherwise stable electric grid could trigger a severe imbalance between power generation and consumption causing a sudden reduction in frequency and voltage of the transmission system [116]. This could even cascade into the collapse of the local transmission system if additional power sources are not connected in sufficient time [116].

2.3.8 Influence of grid disturbances on nuclear power plants

Sources [117] and [118] describe the effects of grid disturbances on NPPs; some of these effects are detailed below:

Load rejection and complete loss of load. A load rejection is a sudden interruption in the electric power demanded. This can be caused by the sudden opening of another part of the system carrying a heavy load [117]. An NPP is usually designed to withstand load rejections up to a certain limit without tripping the reactor. The ability to deal with load rejections depends on the speed of the reactor power being restored to the pre-fault value [117]. Load rejections of 50% can be accommodated by: rapidly running back the steam turbine to the lower demand level; diverting excess steam from the turbine to the main steam condenser unit and reducing reactor power via insertion of control rods without a reactor scram [117]. A complete loss of load (100%) is a full load rejection, where the breaker at the station's generator output is opened or a circuit within the AC system [117]. Under this condition, it may still be possible to "island" the NPP so that it powers only its own auxiliary systems.

Degraded grid voltage or frequency. Transmission systems are controlled to assure that a particular frequency, either 50 or 60 Hz, is maintained within $\pm 1\%$ [118]. When an imbalance is created between generation and load, system frequency drops if the load exceeds generation and increases when generation exceeds the load. A fall in system frequency is caused by: a fault or a trip; loss of a major generating unit; or inadequate generation available to meet load demand [118]. A small drop in frequency caused by the loss of generation can be controlled by the following:

- Starting up additional generation capacity, such as gas turbines or hydroelectric power.
- Quickly activating the grid's available "spinning reserve", either automatically or manually.
- Disconnecting selected loads from the transmission system (load shedding).

Isolating the NPP from the rest of the system (islanding) can reduce its load, requiring its generation be reduced accordingly [118]. Islanding will help prevent the NPP from tripping but may in turn further aggravate the power imbalance on the rest of the system [118].

In [119] it is stated that a plant trip including reactor shutdown should be considered as a last resort. During a trip, the plant will be subjected to varying changes in power, pressure and temperature, which shortens the lifetime of the plant. Moreover, if the NPP is immediately disconnected from the NETS, then the lost generation will exacerbate the already degraded conditions on the system [119].

In [120] any associated change in system frequency will have an effect on the NPP's operation by changing the speed of the NPP's turbo generator and the speed of the pumps that circulate coolants through the reactor and the secondary cooling circuits. The main reactor circulating pumps, steam generator feed-water pumps and long-term decay heat removal systems rely on stable electric power in order to function properly [120]. Apparently the speed of the reactor's main coolant pumps is directly proportional to the frequency of the electrical power supply. If the frequency within the AC grid drops low enough, the reactor coolant pumps will slow [120]. This can result in inadequate cooling of the core, resulting in the subsequent reactor/reactors tripping to prevent overheating and a potential explosion from happening [120].

Other AC motors in the NPP may trip due to rising currents and resulting overheating caused by frequency reduction [120]. The performance of AC motors is directly affected by the voltage and frequency of their respective power supplies [120]. Apparently if system voltages are not sufficient, motors cannot develop sufficient motor torque to start. If the frequency drops below a certain value, excessive current will be being drawn by the motor and in turn can lead to overheating.

In [120] the voltage and frequency operational ranges of large AC motors can be narrow and in abnormal conditions, safety systems within NPPs are required to take protective actions such as tripping the reactor and turbine [120]. These actions protect the NPP by safely shutting it down and keeping it cooled. Any sudden automatic shutdown of a large base-load nuclear unit during periods where there is already a mismatch between generation and load on the grid can only further degrade the grid's condition, potentially leading to a partial or full collapse [120].

Loss of off-Site power. Any loss of off-site power can be caused by external events beyond the NPP's switchyard, such as transmission line faults and weather events such as lightning strikes, ice storms and hurricanes [121]. A loss of off-site power interrupts supplies to all in-plant loads such as pumps, motors, and safety systems. As a protective action, safety systems will trigger multiple commands for protective trips (turbine and generator trip, low coolant-flow trip, and loss of feed-water flow trip) [121]. The reactor protection system will attempt to switch to an alternate off-site power source in order to remove residual heat away from the reactor core. If this fails, in-plant electrical loads must be temporarily powered by batteries and standby diesel generators until off-site power is restored [121]. Diesel generators may not be as reliable as off-site power from the grid in normal conditions. Diesel generators can fail to start or run 1% of the time [121].

In [121] the system operator's response over time to the sudden loss of the NPP can be modelled by computer simulations, conditioned by the capacity and interconnectivity of the system and the size of the lost NPP generation. Large MITS can usually meet the requirements of providing reliable off-site power to NPPs connected to the system [121]. However, in some scenarios involving poorly interconnected or controlled transmission systems, the sudden shutdown of a large NPP, or any other large generation station elsewhere on the system, might result in severe degradation of the system voltage and frequency [121].

When an NPP is sited on a well maintained but small and isolated grid of limited generating capacity (on an island for example), then the sudden loss of its generation may lead to the same outcome [122].

2.3.9 History of nuclear power plant disturbances

Throughout history, there have been numerous records of grid disturbances that have had some effect on an NPP which is located in the particular area of the disturbance. The effect that these plant disturbances can have on a particular NPP (In this instance, in America) can rapidly vary, as displayed in Table 2 [111].

Table 2: Grid disturbance effects on NPP 1993–2003 [20]

Action taken by NPP	Number of occurrences	Percentage of occurrences
Scram	69	56
No scram	51	42
Emergency Diesel Generators (EDG) energise bus	19	16
Another source energises bus	11	9
EDGs started but not loaded	8	7
No action taken	9	7
Power reduction	4	3
Unknown	3	2

It can be seen that the NPP located within America has been “tripped off” supply (scram) for 56% of the total system disturbances. EDGs were called upon to operate for 16% of the total occurrences. A range of different system conditions that had an effect on these NPPs is shown in Table 3 [111].

Table 3: Grid conditions affecting NPP 1993–2003 [111]

Grid condition	Number of occurrences	Number of scrams
No power on line	40	13
Undervoltage	34	14
Overcurrent	28	19
Overvoltage	15	8
Voltage fluctuation or drop	13	7
Underfrequency and overfrequency	8	8
Swing on-load demand	3	2
Other	2	2

Of these system conditions, 40 of them involved no power on the AC lines, while 34 occurrences resulted due to undervoltage conditions, of which 14 scrams were encountered. Different system conditions that acted as initiating events for the actions of the NPP are shown in Table 4.

Table 4: Initiating events for NPP actions [111]

Initiating event	Number of occurrences	Number of scrams
Equipment failures (on the grid)	37	25
Grid perturbations (excluding weather-induced)	35	23
Weather	32	16
Human errors	23	11
Fire (and resulting smoke)	5	0
Animals	3	0

Of these initiating events, 37 occurrences were due to equipment failures on the transmission system. Secondly, 35 occurrences were a result of system perturbations which had no relation to the weather-induced conditions. A combination of weather, human error, fires and animals made up the rest of the initiating events which resulted in those control actions of the NPP. The above analysis has shown how crucial the interaction between the NPP and the NETS is. When analysing this interaction, it is vital that the transmission system is able to supply the NPP in a safe and secure manner, just as vital as it is for the system to rely on the NPP.

2.4 Chapter 2 summary

A detailed literature review of both CSC- and VSC-HVDC technology has been carried out. From the literature review, it is apparent that no NPP in the world has ever been connected by HVDC technology before. If such a solution were to be implemented, then this would represent a world's first and hence there is limited existing technical knowledge on such an application. From the review, if an NPP were to be connected solely by HVDC technology, then the frequency must be maintained by the control system.

The work carried out in the thesis will provide new technical knowledge and learning for an NPP HVDC connection and allow conclusions to be drawn surrounding the suitability of both CSC- and VSC-HVDC technology for such an application.

Chapter 3: Connecting NPPs by AC Technology

In this chapter a technical assessment of an NPP power system connection using AC technology is performed. The impact of AC system faults on the NPP is analysed through power system simulations carried out in PSCAD. Detailed descriptions of the NPP and AC power system models used in PSCAD are presented.

3.1 Introduction

As discussed previously in chapter 2, modern NPPs are connected to the power system by AC technology. This could be in the form of AC overhead lines, cables or a combination of both. Both three-phase and single-phase faults can occur on any part of the power system. These faults will result in the flow of high currents and depressions in AC voltages [123]. In particular, the three-phase fault can result in zero voltage at the point of issue and result in cascading voltage depressions further down the power system. In section 2.2.9, the effects of power system disturbances on an NPP are introduced. When assessing AC technology for a generator connection, the effects of single and three-phase faults on NPP operation need to be ascertained. Power system simulations are a useful tool for carrying out such an analysis.

In the following section simulations are carried out in PSCAD to analyse the effects of power system faults on an NPP connected by AC technology. Models of both an NPP and an AC grid have been developed in PSCAD. A load flow analysis was carried out in Power World Simulator 16 to ascertain the steady-state voltage, active and reactive power parameters of the overall power system. Within the power industry the impacts of three-phase faults on the power system compared to that of single-phase faults are well established [124]. Three-phase faults were placed at different points around the power system, shown in Figure 43, to establish those locations which had the biggest impact on the steady-state parameters. Those which showed the most adverse effects were then analysed in greater detail through further simulations carried out in PSCAD.

3.2 Modelling of an NPP connected by AC technology

In the following sections each of the AC components used in the PSCAD model is described.

3.2.1 AC generator model

Within PSCAD if one or more synchronous generators are connected into the network, the load flow process is simple (even if the generator setup is more complex) [125]. Each generator can start the case during initialisation with a three-phase fundamental voltage source connected to its terminals.

The magnitude and phase is fixed as designated within the machine's data input sheets. An example of this is shown in Figure 31.

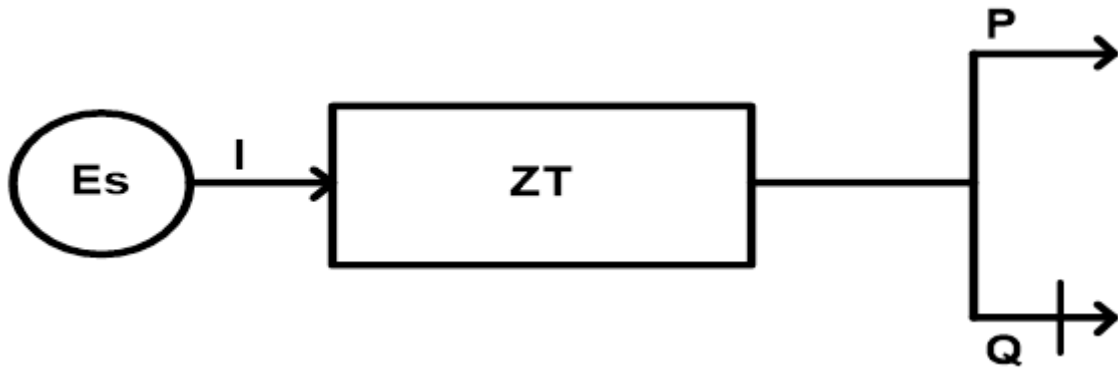


Figure 31: Fundamental voltage source connected to an impedance source.

The source impedance is entered in the format shown in Equation 3.1. The source voltage is given by Equation 3.2 and the current flowing through the impedance Z_T is given by Equation 3.3 [125].

$$Z_s = Z[\phi] = R1 + R2 \text{ll}L = R1 + \frac{R2 \cdot jXL}{R2 + jXL} \quad (3.1)$$

$$E_s = V_T + I * Z_T \quad (3.2)$$

$$I = P - \frac{jQ}{V_T} \quad (3.3)$$

The AC networks are modelled as equivalent R–R/L circuit impedances which represent the strength of the grid connection points. In Figure 32 the Short Circuit Level (SCL) and model representation of the NPP is presented.

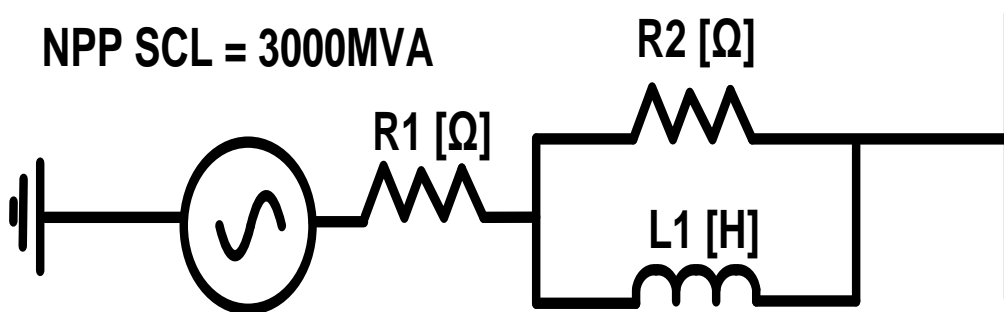


Figure 32: Short circuit level at the NPP

The SCL of the NPP model is 3000 MVA and has been provided by National Grid. The component values of the R–R/L circuit can be calculated using the SCL and Short Circuit Ratio (SCR) of the system [126]. The SCR is discussed and calculated in further detail in chapters 4 and 5, when the connection of the HVDC link is considered. The combined series resistance (R_1), parallel resistance (R_2) and inductance (L_1) represent the AC system and short circuit impedance. The NPP SCL of 3000 MVA corresponds to a single generator unit rating of 1200 MVA. The SCL representation of the AC grid model is shown in

Figure 33.

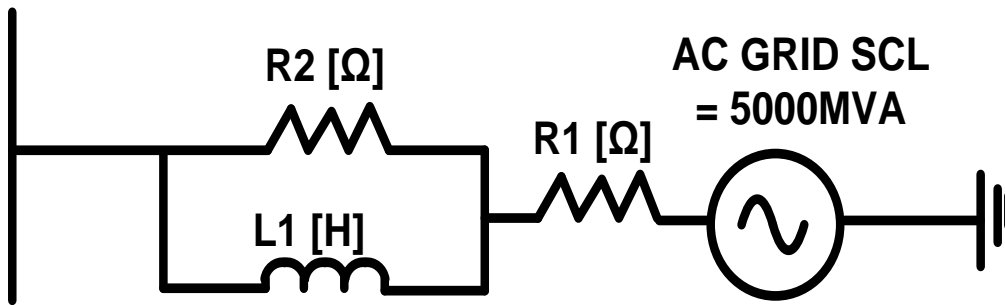


Figure 33: Short circuit level of the AC grid

The SCL of the AC grid is 5000 MVA and represents a strong connection.

3.2.2 AC double-wound transformer model

The AC double-wound transformer can be represented in many different forms within the PSCAD software. Both three-phase and single-phase transformers can be selected with different winding configurations. These can be a combination of star-star, star-delta, delta-star or Y configurations. Primary, secondary and tertiary voltages can be entered manually by the user. Winding resistance and leakage reactance data can also be selected. The AC double-wound transformer used in the power system model is shown in Figure 34.

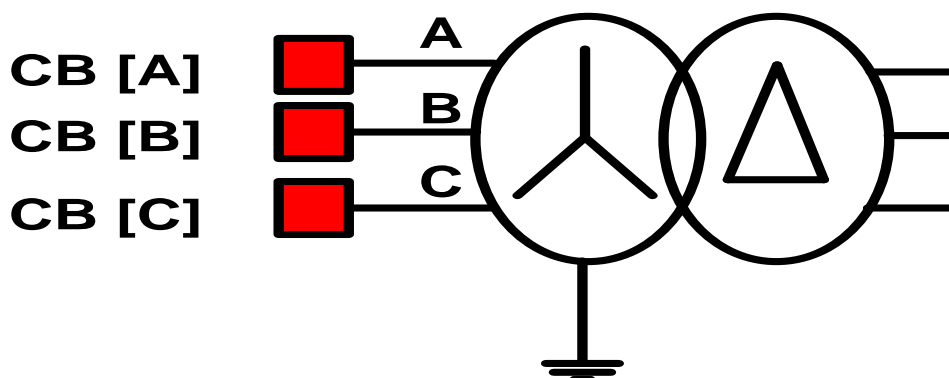


Figure 34: AC transformer with circuit breakers

This component is a single-phase two-winding transformer, and is based on the classical modelling approach [126]. This component is the equivalent of three single-phase, two-winding transformers connected in a three-phase bank. Here the user can select the winding interconnections to be star or delta configuration on either side. PSCAD computes the inductances based on the open circuit magnetising current, the leakage reactance and their rated winding voltages [126]. To demonstrate how the parameters are derived for use by EMTDC, the data for a transformer is shown in Table 5.

Table 5: Data for the transformer shown in Figure 34 [126]

Parameter	Description	Value
TMVA	Transformer single-phase MVA	100 MVA
f	Base frequency	50 Hz
X1	Leakage reactance	0.1 pu
NLL	No load losses	0.0 pu
V1	Primary winding voltage (RMS)	132 kV
Im1	Primary side magnetising current	1%
V2	Secondary winding voltage (RMS)	23 kV
Im2	Secondary side magnetising current	1%

If the resistance in Table 5 above is ignored, then the (approximate) value for L1+L2 from the short circuit test is [126]:

$$L1 + L2 = \frac{0.1 \cdot Z_{base1}}{\omega_{base1}} = 55.462 \text{ mH} \quad (3.4)$$

Where:

$$Z_{base1} = \frac{(132 \cdot \text{kV})^2}{(100 \text{ MVA})} = 174.24 \quad (3.5)$$

Assuming nominal turns ratio for “a”, which is given by [127]:

$$a = \frac{132 \text{ .kV}}{23 \text{ .kV}} = 5.7 \quad (3.6)$$

Taking into account the primary and secondary base currents [127]:

$$I_{base1} = \frac{(100 \text{ .MVA})}{(132 \text{ .kV})} = 0.75kA \quad (3.7)$$

$$I_{base2} = \frac{(100 \text{ .MVA})}{(23 \text{ .kV})} = 4.34kA \quad (3.8)$$

Thus, by energising the primary side with 132 kV, the following magnetising current is [127]:

$$I_{m1} = 1\% \cdot I_{base1} \quad I_{m2} = 1\% \cdot I_{base2} \quad (3.9)$$

Including the following expression from the equivalent circuit [127]:

$$\frac{I_{m1}}{I_{m2}} = \frac{V_{base2}}{V_{base1}} = \frac{1}{a^2} \cdot \frac{(L2 + a \cdot L12)}{L1 + a \cdot L12} \quad (3.10)$$

Where [127]:

$$\frac{V_{base1}}{I_{m1}} = \omega_{base} \cdot (L1 + a \cdot L12) \quad (3.11)$$

$$\frac{V_{base2}}{I_{m2}} = \frac{\omega_{base}}{a^2} \cdot (L2 + a \cdot L12) \quad (3.12)$$

Therefore, since:

$$\frac{I_{m1}}{I_{m2}} \cdot \frac{V_{base2}}{V_{base1}} = \frac{1}{a^2} \quad (3.13)$$

By combining Equations 3.4 and 3.13 we obtain $L1-L2 = 27.731 \text{ mH}$ and from Equation 3.10 we obtain a $L14= 55.4 \text{ H}$. The values for the parameters are obtained as follows [127]:

$$L11 = L1 + a \cdot L12 = 55.4 \text{ H} \quad (3.14)$$

$$L_{22} = \frac{L_2 + a \cdot L_{12}}{a^2} = 13.86 \text{ H} \quad (3.15)$$

$$L_{12} = 27.5 \text{ H} \quad (3.16)$$

3.2.3 Autotransformer model

This component models a three-phase autotransformer bank comprised of three single-phase banks [127]. Options are provided so the user may select between either a magnetising branch or a current injection routine to model the magnetising currents. The magnetising branch can be eliminated altogether, leaving the transformer in “ideal” mode, where all that remains is a series leakage reactance [127]. External connections to the component are shown in Figure 35.

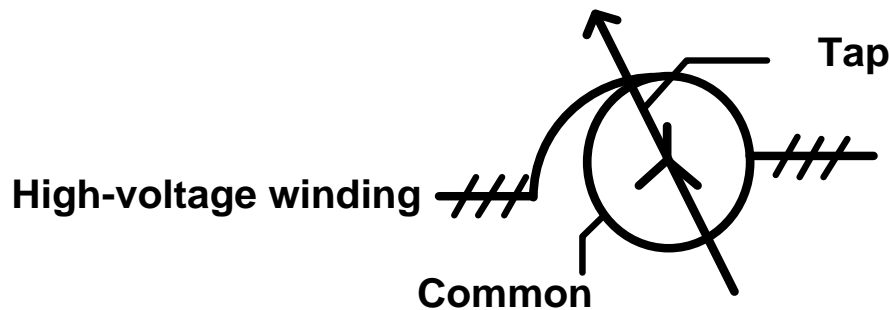


Figure 35: Autotransformer model used in PSCAD

Usually a single winding per phase, the low voltage terminal is made from a tap part-way down the winding. The autotransformer is more economical than a two-winding transformer for a voltage ratio up to 3:1. Autotransformers are usually star connected and share the same neutral, which is often undesirable except in transmission systems where solid earthing is applied at most voltage levels [128].

The turns ratio for the above autotransformer are given by [128]:

$$\frac{V_1}{N_1 + N_2} = \frac{V_2}{N_2} \quad (3.17)$$

$$I_1 \cdot N_1 = (I_2 - I_1) \cdot N_2 \quad (3.18)$$

A star-delta configuration is employed in PSCAD. This results in the following advantages [127]:

- A neutral point is available for earthing.
- A reduced insulation level of the neutral is permitted.
- This is more economical for a high voltage winding.
- This permits a tap changer to be located near the neutral.

3.2.4 On-load tap changer model

An on-load tap changer is employed with the autotransformer. The operation principle of the model used in PSCAD is shown in Figure 36.

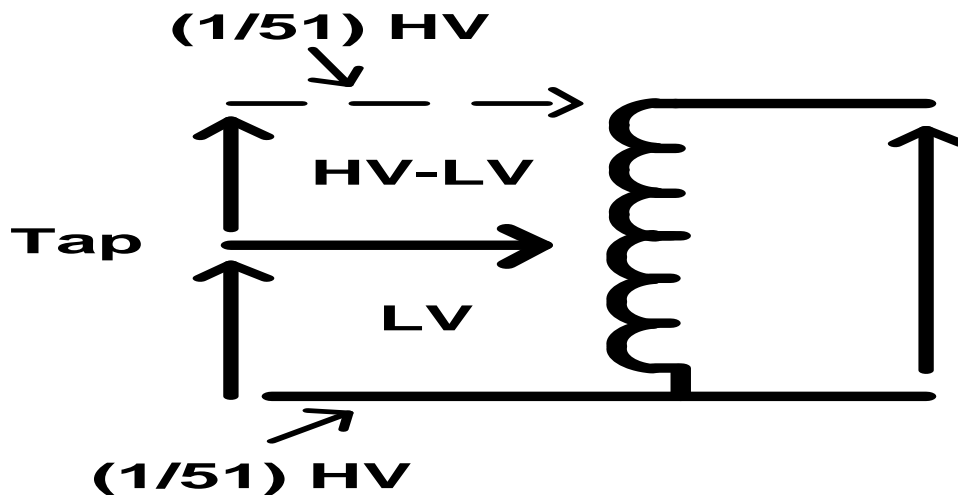


Figure 36: On-load tap changer principle of operation

The tap value is limited internally so that the (HV-LV) and LV voltage ratios never exceed 50. This translates to tap position limits that maintain the LV side voltage between:

$$LV \cdot \left(1 + \frac{1}{50}\right) < HV < 51 \cdot LV \quad (3.19)$$

For example, the tap limits for the 132 kV / 400 kV autotransformer model shown in Figure 36 are:

$$\frac{400}{\left(1 + \frac{1}{50}\right)} = 392.15kV \quad (3.20)$$

And

$$\frac{400}{51} = 7.84kV \quad (3.21)$$

This translates to tap input signal limits of [128]:

$$\frac{400/132}{(1 + \frac{1}{50})} = 2.97pu \quad (3.22)$$

$$\frac{400/132}{5} = 0.05pu \quad (3.23)$$

The tap limits for the autotransformer are not fixed, but are dependent on the HV and LV values.

3.2.5 AC overhead transmission line model

Within PSCAD the direct connection mode has been used for all AC overhead line connections. Here, both the interfaces and the segment properties are housed within a single component, shown in Figure 37

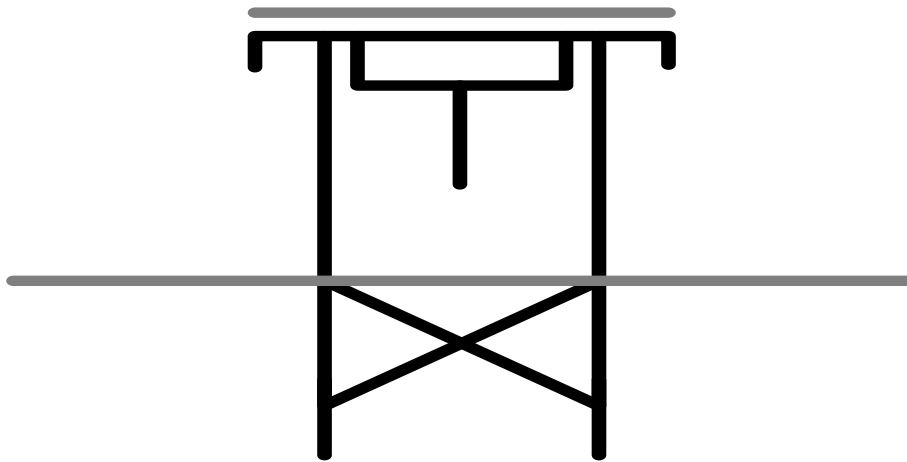


Figure 37: AC overhead transmission line model used in PSCAD

When modelling aerial transmission lines and cables the difficulty arises due to the fact that they are highly nonlinear in nature. This is due to the frequency dependency of the conductors (skin effect), as well as the ground or earth return path [128]. The ability to represent these systems accurately and efficiently is an essential part of the electromagnetic transient simulation of power systems as a whole [128].

Transmission systems are frequency-dependent and so it makes sense to solve their parameters in the frequency domain [129].

To accurately represent a frequency-dependent line when simulating EMTDC (which operates in the time domain), these parameters must be convolved into their equivalent time-domain characteristics [127]. For the model shown in Figure 37, the frequency-dependent (phase) model is used in PSCAD – it is one of the most precise methods available within the software [127].

The frequency-dependent (phase) model is numerically robust and more accurate than any commercially available line/cable model, and is the preferred model to use [127]. It is useful for studies when ever the transient or harmonic behaviour of the line or cable are important. The frequency-dependent (phase) model operates on the principle that the full frequency-dependence of a transmission system can be represented by two matrix transfer functions [127]. The propagation function H , and the characteristic admittance Y_c . The model is shown in Figure 38.

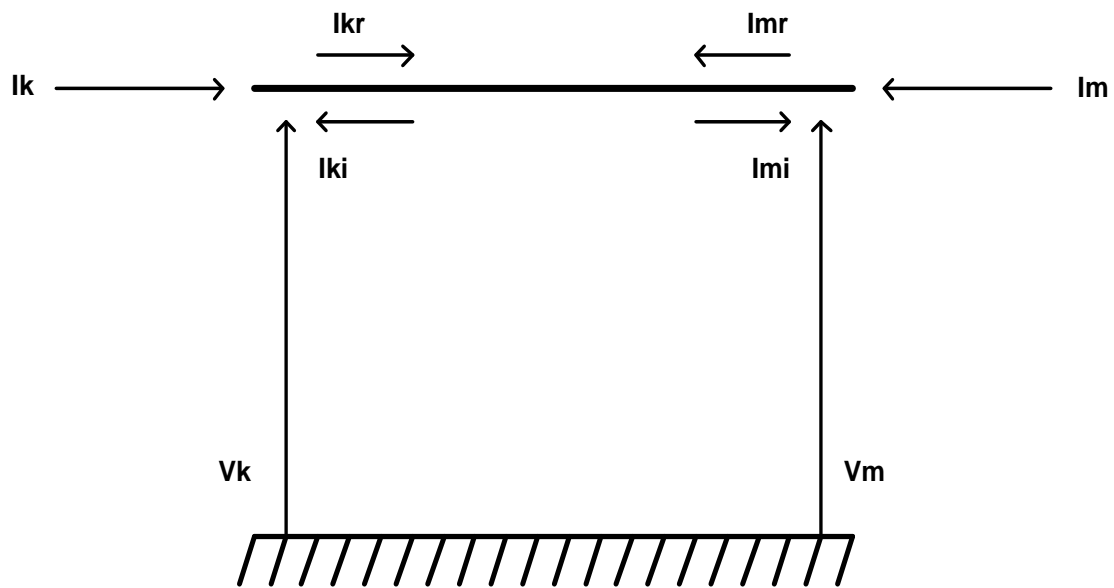


Figure 38: Voltages and currents in an N-conductor transmission line

The following can be derived directly from the “telegraphers” equations as follows [130]:

$$Y_c . V_k - I_k = 2 . HT . I_{mr} = 2 . I_{ki} \quad (3.24)$$

$$Y_c . V_m - I_m = 2 . HT . I_{kr} = 2 . I_{mi} \quad (3.25)$$

Where [130]:

$$H = e^{-\sqrt{ZY}t} \quad (3.26)$$

$$Y_c = Z^{-\tau} - t\sqrt{Z}Yt \quad (3.27)$$

And [130]:

- V_k / V_m = The node voltage vectors at ends k and m
- I_k / I_m = The injected current vectors at ends k and m
- I_{ki} / I_{mi} = The incident current vectors at ends k and m
- I_{kr} / I_{mr} = The reflected current vectors at ends k and m

H and Y_c are calculated multiple times at discrete points in the frequency domain, and then approximated and replaced by equivalent low-order rational functions.

The frequent-dependent (phase) model interfaces with the EMTDC electric network by means of a Norton equivalent circuit, as shown in Figure 39.

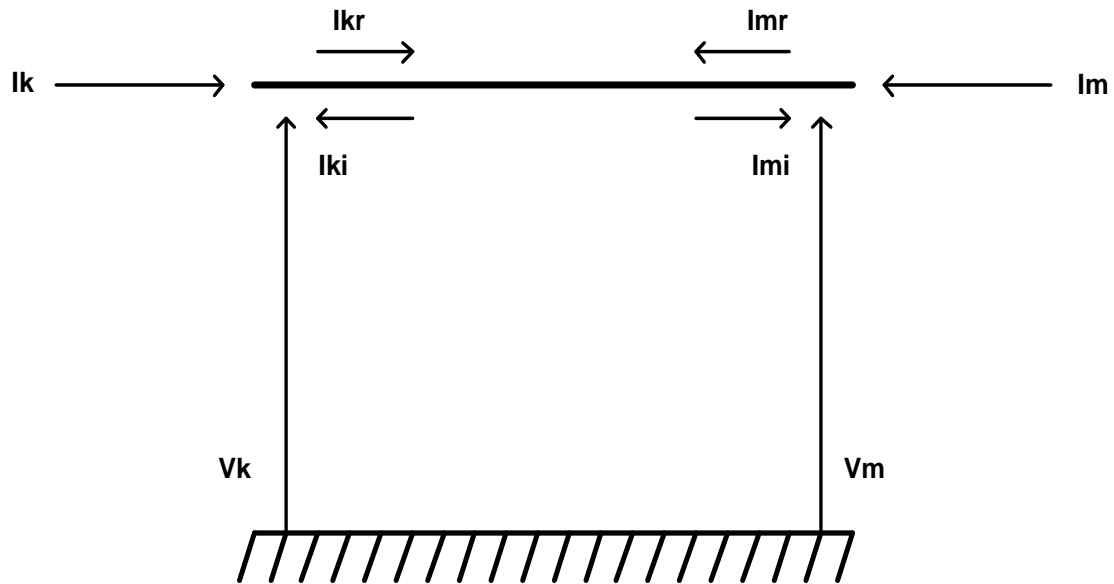


Figure 39: EMTDC frequency-dependent (phase) model time-domain interface

The historical current source injections I_{hisk} and I_{hism} are updated each time step, given the node voltages V_k and V_m , as calculated by EMTDC [127]. The steps by which this is accomplished by the frequency-dependent (phase) model time-domain interface routine are as follows: [127]

$$I_k(n) = G \cdot V_k(n) - I_{hisk}(n) \quad (3.28)$$

$$I_{kr}(n) = I_k(n) - I_{ki}(n) \quad (3.29)$$

$$I_{ki}(n+1) = H * I_{mr}(n - \tau) \quad (3.30)$$

$$I_{hisk}(n + 1) = Y_c * V_k(n) - 2 \cdot I_{ki}(n + 1) \quad (3.31)$$

Where:

- i = Denotes travelling waves
- r = Denotes reflected waves
- $*$ = Indicates a convolution integral

3.2.6 AC induction motor model

The squirrel-cage induction motor is modelled as a double-cage machine to account for the deep-bar effect of the rotor cage [130]. Both the direct and quadrature-axes are identical and are as shown in Figure 40.

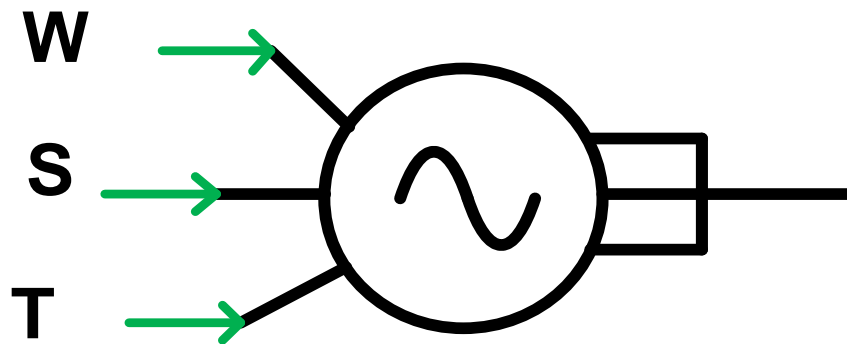


Figure 40: AC induction motor model used in PSCAD

The induction motor can be operated in either speed or torque control mode. In speed control mode, the machine rotates at the speed specified at the input W . In torque control mode, the speed is calculated based on the machine inertia, damping, the input torque and the output torque [130].

Normally the machine is started in speed control mode with the W input is set to the rated per unit value. Once the machine reaches steady state it is changed over to torque control mode. The switch, S , allows the user to select speed control mode (1) or torque control mode (0) [130]. In the case of this model in Figure 40, speed control mode is selected to represent the starting characteristics of an 11 kV motor.

3.2.7 AC circuit breaker model

This component simulates a three-phase circuit breaker operation. The “on” (closed) and “off” (open) resistance of the breaker must be specified, along with its initial state [130]. The breaker model used in PSCAD is shown in

Figure 41.

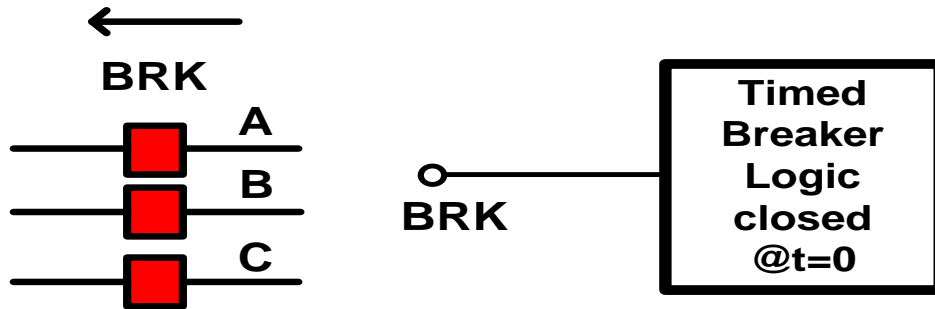


Figure 41: AC circuit breaker component used in PSCAD

This component is controlled through a named input signal (default is BRK), where the breaker logic is [130]:

- 0 = on (closed)
- 1 = off (open)

The breaker control can be configured automatically by using the timed breaker logic component [130]. The user may initially set the state of the breaker being controlled to “off” (open) or “on” (closed). One or two breaker operations may also be selected [130]. The first and second operations will either be “off” (open) or “on” (closed), depending on the initial state. The output of this block should be connected to a data label with the breaker name of the device being controlled [130]:

3.2.8 Load model

This component models a three-phase, passive linear branch. Its resistance value is calculated from the user-entered rated conditions, and remains fixed throughout the simulation. The type of load can be selected to be resistive, inductive or passive. The power ratings of the loads are in MW and the parameters of resistance or inductance can be specified.

All the loads in the PSCAD model are resistive according to the data provided by National Grid.

A resistive load component is shown in Figure 42.

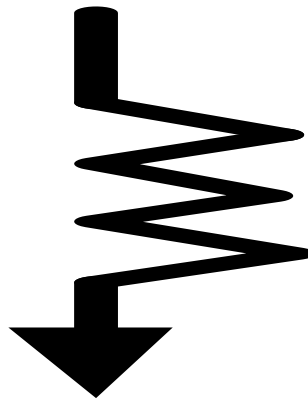


Figure 42: Resistive load

This component is only available in a three-phase (single-line view) configuration.

3.3 Power system setup

The power system model developed in PSCAD is shown in Figure 43. The data for all components used in the PSCAD model has been provided by National Grid Electricity Transmission (NGET).

3.3.1 NPP model

The NPP model has been designed based upon the literature review carried out in chapter 2 and site visits undertaken to several NPPs within the UK. Two individual nuclear reactor stations provide a combined active power rating of 2400 MW; each is electrically independent from the other for safety reasons and a fault or emergency situation in one will not affect the other.

Several step-up transformers are used to provide the required voltage levels within the NPP. The total impedance of all the transformers can influence the effects of voltage disturbances within the NPP and must be included within the model [131]. Two autotransformers (AT1 and AT2) are used to step up the voltage within the NPP from 132 kV to 400 kV for connection into the AC transmission grid. Autotransformers are used due to these being more economical for a 3:1 voltage turns ratio compared with a double-wound transformer [132].

Four 11 kV three-phase motors represent the motors that are used to drive the pumps of the reactor cooling system. The motors are each connected to individual 11 kV busbars, which are supplied from the 23/11 kV transformers. The motors are each rated at 5000 BHP (Brake Horse Power). Circuit Breakers have been installed on either side of the transformers and generators to enable opening during the simulations.

3.3.2 AC grid

The AC grid is based upon the NGET transmission network shown in [1]. Four separate AC systems are interconnected by 400 kV AC overhead lines. The voltage and power ratings of the generators, overhead lines and system loads are shown in Table 6.

Two separate 400 kV double circuit AC overhead lines connect the two individual reactor stations into the northern and southern part of the AC grid as shown in Figure 43.

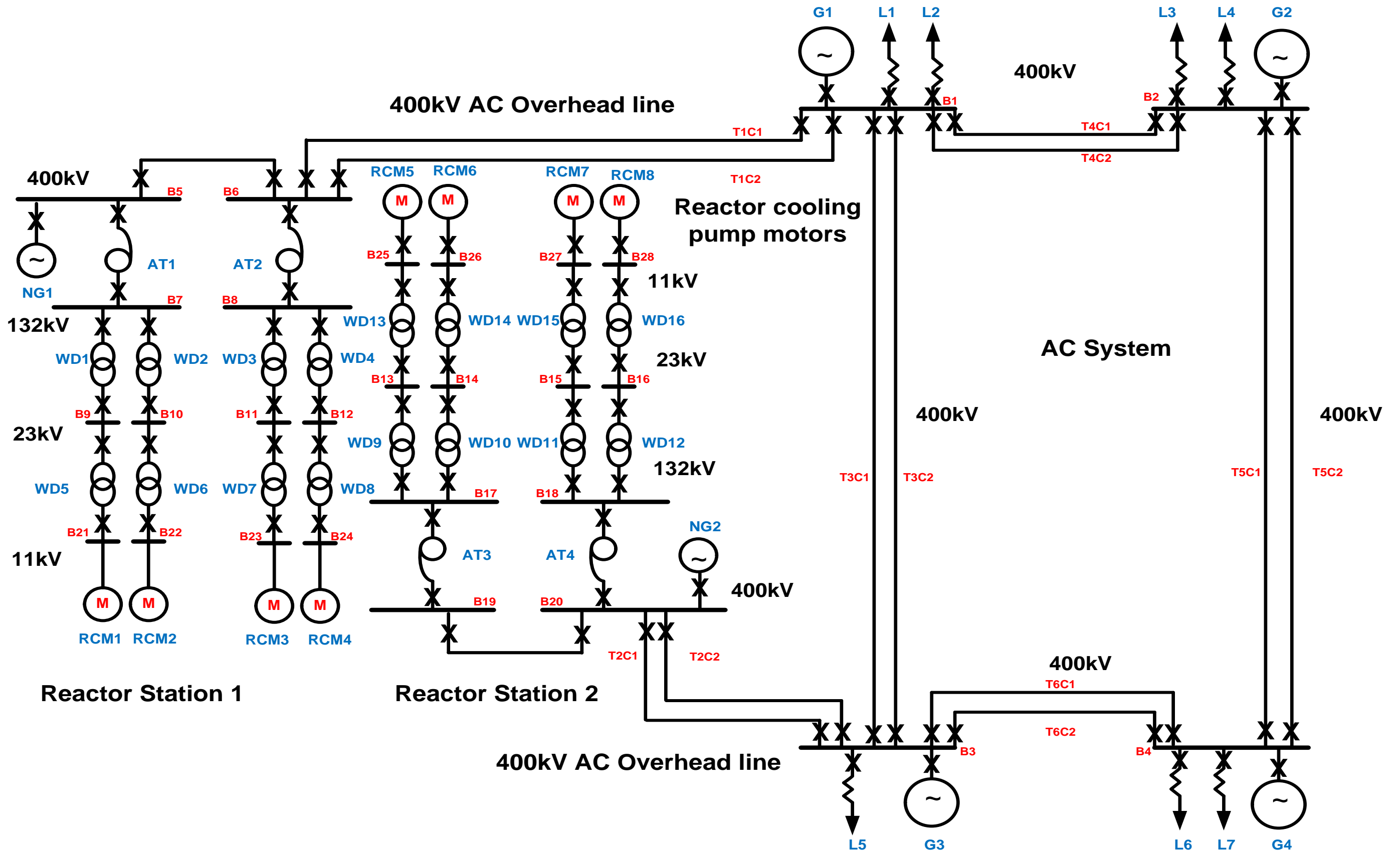


Figure 43: Overall power system setup in PSCAD

Table 6: Table showing PSCAD component data for Figure 43

Component	Description	Connection location	Power rating (MVA)	Voltage rating (kV)
NG1	Nuclear generator 1	B20	1200	23
NG2	Nuclear generator 2	B5	1200	23
G1	AC generator 1	B1	2000	400
G2	AC generator 2	B2	2500	400
G3	AC generator 3	B3	1500	400
G4	AC generator 4	B4	2000	400
AT1/AT2	Autotransformers 1 & 2	B5/B6	700	400/132
AT3/AT4	Autotransformers 3 & 4	B19/B20	700	400/132
DW1/DW2	Double-wound transformer 1 & 2	B9/B10	600	132/23
DW3/DW4	Double-wound transformer 3 & 4	B11/B12	600	132/23
DW5/DW6	Double-wound transformer 5 & 6	B21/B22	500	23/11
DW7/DW8	Double-wound transformer 7 & 8	B23/B24	500	23/11
DW9/DW10	Double-wound transformer 9 & 10	B13/B14	600	132/23
DW11/DW12	Double-wound transformer 11 & 12	B15/B16	600	132/23
DW13/DW14	Double-wound transformer 13 & 14	B25/B26	500	23/11
DW15/DW16	Double-wound transformer 15 & 16	B27/B28	500	23/11
T1C1	Transmission line 1 circuit 1	B1/B6	2200	400
T1C2	Transmission line 1 circuit 2	B1/B6	2200	400
T2C1	Transmission line 2 circuit 1	B3/B20	2200	400
T2C2	Transmission line 2 circuit 2	B3/B20	2200	400
T3C1	Transmission line 3 circuit 1	B1/B3	2200	400
T3C2	Transmission line 3 circuit 2	B1/B3	2200	400
T4C1	Transmission line 4 circuit 1	B1/B2	2200	400
T4C2	Transmission line 4 circuit 2	B1/B2	2200	400
T5C1	Transmission line 5 circuit 1	B2/B4	3200	400
T5C2	Transmission line 5 circuit 2	B2/B4	3200	400
T6C1	Transmission line 6 circuit 1	B3/B4	2200	400
T6C2	Transmission line 6 circuit 2	B3/B4	2200	400
L1	Load 1	B1	1000	400
L2	Load 2	B1	1000	400
L3	Load 3	B2	1000	400
L4	Load 4	B2	2000	400
L5	Load 5	B3	2000	400
L6	Load 6	B4	2000	400
L7	Load 7	B4	1000	400
RCM1-RCM8	Reactor cooling motors 1-8	B21-B28	200	11

3.4 Load flow analysis

Models of both the NPP and AC transmission system are created in Power World Simulator version 16. The data used for each of the individual power system components is identical to those employed in PSCAD. A load flow analysis is carried out on both Power World Simulator 16 and PSCAD to ascertain the steady-state parameters of the two models. A detailed description of both software is given in Appendix A (PSCAD) and Appendix B (Power World).

3.4.1 PSCAD load flow results

The results obtained for the load flow analysis in PSCAD are shown in Table 7.

Table 7: PSCAD load flow analysis results

Bus no.	Voltage (kV)	Power (MW)	Reactive power (Mvar)
B1	397	860	1000
B2	395	1928	800
B3	396	970	516
B4	395	1095	324
B6	397	705	47
B20	398	730	98

3.4.2 Power World Simulator load flow results

The results obtained for the load flow analysis are shown in Table 8.

Table 8: Power World Simulator load flow analysis results

Bus no.	Voltage (kV)	Power (MW)	Reactive power (Mvar)
B1	395	865	996
B2	392	1930	802
B3	397	976	518
B4	392	1092	321
B6	394	700	47
B20	396	727	98

3.4.3 Load flow analysis comparison

A statistical analysis using standard deviation, absolute and relative error calculations is carried out to compare the difference between the two sets of results. An example calculation for the voltage at B1 is given:

The Absolute Error (AE) is the amount of physical error in a measurement and is given by the formula [133]:

$$AE = [x \text{ measured} - x \text{ accepted}] \quad (3.32)$$

The Relative Error (RE) is the ratio of the AE of the measurement to the accepted measurement. The relative error expresses the “relative size of the error” of the measurement in relation to the measurement itself, where [134]:

$$RE = \left(\frac{[\text{Measured Value} - \text{Actual Value}]}{[\text{Actual Value}]} \right) \quad (3.33)$$

The standard deviation (σ) is a measure of the spread of data where [134]:

$$\sigma = \left(\frac{[397 + 395]}{[2]} \right) = 396 \quad (3.34)$$

And [134]:

$$(397-396) = (1^2) = 1 \quad (3.35)$$

$$(395-396) = (-1^2) = 1 \quad (3.36)$$

$$(1+1) = \sqrt{2} \quad (3.37)$$

Hence the following results are obtained [134]:

$$\text{Absolute Error} = (397-395) = 2 \text{ MW} \quad (3.38)$$

$$\text{Relative error} = (2/397) \times 100 = 0.5 \% \quad (3.39)$$

The above calculation was applied to the remainder of the load flow results with the resultant outcomes shown in Table 9.

The relative error for the values shown is less than 1% which is within the $\pm 1\%$ tolerance level acceptable to National Grid and in particular the Grid Code [135].

Table 9: Resultant outcomes of load flow analysis comparison

Bus No	VOLTAGE (kV)			POWER (MW)			REACTIVE POWER (Mvar)		
	Standard Deviation	Absolute error	Relative error (%)	Standard Deviation	Absolute error	Relative error (%)	Standard Deviation	Absolute error	Relative error (%)
B1	1.414213562	2	0.5	3.535533906	-5	-0.58	2.828427125	4	0.4
B2	2.121320344	3	0.75	1.414213562	-2	-0.1	1.414213562	-2	-0.25
B3	0.707106781	-1	-0.25	4.242640687	-6	-0.61	1.414213562	-2	0.39
B4	2.121320344	3	0.75	2.121320344	3	0.27	2.121320344	3	0.93
B6	2.121320344	3	0.75	3.535533906	5	0.71	0	0	0
B20	1.414213562	2	0.5	2.121320344	3	0.41	0	0	0

3.5 Transient analysis of an NPP connected by AC technology

A transient analysis of AC technology for connecting an NPP was carried out in PSCAD. Due to the large scale of the power system in PSCAD, a general fault analysis was carried out initially. The aim was to identify those fault locations which had the worst effect on the voltage and power profiles of the various busbars. Here, both single-phase and three-phase faults were analysed around the system at the multiple locations shown in Figure 44. The faults which influenced the NPP voltage and power profiles were then selected for a more detailed analysis in PSCAD.

3.5.1 General transient analysis

System variables consisting of both voltage and current were measured at the point of fault both before (pre-fault) and during the transient event. The active power output of the reactor was also monitored during each fault to analyse the behaviour during each simulation. Three-phase faults had the worst effect on the NPP and so only the results for these are shown in Table 10. Several of the fault locations showed very similar effects. In most places, the severity of the three-phase fault has resulted in complete voltage collapse at all the nodes. The current during the fault ranges from 4 kA to 27 kA. The reactor power has remained constant for some, but has power spikes as high as 1600 MW for others is observed. This behaviour will be analysed further during the detailed transient simulations.

Table 10: General fault analysis results

Fault number	Pre-fault voltage (kV)	Pre-fault reactor power (MW)	Pre-fault current (kA)	Voltage during fault (kV)	Reactor power during fault (MW)	Current during fault (kA)
F1	397	500	3	0	500	5
F2	399	400	2	0	500	4
F3	398	300	2	0	500	6
F4	395	800	2	0	500	10
F5	396	600	2	0	550	8
F6	396	300	2	0	500	8
F7	394	400	2	0	520	6
F8	395	300	22	0	500	6
F9	395	1096	2	0	500	11
F10	400	1000	2	0	500	12
F11	398	600	2	0	550	9
F12	399	500	3	0	550	9
F13	399	600	4	0	500	12
F14	396	900	4	0	550	11
F15	398	800	3	0	550	8
F16	398	700	3	0	500	8
F17	398	600	2	0	500	9
F18	397	600	2	0	0	9
F19	398	700	2	0	500	6
F20	397	500	2	0	500	7
F21	397	500	2	0	500	7
F22	397	550	2	0	550	8
F23	23	650	2	0	550	10
F24	11	550	3	0	500	10
F25	398	450	2	0	500	9
F26	398	600	2	0	500	9
F27	398	500	2	0	1300	7
F28	11	500	4	0	500	14
F29	22	600	4	0	500	12
F30	130	500	3	0	500	10
F31	130	600	3	0	500	10
F32	11	700	4	0	200	13
F33	22	500	4	0	0	14
F34	131	650	2	0	0	12
F35	397	700	4	0	0	27
F36	398	800	2	0	1600	12
F37	397	800	4	0	1600	15
F38	397	900	4	0	0	24
F39	131	700	4	0	1600	21
F40	400	800	4	0	0	20
F41	22	900	4	0	200	22
F42	11	500	4	0	0	9

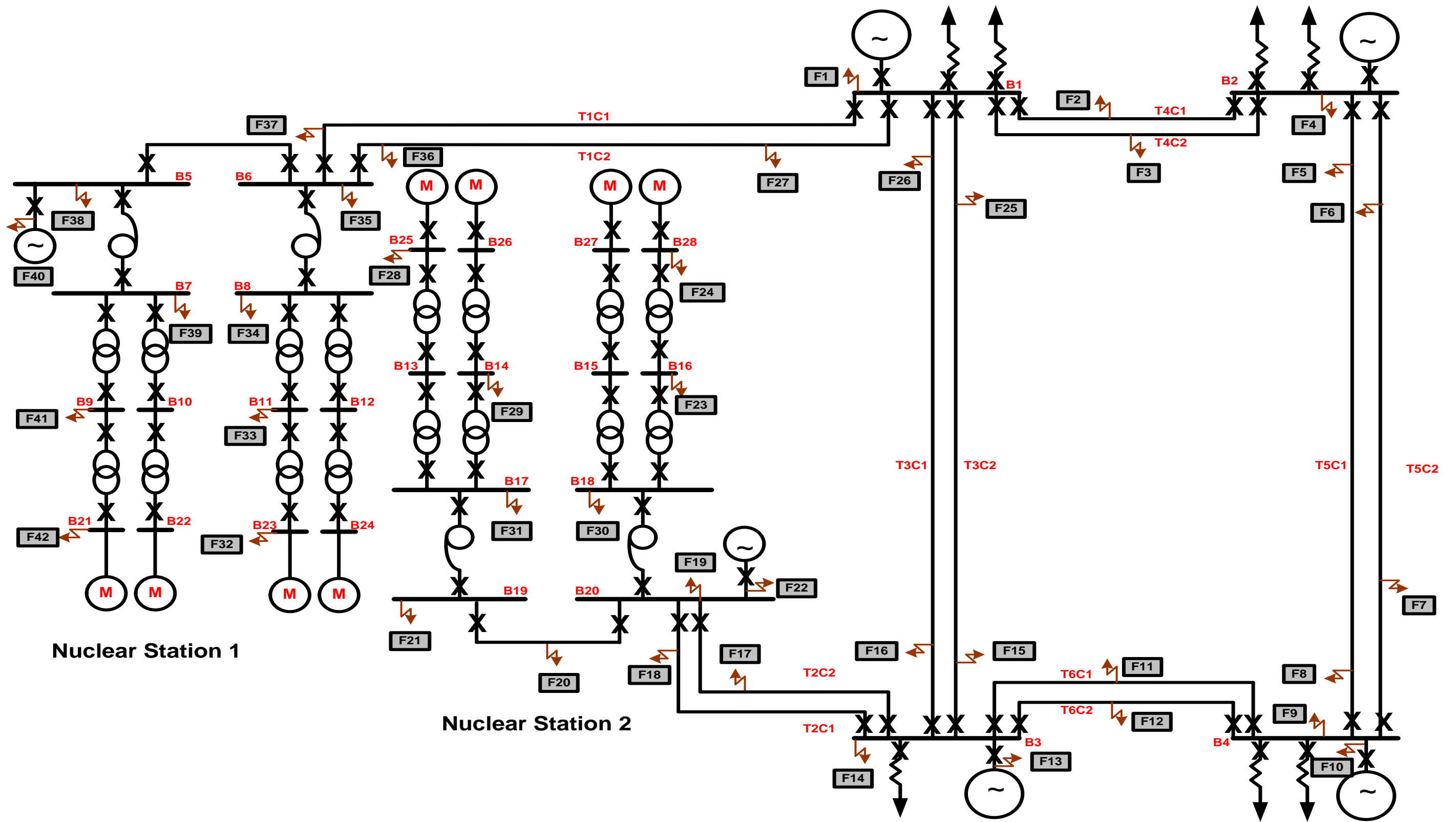


Figure 44: General fault analysis for NPP connected by AC technology

The decision to select which faults merited further detailed analysis was based upon a combination of severe voltage and reactor power variations before and during the fault.

One such example is the fault at location F42, where the reactor active power drops from 900 MW pre-fault to 200 MW during the fault. The pre-fault current increases from 4 kA to 22 kA during the fault and the voltage has collapsed to zero during the fault. Due to this change in system variables, the author has selected this fault at location F42 scenario for further detailed analysis.

3.5.2 Detailed transient analysis

Those fault locations which merited further detailed transient analysis are described and analysed in the following sections. In some cases, AC circuits were switched out before occurrence of the faults to mimic circuit outages on the network. This has the potential to make the impact of the fault greater and cause the SCL of the AC system to change [136]. In one situation, two successive faults were applied one after the other to replicate an incipient fault (intermittent) developing into a permanent fault [137].

The Grid Code is a public document which describes the conditions and technical requirements for any generator wishing to connect to the NETS [135]. The maximum fault clearance time on the UK 400 kV transmission system is 140 ms to ensure system stability is maintained and damage to plant is avoided [135]. For the detailed transient analysis below, all faults at 400 kV transmission voltage level were cleared within the 140 ms stipulation time of the Grid Code. For those faults occurring at lower voltages within the NPP, the total fault clearance times are longer and are based on the information contained in the literature review in chapter 2.

In the simulation plots, selected busbars within the NPP are monitored to observe whether the faults have any impact on those busbar voltage profiles. The reactor output power is also monitored to assess its behaviour both pre and post fault.

3.5.2.1 Successive A–G faults on TL1C1 and TL1C2

A phase A–G fault occurred on transmission line 1, circuit 1 (TL1C1) at a time of 0.3 secs. Approximately 100 ms after the occurrence of the first fault, a second fault occurred on transmission line 2, circuit 2 (TL1C2) at a time of 0.4 secs. The delay of 100 ms between the two was chosen to allow a sufficient margin for the first fault to fully take effect before the occurrence of the second [138]. The main line feeder protections were successful in clearing both faults within 140 ms. Fault 1 was cleared within 0.44 secs and fault 2 within 0.54 secs respectively. The simulation results are shown in Figure 45.

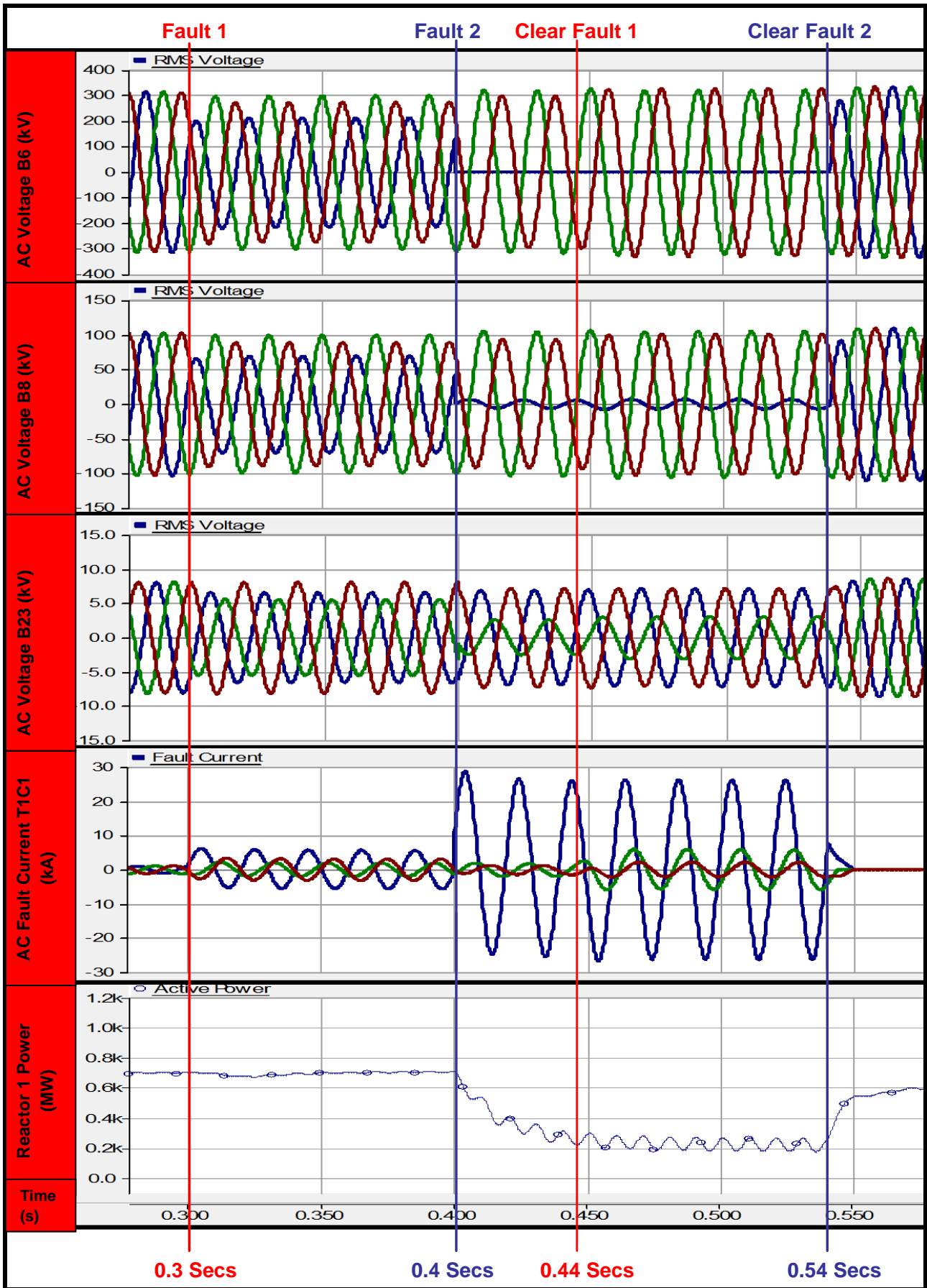


Figure 45: AC system profiles for successive A–G faults on transmission line 1 circuits

When fault 1 occurs at a time of 0.3 secs, the peak current on the faulted phase is approximately 6.0 kA. Voltage depressions on the red A phase (blue) at busbar 6 can also be observed. This voltage depression propagates into the AC switchyard, affecting busbars 6 and 8. The reactor generator output power is held constant by governor control [139] due to the remaining healthy circuit (TL1C2) providing an alternate path for the power to flow into the AC system on busbar B1. The second fault appears at a time of 0.4 secs on the remaining healthy circuit (TL1C2), with both system faults now occurring simultaneously. The fault current measured on transmission line 1 circuit 1 (TL1C1) now exceeds 15 kA due to multiple circuit infeeds to both faults. The same fault current values were observed on both TL1C1 and TL1C2 circuit 1, so only one display is shown in Figure 45 (TL1C1).

The A phase voltage on busbar 6 collapses to zero. Voltage propagation penetrates onto busbar 23 where reactor cooling motor number 3 is connected. As discussed in chapter 2, this could result in the cooling motor being tripped by the overvoltage protection, depending on the setting. This would result in the loss of this cooling motor to the nuclear reactor [102].

The severity of both faults has caused the output power of the reactor to drop significantly and power transfer through the AC lines has been reduced due to the bottleneck representing a load rejection scenario [102]. Some power is supplied from the nuclear reactor generator to the cooling motors and to both faults due to it still being connected. When the first fault is cleared at a time of 0.44 secs, full active power recovery of the generator is not possible due to the voltage depression. Once the second fault has been cleared at a time of 0.54 secs, the voltage recovers and governor control commences. The active power output of the reactor generator (NG1) is restored to nominal within 50 ms and successful fault ride through is achieved.

From the above analysis, it is shown that the severity of voltage propagations into the NPP AC switchyard has the potential to cause the undervoltage protections on the cooling motors to trip, thus removing essential cooling supplies to the reactor [106]. The fault currents can rise exponentially and must be cleared within the maximum fault clearance times or damage could occur to plant and equipment, leading to long-term outages for repairs [120].

3.5.2.2 Three-phase fault on busbar 21

In this particular scenario, a three-phase fault has occurred on busbar 21, where reactor cooling motor number 1 (RC1) is connected. The fault was cleared by the motor protection within 200 ms. A longer fault clearance time was due to the much slower operation usually associated with motor protection relays [140]. The aim of this study is to determine the impact of a three-phase fault within the vicinity of the reactor cooling motor. The simulation results are shown in Figure 46.

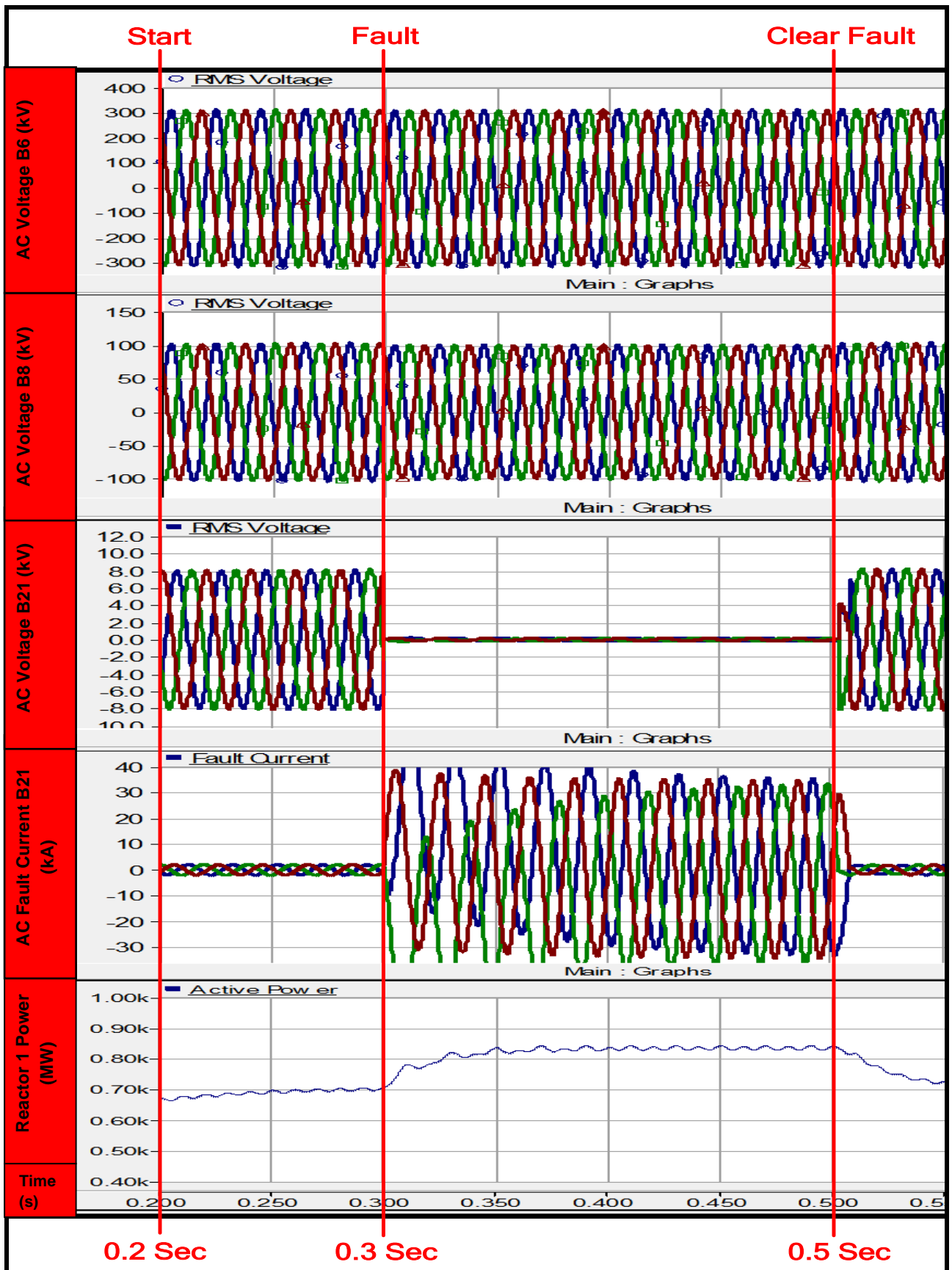


Figure 46: AC system profiles for three-phase fault on busbar 21

In Figure 46, the voltage on busbar 21 has completely collapsed due to the severity and close proximity of the three-phase fault. In reality this would cause the reactor cooling motor undervoltage protection to operate and trip off power supplies, depending on the setting applied [102]. This will result in the loss of power to the motor and consequently the loss of a source of cooling to the nuclear reactor. The voltage profiles on busbars 6 and 8 have been unaffected due to the large impedance, mainly formed of power transformers, between busbar 21 and the point of fault, which limits the voltage depression through the network [141].

The peak fault current rises to 40 kA on busbar 21 and would cause considerable damage if this was not cleared by the motor protection systems within the tolerance of the settings [135]. The output power of the reactor has increased to 850 MW and continues to feed the fault and AC system demand until successful clearance is achieved at 0.5 secs. Once the fault has been cleared, the output power of the reactor is restored to nominal by the governor control after 50 ms [139]. The recovery of the reactor here is slow due to the close proximity of the fault within the AC switchyard, which results in a much longer recovery time of 50 ms for the generator output power to return to normal.

From the above analysis, the level of voltage depression within the NPP AC switchyard will depend on the total impedance of the transformers and equipment between the nuclear reactor and point of fault [141]. Higher impedance will limit the voltage depression but the severity of the three-phase fault will be sustained until the protection system has operated and achieved successful clearance.

3.5.2.3 Three-phase fault on busbar 1

A three-phase fault occurred on busbar 1 and was cleared within 140 ms. The aim of this study was to monitor the impact of the three-phase fault on the NPP when the distance between the two is increased. In this case the fault is over 100 km away from the NPP. The 400 kV voltage profiles on busbar 5 and 132 kV on busbar 6 are monitored to see if a voltage depression occurs within the NPP.

In Figure 47, despite the distance between busbar 5 and the point of fault, the voltage has collapsed to zero. The voltage depression has propagated into the NPP AC switchyard and has reduced the voltage profile on busbar 8 by nearly 50%. In reality, depending on the settings of the motor undervoltage protections, a trip would result in a loss of power supply to the reactor cooling pumps and consequently could compromise the security of the NPP [135].

The fault current on busbar 5 has risen to 5 kA and has been limited by the large impedance of the transformers and length of distance to the point of fault [141]. The output power of the reactor has reduced significantly due the collapse in voltage on busbar 5.

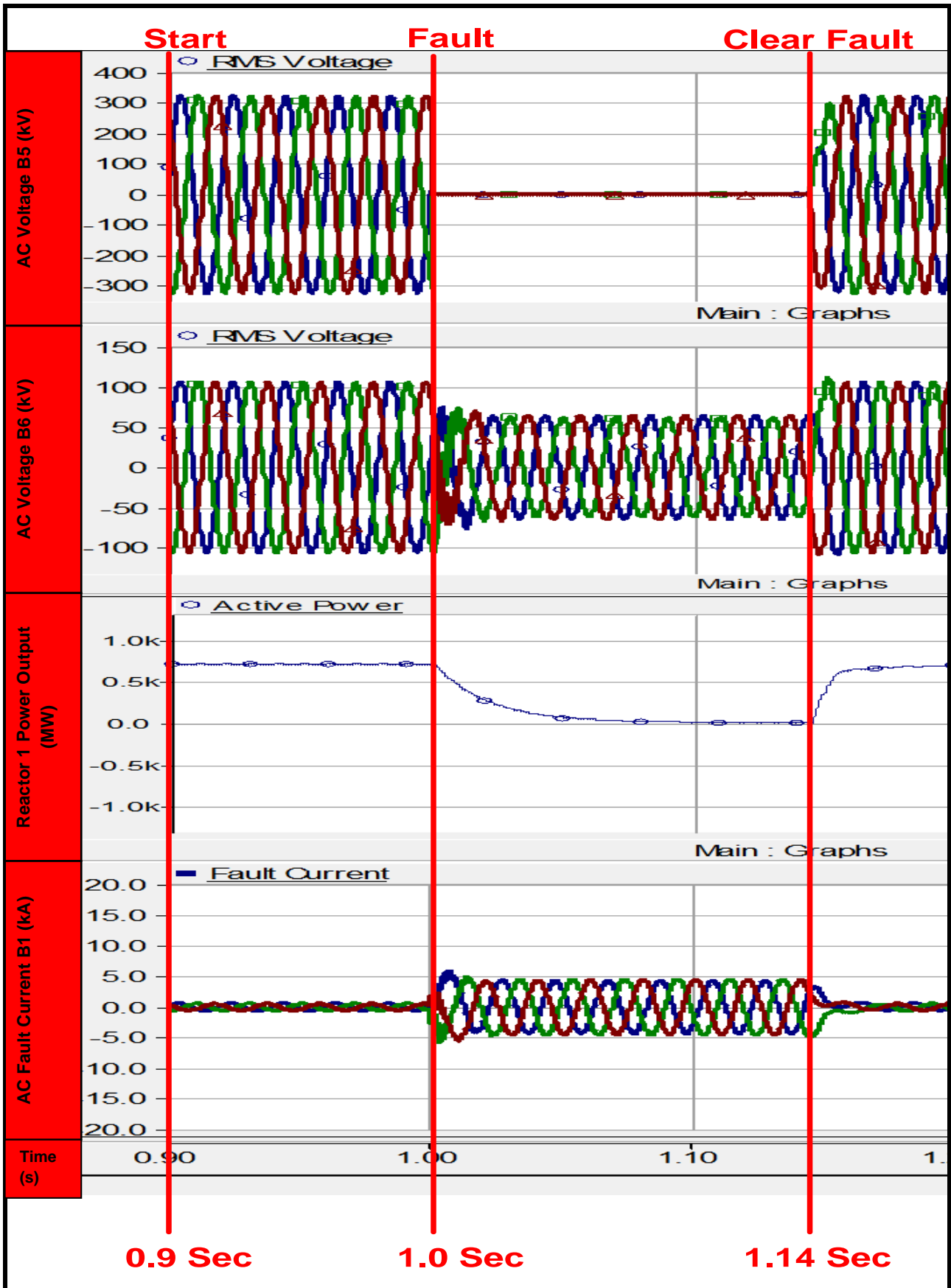


Figure 47: AC system profiles for three-phase fault applied to busbar 1

Once the fault is cleared within 140 ms the governor control restores the reactor output power back to nominal within 20 ms. The recovery of the reactor generator this time around is much quicker compared to the previous case in scenario 2. With the fault being further away from the generator the impact within the AC switchyard is less severe and system recovery is much faster [142].

The recent analysis has demonstrated the severity and impact of the three-phase fault on the NPP, even when the distance between the two is long. Voltage depressions can propagate through the AC network and affect the voltage profiles within the NPP. The fault current will be lower within the NPP compared to that encountered on the AC grid due to the distance involved and much lower impedance encountered [142]. Any voltage collapse encountered on the main 400 kV (B5) interface busbars will result in the reactor output power being significantly reduced until fault clearance has been achieved.

3.5.2.4 Three-phase fault on TL2C1 with outage of TL2C2

In this analysis TL2C2 has been taken out of service for maintenance, while a three-phase fault has occurred on TL2C1 at a time of 0.4 secs. The aim of the study was to assess the impact of the three-phase fault on reactor station 2 when only one circuit connection to the AC grid is available. The voltage profiles on busbars 18, 20 and 23 are monitored to assess any impact experienced as a consequence of the three-phase fault.

In Figure 48, the effect of the three-phase fault upon the busbar voltages has been considerable. The three-phase voltages on busbars 18, 20 and 27 have completely collapsed. The depressions have caused the voltage of the reactor cooling motors to drop and in reality this has the potential to cause tripping of the local motor protection systems, depending on the settings applied [102]. Transmission line circuit one (TL2C1) is the sole means of connecting reactor 2 generator to the AC. grid. With then other circuit (TL2C2) out for maintenance the total line impedance pre-between the point of fault and NPP is halved. Thus the voltage depression through the circuit is more severe and much faster with the fault being closer [102].

Fault current oscillations can be observed on busbar 27 where reactor cooling motor 27 is connected. The motor is over speeding and in practice over speed protection will trip the motor resulting in the loss of one cooling supply to the reactor [3].

A combination of voltage depressions and the faulty circuit has created a large bottleneck, preventing any power transfer to the AC grid. The reactor output power has dropped significantly as a direct result. When the fault is eventually cleared, governor control restores the reactor output power back to nominal within 20 ms.

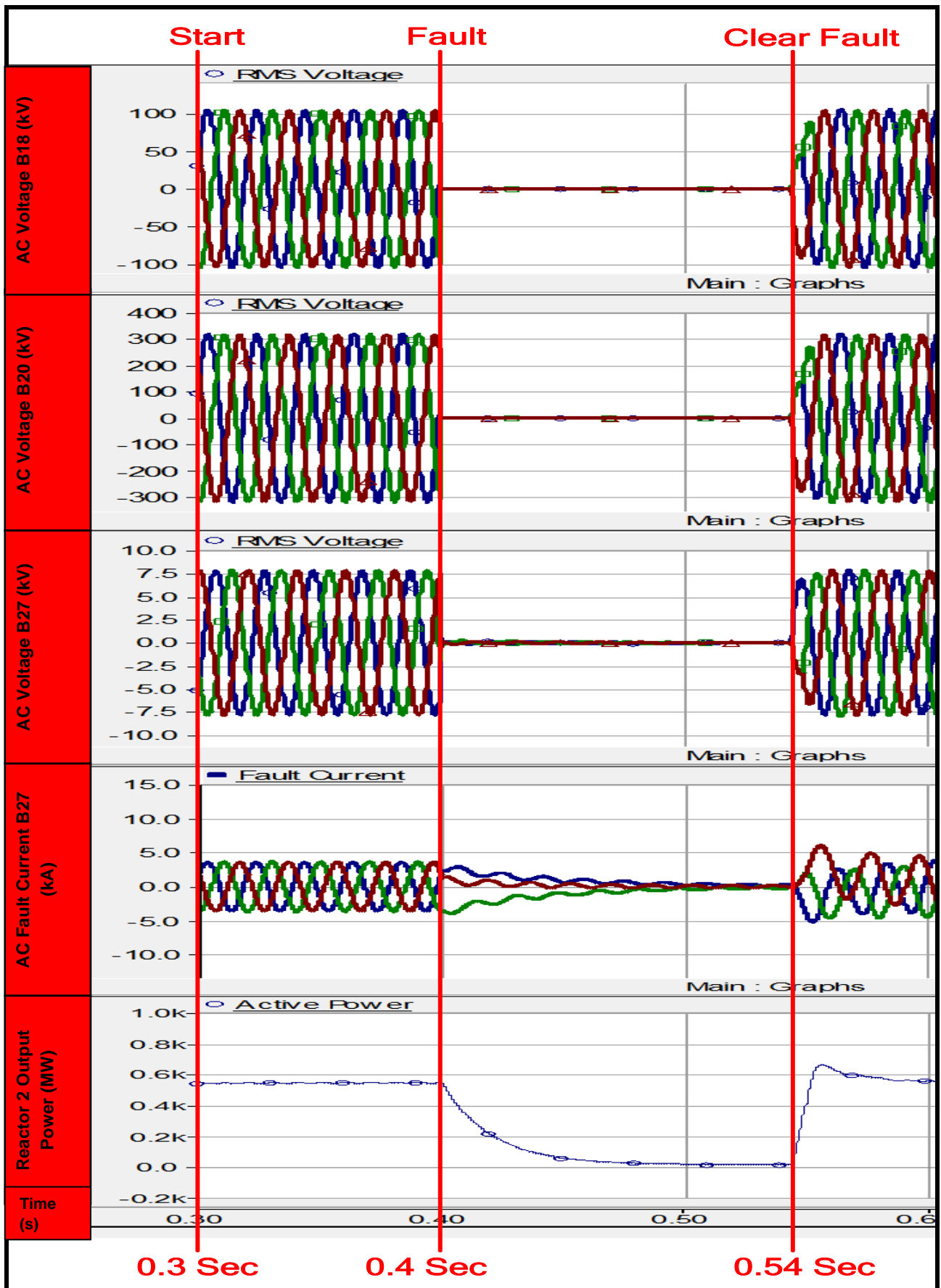


Figure 48: AC system profiles for three-phase fault on TL1C1

The recent analysis has shown the vulnerability of the NPP when only one connection to the AC grid is provided. With one of the AC circuits is out for maintenance, the impedance between the NPP and AC grid is increased through the healthy circuit being in service [142]. Following the occurrence of a three-phase fault on the remaining healthy circuit, voltage collapse occurs and propagates further into the NPP. In reality the voltage depression could be so severe that over speeding of the reactor cooling motors is experienced and this results in the operation of protection systems [100].

A bottleneck in active power is encountered and the NPP will be temporarily islanded from the AC grid until the fault is cleared. Reactor recovery will depend on the severity of the fault and voltage depressions encountered [100].

3.5.2.5 Three-phase fault applied on busbar 2

In this study a three-phase fault has occurred on busbar 2. The aim of the study was to analyse the impact on nuclear reactor station 1 for a distant three-phase fault within the AC grid on busbar 2. The distance of the three-phase fault on busbar 2 from reactor station 1 is over 200 km away. Hence the voltage profiles of busbar 5 (400 kV) and busbar 8 (132 kV) is monitored to assess the impact of the fault.

In Figure 49, despite the distance of the fault from reactor station 1, voltage depressions are encountered on busbar 5 and busbar 8. The voltage depressions are not as severe as in previous simulations, where the fault was much closer. In reality, the voltage depressions are still low enough to cause protection systems within the nuclear reactor station to operate, dependent upon the settings employed [102]. This will result in the disconnection of essential cooling supplies to the nuclear reactor.

With the reduction in voltage, the reactor output power has dropped below 500 MW but recovers once the fault has been cleared. This represents a stable situation for the NPP, (except for the voltage depressions), and despite this reduction, the majority of the power is still being supplied to the AC grid during the fault.

The fault current measured at busbar 5 reaches 5.0 kA and is limited due to the distance and impedance between the point of fault and the nuclear reactor station [142]. Despite this, the fault must be cleared within the required clearing times to prevent potential damage to equipment and plant within the NPP [120].

The analysis carried out has demonstrated the effect of a three-phase fault when this is located further away from the NPP within the AC network and has shown that voltage depressions may be encountered within the NPP, but at a much reduced level.

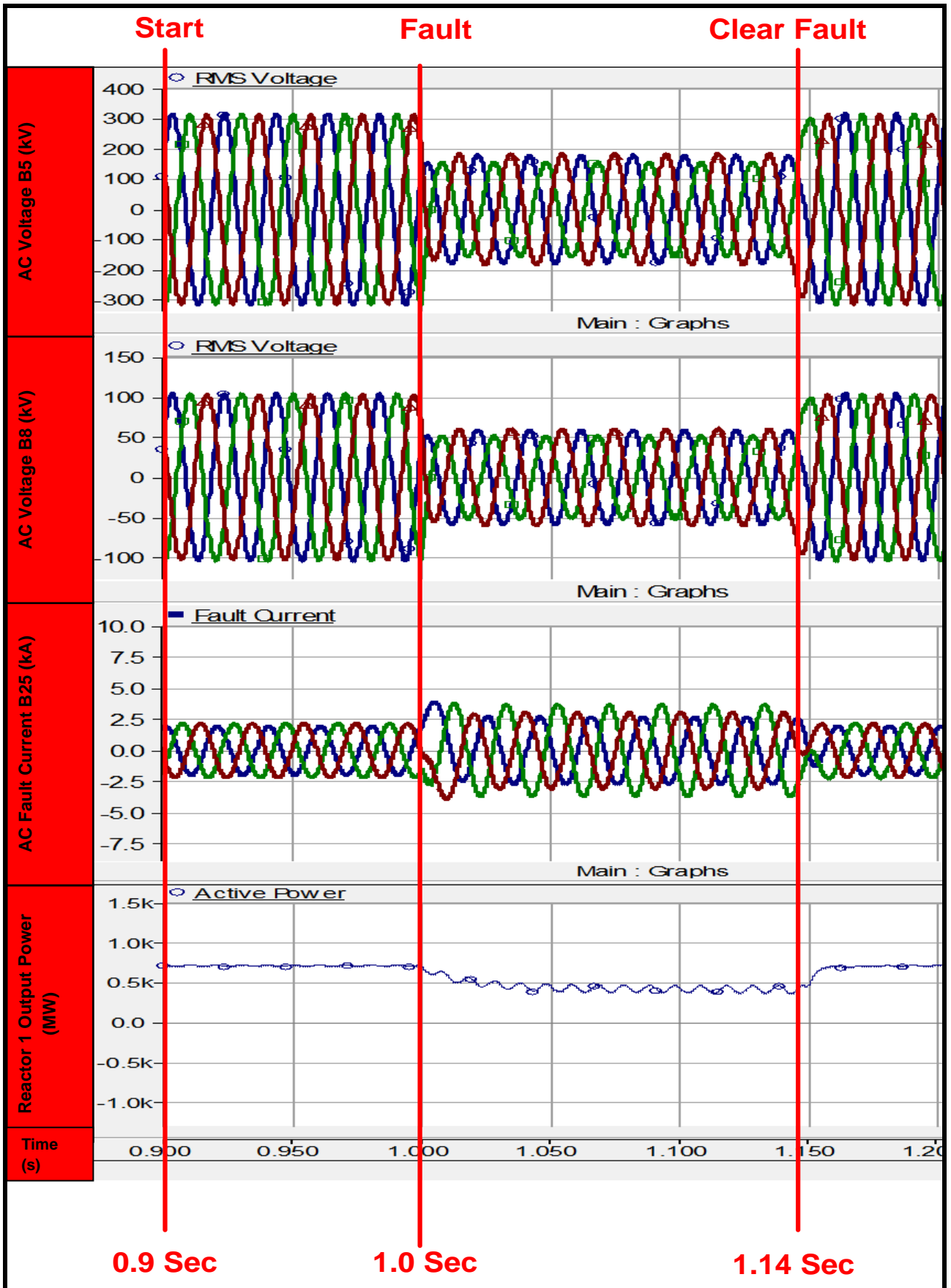


Figure 49: AC system profiles for three-phase fault on busbar 2

The depression may still be low enough to cause the operation of protection relays, depending on the settings applied. The fault current within the NPP will be lower due to the much higher impedance as a function of the greater distance encountered. The output power of the reactor generator may drop, but the NPP is still able to ride through the fault, as long as the voltage recovers on all affected busbars. If the voltage does not recover, this can impact the stability and security of supply to both the NPP and AC grid.

3.6 Chapter 3 summary

The common and proven method of connecting a modern NPP to the NETS via 400 kV AC overhead line technology has been presented.

From the analysis carried out, the following technical issues have been found:

- *Three-phase faults can cause voltage depressions within the NPP. The intensity and penetration is dependent upon the amount of impedance between the fault location and the NPP as well as the configuration of the power system.*
- *The vulnerability of the NPP when connected by a single AC circuit is an important consideration; in such a case, the impedance between the NPP and AC grid is increased and the voltage propagation can be faster and more prominent.*
- *For the above conditions, in practice, the protection systems of the reactor cooling motors will operate and remove the essential cooling supplies to the NPP. A switch over to alternate power supplies such as Diesel Generators will be initiated.*
- *When voltage dips are present AC motors may overspeed, resulting in protection operation and loss of cooling to the nuclear reactor.*
- *The reactor and generator must be able to survive load rejection by appropriate control actions until the fault has been cleared and power transfer has recommenced.*

Based upon the above, the following recommendations are made:

- *For secure and stable NPP operation, sufficient redundancy in connections to the AC grid is needed.*
- *The settings of protection systems need to be considered to ensure faults are successfully cleared within the critical times needed for stability, while ensuring the NPP achieves fault ride-through capability.*

The next chapter provides analysis of the new application of connecting of an NPP to an AC grid by CSC-HVDC technology.

Chapter 4: Connecting NPPs by CSC-HVDC Technology

In this chapter a technical assessment of connecting an NPP to a power system by Current Source Converter (CSC) HVDC technology is performed. Detailed descriptions of the CSC-HVDC model and individual components used in PSCAD are provided. The impact of changing the Effective Short Circuit Ratio (ESCR) at the Point of Common Coupling (PCC) on the operation of the HVDC link during steady-state conditions is investigated through simulation. The impact of both AC and DC system faults on the NPP and CSC-HVDC link are analysed using PSCAD simulation. Contingency analysis is performed to study the impact of the high-level HVDC controls on frequency control and active power modulation.

4.1 Introduction

As described previously in chapters 2 and 3, modern NPPs are connected to the power system by AC technology. This could be in the form of AC overhead lines, cables or a combination of both. In some situations, the distance of connection from the NPP to the AC grid could be 70 km or more [1]. If the circuit routes involve crossing environmentally sensitive areas – where overhead lines are not welcomed – then other technologies may have to be considered. Such technologies could be in the form of underground or subsea cables. However, up to certain distances (60 km or more), the capacitive current limitations of AC cables may prove to be an obstacle [1]. For such a situation, HVDC technology may provide an alternate solution.

HVDC technology has never been used to connect an NPP to the AC grid before. This represents an unproven and high technological risk for an NPP connection [2]. Any Transmission System Operator (TSO) considering HVDC technology for such an application needs to fully understand both the technical challenges and the risks involved. The high-level controls of CSC-HVDC technology and their impact on NPP operation and security need to be understood [2]. The response of the HVDC controls during both AC and DC system faults during transient conditions needs to be ascertained [2]. Equally important is the strength or ESCR of the AC system and NPP connection and their effect on the operation of CSC-HVDC technology during steady-state conditions. These areas will be investigated through means of power system simulation in PSCAD and are covered in the following sections of this chapter.

4.2 Modelling of an NPP connected by CSC-HVDC technology

In the following section each of the individual components which make up the CSC-HVDC model in PSCAD is described.

4.2.1 Six-pulse bridge

This component is a compressed representation of a DC converter, which includes a built-in six-pulse Graetz bridge (can be inverter or rectifier), an internal Phase Locked Oscillator (PLO), firing and valve blocking controls, and firing angle (α) and extinction angle (γ) measurements [130]. Snubber circuits are also incorporated into each thyristor [130]. Representation of the model in PSCAD is shown in Figure 50.

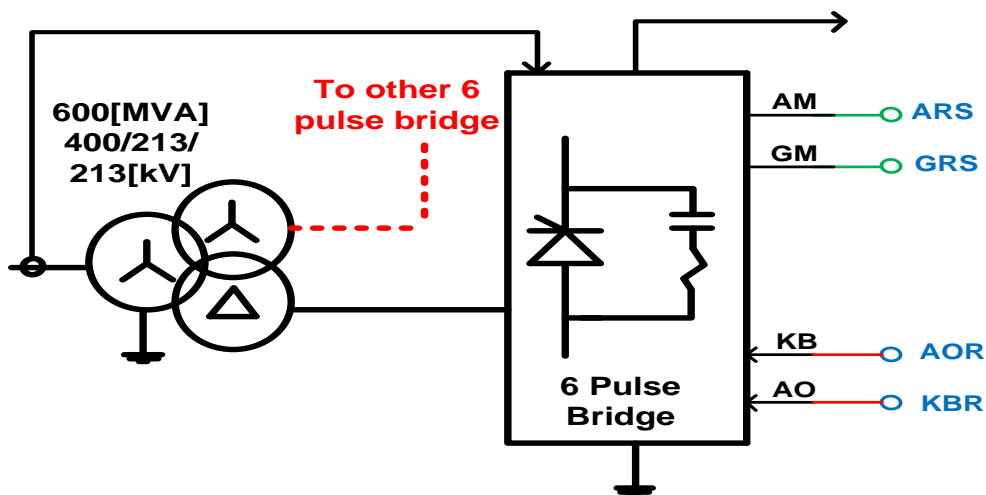


Figure 50: Six-pulse bridge model used in PSCAD

The general idea is to eliminate the complex and tedious process of building a thyristor bridge, putting together controls, and coordinating the valve firing pulses involved in modelling an HVDC converter [130].

The six-pulse bridge model possesses the following external inputs and outputs [127]:

- Combus: input signal to the internal PLO.
- AO: input alpha order (firing angle) for the converter.
- KB: input block/deblock control signal.
- AM: measured alpha (firing angle) output (in rads).
- GM: measured gamma (extinction angle) output (in rads).

4.2.2 Firing and blocking control

The actual firing is accomplished for each valve by comparing the alpha order input (AO) to the value of the ramp. The interpolated firing time is calculated and passed to the thyristor component routine so that the system may be interpolated to this point [127].

The firing is delayed until the voltage is exactly equal to the forward voltage drop across the thyristor. The firing pulse is maintained across each valve for 120° [127].

When the default internal firing controls are used, the user supplies the AO for firing. The Externally generated firing pulses can be inputted directly to each of the thyristors [127]. The measured firing angle output (AM) and the measured extinction angle (GM), are calculated for both modes (inverter/rectifier) of operation. The firing angles of the converter relate to the following steady-state converter equations [127]:

$$\beta = 180.0 - \alpha \quad (4.1)$$

$$\gamma = \beta - \mu \quad (4.2)$$

The advance angle β is then time-expressed in electrical angular degrees measured from the starting point of the forward current conduction to the next zero crossing of the idealised sinusoidal commutating voltage. The angle of advance β is related in degrees to the angle of delay α [127].

The overlap angle μ is the duration of commutation between two converter arms, and is expressed in electrical angular degrees.

The extinction angle γ is the time, expressed in electrical angular degrees, measured from the end of the conduction to the next zero crossing of the idealised sinusoidal commutating voltage. The extinction angle depends on the angle of advance β and the overlap angle μ [41].

It is useful to express the commutating reactance of a six-pulse converter bridge in per unit of the converter transformer rating SN where [127]:

$$SN = \sqrt{2} U_{vn} \cdot I_{dn} \quad (4.3)$$

Where:

- I_{dn} : is the rated direct current.
- U_{vn} : is the rated phase-to-phase voltage on the valve or secondary side of the converter transformer.

The blocking logic is controlled by the KB external in/out signal, and is effective regardless of whether the user has supplied the pulse or if internal firing controls are used. In this model, no blocking is used as the protective functions are carried out within the control logic [127].

4.2.3 Converter transformer tap changer

The tap changer has already been covered in chapter 2; however, there are some subtle differences for the type used on the CSC-HVDC model. The model of the converter transformer has been shown previously in Figure 50. AC circuit breakers are connected to the converter transformer for fault current interrupting purposes.

The converter transformer online tap changer will adjust the delay angle α at the rectifier to its desired normal operating range [127]. At the inverter, the online tap changer will adjust to maintain the inverter operation at its desired level of DC voltage U_d or extinction angle γ [127]. Knowing the desired levels of DC voltage (U_d), DC current (I_d), the nominal turns ratio TR_n of the converter transformer, the operating level of the primary side AC voltage (U_L), and the extinction angle γ (if an inverter) or delay angle α (if a rectifier), the per unit turns ratio TR of the converter transformer can be determined [127]:

At a rectifier [127]:

$$\cos(\alpha + \mu) = \cos(\alpha) - X_c \cdot I_d / I_{dn} \quad (4.4)$$

At the inverter [127]:

$$\cos(\gamma + \mu) = \cos(\gamma) - X_c \cdot I_d / I_{dn} \quad (4.5)$$

And [127]:

$$\alpha = 180^\circ - (\gamma + \mu) \quad (4.6)$$

It may also be necessary to determine the overlap angle μ . At the rectifier, an approximate expression can be applied when the delay angle α , per unit commutating reactance X_c and DC load current I_d are known [127].

Similarly, at the inverter, the extinction angle γ is usually known for steady-state operation and a similar expression involving μ can be determined [127].

It is also possible to determine the nominal turns ratio of the converter transformer, once the rated secondary (DC valve side) voltage U_{VN} is known, if the primary side rated phase-to-phase AC bus voltage U_{LN} is also known [127].

Based on the phase-to-phase voltages, the nominal turns ratio of the converter transformer TR_n is determined [127]:

$$TRN = \frac{UVN}{ULN} \quad (4.7)$$

And [127]:

$$TR = \frac{UD + UDN \frac{Id}{Idn} \cdot \frac{Xc}{(2Cos(\varphi) - Xc)}}{1.35 \cdot TRN \cdot UL \cdot Cos(\varphi)} \quad (4.8)$$

Where [127]:

- Xc: is the commutating reactance of the converter bridge in per unit.
- Φ : represents α for a rectifier and γ if an inverter.
- Idn: is the rated DC current for the converter bridge.
- UDN: is the rated DC voltage for the converter bridge.

4.2.4 AC filters

For CSC-HVDC links, AC filters are one of the most important components for successful operation of the converter [41]. Their main purpose is to dampen out current and voltage harmonics produced by the HVDC converter during the conversion process. Their other purpose is to supply the reactive power demand of the HVDC converter during operation. Two types of filters are used in the CSC-HVDC PSCAD model. They are the C-type filter and a high-pass RLC type. Both filter models used in PSCAD are described in the following sections.

4.2.4.1 C-type AC filter

The significance of this filter is that its elements are purely capacitive at fundamental frequency and the power loss is reduced to a minimum. Within PSCAD, this component can be used in single-phase or three-phase single-line circuits. Each of the various components relate to the following equations [143]:

$$C1 = \frac{Q}{2 \cdot \Pi \cdot f1 \cdot U^2} \cdot \frac{(1 - \frac{1}{n^2})}{(1 - \frac{1}{na^2} - \frac{1}{nb^2})} \quad (4.9)$$

$$L = \frac{1}{(2 \cdot \Pi \cdot f1 \cdot na)^2 \cdot C1} \quad (4.10)$$

$$C2 = \frac{1}{(2 \cdot \Pi \cdot f1 \cdot nb)^2 \cdot L} \quad (4.11)$$

$$R = \sqrt{\frac{L}{C1}} \cdot q \quad (4.12)$$

Where:

- n is the number of the associated harmonic (1,2,3,4..)
- n_a and n_b are orders of filter tuning harmonics.
- f_1 is the fundamental frequency value.
- L is the filter inductance.
- R is the filter resistance.
- C is the filter capacitance.
- Π is the tuned angular frequency.

The C-type AC filter models used in PSCAD for both the rectifier and inverter are shown in Figures 51 and 52 below:

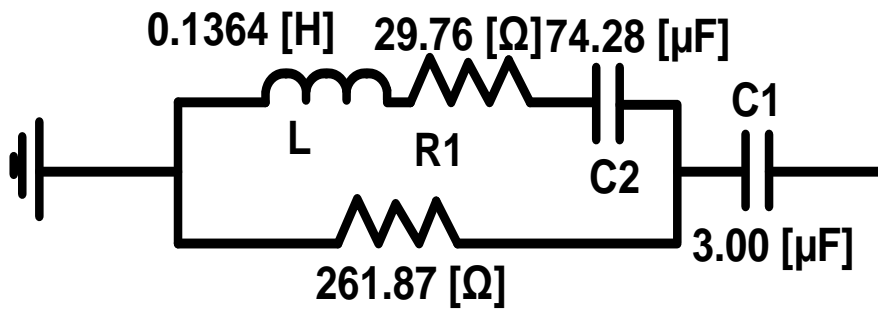


Figure 51: Rectifier 150 Mvar C-type filter

The lower L-C is series-resonant at the fundamental frequency and so is bypassed by the resistor to greatly reduce filter losses.

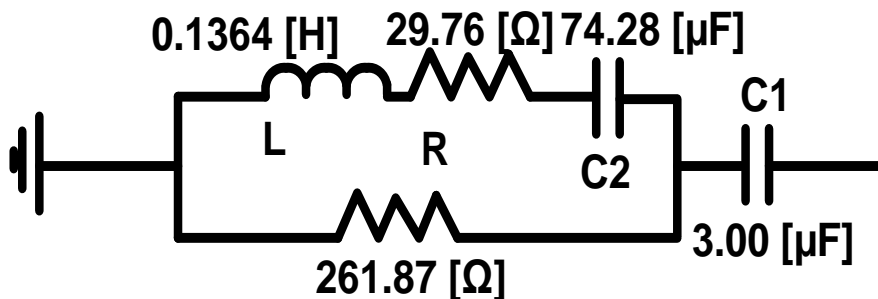


Figure 52: Inverter 150 Mvar C-type filter

This low-order high-pass filter is primarily for 3rd, 5th and 7th harmonic filtering purposes. Each AC filter supplies 150 MVAR of the reactive power demand of the HVDC converters and is given by [143]:

$$Q_c = \frac{400 \text{ kV}^2}{\frac{1}{\frac{2 \cdot \pi \cdot 50 \cdot 3.0 \mu\text{F}}{1}}} = 150 \text{ Mvars} \quad (4.13)$$

4.2.4.2 High-pass AC filter

The branch impedance of this filter decreases with increasing frequency.

Placing the branch between line and ground will absorb frequencies above the “cut-off” frequency. This type of filter can be designed with high Q-values for 11th and 13th harmonics with lower fundamental losses. The parallel resistor can be expensive [144]. The high-pass AC filter models used in PSCAD for the rectifier and inverter are shown in Figures 53 and 54.

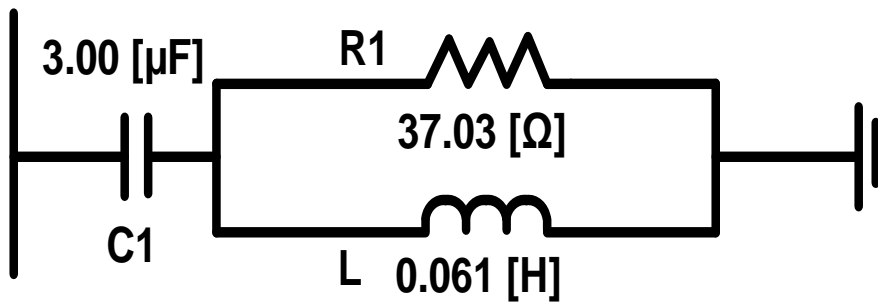


Figure 53: Rectifier 150 Mvar high-pass RLC filter

Each filter provides 150 Mvar of reactive power demand to the HVDC converters and is given by [143]:

$$Q_c = \frac{400 \text{ kV}^2}{\frac{1}{\frac{2 \cdot \pi \cdot 50 \cdot 3.0 \mu\text{F}}{1}}} = 150 \text{ Mvars} \quad (4.14)$$

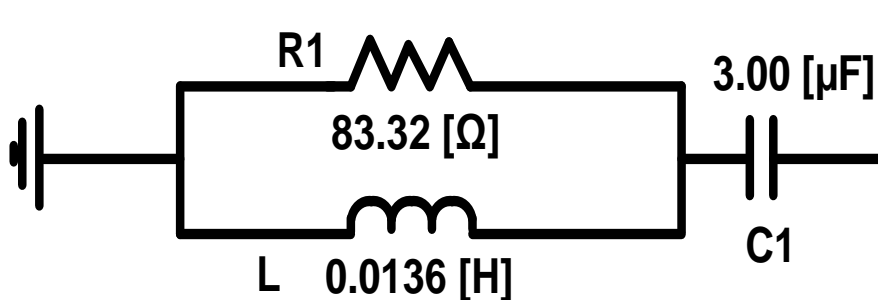


Figure 54: Inverter 150 Mvar high-pass RLC filter

The level of tuning is given by the following equations [143]:

$$C1 = \frac{Q}{2 \cdot \Pi \cdot f1 \cdot U^2} \cdot \left(1 - \frac{1}{n^2}\right) \quad (4.15)$$

$$L1 = \frac{1}{(2 \cdot \Pi \cdot f1 \cdot n)^2 \cdot C1} \quad (4.16)$$

$$R1 = 2 \cdot \Pi \cdot f1 \cdot n \cdot L1 \quad (4.17)$$

The broadband filter can take care of all harmonics from the 23rd and upwards, tuned to near the 24th harmonic.

4.2.5 Shunt capacitor

The shunt capacitor's main function is to provide the reactive power demand (301 Mvar) of the HVDC converter station. The shunt capacitor models used in PSCAD are shown in Figures 55 and 56.

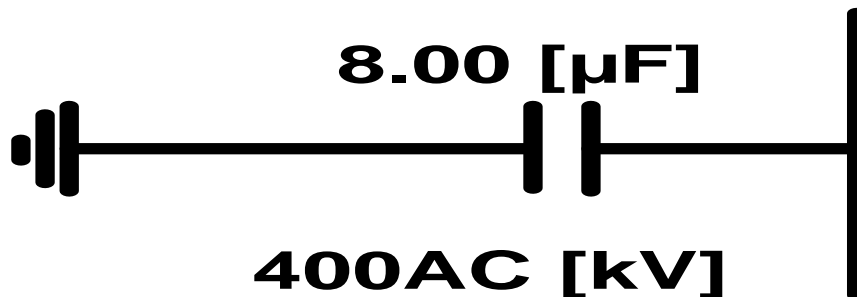


Figure 55: Rectifier 301 Mvar shunt capacitor

The formula to take into account the contribution of reactive power demand of both the rectifier and inverter is given by [143]:

$$Qc = \frac{Vs^2}{\frac{1}{2\Pi fc}} \quad (4.18)$$

Where:

$$Qc = \frac{400 \text{ kV}^2}{\frac{1}{2 \cdot \Pi \cdot 50 \cdot 6.0 \mu F}} = 301 \text{ Mvars} \quad (4.19)$$

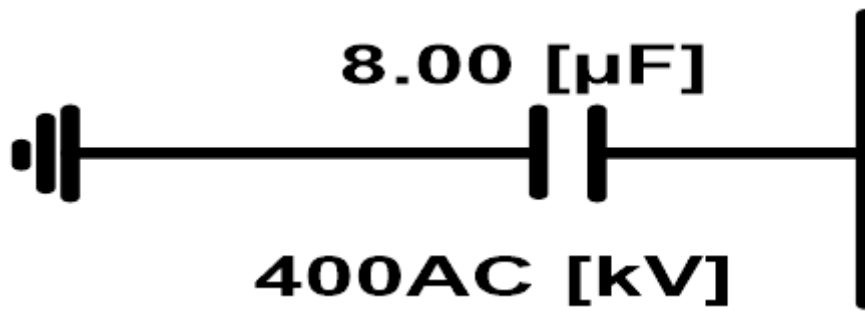


Figure 56: Inverter 301 Mvar shunt capacitor

Hence each shunt capacitor contributes 50% of the total reactive power supplied to the HVDC converters.

With the contribution of both the C-type and high-pass RLC filters, the total reactive power supplied to each end of the HVDC link is $(301+150+150) = 601$ Mvar. This is the maximum 60% reactive power demand required for successful converter operation as mentioned previously in chapter 2. The filters supply the required reactive power independent of the AC system, which prevents the absorption of reactive power from the AC network and the possibility of draining the AC system's reactive reserves.

4.2.6 DC cable

The frequency-dependent (phase) model has been selected in PSCAD due to the reasons mentioned previously in section 3.2.5. The frequency-dependent (phase) model is numerically robust and more accurate than any commercially available line/cable model, and thus, is the preferred model to use [143]. The model is shown in Figure 57.

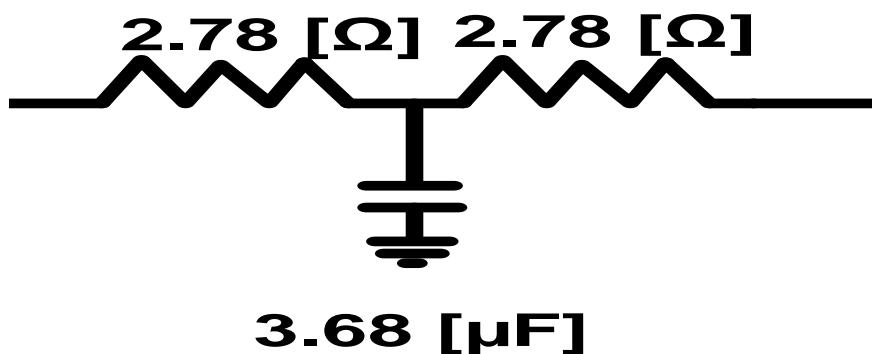


Figure 57: DC cable model used in PSCAD

DC cables are predominantly resistive [145] and this has been replicated in the model. Shunt capacitance has also been included.

The power rating of each cable is 600 MW. These parameters have been supplied by National Grid Electricity Transmission (NGET) and are based upon a 100 km Mass Impregnated (MI) submarine cable with a nominal DC voltage of 500 kV.

4.2.7 Short circuit ratio

As discussed previously in chapter 3, the component values of the R–R/L circuit for both the rectifier and inverter point of connection can be calculated using the Short Circuit Ratio (SCR) of the system. A strong AC system is defined to have an SCR of 2 or greater, while a weak AC system is defined to have an SCR of between 1 and 2 [41]. The impedance of the AC system can be solved using Equations 4.20 and 4.21 [41]:

$$Z_{ac} = \frac{E^2_{ac}}{SCR \cdot Pd} \quad (4.20)$$

$$Z_{ac} \angle \theta = Z_{ac} \left[\tan^{-1} \frac{X}{R} \right] = a + jb \quad (4.21)$$

In order to calculate the component values, the R–R/L circuit can be expressed in Equation 4.22 [41]:

$$\begin{aligned} Z_{ac} \angle \theta &= R1 + R2 \parallel jXL = R1 + \frac{R2 \cdot jXL}{R2 + jXL} \\ &= R1 + \frac{XL^2 \cdot R2 + jXL \cdot R2^2}{R2^2 + XL^2} \\ &= R1 + \frac{XL^2 \cdot R2}{R2^2 + XL^2} + j \frac{XL \cdot R2^2}{R2^2 + XL^2} \end{aligned} \quad (4.22)$$

The HVDC power rating = 1200 MW.

Hence the following SCRs are calculated for the rectifier (Equation 4.23) and inverter (Equation 4.24) as follows [41]:

$$SCR (Rectifier) = \frac{3000MVA}{1200MW} = 2.5 \quad (4.23)$$

$$SCR (Inverter) = \frac{5000MVA}{1200MW} = 4.1 \quad (4.24)$$

The AC impedance can then be calculated at each end of the HVDC link for the rectifier end (Equation 4.25) and inverter (Equation 4.26):

$$Z_{ac} (Rectifier) = \frac{400kV^2}{2.5 \cdot 1200 MW} = 53.33\Omega \quad (4.25)$$

$$Z_{ac} (Inverter) = \frac{400kV^2}{4.1 \cdot 1200MW} = 32.52\Omega \quad (4.26)$$

The moderational X/R ratio for both the NPP and AC system is 14, which is a typical value for a semi-weak system [41], and has been provided by National Grid. By using Equation 4.22 and the figures calculated previously the following values are obtained:

$$Rectifier = 53.33[\tan^{-1}(14)] = 53.33[85.91^\circ] \quad (4.27)$$

$$Inverter = 32.52[\tan^{-1}(14)] = 32.52[85.91^\circ] \quad (4.28)$$

Converting to Cartesian form yields:

$$Rectifier = 3.80+j53.19$$

$$Inverter = 2.31+j32.43$$

From Equation 4.22 the values of R1 and L1 can be found, where the value R2 is the constant value of 2160 Ω .

$$Rectifier (3.80) = R1 + \frac{XL^2 \cdot R2}{R2^2 + XL^2} \quad (4.29)$$

And:

$$Rectifier (j53.19) = j \frac{XL \cdot R2^2}{R2^2 + XL^2} \quad (4.30)$$

Likewise, for the inverter:

$$Inverter (2.31) = R1 + \frac{XL^2 \cdot R2}{R2^2 + XL^2} \quad (4.31)$$

And:

$$Inverter (j32.43) = j \frac{XL \cdot R2^2}{R2^2 + XL^2} \quad (4.32)$$

The following values are calculated for both the rectifier and inverter connections, as shown in Table 11:

Table 11: Parameters for CSC-HVDC link model used in PSCAD

Location	SCL [MVA]	SCR	L1 [H]	R1 [Ω]	R2 [Ω]
NPP (rectifier)	3000	2.5	0.151	1.59	2160
AC grid (inverter)	5000	4.1	0.151	3.25	2160

The R–R/L arrangements for both the rectifier and inverter AC sources are shown in Figures 58 and 59: The SCR at the rectifier is lower than at the inverter because the only voltage source available is a single NPP generator. The higher SCR can be explained by the inverter being connected to the main AC grid, with several other sources of circuit infeed available [41].

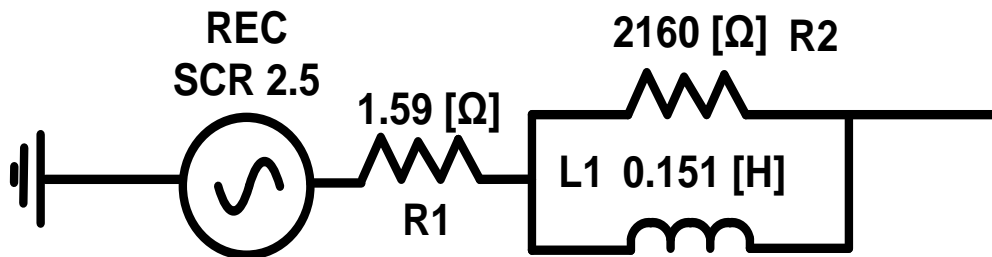


Figure 58: Parameters for rectifier AC connection

The series resistance R1 of each model can be changed to alter the SCR value at the PCC.

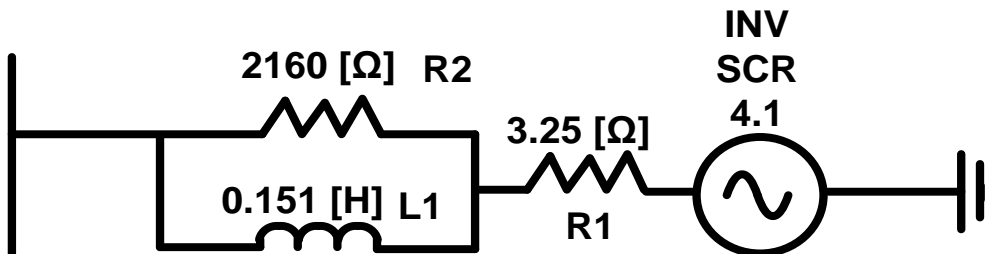


Figure 59: Parameters for inverter AC connection

Alternately, at the inverter, switching out of AC circuits can also be used to change the SCR value [41].

4.2.8 CSC-HVDC bipole model in PSCAD

All of the components described in this chapter have been combined to form the CSC-HVDC CIGRE benchmark bipole model shown in Figure 60. The design is based upon the CIGRE benchmark system which has been validated by CIGRE as a suitable model for carrying out HVDC studies for educational, research and consultancy purposes [146], [147].

A monopole HVDC link has been modified to represent a bipole model by adding an extra six-pulse bridge in series with the existing one.

The bipole option has been developed in PSCAD to represent the best practical option if this was used for real industry application [60] and in particular an NPP connection. The advantage of a bipole construction is that 50% active power transfer is available when one pole is out of service due to fault or maintenance purposes. For an NPP connection in industry, this would increase the security of supply and provide redundancy for power transmission to the AC grid [17].

The combined power rating of the link is 1200 MW (600 MW per pole) and matches the rating of the NPP in reactor station 2. The equivalent full bipole DC current is 1200 A at a voltage level of ± 500 kV. An earth is provided at the rectifier end to provide the reference for power flow from the rectifier to the inverter.

The two Mi cables include the resistance and shunt capacitance values shown previously in section 4.2.5. The DC smoothing reactors have an inductance of 0.5 H and are connected in series with the DC cables.

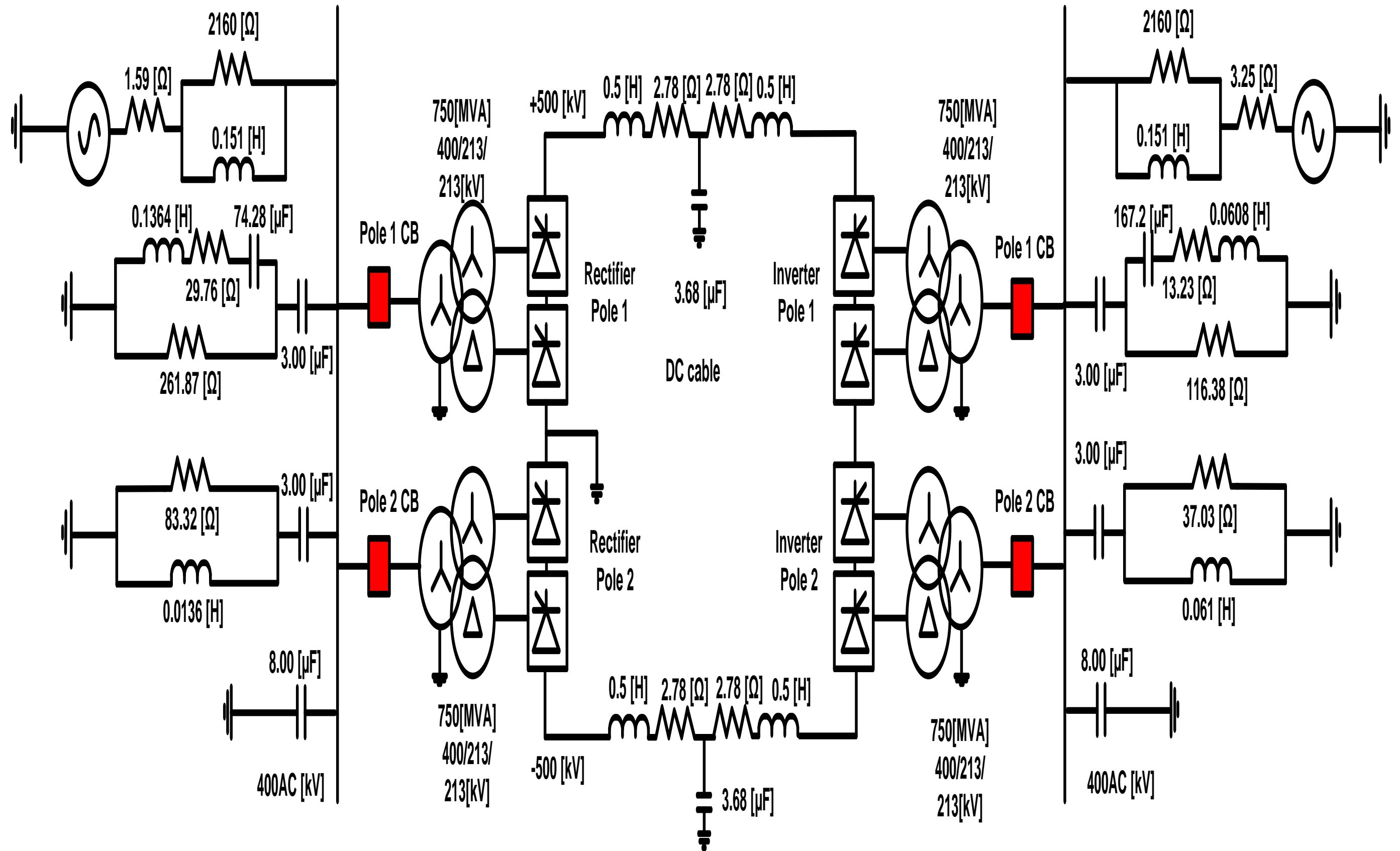


Figure 60: CSC-HVDC bipole model used in PSCAD

4.2.9 CSC-HVDC controls

In the following section the controls employed in the PSCAD CSC-HVDC model are presented. The rectifier firing controls are described first and gamma and current control are defined for the inverter.

4.2.9.1 Rectifier controls

In Figure 61 the control circuitry for the rectifier is presented.

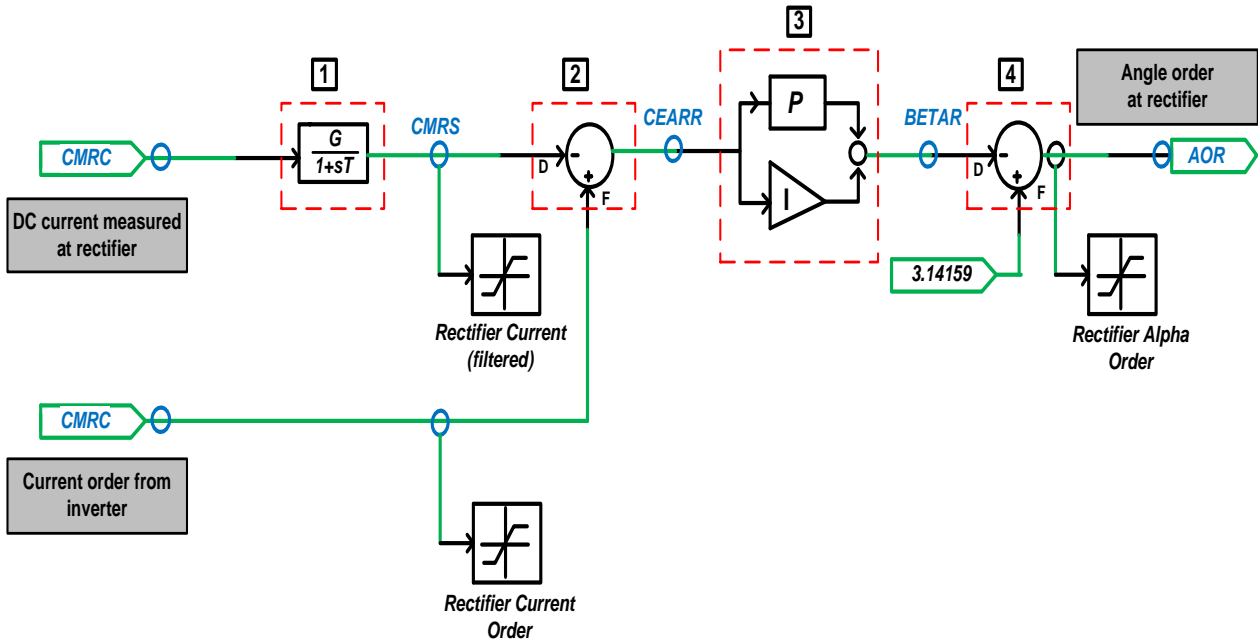


Figure 61: Rectifier controls used in the PSCAD CSC-HVDC model

In stage 1 the DC current measured at the rectifier is fed in to a transfer function block. This function simulates a lag or “real pole” function, where the output can be reset to the user-specified value at any instant. The input signal is scaled by the gain factor $G(t)$ before it is processed. In this case the transfer function block sets the DC current level via the function $(1/0.83) = 1200$ A. The current is filtered (CMRS) and can be used to produce a graph to visually display the output.

The measured current is then fed into a summing block at stage 2. Here it is subtracted from the inverter current order to produce a current order error (CERRR). This error is then fed into a PI controller at stage 3. This function performs a PI action (i.e. the output is the sum of proportional and integral gains of the input signal).

Either trapezoidal or rectangular integration may be used for the time-domain computation of the integral function. An adjusted output error (BETAR) is fed into a final summator at stage 4. Component F represents a real constant value which can be assigned to a data signal wire, or a component input. In this case the value $\text{PI} = 3.141592653589793$ provides the reference angle from which the adjusted value (BETAR) is subtracted to generate the final angle order for the rectifier.

4.2.9.2 Inverter controls

In Figure 62 the inverter gamma control circuitry for the inverter end of the CSC-HVDC link is shown.

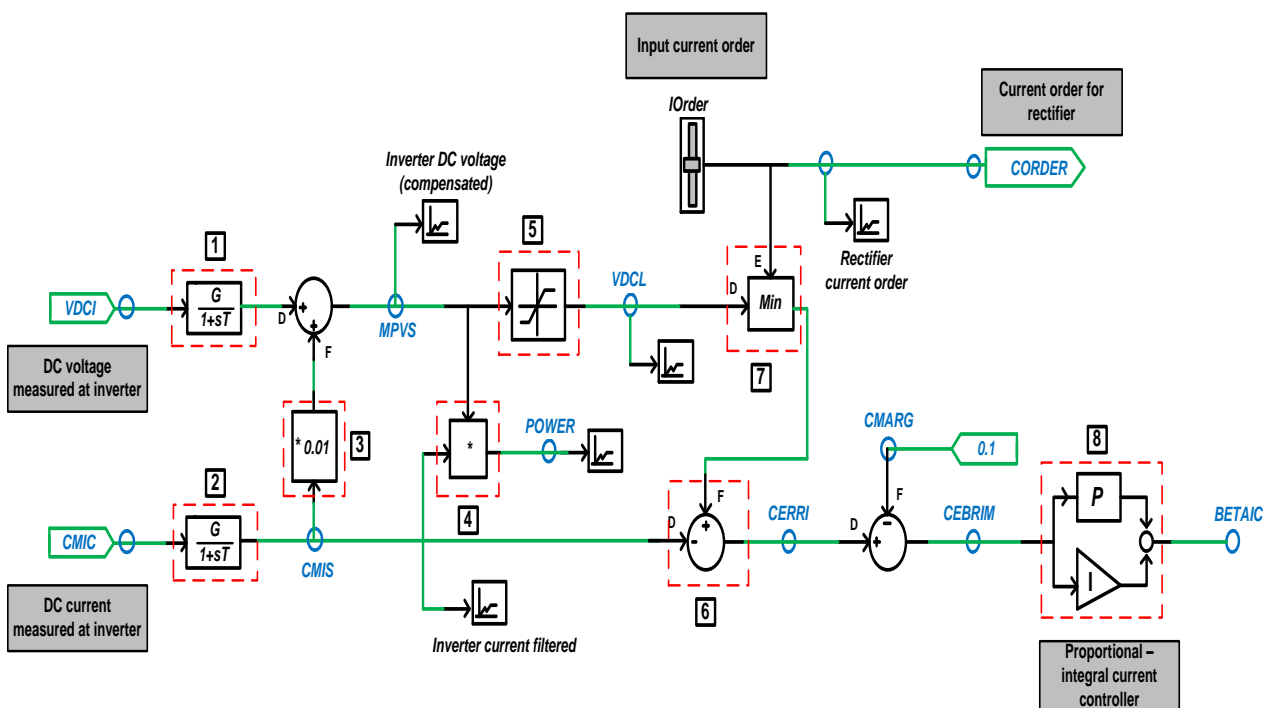


Figure 62: Inverter gamma control

The process starts with the DC voltage measured at the inverter in stage 1. Here it is fed into a transfer function block to give the voltage level via the calculation $(1/0.002) = 500 \text{ kV DC}$. The DC current measured at the inverter at stage 2 is fed through a transfer function block $(1/0.83 = 1200 \text{ A})$ and multiplied by the resistance value of the DC cable/line at stage 3 to give the total voltage drop between the rectifier and inverter. This is fed into a summing junction where the voltage drop is subtracted from the measured inverter DC voltage and compounded (back calculated) to give the DC voltage at the rectifier. The calculated rectifier DC voltage is then fed into the voltage dependent current limiter transfer function at stage 5. This DC voltage is then combined with the required input current order at stage 7 to give the minimum current order for the rectifier.

At stage 7 the current value can be changed from per unit to kA if required.

At stage 4 the DC current measured at the inverter is multiplied by the calculated rectifier DC voltage from stage 5 to give the user a power output display if needed. In stage 6 the measured current at the inverter is subtracted from the minimum rectifier current order to produce a current error (CERRI).

At stage 8 the current error is multiplied by the set current margin to give an error (CERRM). A PI controller is then used in an attempt to reduce this error to zero.

In Figure 63 the inverter current control for the CSC-HVDC model is shown:

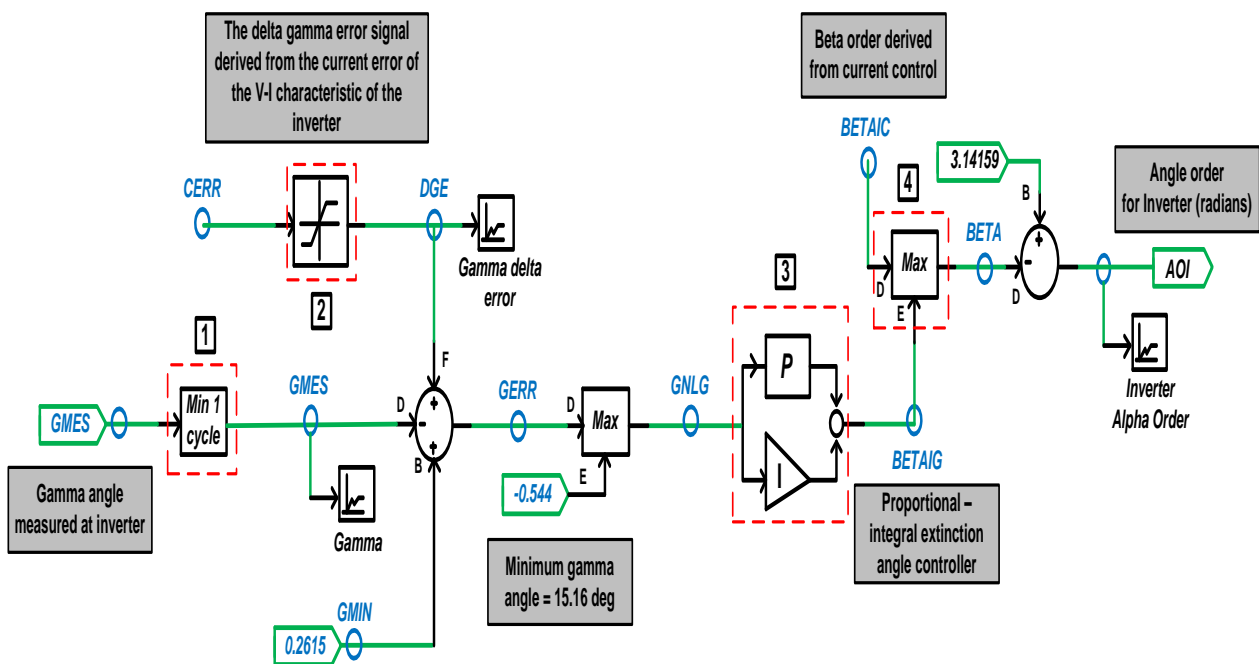


Figure 63: Inverter current control

During stage 1 the gamma angle measured at the inverter is fed into a summator. At stage 2 the current error (CERRI) is fed through an up ramp transfer function. The output of this component will ramp from 0 to a specified output level as the input value increases, which will in turn produce a delta gamma error for the inverter. The measured gamma angle at the inverter is fed into a minimum gamma measurement block; this component measures the input gamma signal and outputs the minimum value from the past full cycle of fundamental frequency. The output is updated every 30 electrical degrees (1/12 of a cycle) so that the output is the minimum of the last twelve 30-degree periods. The measured value is then subtracted from the delta gamma error at stage 2 and added to the minimum gamma angle to produce the gamma error (GERRI).

This error is then fed through a PI controller at stage 3 where the error will be reduced to zero (if possible) before being summed with the adjusted current margin error from stage 4 to give the maximum output angle (BETA) at stage 3. Finally, this maximum value is subtracted from the reference value $P_i = 3.141592653589793$ to give the angle order for the inverter.

4.3 Impact of effective short circuit ratio on CSC-HVDC operation

The SCR is an important factor in determining the stability and steady-state operation of an AC power system [41]. For CSC-HVDC technology, the reactive contribution of the AC filters needs to be taken into account. The ESCR is used, as calculated by Equation 4.33, to estimate the system strength taking into account the effect of the reactive shunt compensation on the system impedance (as seen by CSC-HVDC converters) [41].

$$ESCR = \frac{S_{sc} - Q_c}{P_{dN}} \quad (4.33)$$

Where [41]:

- S_{sc} is the short circuit capacity of the commutations bus.
- Q_c is the reactive contribution from the shunt compensation (filters).
- P_{dN} is the rated power of the converter station.

AC filters can reduce the strength of the AC system, despite their reactive power contribution [41]: the SCR may be high, but the ESCR could be lower. Analysis of ESCR on the impact of CSC-HVDC technology has already been carried out in [148], [149], and [150] but the impact of ESCR on CSC-HVDC technology operation for an NPP connection has yet to be studied.

In the following section the impact of ESCR on CSC-HVDC operation for an NPP connection during steady-state conditions is analysed [148]. First the ESCR at the rectifier connection to the NPP is reduced while keeping the inverter ESCR constant. In reactor station 2 the series impedance of nuclear generator 2 is adjusted to reflect the corresponding value of ESCR before the reverse scenario (rectifier ESCR is kept constant and the inverter ESCR is reduced) is analysed. Due to multiple AC circuits connected to the inverter busbar the ESCR is reduced by switching out the corresponding overhead lines one at a time. The reference value of the DC current and voltage orders is shown in the reference plots and the DC current can also provide an indication of the active power transmission from the Ohm's law relationship [41].

4.3.1 Rectifier ESCR 1.8 and inverter ESCR 3.5

In Figure 164 the CSC-HVDC link is able to function correctly with nominal ESCRs at both the rectifier and inverter.

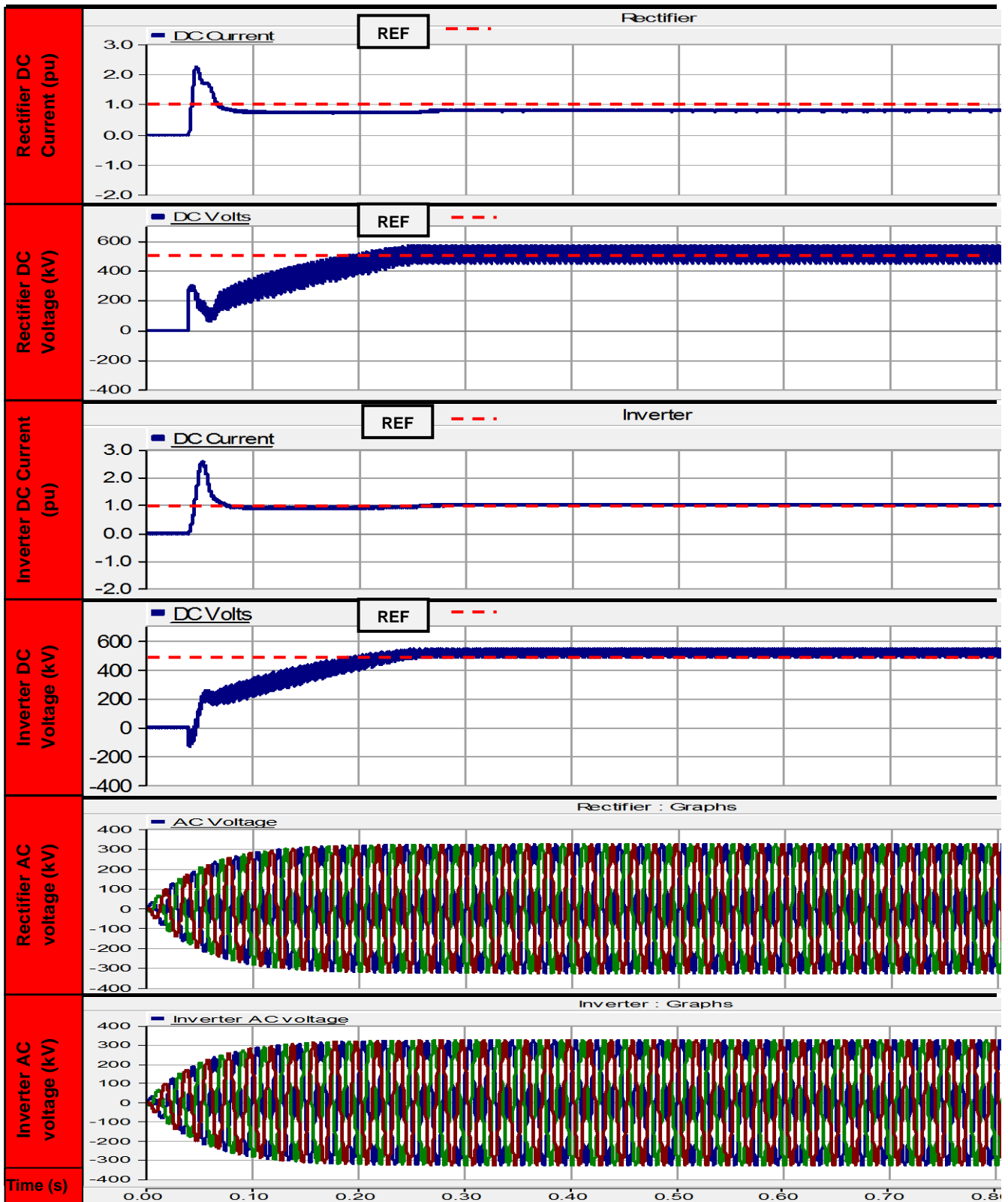


Figure 64: Rectifier ESCR 1.8, inverter ESCR 3.5

There are no deviations in DC current or voltage, and the reference values are maintained. The AC voltage profiles at both the rectifier and inverter are constant and the CSC-HVDC link is able to supply full power to the AC system.

4.3.2 Rectifier ESCR 1.4 and inverter ESCR 3.5

The CSC-HVDC link profiles for a reduction in ESCR at the rectifier are shown in Figure 65.

The ESCR reduction has affected the operation of the CSC-HVDC link. The voltage profile at the rectifier experiences a minor voltage distortion caused by the increase in NPP generator series impedance and reduction in ESCR. After initial startup, the DC currents at both the rectifier and inverter take nearly 30 ms to reach a steady-state value of 0.8 pu – due to the reduction in ESCR at the rectifier the currents have dropped below their reference values by 20%.

At 0.3 secs the rectifier current controller attempts to increase its output to meet the full target references, but due to the lower ESCR, and voltage distortion, these cannot be met. A maximum of 0.8 pu is supplied, hence the active power delivered into the AC system has also dropped:

$$P = VDC.IDC \quad (4.34)$$

Similar results are experienced in the work carried out in [150], where a reduction in ESCR at the rectifier results in a reduction in active power transfer capability within the CSC-HVDC link.

Since a reduction in DC current translates to a drop in active power transmission, in reality, the full active power output of the NPP cannot be delivered to the AC network. Such a constraint in active power transmission could be costly if the full generation cannot be supplied to the AC system [151].

Despite the AC voltage distortion at the rectifier, the DC voltage profile is held constant. This allows the CSC-HVDC link to successfully deliver 0.8 pu DC current.

The strong ESCR at the inverter has helped to keep the AC voltage profile constant, which enables successful valve commutation. Equally, the DC voltage has been unaffected and allows delivery of DC current to the AC system.

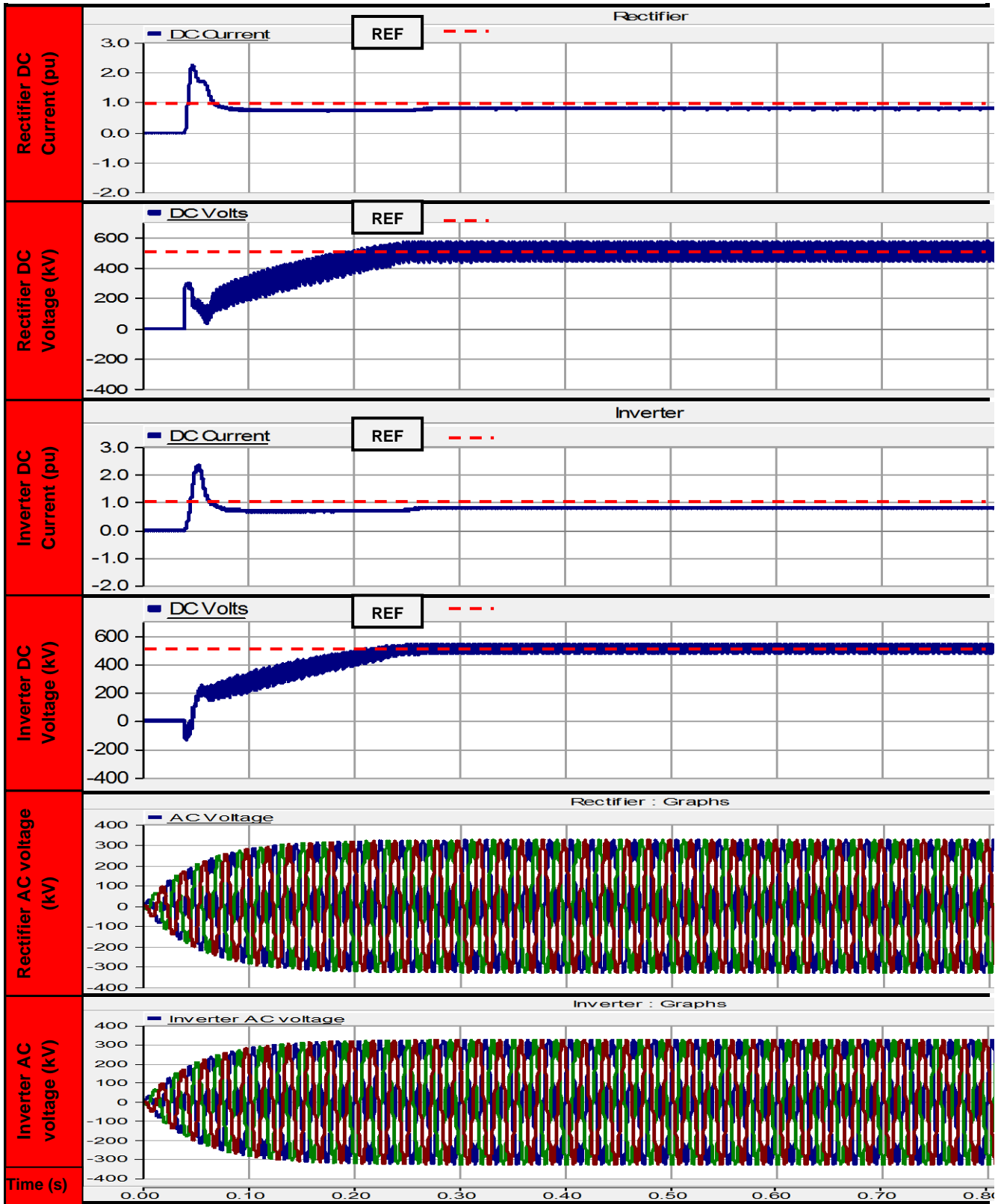


Figure 65: Rectifier ESCR 1.4, inverter ESCR 3.5

4.3.3 Rectifier ESCR 1.0 and inverter ESCR 3.5

The CSC-HVDC link profile for an ESCR of 1.0 at the rectifier is shown in Figure 66. Here the AC voltage distortion at the rectifier has remained.

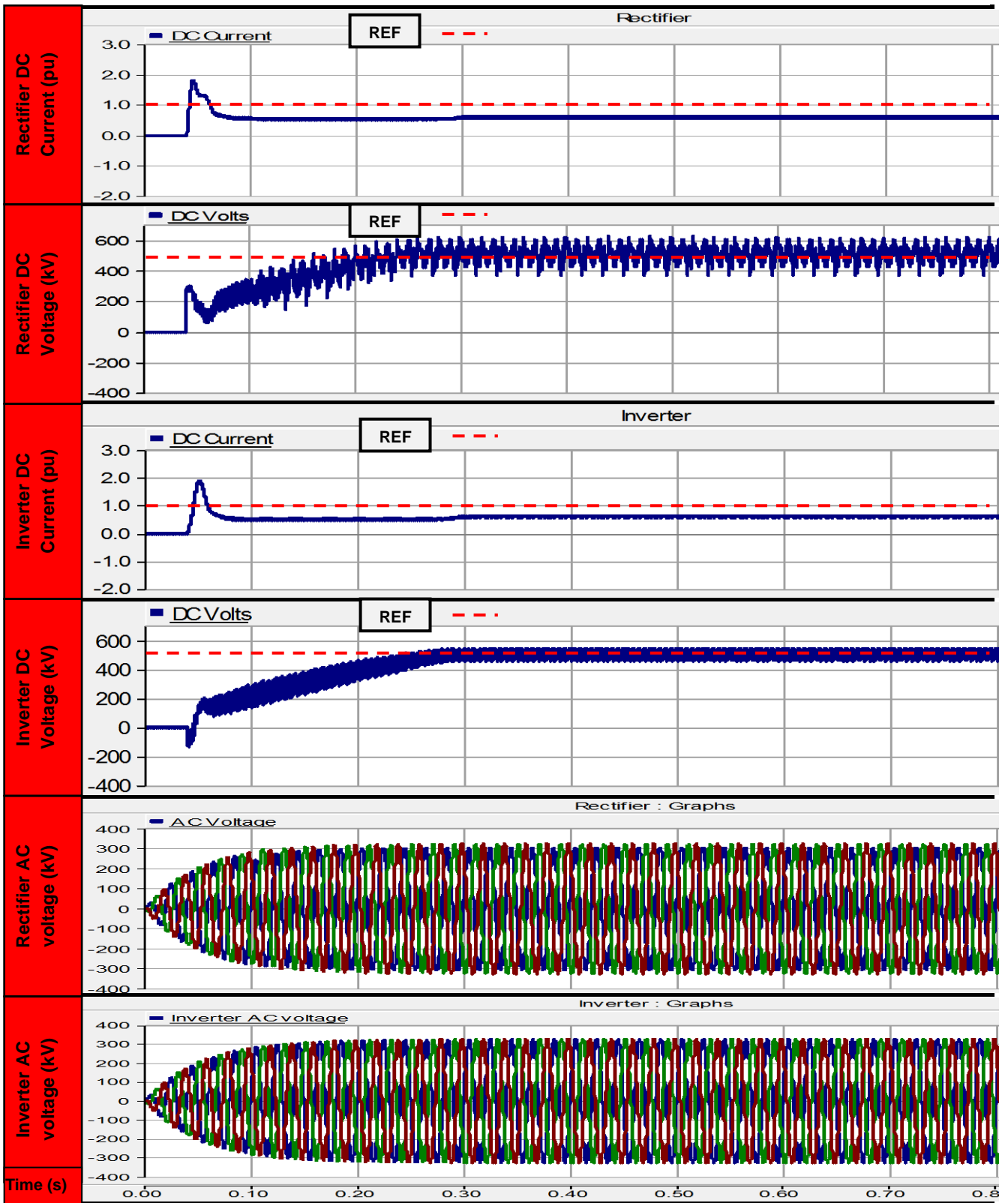


Figure 66: Rectifier ESCR 1.0, inverter ESCR 3.5

In combination with the reduction in ESCR, the DC voltage profile at the rectifier has become severely distorted, which has caused the DC currents at both the rectifier and inverter to reduce to 0.6 pu.

At a time of 0.3 secs, the rectifier current controller attempts to increase its output to meet the DC current reference target of 1.0 pu but is unable to achieve this due to the exacerbated conditions at the NPP generator source.

A slight AC voltage distortion is present at the inverter, but the DC voltage is held constant. The strong ESCR (3.5) of the AC network has allowed successful valve commutation to take place, and DC current (active power) to be supplied to the AC network. For an ESCR of 1.0, the CSC-HVDC system is on the very limit of its operation before instability may be encountered.

4.3.4 Rectifier ESCR 1.8 and inverter ESCR 2.4

The CSC-HVDC profile for a reduction in ESCR at the inverter to 2.4 is shown in Figure 64.

All reference values have been met, but minor distortions in the DC voltage profile at the inverter can be observed. The AC voltage profile at the inverter is unaffected, and successful valve commutation has taken place.

The AC voltage profile at the rectifier is stable and the current controller allows the full DC reference current to be delivered to the AC network; this translates into 100% of the active power also being supplied.

The profile of Figure 64 represents a stable and manageable situation for the CSC-HVDC link and would in reality; result in a secure and stable connection to the AC grid.

Similar results have been encountered in work already carried out in [149] and [150] where full active power was able to be delivered to the AC grid, and the CSC-HVDC link performed well for a low ESCR at the rectifier (1.5) and strong value (3.0) at the inverter. As the ESCR values were reduced even further, the ability of the CSC-HVDC link to maintain the DC current and active power references were exacerbated even further.

In the next simulation the ESCR is reduced even further at the inverter and the ESCR values at both ends of the CSC-HVDC link are the same.

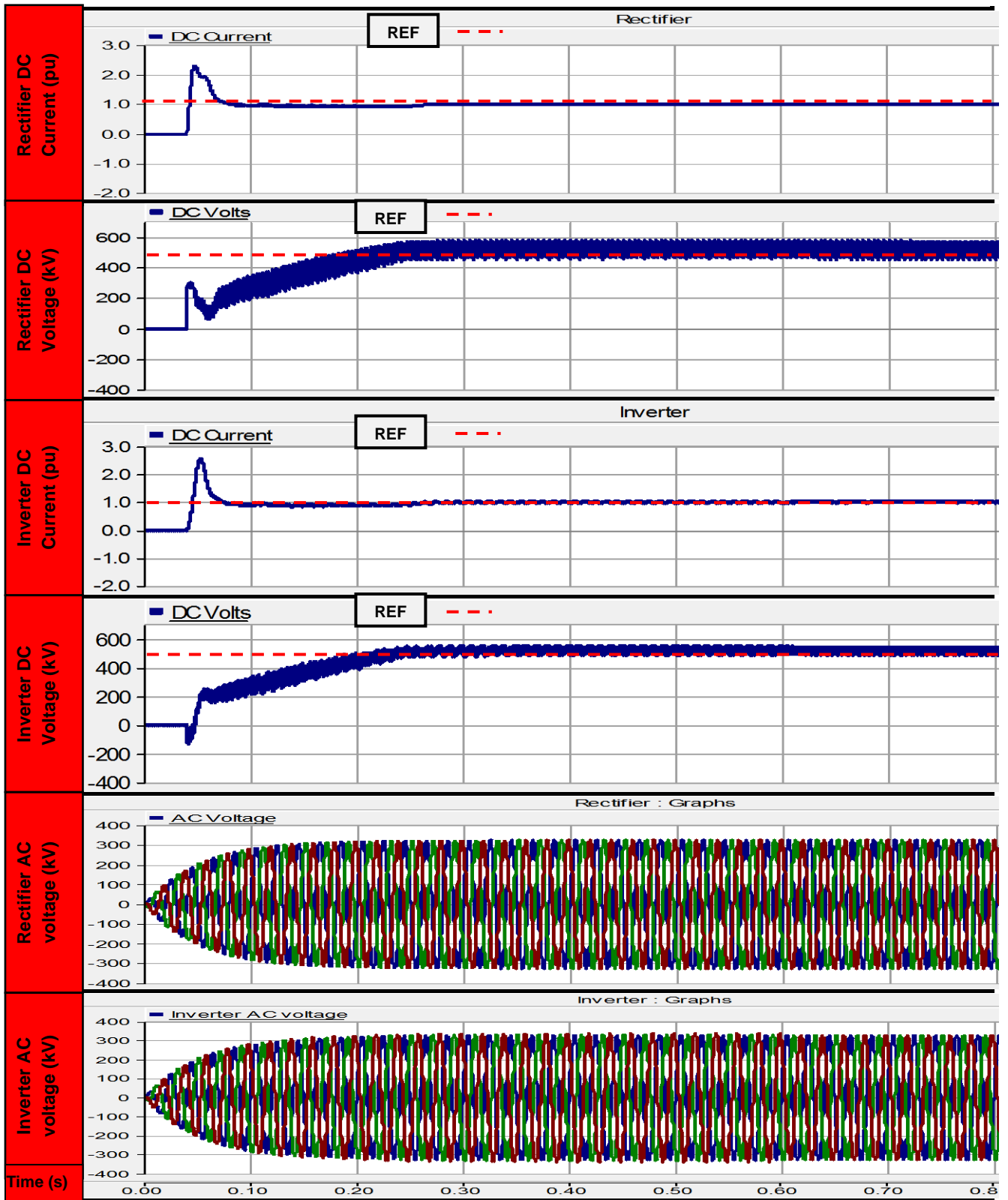


Figure 67: Rectifier ESCR 1.8, inverter ESCR 2.4

4.3.5 Rectifier ESCR 1.8 and inverter ESCR 1.8

In Figure 68 the drop in ESCR at the inverter has had some noticeable effects on the CSC-HVDC link operation.

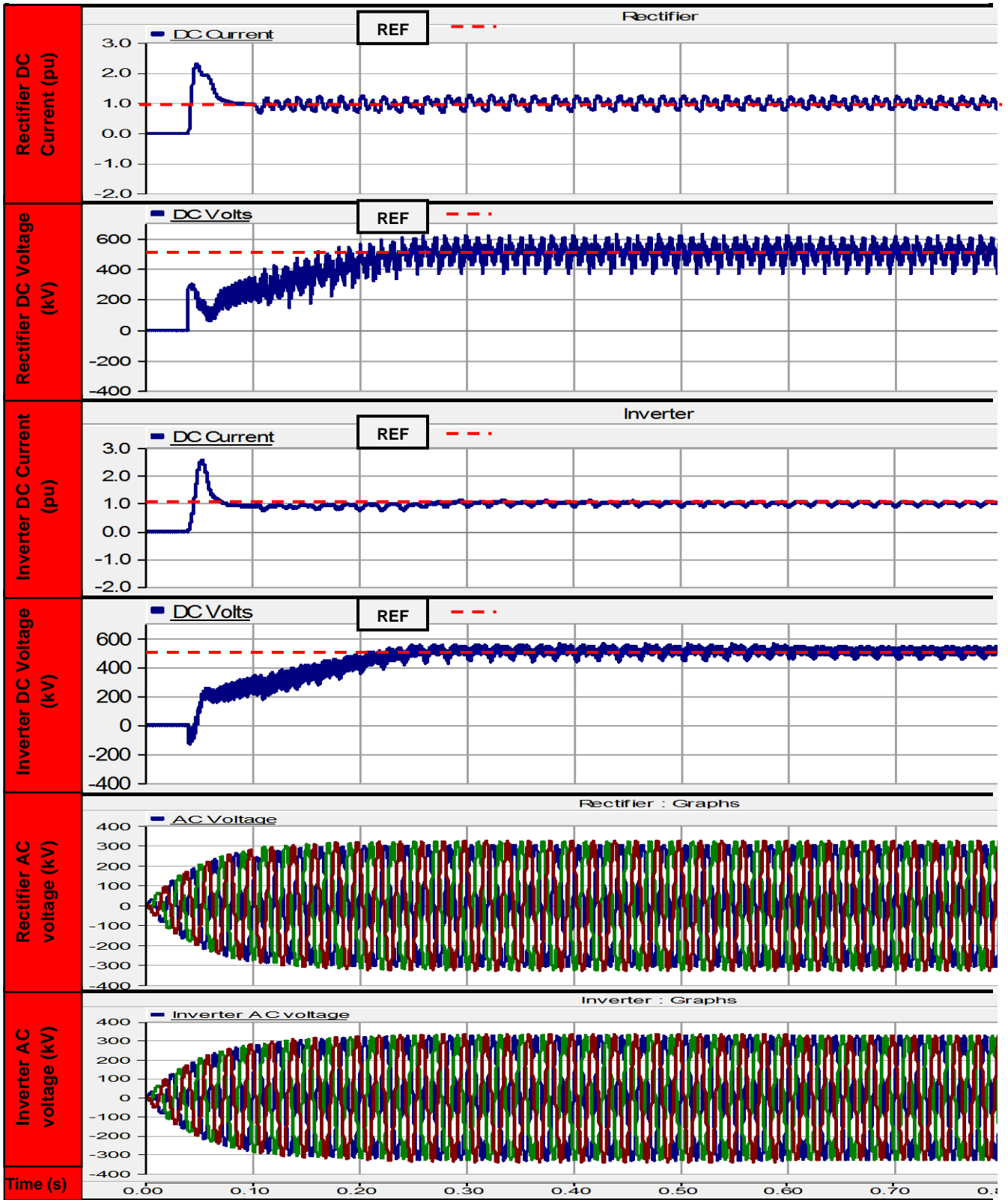


Figure 68: Rectifier ESCR 1.8, inverter ESCR 1.8

Distortions in DC currents at both the rectifier and inverter can be observed. The DC current reference at the rectifier is fully met despite the oscillations encountered. At the inverter, the DC current supplied is below the reference demand.

This recovers once the output is increased by the rectifier current controller at a time of 0.3 secs; once this is completed, then full active power delivery to the AC grid is possible.

Severe distortions in both DC voltage profiles at the rectifier and inverter are present. The level of DC harmonic content has also increased, and the oscillations have worsened since the ESCR at the inverter has been reduced.

The AC voltage profiles at the rectifier and inverter experience some minor distortions, but successful valve commutation takes place and the full output of the NPP is delivered to the AC system.

For an ESCR value of 1.8 at both ends of the CSC-HVDC link, perturbations are encountered. With the inverter operating in either constant extinction angle or DC voltage control any disturbance will also be reflected at the rectifier end [150].

For the above ESCR value at the inverter, the simulations have indicated the boundary at which successful operation can be achieved at full current output. If the ESCR is reduced further, then the possibility of instability cannot be ruled out [150].

For the final example the ESCR is reduced even further in order to fully ascertain the stable operating limit of the CSC-HVDC link.

4.3.6 Rectifier ESCR 1.8 and inverter ESCR 1.4

In Figure 69 the further reduction in ESCR at the inverter has resulted in complete system collapse.

Distortions in AC voltages at both the rectifier and inverter can be observed and the drop in ESCR has resulted in commutation failure at the inverter. Valve commutation takes place but the AC voltage is too low for it to continue. The voltage depression continues until 0.6 secs after initial startup before complete collapse is observed. A large harmonic content is visible in the voltage distortions, which could exacerbate conditions within the AC network even further. Voltage depressions also occur in the rectifier due to the commutation failure at the inverter. Here the harmonics could exacerbate voltages within the NPP and affect its operation. The filters are unable to supply the required reactive power and this may be exacerbated even further within the AC network [150]. Despite the severity of the voltage depressions, and the drop in ESCR, the rectifier current controller is able to meet the DC current reference until 0.5 secs into operation. Eventually the DC voltage at both the rectifier and inverter collapse and the DC current severely oscillates and instability is encountered.

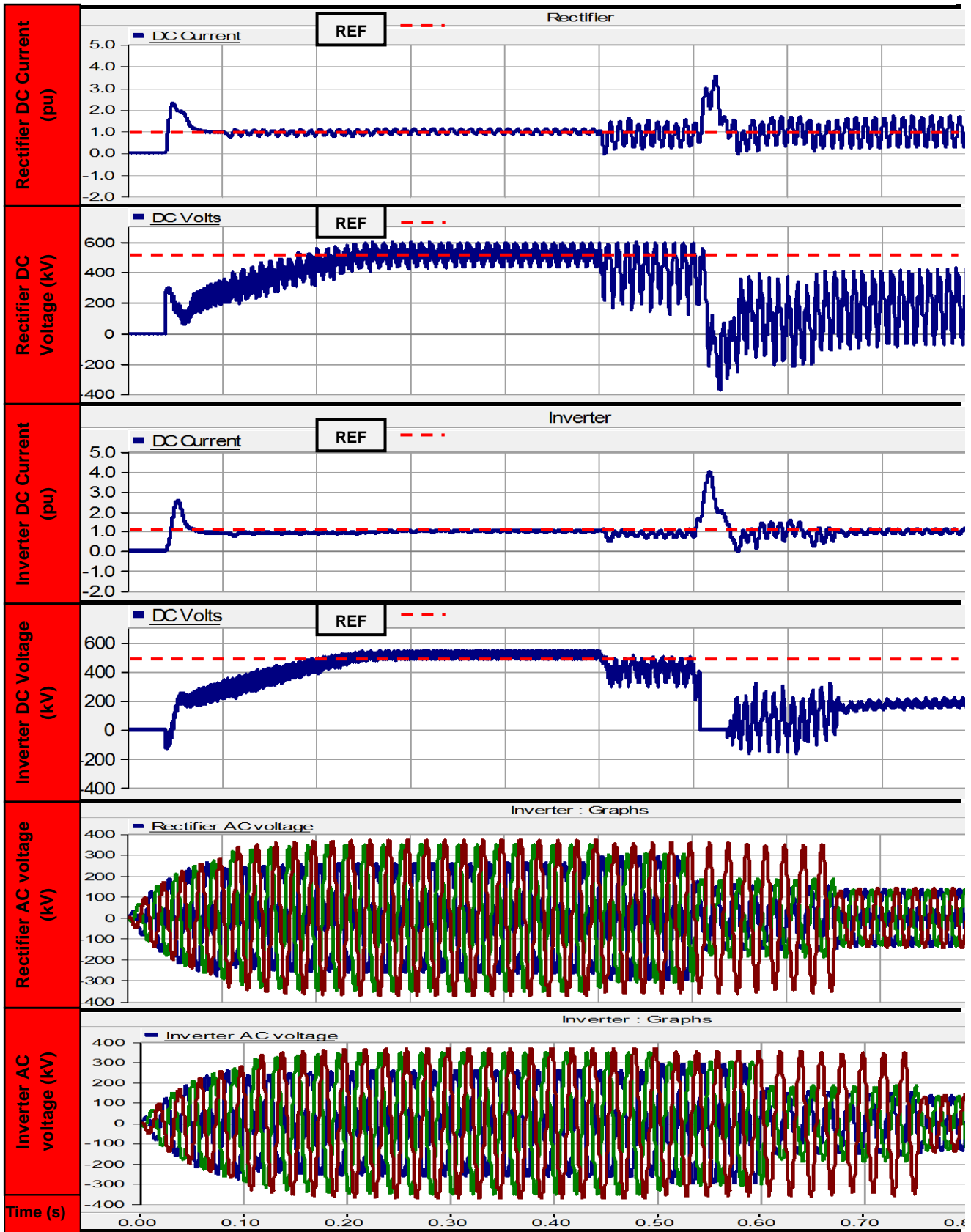


Figure 69: Rectifier ESCR 1.8, inverter ESCR 1.4

DC current spikes of 4.0 pu can be observed at the time of 0.6 secs when the DC voltage has completely collapsed due to inverter commutation failure.

The above situation would result in the NPP being islanded from the AC network and a shutdown of the reactor may be required [103]. The large oscillations could cause damage to the NPP and AC system where in industry the DC protection and control system would trip and isolate the CSC-HVDC link for safety purposes [41].

4.3.7 Summary

The effect of the ESCR value on the operation of a CSC-HVDC link connected to an NPP has been investigated. A summary of the results obtained is provided in Table 12.

Table 12: Summary of results for ESCR variation

Rectifier SCR	Rectifier ESCR	Inverter SCR	Inverter ESCR	Instability	Full load supplied
2.5	1.8	4.1	3.5	No	Yes
2.0	1.4	4.1	3.5	No	No (80%)
1.6	1.0	4.1	3.5	No	No (60%)
2.5	1.8	3.0	2.4	No	Yes
2.5	1.8	2.5	1.8	Yes	Yes
2.5	1.8	2.0	1.4	Yes	No (system collapse)

If the value of ESCR at the rectifier is lowered, then the CSC-HVDC link has difficulty in delivering the full output of the NPP to the AC system. For the conditions analysed in the previous section for ESCR values of 1.4 or lower, a drop in DC current and active power will be experienced, along with distortion in the rectifier AC voltage, indicating the maximum permissible operational limits of the CSC-HVDC have been reached.

In summary, the effect of the ESCR on the operation of CSC-HVDC NPP connection needs to be carefully considered. To improve the operational range of the CSC-HVDC link and increase reliability during a low ESCR the inclusion of a STATCOM or synchronous condenser at the rectifier end is worth investigating and has been proven successful for previous work carried out in [152], [153], and [154].

4.4 Transient analysis of a CSC-HVDC NPP connection

A transient analysis is carried out in PSCAD to analyse a CSC-HVDC NPP connection. As in chapter 3, a general fault analysis is carried out to identify fault locations with the worst case effect on the voltage and power profiles of the various busbars. A combination of both AC and DC faults are studied at the multiple locations shown in Figure 70. DC currents and voltages are monitored before and during the faults along with the reactor output power to assess the system behaviour.

The faults with the worst case effects on the system profile are then selected for further detailed analysis in PSCAD. Plots displaying the profiles of both the CSC-HVDC link and the areas monitored within the NPP are produced.

Following the detailed transient analysis, further simulations are carried out for different system contingencies. Here the response of the HVDC controls to different system conditions is analysed and in particular, the use of active power modulation to reduce system oscillations and control frequency during the contingencies is studied.

4.4.1 General transient analysis

Within PSCAD system variables consisting of both DC voltages and current along with the active power output of the reactor were measured at the point of fault both before (pre-fault) and during the transient event. The locations of the faults are shown in Figure 70 and the fault cases and the results obtained from each simulation are shown in Table 13.

The three-phase faults at the rectifier (F19) and inverter (F14) have noticeable effects on the CSC-HVDC link variables. Both the DC and AC voltages are significantly reduced and the reactor output power increases during the faults. Due to the effects on the reactor output power, both of these fault cases are selected for further analysis.

The pole-ground and pole-pole DC faults show similar results, with high fault currents present. The DC voltages are seriously reduced, indicating the possibility of commutation failure [41]. Due to the nature of the faults and the known effects that they can have on the power system these fault cases are selected for further analysis.

Table 13: General fault analysis results

Fault Number/Location	Fault Type	Duration (msecs)	REC DC Pre-fault current (pu)	INV DC Pre-fault current (pu)	REC Pre-fault DC Voltage (kV)	INV Pre-fault DC Voltage (kV)	AC Pre-fault voltage (kV)	Pre-fault Reactor power (MW)	REC DC Current During fault (pu)	INV DC Current during fault (kA)	REC DC Voltage During Fault (kV)	INV DC Voltage During Fault (kV)	AC Voltage During fault (kV)	Reactor power During fault (MW)
F1	3Φ	140	1	1	500	500	400	500	1	1	500	500	0	500
F2	3Φ	140	1	1	500	500	400	400	1	1	500	500	0	500
F3	3Φ	140	1	1	500	500	400	300	1	1	500	500	0	500
F4	3Φ	140	1	1	500	500	400	800	1	1	500	500	0	500
F5	3Φ	140	1	1	500	500	400	600	1	1	500	500	0	500
F6	3Φ	140	1	1	500	500	400	300	1	1	500	500	0	500
F7	3Φ	140	1	1	500	500	400	400	1	1	500	500	0	500
F8	3Φ	140	1	1	500	500	400	300	1	1	500	500	0	500
F9	3Φ	140	1	1	500	500	400	600	1	1	500	500	0	500
F10	3Φ	140	1	1	500	500	400	800	1	1	500	500	0	500
F11	3Φ	140	1	1	500	500	400	500	1	1	500	500	0	500
F12	3Φ	140	1	1	500	500	400	500	1	1	500	500	0	500
F13	3Φ	140	1	1	500	500	400	600	2	3	500	300	0	1600
F14	3Φ	140	1	1	500	500	400	1000	3	4	200	400	0	2000
F15	3Φ	140	1	1	500	500	400	1000	1	2	500	400	0	1400
F16	3Φ	140	1	1	500	500	400	1000	1	2	500	400	0	1460
F17	3Φ	140	1	1	500	500	400	1000	3	4	200	0	0	2000
F18 (a)	Pole-G	140	1	1	500	500	N/A	1000	2.8	1.6	0	300	N/A	500
F18 (b)	P-P	140	1	1	500	500	N/A	1000	2.8	0	100	0	N/A	0
F19	3Φ	140	1	1	500	500	400	1000	1	0	0	0	400	2000
F20	3Φ	140	1	1	500	500	400	1000	1	1	0	0	0	500
F21	3Φ	140	1	1	500	500	400	600	2	2	500	500	0	500
F22	3Φ	140	1	1	500	500	400	600	2	2	500	500	0	520
F23	3Φ	140	1	1	500	500	132	500	1	1	500	500	0	550
F24	3Φ	140	1	1	500	500	23	500	1	1	500	500	0	500
F25	3Φ	140	1	1	500	500	11	500	1	1	500	500	0	500
F26	3Φ	140	1	1	500	500	400	600	1	1	500	500	0	500
F27	3Φ	140	1	1	500	500	400	700	1	1	500	500	0	1800
F28	3Φ	140	1	1	500	500	400	500	1	1	500	500	0	500
F29	3Φ	140	1	1	500	500	11	600	1	1	500	500	0	500
F30	3Φ	140	1	1	500	500	23	600	1	1	500	500	0	500
F31	3Φ	140	1	1	500	500	132	500	1	1	500	500	0	500
F32	3Φ	140	1	1	500	500	132	500	1	1	500	500	0	200
F33	3Φ	140	1	1	500	500	11	800	1	1	500	500	0	0
F34	3Φ	140	1	1	500	500	23	900	1	1	500	500	0	0
F35	3Φ	140	1	1	500	500	132	800	1	1	500	500	0	0
F36	3Φ	140	1	1	500	500	400	900	1	1	500	500	0	1800
F37	3Φ	140	1	1	500	500	400	700	1	1	500	500	0	1800
F38	3Φ	140	1	1	500	500	400	800	1	1	500	500	0	0
F39	3Φ	140	1	1	500	500	400	900	1	1	500	500	0	1600
F40	3Φ	140	1	1	500	500	132	900	1	1	500	500	0	0
F41	3Φ	140	1	1	500	500	400	1000	1	1	500	500	0	0
F42	3Φ	140	1	1	500	500	23	900	1	1	500	500	0	300
F43	3Φ	140	1	1	500	500	11	850	1	1	500	500	0	300

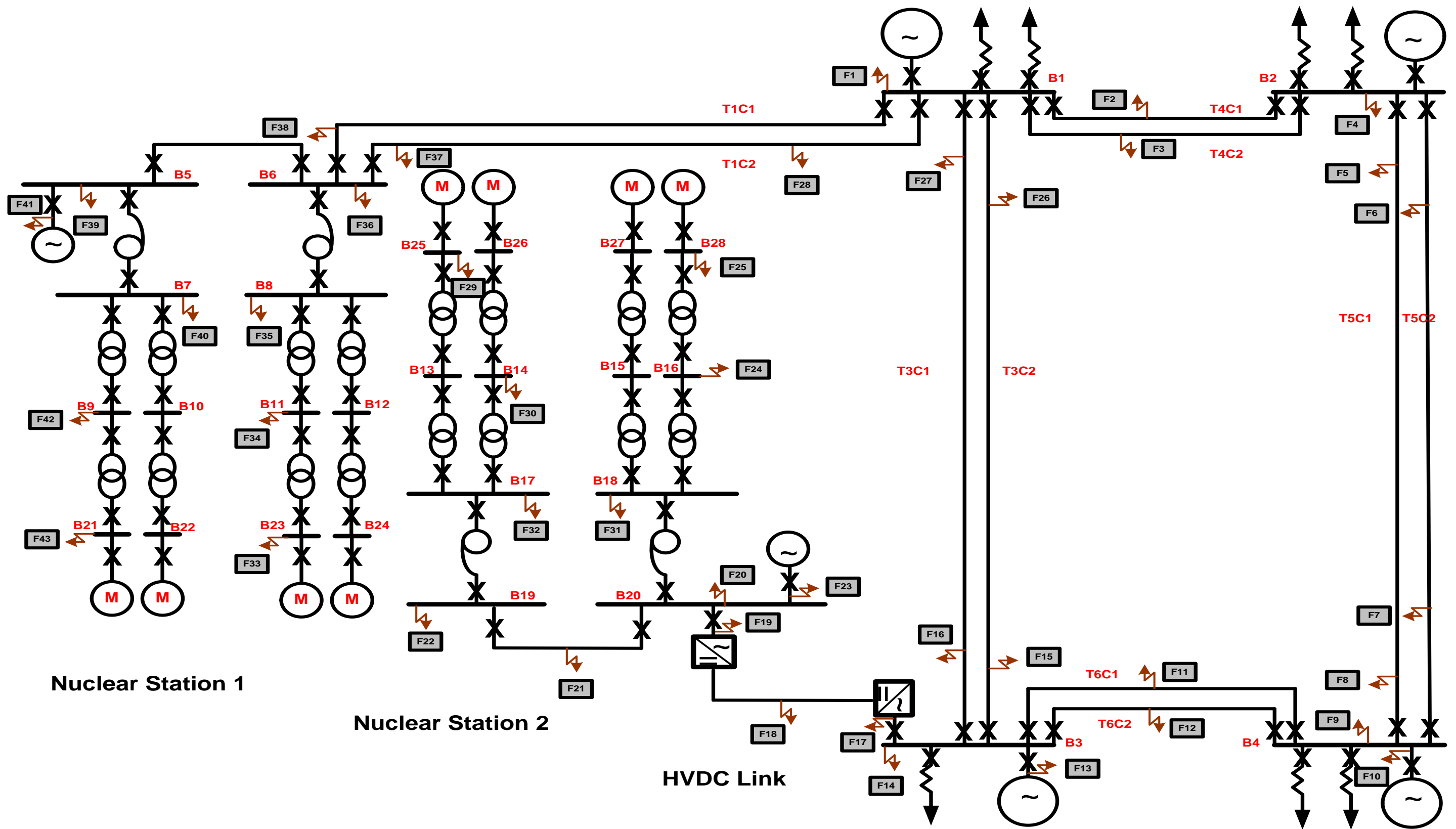


Figure 70: General fault analysis for NPP connected by HVDC technology

4.4.2 Detailed transient analysis

Those fault locations which merited further detailed transient analysis are described in the following sections.

For the detailed transient analysis, all faults at 400 kV were cleared within the 140 ms stipulation time of the Grid Code [135]. For DC faults these are assumed to be permanent and were present for the full simulation to demonstrate the effects of their non-clearance by protection or controller action. In the simulation plots, busbar 27 was monitored to observe the impact of the faults on the voltage profiles of the reactor cooling motors. The reactor output power is also monitored to assess the effects of the faults on its behaviour.

In addition to the above simulations, the response and impact of the CSC-HVDC controls to system contingencies within the NPP and AC grid are assessed.

4.4.2.1 Three-phase fault on busbar 3

In this scenario, a three-phase fault is placed on busbar 3 and is cleared by the AC protection within 140 ms.

The DC profiles are shown in Figure 71. The rectifier firing angle is forced to 90° to coincide with the collapse in DC voltage, which ensures that no further unnecessary control actions are initiated to avoid further system exacerbation [41]. The Voltage Dependent Current Order Limiter (VDCOL) function becomes active as soon as the fault occurs and the inverter firing angle is significantly reduced during the disturbance to help reduce reactive power absorption from the AC system and increase the extinction angle to aid the recovery of the system once the fault has been cleared [41]. The DC current is limited by the rectifier current controller during the fault.

Once the fault has been cleared, large current spikes re-occur at both the rectifier and inverter. The rectifier controller attempts to reduce the DC current spike by increasing its firing angle to 130° and enters inversion mode for 10 ms [155]. The inverter firing angle is reduced to 90° during the same time period by the VDCOL to reduce the stress on the system and ensure that no further unnecessary controller actions are encountered. The DC current is restored 40 ms later and the rectifier and inverter firing angles return to nominal values to aid system recovery.

After system recovery, large oscillations and harmonics are present in all the DC profiles; this shows the severity of an inverter commutation failure when a three-phase fault occurs [41].

In Figure 71 the AC currents on the valve winding side of the converter transformer are significantly reduced due to the collapse of DC voltage and cessation of power transfer.

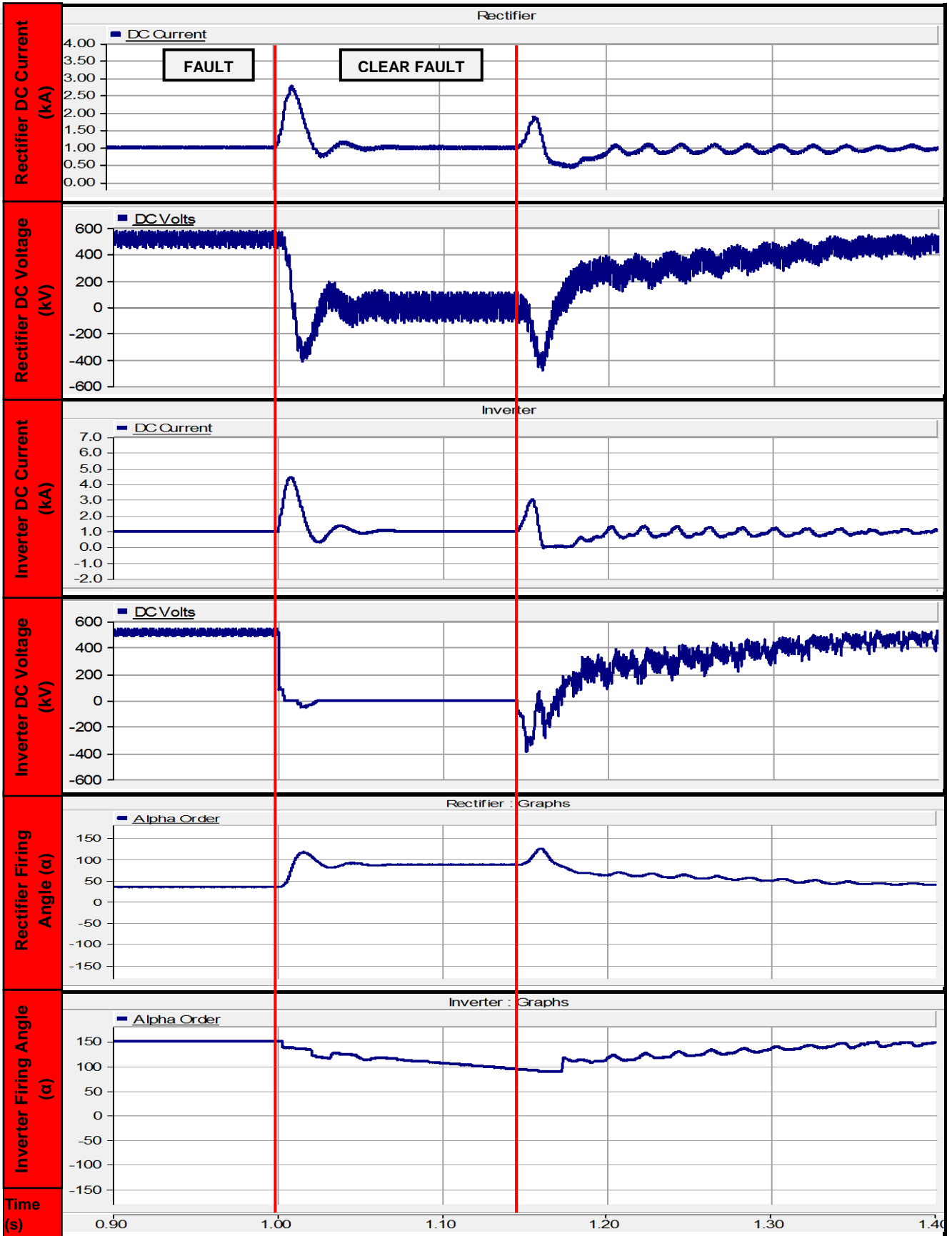


Figure 71: DC profiles for three-phase fault on busbar 3

Temporary AC current spikes can be observed on the valve windings when the fault occurs.

At the inverter the current reaches over 9 kA.

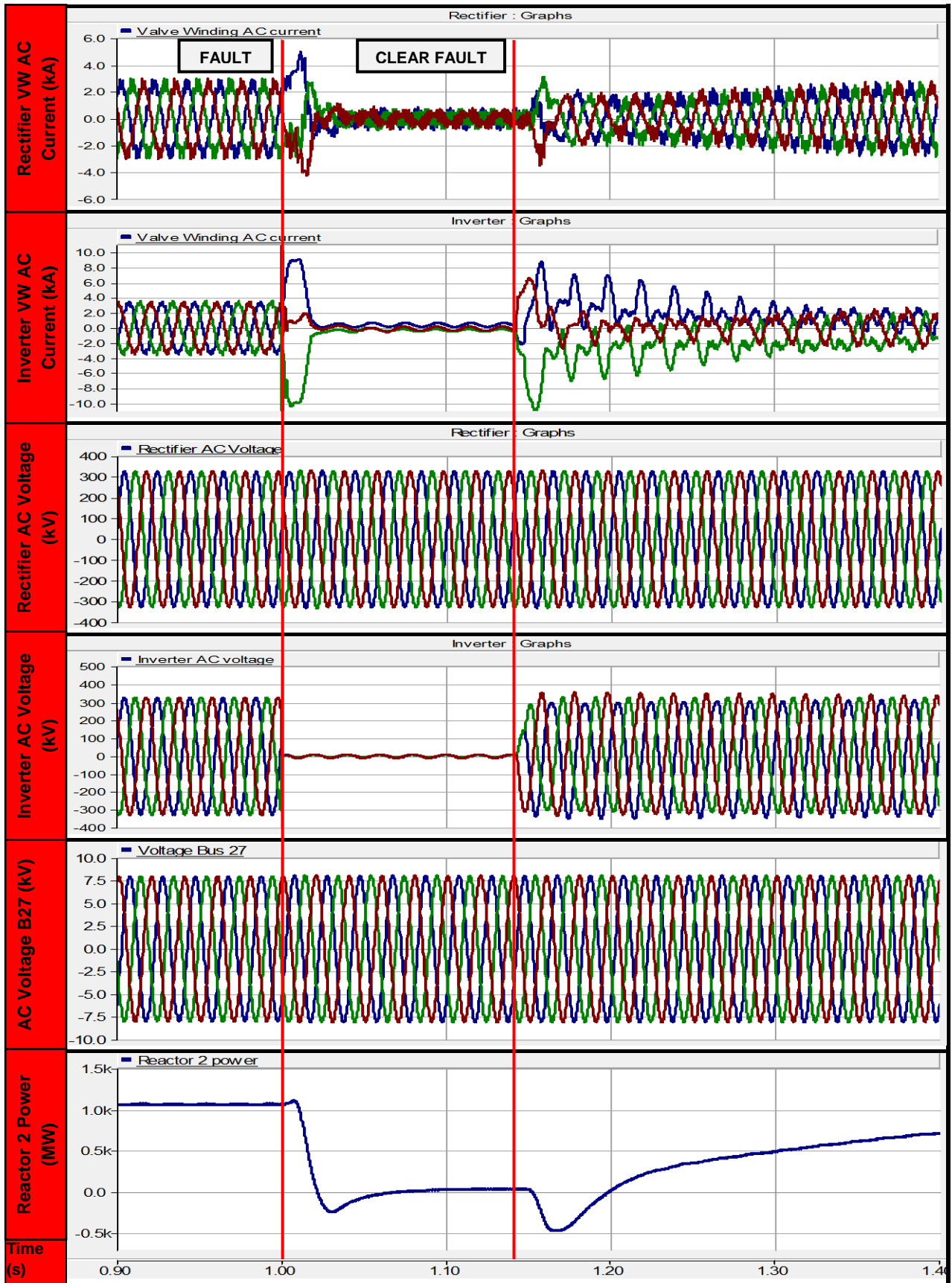


Figure 72: DC profiles for a three-phase fault on busbar 3

The AC voltage profiles of the rectifier and busbar 27 are unaffected by the three-phase fault due to the firewall function provided by the CSC-HVDC link [41]. The inverter AC voltage profile has collapsed to zero, but recovers once the fault has been cleared, ensuring the operational safety of the reactor cooling motors and a constant supply of power [103].

In summary, the three-phase fault on busbar 3 has caused a commutation failure at the inverter end of the CSC-HVDC link resulting in DC voltage collapse and high DC currents. The valve winding AC currents reach values of over 9 kA, which can cause considerable damage if the fault is not cleared. The DC control system is able to cope with the commutation failure by taking appropriate controller action: the firing angle at the inverter is reduced to increase the extinction angle and help the valves recover once the fault has been cleared [40]. The firewall functions of the HVDC link prevent the voltage depression from propagating into the NPP and ensure that the reactor cooling motors are unaffected. The reactor is able to ride through the disturbance, and the governor control restores the output power once the fault has been cleared.

4.4.2.2 Three-phase fault on busbar 20

In this scenario, a three-phase fault is placed on busbar 20 and is cleared by the AC protection within 140 ms.

The DC profiles are shown in Figure 73. The rectifier firing angle reduces in an attempt to increase the DC voltage [155]. The DC current is reduced by the VCDOL to help system stability. The rectifier DC voltage falls below the minimum limit, causing the inverter to take control of the current 10 ms after the fault occurred [155]. The inverter firing angle reduces during the disturbance which helps to reduce reactive power absorption from the AC system and increase the extinction angle to aid the recovery of the system once the fault has been cleared. The DC currents at both the rectifier and inverter are constrained by the VDCOL to 0.9 pu until the fault has been cleared. Immediately after fault clearance, DC current spikes are observed at both the rectifier and inverter due to the sudden recovery in active power transmission. The firing angles at both the rectifier and inverter are temporarily increased to discharge the DC current and limit the spikes [156]. The rectifier takes back control of current 30 ms after fault clearance.

The DC voltage at the rectifier collapses and causes a temporary commutation failure at the inverter. DC harmonics are present in both of the DC voltage profiles. Recovery is achieved 50 ms after fault clearance, although large oscillations are present due to the impact of the fault at the rectifier.

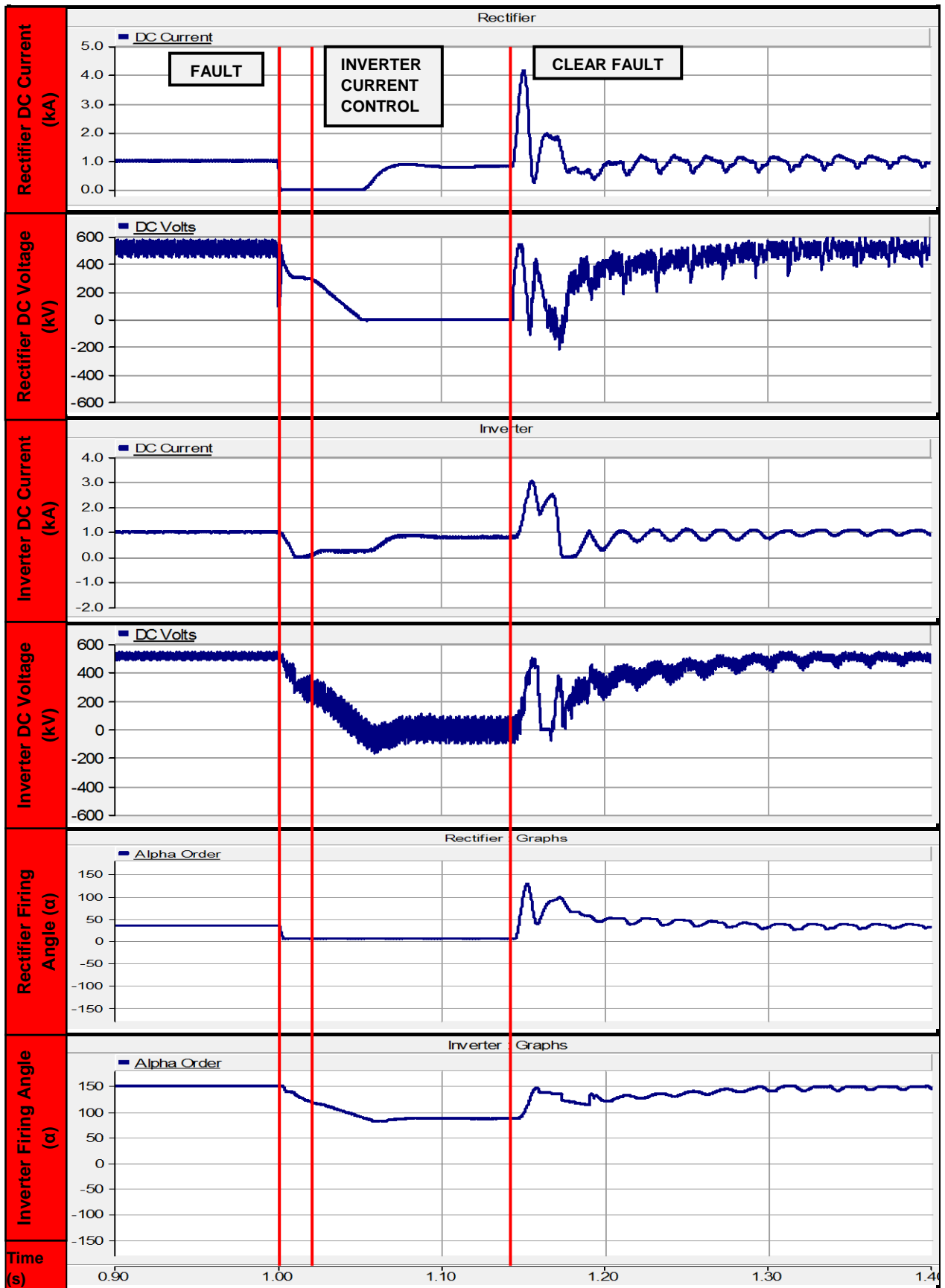


Figure 73: DC profiles for a three-phase fault on busbar 20

These oscillations will need to be damped by the HVDC control system otherwise further instability may occur in both the NPP and AC grid [156].

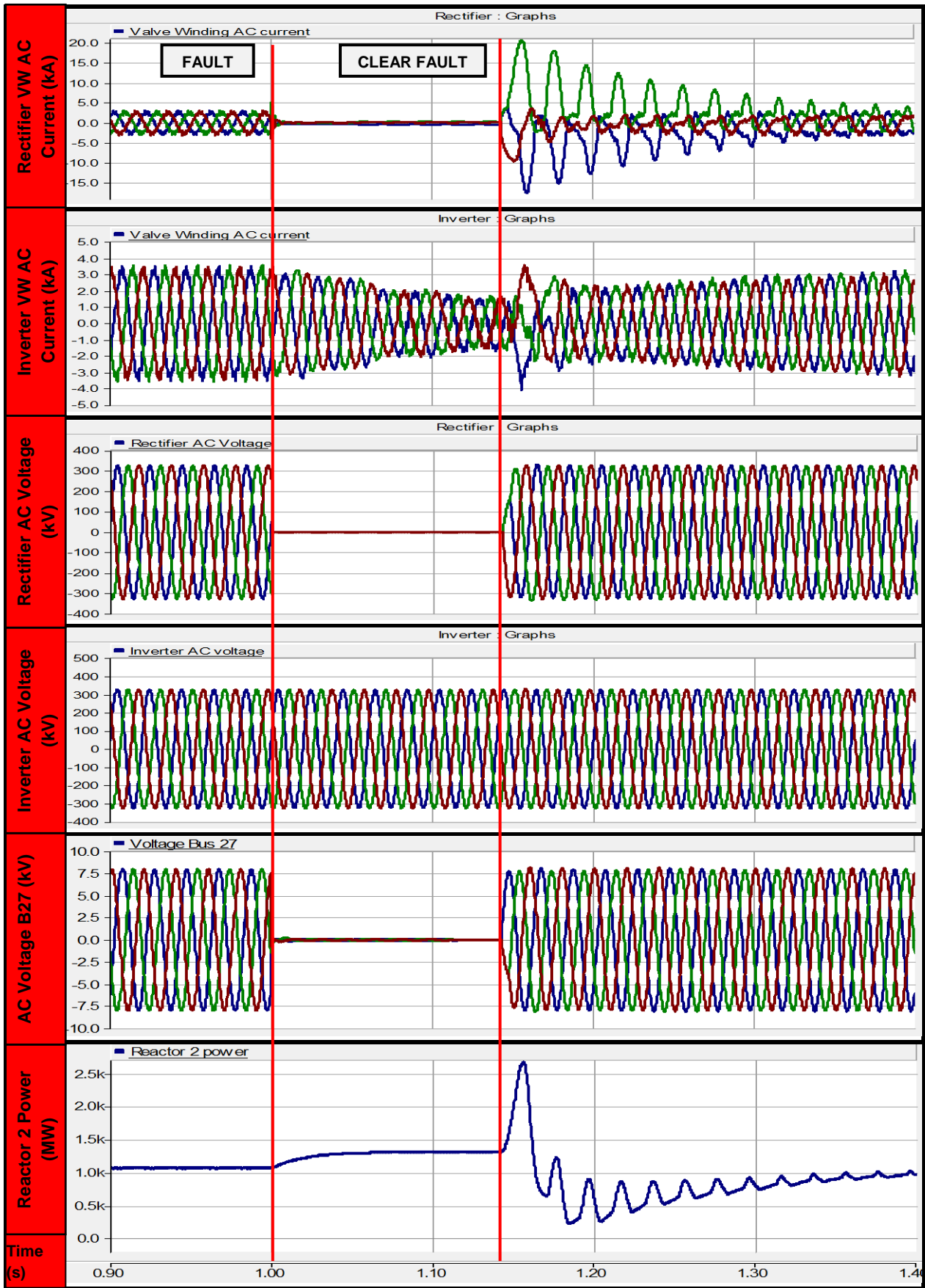


Figure 74: AC profiles for three-phase fault on busbar 20

In Figure 74 the rectifier AC valve winding current is reduced to zero due to the cessation in active power transfer caused by the fault.

At the inverter, the valve winding current is gradually reduced by the control system but continues to feed the fault through the CSC-HVDC link. Once the fault is cleared, the valve winding current at the inverter recovers. Following active power recovery, a large current spike of 20 kA magnitude is observed on the rectifier valve winding. In reality the primary equipment must be rated for such a current value and it is common for excessive current ratings to be tolerated for at least 500 ms [41]. The current eventually decays following successful fault clearance.

The firewall function of the HVDC link ensures that the inverter AC voltage is unaffected by the fault [156]. The AC voltage at the rectifier and busbar 27 collapses due to its close proximity to the fault, and the severity level. In practice this will seriously affect the reactor cooling motors and may result in a loss of power supplies due to undervoltage protection operating [103].

The output power of reactor 2 generator increases and feeds the fault until clearance has been achieved. Large oscillations are present post-fault, which take 200 ms to settle down once the reactor governor control has been applied.

In summary, a three-phase fault at the rectifier causes the AC and DC voltages to collapse, commutation failure to occur, and high current spikes on the inverter valve winding once the fault is cleared of 20 kA magnitude. The HVDC control system adjusts the firing angles via the VDCOL and helps the system to recover post fault. The inverter takes over current control when the rectifier DC voltage drops below the minimum limit, which is essential to prevent the DC currents from being uncontrolled and reaching large values which could exacerbate conditions even further [40]. The AC voltage profile of the reactor cooling motor collapses but recovers once the fault has been cleared. In practice, time delays on the undervoltage protection will need to be set above 140 ms to ensure that fault ride through is achieved and to prevent the tripping of supplies [103]. The governor control on the nuclear reactor enables fault ride through to be achieved, but oscillations occur and take a long time to settle down due to the severity of the three-phase fault.

4.4.2.3 Three-phase fault on busbar 4

In this scenario, a three-phase fault is placed on busbar 4 and is cleared by the AC protection within 140 ms; the fault ride-through capability of the CSC-HVDC converter is analysed. In Figure 75 the DC voltage profiles at both the rectifier and inverter have dropped. The three-phase fault on busbar 4 has created a bottleneck situation, where the active power from reactor station 2 flowing through the CSC-HVDC link into busbar 3 cannot enter busbar 4 via T6C1 and T6C2.

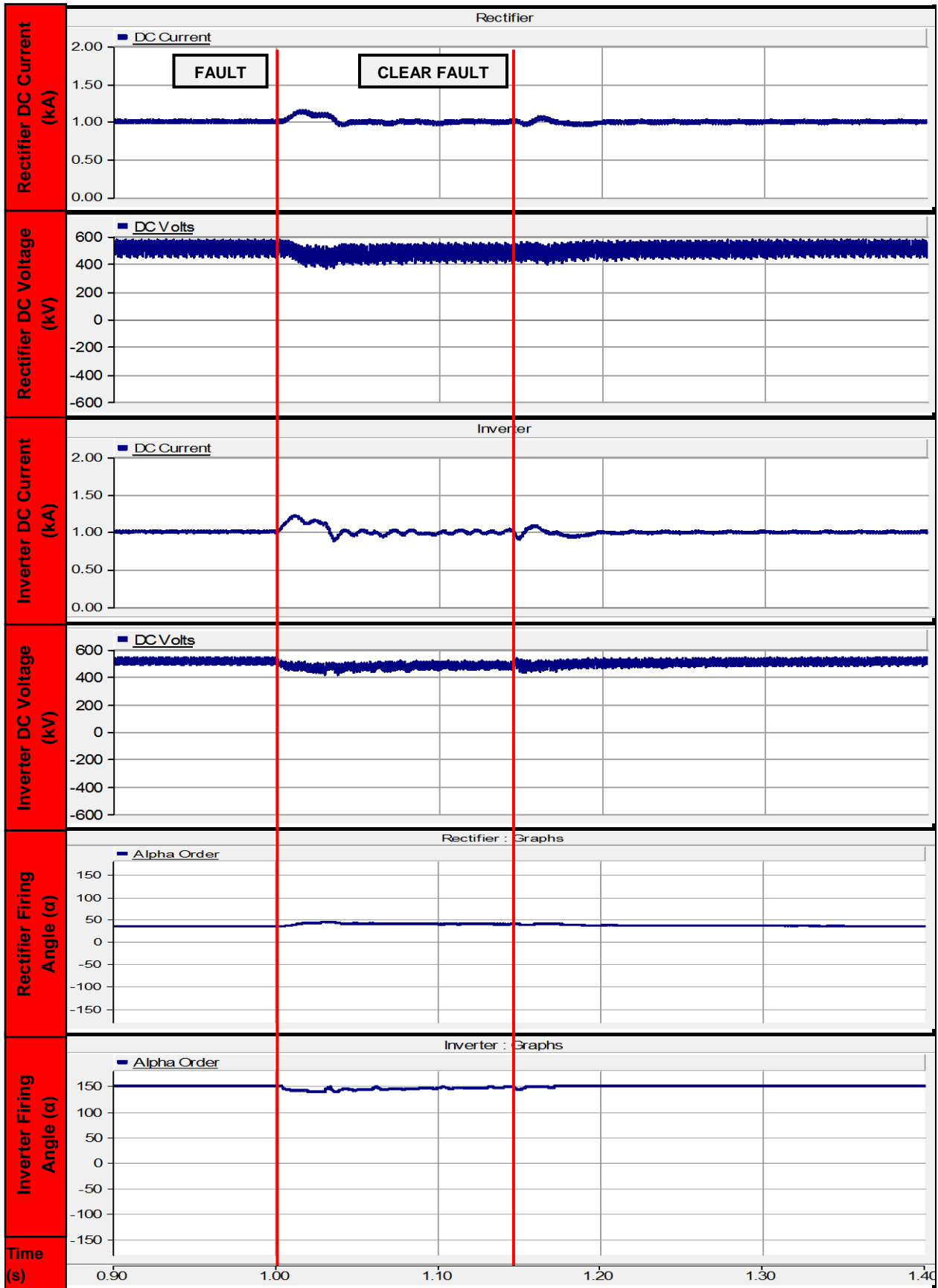


Figure 75: DC profiles for three-phase fault on busbar 4

The firing angle is increased at the rectifier and decreased at the inverter to aid system stability.

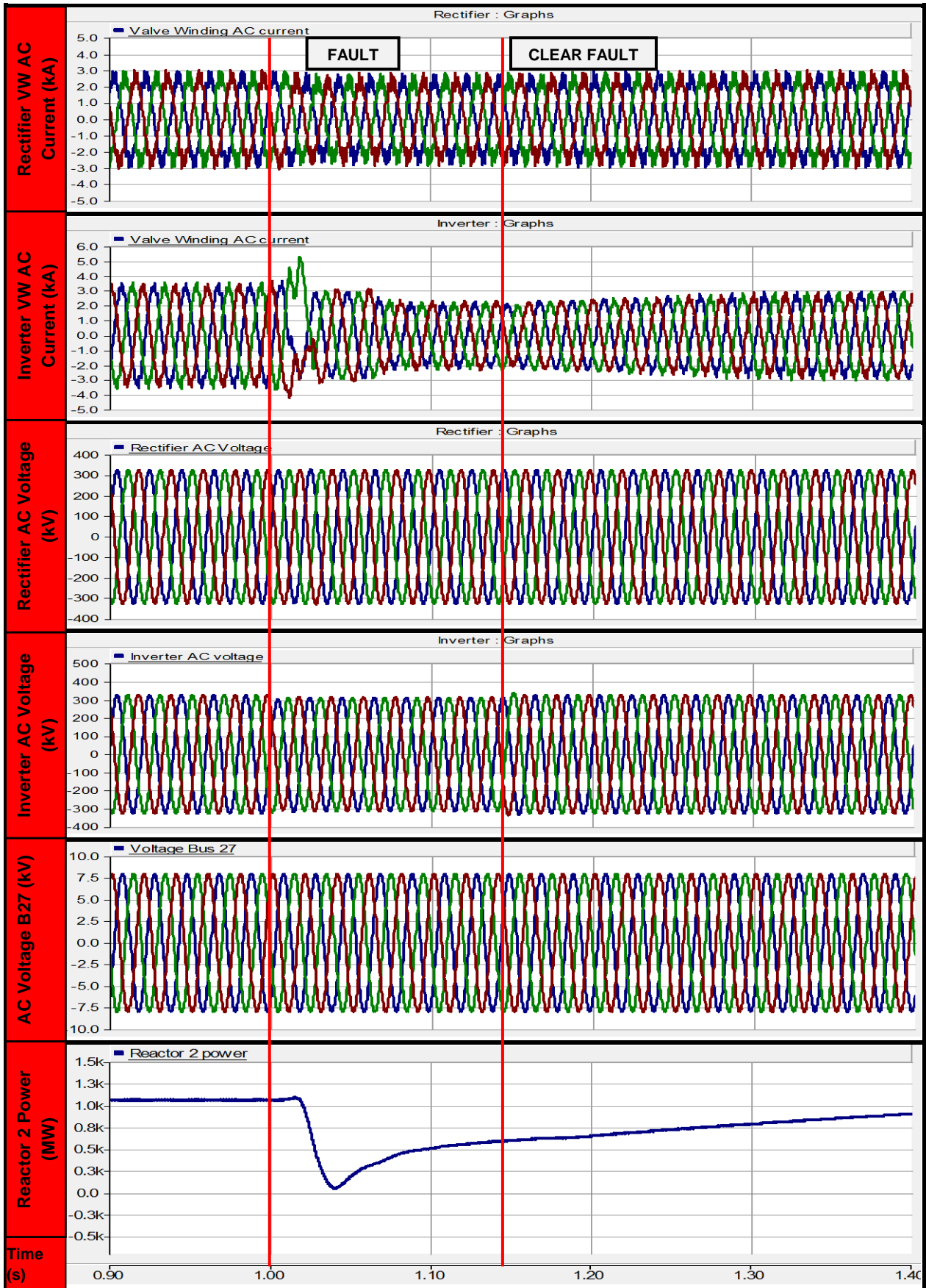


Figure 76: AC profiles for three-phase fault on busbar 4

In Figure 76, none of the AC voltage profiles are affected by the three-phase fault on busbar 4, due to the firewall capability of the CSC-HVDC link [156]. The strong ESCR at the inverter provides the commutation voltage required for successful operation and the AC voltage profile of busbar 27 is stable, ensuring the integrity of power supplies to the nuclear reactor cooling motors through non-protection operation [103]. At the inverter, a brief current spike of 5 kA magnitude is observed due to the sudden interruption in operation caused by the three-phase fault. This recovers within 20 ms once firing angle control has been re-established by the DC control system. The output power of the nuclear reactor generator is reduced due to the sudden load rejection in the system and governor control restores the output power to nominal value 100 ms post fault and allows fault ride-through capability to be achieved.

In summary, the fault ride-through capability of the CSC-HVDC link for a three-phase fault within the AC grid is successfully demonstrated. Firing angle control within the DC link is adjusted to suit the changes in system state and control the DC currents and voltages, and the AC voltage profiles within the NPP are unaffected due to the firewall capability of the CSC-HVDC link which preserves the security of reactor station 2 and prevents the integrity of power supplies to the reactor cooling systems from being compromised [102]. The strong ESCR at the inverter prevents commutation failure and ensures that the operational stability of the CSC-HVDC link is maintained following successful fault clearance. The nuclear reactor is able to ride through the fault via appropriate governor control and stable operation post fault is ensured.

4.4.2.4 DC pole-to-ground fault

In Figure 77, a permanent pole-to-ground fault occurs on the CSC-HVDC link without protection clearance to show the resultant effects if not cleared. The DC voltage collapses to zero at both the rectifier and inverter. The DC fault is detected by the control system and the rectifier firing is temporarily forced beyond 100° into inverter operation to discharge and reduce the fault current to zero [41]. The DC voltage at the inverter becomes negative, where the energy stored in the DC cable is also discharged into to the AC network in an attempt to extinguish the fault current at the next zero crossing [155]. The VDCOL at both ends of the HVDC link becomes active, and the firing angles at both the rectifier and inverter are held at 90° to prevent any further inadvertent control actions which may further exacerbate the situation [156].

The current controller at the rectifier clamps the DC current as it continues to feed the pole-to-ground fault. The commutation failure causes large oscillations in DC current at the inverter with magnitudes in excess of 8 pu present. In reality this would cause damage to equipment and may cause further instability within the NPP and AC grid [19].

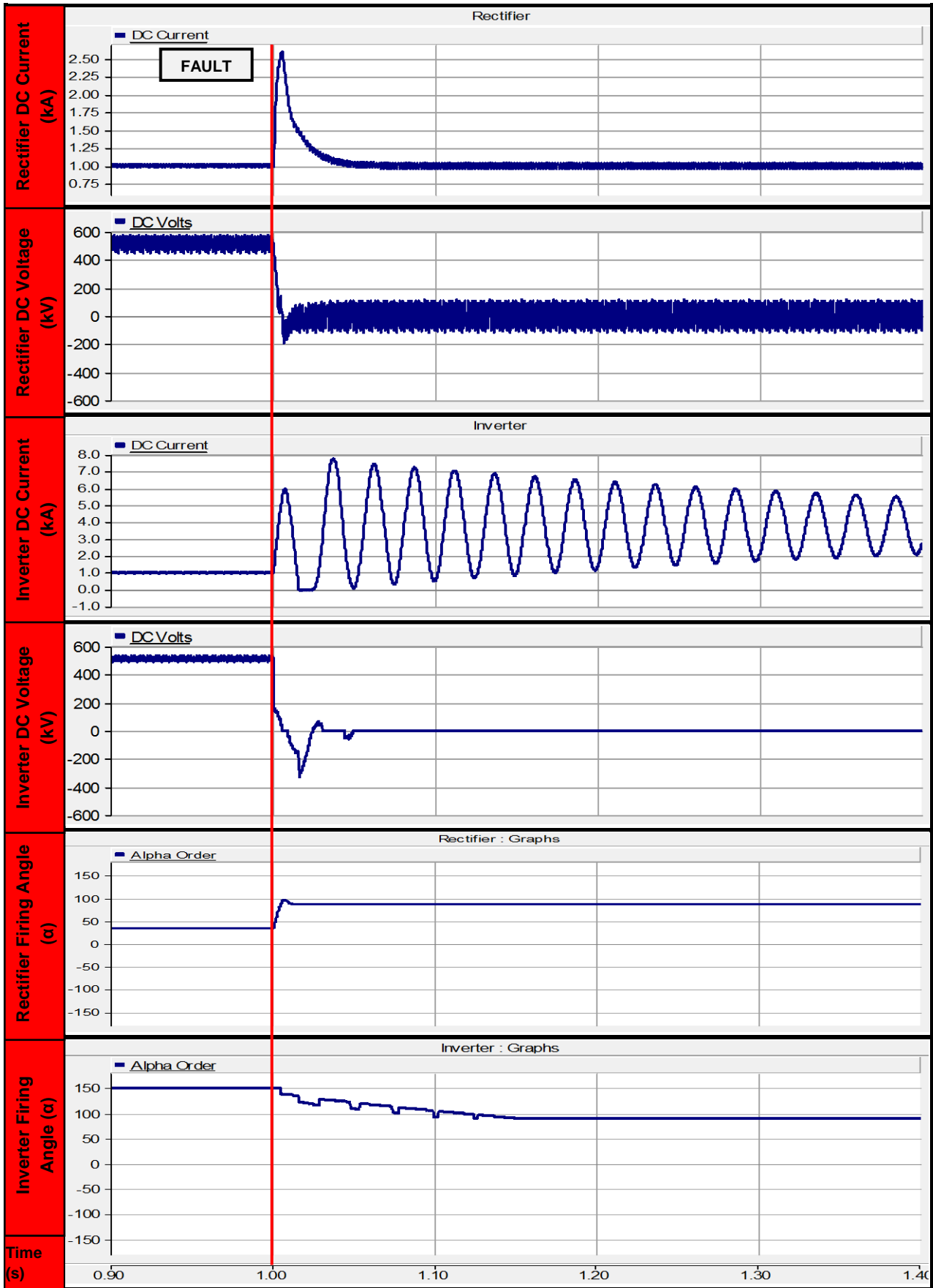


Figure 77: DC profiles for permanent pole-to-ground fault

The AC voltage profiles are shown in Figure 78.

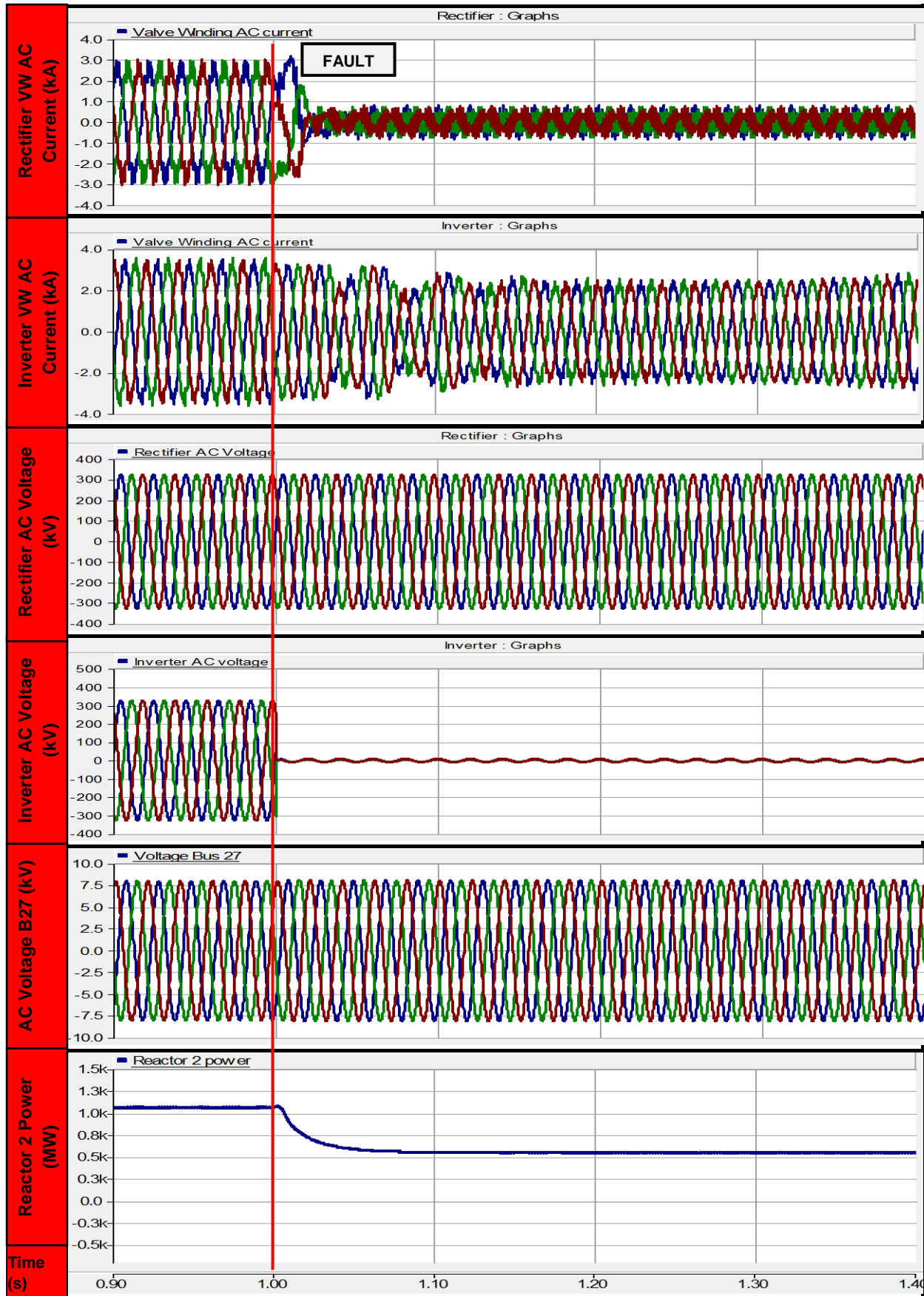


Figure 78: AC profiles for permanent pole-to-ground fault

In Figure 78, the AC voltage at the inverter has collapsed due to commutation failure caused by the DC fault. The AC voltages at both the rectifier and busbar 27 have been unaffected due to reactor generator 2 remaining online and supporting reactive power within the vicinity [102].

With active power transfer through the link ceasing, the valve winding currents are also reduced but continue to feed the uncleared DC fault. The active power output of reactor 2 generator has decreased due to the bottleneck but continues to feed the fault and maintains power supplies to the cooling motors. This at first may seem advantageous due to the reactor cooling motors still being operational but an uncleared DC fault can be of major detriment to primary and secondary systems and may compromise the security of the NPP [102], [103].

This analysis shows that a permanent single-pole-to-ground fault can cause considerable disruption to the CSC-HVDC link and NPP. Commutation failure may occur at the inverter with a complete collapse in DC voltages at both ends of the CSC-HVDC link. Considerable oscillations in DC current with magnitudes in excess of 8 pu are observed. In reality, the combination of these would damage equipment and could lead to further system instability within the NPP and AC system [103]. The output power of the reactor is reduced, but it continues to supply the reactor cooling motors. In practice, this prevents a scram of the reactor during the islanding of the NPP from the AC grid but, if the DC protection and control system does not clear the fault as fast as possible, then system instability and equipment damage could occur [102].

4.4.2.5 DC pole-to-pole fault

A permanent DC pole-to-pole fault was applied on the CSC-HVDC link and was not cleared (no protection operation) to analyse the effects on both the NPP and AC grid.

In Figure 79, the DC voltage profiles at both the rectifier and inverter have collapsed due to complete commutation failure in all of the converter valves. The firing angle at the rectifier is forced beyond 90° to act as a temporary inverter for discharging the DC fault current. Following the discharging of the DC current, the firing control orders the angle to remain at 90° so that no further inadvertent actions compromise the current state of the system [156]. Due to the absence of protective action, a constant DC current is supplied to the fault.

The VDCOL at the inverter becomes active and reduces the firing angle in order to limit the DC current and reduce the impact on the power system. A DC current spike appears the rectifier due to the sudden load rejection caused by the fault but is limited to 2.5 pu. A large harmonic content can be observed in the DC voltage profiles cause by the commutation failure [41].

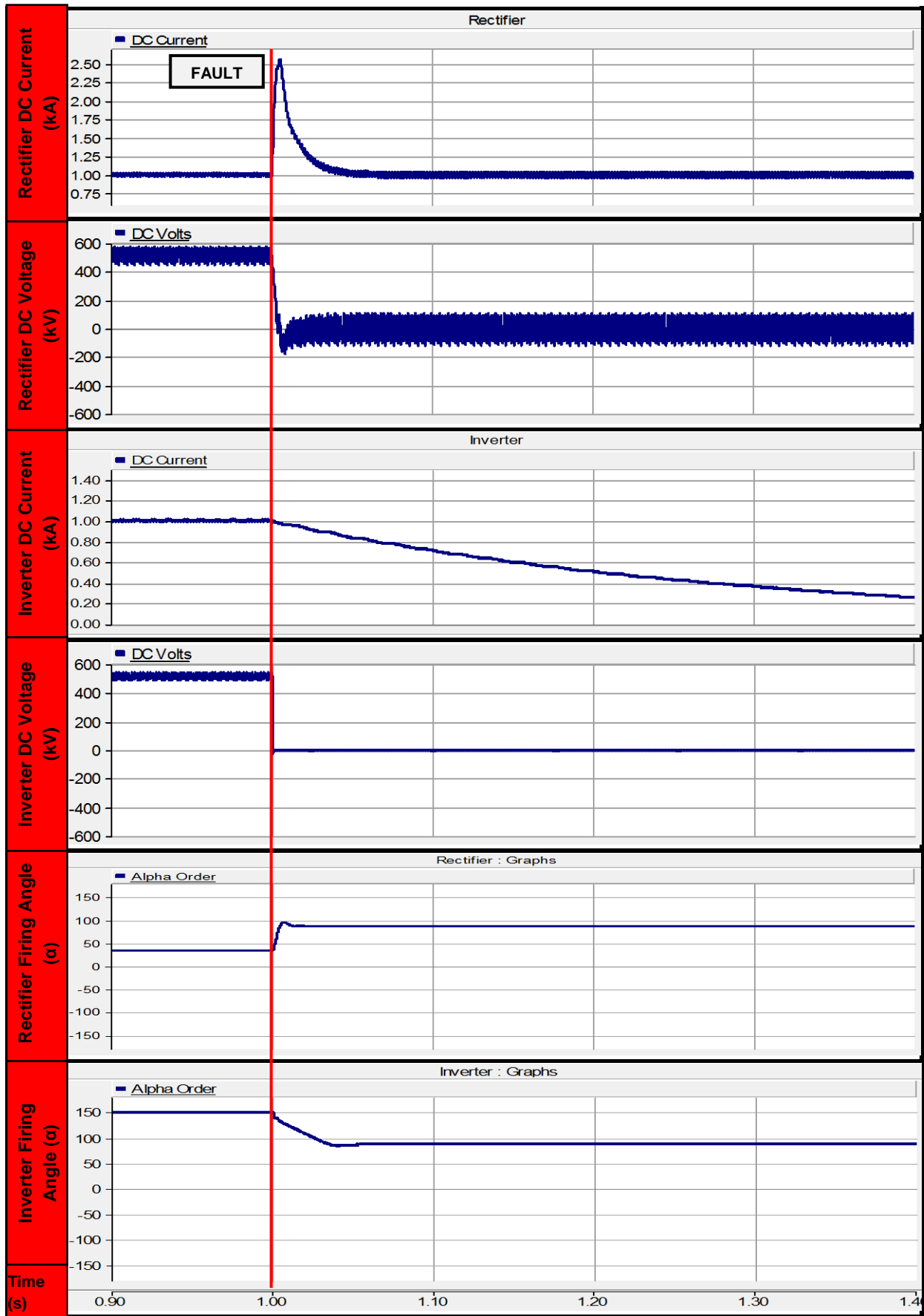


Figure 79: DC profiles for a permanent DC pole-to-pole fault

The AC profiles are shown in Figure 80.

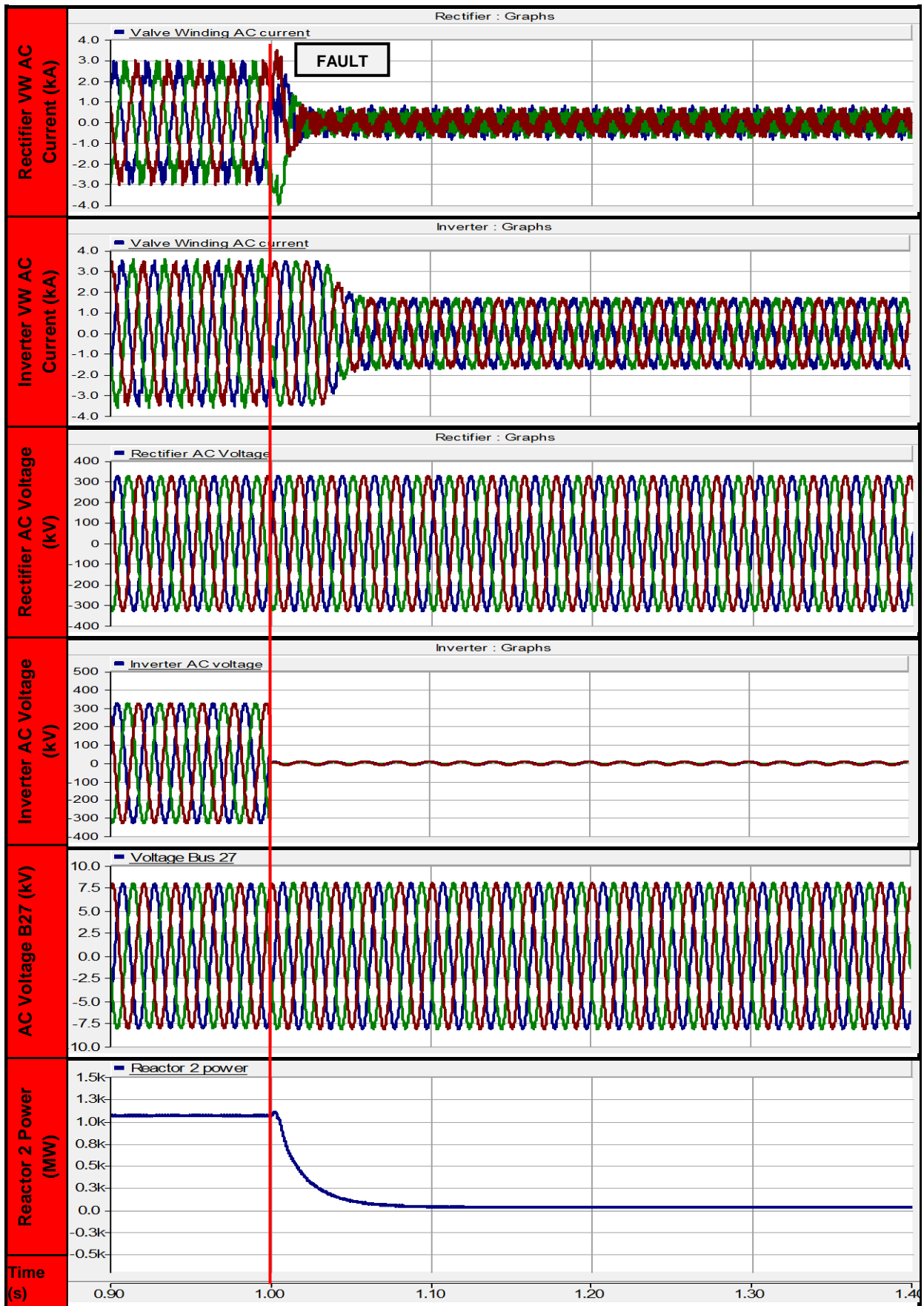


Figure 80: AC profiles for a permanent DC pole-to-pole fault

The results in Figure 80 are very similar to the DC profiles: commutation failure occurs at the inverter, the AC voltage has collapsed and the valve winding current is reduced but continues to feed the DC fault. The AC voltage profiles at both the rectifier and busbar 27 are unaffected due to the voltage source supplied by reactor 2 station generator [103]. In practice this preserves the integrity of the reactor cooling motor power supplies and prevents any undervoltage protections from operating. However, due to the DC fault not being cleared further detriment to the system will occur in the long term [3].

The active power output of the nuclear reactor generator is reduced due to the bottleneck created through the CSC-HVDC link to the AC grid. The governor control ensures power is supplied to the reactor cooling motors during the fault.

A permanent DC pole-to-pole fault is shown to have a profound effect on the operation of the CSC-HVDC link; collapsing the DC voltages at both ends of the CSC-HVDC resulting in permanent commutation failure. The HVDC control system adjusts the firing angles to prevent further instability from occurring but 100% power transmission to the AC grid has halted. The VDCOL helps to reduce the current at the inverter during the disturbance to aid recovery but without any protective action it makes little difference to the situation. The NPP is islanded but the reactor continues to supply power to the cooling motors for safe operation. The voltage profiles at the rectifier and within the NPP are unaffected, but in reality the HVDC protection and control systems will need to clear the fault to prevent further instability within the NPP and AC system [102], [103].

4.4.3 CSC-HVDC contingency analysis

In the following section, three system contingencies within the AC network and NPP are created to analyse the response of the HVDC control system. The analysis aims to determine whether the HVDC controls can be of benefit to the NPP or AC network during the contingency. Specifically, the studies examine the suitability of the CSC-HVDC link to supply power to the NPP and evaluate the effectiveness of the active power modulation function.

4.4.3.1 CSC-HVDC contingency 1

In this particular contingency the CSC-HVDC link is supplying power to the NPP from the AC grid through a change in DC voltage polarity. Reactor generator 2 is in service with no power being generated but it is supplying the commutation voltage needed by the inverter for operation. At a time of 1.0 sec, the reactor generator is scrambled due to human error. The DC link still needs to supply power to the reactor cooling motors from the AC grid to prevent an emergency situation from occurring. The results of the simulations are shown in Figures 81 and 82.

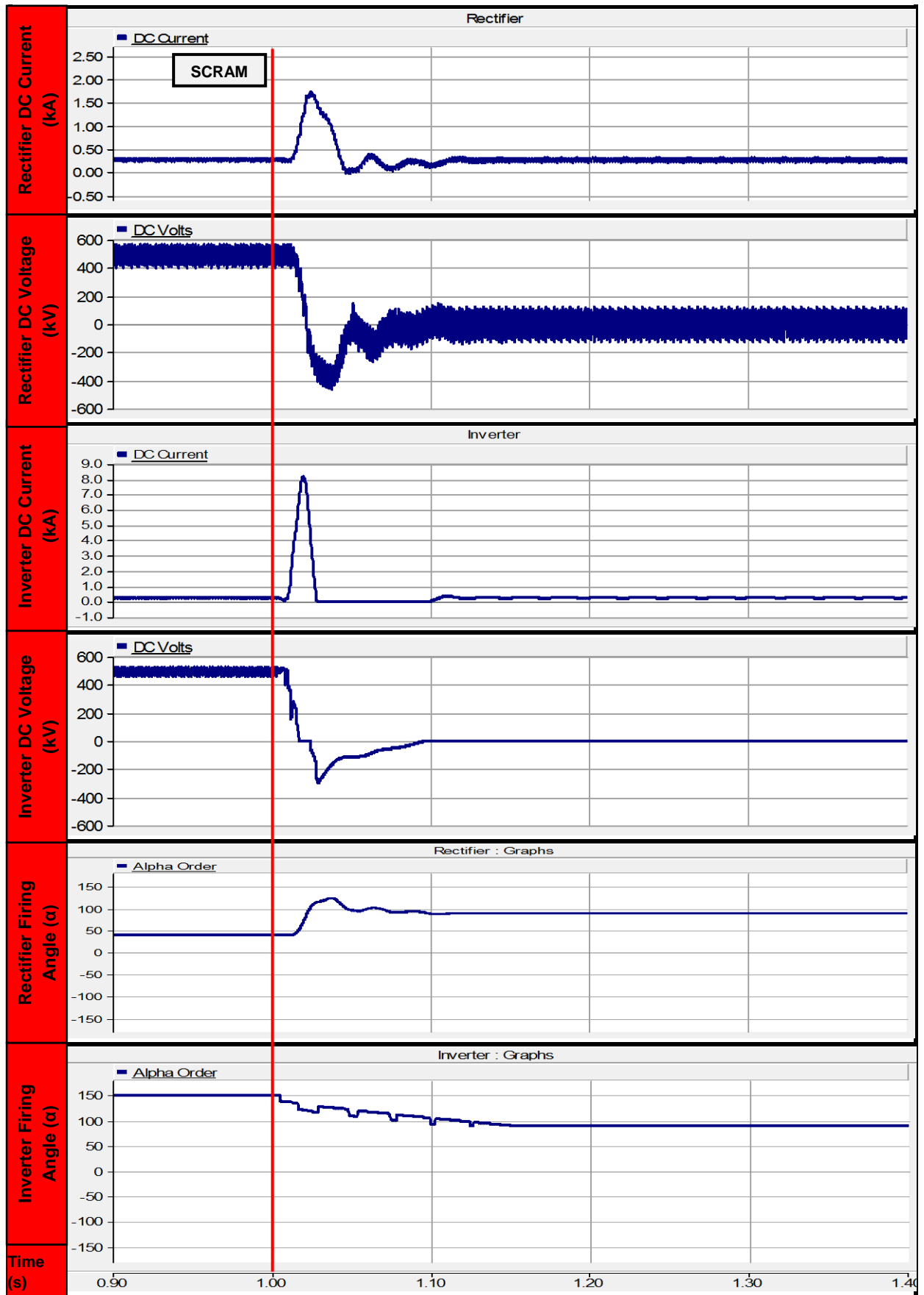


Figure 81: DC profiles for contingency 1

In Figure 81, a permanent commutation failure at the inverter and rectifier occurs when the reactor generator is tripped; the DC voltages at both the rectifier and inverter collapse and large spikes in the current are observed due to the sudden load rejection.

The firing angle at the rectifier is increased (forced inversion) to discharge and help reduce the fault current. The VDCOL is activated at the inverter and the firing angle is reduced in an attempt to help the system recover and alleviate the instability. DC current still flows into the fault from the HVDC link due to no converter blocking and the lack of opening of the AC pole circuit breakers.

The level of DC harmonic content is vastly increased during the commutation failure; this has the potential to cause severe overheating and equipment stress to both the HVDC link and NPP [41].

In Figure 82, the AC voltage at the inverter collapses due to permanent commutation failure. The Root Mean Square (RMS) voltage on busbar 27 drops by 50%. In industry, such a voltage depression has the potential to cause the operation of undervoltage protections on the reactor cooling motors; these would remove the affected motors from service, which would affect the cooling supplies to the nuclear reactor [103], leaving the NPP in a serious situation requiring a switch over to backup diesel generators, batteries or gas turbines in order to power the reactor cooling and emergency safety systems.

The valve winding currents reduce, but continue to feed the fault within the NPP. The rectifier AC voltage is unaffected due to the strong ESCR within the AC grid and the active power output of the reactor is zero due to the scram.

This scenario highlights the risk when a CSC-HVDC link is used to supply power to an NPP when only one voltage source is available for valve commutation. If only a single reactor generator is available and trips, then a commutation failure will occur, high DC currents will appear, and a complete collapse in DC voltages will be experienced. The HVDC firing controls will respond to alleviate this situation, but if protective actions are not initiated straight away, then system instability could occur and equipment may become permanently damaged, a large load rejection will be created, and the NPP will be islanded from the AC network. An emergency switch over to alternate power supplies such as diesel generators or batteries will be required to maintain power supplies to the reactor safety systems [103].

In order to aid the above situation, a STATCOM (Static Compensator) or synchronous condenser is recommended in order to provide the commutation voltage required for successful operation. Failing this, more generators and an NPP with a stronger ESCR will be needed. Based upon the above results a CSC-HVDC NPP should be operated in normal mode where active power only flows to the AC grid from the NPP.

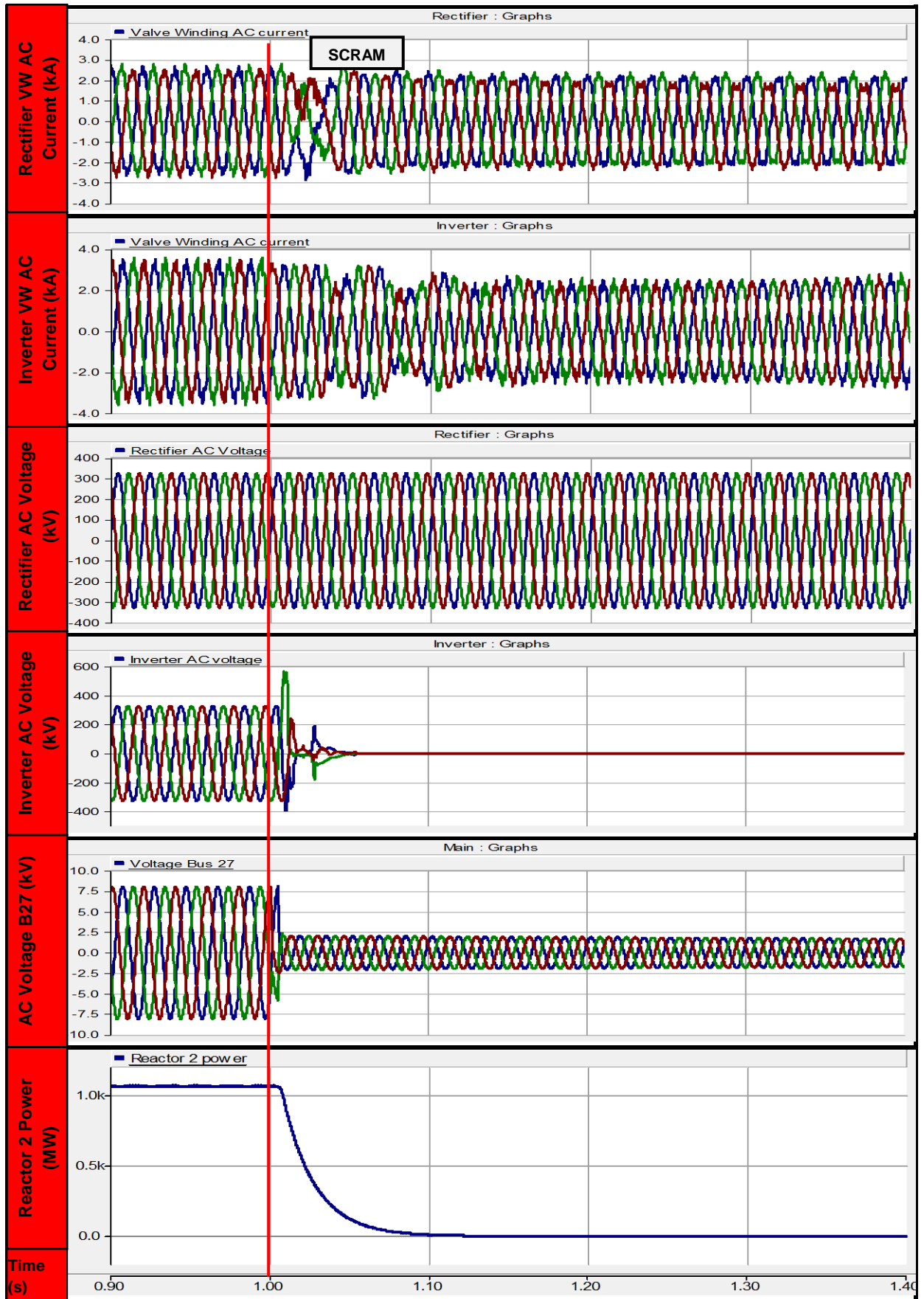


Figure 82: AC profiles for contingency 1

Power should not under any circumstances be supplied to the NPP unless the ESCR is very high and FACTS devices are used to provide backup commutation voltage needed for secure operation.

4.4.3.2 CSC-HVDC contingency 2

In contingency 2 the CSC-HVDC link is supplying power to the AC grid. At a time of 1.0 sec the inverter AC circuit breaker trips due to a local fault within the AC grid. The rectifier end is unaffected and remains in service. Following the trip of the inverter, an analysis is undertaken to study the effects of the inverter trip and load rejection encountered on both the NPP and AC grid.

In Figure 83, once the inverter has tripped the DC voltage profiles at both ends of the CSC-HVDC link increase to over 600 kV. The inverter experiences the largest voltage rise, and oscillations in the DC voltage can be observed. Following the trip of the inverter circuit breaker the AC filters are still in service and contribute maximum reactive power to the converter. The load rejection causes a cessation in active power transmission and a resultant overvoltage occurs [157].

The CSC-HVDC firing controls reduce both angles at the rectifier and inverter to reduce the current (VCDOL) and help alleviate the situation. Once the current has been reduced, the firing angle at the rectifier settles to prevent any further inadvertent operation.

To alleviate the overvoltage, the AC filters at both ends of the CSC-HVDC link are tripped by their protective systems 100 ms after occurrence. During the inverter trips, a large spike in the DC currents is observed which the rectifier control responds to by forcing the firing angle past 90° to discharge the DC current and reduce the current spikes.

The DC voltage becomes negative and is returned to the AC system during the forced inversion process [41]. Following the removal of the AC filters, the reactor is scrambled 30 ms after the event due to voltage instability [103]. Following this the rectifier reduces its firing angle to ramp the DC current down to prevent any further instability from occurring.

System oscillations are present during the disturbance and have the potential to cause damage to both the NPP and AC grid [102]. Large DC harmonic content is present within the DC voltage profiles as a direct consequence of the disturbances encountered.

Active power transmission through the CSC-HVDC link has stopped and the NPP is now in an islanded situation where emergency backup power supplies are needed to power the reactor safety systems.

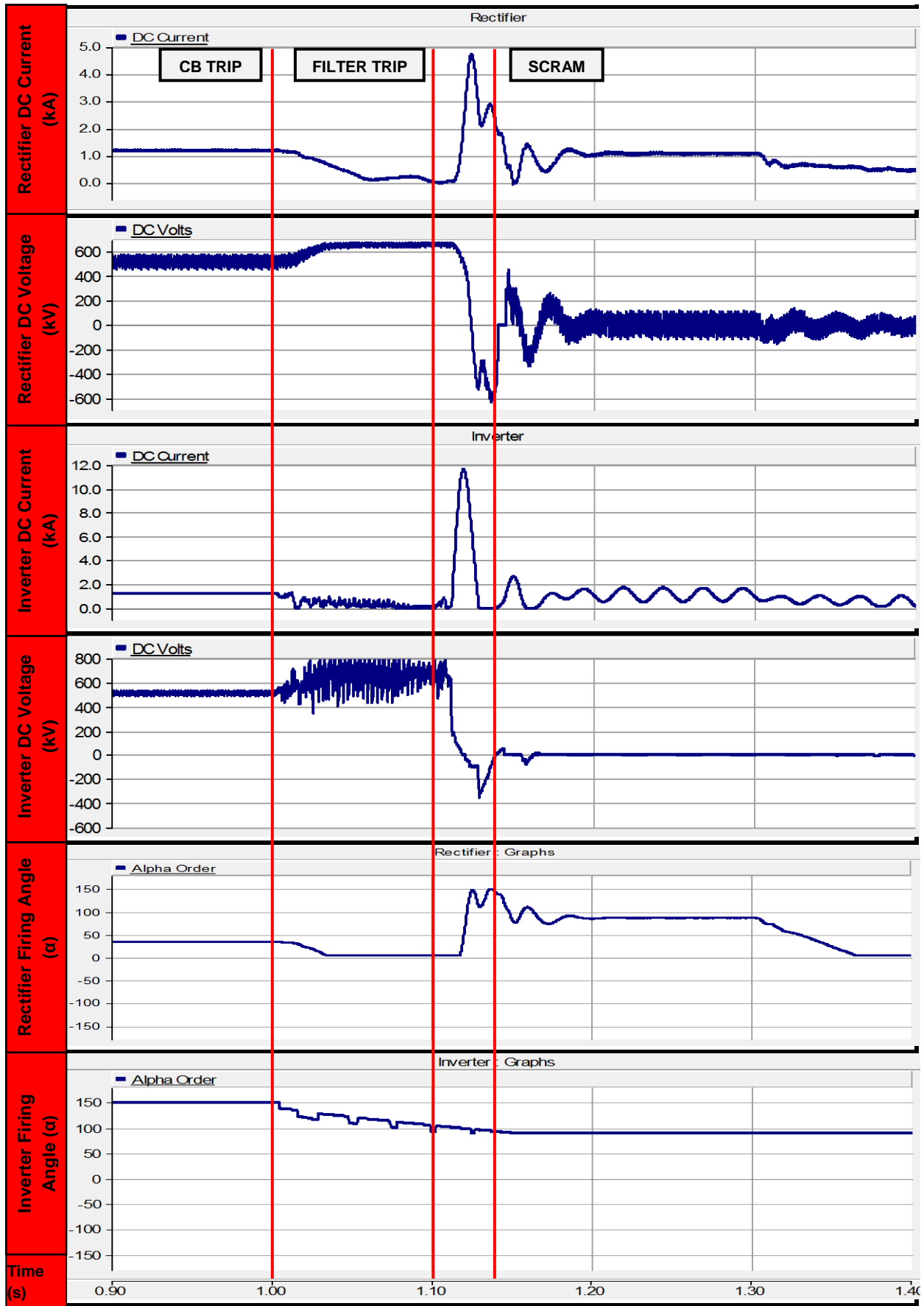


Figure 83: DC profiles for CSC-HVDC contingency 2

The AC profiles are shown in Figure 84.

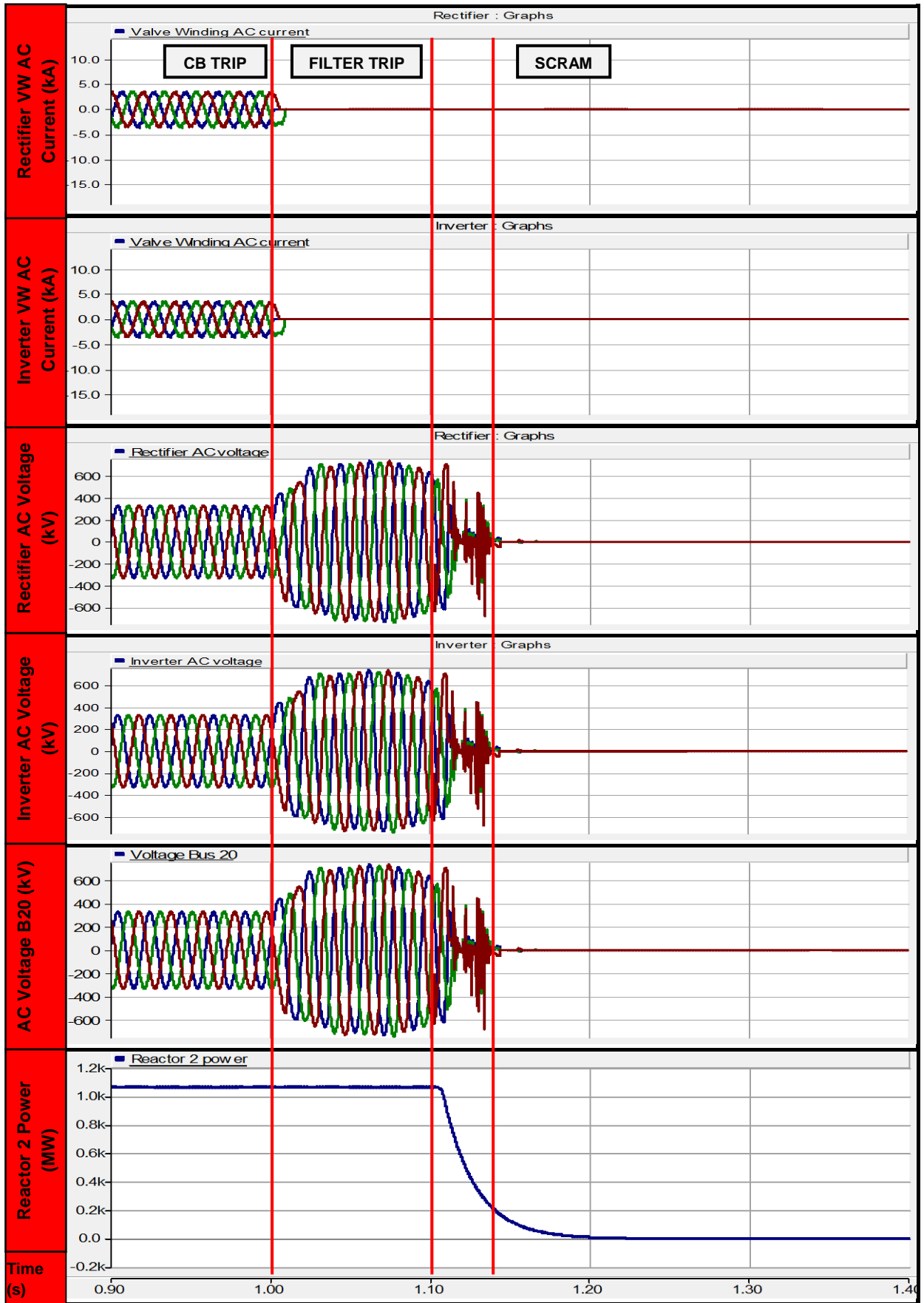


Figure 84: AC profiles for CSC-HVDC contingency 2

In Figure 84, large AC overvoltages at both the rectifier and inverter can be observed. The rms values reach over 600 kV and could seriously damage equipment if the filters are not tripped by the protection [25]. The governor control automatically reduces the active power output of the reactor following the detection of zero AC voltage following the filter trip and the reactor scram causes the active power to reduce to zero.

In summary, during contingency 2, the trip of the inverter AC circuit breaker causes large rises in both the DC and AC voltage profiles at both ends of the CSC-HVDC link. With the AC filters supplying the full reactive power demand of the converter station, the corresponding AC pole circuit breakers must be tripped by protective action to alleviate the situation. With this the sudden load rejection, the power flow through the CSC-HVDC link becomes unbalanced and the HVDC controls system adjust the rectifier and inverter firing angles to aid system recovery. Following tripping of the AC filters, the reactor may scram due to zero voltage detection and system instability. For the above system, in industry practice, a switch over to backup power supplies will be needed to keep the reactor cooling systems active and prevent possible overheating of the core [106].

4.4.3.3 CSC-HVDC contingency 3

In Figure 86, a single generator (G4) and the four AC circuits shown are out of service due to either maintenance or fault reasons. The NPP is operating at full output power and generation matches system load, resulting in a stable power system. A fault occurs on generator G3 which causes the protection to trip its own AC circuit breaker and the other two AC feeder circuits between busbar 3 and busbar 4 (T6C1 and T6C2). Nuclear reactor station 2 is now supplying surplus generation to the load on busbar 3. There is a sudden 500 MW mismatch between generation and load until auto-reclosure of the feeder circuits T6C1 and T6C2 is accomplished and generation matches the load to retain system equilibrium.

In this contingency, the effectiveness of the HVDC active power modulation control is analysed to ascertain any benefits this could offer to the NPP and AC grid during the disturbance.

Following the mismatch between generation and load, the frequency measured on busbar 20 within the NPP is shown in Figure 86. Large oscillations occur and the frequency fluctuates violently. Despite the auto-reclosure of the AC feeder circuits following successful fault clearance, the frequency has become unstable and the power system enters instability with unsuccessful recovery.

In practice this condition would normally result in a reactor scram to prevent any further degradation to the NPP and preserve the integrity of the power supplies to the reactor cooling system [102], [106].

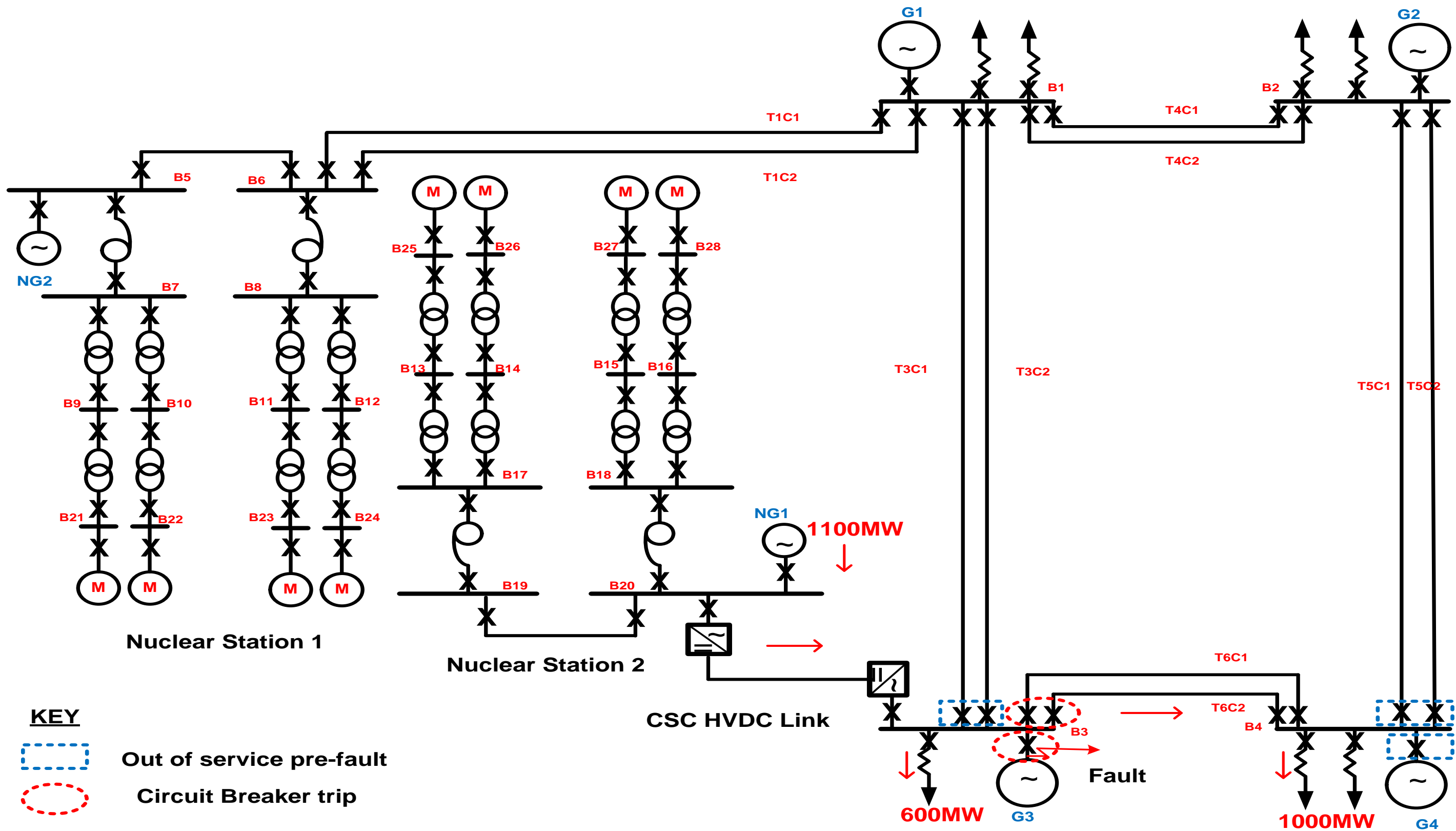


Figure 85: Power system state for contingency 3

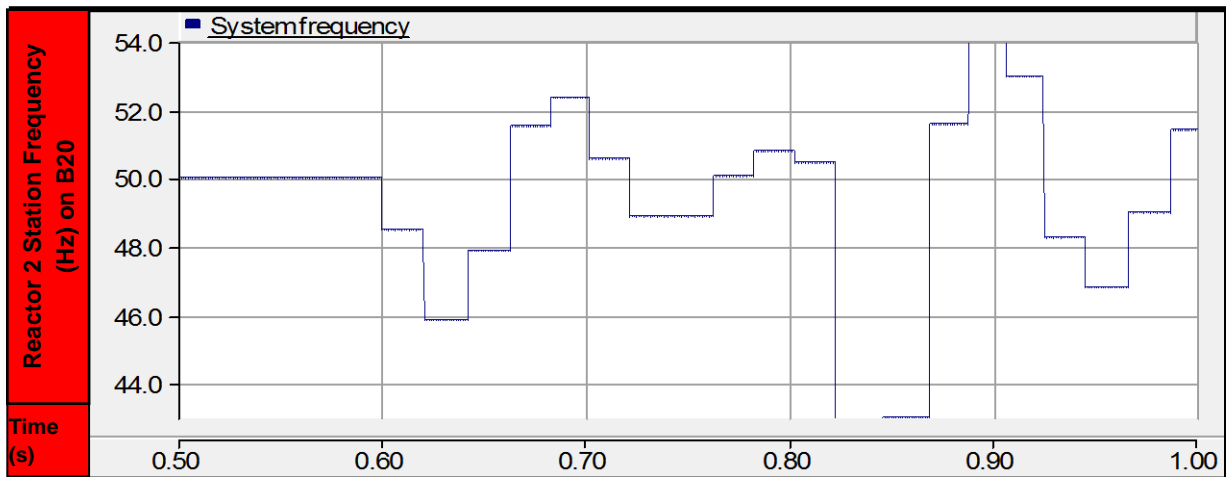


Figure 86: Measured frequency on busbar 20 reactor station 2 with no DC control action

In Figure 86, the frequency has exceeded the normal 48 Hz limit imposed on some NPP stations for safe operation and as a direct consequence the nuclear reactor will be scrambled [106].

The same scenario is repeated but with DC control action initiated. In Figure 87, at a time of 0.6 secs, the fault on generator G3 occurs and trips the AC circuit breaker to clear the fault. As soon as the rise in frequency within the NPP is detected, at 0.8, secs the CSC-HVDC control system performs an active power runback. As soon as the runback is activated the DC current profiles drop to 50% and hence the active power is also reduced. The DC voltage profiles experience a small dip following the runback activation, but maintain a steady value during the process. The firing angle controls at both the rectifier and inverter are adjusted to accommodate the required runback order of 500 MW.

Approximately 70 ms after occurrence, the generator fault has been cleared and the autoreclose protection of the AC feeder circuits T6C1 and T6C2 is achieved; the load now matches the generation. The active power runback is deactivated at time of 1.28 secs and is immediately ramped back to the pre-fault value of 1100 MW to ensure the frequency within reactor station 2 is restored. This is achieved within 10 ms of the deactivation order being given.

In industry, the rise in frequency may cause the overfrequency protection on the reactor 2 system to operate and initiate a tripping action [103], which could result in a reactor scram and backup power supplies being called upon to keep the safety systems powered up to allow sufficient cooling to take place. This rise in frequency would also have a direct impact on the motors and pumps within the NPP, resulting in excess current being drawn and possible stall [102].

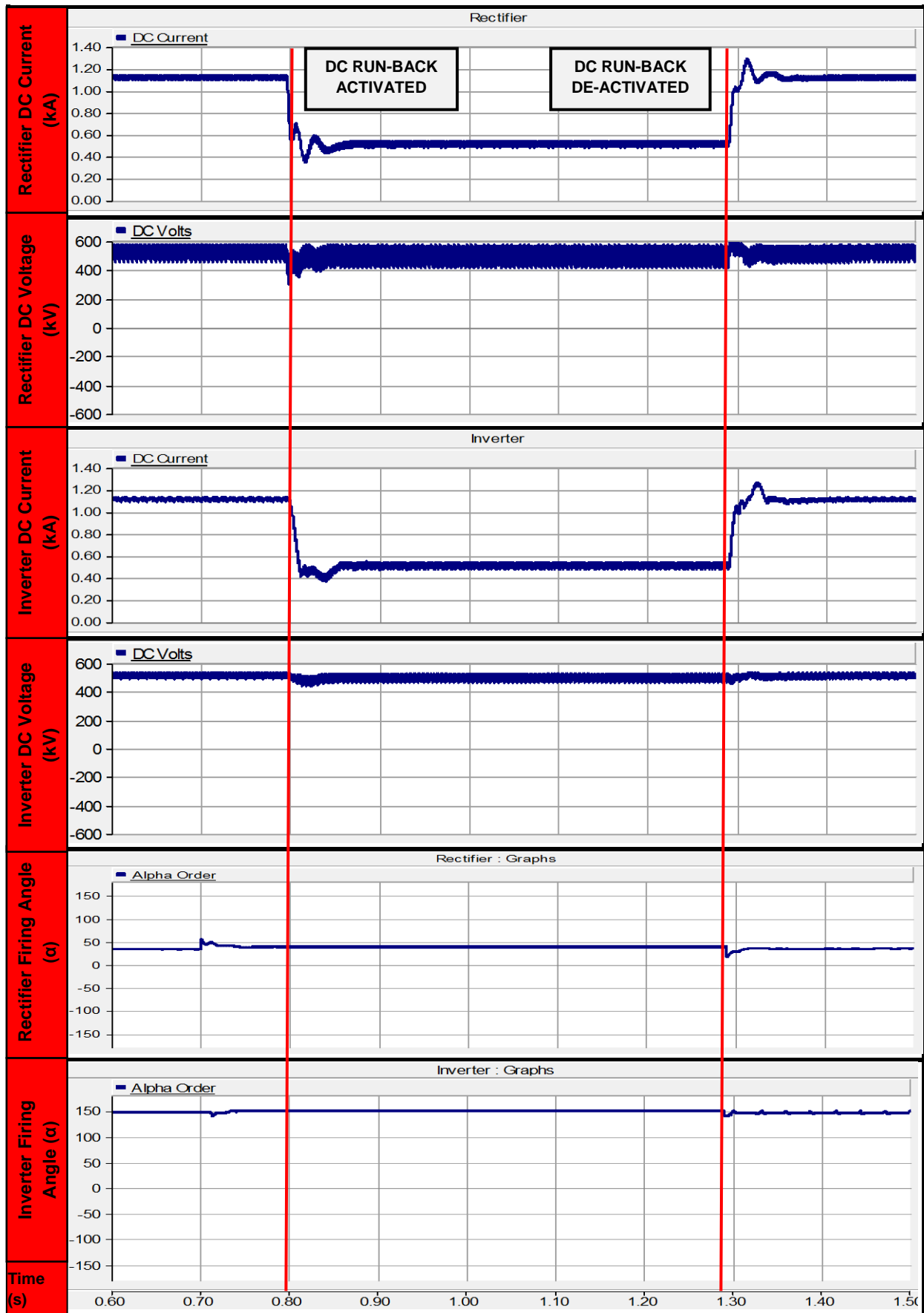


Figure 87: DC profiles for contingency 3 with active power runback activated

The post-fault frequency in reactor station 2 following the active power runback is shown in Figure 88.

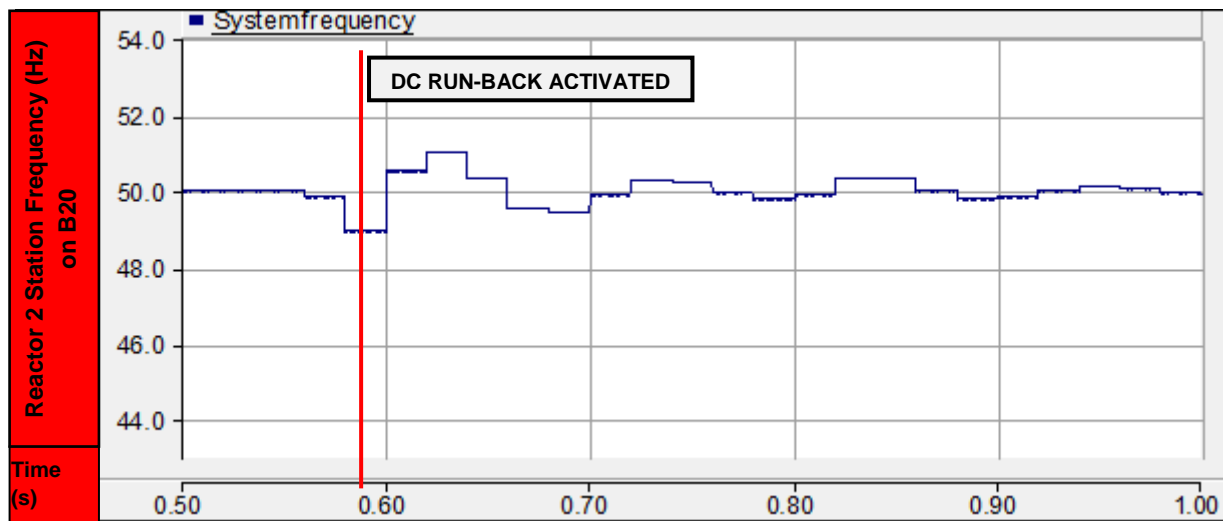


Figure 88: Post-fault frequency profile in reactor 2 station

Small oscillations are still present within the frequency profile of reactor station 2. Despite this the majority of oscillations are damped out and the frequency is restored to within the nominal operating range of $\pm 1\%$. In practice, a more detailed and accurate frequency controller with customised modulation control loops may damp out the full range of oscillations.

This contingency analysis has analysed the effectiveness of the fast DC active power modulation control of CSC-HVDC technology and shown that a fast DC active power runback can help to restore the frequency within the NPP and damp out oscillations which could otherwise damage equipment and cause system instability [103]. In practice, with a detailed frequency controller and customised modulation control loops, the response achieved becomes more prominent. The speed of response and active power ramp rates are determined by the ESCR of the power system and the preloading of the CSC-HVDC link [41].

4.5 Chapter 4 summary

In chapter 4 the unproven method of connecting a modern NPP to the NETS via CSC-HVDC technology has been analysed. From the analysis carried out the following findings have been made:

- *For a low ESCR at the NPP connection, the performance of the CSC-HVDC link under fault conditions can be affected and active power transfer capability is limited.*
- *Failure to clear DC faults puts the operation of the CSC-HVDC link at risk and may cause instability to both the NPP and AC system.*

- *For distant faults further in the AC system, CSC-HVDC technology is able to provide fault ride-through capability and a firewall function to the NPP, shielding it from the effects.*
- *The fast DC active power modulation capability of CSC-HVDC technology can be used to damp oscillations and provide frequency response under a situation where generation and system load do not match.*

If a CSC-HVDC link is considered for an NPP connection, then the following recommendations are made:

- *Further analysis is required to study the effects of installing a STATCOM or synchronous condenser for a weak NPP connection; these devices have the potential to increase the ESCR and could improve the performance of the CSC-HVDC link [150].*
- *A CSC-HVDC link should not be used to supply power to the NPP if the ESCR at the PCC is weak, otherwise the security of the NPP may be compromised through possible commutation failure.*
- *Extra circuit connections from the NPP to the AC grid are recommended to provide additional redundancy to alleviate active power bottlenecks during commutation failure of the CSC-HVDC link and prevent islanding of the NPP.*

From a technical perspective, the author recommends not adopting CSC-HVDC for such a critical application. If CSC-HVDC technology is considered for NPP connections, then the above technical requirements must be considered and studied in further detail when evaluating a first-time and unproven technical solution.

Chapter 5 analyses the impact of connecting an NPP by VSC-HVDC technology.

Chapter 5: Connecting NPPs by VSC-HVDC Technology

This chapter provides a technical assessment of connecting an NPP to a power system by Voltage Source Converter (VSC) HVDC technology. Detailed descriptions of the VSC-HVDC model and individual components used in PSCAD are covered and the impact of changing the AC system Short Circuit Ratio (SCR) on VSC-HVDC operation is analysed through simulation. The impact of AC and DC system faults on both the NPP and VSC-HVDC link are studied through power system simulations carried out in PSCAD and contingency analysis is used to study the benefits of the high-level VSC-HVDC controls for frequency control and active power modulation.

5.1 Introduction

Chapter 4 provided a technical analysis of connecting an NPP to an AC power system by CSC-HVDC technology. VSC-HVDC technology is now becoming the preferred choice for connecting new forms of generation to the AC grid, interconnecting different countries, and providing power supplies to offshore gas locations, just to name a few of its applications [5].

In this chapter, the evolving VSC-HVDC technology will be studied for an NPP connection. For the application of connecting an NPP to the AC grid, just like CSC-HVDC technology, this is also unproven and presents a technological risk to any project [1]. However, for new NPPs, this technology is being considered as part of the technology assessment process for projects in [1] and [2]. It is extremely important to gain an understanding of the key technical issues with VSC-HVDC technology for an NPP connection. A similar analysis to that which was carried out in chapter 4 with CSC-HVDC technology will be performed in this chapter to assess the impact on VSC-HVDC operation of changing the AC network SCR during steady-state conditions. This is an important factor that is vital to understand from a system operation perspective [158], along with the response of the VSC-HVDC controls to both AC and DC faults [159].

5.2 Modelling of an NPP connected by VSC-HVDC technology

In the following section, each of the key components that make up the VSC-HVDC model used in PSCAD is described and, where applicable, mathematical analysis of the models and control systems is presented.

5.2.1 VSC-HVDC converter bridge model

The six-pulse converter bridge makes up one pole of the VSC-HVDC link used in PSCAD. Two of these can be connected in series to form a bipole solution.

The six-pulse converter bridge used in PSCAD is shown in Figure 89.

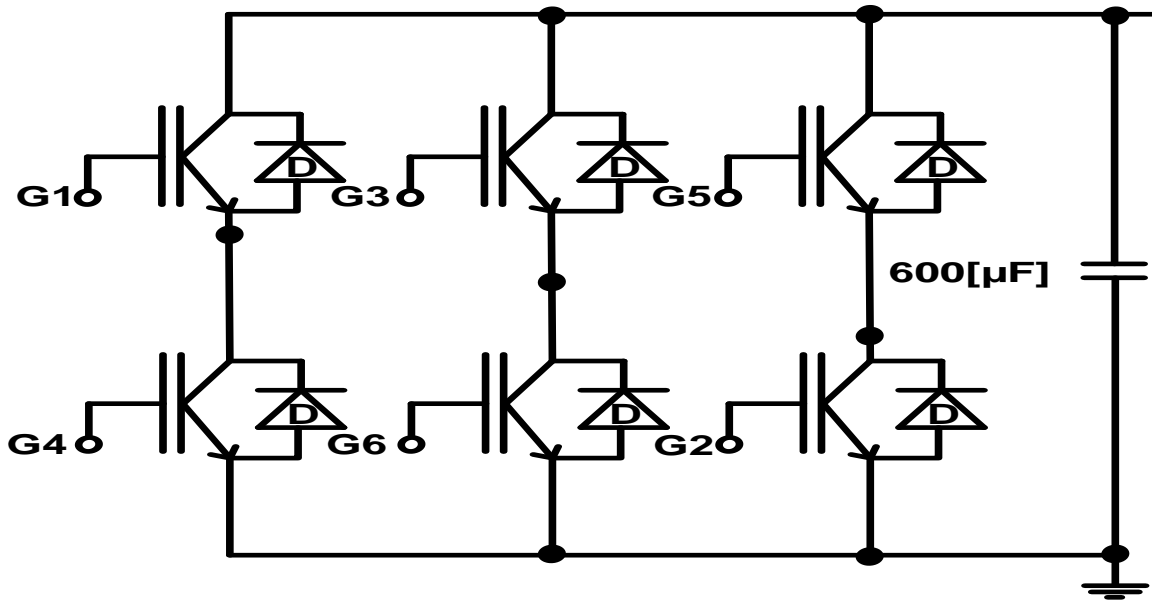


Figure 89: VSC-HVDC six-pulse Converter Bridge used in PSCAD

Here, six Insulated Gate Bipolar Transistors (IGBTs) with associated anti-parallel diodes make up the six-pulse converter bridge. Two of these are connected together to form a bipole link as shown in Figure 94. Compared to the twelve-pulse CSC-HVDC configuration used in chapter 4, in industry the six-pulse is generally adopted for VSC-HVDC converters due to lower harmonic productions [75]. The Gate Turn-Off (GTO) or IGBT models are essentially the same. They are usually turned on and off by firing pulses supplied to a gate terminal. An external control signal is required to generate the gate firing pulses. The characteristic of the GTO/IGBT are very similar to the thyristor except that the GTO/IGBT can be forced off with a gate pulse of 0, while the device is forward biased. The V-I characteristic for the GTO/IGBT model is shown in Figure 90.

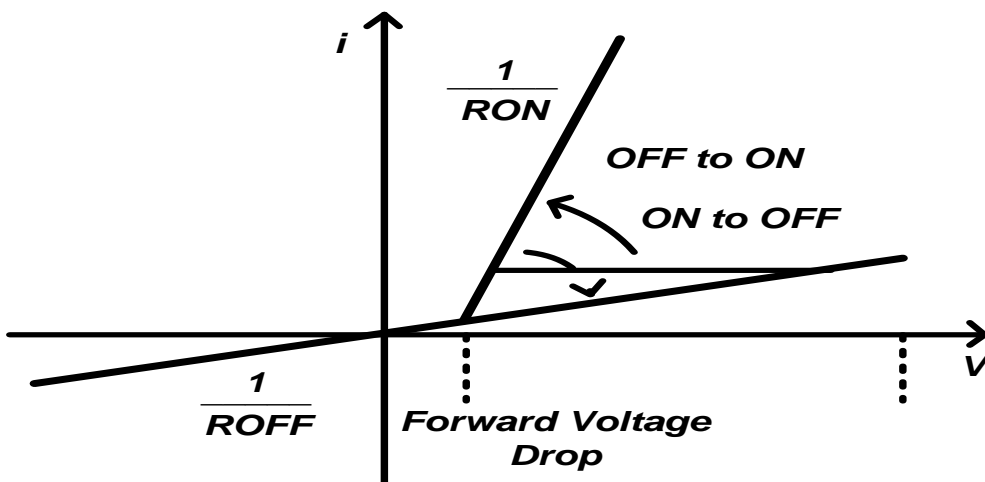


Figure 90: V-I characteristic for the GTO/IGBT model used in PSCAD

The interpolation algorithm is automatically invoked during all naturally commutated on and off events (including forward break-over), to calculate the exact instant of switching. Reverse recovery time (i.e. the time for which a finite reverse current flows in the device, following a turn-off) of the diode is assumed to be zero. If the on resistance is zero, or smaller than the switching threshold value, then the closed state will be modelled as a short circuit.

5.2.2 VSC-HVDC converter transformer model

The analysis of the transformer models carried out in chapter 3 is still valid for the VSC-HVDC interface model used in PSCAD [127]. The converter transformer shown in Figure 91 is rated at 750 MVA per pole and has a voltage rating of 400/230 kV.

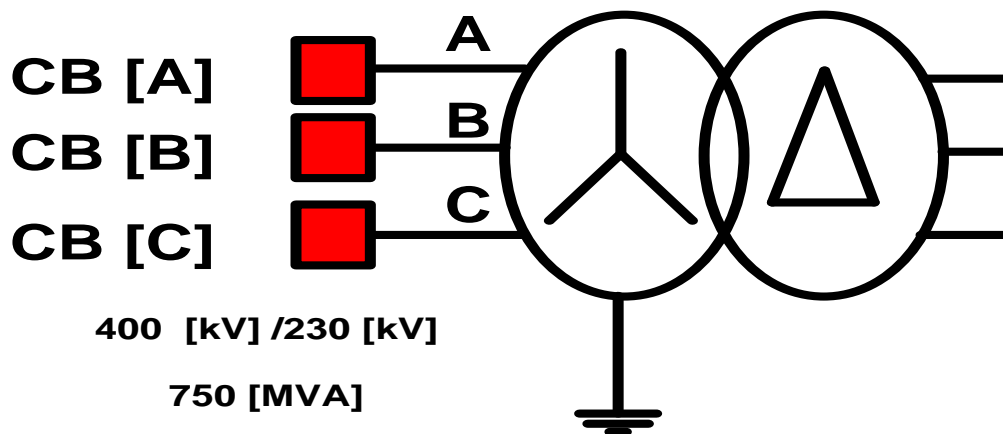


Figure 91: VSC-HVDC converter transformer model used in PSCAD

This component is a single-phase two-winding transformer and is based on the classical modelling approach. This component is the equivalent of three, single-phase, two-winding transformers connected in a three-phase bank. The AC circuit breakers perform the function of breaking high currents during a fault. Due to harmonics, the converter transformers used in bipolar configurations will be subject to 50% of the DC offset voltage and have strict design criteria on the level of DC insulation required [19].

5.2.3 High-pass filter model

The high-pass filter shown in Figure 92 is used to filter out the high switching harmonics produced by the Pulse Width Modulation (PWM) switching of the converter. Despite the ability of the VSC-HVDC converter to control reactive power, the high-pass filters may also contribute towards the overall value applied. This factor needs to be considered when specifying the reactive power generation or absorption requirements of the AC network, in order to avoid possible overvoltages and changing of the steady-state modulation index [22].

The analysis of the high-pass filter used for the CSC-HVDC model is also valid for the VSC-HVDC converter [127].

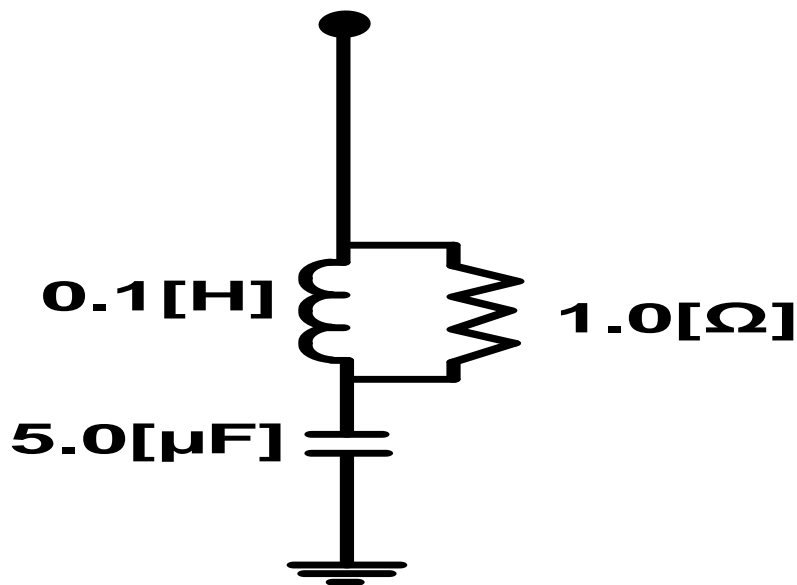


Figure 92: High-pass filter used in VSC-HVDC model

The value of each of the components is adjusted to represent the level of harmonic content produced by the high frequency switching (1200 Hz or higher) of the two-level VSC-HVDC converter. A total of one filter per phase, three per pole is connected between the AC converter transformer and the valve bridge as shown in Figure 94.

5.2.4 DC cable model

The DC cable shown in Figure 93 is modelled in the same way as the CSC-HVDC system presented in chapter 4, with the exception that the values of both resistance and shunt capacitance are contained within the cable model in a black-box formation.

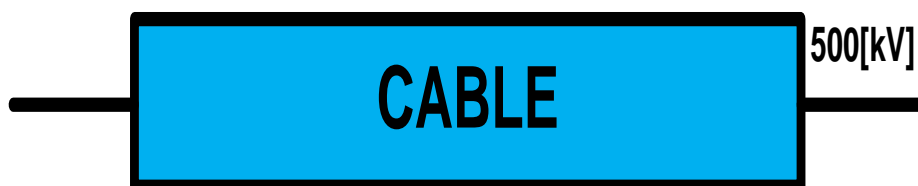


Figure 93: VSC DC cable model used in PSCAD

This does not change the behaviour of the model during simulation but is just another feature available within PSCAD to save space within the main circuit design area [127]. The same frequency-dependent (phase) model used in chapter 4 is used due to its robustness and accuracy [127].

5.2.5 PSCAD VSC-HVDC bipole model

The VSC-HVDC bipole model used in PSCAD is shown in Figure 94. A bipole configuration has been selected to match the CSC-HVDC link in chapter 4. As discussed in chapters 2 and 4, the advantage of a bipole construction is that 50% active power transfer is available when one pole is out of service due to fault or maintenance purposes [22].

The total power rating of the VSC-HVDC link is 1200 MW (600 MW per pole) and matches the rating of the NPP in reactor station 2. The equivalent full bipole DC current is 1200 A at a voltage level of ± 500 kV. An earth is provided at the rectifier end only as no electrode return is used in the model.

The short circuit levels at both the rectifier and inverter are identical to those in chapter 4 as are the series and parallel resistance/impedances.

The total reactive power rating is ± 250 Mvar per pole, which yields a total rating of 500 Mvar when in bipole mode. During STATCOM operation, when the VSC-HVDC link is in AC voltage control mode, this may rise to ± 600 Mvar, especially when the active power is zero and full reactive current is available within the PQ envelope [160].

Two six-pulse converters are connected in series to provide the ± 500 kV voltage level. The bipole is earthed at the rectifier to provide the voltage reference with respect to the direction of power flow [22].

The high-pass AC filters covered in section 5.2.3 are installed between the converter transformers and the valve bridge to reduce the characteristic harmonics produced from the high frequency PWM switching pattern of the valves.

The IGBTs are numbered accordingly and the DC pole capacitors maintain the DC voltage during power transmission.

The 500 kV Mass Impregnated Non Draining (MIND) cables connect the rectifier to the inverter and are contained within the black-box function.

The AC pole circuit breakers provide the interruption of fault current during protection operation and are essential in half-bridge configurations to prevent free-wheeling diode rectification during DC fault conditions [59].

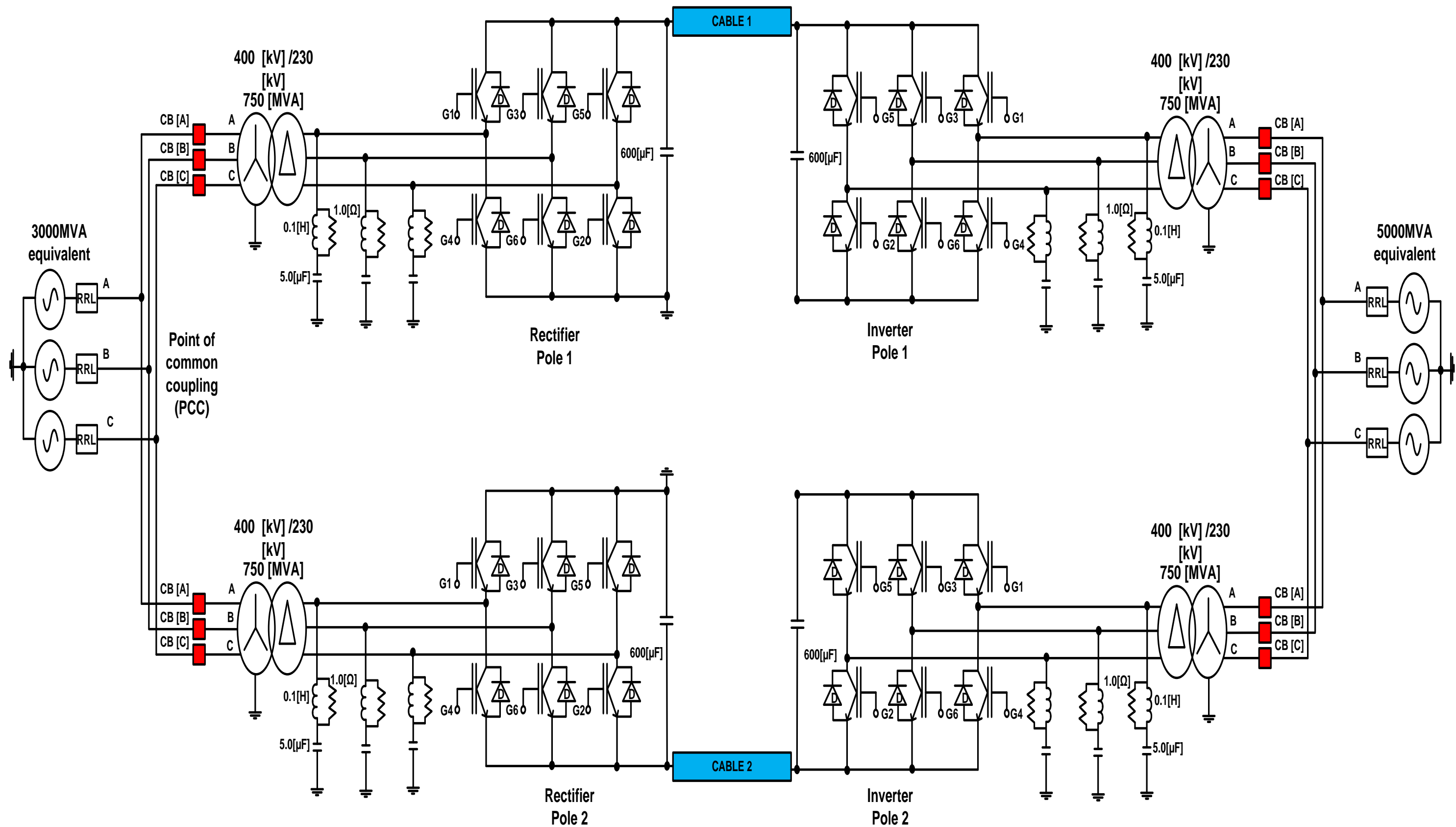


Figure 94: VSC-HVDC bipole model used in PSCAD

5.2.6 Controls used in the PSCAD VSC-HVDC model

In the following section, the controls employed in the PSCAD VSC-HVDC model are presented. First the rectifier firing controls are described, followed by the inverter firing controls.

5.2.6.1 Detailed VSC-HVDC control model

The detailed VSC-HVDC control model used in PSCAD is shown in Figure 95.

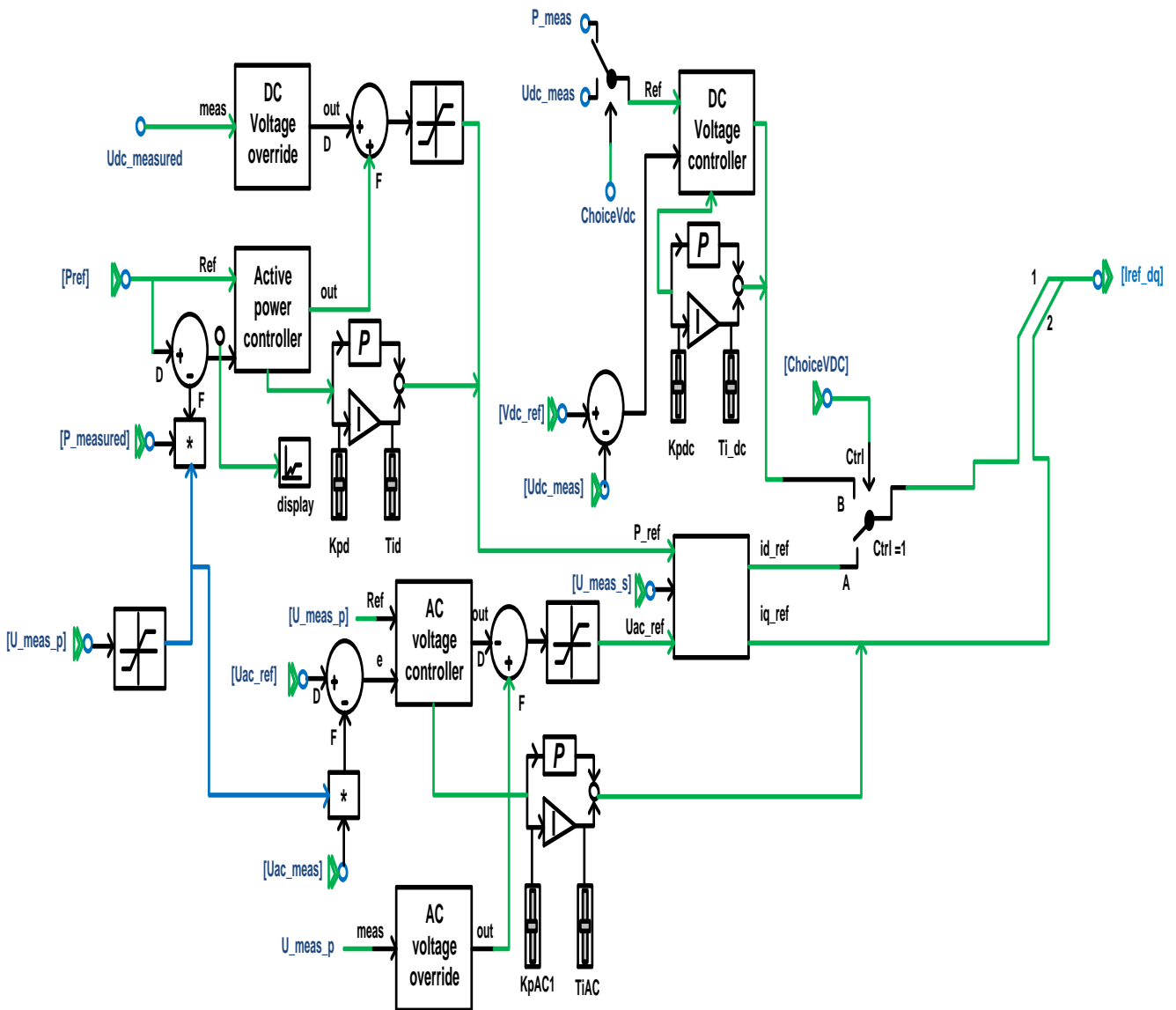


Figure 95: Detailed VSC-HVDC control model used in PSCAD

The outer controllers consist of: active power controller; DC voltage controller; and AC voltage controller. A criterion when designing the outer controllers is that the outer control loop must be slower than the inner control loop to ensure stability [161].

The inner current control loop can then be considered instantaneous, so the current controller can be represented as [162]:

$$idq = idq_{ref} \tag{5.1}$$

The outer control module includes two integral controllers. One of the two integral controllers is for the active power control and the other for the AC voltage control. In addition, both have voltage control override implementation. The system can switch between active power control and direct voltage control, both of which use PI controllers as shown. The parameters for each of the PI controllers can be changed via the slider mechanism controls. The PI controller constants shown in Figure 95 are designated in Table 14.

Table 14: Abbreviations for PI controller constants used in VSC-HVDC model

Term	Definition
Kpdc	DC voltage controller gain
Ti_dc	DC voltage controller time constant
Kpd	Active power controller gain
Tid	Active power controller time constant
Kpq	Reactive power controller gain
Tiq	Reactive power controller time constant

The rectifier slider controls with optimum control constants for stable operation are shown in Figure 96.

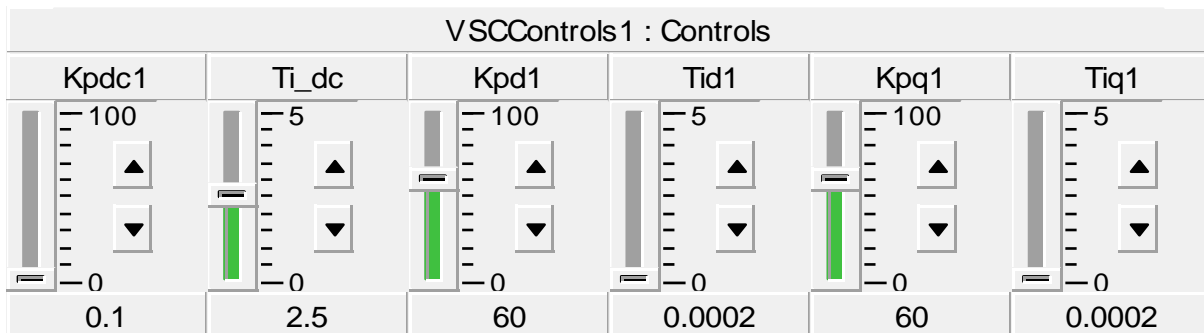


Figure 96: Optimal controller gains/constants for the VSC-HVDC rectifier

The inverter slider controls with optimal gains are shown in Figure 97.

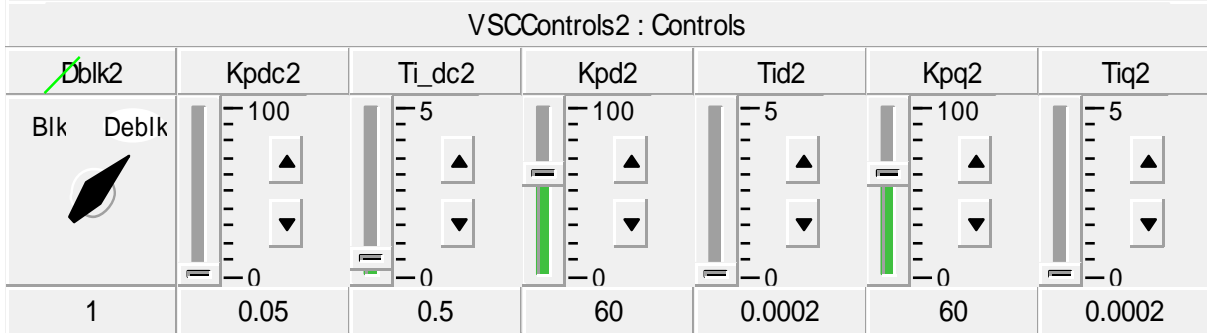


Figure 97: Optimal controller gains/constants for VSC-HVDC inverter

The sliders can be adjusted before, during, or after a simulation. A blocking/de-blocking control is included and allows the user to perform a protective block or de-block action when desired.

5.2.6.2 VSC-HVDC rectifier/inverter controls

In Figure 98 the control references for the rectifier end of the VSC-HVDC link can be changed before or during a simulation.

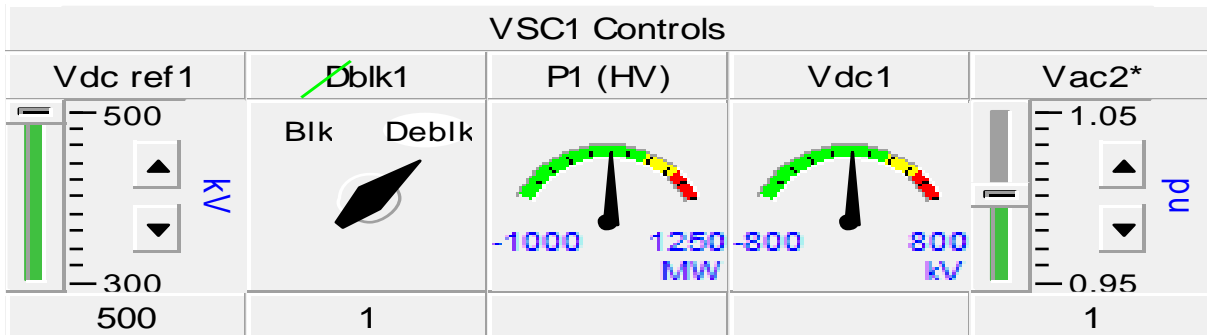


Figure 98: Rectifier controls used in VSC-HVDC PSCAD model

The DC voltage reference (Vdc ref1) allows the user to adjust this parameter via the slider controls. The nominal voltage of the model is ± 500 kV but can be lowered to a minimum of ± 300 kV if the user selects this option. By doing this the modulation index (ratio between AC converter voltage and DC voltage) can be changed. The modulation index is given by the following equation [84]:

$$m = \frac{V1 (kV)}{\frac{VDC (kV)}{2}} \quad (5.2)$$

Where:

- V_1 = Peak value of fundamental component valve phase-ground voltage in kV.
- V_{dc} = Maximum pole-to-pole DC voltage.

This enables a larger transfer of active power within the converter rating and allows modelling of lower voltage HVDC links. However, if the DC voltage is lowered, then the gains may need to be changed to compensate for the change and prevent possible instability in control system response [159]. The AC voltage reference ($V_{ac} 2^*$) can also be changed and will provide the target value for both ends of the VSC-HVDC link and inject reactive power during system disturbances. The converter valves can also be blocked and de-blocked during fault simulations, and meters displaying the active power (P_1) and DC voltage (V_{dc1}) are available.

A slider for active power control is available where the power reference can be changed from +1200 MW to -1200 MW through the full operating range of the converter. This control function is a useful tool when fast power reversals or modulation changes are required [78].

The rectifier controls shown in Figure 98 are identical those for the inverter and are not shown here.

5.2.6.3 Valve firing pulses

The VSC-HVDC valve firing controls use PWM switching. The PWM method requires the carrier signal to be mixed with the fundamental frequency signal. This defines the AC wave shape. In Figure 99, the PWM carrier signal is compared with the sine wave signal and both turn-on and turn-off pulses are generated for interpolated switching [22].

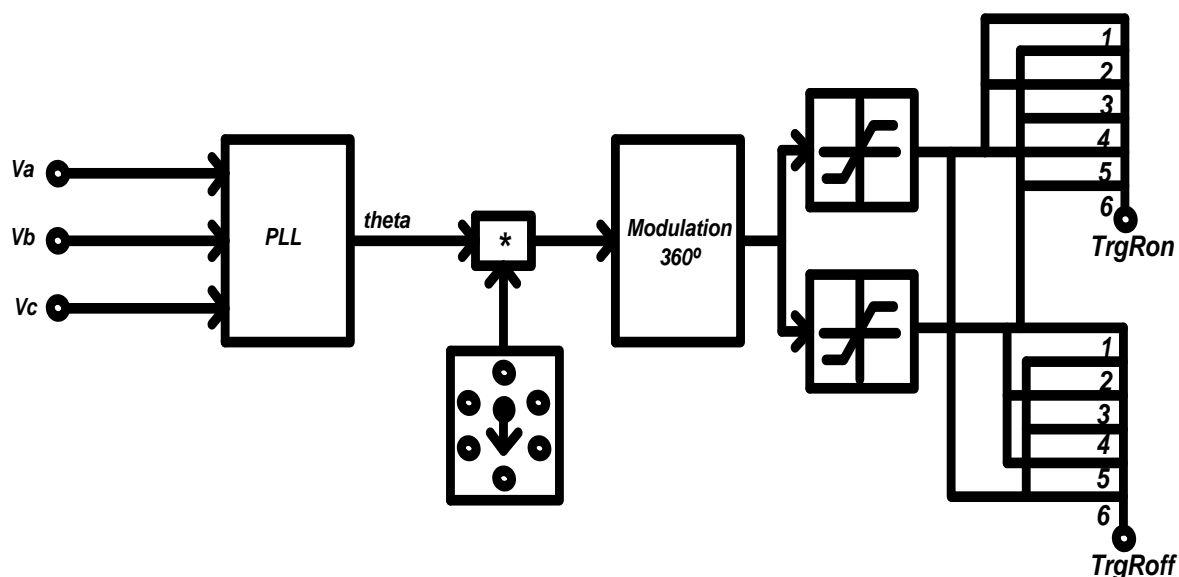


Figure 99: Firing pulse controls

In the EMTDC model shown, a Phase Locked Oscillator (PLO) is synchronised to the three-phase AC system voltage. The ramp output is synchronised to phase A and ramping between 0° and 360° over one cycle of the fundamental frequency takes place [163]. For a phase A angle range of 0° to 360° the ramp is converted to the required PWM frequency, then to a triangular signal between -1 and +1 [163]. Finally, this is allocated to each valve for both interpolated switching turn-on and turn-off. PWM is applied to the VSC valves, which results in high switching frequencies of 2000 Hz or more [163].

The PLO plays a key role in synchronising the valve switching to the AC system voltage [163]. First, a single 0° – 360° ramp is locked to phase A at fundamental frequency. This is used to generate the PWM triangular carrier signal. Its frequency is then multiplied by the PWM switching frequency, and converted to a triangular signal whose amplitude is fixed between -1 and +1 [163]. If the PWM frequency is divisible by three, then it can be applied to each valve in the two-level converter.

The 0 – 360° ramp signals generated by the six-pulse PLL are applied to generated sine waves at the designated fundamental frequency [163].

5.2.6.4 Inner current control loops

The inner current loop control employed in PSCAD is shown in Figure 100.

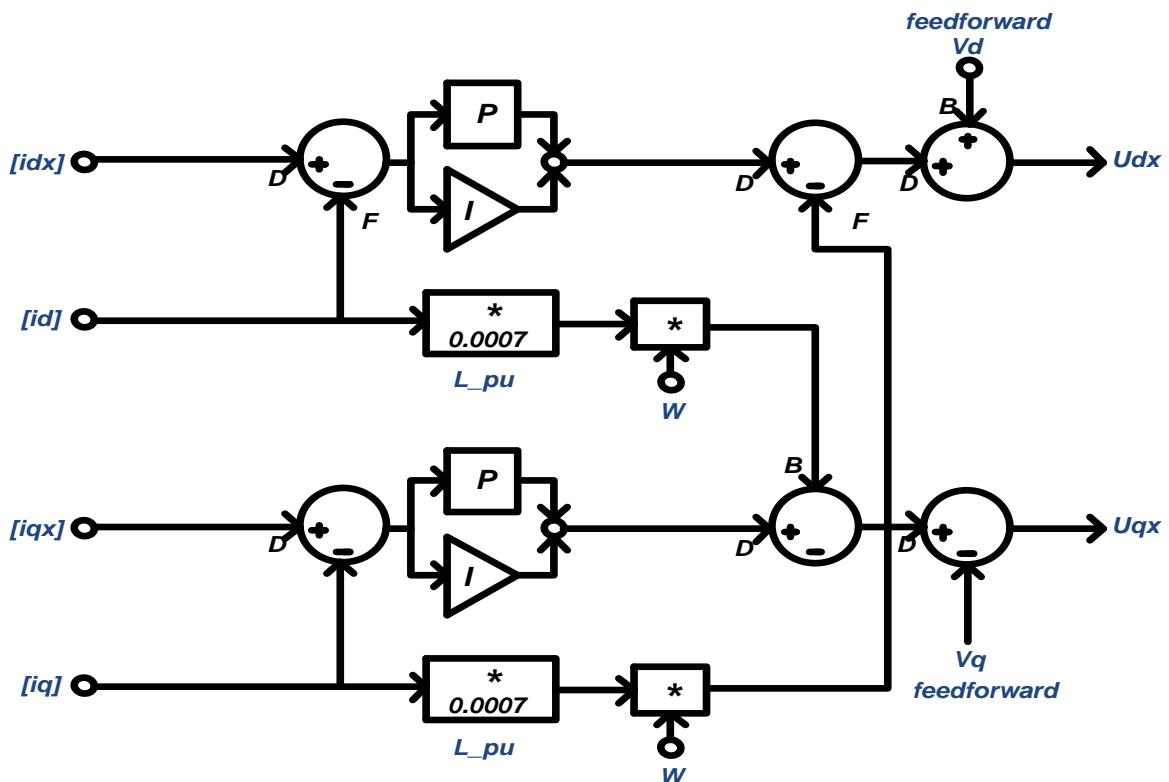


Figure 100: VSC inner current control loops

The time constant T_i is given by [62]:

$$T_i = r = \frac{L_{pu}}{r_{pu}} = \frac{0.0009}{0.07} = 0.013 \text{ s} \quad (5.3)$$

The cut-off frequency is given by [62]:

$$\omega = \frac{4500}{2} = 2250 \text{ Hz} \quad (5.4)$$

The proportional gain becomes [62]:

$$K_p = \omega c T_i r (1 + \tau a^2 \omega c^2)^{1/2} \quad (5.5)$$

Where [62]:

- $\omega c = 5000\pi \text{ rad/s}$
- $T_i = 0.012 \text{ sec}$
- $r = 0.01 \text{ pu}$
- $T_s = 0.000006 \text{ sec}$

Substituting the values into Equation 3.72 gives:

$$K_p = 4 \quad (5.6)$$

The inner controller input takes the error between the reference and measured current, and carries it through the PI regulator [60]. Decoupling terms are compensated by feed-forward control. As a result, the desired converter voltage is obtained in the dq reference frame. The feed-forward control is used to minimise the slow dynamic response of cascade control. The reference values of the inner loop variables are often available and are fed forward for a faster and safer operation [60].

5.2.6.5 Phase locked loop

The PLL is a circuit that synchronises a local oscillator with a reference sinusoidal input. This ensures that the local oscillator is at the same frequency and is in phase with the reference input and output. The PLL block measures the system frequency and provides the phase synchronising angle θ . In steady state, $\sin(\theta)$ is in phase with the fundamental (positive sequence) of the component and phase A of the Point of Common Coupling (PCC), the AC busbar voltage.

The PLL used in the VSC control system is shown in Figure 100.

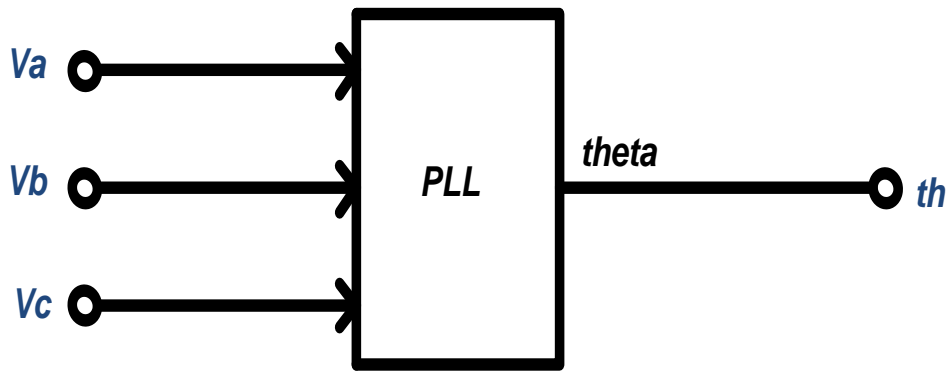


Figure 101: PLL used for generating the synchronising angle (θ)

If a VSC-HVDC link is connected to a passive network, then there is only one source of AC voltage available (the VSC itself) and there is no issue of synchronisation. In a passive network, the VSC-HVDC PWM obtains its sinusoidal signal from a fixed oscillator circuit. For all other cases, where the VSC-HVDC link is connected to an active AC system, frequency and phase must be detected and the converter should be synchronised accordingly [21].

5.2.6.6 Frequency controller

The VSC-HVDC link has a frequency control function which can be used to modulate the active power to provide support during an unbalance in the power system. The controller is shown in Figure 102.

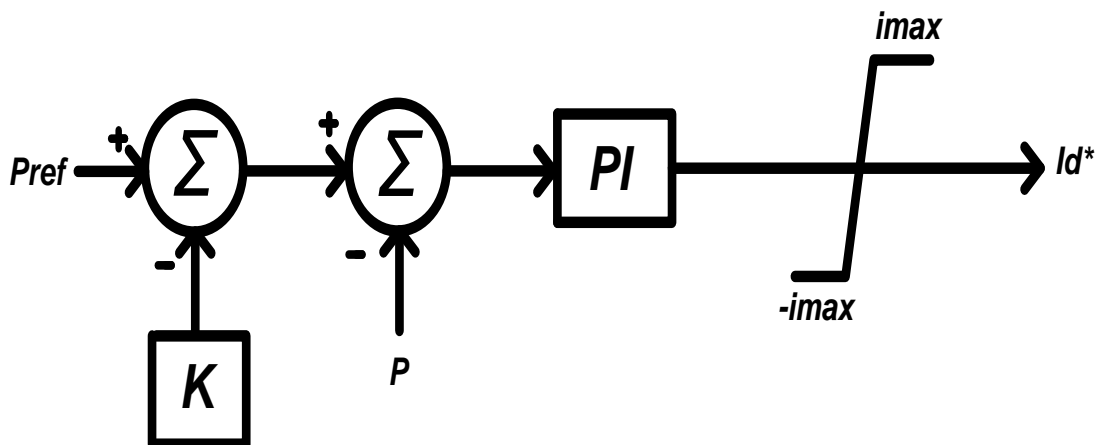


Figure 102: VSC frequency controller

The power reference is fed into a summatior where a gain constant (K) can be selected to provide a modulated signals reference. The measured power is then subtracted from the reference quantity to provide the input and output to the PI controller. The output signal of the PI controller is then passed through a current limiter function before the active current reference (I_d) is generated.

5.2.6.7 Active power controller

The active power injection can be given by the following Equation [62]:

$$P = Vd \cdot id + Vq \cdot iq \quad (5.7)$$

And power flow [62]:

$$Vxd = Vx \quad (5.8)$$

Where Vx is the resultant voltage in dq reference frame and is desired to have a constant value [62]. Active power flow can be controlled by the active current (id) and the active power controller shown in Figure 103.

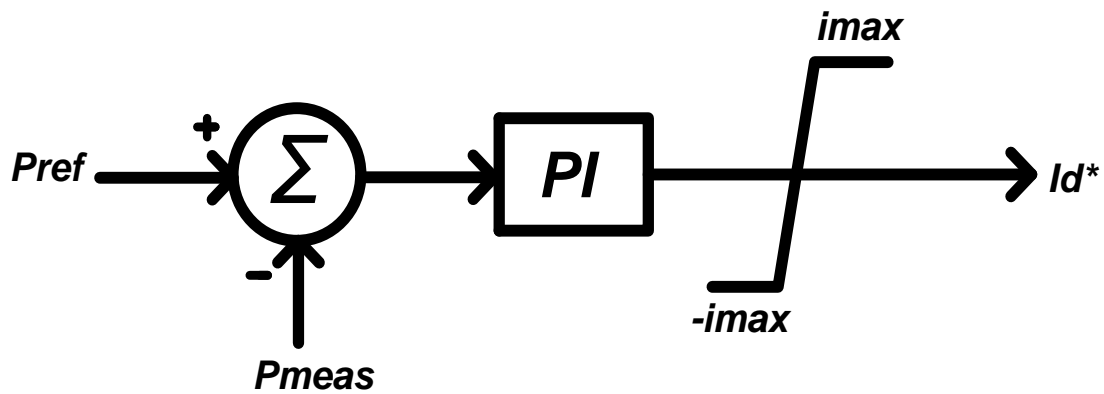


Figure 103: VSC active power controller

The output of the active power controller (id) will be the reference ($nout$) to the d axis current controller of the inner current loop. In order to limit the magnitude of the current in the VSC-HVDC to a maximum level, the output of the active power controller is followed by a limiter function of +/- limits where [62]:

$$imax = irated \quad (5.9)$$

5.2.6.8 DC voltage controller

The DC voltage controller implemented in PSCAD is shown in Figure 104.

From the energy balance in the VSC-HVDC terminal [62]:

$$Pac + PDC + Pcap = 0 \quad (5.10)$$

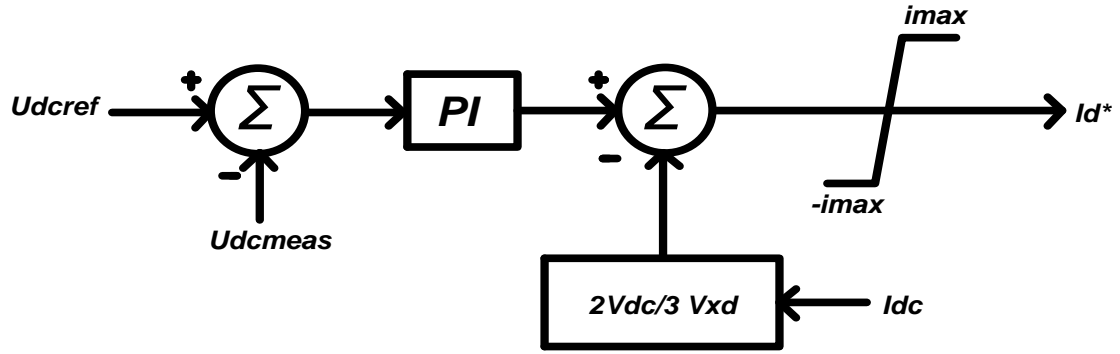


Figure 104: VSC DC voltage controller

Where:

$$\frac{3}{2}Vd \cdot +VDC \cdot IDC + VDC \cdot icap = 0 \quad (5.11)$$

From Equation 5.11, the current through the capacitor will be [62]:

$$icap = -\left(\frac{3V \, xd \, id}{2VDC} + IDC\right) \quad (5.12)$$

The same current in terms of voltage across the capacitor is given by:

$$icap = C \frac{d \cdot VDC}{dt} \quad (5.13)$$

From Equations 5.12 and 5.13, the differential equation for the DC voltage becomes:

$$\frac{d \, VDC}{dt} = \frac{1}{C} \left(\frac{3V \, xd \, id}{2VDC} + IDC \right) \quad (5.14)$$

$$\frac{d \, VDC}{dt} = \frac{-3V \, xd \, id}{2VDC} \left(id + \frac{2VDC}{3V \, xd} IDC \right) \quad (5.15)$$

From the above equations, the DC voltage can be regulated by control of the active current (*id*). The IDC term is compensated by feed-forward control in the DC voltage regulator.

5.2.6.9 AC voltage controller

AC voltage control is implemented in the VSC- HVDC model for transient purposes and is shown in Figure 105.

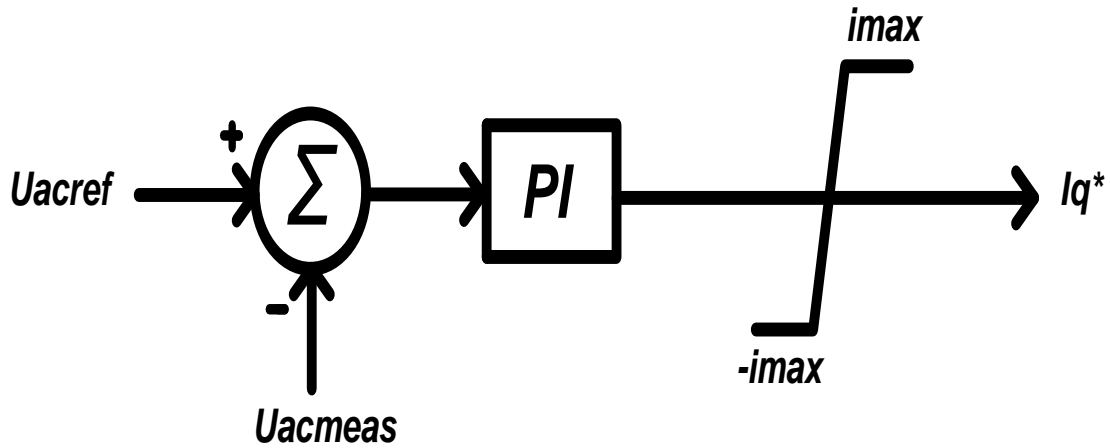


Figure 105: VSC AC voltage controller

This type of control is normally used where the AC grid connection is weak [79] – with significant AC network resistance and inductance. This creates considerable fluctuations with a change in the active power flow.

For a weak grid connection, the AC voltage must be controlled by the converter at the PCC. Under dynamic conditions, AC voltage control is faster and more effective than the much slower reactive power (Q) control loop. The quadrature axis change in voltage due to active and reactive power has little effect on the resultant voltage magnitude V_x . Therefore, V_x is approximately [79]:

$$V_x = V: \left(\frac{Pr(ac\ system) + Q\omega (ac\ system)}{V_x} \right) \quad (5.16)$$

In Equation 5.16, P is determined by the desired amount of active power flow and hence voltage V_x can be maintained constant by reactive power injection. This relation is mathematically given by [79]:

$$V_x = \frac{\omega (a.c.\ system)}{V_x} \Delta Q \quad (5.17)$$

The time constant will determine the speed of the applied step response.

In some applications AC voltage control is permanently applied in normal operation and not just during dynamic situations [9]. The enhanced performance of AC voltage control compared to that of the slower reactive power (Q) control can help improve the operation of neighbouring AC systems [161].

5.2.7 Comparison of PSCAD/MATLAB VSC-HVDC models

A comparison between the VSC-HVDC model used in PSCAD and a similar one developed in MATLAB/Simulink is performed to compare their behaviour during transient conditions. The aim of the analysis is to compare the responses, as some minor differences are employed in the respective control philosophies employed within the two models. In particular, the PSCAD model utilises AC voltage control during disturbances whereas MATLAB uses reactive power (Q) control. From the literature survey carried out in chapter 2, it has become evident that the two different control strategies may yield different behaviours during transient conditions [160].

5.2.7.1 VSC-HVDC bipole model developed in MATLAB/Simulink

The VSC-HVDC bipole model developed in MATLAB is shown in Figure 106. The same system parameters used in the PSCAD model was also employed in the MATLAB/Simulink version. The converter transformer voltage, configuration and power ratings are also identical and can be changed by the user if desired.

A two-level, six-pulse converter is used for each pole and the same parameters for the AC filters and DC cable are adopted. In this model, black-box functions are used to hide the inner details and to save on space within the main drawing area.

The SCLs (Short Circuit Levels) at both the rectifier and inverter can be adjusted to reflect the SCR of the AC connections if required.

The VSC-HVDC control system is described in section 5.2.7.2.

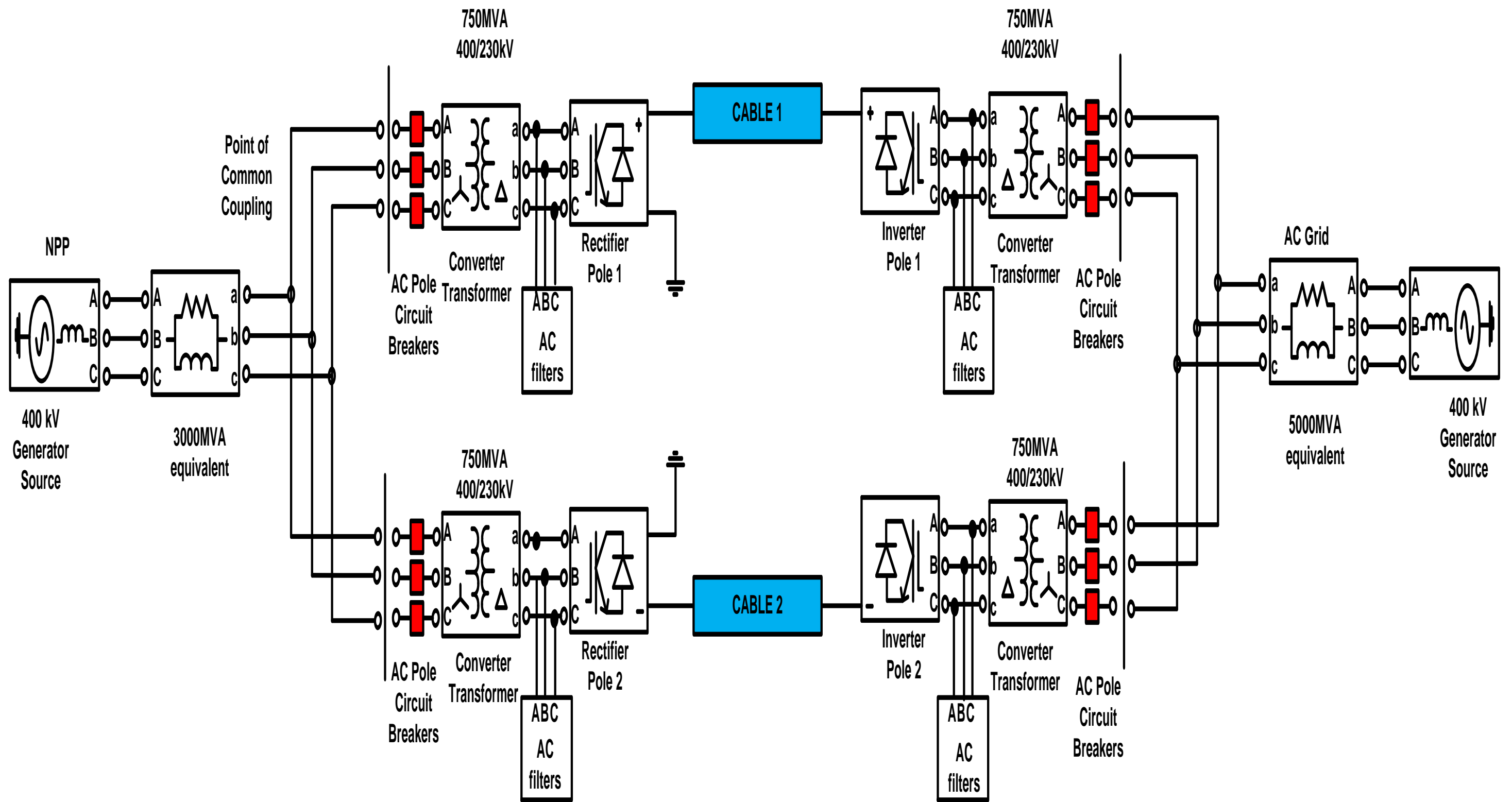


Figure 106: VSC-HVDC bipole model developed in MATLAB/Simulink

5.2.7.2 MATLAB/Simulink VSC-HVDC control philosophy

An overview of the control system used for the VSC-HVDC model in MATLAB/Simulink is shown in Figure 107.

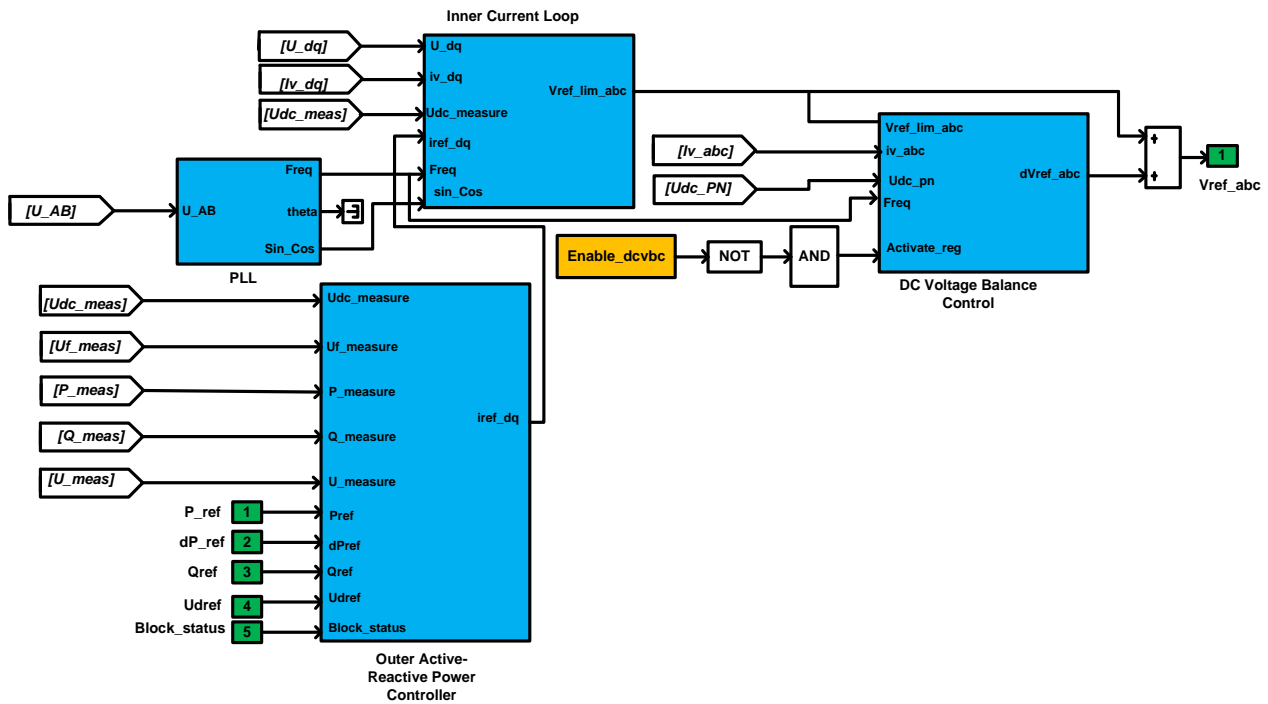


Figure 107: VSC-HVDC control loops used in MATLAB/Simulink

Just like the PSCAD model, the Clark-transformation block transforms the three-phase quantities to space vector components α and β (real and imaginary part). The dq transformations block then computes the direct axis d and the quadratic axis q (two-axis rotating reference frame) from the α and β quantities [160]. The signal calculations block calculates and filters the quantities used by the controller (e.g. active and reactive power, modulation index, DC current and voltage) [160].

The PLL measures the system frequency and provides the phase synchronising angle θ .

The active power, reactive power and voltage loop contains the outer loop regulators, which calculate the reference value of the converter current vector (I_{ref_dq}) and forms the input to the inner current loop [160]. The reactive power control regulator block combines PI control with a feed-forward control to increase the speed of the response. AC voltage control is not available within this model and an extra regulator is required to implement such a function [164]. The active power control block is similar to the reactive power control block, which ramps the power order towards the reference value at an adjusted rate [164].

The DC voltage control block uses a PI regulator and is enabled when the active power control block is disabled [164].

The DC voltage control block provides a reference value, for the d component of converter vector current control. The current reference calculation block transforms the active and reactive power references, calculated by the P and Q controllers, to current references, according to the measured voltage at the AC filter bus [164]. The current reference is approximated by dividing the power reference by the voltage. The current reference limitation block limits the current vector to a maximum value (1200 A DC).

The AC current control block tracks the current reference vector (d and q components) with a feed-forward scheme to achieve a fast control of the current at load changes and disturbances. [164].

The reference voltage controlling block takes into account the actual DC voltage and the theoretical maximum peak value of the fundamental bridge phase voltage to generate the new optimised reference voltage vector [164].

5.2.7.3 Transient response comparison between MATLAB/Simulink and PSCAD

During transient faults, a difference in protective controller action is employed between the two models. In the VSC-HVDC MATLAB model, the inverter controller will perform a fast ramp down in DC current to reduce system instability. This particular function is a default function in the MATLAB model and was previously implemented when the inverter was connected to weak AC systems [81]. At the rectifier, the current is clamped before it reaches a dangerously high value as was previously implemented for strong AC systems. In the PSCAD model, the more conventional current clamping control is implemented at both the rectifier and the inverter. In industry either one, or a combination of the above, protective control strategies can be employed within a VSC-HVDC link. The decision will be based upon network strength, rating and the operational strategy of the interconnection [61], [75].

As mentioned previously in section 5.2.7, the VSC-HVDC PSCAD model utilises the default setting of AC voltage control for both steady-state and transient system conditions.

The literature survey in chapter 2 described how AC voltage control is more effective than conventional reactive power (Q) control for weak AC systems, or during transient conditions [160]. Some differences in the following transient comparisons are expected based upon the different strategies employed in each model. In MATLAB/Simulink, the reactive power reference is 0.2 and will not be changed during the fault analysis. This allows the key difference between reactive power and AC voltage control during transient disturbances to be distinguished from the results obtained. Both single-phase and three-phase faults were placed at each end of the HVDC links at a time of 1.0 secs for 300 ms duration. The extended fault duration times allowed a more detailed analysis of the plots to be studied. The measurements for each of the variables are shown in Table 15. For most of the faults, the differences between the measured variables between the two models are less than $\pm 1\%$. In other cases, they are identical.

In Appendices A–D, the profiles for a three-phase fault at the rectifier are presented. When the fault occurs, the rectifier clamps the current in both the PSCAD (Figure 175) and MATLAB/Simulink (Figure 173) VSC-HVDC models. The values in current have a 0.4 pu difference and are dependent upon how quickly the clamping control is activated within each of the models. In MATLAB, the inverter (Figure 174) controller ramps down the DC current to 0.2 pu. In PSCAD (Figure 176) this is clamped straight away, which highlights the difference in protective strategies. The AC voltage collapses at the rectifier in both models due to the severity of the fault and the active power transfer is halted until fault clearance is achieved. The AC voltage (1.0 pu) and active power profiles (0.2 pu) are identical in both models, as are the DC voltage measurements. The DC active power transfer is dependent on the charge and discharge of the DC capacitors in controlling the DC voltage [81]. As the capacitors discharge, the DC voltage is reduced, which in turn causes a drop in active power.

In Figure 174, the most noticeable difference is at the inverter, where in MATLAB the 0.2 pu reference order for the reactive power is maintained during the fault. In Figure 176 the PSCAD measurement is 0.9 pu with the AC voltage control mode applied. A large difference in reactive power injected (STATCOM mode) highlights the effectiveness of AC voltage control during transient conditions [160]. This becomes more evident once the fault has been cleared. The reactive power profiles at both the inverter and rectifier in MATLAB/Simulink display oscillatory response due to the slow feedback order applied to the control system. In PSCAD the reactive power is restored through a fast injection via the AC voltage control STATCOM function [160].

In summary both VSC-HVDC models display good control responses during the different faults. The more detailed control loops in PSCAD help the responses to be much smoother with less oscillatory behaviour than the MATLAB/Simulink VSC-HVDC models [164].

Table 15: Comparison between PSCAD and MATLAB VSC-HVDC models for AC faults

Model	Fault type	Location	Fault duration (ms)	Measurement location	AC current (Iabc/pu)	AC voltage (Uabc/pu)	Reactive power (Q/pu)	AC active power (P/pu)	DC voltage (Udc/pu)	DC active power (Pdc/ pu)
MATLAB	Single-phase	Rectifier	300	Rectifier	1.4	0.4	0	0.6	0.9	0.6
				Inverter	1.	1.0	0.2	1.0	1.0	1.0
MATLAB	Three-phase	Rectifier	300	Rectifier	1.4	0	0	0	0.9	0.1
				Inverter	0.2	1.0	0.2	0.2	0.9	0.05
MATLAB	Single-phase	Inverter	300	Rectifier	1.0	1.0	0.2	1.0	1.0	1.0
				Inverter	1.4	0.4	0	0.6	0.9	0.6
MATLAB	Three-phase	Inverter	300	Rectifier	1.4	0	0	0	0.9	-0.1
				Inverter	0.2	1.0	0.2	0.2	0.9	0.05
PSCAD	Single-phase	Rectifier	300	Rectifier	1.4	0.4	0	0.6	0.9	0.6
				Inverter	1.	1.0	0.6	1.0	1.0	1.0
PSCAD	Three-phase	Rectifier	300	Rectifier	1.8	0	0	0	1.0	0
				Inverter	1.0	1.0	0.9	0.2	1.0	0.2
PSCAD	Single-phase	Inverter	300	Rectifier	1.0	1.0	0.2	1.0	1.0	1.0
				Inverter	1.4	0.4	0	0.6	0.9	0.5
PSCAD	Three-phase	Inverter	300	Rectifier	1.8	0	0	0	1.0	0
				Inverter	1.0	1.0	0.9	0.2	1.0	0.2

5.3 Impact of short circuit ratio on VSC-HVDC operation

The SCR is an important factor in determining the stability and steady-state operation of an AC power system [158]. For CSC-HVDC technology the reactive contribution of the AC filters needs to be taken into account. For VSC-HVDC technology, since there is no reactive power demand, AC filters do not normally need to be considered [158].

The SCR is given by the following formula:

$$SCR = \frac{S_{sc}}{PdN} \quad (5.18)$$

Where:

- S_{sc} is the short circuit capacity of the commutations bus.
- PdN is the rated power of the converter station.

Analysis of SCR on the impact of VSC-HVDC technology has already been carried out in [165] and [166], but the impact of VSC-HVDC technology operation for an NPP connection has yet to be studied.

In the following section, the impact of changing SCR on VSC-HVDC operation for an NPP connection during steady-state conditions is analysed. First the SCR at the rectifier connection is reduced while keeping the inverter SCR constant. In reactor station 2 the series impedance of nuclear generator 2 is adjusted to reflect the corresponding value of SCR. In the opposite scenario the rectifier SCR is kept constant and the inverter SCR is reduced and then analysed. Due to multiple AC circuits being connected to the inverter busbar, the SCR is reduced by switching out the corresponding overhead lines one at a time. In each of the simulation plots the reference values of DC current and voltage orders are shown.

Previous work has suggested the need to consider optimising the VSC-HVDC control parameters each time that the SCR is changed for a simulation [165], [166]. If this is not done, then the control response may become unstable. For each change in SCR, the control response of the VSC-HVDC link is studied and if instability was encountered, the control parameters shown in Figures 97 and 98 were adjusted by trial and error until a steady-state response was attained. After some initial testing, a rigorous procedure was developed to finetune the control parameters for each change in SCR. The procedure starts with setting the power controller (DC voltage/active power/AC voltage) gain (K_p) to zero; then the time response (T_i) is set to zero and the gain (K_p) is increased until the control loop obtains a good stability response in the measurement signal.

Alternatively, the gain (K_p) is set to 1 and then either increased or decreased until some overshoot is observed or a barely observable undershoot in the opposite scenario is encountered. It is important that the control signal is not driven to any saturation limit (maximum or minimum value) during the experiment. If such limits are reached, then the gain K_p may not be at a sensible value [167]. The integral time T_i is set equal to 1, where the duration between the overshoot and undershoot of the step response produces the required time interval.

The optimised control parameters for the standard SCR values of the power system are summarised in Table 16.

Table 16: Control parameter settings for fixed SCR values

Parameter	Definition	Rectifier (SCR 2.5)	Inverter (SCR 4.1)
K_{pdc}	DC voltage controller gain	0.1	0.05
T_{i_dc}	DC voltage controller time constant	2.5	0.5
K_{pd}	Active power controller gain	60	60
T_{id}	Active power controller time constant	0.0002	0.0002
K_{pq}	AC voltage controller gain	60	60
T_{iq}	AC voltage controller time constant	0.0002	0.0002

For each simulation the target reference values for each power system variable are shown; this helps to distinguish any deviations in setpoint from the reference value during the simulations.

5.3.1 Rectifier SCR 2.5 and inverter 4.1

In this particular scenario, the normal system SCRs of 2.5 (rectifier) and 4.1 (inverter) are used with the optimised parameter settings shown in Table 16. The simulation results are presented in Figure 108.

The DC voltages are held constant by the HVDC control system and reactive power is maintained at both ends of the VSC-HVDC link to keep the AC voltage profiles constant. The DC active powers at both the rectifier and inverter reach the target reference values, while a slighter lower value is encountered at the inverter due to the losses over the entire length of the connection.

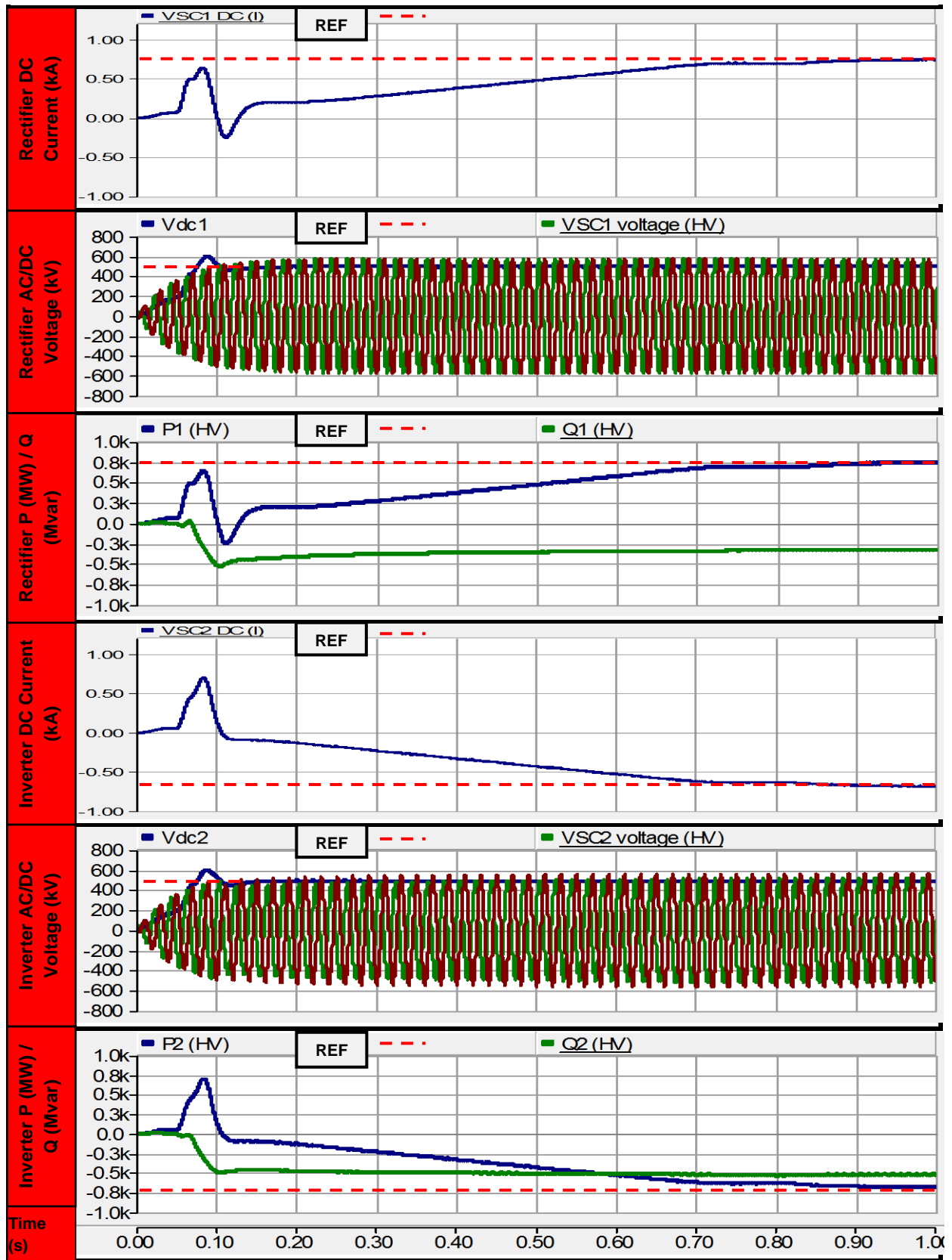


Figure 108: Profiles for rectifier SCR 2.5 and inverter 4.1

The run-ups in DC current are maintained with no signs of instability in the control response; the responses have shown good stability and the target reference values have been met.

5.3.2 Rectifier SCR 2.0 and inverter 4.1

In Figure 109, the SCR of the rectifier is decreased to 2.0 while the inverter is kept constant.

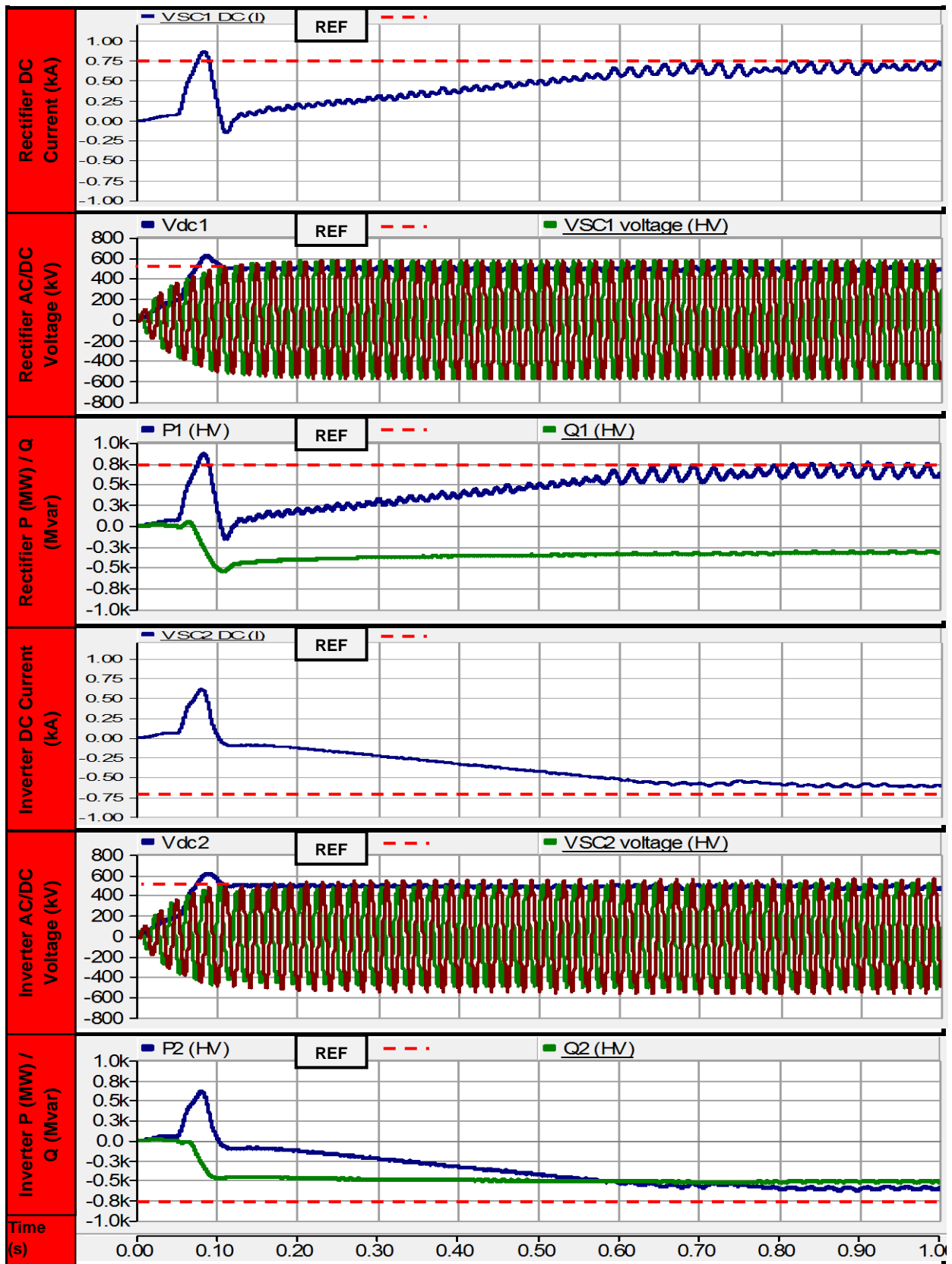


Figure 109: Profiles for rectifier SCR 2.0 and inverter 4.1 with nominal control parameters

Reducing the SCR at the rectifier leads to some significant changes in control response. Instability in both the DC current and active power profiles are observed. In particular, the active power no longer meets the reference target of 800 MW, reaching only 600 MW. Once the run-ups are complete, 600 ms after initial startup, the instability intensifies once the 600 MW capability has been reached.

The reactive power plots show a minor oscillatory response but the AC voltages at both the rectifier and inverter remain constant. Due to the oscillations in active power, minor instability is present in the DC voltage profiles at both the rectifier and inverter but the DC voltage references are maintained and the VSC-HVDC link is able to deliver active power to the AC system from the NPP. The reduction in SCR at the rectifier has distorted the AC voltage at the PCC, which makes it harder for the Phase Locked Loop (PLL) of the VSC-HVDC control to synchronise to the AC system and causes instability within the inner current control loops [77].

The simulation is repeated with the gains and time constants for DC voltage, active power and AC voltage controllers adjusted until an acceptable control response is obtained. The gains which result in the best optimised control response is shown in Table 7. In Figure 110 the simulation shows how the adjusted gains have improved the stability and control response of the VSC-HVDC control system.

The active power controller gains have been reduced and the speed of response is slower. This allows the active power reference values to be met and a reduction in the oscillatory behaviour experienced previously.

The oscillations in DC voltage at both the rectifier and inverter disappear as the DC voltage controller gains are increased; the speed of response is thereby quicker, and instability is alleviated [77].

A slight reduction in the gain of the AC voltage controllers has reduced the small signal instability experienced previously. Reactive power support is maintained, as are the AC voltage profiles at both the rectifier and inverter.

Through adjustment of the different controller gains and time constants, the VSC-HVDC link is able to supply the maximum active power reference to the AC system. The potential instability due to the interaction of the inner control loop with the low-frequency resonance of the weakened rectifier at the PCC has been alleviated by slowing down the active power run-up response [77]. An increase in the DC voltage controller gain has resulted in a faster response of the outer control loop and helped overcome the oscillatory behaviour caused by the lower rectifier SCR [161].

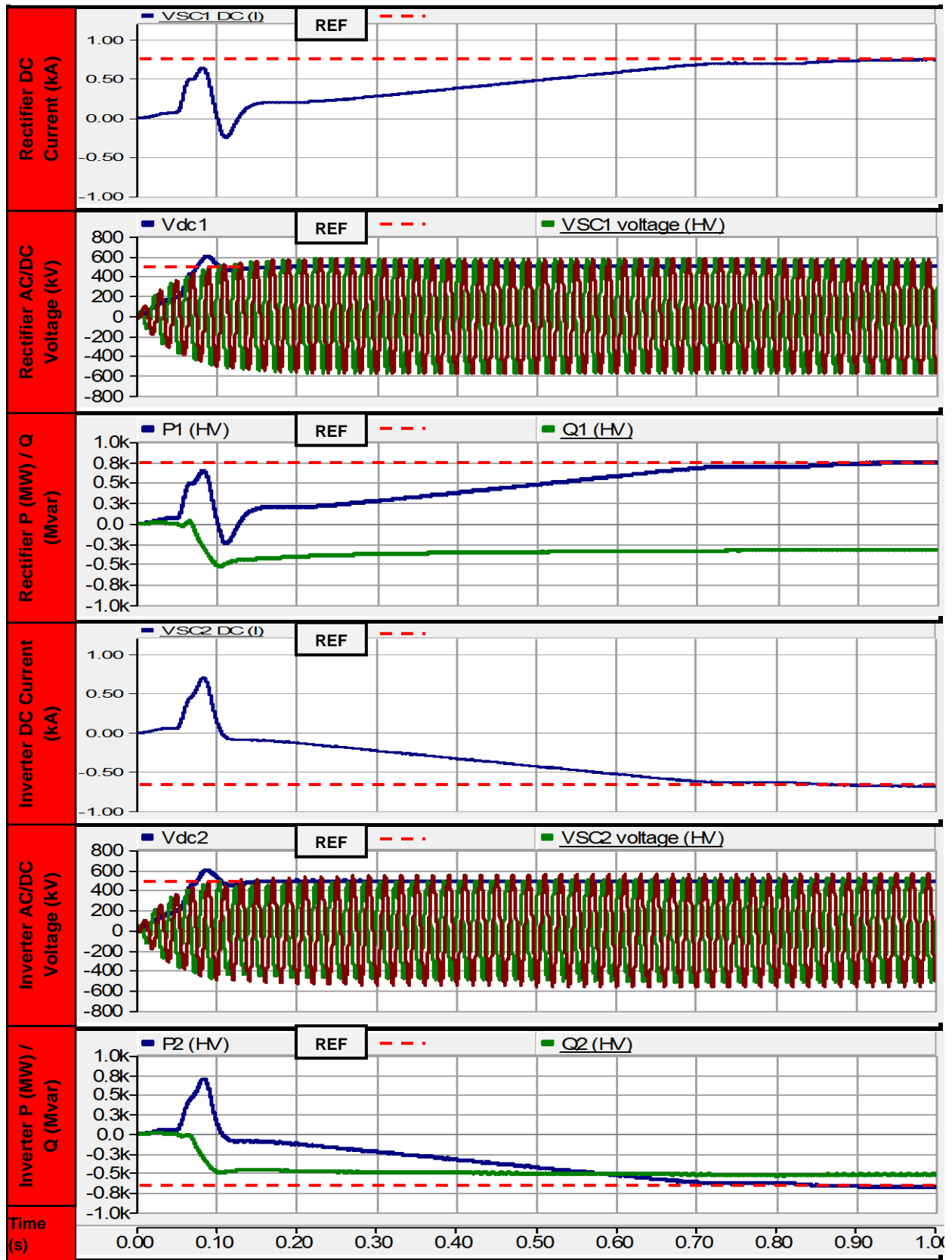


Figure 110: Profiles with rectifier SCR 2.0 and inverter 4.1 with adjusted control parameters

The simulations are displaying satisfactory responses and system stability is maintained.

5.3.3 Rectifier SCR 1.6 and inverter 4.1

In Figure 11 the simulation results for a rectifier SCR of 1.6 and inverter 4.1 are presented.

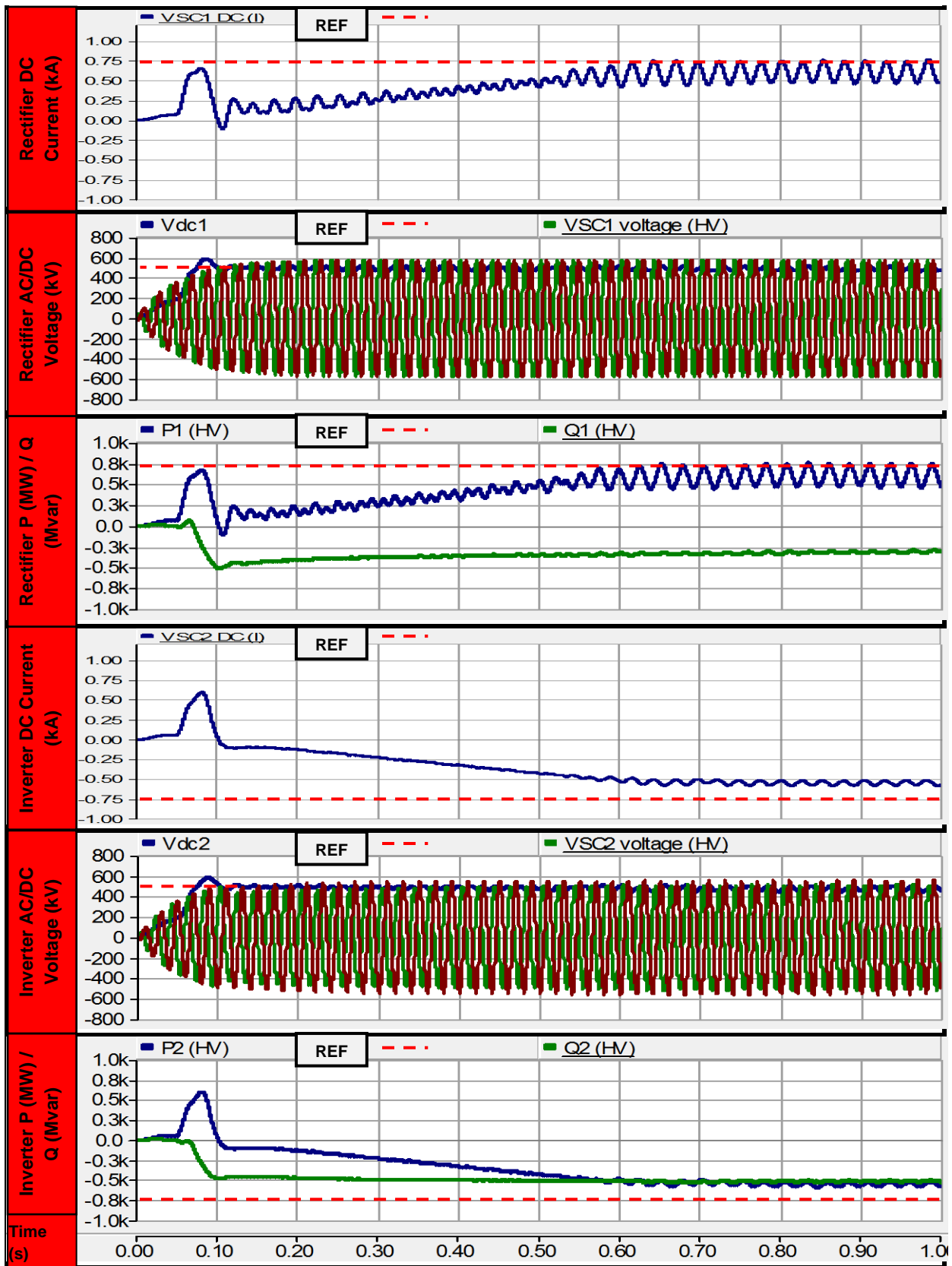


Figure 111: Profiles for rectifier SCR 2.0 and inverter 4.1 with nominal control parameters

The active power transfer reduces to a maximum capability of 500 MW as the rectifier SCR is reduced to 1.6. Large oscillations are present which indicates instability encountered in the fast inner control loops of the VSC-HVDC and interaction with low frequency resonance [161].

The reactive power helps to maintain the AC voltage profiles at both the rectifier and inverter but despite this, an oscillatory response is observed and is most onerous at the rectifier.

The DC voltage profiles at both the rectifier and inverter display oscillations, indicating some difficulties in the outer control loop of the VSC-HVDC converter. The gains and time constants on each of the PI controllers are adjusted to obtain the most optimised system response, giving the results shown in Figure 112.

A decrease in active controller gains slows down the power run-ups and the output obtained is 700 MW. This is 200 MW more than the previous value of 500 MW in Figure 11, where the nominal system gains were applied. In Figure 112 the oscillatory response is vastly improved despite small traces still present, indicating the persistence of a slight issue with the inner control loop. The DC currents also increase alongside the increase in active power and no oscillatory response remains.

An increase in DC voltage controller gain has improved the performance of the outer control loop of the VSC-HVDC link: a faster response is achieved, while maintaining stability.

The oscillatory behaviour that was experienced in the reactive power profiles previously has disappeared since the controller gain was adjusted. The AC voltage profiles are maintained and instability is avoided.

With the adjustment in controller gains, the performance of the VSC-HVDC system is improved, which helps the VSC control system to adapt to the drop in rectifier SCR. Despite this, the active power output delivered is still below the reference value of 800 MW. The drop in SCR has now reached the minimum limit where the VSC-HVDC link is able to supply and meet 100% of the active power reference demand.

With a strong ESCR at the inverter, the VSC-HVDC link is able to receive the power transferred from the NPP. However, the rectifier cannot physically transmit the active power from the NPP due to the weaker connection caused by an increase in system impedance through reduction in rectifier SCR [161].

Despite the increase in controller performance, the reduction in active power suggests the minimum operating limit of the VSC-HVDC link is close.

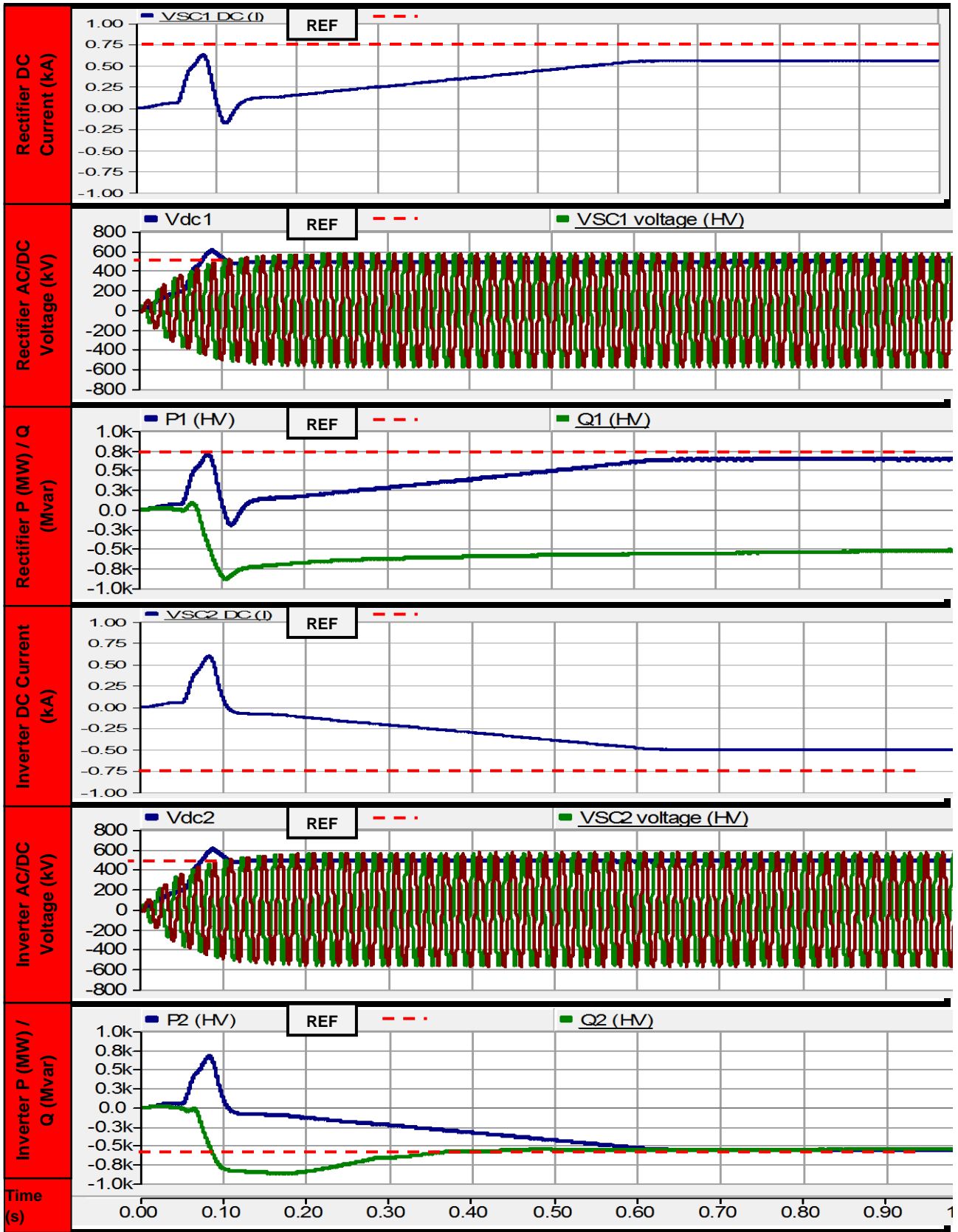


Figure 112: Profiles for rectifier SCR 2.0 and inverter 4.1 with adjusted control parameters

In the final example, the SCR is reduced even further and the effect on operational performance of the VSC-HVDC link is studied.

5.3.4 Rectifier SCR 1.0 and inverter 4.1

The simulation results for a rectifier SCR of 1 and inverter 4.1 is shown in Figure 113.

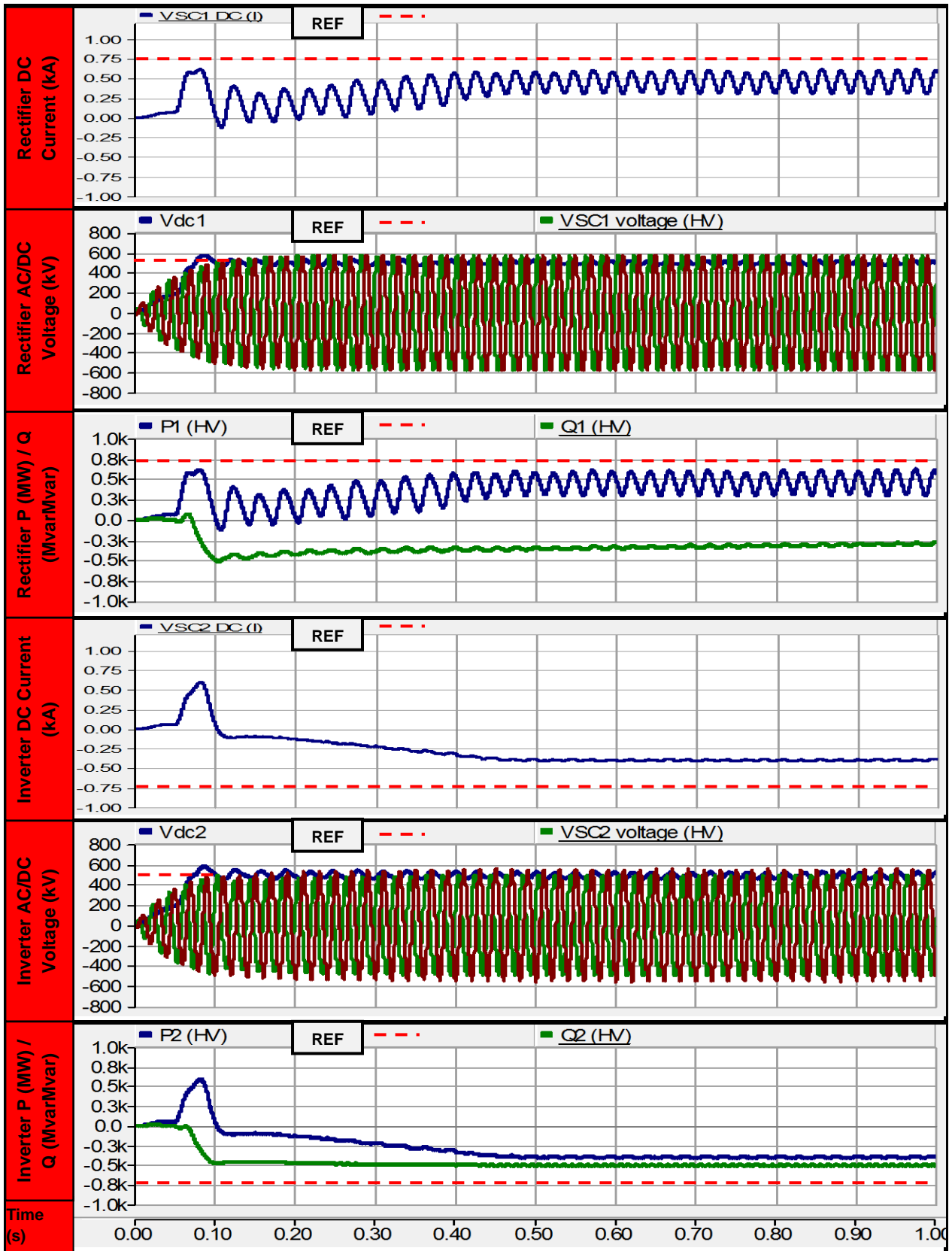


Figure 113: Profiles for rectifier SCR 1.0 and inverter 4.1 with nominal control parameters

Large oscillatory responses in the active power and DC current profiles at the rectifier are observed, which indicates the possibility of low frequency resonance in the weak AC connection causing instability with the inner current control loop of the VSC-HVDC link [161].

Some minor oscillatory response on both the active power and DC current profiles is present in the inverter. The stronger SCR at the inverter reduces the impact of the lower frequency resonance in the inner current control loop of the VSC-HVDC link but despite this, the value of active power delivered to the AC grid from the NPP has reduced to 400 MW. This is 50% less than the active power reference order of 800 MW. Small oscillatory responses occur in the reactive power profiles at both the rectifier and inverter but reactive power and the AC voltage profiles are maintained at both ends of the VSC-HVDC link. This aids the VSC-HVDC link in maintaining some active power transfer to the AC grid [77].

Instability in the VSC outer control loop is evident from the oscillations encountered in the DC voltage profiles at the rectifier and inverter but DC voltage references are maintained.

The gains and time constants of the PI controllers are adjusted until the best optimal control response is found. The simulation result in Figure 114 shows a vast improvement to the stability of the VSC-HVDC link.

The oscillatory response in both the DC current and active power profiles has diminished. The active power transfer capability has increased to 500 MW which is a shortfall of just over 40% of the 800 MW target reference.

The DC voltage profiles have stabilised due to the increase in controller gain, allowing a slower, more stable control response to be obtained. The reference values are met, which helps active power to be transferred through the VSC-HVDC link to the AC system. The small oscillatory response previously encountered with the reactive power profiles has disappeared. The improved response helps to maintain the AC voltage profiles and reduces the risk of instability caused by reduction in rectifier SCR.

In this scenario the vast reduction in rectifier SCR has posed challenges for the VSC-HVDC control system, making it difficult to deliver the full 800 MW output to the AC grid. With nominal control parameters major instability has been encountered but by adjusting the gains and time constants of the PI controllers, the responses are vastly improved but over 40% of the active power transfer capability has been lost. The low frequency resonance of the weak rectifier connection causes instability in the fast inner current control loop of the VSC-HVDC link. The PLL is also affected due to the delay and difficulty of synchronising the firing control to the phase angle of the AC busbar voltage.

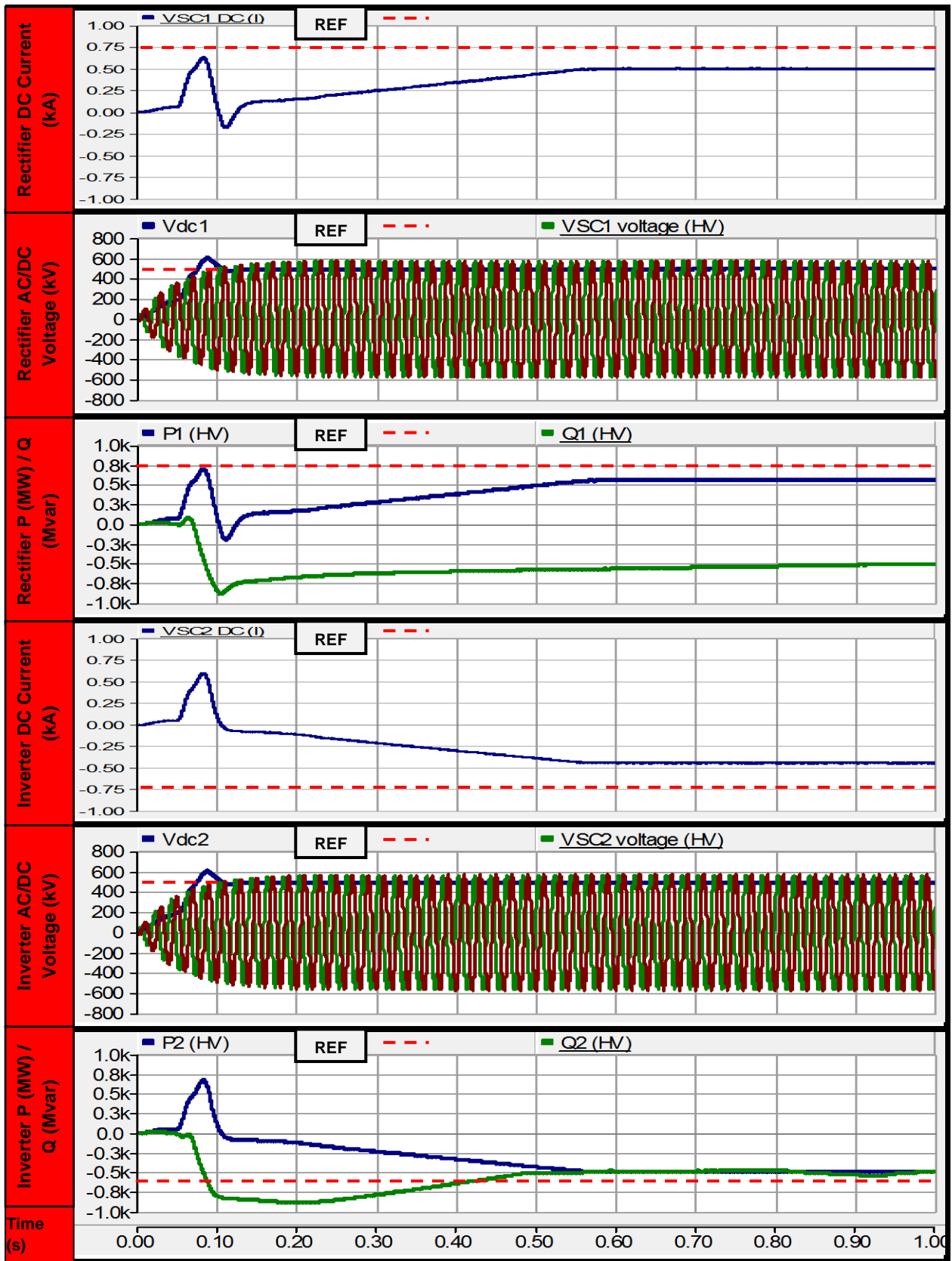


Figure 114: Profiles for rectifier SCR 1.0 and inverter 4.1 with adjusted control parameters

For the above situation, despite the capability of VSC-HVDC technology to operate in weak AC systems, limitations in active power transfer capability have been observed.

5.3.5 Rectifier SCR 2.5 and inverter 3.0

In Figure 115, simulation results for a rectifier SCR is 2.5 and the inverter 3.0 are presented.

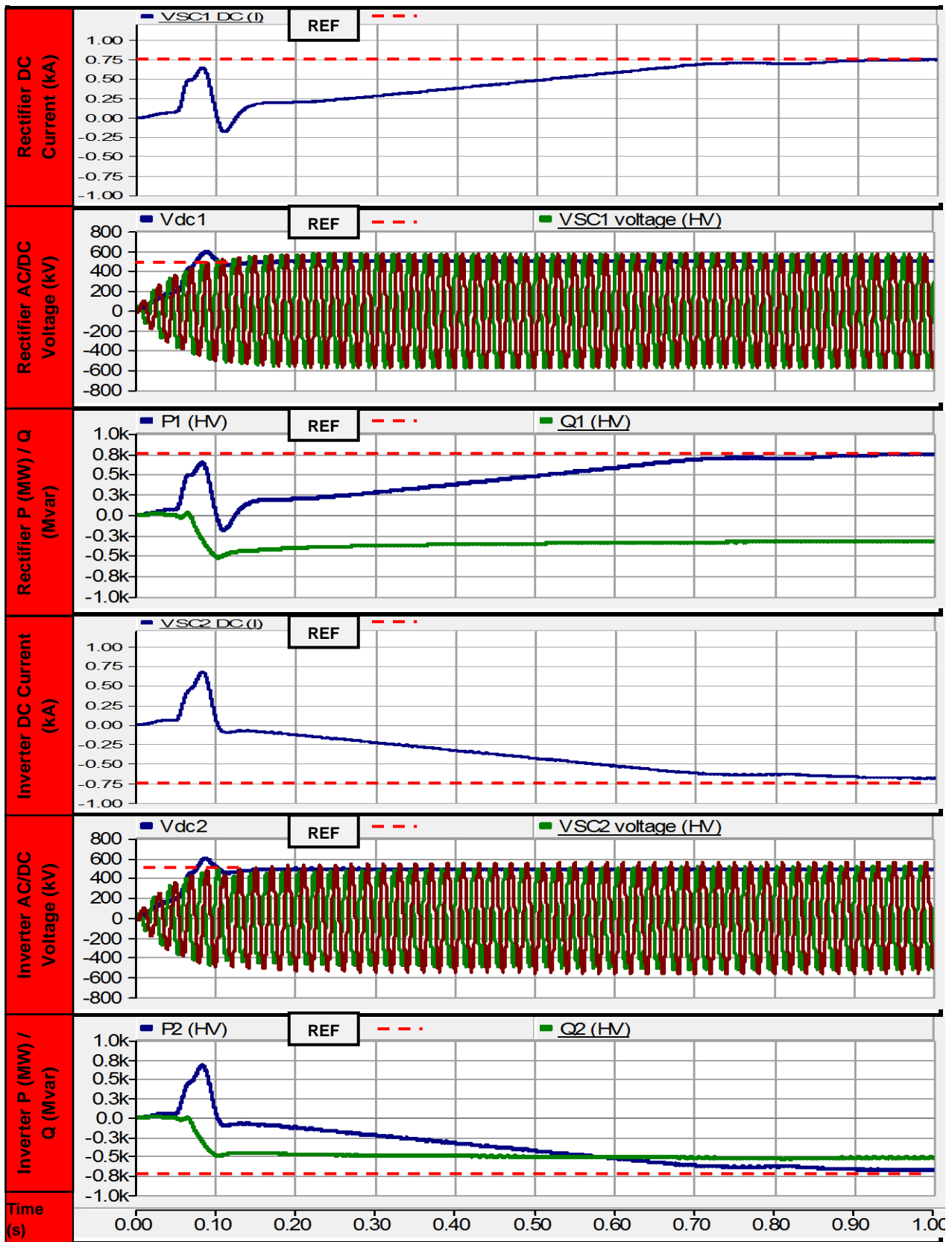


Figure 115: Profiles for rectifier SCR 2.5 and inverter 3.0 with nominal control parameters

Minor oscillatory responses are present in both the reactive power and DC active power profiles. At the inverter the active power delivered to the AC grid has dropped due to the losses over the length of the VSC-HVDC link [9].

The DC current references are maintained at both the rectifier and inverter, despite a minor oscillatory response being present in the profiles.

The DC voltage references are met and a stable response is achieved from the outer control loops.

The reactive power at each end of the VSC-HVDC link helps to keep the AC voltage profiles constant and ensures that stability is maintained during power transfer. Since no major instability has been encountered, the gains of the PI controllers have not been adjusted.

5.3.6 Rectifier SCR 2.5 and inverter 2.5

In this scenario the SCR (2.5) at both the rectifier and inverter are equal. The simulation results with nominal control parameters applied is shown in Figure 116.

The DC active power reference of 800 MW is achieved with minor oscillatory responses present in the profiles shown. As with previous simulations, the DC active power at the inverter is reduced due to the losses encountered over the VSC-HVDC link.

The DC current profiles at both the rectifier and inverter are stable with negligible oscillatory responses present.

The reactive power profiles are constant and help to maintain the AC voltages at both the rectifier and inverter.

The strong SCR at the rectifier helps the VSC-HVDC link to deliver the full active power reference of 800 MW from the NPP to the AC grid. Having the same strong SCR value at the inverter ensures that the active power can be received safely without any stability issues [77].

The PI controller gains and time constants are adjusted to see if a better system response can be achieved. The simulation results shown in Figure 117 are with optimal control parameters applied. The responses of the system have not changed compared to those shown previously in Figure 116; all reference values have been met and minor oscillatory responses are present in the profiles, suggesting that the requirement to change PI controller gains only exists if the control response shows high levels of instability [86].

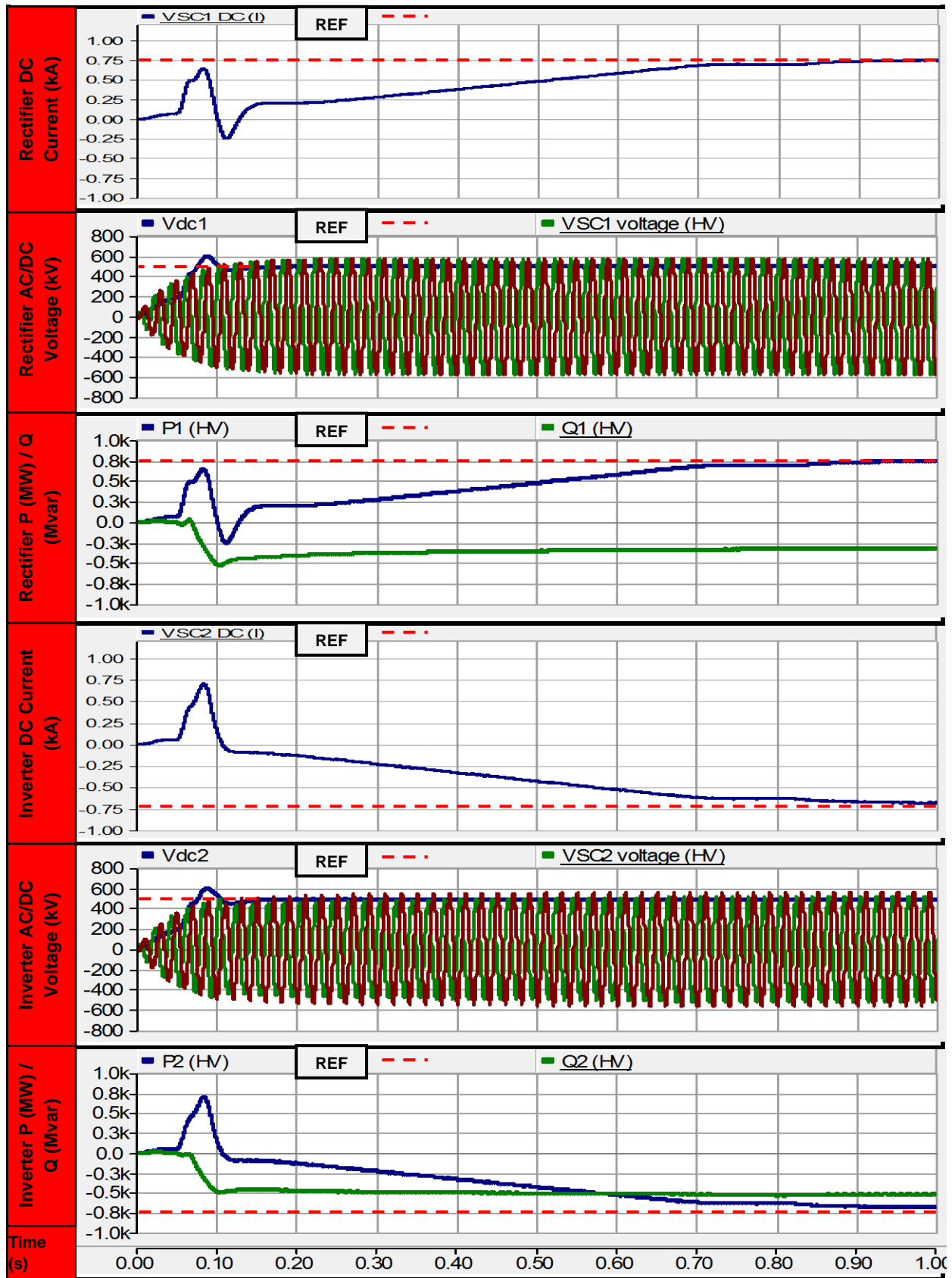


Figure 116: Profiles for rectifier SCR 2.5 and inverter 2.5 with nominal control parameters

The system is stable due to the SCR at both the rectifier and inverter being strong and no improvements in the responses can be achieved through the adjustment of the control parameters.

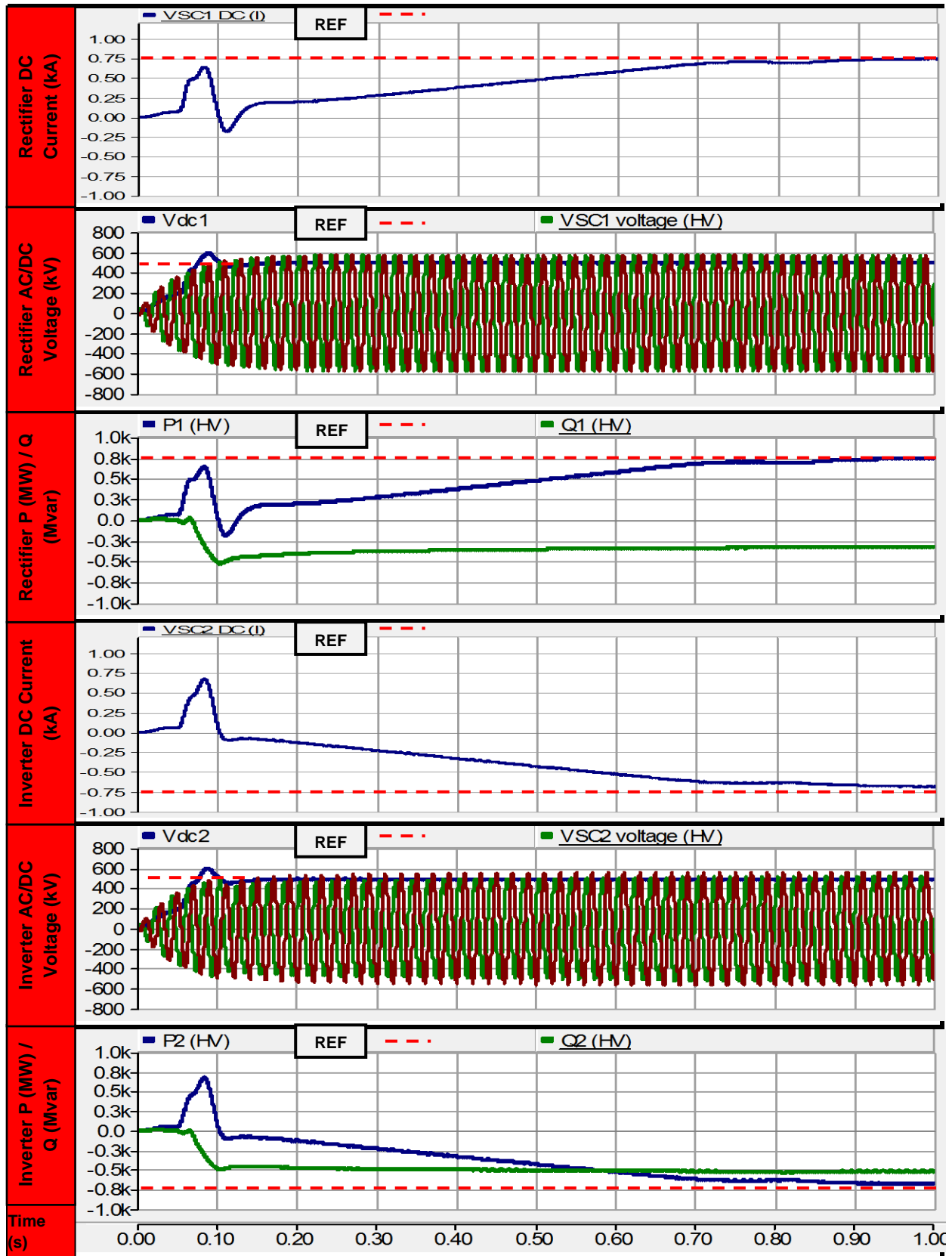


Figure 117: Profiles for rectifier SCR 2.5 and inverter 2.5 with adjusted control parameters

5.3.7 Rectifier SCR 2.5 and inverter 2.0

The inverter SCR was reduced further with nominal control gains applied.

The simulation results are shown in Figure 118.

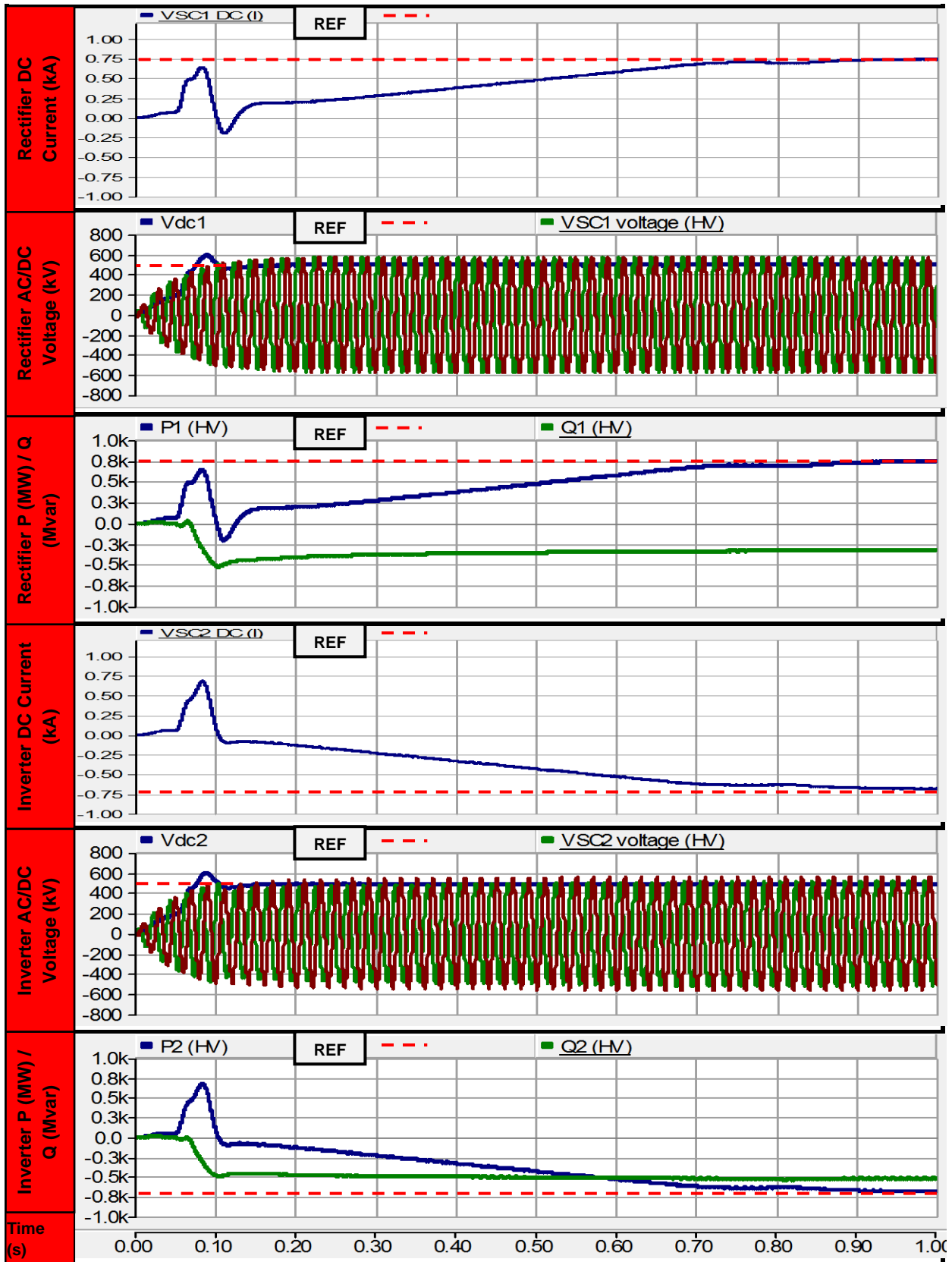


Figure 118: Profiles for rectifier SCR 2.5 and inverter 2.0 with nominal control parameters

Some minor oscillations are present in the profiles shown. The main difference here, compared to the previous simulations, is the time taken for the active power run-up to reach the reference target

of 800 MW – 750 ms compared to 100 ms in Figure 117.

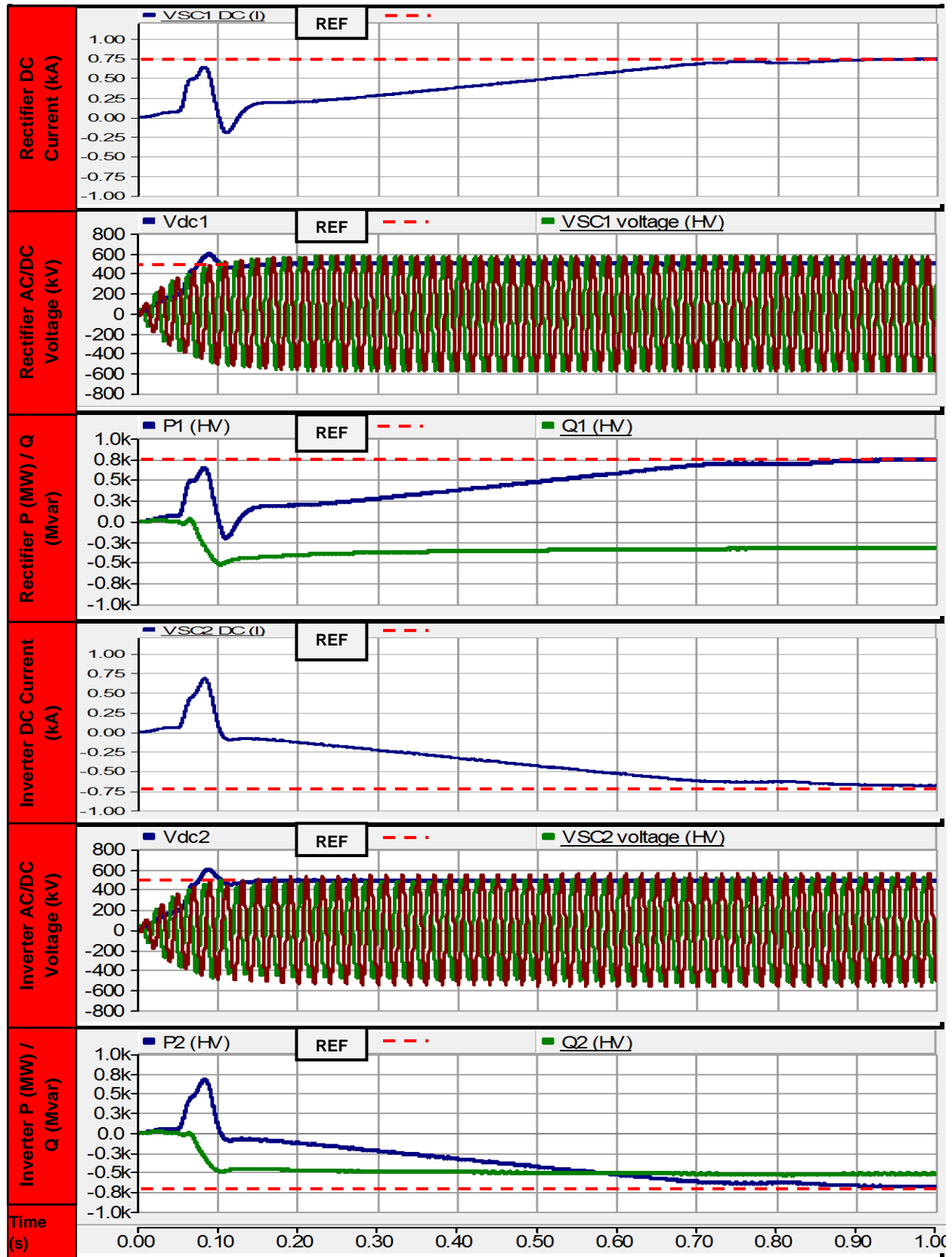


Figure 119: Profiles for rectifier SCR 2.5 and inverter 2.0 with adjusted control parameters

The control responses have not improved, which demonstrates the importance, when adjusting the parameters of PI controllers, of system strength in determining the possibility of achieving a

successful response.

Adjustments should only be made if the controller responses show large instability or if the physical transfer limits of the VSC-HVDC link are impacted; no benefits are found by adjusting the control parameters for a stable system [86].

5.3.8 Rectifier SCR 2.5 and inverter 1.6

In Figure 120 the inverter SCR is reduced to 1.6 with nominal control parameters applied. The response of the system changes significantly compared to the previous scenario where the SCR at the inverter was 2.0.

The active power reference of 800 MW cannot be achieved due to the weak point of connection at the inverter. Once the physical capability limit of 500 MW is reached, the active power level can no longer be maintained and the level drops significantly before becoming unstable, 900 ms after initial startup. Instability in the fast inner current control loops of the rectifier occur at the same time. Even though the rectifier SCR is kept strong, because of the weaker connection at the inverter, the sending end current is unable to be delivered to the receiving end [77].

As soon as the physical transfer capability of the VSC-HVDC link is reached, instability in the inner control loops is encountered and is affected by the inverter end. An adjustment in PI control parameters at the rectifier may improve the situation.

The nominal PI control parameters at the inverter provide a more stable response and require a smaller adjustment than the rectifier.

Reactive power is maintained at both ends of the VSC-HVDC link, which helps to keep the AC voltages stable. Despite this, minor instability in the reactive and active power control responses occur within 900 ms after initial startup.

The much slower outer control loops respond well and manage to keep the DC voltage references constant until active power transfer limits are reached, with only small oscillations appearing in the DC voltage profiles.

The profiles shown in Figure 120 have highlighted the need to adjust the PI controllers to obtain a more stable and improved control response from the VSC-HVDC link. Such adjustments are made through trial and error, giving the simulation results shown in Figure 121.

The control responses achieved are more stable and the instability observed in the previous simulation has been damped out.

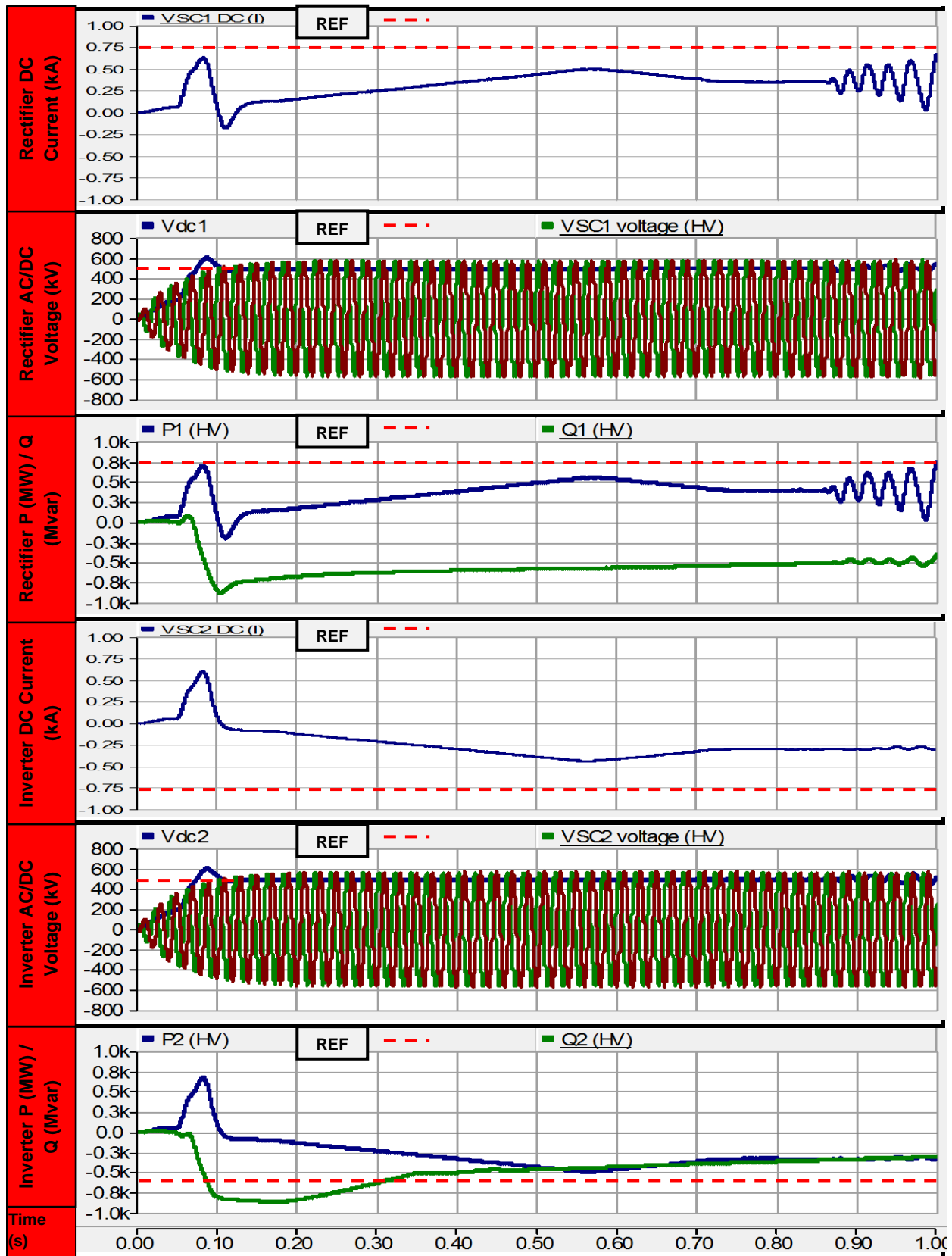


Figure 120: Profiles for rectifier SCR 2.5 and inverter 1.6 with nominal control parameters

The physical transfer capability of the VSC-HVDC link remains unchanged. Both the DC active power and current references cannot be met; for the active power transfer only 300 MW is achieved, which is nearly 40% less than the required reference of 800 MW.

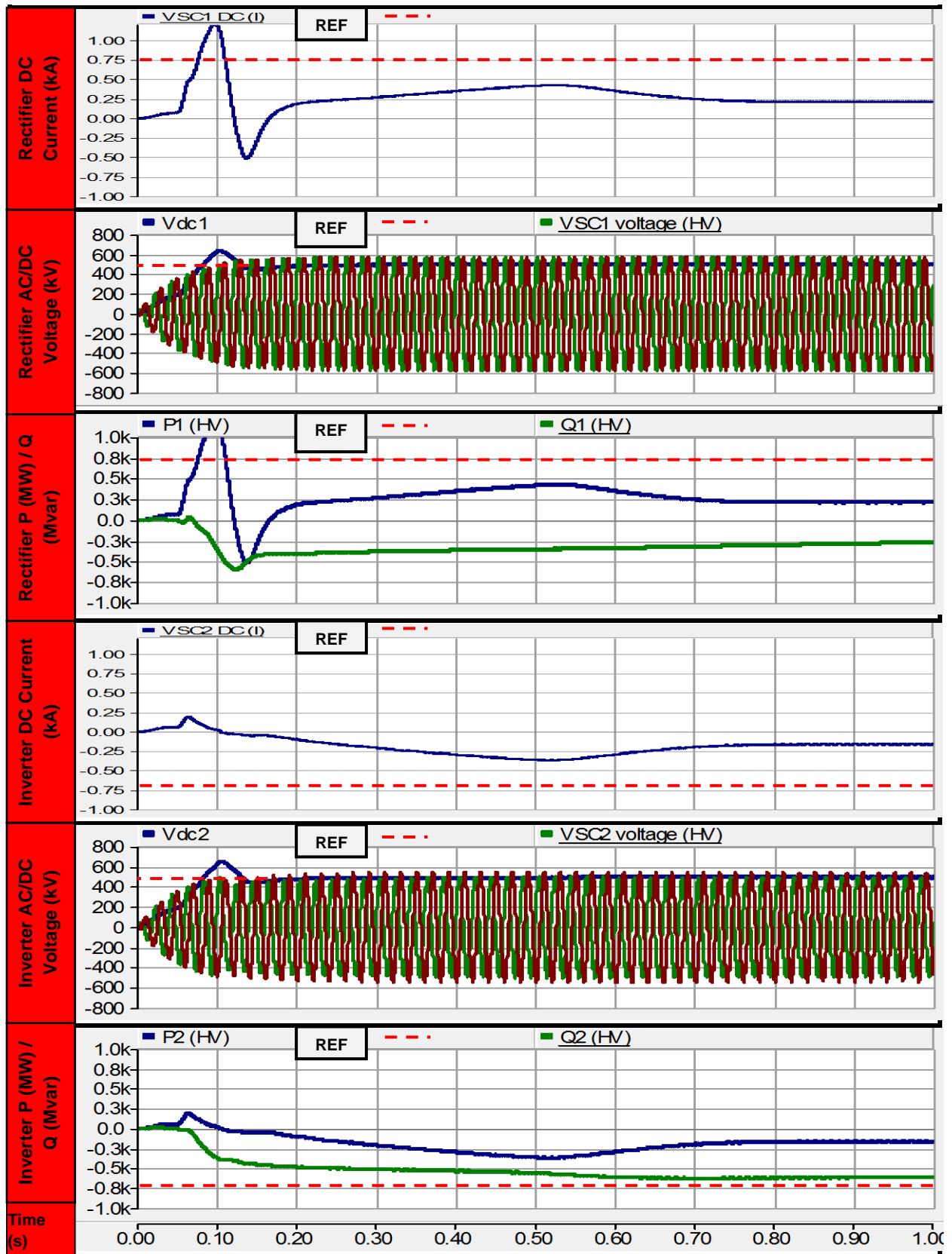


Figure 121: Profiles for rectifier SCR 2.5 and inverter 1.6 with adjusted control parameters

The adjustments in the DC voltage PI controller parameters have eliminated the oscillations encountered previously.

5.3.9 Rectifier SCR 2.5 and inverter 1.0

Using nominal controller parameters, the SCR at the inverter was reduced to 1.0. The simulation results are shown in Figure 122.

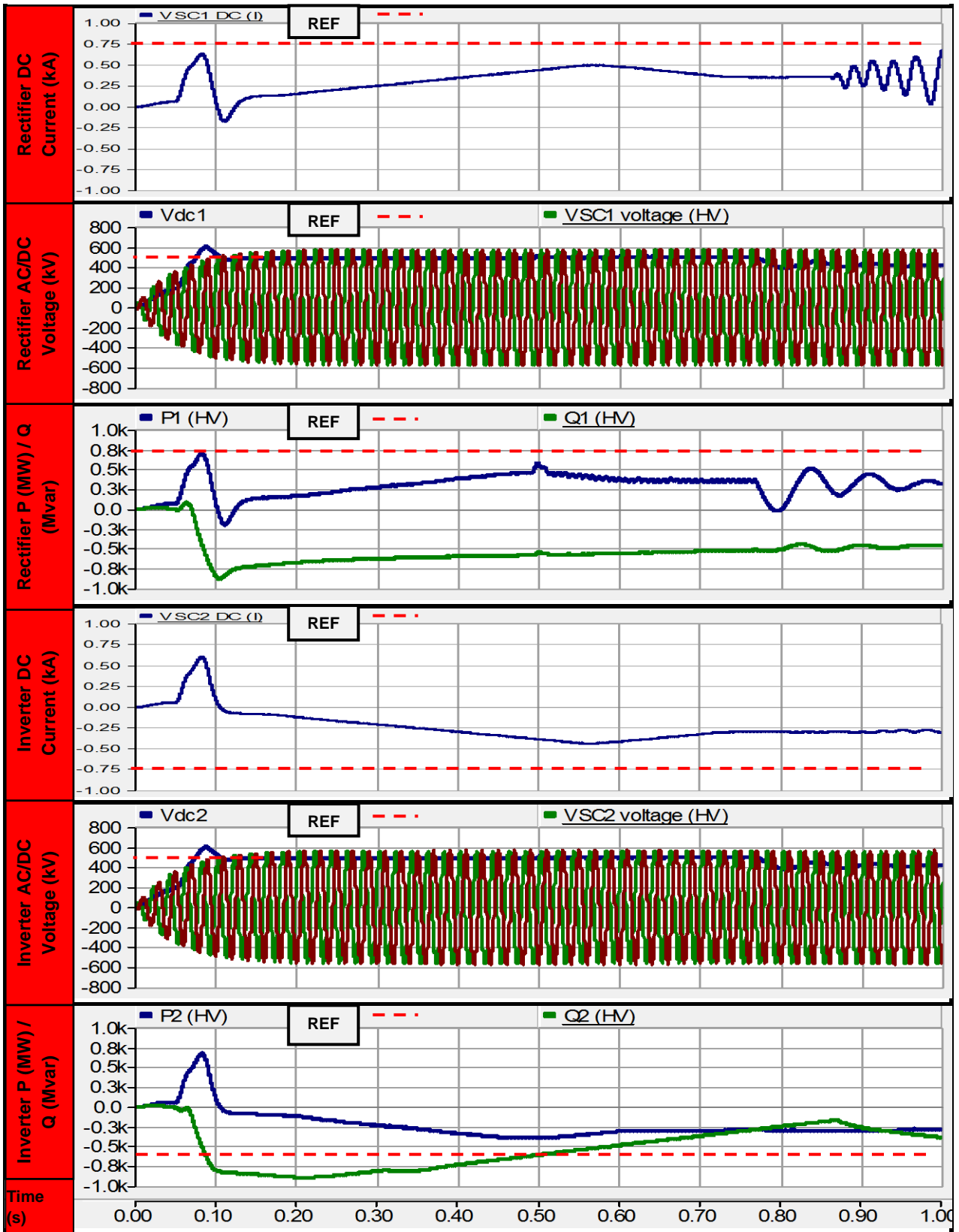


Figure 122: Profiles for rectifier SCR 2.0 and inverter 1.0 with nominal control parameters

The reduction in inverter SCR has caused large control instability in the responses obtained. The physical DC active power transfer capability of the VSC-HVDC link is limited to 500 MW for only 50 ms before the value drops further to 350 MW.

Once the active power level drops, the VSC pole capacitors discharge and the corresponding DC voltages at both the rectifier and inverter reduce to 400 kV. This in turn exacerbates the active power transfer further and leads to large oscillations within 800 ms after initial startup. Eventually the system becomes unstable.

The low frequency resonance at the inverter causes instability in the inner current control loops and is encountered within 800 ms after the initial startup of the system. The reference target has not been met.

The reactive power at the rectifier starts to oscillate 800 ms after startup but assists in keeping the AC voltage profile constant. The reactive power at the inverter is able to support the AC voltage but starts exhibiting instability 900 ms after startup once the overall system has become unstable. The AC voltage profiles increase due to the weaker inverter connection and increased impedance in the AC grid. In practice this issue would need to be studied as the overvoltage rating of the equipment could be exceeded and insulation may become damaged. The modulation index could be changed but this in turn could affect the dynamic capability of the VSC-HVDC link within the limits of the P–Q curve [75].

The PI controller gains were adjusted through trial and error to obtain a better control response for the weaker system connection at the inverter. The simulation results are shown in Figure 123. The overall system has become more stable and the oscillations present in the previous simulations shown in Figure 122 have disappeared.

The DC active power profiles display a more stable response but the transfer capability of the VSC-HVDC link is limited to 300 MW due to the lower SCR at the inverter.

Reactive power is maintained at both ends of the VSC-HVDC link and minor oscillations are present at the inverter. The AC overvoltage that was experienced at the inverter previously in Figure 122 has been reduced by the adjustment of the AC voltage controller gains, but the AC voltage at the rectifier is still high and this would need to be considered during the design stage of a real-life project [22].

The outer control loop response is vastly improved due to a more stable DC voltage response being obtained at both ends of the VSC-HVDC link.

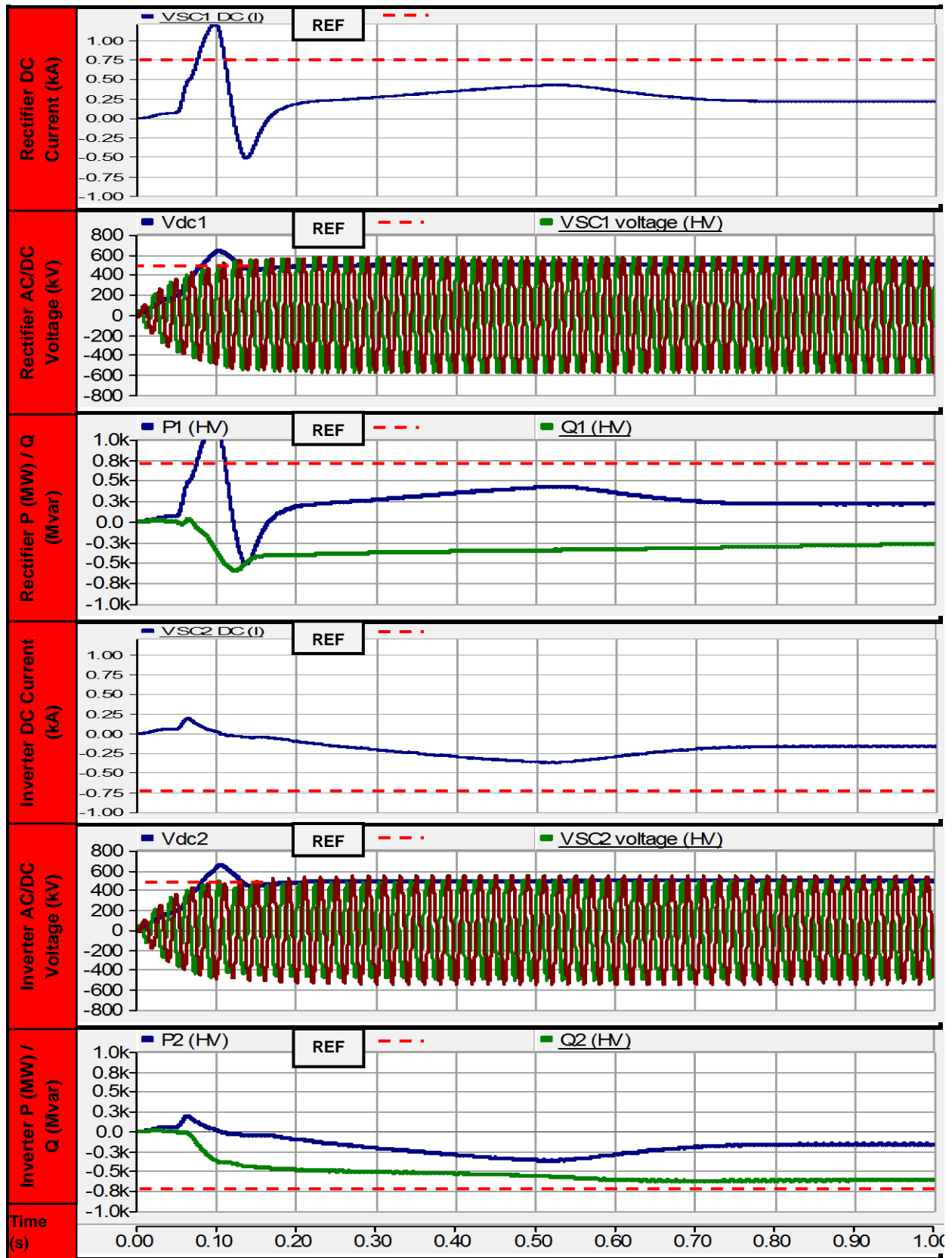


Figure 123: Profiles for rectifier SCR 2.5 and inverter 1.6 with adjusted control parameters

5.3.10 Rectifier SCR 1.0 and inverter 1.0

Simulation results for an SCR of 1.0 at the rectifier and inverter is shown in Figure 124.

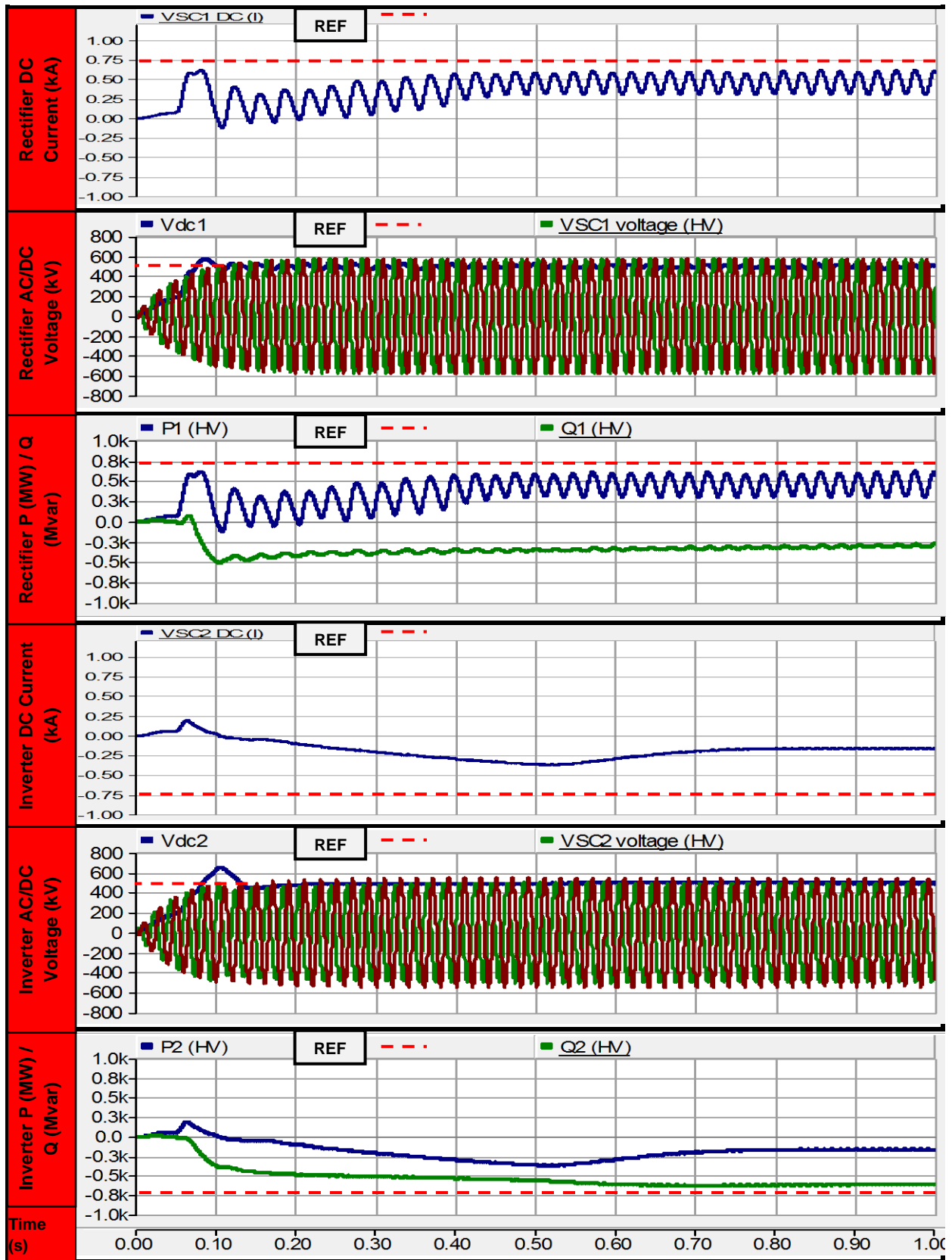


Figure 124: Profiles for rectifier SCR 1.0 and inverter 1.0 with adjusted control parameters

Due to the weak connection at the rectifier, instability is encountered in both the DC active power and current profiles. At the inverter, the profiles are more stable but the active power transfer capability is reduced to less than 300 MW and the current reference targets cannot be met.

The reactive power is maintained at both ends but minor oscillations are present at the rectifier. The AC voltages are held stable but the overvoltage at the rectifier is still present.

The oscillations in active power have caused instability in the DC voltage profile at the rectifier, and this propagates through the inverter.

The PI controller gains have been adjusted to improve the control response of the system. The simulation results in Figure 125 display a vast improvement in control response, and instability is reduced.

Despite the adjustment in active power controller gain, the physical transfer capability is still limited to a maximum of just over 300 MW. The weakened AC systems at both the rectifier and inverter have created issues for the PLL in synchronising with the bus voltages [161]. This produces delays and instability in the firing angle controls and affects the active power transfer capability of the VSC-HVDC link.

The DC current profiles are unable to meet the reference targets, despite a stable response being achieved.

The reactive power profiles are maintained, but at the inverter minor instability is encountered due to the lower SCR value. The AC voltage profiles remain unchanged from the previous simulations of Figure 124. The overvoltage at the rectifier is still present and would need to be considered during the design stage of a real-life project.

The changes applied to the PI controller have improved the overall system response but the maximum capability of the VSC-HVDC link has been reached.

The simulations have indicated the minimum SCR threshold of (1.0) on which successful power transfer can be achieved; any further reductions in SCR could further affect the stability of the system [161].

For the previous scenario, a statom or synchronous condenser will be required in practice to increase the SCR at both ends of the VSC-HVDC link and improve the active power transfer capability. In the present condition the VSC-HVDC link is unable to provide 100% usefulness and the cost investment in such technology may not be justified. With weak SCRs at both ends of the VSC-HVDC link, the low frequency resonance in the AC system is increased [81]. This causes instability within the fast inner current control loops at both ends of the VSC-HVDC link which can be improved by adjusting gains to slow down the control response.

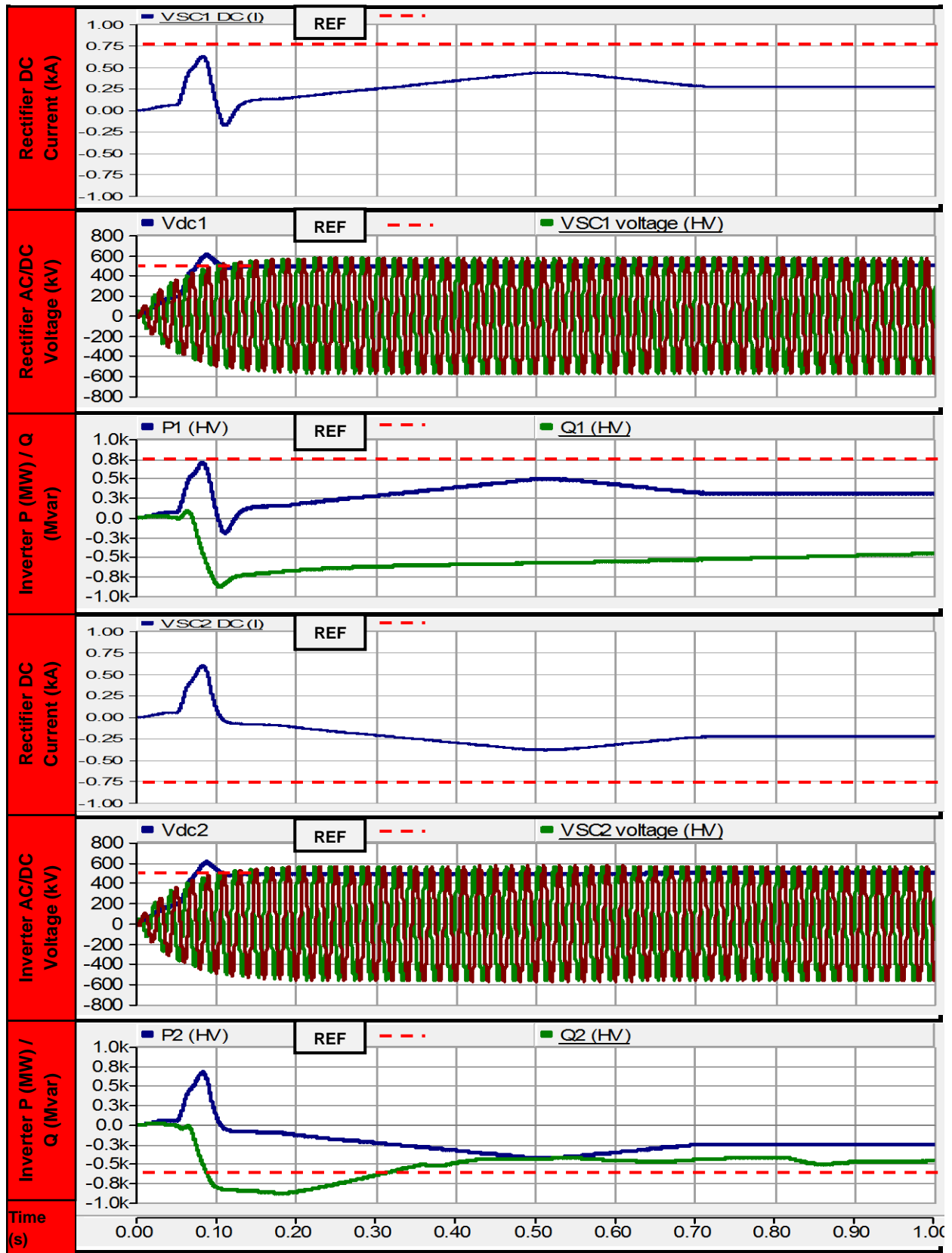


Figure 125: Profiles for rectifier SCR 1.0 and inverter 1.0 with adjusted control parameters

The optimised PI control parameters which provide the optimal control response for each of the different SCR combinations are shown in Table 17.

Table 17: Optimised PI controller gains for different combination of SCRs

SCR		DC voltage controller gain (Kpdc)		DC voltage controller time constant (Ti_dc)		Active power controller gain (Kpd)		Active power controller time constant (Kpd)		AC voltage controller Gain (Kpq)		AC voltage controller time constant (Tiq)	
Rectifier	Inverter	Rectifier	Inverter	Rectifier	Inverter	Rectifier	Inverter	Rectifier	Inverter	Rectifier	Inverter	Rectifier	Inverter
2.5	4.1	0.1	0.05	2.5	0.50	60	60	0.0002	0.0002	60	60	0.0002	0.0002
2.0	4.1	0.3	0.06	3.0	0.70	55	55	0.0001	0.0001	57	57	0.0002	0.0002
1.6	4.1	0.4	0.06	2.8	0.70	52	53	0.0001	0.0001	55	55	0.0001	0.0001
1.0	4.1	0.42	0.07	2.5	0.64	50	51	0.0015	0.0015	54	53	0.0015	0.0015
2.5	3.0	0.43	0.07	2.2	0.62	48	49	0.0012	0.0012	52	52	0.0013	0.0013
2.5	2.5	0.44	0.08	2.0	0.60	46	47	0.0010	0.0010	50	50	0.0011	0.0011
2.5	2.0	0.45	0.09	1.8	0.50	44	45	0.0010	0.0010	49	49	0.0010	0.0010
2.5	1.6	0.44	0.09	1.6	0.48	43	44	0.009	0.009	47	47	0.008	0.008
2.5	1.0	0.46	0.010	1.4	0.46	42	43	0.008	0.008	47	45	0.007	0.007
1.0	1.0	0.45	0.011	1.3	0.44	41	42	0.007	0.007	45	43	0.006	0.006

5.3.11 VSC-HVDC SCR analysis summary

The impact of the SCR on VSC-HVDC operation has been investigated through means of power system simulation carried out in PSCAD. Despite the capability of VSC-HVDC technology to operate down to very low SCLs, the SCR can have a profound effect where a vector current control strategy is employed [81]. With a reduced SCR, the AC system becomes weaker, and this increases the level of low frequency resonance [81]. The higher the low frequency resonance, the greater the impact on the fast inner current control loops of the VSC-HVDC system, which can cause unstable or oscillatory responses within the control system and affect VSC performance.

The VSC-HVDC PLL also has issues synchronising to the AC system and obtaining the phase angle reference for the valve firing control with a reduced SCR [161]. If the SCR at the rectifier reduces while the inverter remains constant, then power transfer can still be achieved down to a level of between 1.6 and 1.0.

The DC active power transfer capability of the VSC-HVDC link will reduce due to the weaker connection at the PCC. In the opposite scenario, where the SCR is constant at the rectifier and reduced at the inverter, a similar outcome is observed.

The gains and time constants for the PI controllers can be adjusted to improve the control response and system performance of the VSC-HVDC link. Care must be taken in selecting the correct PI controller values, as there could be no improvement in control response if the maximum transfer capabilities of the VSC-HVDC link for a given SCR level are reached.

5.4 Transient analysis of a VSC-HVDC NPP connection

Transient analysis is carried out in PSCAD to analyse a VSC-HVDC NPP connection. First a general fault analysis is carried out to identify those fault locations with the worst case effect on the voltage and power profiles of the various busbars. Here, a combination of both AC and DC faults are placed at multiple locations around the power system in Figure 70. Both the DC currents, DC voltages and reactor output power are monitored both before and during the faults. The faults with the worst case effects on the profiles are then selected for further detailed analysis in PSCAD.

Further simulations are then carried out to assess the impact of the VSC-HVDC control systems on the NPP connection and AC grid. System contingencies are created to analyse the potential benefits of the high-level VSC-HVDC controls on system operation.

5.4.1 General transient analysis

Within PSCAD, system variables consisting of both DC voltages and current are measured at the point of fault both before (pre-fault) and during the transient event.

The active power output of the reactor is also monitored during each fault to assess the simulated behaviour. The same power system layout and fault location shown in Figure 70 is used for the analysis. Table 18 shows the effects of the three-phase faults at both the rectifier (F19) and inverter (F14) on the VSC-HVDC link profiles; both the DC and AC voltages are significantly reduced and the reactor output power is increased during the faults.

The pole-ground and pole-pole DC faults show similar results, with a reduction in the DC voltage profiles. The DC pole-pole fault shows the most considerable effect, with voltages collapsing to zero. The reactor output power also reduces to zero, indicating a potential bottleneck during the simulation.

These faults are then selected for further detailed transient analysis studies in PSCAD.

Table 18: Results for VSC-HVDC general transient analysis

Fault Number/Location	Fault Type	Duration (msecs)	REC DC Pre-fault current (pu)	INV DC Pre-fault current (pu)	REC Pre-fault DC Voltage (kV)	INV Pre-fault DC Voltage (kV)	AC Pre-fault voltage (kV)	Pre-fault Reactor power (MW)	REC DC Current During fault (pu)	INV DC Current during fault (kA)	REC DC Voltage During Fault (kV)	INV DC Voltage During Fault (kV)	AC Voltage During fault (kV)	Reactor power During fault (MW)
F1	3Φ	140	1	1	500	500	400	500	1	1	500	500	0	500
F2	3Φ	140	1	1	500	500	400	400	1	1	500	500	0	500
F3	3Φ	140	1	1	500	500	400	300	1	1	500	500	0	500
F4	3Φ	140	1	1	500	500	400	800	1	1	500	500	0	500
F5	3Φ	140	1	1	500	500	400	600	1	1	500	500	0	500
F6	3Φ	140	1	1	500	500	400	300	1	1	500	500	0	500
F7	3Φ	140	1	1	500	500	400	400	1	1	500	500	0	500
F8	3Φ	140	1	1	500	500	400	300	1	1	500	500	0	500
F9	3Φ	140	1	1	500	500	400	600	1	1	500	500	0	500
F10	3Φ	140	1	1	500	500	400	800	1	1	500	500	0	500
F11	3Φ	140	1	1	500	500	400	500	1	1	500	500	0	500
F12	3Φ	140	1	1	500	500	400	500	1	1	500	500	0	500
F13	3Φ	140	1	1	500	500	400	600	2	3	500	300	0	1600
F14	3Φ	140	1	1	500	500	400	1000	3	4	200	400	0	2000
F15	3Φ	140	1	1	500	500	400	1000	1	2	500	400	0	1400
F16	3Φ	140	1	1	500	500	400	1000	1	2	500	400	0	1460
F17	3Φ	140	1	1	500	500	400	1000	3	4	200	0	0	2000
F18 (a)	Pole-G	140	1	1	500	500	N/A	1000	2.8	1.6	0	300	N/A	500
F18 (b)	P-P	140	1	1	500	500	N/A	1000	2.8	0	0	0	N/A	0
F19	3Φ	140	1	1	500	500	400	1000	1	0	0	0	400	2000
F20	3Φ	140	1	1	500	500	400	1000	1	1	0	0	0	500
F21	3Φ	140	1	1	500	500	400	600	2	2	500	500	0	500
F22	3Φ	140	1	1	500	500	400	600	2	2	500	500	0	520
F23	3Φ	140	1	1	500	500	132	500	1	1	500	500	0	550
F24	3Φ	140	1	1	500	500	23	500	1	1	500	500	0	500
F25	3Φ	140	1	1	500	500	11	500	1	1	500	500	0	500
F26	3Φ	140	1	1	500	500	400	600	1	1	500	500	0	500
F27	3Φ	140	1	1	500	500	400	700	1	1	500	500	0	1800
F28	3Φ	140	1	1	500	500	400	500	1	1	500	500	0	500
F29	3Φ	140	1	1	500	500	11	600	1	1	500	500	0	500
F30	3Φ	140	1	1	500	500	23	600	1	1	500	500	0	500
F31	3Φ	140	1	1	500	500	132	500	1	1	500	500	0	500
F32	3Φ	140	1	1	500	500	132	500	1	1	500	500	0	200
F33	3Φ	140	1	1	500	500	11	800	1	1	500	500	0	0
F34	3Φ	140	1	1	500	500	23	900	1	1	500	500	0	0
F35	3Φ	140	1	1	500	500	132	800	1	1	500	500	0	0
F36	3Φ	140	1	1	500	500	400	900	1	1	500	500	0	1800
F37	3Φ	140	1	1	500	500	400	700	1	1	500	500	0	1800
F38	3Φ	140	1	1	500	500	400	800	1	1	500	500	0	0
F39	3Φ	140	1	1	500	500	400	900	1	1	500	500	0	1600
F40	3Φ	140	1	1	500	500	132	900	1	1	500	500	0	0
F41	3Φ	140	1	1	500	500	400	1000	1	1	500	500	0	0
F42	3Φ	140	1	1	500	500	23	900	1	1	500	500	0	300
F43	3Φ	140	1	1	500	500	11	850	1	1	500	500	0	300

5.4.2 Detailed transient analysis of a VSC-HVDC NPP connection

Those fault locations which merited further detailed transient analysis are analysed and presented.

For the detailed transient analysis, all AC faults at 400 kV are cleared within the 140 ms stipulation time of the Grid Code [135]. For DC faults, these are permanent and are cleared by VSC-HVDC protection and control actions to prevent system instability. In the simulation plots, AC busbars 3, 18, 20 and 27 are monitored to observe whether the impact of the faults on the voltage profiles of reactor station 2. The reactor output power is also monitored to assess the effects of the faults on control operation.

In the following sections the rectifier, referred to as VSC1, is in DC voltage control mode and the inverter, VSC2, is in active power (P) control mode [22]. Both ends are in AC voltage control mode and will control the reactive power to maintain the reference voltage limit of 1.0 pu.

5.4.2.1 Three-phase fault on busbar 3

In this particular scenario a three-phase fault occurs on busbar 3, and is cleared by the AC protection within 140 ms.

In Figure 126, the AC voltage at VSC1 is unaffected by the fault due to the firewall function provided by the VSC-HVDC link and the reactive power, which is being maintained via Statcom operation [22]. The severity of the three-phase fault limits the reactive power at VSC2. Once the fault is cleared, a fast reactive power injection via Statcom operation is provided by VSC2 which allows the AC voltage at busbar 3 to fully recover within 20 ms.

The active power is temporarily reduced due to the collapse in AC voltage at VSC2. The DC current transfer reduces during the fault and is clamped by the current limiter control to limit the system impact [91].

With VSC2 being in active power (P) control mode, the temporary disruption causes the DC capacitors to charge and the voltage increases until the fault has been cleared; they then discharge back to nominal value [91]. At VSC1, the DC voltage is maintained throughout the simulation.

Harmonics are present within the DC current profiles and further tuning of the AC filters may be required in practice [19].

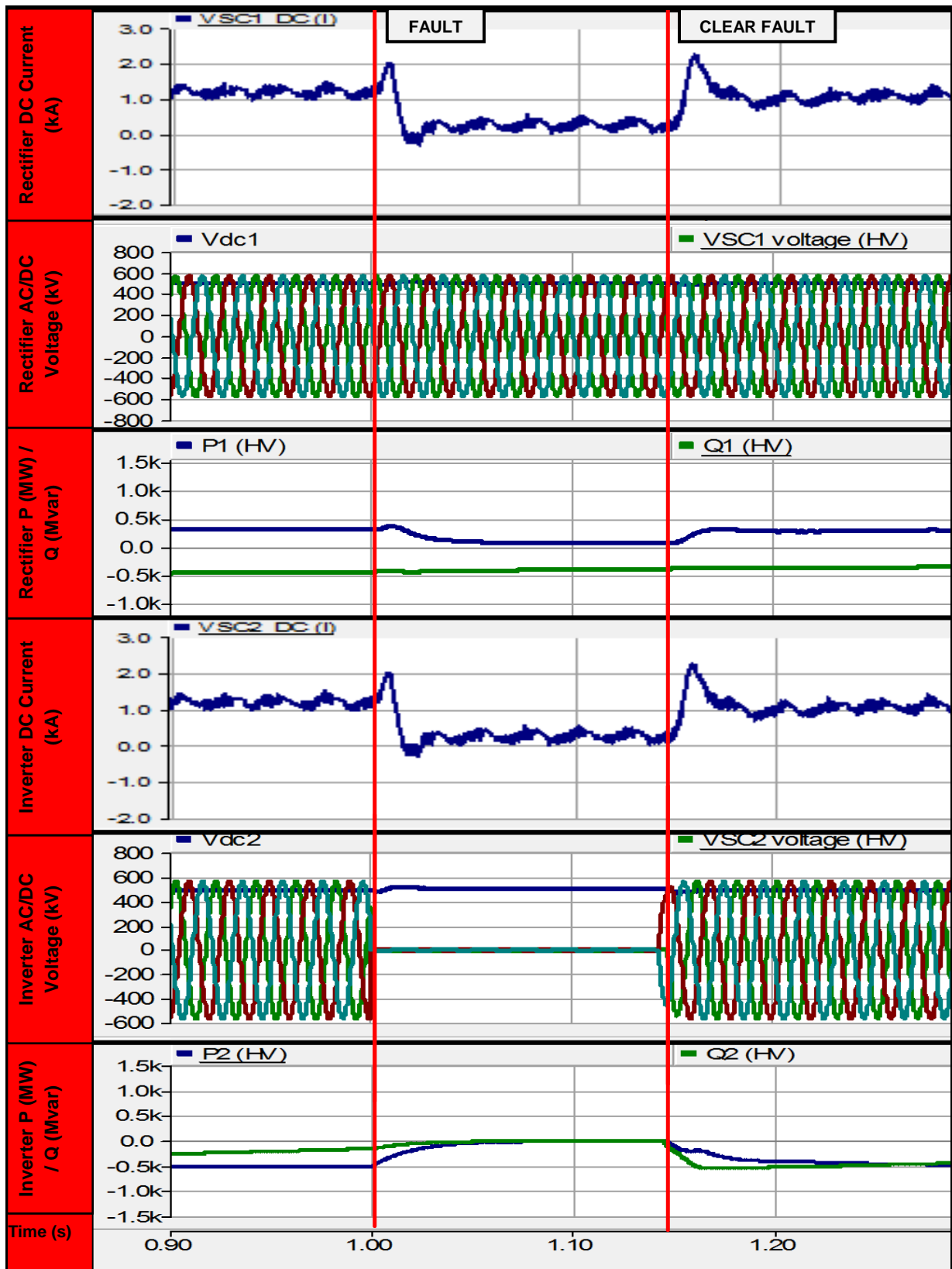


Figure 126: VSC profiles for three-phase fault on busbar 3

In Figure 127 the AC voltage at busbar 3 has collapsed due to the severity of the three-phase fault.

The AC current measured at both of the converter transformer valve windings is held constant due to the clamping of the DC current by the VSC-HVDC control system [5].

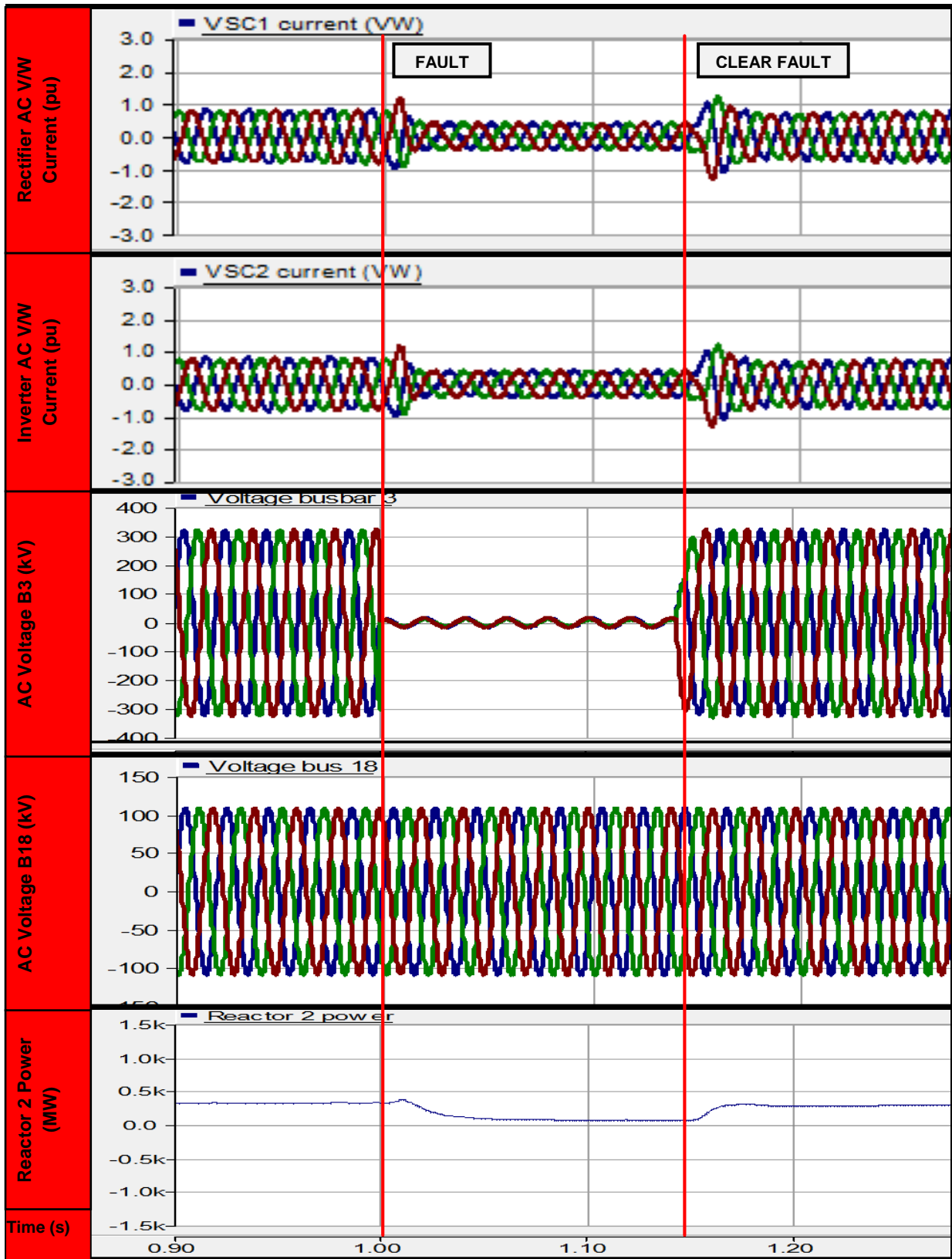


Figure 127: AC/DC profiles for three-phase fault placed at busbar 3

The busbars within the NPP have not been affected, due to a combination of the firewall function provided by the DC link and the Statcom functionality within VSC1 [19]. The power transfer from the reactor through the link has decreased during the fault due to the active power bottleneck, but recovers back to full transfer within 20 ms after the fault is cleared.

In summary, the AC side is not affected due to the firewall functionality of VSC-HVDC technology. The Statcom capability enables the AC voltage profile within the NPP to be maintained via control of the reactive power. A voltage depression is avoided and the security of supplies to the reactor safety systems is maintained. The current clamping capability of the HVDC control system reduces the impact and helps the system to recover. A combination of stable DC voltage control and fast reactive power injection post fault allows the nuclear reactor to ride through the fault and recover.

5.4.2.2 Three-phase fault on busbar 20

In this particular scenario a three-phase fault is placed on busbar 20 and is cleared by the AC protection within 140 ms.

In Figure 128, the AC voltage at VSC2 is not affected due to the decoupling provided by the DC link between busbar 20 and the AC grid [22]. Full Statcom functionality is provided, and helps to maintain the voltage profiles within the AC system connected to busbar 3. The reactive power at VSC1 is reduced during the fault but once cleared, a fast reactive power injection through Statcom operation is applied and the AC voltage recovers within 20 ms.

The DC voltage at VSC1 has increased due to the capacitors being charged. Once fault clearance has been achieved, the capacitors discharge and stable operation is resumed. At VSC2 the DC voltage reduces due to the capacitors discharging until active power recovery has been attained.

The DC current is clamped by the VSC control system to prevent system instability; aiding system recovery once the fault is cleared. DC harmonics are present within the current profiles and in practice the filters will need additional tuning to damp these out [19].

Active power transfer through the HVDC link is halted during the fault but once cleared the system recovers within 50 ms.

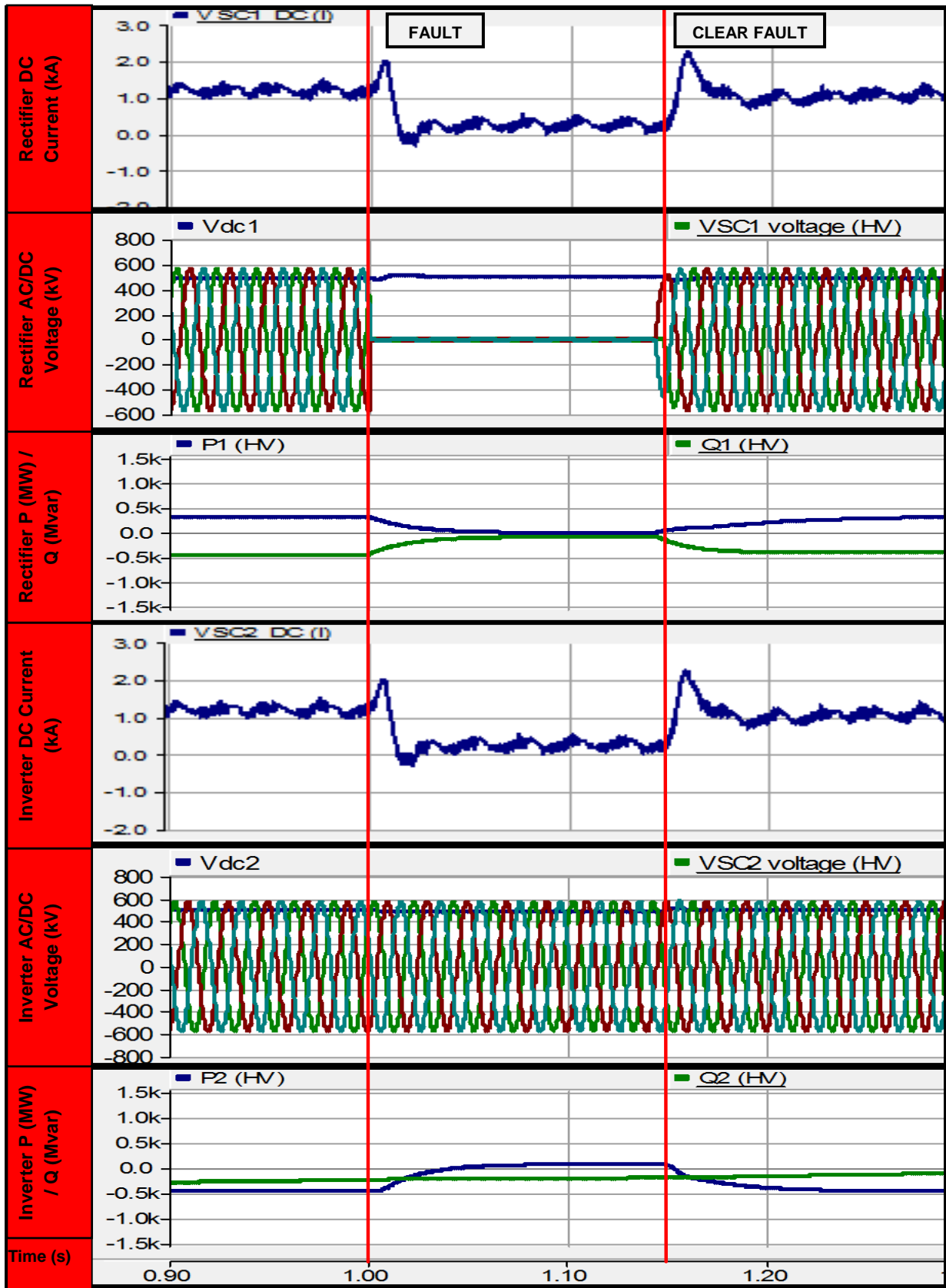


Figure 128: VSC system profiles for three-phase fault at busbar 20

In Figure 129 the AC valve winding currents are reduced and clamped during the fault.

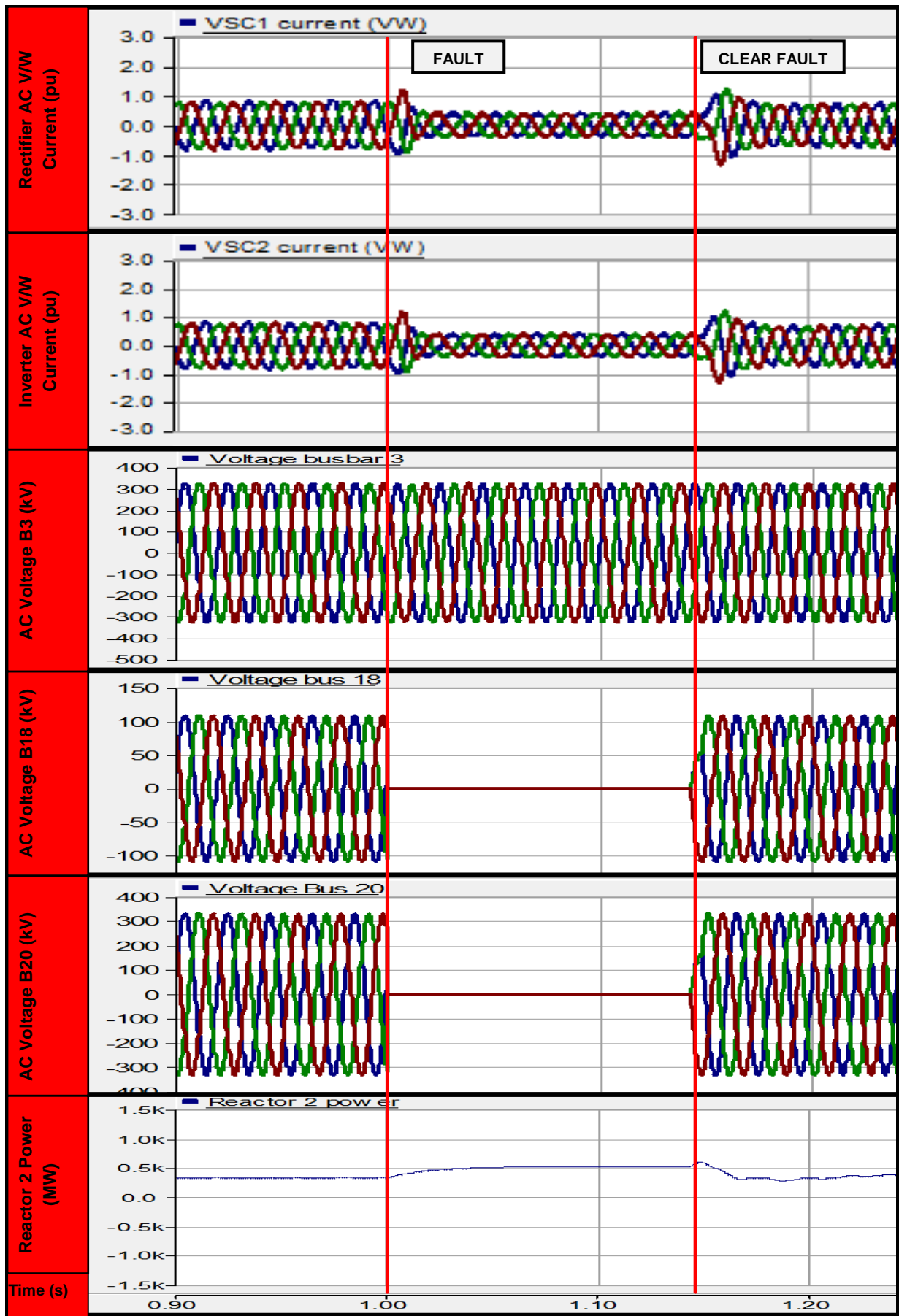


Figure 129: AC/DC profiles for three-phase fault at busbar 20

The firewall function provided by the VSC-HVDC link has prevented the voltage depression from penetrating into the AC network. The voltage has collapsed on busbars 18 and 20 and in practice, this would cause the undervoltage protection to operate, tripping the motors and compromising the safety of the NPP [106]. Provided that sufficient time delays are applied to the motor protection settings, then the Statcom operation at VSC1 will be able to restore the AC voltages back to nominal before protective tripping takes place [111].

The active power output from the reactor generator increases and feeds the fault until the governor control restores the value to the nominal level 160 ms after the fault.

In summary, the voltage depression occurs at busbar 20 and propagates into reactor station 2. The fast post-fault reactive power injection provided by the Statcom operation can help to restore the AC voltage. In practice, provided that suitable time delays are employed on the motor undervoltage protections, then these can be delayed from operating in order to allow the VSC to restore AC voltages back to nominal.

The AC voltage at the inverter remains unaffected due to the firewall function provided by the VSC-HVDC link and helps to maintain stability within the AC grid [75]. The nuclear reactor is able to ride through the fault provided that the governor control responds quick enough post fault.

5.4.2.3 Three-phase fault on busbar 4

A remote three-phase fault is placed on busbar 4 and is cleared by the local protection within 140 ms and in this scenario the fault ride-through capability of the VSC-HVDC link is analysed.

In Figure 130, most of the profiles on the AC side of VSC1 have been unaffected by the fault, due to the firewall function provided by the DC link. The DC and AC voltages have remained constant throughout except for some capacitor charging at VSC2. The Statcom functionality is available at VSC1 and helps to keep the AC voltage profiles within the NPP constant.

Once the fault clears, full active power is restored 40 ms after the event. The DC current is clamped by the VSC control system upon occurrence of the fault.

In Figure 131, the reactor output power has decreased due to the temporary cessation of active power transfer through the link. Following successful fault clearance, the power supplies to the reactor 2 nuclear station are restored. The AC voltage profiles on busbars 18 and 27 within the NPP are unaffected and the integrity of the reactor station 2 safety systems is retained. The active power of the reactor has decreased due to the bottleneck in active power transfer created by the three-phase fault.

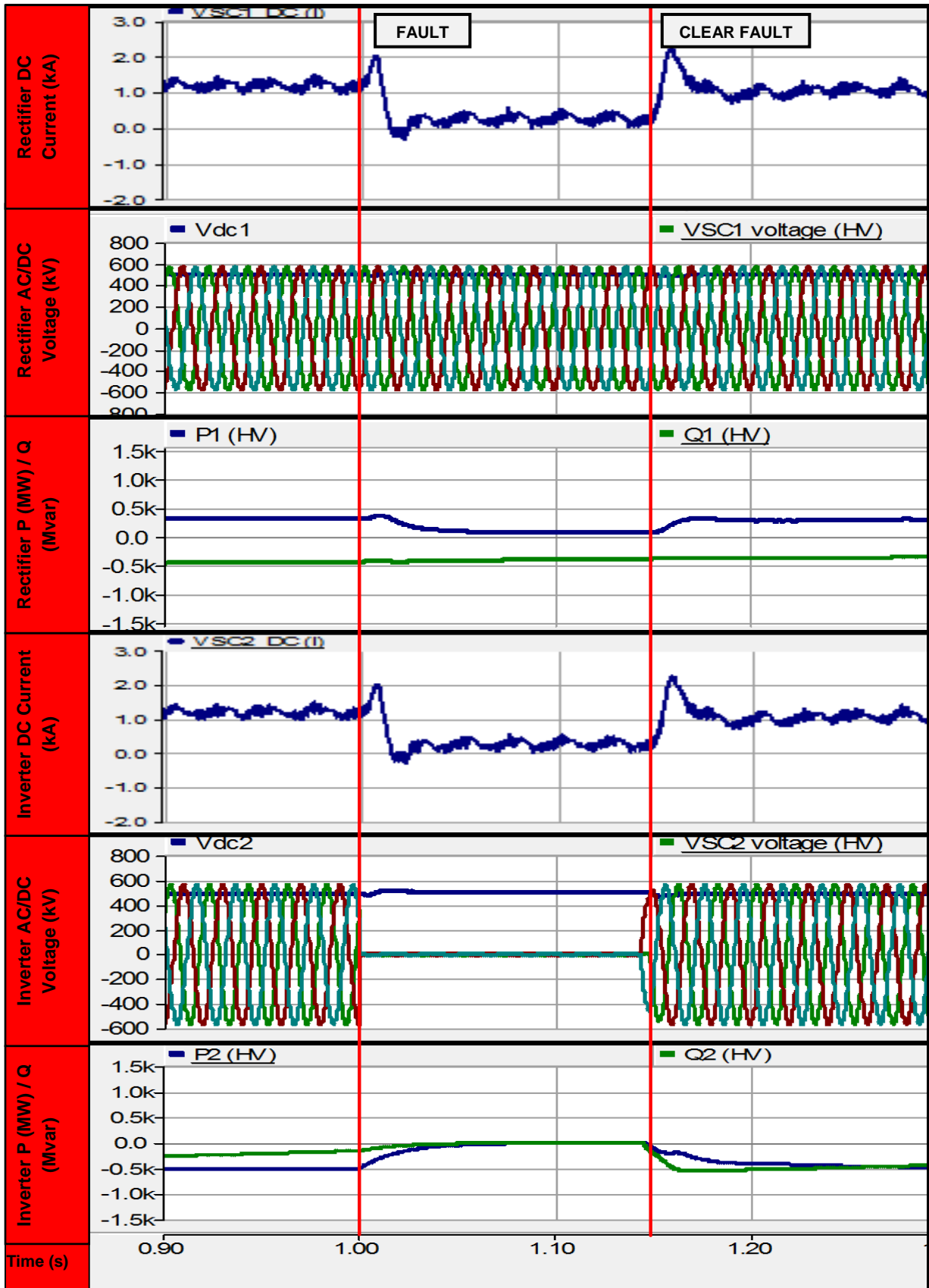


Figure 130: VSC profiles for three-phase fault applied on AC side of VSC2

Once the fault has been cleared, the output power returns to nominal within 20 ms.

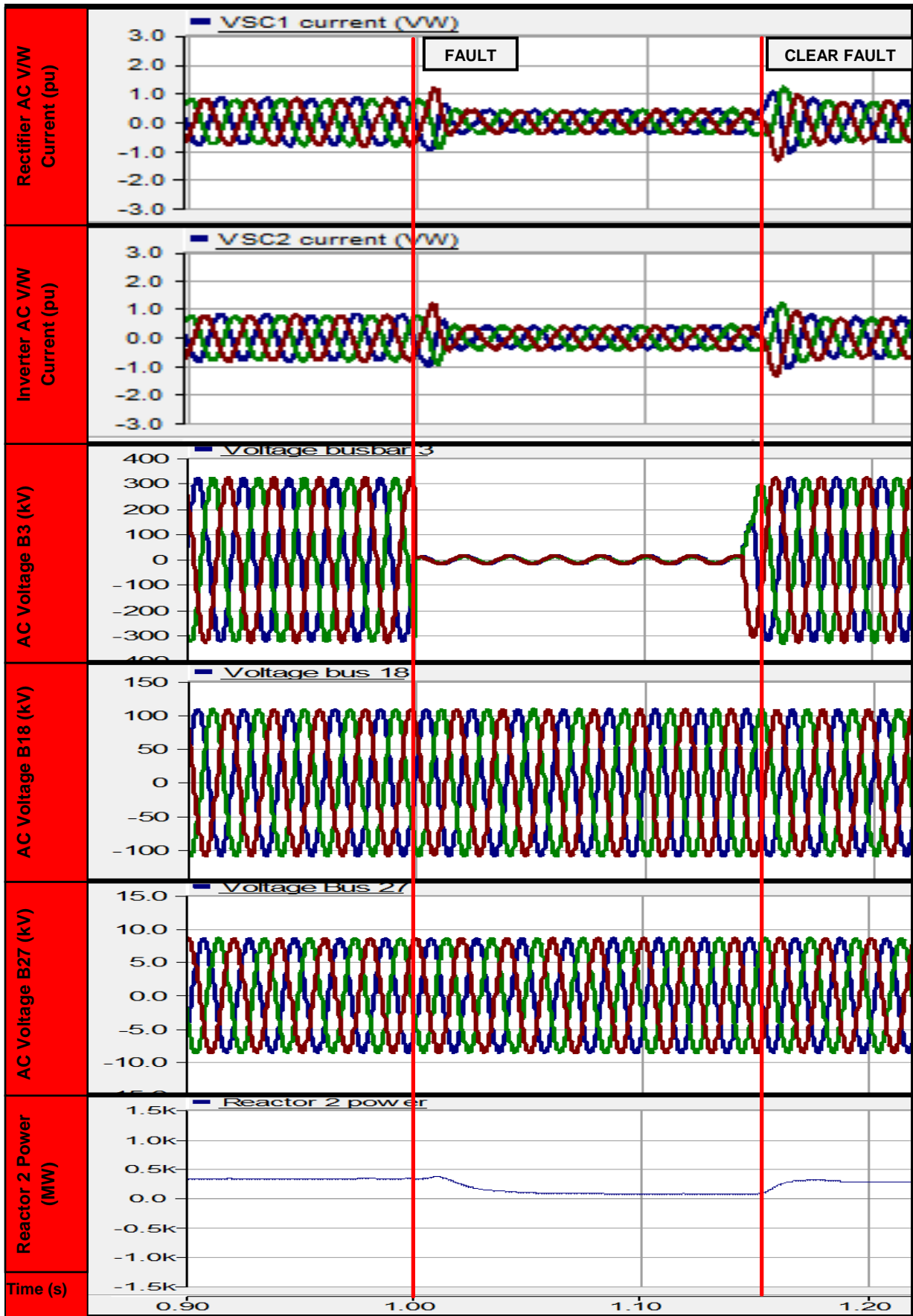


Figure 131: AC/DC Profile for three-phase fault applied on AC side of VSC2

In the recent scenario the fault-ride-through capability of VSC-HVDC technology for a remote three-phase AC fault has been analysed.

During the fault, the active power transfer decreases but then recovers post fault. The Statcom functionality at both ends of the VSC-HVDC link help the system to maintain voltage stability and the fast reactive power injection at VSC2 helps the AC voltage to recover post fault.

The DC control system clamps the DC current to a low value and allows full recovery once the system has regained equilibrium [22]. Despite the charging and discharging of the capacitors, both during and after the fault, the DC voltage is maintained. The reactor generator is able to ride through the fault and the governor is successful in restoring the active power back to nominal.

5.4.2.4 DC pole-to-ground fault

A pole-to-ground fault is applied on the DC side of the VSC-HVDC link at a time of 1.0 secs. The fault is cleared by applying protective blocks to both the rectifier and inverter, followed by opening of the pole AC circuit breakers. Total fault clearance is achieved within 140 ms.

In Figure 132, as soon as the fault is applied, the DC voltages at VSC1 and VSC2 are reduced and a large spike caused by the sudden interruption in power flow occurs. The AC voltages at both VSC1 and VSC2 are not affected.

The DC current approaches 8 kA in magnitude. As soon as the fault is detected, the converter valves are blocked within 20 ms, and then a tripping command is issued to all AC pole breakers. Fault clearance is then achieved within 140 ms of the tripping command, with all the AC pole breakers fully open. The current is reduced to zero and active power transfer ceases.

The active power and reactive power at VSC2 drop to zero during the fault and the Statcom functionality is unavailable once the converter valves have been blocked. In Figure 133, the AC voltages remain unaffected due to the fast fault clearance.

Large AC current spikes are present at both converter transformer valve windings, but are alleviated when the protection system has applied all of the necessary actions required to clear the DC fault.

The output power of the reactor fluctuates violently due to the disturbance, before normal operation is restored after the fault has been cleared. The reactor generator now supplies its own demand due to the VSC-HVDC link being removed from service [106].

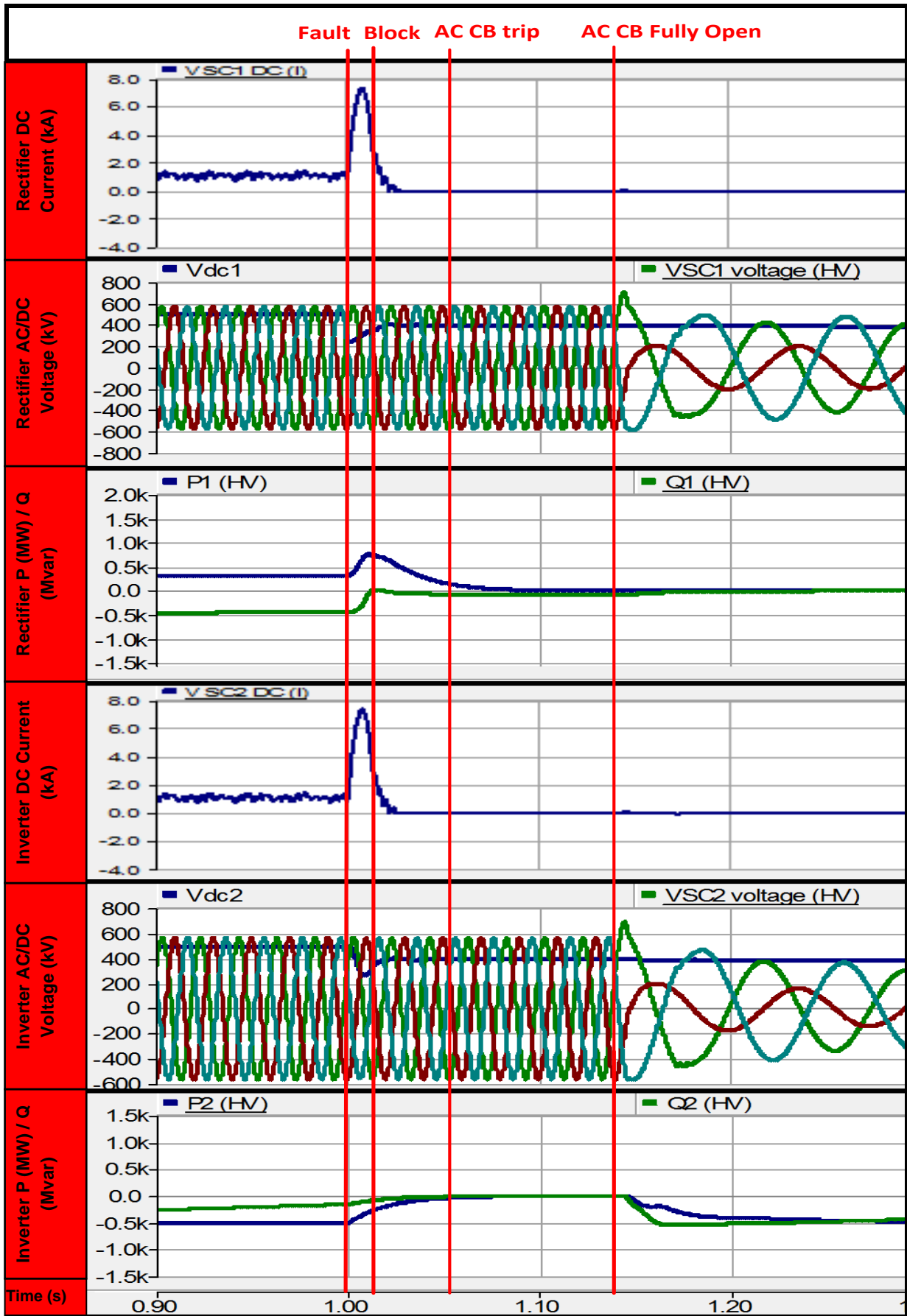


Figure 132: VSC system profiles for pole-to-ground fault

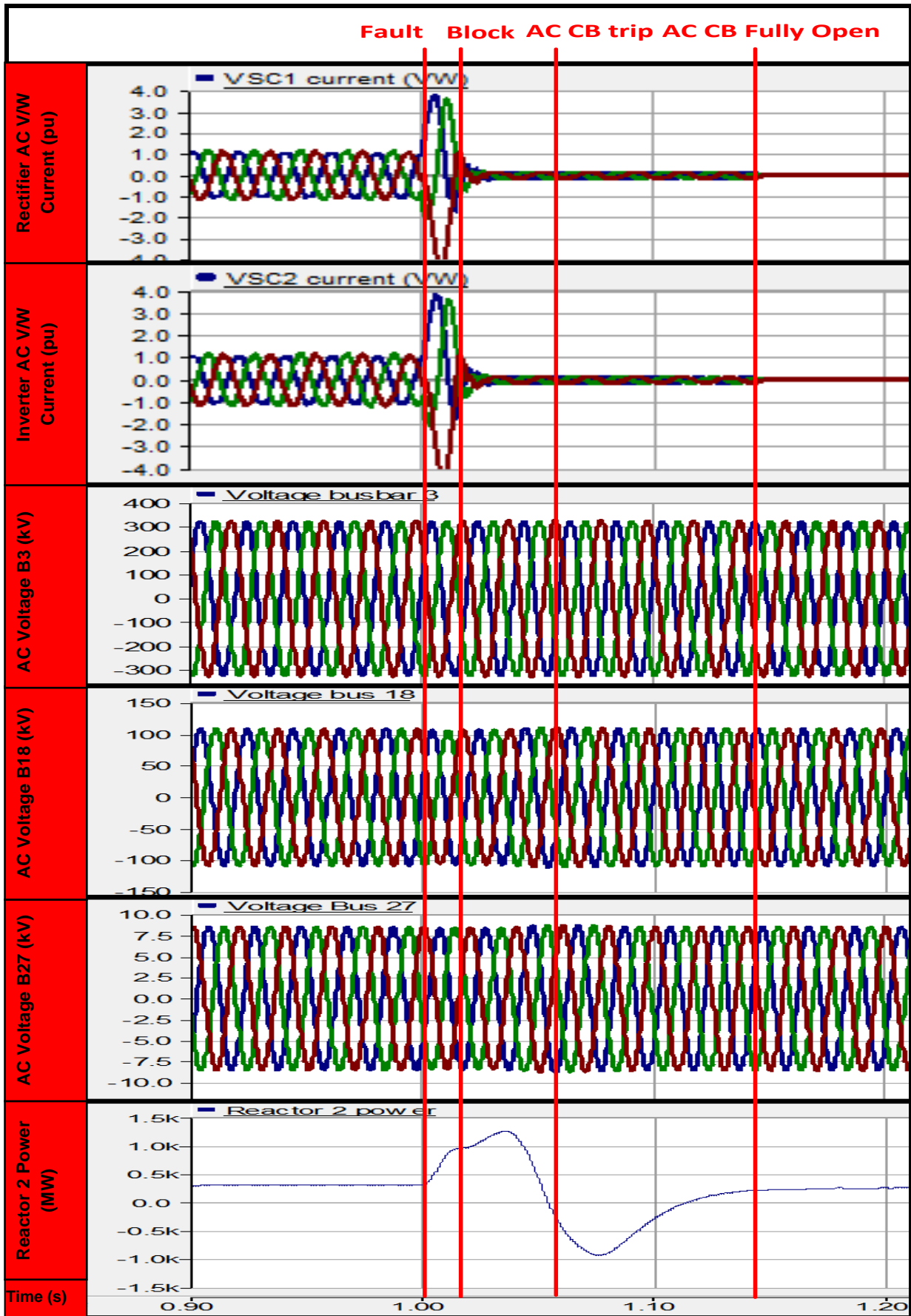


Figure 133: AC system profiles for DC pole-to-ground fault

In summary, a DC pole-to-ground fault has been successfully cleared by the HVDC protection and control system. Full clearance must be achieved as soon as possible to prevent system instability and large DC fault currents from damaging equipment [5]. Following the blocking of the converter valves, the DC current starts to decay and Statcom functionality becomes unavailable. Following successful fault clearance, the VSC-HVDC link is removed from service and the reactor generator must stay connected in order to supply its own in-house demand.

5.4.2.5 DC pole-to-pole fault

A pole-to-pole fault is applied on the DC side of the VSC-HVDC link at a time of 1.0 secs. The fault was cleared by applying protective blocks to both the rectifier and inverter, followed by the opening of all pole AC circuit breakers. Total fault clearance is achieved within 140 ms.

In Figure 134, as soon as the fault is applied, DC voltage collapse occurs at both VSC1 and VSC2. Free-wheeling rectification is encountered and the DC current remains uncontrolled until the pole AC circuit breakers have been fully opened following the application of protective blocks to both converters [61]. Large oscillations in both the active, reactive power and DC current profiles are present during the uncontrolled free-wheeling rectification. If this type of fault was not cleared by the DC protection system this could have a major impact on the NPP and cause instability.

The DC current reaches 8 kA at both VSC1 and VSC2 and must be limited otherwise this could damage the IGBTs and equipment due to overload tolerance limitations [61].

As soon as the converter valves are blocked, the ability to provide Statcom support to both the NPP and AC network is removed. Once the fault has been cleared, the active power transfer ceases and the VSC-HVDC link is out of service.

In Figure 135, the uncontrolled free-wheeling diode rectification can be seen in the AC valve winding currents. After both converter valves have been blocked, the current still remains uncontrolled due to the path through the IGBT protective diodes associated with half-bridge VSC-HVDC configurations [22]. This is prevented once the pole AC circuit breakers have fully opened.

The AC voltages within the NPP have been unaffected due to the fast protective actions carried out by the DC link. Oscillations appear in the active power profile of reactor 2 as soon as the DC fault occurs. Once the fault has been cleared, the oscillations gradually decay and eventually disappear.

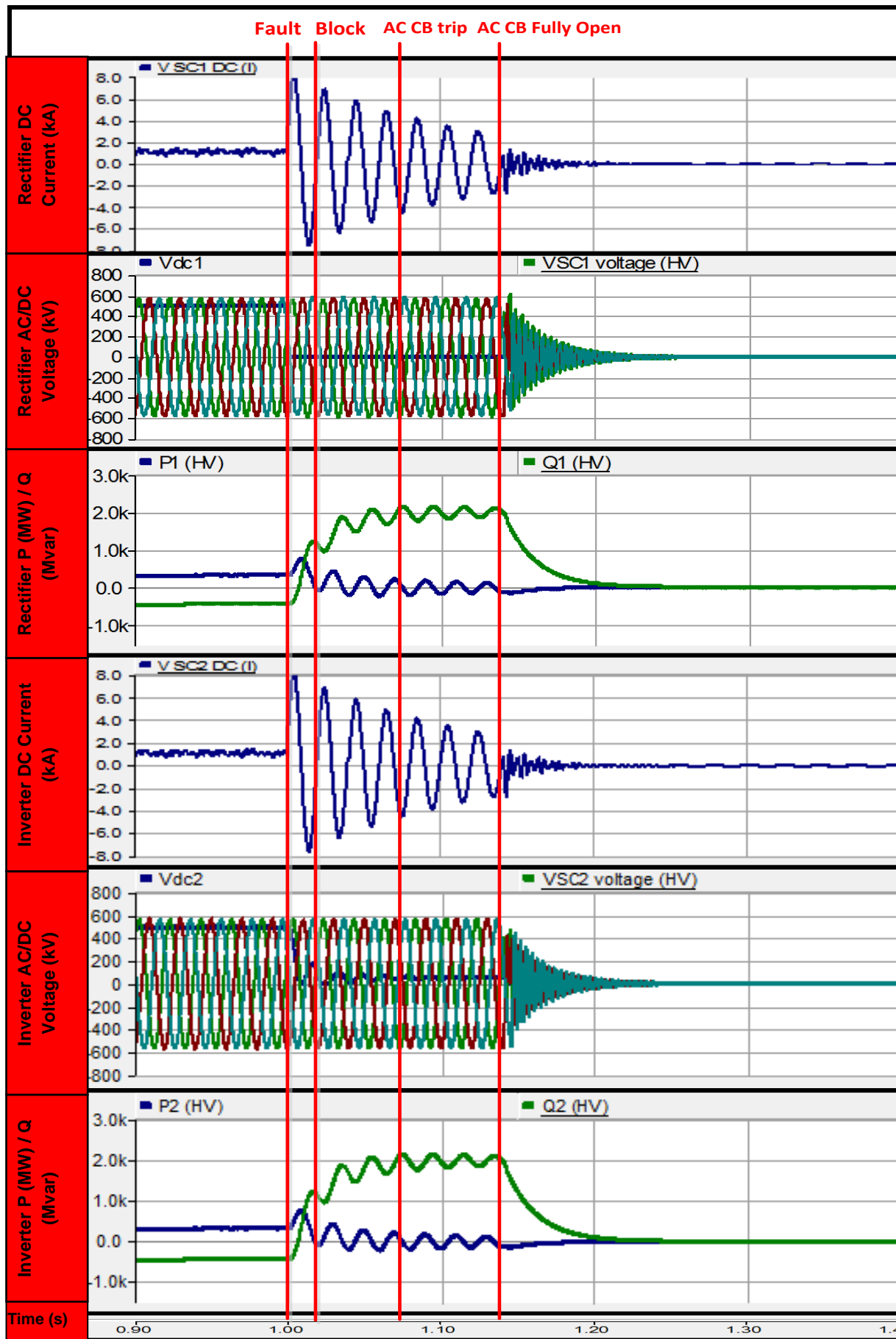


Figure 134: VSC profiles for DC pole-to-pole fault

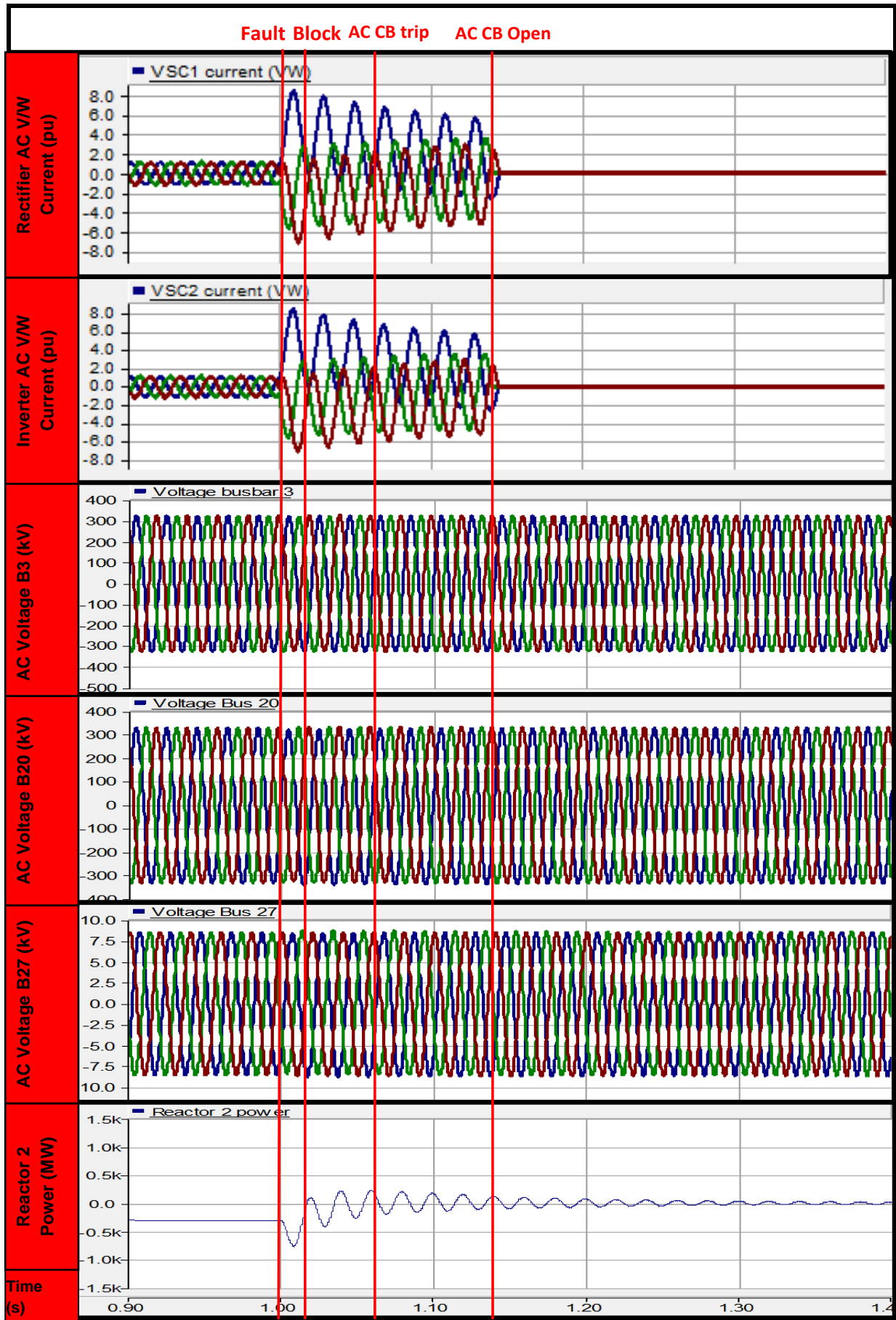


Figure 135: AC/DC profiles for DC pole-to-pole fault

In summary, a DC pole-to-pole fault is successfully cleared by the HVDC protection and control system. Full clearance must be achieved as soon as possible, in order to prevent system instability due to the uncontrolled free-wheeling diode current rectification. Following blocking of the converter valves, the DC current starts to decay and Statcom functionality becomes unavailable. In half-bridge VSC-HVDC converters, blocking of the valves reduces (but does not stop) the free-wheeling effect [5]. The AC pole breakers must be opened to fully suppress DC side faults. Following successful fault clearance, the VSC-HVDC link is removed from service and the reactor generator must stay connected, in order to supply its own in-house demand islanded from the AC grid.

5.4.3 Contingency analysis

Three system contingencies within the AC network and NPP are created to analyse the response of the VSC-HVDC controls. The aim of the analysis is to determine whether any of the control functions can be of benefit to the NPP or AC grid for different system contingencies. These studies help to assess the suitability of the VSC-HVDC link for the supply of power to the NPP and evaluate the effectiveness of the active power modulation control functionality.

5.4.3.1 VSC-HVDC contingency 1

In the following contingency the VSC-HVDC inverter AC pole breaker is tripped due to a local fault within the AC network. Simultaneously, a three-phase busbar fault has occurred on busbar 19 within the switchyard of reactor 2 nuclear station. A single-phase-to-ground fault occurs soon after on busbar 19. The rectifier remains connected to reactor station 2 in Statcom operation following the removal of load due to the tripping of the inverter. This particular contingency is devised based on the learning from the literature review in chapter 2 and the author's personal industry experience gained from NPP visits.

In Figure 136, the DC voltage is held constant at VSC1, allowing Statcom operation and control of the reactive power in order to keep the AC voltages within reactor station 2 constant, despite the fault on busbar 19. In industry, by helping to control the AC voltage at the PCC, this will help prevent potential operation of undervoltage protections on the reactor cooling pumps and motors. This allows power supplies from the NPP generator to the essential safety systems to be maintained and ensures that reactor cooling is provided [3]. Following the trip of the inverter AC pole breaker at VSC2, Statcom operation is lost and both the reactive and active power profiles drop to zero. The DC voltage is held constant, and if the circuit breaker is reclosed for a transient fault, then power operation could be started up again by operator action. As soon as the inverter AC pole breaker is opened, then the voltage decays.

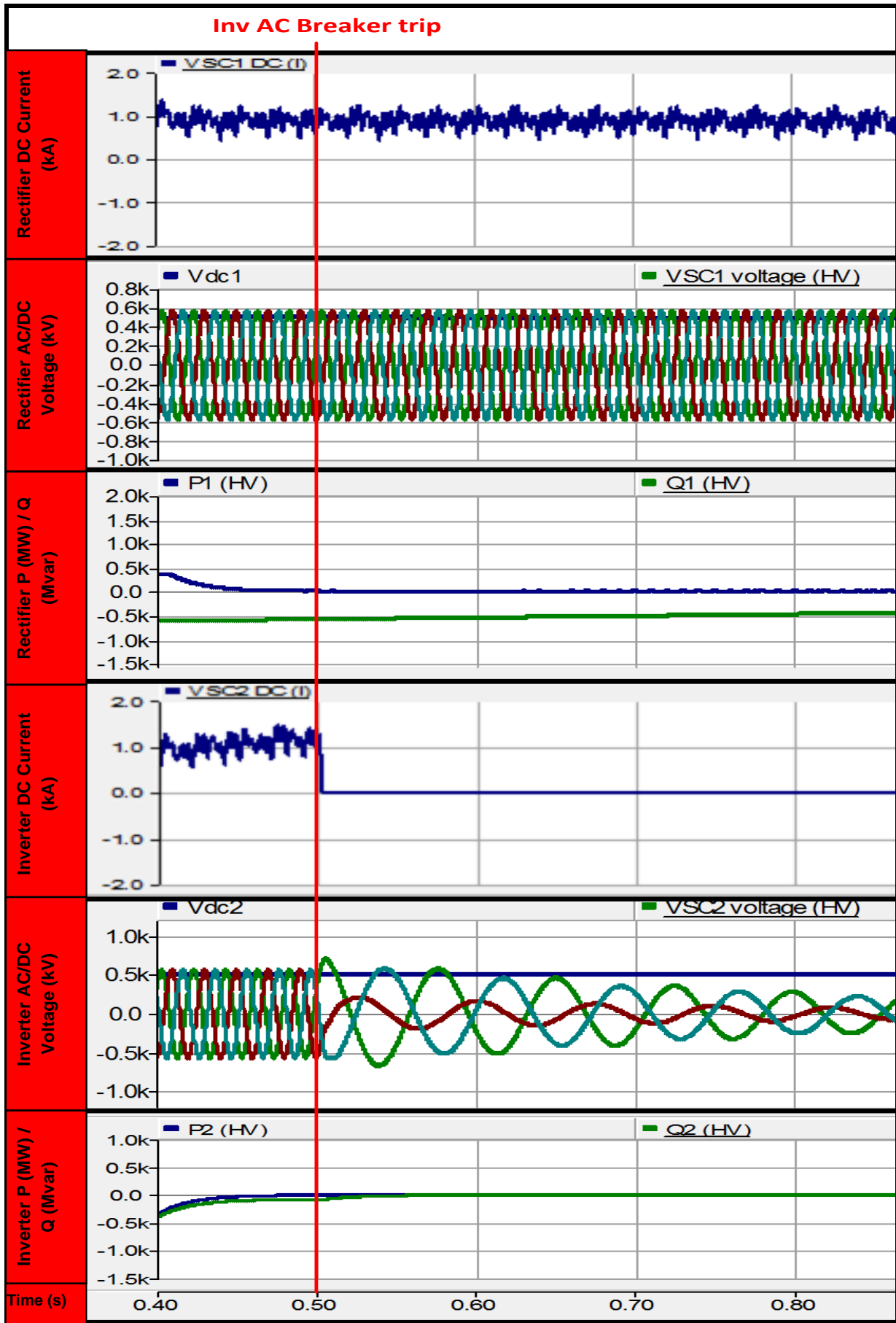


Figure 136: VSC profiles for inverter AC pole breaker trip

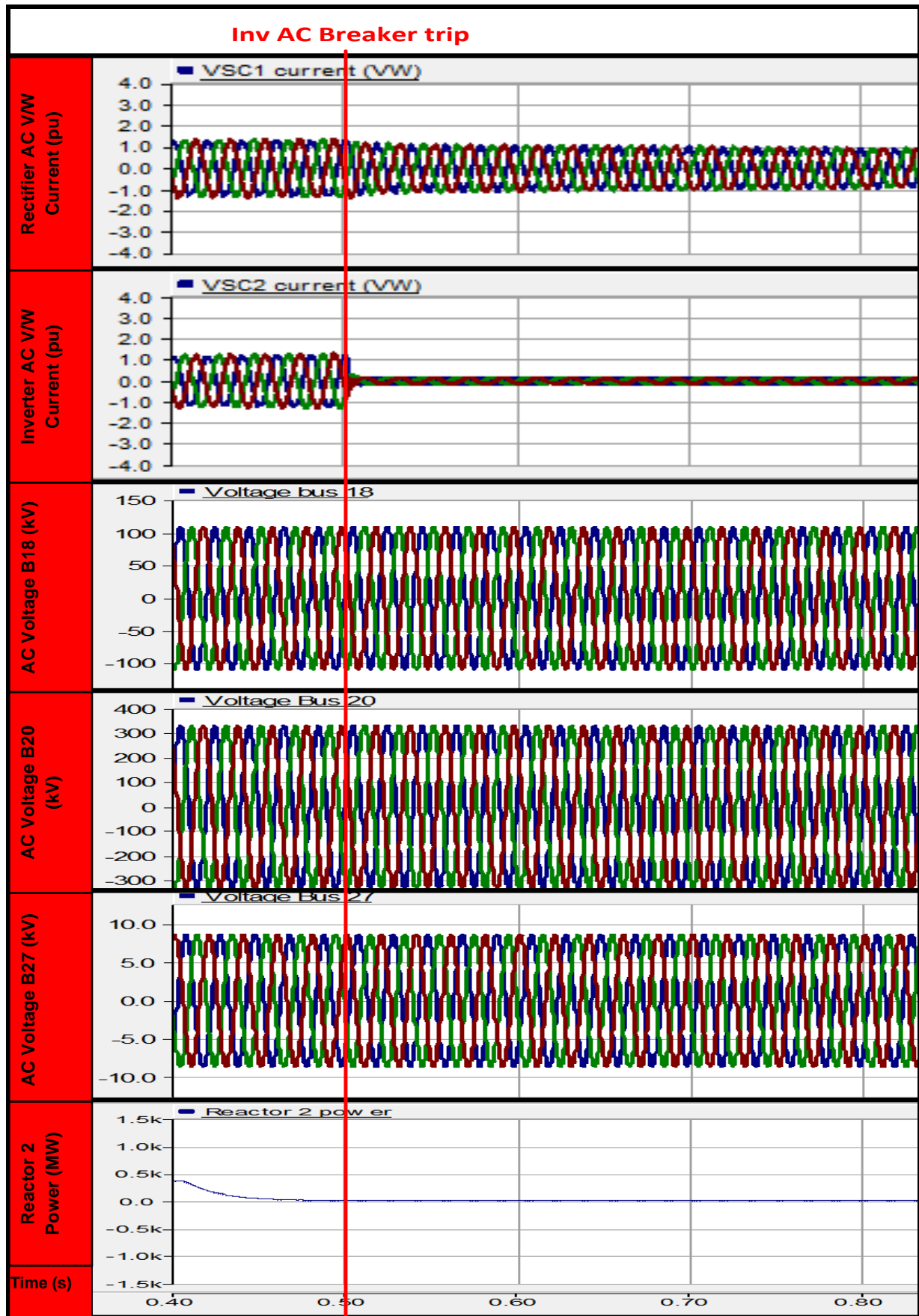


Figure 137: AC system profiles after inverter AC pole breaker trip

In Figure 137, the AC voltage profiles are maintained during the trip of the inverter and phase-to-ground fault on busbar 19. The AC valve winding current at VSC1 is clamped by the DC current limiter control once the VSC2 has tripped.

The reactor output power has reduced significantly due to the removal of the load from VSC 2, but power is still able to be supplied to the reactor cooling motors and essential safety systems.

In summary, during this contingency the independent Statcom functionality available within VSC-HVDC converters has proven to be effective. Following the trip of the AC pole breaker at VSC2, Statcom functionality is available within VSC1 since this converter remains connected to the NPP during the disturbance. The AC voltage within the reactor station 2 is maintained through the control of reactive power, despite the additional fault on busbar 19. This prevents a voltage depression and allows reactor generator 2 to maintain stable power supplies to the cooling motors, ensuring the security and stability of the NPP.

5.4.3.2 VSC-HVDC contingency 2

In scenario 2, the VSC-HVDC link is about to supply power to reactor station 2 when a single-phase-to-ground fault occurs on busbar 20. This causes the reactor AC circuit breaker to trip and disconnects the generator from the system.

Following the trip of the reactor generator, the NPP frequency measured at busbar 20 fluctuates, as shown in Figure 138.

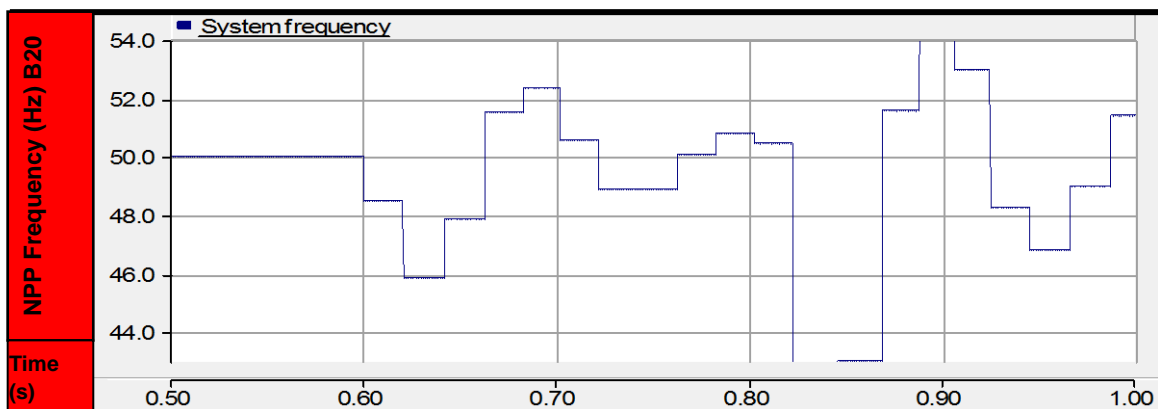


Figure 138: NPP frequency after reactor generator trip

Large oscillations occur, and in practice would cause the reactor cooling motors to trip via their over/under-frequency protection systems [3]. The same situation is repeated, but this time, around 30 ms after the trip, an active power run-up order is activated by the HVDC control system as shown in Figure 139.

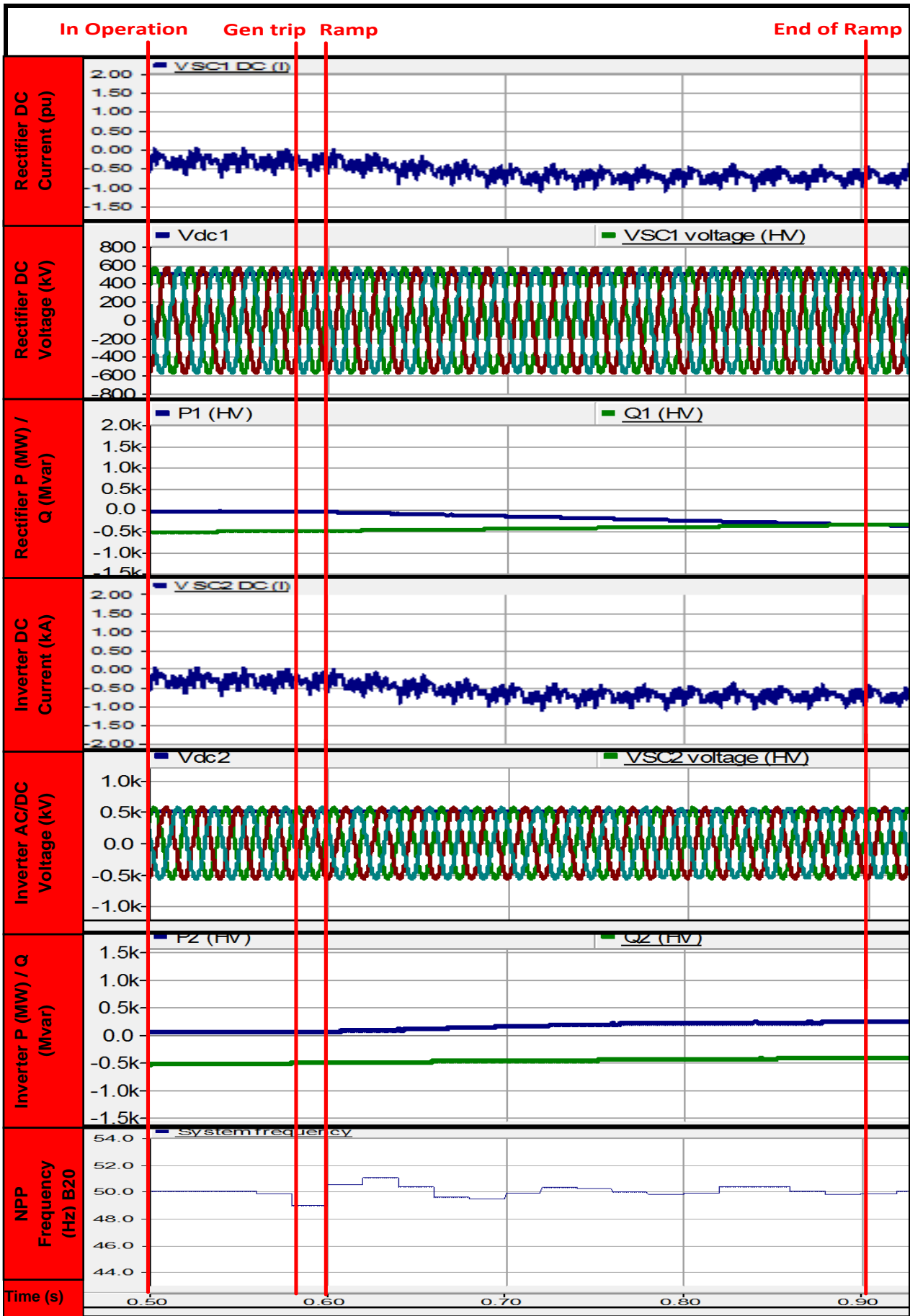


Figure 139: VSC profiles for single-phase-to-ground fault on busbar 20

The active power run-up is completed within 300 ms of activation and is completed in a smooth manner, with limited oscillations present. The reactive power is kept constant throughout, which ensures that the voltage profiles remain stable during the active power run-up.

The DC voltage remains constant but harmonics are present in the current profiles; DC filters may be required to filter out such harmonics in practice.

In summary, for this scenario, a trip of reactor generator 2 occurs. During the instance when no Emergency Power Control (EPC) is activated, the VSC-HVDC link has the responsibility to maintain equilibrium: frequency fluctuates and large oscillations are present.

A repeat of the same event is carried out with EPC activated. The frequency within the NPP has been restored and most of the oscillations have been damped out. In reality, the EPC can prevent the tripping of the reactor cooling system motors and allow nuclear reactor generator 2 to continue supplying power to the vital safety and cooling systems.

5.4.3.3 VSC-HVDC contingency 3

In this contingency the fast current reversal and black-start functionality of the VSC-HVDC link are analysed. The VSC-HVDC link is initially supplying power from reactor station 2 to the AC grid. Reactor station generator 2 trips and a blackout of the NPP occurs at a time of 0.3 secs. The black-start process for a VSC-HVDC link has been covered in [67].

In Figure 140, as soon as the blackout is detected, then VSC1 HVDC converter is blocked, the AC pole breaker is opened and the converter is switched over to black-start control. With black start activated, VSC1 converter is de-blocked and the AC voltage is ramped up smoothly to the required reference value [67]. VSC1 AC pole breaker is closed at a time of 0.48 secs and an instant current reversal is initiated 180 ms after the initial blackout was detected.

Full power reversal is completed within a time of 0.70 secs, in a smooth and controlled manner. The total time taken for this function was 110 ms and the time duration of the overall sequence from blackout detection to full current reversal is 400 ms [67]. During the black-start sequence the reactive power is controlled, which enables the process to be completed while maintaining voltage stability. Once full current reversal has been achieved, power is supplied to reactor station 2 and the security of the NPP is ensured.

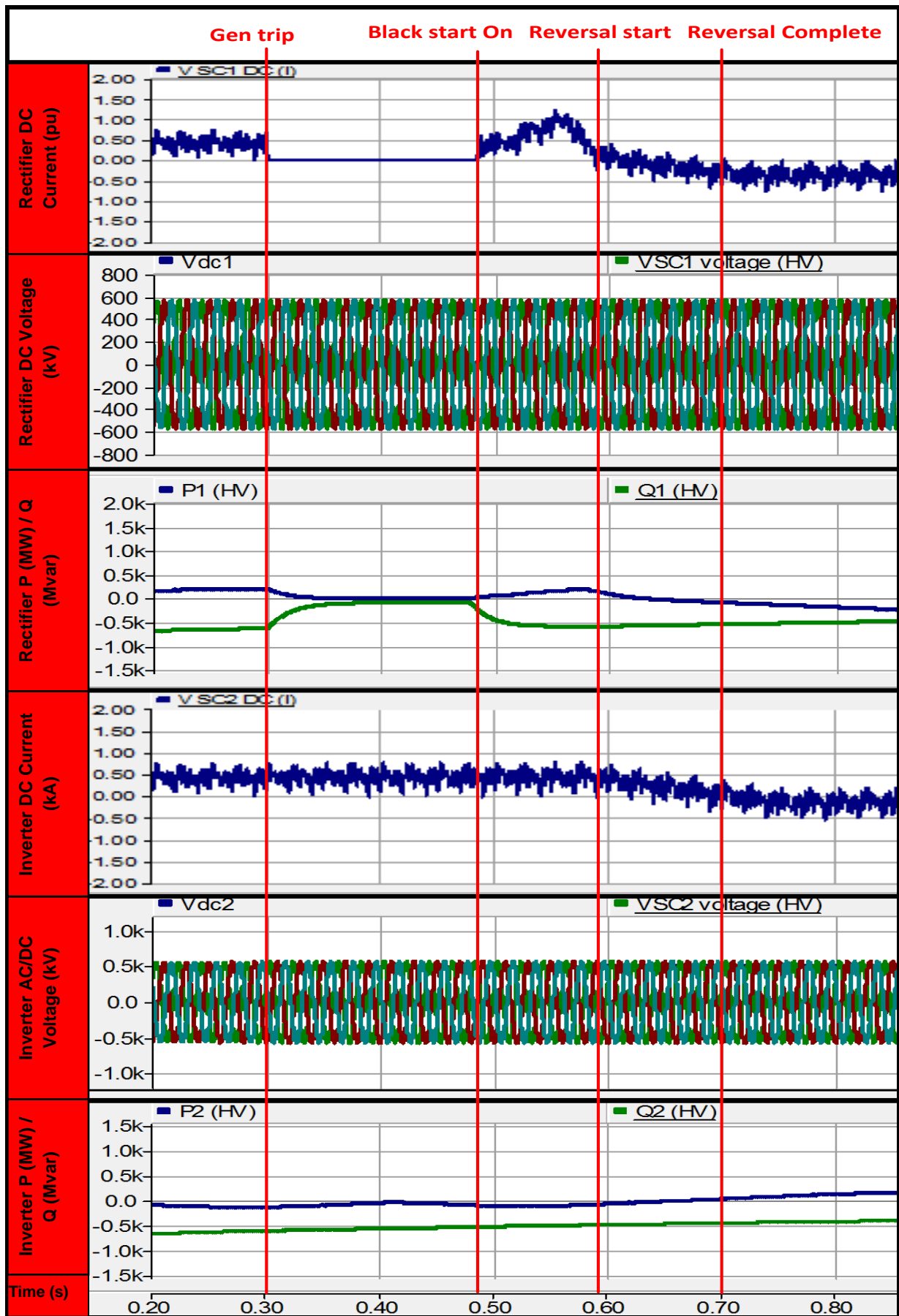


Figure 140: VSC system profiles for reactor 2 generator trip and black start

In summary, this contingency demonstrates the black-start functionality and fast current reversal functionality of the VSC-HVDC link. These functions are used to supply emergency power to reactor station 2 following a reactor scram. The control features of the PSCAD VSC-VDC model are used to create the above contingency and to analyse the response obtained.

Through appropriate control action and the correct energisation sequence, the reactor station is restarted. A fast current reversal is achieved in a smooth manner, while independent reactive power control within the converter maintains voltage stability during the process. In practice, the speed and ramp rate of current reversal will be determined by the SCR and stability limits of the AC network [9]. The sequence of black-start energisation may vary from project to project and will also depend on the AC network SCR level and stability limits [67]. VSC-HVDC technology has the potential to provide the NPP with these emergency control functions and improve security during transient conditions.

5.5 Chapter 5 summary and conclusions

In chapter 5 the unproven method of connecting a modern NPP to the NETS via VSC-HVDC technology has been analysed. From the analysis the following findings are ascertained:

- *The impact of SCR on the operation of the VSC-HVDC link is important: for a low SCR, the active power transfer capability of converters employing vector current control can be limited due to the impact of the low frequency resonance within a weak AC system on the control response. The PI controller parameters may need to be adjusted to obtain a better control response and to alleviate the instability in the PLL.*
- *DC faults must be cleared by protection and control action as quickly as possible. Failure to do so will put the operation of the NPP at risk and may cause instability and damage within the power system.*
- *The VSC-HVDC link is able to provide fault ride through for remote three-phase faults on the AC network, enabling system recovery through appropriate DC controller action and a fast reactive power injection via Statcom operation.*
- *For different system contingencies, the fast DC active power modulation capability of VSC-HVDC technology can be used to damp oscillations and to provide frequency response in the situation where generation and load do not match.*
- *Fast current reversal and black-start control functionality could offer some key benefits to the NPP under transient conditions.*
- *The independent Statcom functionality within the converters can provide fast reactive power injection to maintain the NPP AC voltage during transient conditions.*

Following the findings from the work, if a VSC-HVDC NPP connection is considered, then the following recommendations are made:

- From a technical perspective, the author recommends VSC-HVDC technology in preference to CSC-HVDC converters for an NPP connection.*
- VSC-HVDC technology can offer many benefits as discussed previously for an NPP HVDC connection. However, the above technical requirements must be considered and studied in further detail when evaluating such an unproven application.*
- For low SCR values, the inclusion of a FACTS (Flexible AC Transmission) device such as a Synchronous Condenser or Statcom may be necessary to improve the active power transfer capability of VSC-HVDC technology and should be evaluated.*
- The speed and sequence of the VSC-HVDC operation will need to be studied in detail during the project delivery phase to ascertain accurate control timings and responses.*

Chapter 6: Design of Nuclear Power Plant Connections

This chapter presents technical designs for a nuclear power plant connection. Three different technologies are considered for the NPP connection: a design adopting conventional AC overhead line technology; a design involving Current Source Converter (CSC) HVDC technology; and a design utilising Voltage Source Converter (VSC) HVDC technology. For each of the technology options, a standard NPP design is considered. Two 400 kV AC double busbar substation designs are presented for interfacing both the AC and DC connections to the AC grid and NPP. Finally, a frequency controller design and a study of HVDC control actions in relation to contingencies within an AC power system are presented.

6.1 Design of an NPP connection utilising AC technology

A design utilising AC technology for connecting a 4500 MW NPP with three reactor generators to an AC grid is presented. This represents the largest rated NPP which can be physically connected by the maximum rated AC overhead line circuits currently available in the UK market [1]. Designs for two separate 400 kV double busbar AC substations providing a connection interface from the NPP to the transmission system are presented, with full protection scheme designs for the substations. Finally, all the designs are combined into one overall design option to provide a connection into the AC grid for the 4500 MW rated NPP.

6.1.1 Design of a 4500 MW rated NPP

In Figure 141, a design for a 4500 MW rated NPP utilising three reactor generators is presented. Each reactor is rated at 1500 MW, has a main isolator, and is rated at 22 kV – which is stepped up to a transmission voltage of 400 kV. Here, connection to a local 400 kV NPP AC interface substation via the Main Grid Power Transformer (MGT) is provided. The MGT AC circuit breaker is used to interrupt and clear faults.

The station transformers provide an alternate off-site power supply to the reserve auxiliary transformers in case the reactors are tripped or main supplies are lost. The 400 kV AC grid voltage level is stepped down to 22 kV through an MGT, before reaching the unit auxiliary transformers themselves. The reserve transformers are split into banks of two for redundancy purposes, but the design can vary from station to station. Each bank has a dedicated circuit breaker (RATCB) for fault clearing purposes. Each of the generator circuits are separated from the station transformer supplies for security purposes [106].

6.1.2 Design of a 400 kV NPP AC interface substation

In Figure 142, a 400 kV double busbar AIS (Air Insulated Switchgear) AC substation is used to provide a connection interface for the NPP. A main and reserve busbar provide the connection for both the incoming and outgoing circuits. Main and reserve bus sections split the substation into two separate sections; the split provides redundancy and security so that a fault on one section does not affect the other. Isolator switches allow segregation of different parts of the substation and can only be opened once system load has been removed via the appropriate AC circuit breakers.




Six 400 kV feeder circuits connect the NPP to the local AC interface substation. Three circuits connect the generators GT1, GT2 and GT3 to NPP station transformers ST1, ST2 and ST3. Each circuit connects to a different section of the NPP to improve security of supply and provide additional redundancy [106]. Each circuit can be selected to either main or reserve bar via the appropriate isolators.

Four separate 400 kV AC feeder circuits connect the nuclear AC interface substation into the AC grid. Two 400 kV AC feeder circuits (South 1 and 2), and the northern connections (North C1 and C2) make up the four AC feeder circuits for connection to the grid. Two additional 132 kV emergency supplies circuits (ES1 and ES2) provide off-site supplies to essential safety systems within the NPP in case all feeder circuits to the AC grid are lost. Two Autotransformers are used to step-down the 400 kV transmission voltages to 132 kV levels. Two bus-section couplers, each with dedicated AC circuit breakers allow the main and reserve bars to be paralleled together for additional load sharing if required. Earth switches are provided for earthing of equipment during maintenance or circuit outages.

6.1.2.1 Protection system design for 400 kV NPP AC interface substation

A protection system is required to protect the equipment from power system faults; a design of a protection system for such a purpose is presented in Figure 143.

From an operational point of view, losing the whole substation for a single fault could be detrimental to the power system and result in the unnecessary loss of healthy circuits to the NPP [103]. By splitting the substation into individual protection zones a high level of fault discrimination is provided. Only faults within the protected zones are detected and result in the tripping of all sources of infeed to the restricted area [168]. Any faults outside of a protection zone should not be detected by the relays in the region and AC circuit breaker tripping should be prohibited [169].

Key	
X	AC Circuit Breaker
	Earth Switch
	Auto-Transformer
	Feeder Circuit
ST1C	Station Transformer 1 Circuit
GT1C	Generator Transformer 1 Circuit
MB	Main Busbar
RB	Reserve Busbar
MBS	Main Bus-Section

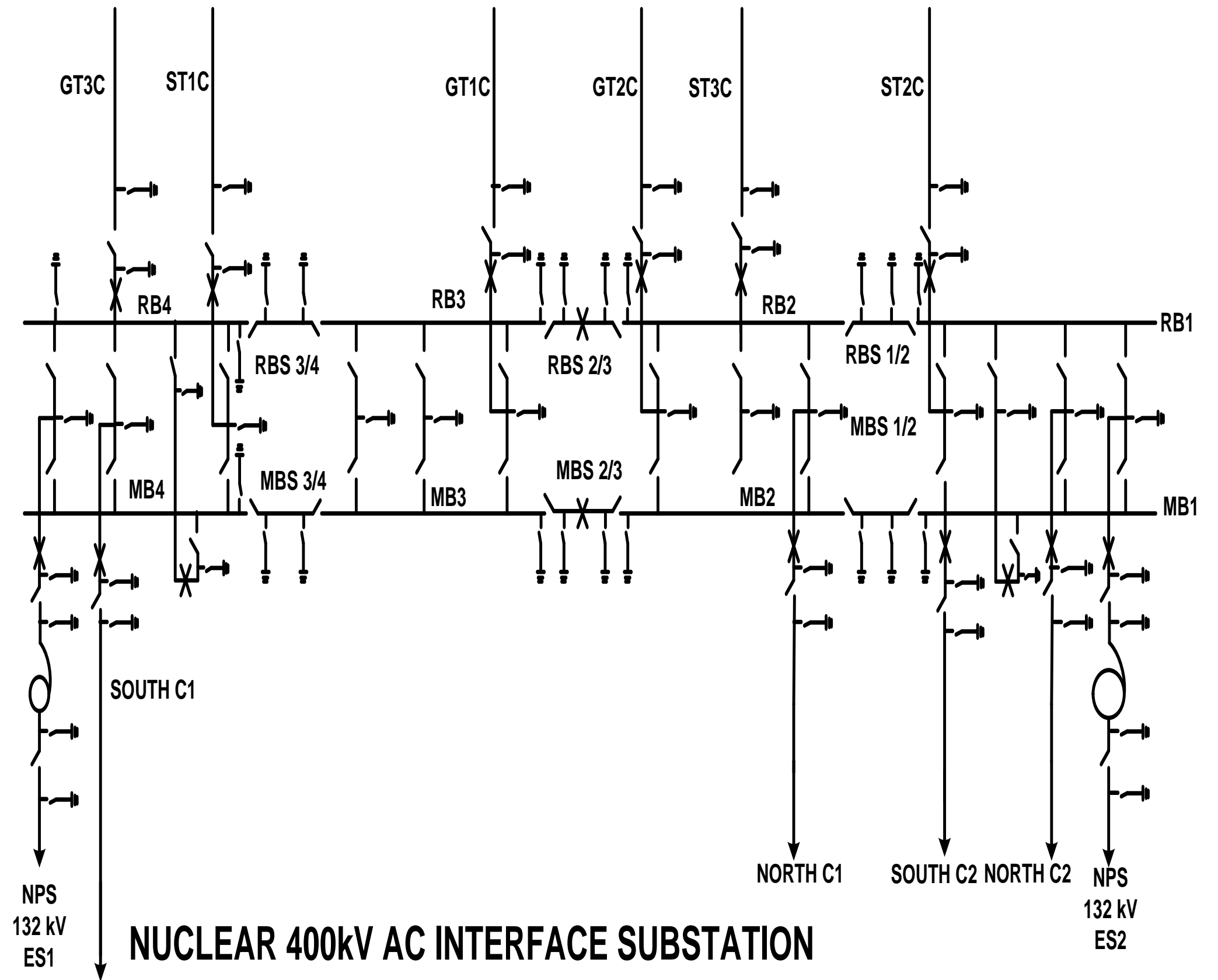


Figure 142: NPP 400 kV AC interface substation

6.1.2.2 Busbar protection system

The main safeguard for the double busbar substation consists of a low impedance protection system. Protective Current Transformers (CTs) measure the primary system current and converts this to a secondary value for the busbar protection relays. The CT secondary wiring presents a low impedance path to the flow of secondary fault current, hence the name applied to such a protection system [168]. The double busbar substation can be split into different protection zones according to CT position; this improves the integrity of the substation where a fault in one zone will only result in the tripping of that region [170]. This configuration can leave half of the substation in service, depending on whether the system is run solid or whether it is split, by opening the bus-section switches. Each isolator can be switched to either main or reserve bar and a CT can be selected to a particular protection zone depending on the position of auxiliary switches within the switchgear [168].

A Main Unit (MU), shown in Figure 143, receives information from each of the Bay Units (BUs). Such information includes current measurement at the bay unit and positional information from switchgear. The MU performs the busbar protection algorithm using the information transmitted from the BU. If the MU detects a fault, then tripping commands will be sent to the affected BU. The BU will then send a trip signal to the appropriate AC circuit breakers to clear the fault. A second main unit (M2) provides redundancy in case MU1 fails. Only one of the MUs has priority at any one time [170].

If a BU becomes faulty, then it can be switched out for maintenance and the system can carry on operating with the existing configuration. Fibre-optic connections installed between each of the devices allow fast data and signal transfer, ensuring busbar faults are cleared within the required fault clearance times [135].

For any of the BU busbars 5–8, additional protective functions can be included within each device. An overcurrent protection element can be used for commissioning purposes when a section of busbar is out of service, allowing for a temporary protection arrangement for safety purposes in case a fault occurs on any section of bar that is energised and at risk of fault during maintenance. Earth fault protection can also be included as additional backup functionality.

6.1.2.3 Circuit breaker fail protection

An AC circuit breaker, just like any mechanical device, has the potential to fail or jam. If a circuit breaker fails to open, then the results can be catastrophic. Protection systems further down the power system could trip unnecessarily and cause widespread disruption. Damage to the substation could result in long circuit outages while damaged equipment is repaired and can be costly. To cater for this contingency, circuit breaker fail protection is implemented [171].

Key	
ξ	Current Transformer
BU	Busbar protection Bay Unit
MU	Busbar protection Main Unit
TP	Transformer protection
FMFP	First Main Feeder protection
SMFP	Second Main Feeder protection
- - -	Busbar Protection Zone 1
- - -	Busbar Protection Zone 2
- - -	Busbar Protection Zone 3
.....	Fibre optic connections
- - -	Feeder protection zone
.....	Auto-transformer protection zone

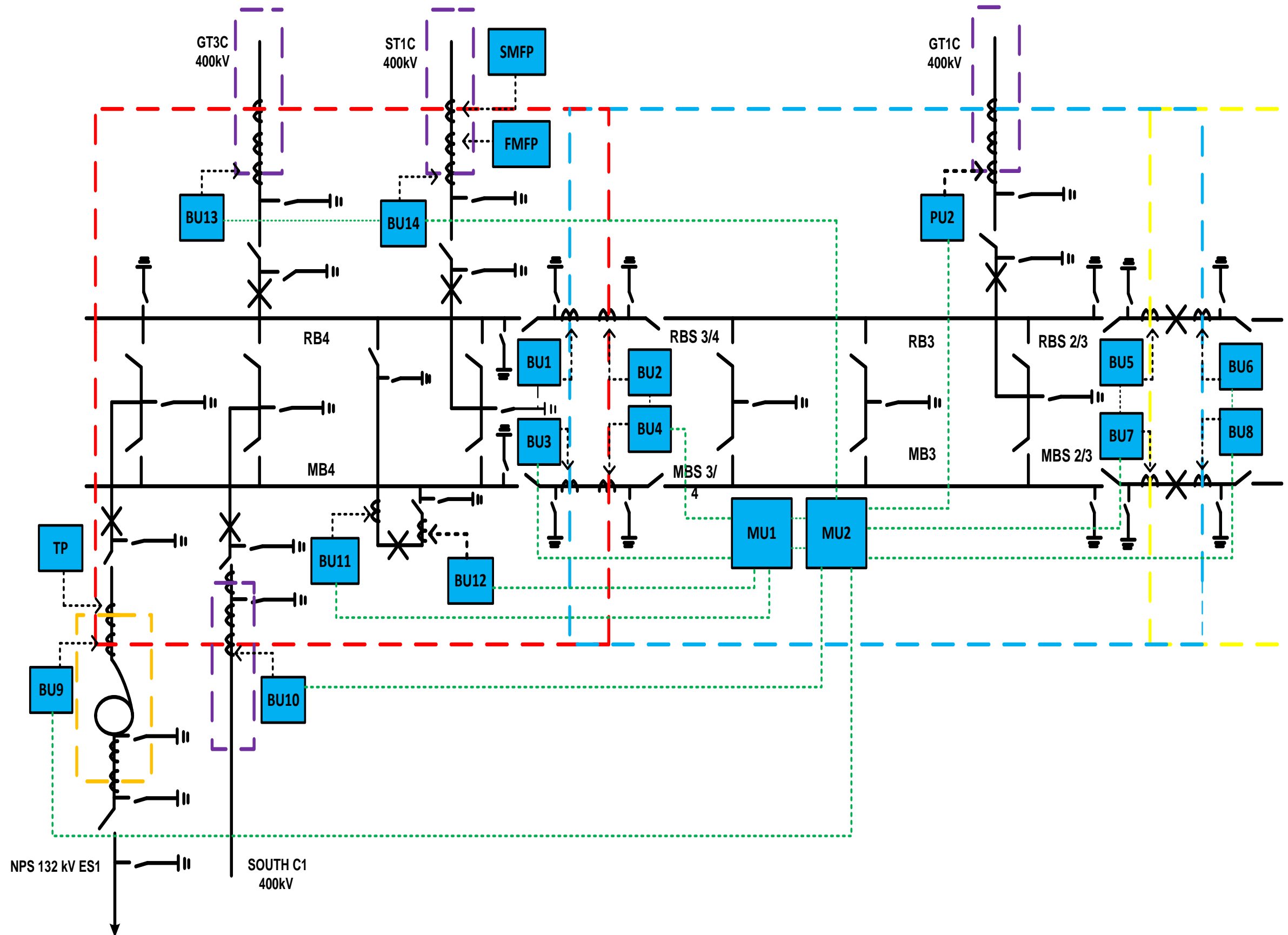


Figure 143: Protection scheme design for NPP AC interface substation

Circuit breaker fail protection is initiated by the tripping contacts of a main primary protection. Once a trip signal reaches the circuit breaker fail protection, a current check element, fed from a separate CT is activated. Detection of current in any phase above its protection setting will start and maintain a timing element. The delay of the timing element should be set long enough to allow a main primary protection to clear the fault. On the UK 400 kV transmission system, this is normally 140 ms [135]. The delay should also include a safety margin and cater for measurement errors in CTs and voltage transformers [171].

If a main protection system manages to clear the fault, then the current flowing through the circuit breaker fail current element will drop off and reset. If a main protection fails to clear the fault, and current is still flowing, then this is a good indication of an AC circuit breaker failing to open. At the end of the timing element, if the current check element is still showing current flow, then signals are sent to the busbar protection system. Upon receipt of these signals, all sources of infeed to the affected zone are tripped by opening all AC circuit breakers on circuits providing a source of fault in-feed. Even though this can result in significant loss of supplies to customers, the main priority is to clear the fault and prevent system instability [171].

The circuit breaker fail protection elements can be included within the busbar protection relays themselves, or in separate cubicles on the feeder circuits. However, in the event of a feeder circuit being taken out of service, the circuit breaker fail function in this leg will not be available. Hence a separate circuit breaker fail system will need to be installed on every single feeder circuit. By including circuit breaker fail functionality within the busbar protection systems, cost savings are made, while still overcoming the previous issue [171].

6.1.2.4 AC feeder protection

For the main AC feeder circuits at transmission voltage levels of 400 kV and 275 kV, more than one protection is employed for redundancy and security purposes. In Figure 143, the 400 kV feeder circuits each comprise two main protection systems, each using a different operating principle for fault detection purposes [172].

The first main feeder protection operates on a current differential principle that compares current entering and leaving the circuit. This principle is called unit protection, and is shown in Figure 144. If the current flowing into the protected zone is equal to that flowing out, then the protection is stable and no operation is encountered. For an in-zone fault, the current is unbalanced and the protection systems will pick-up and trip the AC circuit breakers to clear the fault. Unit protection offers good stability for out of zone faults but relies on the communication between devices to exchange information. If the communication channel is lost or faulted, then the protection is blocked to prevent maloperation [172].

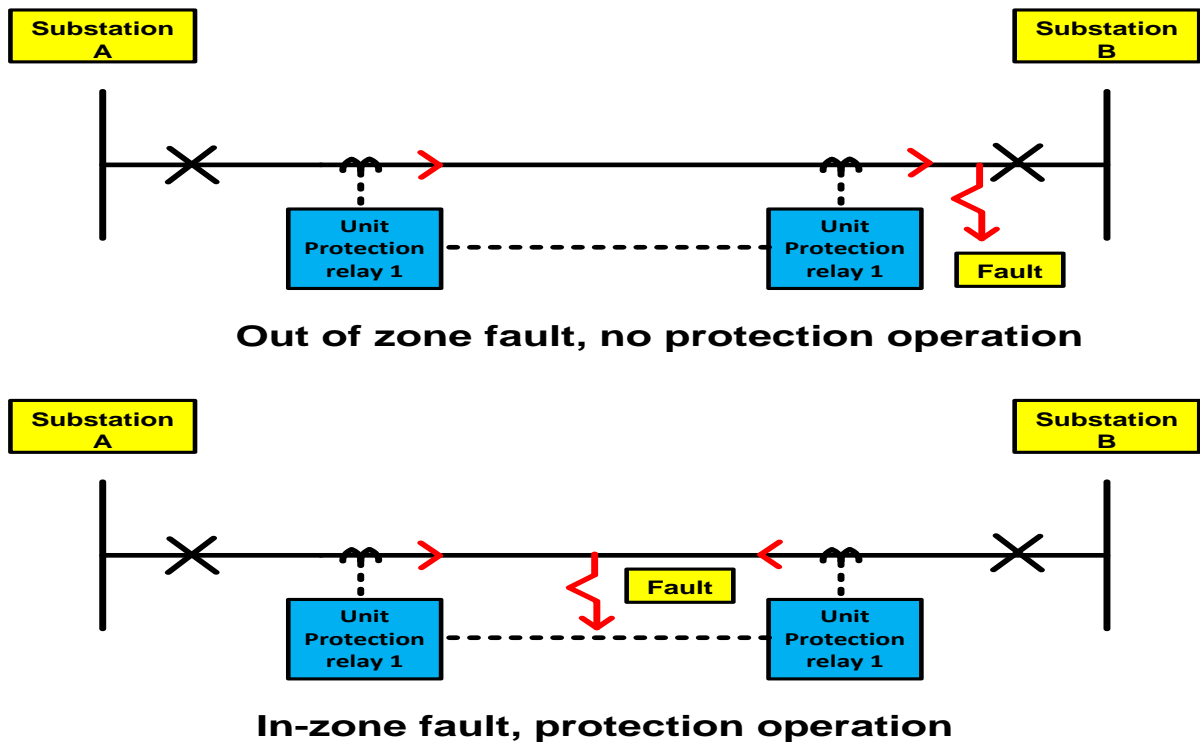


Figure 144: Operation principle of unit protection

To cater for failure of the unit protection, backup functionality may be included in the same or a separate device. One such function includes three-phase overcurrent protection to detect uncleared remote busbar faults outside of the main feeder zone [172]. In addition to this, earth fault protection is also included. High resistance earth faults will be undetectable to the overcurrent protection due to the very low level of sensitivity required. The backup protection is time-delayed to allow the main primary protections to clear the fault. A one second operating time is usually sufficient to provide adequate discrimination between the two systems [172].

The second main feeder protection operates using the distance protection principle shown in Figure 145. Such devices measure the voltage and current of the protected line and calculate the impedance to the fault using the principle of Ohm's law [173]. Different impedance lengths can be used to provide independent protection zones.

Zone 1 is called an under-reaching zone and is deliberately set to not cover the whole 100% of the feeder circuit. The operating time is usually instantaneous, to clear line faults as soon as possible. A setting of 80–85% is usually adopted in practice and caters for relay (5%) and CT (5%) measuring errors, variations in line impedance and a general safety margin of 5%. If such allowances were not made, then the relay could overreach into the next feeder circuit due to an increase in line impedance and may operate for an out of zone fault [174].

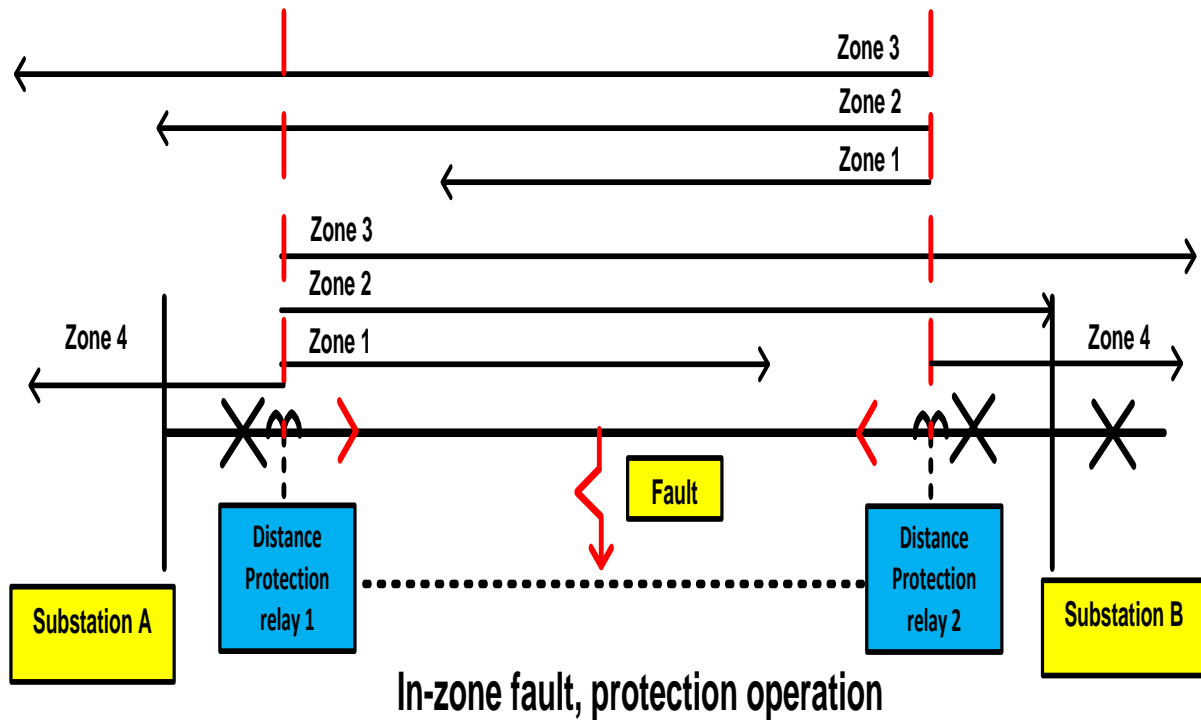


Figure 145: Operation principle of distance protection

Zone 2 can be set to have a longer reach (100–120%) and will provide backup for uncleared remote busbar faults. This function will also cover the remaining 15–20% of the feeder not protected by zone 1. Zone 2 is normally time-delayed to allow faults in the next feeder to be cleared by the local protection [174]. A time delay of 300–500 ms is usually employed. A further forward-reaching zone 3 can be used to cover larger distances, and the time delay is normally adjusted to one second to grade with remote backup protections. A reverse looking zone (zone 4) can be used to detect faults behind the relay. A reach setting of 10% is usually employed to prevent protection maloperation for faults in the next feeder section [175].

Just like unit protection, three-phase overcurrent and earth fault protections can be employed in the same or separate boxes. The zone 2 setting can provide backup for uncleared remote busbar faults due to its reach setting and hence, in some instances, three-phase overcurrent protection may not be required.

For the 132 kV transformer feeder circuit (ES1) shown in Figure 143, one single main protection is employed. This consists of a distance protection relay (not shown) with a separate box for the backup protection incorporating the functions mentioned previously. The choice between one or more main feeder protections for 132 kV circuits and below is a choice between cost and redundancy. With the 132 kV feeder also containing protections for the autotransformer, one main protection is deemed sufficient [174].

6.1.2.5 Autotransformer protection

The autotransformer is a very expensive component, and needs to be protected against power system faults [176]. Faults can cause damage to windings and break down insulation resulting in internal flashovers and even damage external components like bushings. The main protection consists of a biased differential protection with restricted earth fault (REF) covering the earth connection shown in Figure 146. Biased differential protection will restrain relay operation for given set of bias current encountered from the transformer. The steady state level of bias current is calculated and applied to the protection settings. This prevents protection maloperation during transformer energisation. During a fault the level of fault current will increase, the bias setting will be exceeded and protection operation occurs.

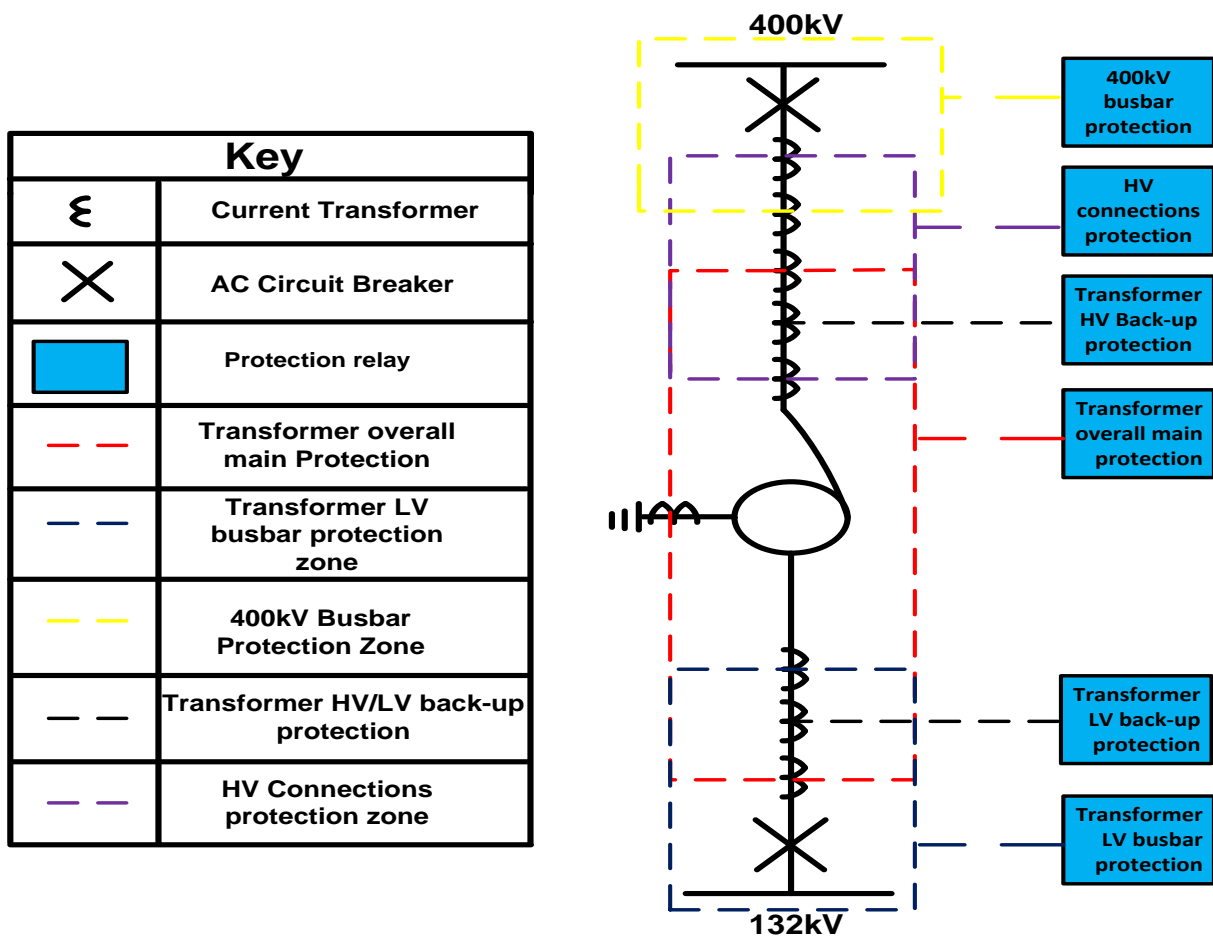


Figure 146: Protection arrangement for 400/132 kV autotransformer

By placing a current transformer on the earth connection of the autotransformer the protection is made more sensitive to internal earth faults (REF). Any fault current will flow back up through the transformer earth and can be measured by the neutral CT. By combining this function with the overall protection, it becomes a highly reliable and effective method of detecting high resistance earth faults that other protections may fail to detect [177].




For the autotransformer HV backup protection, a two-stage overcurrent relay is installed to cover failure of the MUs. The first stage acts as a backup protection for uncleared faults on the 132 kV side and when operated trips the 132 kV AC circuit breaker. The second stage provides backup protection to the transformer HV and LV connections and trips the 400 kV AC circuit breaker. The time delays of each can be set to grade with other protections on the system. A high-set overcurrent relay is also included in the HV backup protection to clear high current faults on the transformer bushing/busbar and is instantaneous in operation. The relay must be set so that it does not operate for faults on the 132 kV sides [177]. A connection's differential protection covers any long busbar connections on the transformer HV side and also provides backup to the main systems. The 400 kV busbar protection CTs are overlapped with the HV connections to ensure that no item is left unprotected within the designated protective zones.

On the autotransformer 132 kV side, an earth fault relay is included in the LV backup protection. This provides backup protection for uncleared earth faults on the 132 kV system. An interlocked overcurrent (ILOC) relay is also utilised in the same box as the earth fault relay. A fault within the LV busbar zone will trip the 132 kV AC circuit breaker but not the 400 kV circuit breaker. The ILOC relay is activated by the 132 kV busbar protection and will trip the 400 kV AC circuit breaker after a time delay to clear the source of infeed from the HV side. An LV overcurrent relay is also installed to detect equivalent faults on the 132 kV network [177].

The autotransformer contains mechanical protections such as the buchholz device. This sits on top of the transformer conservator and detects any gassing or bubbling within the main tank, indicating a potential winding fault. The gassing produces bubbles which work their way up to the buchholz relay and eventually depress a contact, resulting in the tripping of the AC circuit breakers on both the 400 kV and 132 kV side. A winding temperature monitoring system is also included to provide an alarm or trip the LV side of the autotransformer if the temperature exceeds the maximum limit of the equipment [177].

6.1.3 Design of a 400 kV AC grid substation

A design for a new 400 kV AC double busbar substation for connecting the NPP into the transmission grid is presented in Figure 147. Four 400 kV AC feeder circuits (South C1/C2 and North C1/C2) provide connections from the nuclear AC interface substation shown in Figure 142, into the new 400 kV AC grid substation in Figure 147. Four 400 kV AC feeder circuits provide a connection into the existing transmission grid from the NPP AC interface substation. Power flows can be selected to either the main or reserve bar which offers good operational flexibility in design. The protection systems designed for the NPP AC interface substation are identical to those employed for the 400 kV AC grid substation.

Key	
X	AC Circuit Breaker
	Earth Switch
	Auto-Transformer
	Feeder Circuit
SOUTH C1	Southern AC circuit 1 from NPP interface substation
SOUTH C1	Southern AC circuit 2 from NPP interface substation
AC Grid 1	AC feeder connections to AC grid
RB	Reserve Busbar
MBS	Main Bus-Section

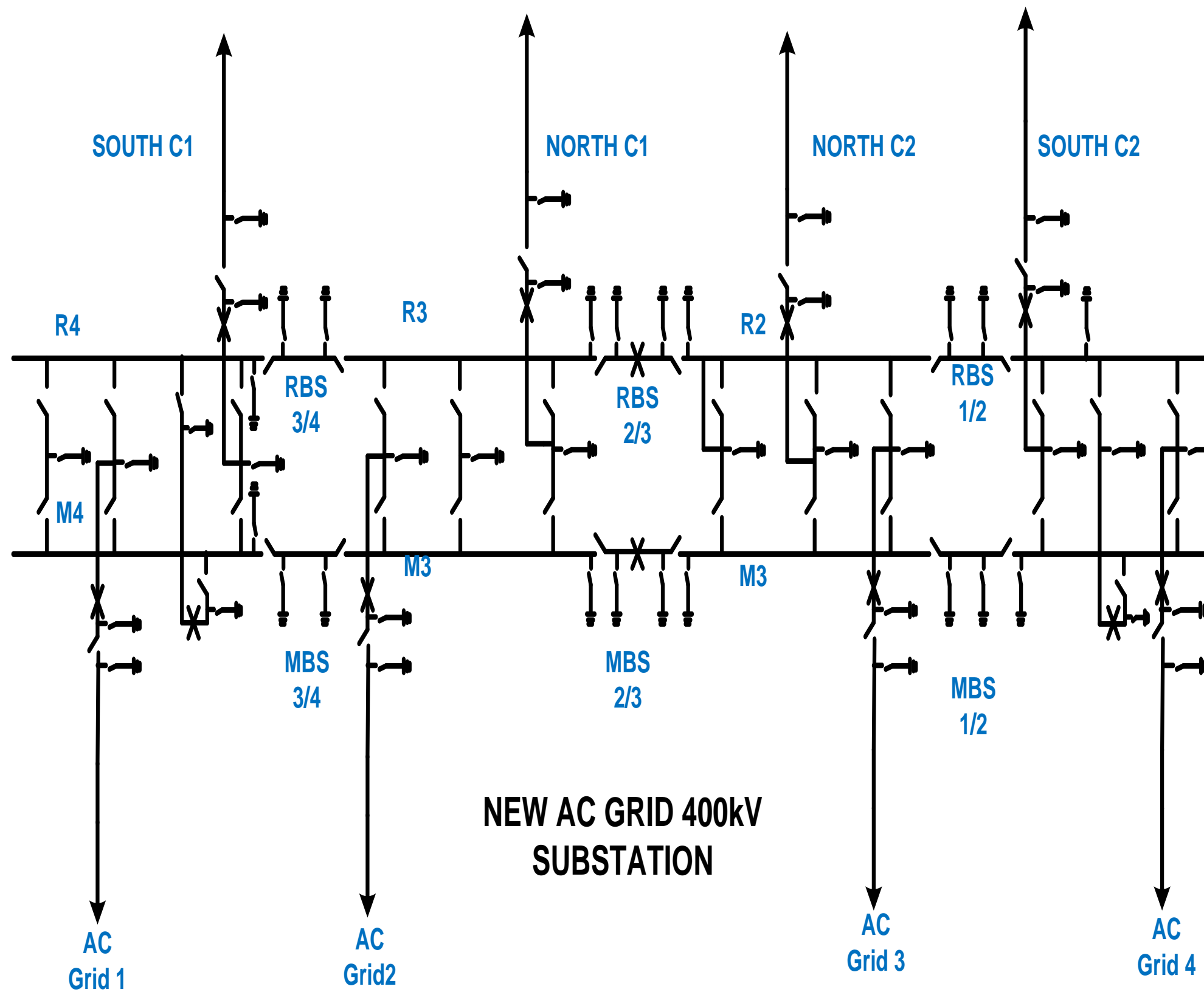


Figure 147: New 400 kV AC grid substation to connect NPP into the 400 kV transmission system

6.1.4 Overall design of an NPP AC connection to the transmission grid

Each of the individual designs presented in section 6.1 combine to form an overall solution for connecting an NPP to the grid by AC technology.

In Figure 148, two 400 kV AC double overhead line circuits, one north (North 1 and 2) and one south (South 1 and 2) are used to connect the 4500 MW NPP via the AC interface substation to the new AC grid substation. All 400 kV feeder circuits include the full list of protection systems discussed previously in section 6.1.2.

Three generators, each 1500 MW in rating, provide power export into the AC grid and supply the in-house demand of 5–10% of the NPP. Individual feeder circuits, owned by the NPP, connect each generator into the 400 kV AC interface substation. Reserve auxiliary transformer circuits import power from the AC grid to supply the essential safety systems of the NPP in the situation of the generators being unable to do so. An example would be if the generator was faulted or out of service for maintenance [106].

The advantage of having three individual reactors instead of the usual two comes in the management of both intertripping schemes and power flow. If a reactor needs to be scrammed, then a smaller block of power (1500 MW) is lost, making it easier to manage power flows under an emergency condition compared to the situation where the loss of one of two larger reactors (1800 MW) would result in an extra 300 MW of loss.

The protection systems discussed previously for both the double busbar 400 kV substations are employed. The NPP has its own protection systems for the generators, busbars, transformers, feeder circuits and low voltage systems; these are the responsibility of the NPP designer/owner and have not been included in the design.

In summary, an overall design for connecting an NPP to the AC grid is presented. A 4500 MW NPP is designed, with all the necessary components required for successful power generation. Two new 400 kV double busbar substations, complete with protection systems, are also designed and described in detail. Finally, all the components are put together to form an overall design.

The design shows the amount of infrastructure required to successfully integrate a large NPP into the AC grid. The overall system design is important to ensure the correct level of circuit redundancy and security is provided for stable NPP operation [102].

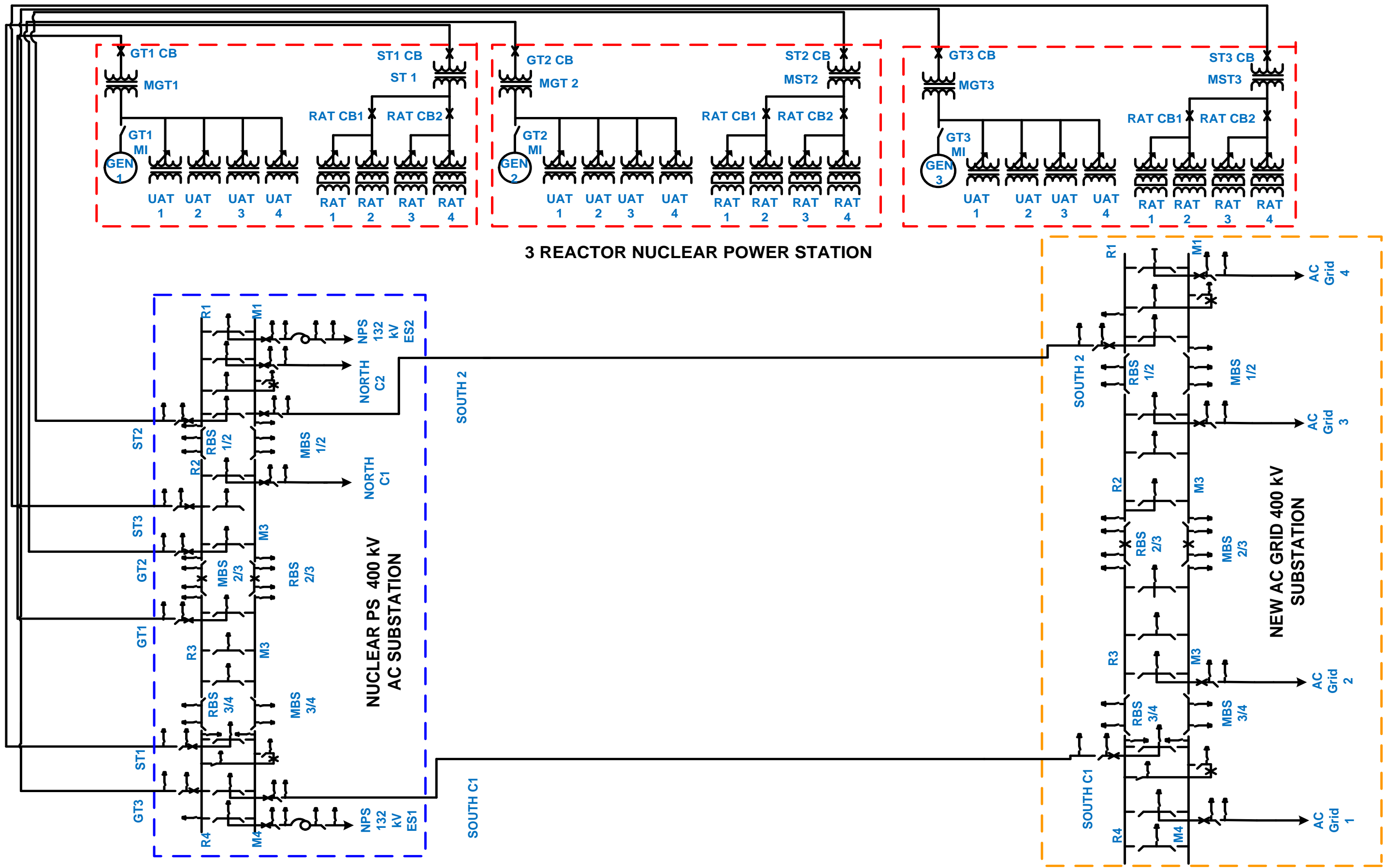


Figure 148: Design for connecting an NPP to the transmission grid by AC technology

6.2 Design of an NPP connection utilising CSC-HVDC technology

In this section, a design utilising CSC-HVDC technology for connecting an NPP to an AC grid is presented. The 4500 MW NPP design used in section 6.1 is included, along with the same two 400 kV double busbar AC substations used in the previous section. A 2250 MW ± 600 kV bipole CSC-HVDC link design is presented, with a full description of the protection systems employed. The design is based upon the maximum rated technology used in the Western HVDC link project [178]. Finally, the designs are combined into one overall solution for an NPP connection to the AC grid via a combination of CSC-HVDC technology and AC circuit connections; the AC circuit connections are included for security purposes since HVDC technology has never before been used in such a critical application [2].

6.2.1 CSC-HVDC bipole converter station design

A design of a ± 600 kV, 2250 MW CSC-HVDC converter station is shown in Figure 149. Both the rectifier and inverter are connected to a single busbar at each end, with two 400 kV AC cable feeder circuits providing an interface connection to the 400 kV AC grid substation. AC filters are connected to the busbar to filter out harmonics and supply the reactive power demand of the converter station.

The converter transformers are connected to the single busbar and can be isolated via the AC circuit breaker and line isolators as required. The three-winding converter transformers are equipped with a tap changer on the primary side to provide coarse control of the AC voltage. One twelve-pulse converter is used for each pole and provides 1150 MW of power transfer capability.

Each pole has a smoothing reactor, with bypass isolators available if one pole needs to be taken out of service, and metallic return mode via the second DC cable is required. DC filters may be required, depending on the performance requirements of the AC grid.

The DC subsea cables connect the rectifier to the inverter, and earth switches are available at either end for discharging the DC cable if required. Neutral bus ground switches are provided to connect both negative poles together for metallic return operation. Various earth switches are available around the link to provide safe isolation and earthing. A high frequency filter is used to reduce the harmonic interference with telephone circuits and power line carrier circuits which could be present within the AC grid. Two bipoles can be connected together to provide higher voltage and power ratings if needed. The protection system for one pole will be identical to that in the other, with full redundancy provided for each.

Key	
	AC Circuit Breaker
ACBB	AC Busbar
ACFC	AC Feeder Circuit
CTFC	Converter Transformer Feeder Circuit
CT	Converter Transformer
12PC	12 Pulse Converter
LVN	Low Voltage Neutral
IR	Interface Reactor
BSMR	Bypass Switch for Metallic Return
DCC	DC Cable
ACF	AC Filter
	AC Busbar
	Earth Switch

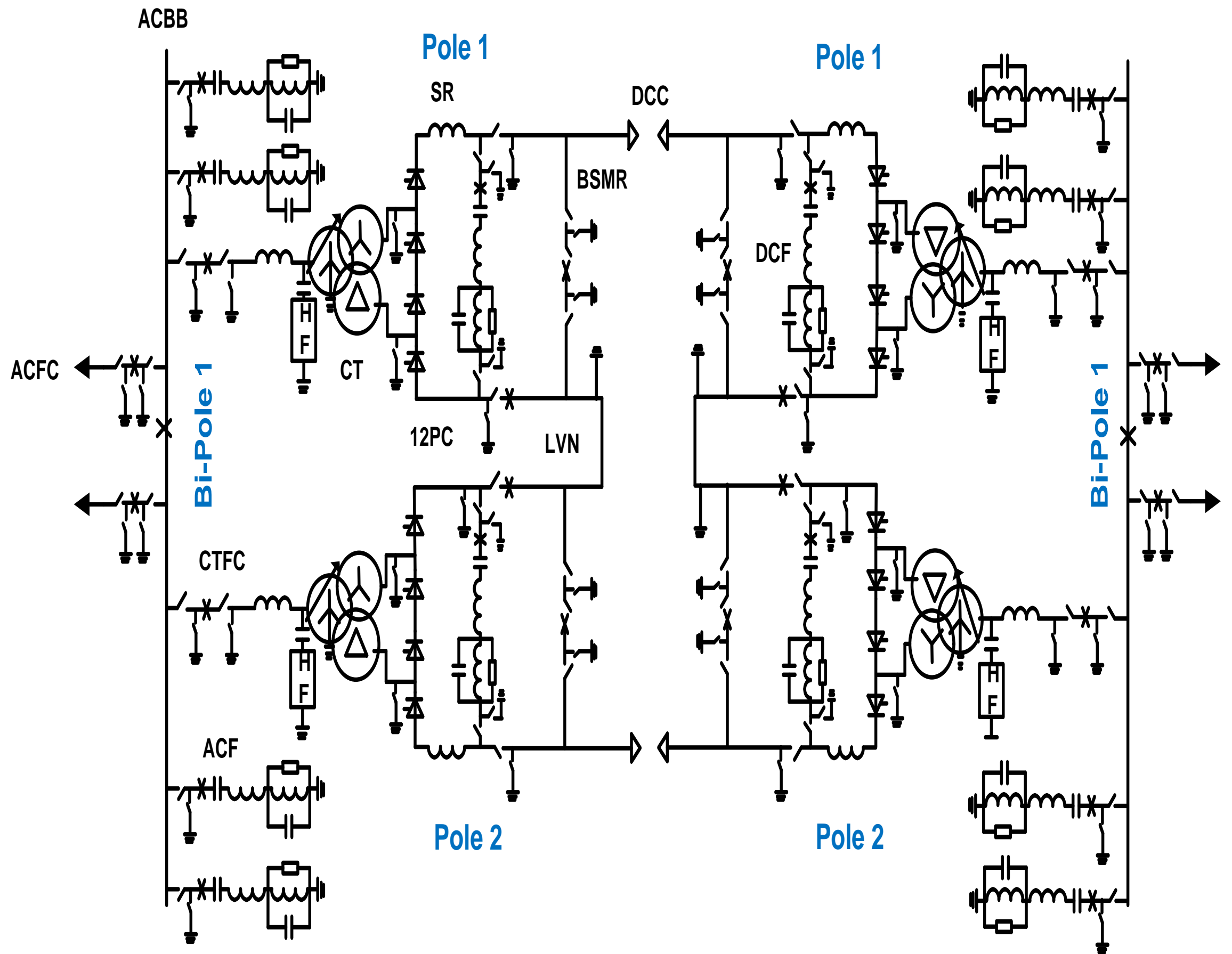


Figure 149: Design of a bipole CSC-HVDC converter station

6.2.1.1 Protection system design for a CSC-HVDC bipole converter station

The DC protection system is provided with complete redundancy to enable safe shutdown and isolation of faulty equipment. Both protection systems are in service simultaneously and thus provide uninterrupted supervision of the HVDC transmission system. The tripping levels and tripping times are set to meet the requirements of the protected zone and the individual protective zones are overlapped by using different transformer cores for each protection system, thereby ensuring that there is no unprotected zone within the HVDC system. The DC protection system is designed to have full redundancy. The duplicated protections are implemented in two different cubicles for system 1 and system 2 on a pole-by-pole basis where both systems incorporate the same protection functions, thereby providing two protection systems per pole [41].

Redundancy is also provided for the measurement in the DC circuits by using separate sensor electronics within a high precision shunt for the individual control and protection systems. The DC protection system is subdivided into the zones as shown in Figure 150. The protection equipment is designed to be fail-safe and incorporates comprehensive monitoring functions to provide a high degree of security to avoid unnecessary shutdowns due to protection equipment failures. For DC faults, the main aim is to detect and clear these as quickly as possible while ensuring that the protection does not malfunction for faults in the AC system [41].

The type and number of DC protections employed can vary according to the manufacturer concerned but there are common protection principles that are used by most of them. Some of these are described in the following sections.

6.2.1.2 DC converter protection

Within the DC converter, short circuits can cause high levels of fault current that can seriously damage the valves. A short circuit protection compares the AC current on the converter transformer valve winding with that flowing on the DC side via the pole and neutral conductors. A short circuit within the converter bridge will cause an imbalance between the AC- and DC side currents. The AC side current will rise substantially and once it rises above the protection setting, the converter blocks, then the pole circuit breakers are opened. An emergency switch-off signal is also initiated and shuts down the pole control [41]. A time-delayed overcurrent protection can be employed as backup to the short circuit protection where the current is measured on the converter transformer valve winding and once above the setting (1.0 pu or higher), the same protective actions as previously described will be initiated. Several time-delayed stages, each with a consecutively higher setting, can be applied to give the control system a chance to alleviate the overcurrent before protective tripping is initiated [41].

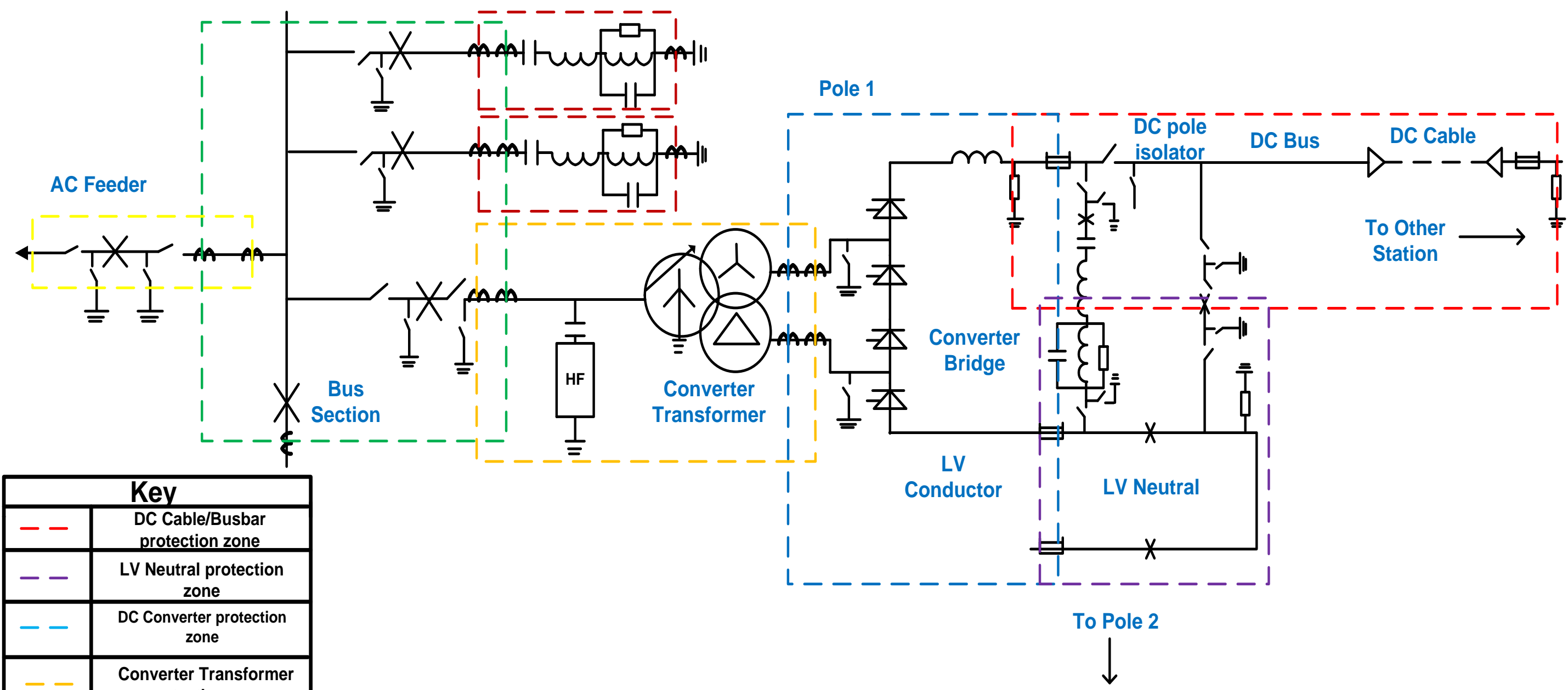
Due to the possibility of commutation failure with CSC-HVDC technology, a differential protection measuring the current on the converter transformer AC valve winding can be employed. A commutation failure results in a high AC current, and once above the protection setting a current reduction can be applied by the DC control system. This provides the system with a chance to recover from the commutation failure without tripping the AC pole breakers. If persistent commutation failure occurs, then the AC pole breakers are opened and an emergency switch-off signal is sent to the pole control [41].

DC differential protection can be used to detect ground faults anywhere within the converter. Extending the protection zone up to the pole isolator provides further coverage. The DC measuring devices compare the current flowing down the positive pole without returning along the neutral connection, and any detected imbalance will cause operation of the protection system which blocks the converter, then opens the AC pole breakers. An emergency switch-off signal is sent to the pole control to safely shut the system down [179].

Both overvoltage and undervoltage protections can be applied by using the Resistive Voltage Dividers (RVD) on the converter DC side to detect abnormal system conditions. If an undervoltage on the DC side is detected, then the converter will be blocked. If no communications are available between the rectifier and inverter, then the fault condition can still be detected. An undervoltage at the inverter will cause the DC voltage to drop and a valve bypass pair will be fired, initiating a protective shutdown. The rectifier undervoltage protection will detect the voltage collapse at the inverter (caused by the shutdown) and will block its own converter. In the opposite scenario, where an undervoltage condition occurs at the rectifier, remote-station fault detection at the inverter will detect the drop in voltage and current, and initiate a protective shutdown. For overvoltage protection, several time delays can be employed to allow the condition to be alleviated by control action. If the condition does not recover, then the HVDC link is tripped and a protective shutdown is initiated [179].

Fundamental frequency protection is used to detect excessive harmonics which could damage the converter. Since these can be reduced during normal converter operation time-delayed stages can be employed so that upon detection, a reduction in current is initiated by the DC control system, and if the situation is not alleviated, then protective shutdown and circuit breaker tripping is applied [179].

Sub-Synchronous Resonance (SSR) protection is included in the converter protection. Upon detection of the frequency range of interest, the DC control system will activate damping control to alleviate the condition. Failing this, the converter will be blocked and the SSR condition will subside. Both AC overvoltage and undervoltage protections on the converter AC busbar are installed and will block the converter if such conditions are detected.



Key	
	DC Cable/Busbar protection zone
	LV Neutral protection zone
	DC Converter protection zone
	Converter Transformer protection zone
	Busbar Protection zone
	Feeder Protection Zone
	DC Current measuring device
	Resistive voltage divider

Figure 150: Protection system design for CSC-HVDC bipole converter station

6.2.1.3 DC cable protection

If a DC cable becomes damaged by a fault, then this can have major repercussions for the CSC-HVDC link. An outage of the converter station is required to locate and repair the damaged cable that could last several months, especially if a subsea cable is damaged. Locating the fault, gaining access to the buried cable and carrying out a repair can be extremely costly. The main DC cable protection must be reliable, sensitive and must clear the fault as quickly as possible while remaining selective. Backup protections can be time-delayed and can pick-up at the same time as the main DC cable protection, operating if the MUs fail to clear the fault [179].

A travelling-wave concept can be used as the primary cable protection where the discharge and reflected waves from a DC fault are detected. To make the protection secure, several stages can be employed before protective actions are initiated. The discharge wave will cause the DC current to rise substantially and the voltage to drop, thus enabling fault identification by measuring these changes over a fixed amount of time. The rate of change of DC voltage and current can also be used as additional security measures so that three of the above detection conditions must be satisfied before protection initiation [179]. The protection will block the converter, open the AC pole breakers and issue an emergency switch-off to the pole control. Automatic isolation of the cable can then be carried out by opening the pole isolators once the load has been removed.

DC undervoltage sensing protection can be used and is slightly different to that included in the converter. The rate of change of voltage can be used to detect fault penetration as a genuine DC fault will cause the voltage to change within milliseconds. A second variable, measuring how long the DC voltage remains below a set limit, makes the protection more stable. A DC undervoltage condition can appear during normal operation temporarily and often recovers, but for a DC cable fault the value will almost be zero, so once the two above criteria have been met, the same protection actions as the travelling-wave protection are initiated to safely shut down the converter [179].

DC cable differential protection can be used for detecting high resistance earth faults by measuring the current in and out of the cable. Any imbalance indicates a potential fault and the same protective actions as described previously are initiated. Due to some DC cables being extremely long, propagation delays can be encountered on communicating signals, increasing the operation time. This protection can be time-delayed and acts as a backup protection to the travelling wave and undervoltage sensing protections. A time delay of 500 ms or more will allow grading with other AC protection systems [179].

6.2.1.4 LV neutral conductor protection

The neutral conductor is essential to CSC-HVDC operation and also needs to be protected against faults. A differential protection can be applied to the LV conductor at both ends of the HVDC link when monopolar operation is required. The current flowing in the LV conductor at the rectifier is compared to that flowing at the inverter. A fault will cause an imbalance in the currents that will result in a shutdown of the converter stations at both ends via protective blocking and tripping of the AC pole breakers [179].

Overvoltages can occur on the neutral conductor due to an open circuit or loss of station grounding when the CSC-HVDC link is in metallic return operation. By using the RVD on the neutral connection to measure the DC voltage, any rise above the protection setting will result in the converters being blocked and the pole control being shut down. The setting corresponds to the maximum insulation level of the neutral conductor [179].

Station ground overcurrent protection can be used to detect overcurrents in the earth connection or earth faults in the LV conductor. The CSC-HVDC link will be shut down by the same protective actions described previously.

When the CSC-HVDC link is in bipole operation, earth faults in the LV conductor can be detected by adopting a differential protection. The current flowing in the pole LV conductor via the DC current measuring device is compared to the equivalent section on pole two. An earth fault will result in an imbalance, and the DC protection system will block the converters at both poles, followed by the opening of the AC pole circuit breakers [179].

6.2.1.5 Converter transformer protection

The converter transformer is one of the most expensive and important items of plant associated with a CSC-HVDC converter station. Some of the protections described in section 6.1.2.5 are also applicable to the double-wound transformer. Only the protection systems which differ from that applied to the autotransformer will be described here.

For the double-wound transformer shown in Figure 151 a main protection is similar to that employed on the autotransformer. In Both HV and LV, restricted earth fault protection is combined with a biased differential protection scheme to define the interior of the transformer as the protected zone. An external fault in the star side will result in current flowing in the line CT of the affected phase and at the same time balanced current flows in the neutral CT; hence the resultant current in the relay is zero. During an internal fault, unbalanced current flows through the relay and tripping takes place. The scheme is extremely sensitive for internal earth faults [180].

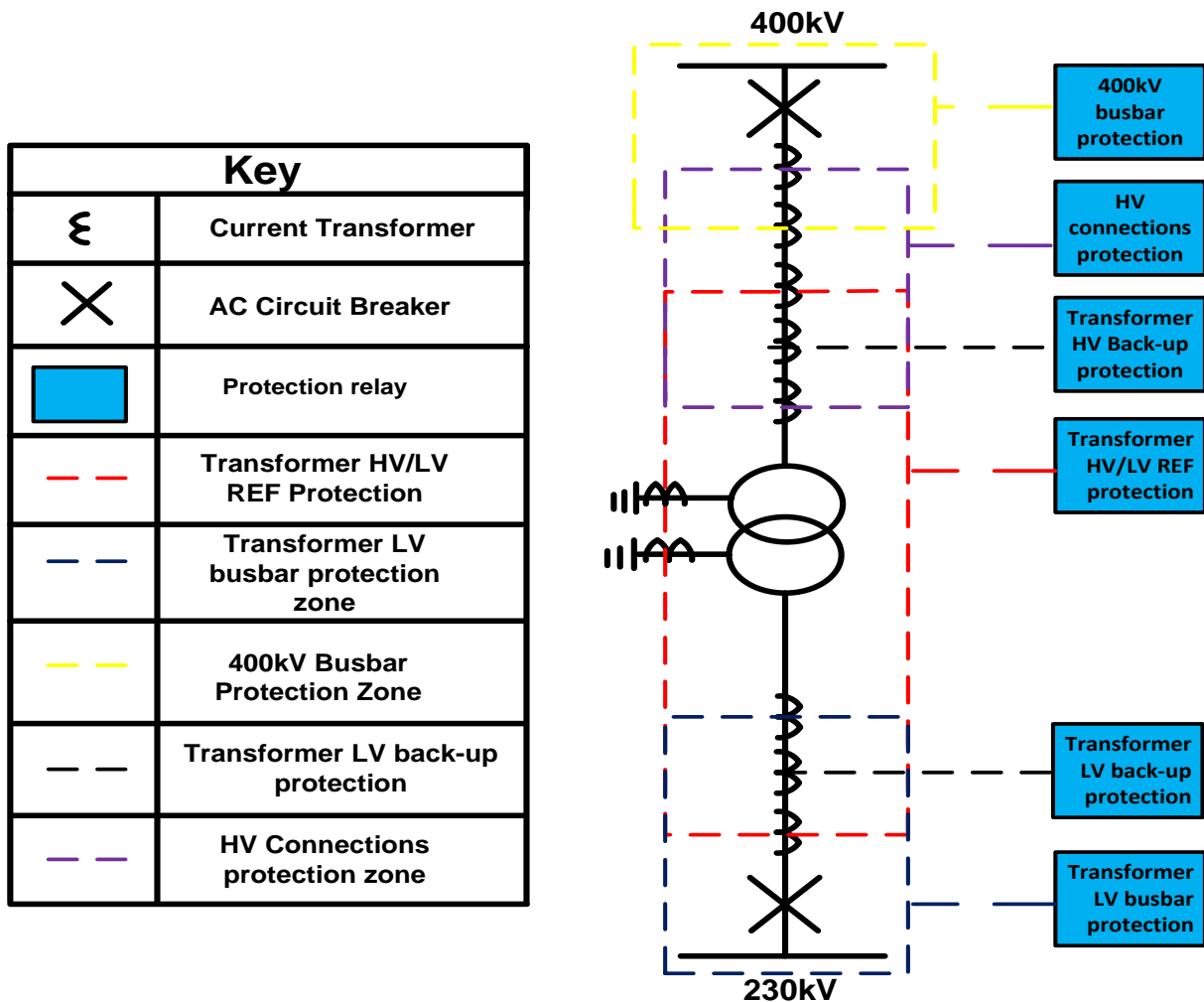


Figure 151: Protection scheme for converter transformer

Over-excitation protection is included to detect overfluxing and protect the transformer core from overheating. This function resides in the same protection relay as the HV and LV restricted earth fault protection. A harmonic restraint function is also provided, which protects the transformer from excessive harmonics and is stable for magnetic inrush during initial startup.

On the LV side, an overcurrent protection is provided for detecting overcurrents. Since the LV REF is provided to detect earth faults, no other form of backup protection is required. The same mechanical protection relays applied to the autotransformer are also used here [180].

6.2.1.6 AC cable feeder protection

Due to the limitations of distance protection on very short cable feeder circuits (<4 km), a double unit protection for both the first and second MUs are applied. Each main system is fed from a different CT and obtained from different suppliers to ensure that any manufacturing defect in one is not common to the other.

Within each MU protection relay, a three-phase overcurrent and earth fault protection are included, for the same reasons mentioned in section 6.1.2.4. Thermal overload protection is included to protect the AC cable feeders from overheating; this uses the cooling and heating characteristics of both cables to determine whether the cable temperature exceeds the nominal setting, initiating an alarm to notify the system operator of the condition. If no control action is taken, or if the condition is not alleviated after a suitable time delay, then a protection trip will be initiated [180].

The busbar protection follows the same principle as that described in section 6.1.2.2 and only applies to the single busbar shown in Figure 150. The busbar CTs overlap with those of the main protections for the AC cable, converter transformer feeder circuits and harmonic filters to ensure that no zone is left unprotected.

6.2.2 Final design CSC-HVDC NPP connection

Each of the individual components presented in chapter 6 have been combined to form a final design for connecting an NPP to the grid by CSC-HVDC technology.

In Figure 152, two 2250 MW CSC-HVDC bipoles are used to connect the NPP AC interface substation to the 400 kV transmission grid. The combined active power transfer capacity of both CSC-HVDC links is 4500 MW and permits the connection of an NPP with the same maximum power rating whilst considering house load supply. The 400 kV AC overhead line circuits (North 1 and 2) provides an additional export route to the AC grid. The design offers great flexibility if either the northern AC or southern DC circuits are unavailable for power export/import purposes. The full output of the NPP can be delivered solely by the northern AC circuits or southern HVDC connections circuits, or via a combination of both.

If one of the DC links is out of service due to a permanent cable fault, with the inclusion of the double 400 kV AC overhead line running north (North 1 and 2), then 100% power transfer from the NPP to the AC system can still be supplied. If one of the 400 kV AC circuits running north is lost due to a permanent fault, then the full output power of the NPP can still be maintained via a combination of both CSC-HVDC bipole links and the remaining, in-service single 400 kV AC overhead line circuit.

Four AC cable feeder circuits connect the two new 400 kV substations to each end of the CSC-HVDC bipole converter stations. Each cable feeder has a rating of 1250 MVA. The protection systems described in section 6.2.1.6 are applied individually to each cable feeder circuit in turn and the other protection systems described previously apply to the final design shown in Figure 150.

The DC converter protection system described in section 6.2.1 is duplicated, providing a main system 1 and 2 for each pole. With an identical arrangement at both ends, full redundancy is provided whether the CSC-HVDC link is in monopolar or bipolar operation.

Mass Impregnated Non Draining (MIND) DC subsea cable technology connects the rectifiers to the inverters through four DC cables, each 1250 MVA in rating, to provide full active power transfer capability from the NPP to the AC grid via the 400 kV substations.

Each bipolar configuration employs appropriate switching mechanisms to allow 50% power to be supplied in the case of either a pole or converter outage.

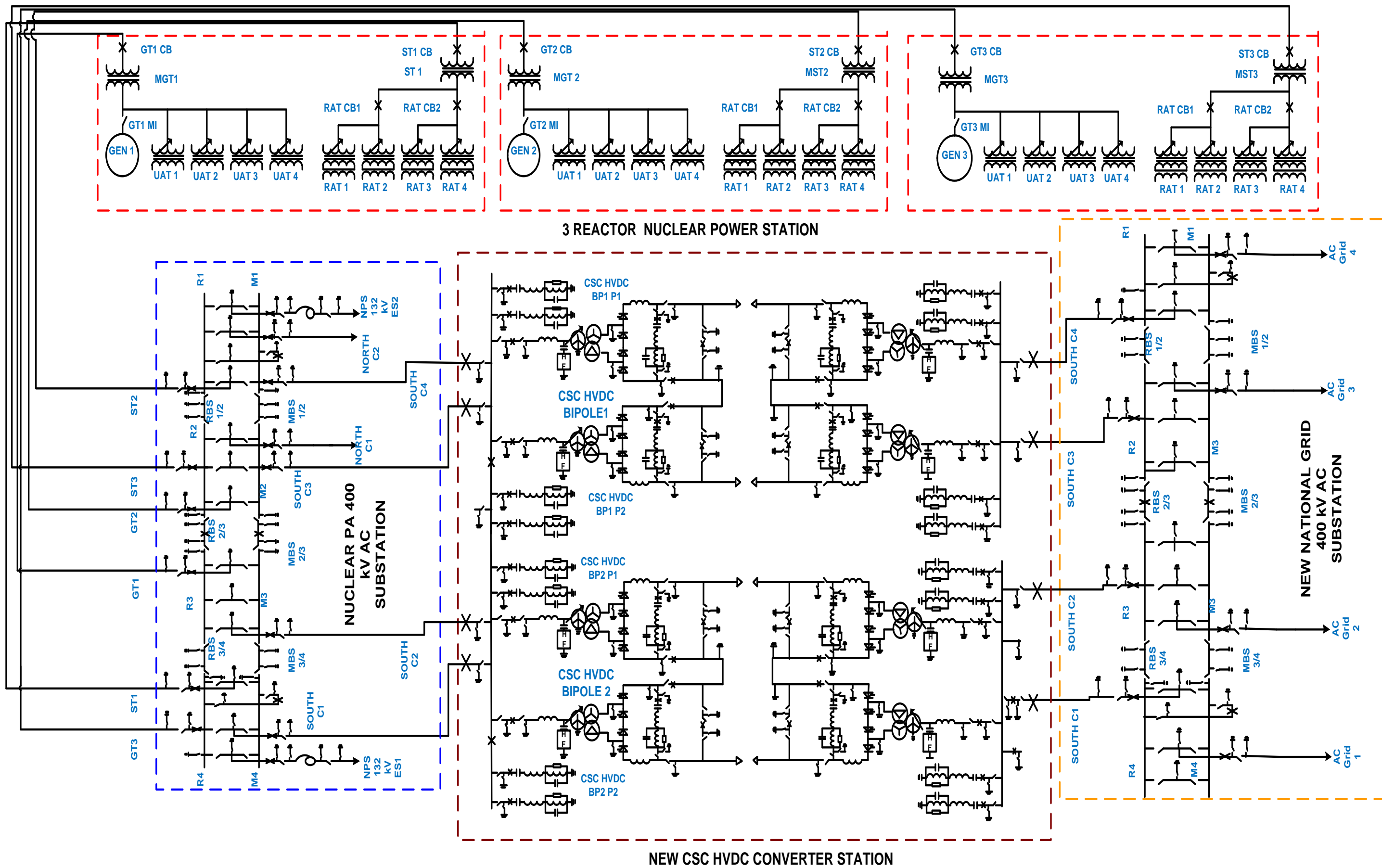


Figure 152: Final design of an NPP connected to the AC grid by CSC-HVDC technology

6.3 Design of an NPP connection utilising VSC-HVDC technology

A design utilising VSC-HVDC technology for connecting the 4500 MW NPP design used in sections 6.1 and 6.2 to an AC grid is presented, employing the same two 400 kV double busbar AC substations used in the previous sections. A 2250 MW, ± 600 kV bipole VSC-HVDC link design is presented, based upon the maximum bipole VSC-HVDC converter [90] and DC cable [178] available within industry at the time of writing. A full description of only those protection systems which differ from those applied to the CSC-HVDC link previously in section 6.2 is included. Finally, the designs are combined into one overall design option for an NPP connection to the AC grid via VSC-HVDC technology.

6.3.1 VSC-HVDC bipole converter station design

A design of a ± 600 kV, 2250 MW VSC-HVDC converter station is shown in Figure 153. Both the rectifier and inverter are connected to a single busbar at each end, with two 400 kV AC cable feeder circuits providing the interface connection to the grid. AC filters are connected to the busbar for filtering out harmonics.

The converter transformers are connected to the single busbar and can be isolated via the AC circuit breaker and line isolators as required. The two-winding converter transformers are equipped with a tap changer on the primary side for providing coarse control of the AC voltage. Each pole provides 1150 MW of power transfer capability.

A DC capacitor is included on each pole for reducing harmonics and voltage ripple. Bypass isolators are available if one pole needs to be taken out of service to enable the use of metallic return mode via the second DC cable. DC filters may be required, depending on the performance requirements of the VSC-HVDC link and the connected AC system.

The converter reactors allow control of active and reactive power and also limit fault currents in the valve.

The DC subsea cables connect the rectifier to the inverter, and earth switches are available at either end for discharging the DC cable if required. Neutral bus ground switches are provided to connect both negative poles together to enable metallic return mode operation.

Two bipoles can be connected together to provide higher voltage and power ratings if needed. The protection system for one pole will be identical to that in the other. The IGBTs are arranged as a six-pulse system per pole, with no reactive power being required.

Key	
	AC Circuit Breaker
ACBB	AC Busbar
ACFC	AC Feeder Circuit
ITFC	Inverter Transformer Feeder Circuit
IT	Interface Transformer
12PC	12 Pulse Converter
LVN	Low Voltage Neutral
IR	Interface Reactor
BSMR	Bypass Switch for Metallic Return
DCC	DC Cable
ACF	AC Filter
	AC Busbar
	Earth Switch

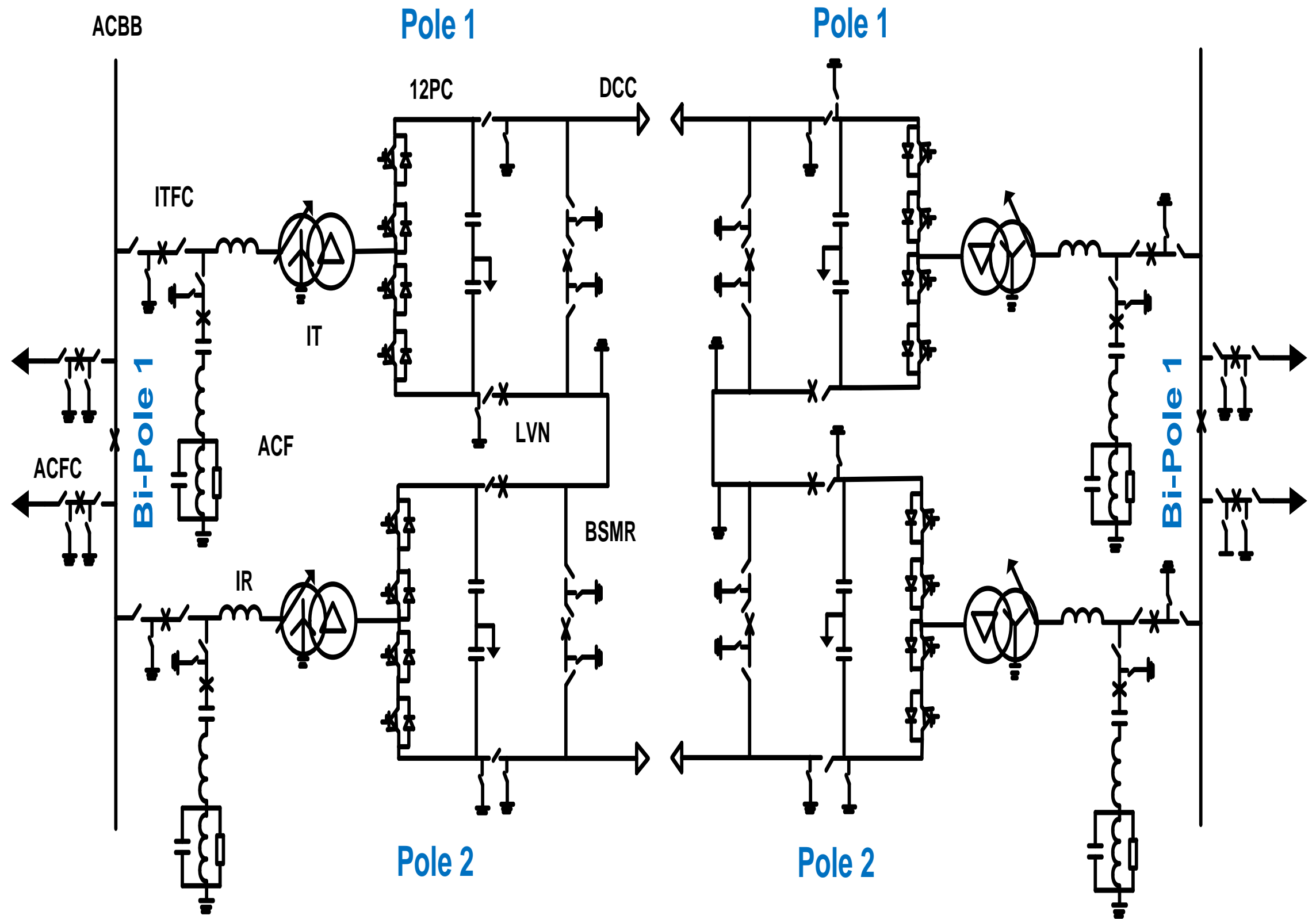


Figure 153: Design for a VSC-HVDC bipole converter station

6.3.1.1 Protection system design for a VSC-HVDC bipole converter station

Just like CSC-HVDC converters, the VSC-HVDC protection system is provided with complete redundancy to ensure a safe shutdown and isolation of the faulty equipment. Both protection systems are in service simultaneously and thus provide uninterrupted supervision of the HVDC transmission system. Each of the protection systems described for the CSC-HVDC link are applied to the VSC design in Figure 153. Two different protections are employed in the converter; these are described below.

A protection system is employed to monitor the number of failed IGBTs. Failure of IGBTs can cause healthy ones to be overstressed by the increased voltage across the valves. When an IGBT fails, it becomes short circuited safely so that power transmission can continue. Once a predetermined number of IGBTs have failed, then the converters are tripped and the components are replaced [182].

The converter cells can be subject to large overvoltages, especially at high currents and with unbalanced voltage due to ground faults. The control system monitors the cell voltage and once this rises above the maximum setting, the converter is blocked. Once the voltage returns to normal, the converter is de-blocked and power transfer recommences. If the condition reappears, then the converter is tripped [182].

6.3.1.2 Final design of an NPP connected by VSC-HVDC technology

Each of the individual components presented in chapter 6 have been combined to form a final design for connecting an NPP to the grid by VSC-HVDC technology.

In Figure 154, two 2250 MW VSC-HVDC bipoles are used to connect the NPP AC interface substation to the 400 kV transmission grid. The combined active power transfer capacity of both VSC-HVDC links is 4500 MW. The 400 kV overhead line circuits (North 1 and 2) provide an additional export route to the AC grid.

Just like the CSC-HVDC link, four AC cable feeder circuits connect the two new 400 kV substations to each end of the VSC-HVDC link. The DC cables are identical to those used in the CSC-HVDC design. MIND cables are used to match the ± 600 kV maximum converter ratings available in [90]. The converter stations also have the potential to be much smaller than those employing CSC-HVDC technology and could offer significant cost savings; this will be explored in chapter 7.

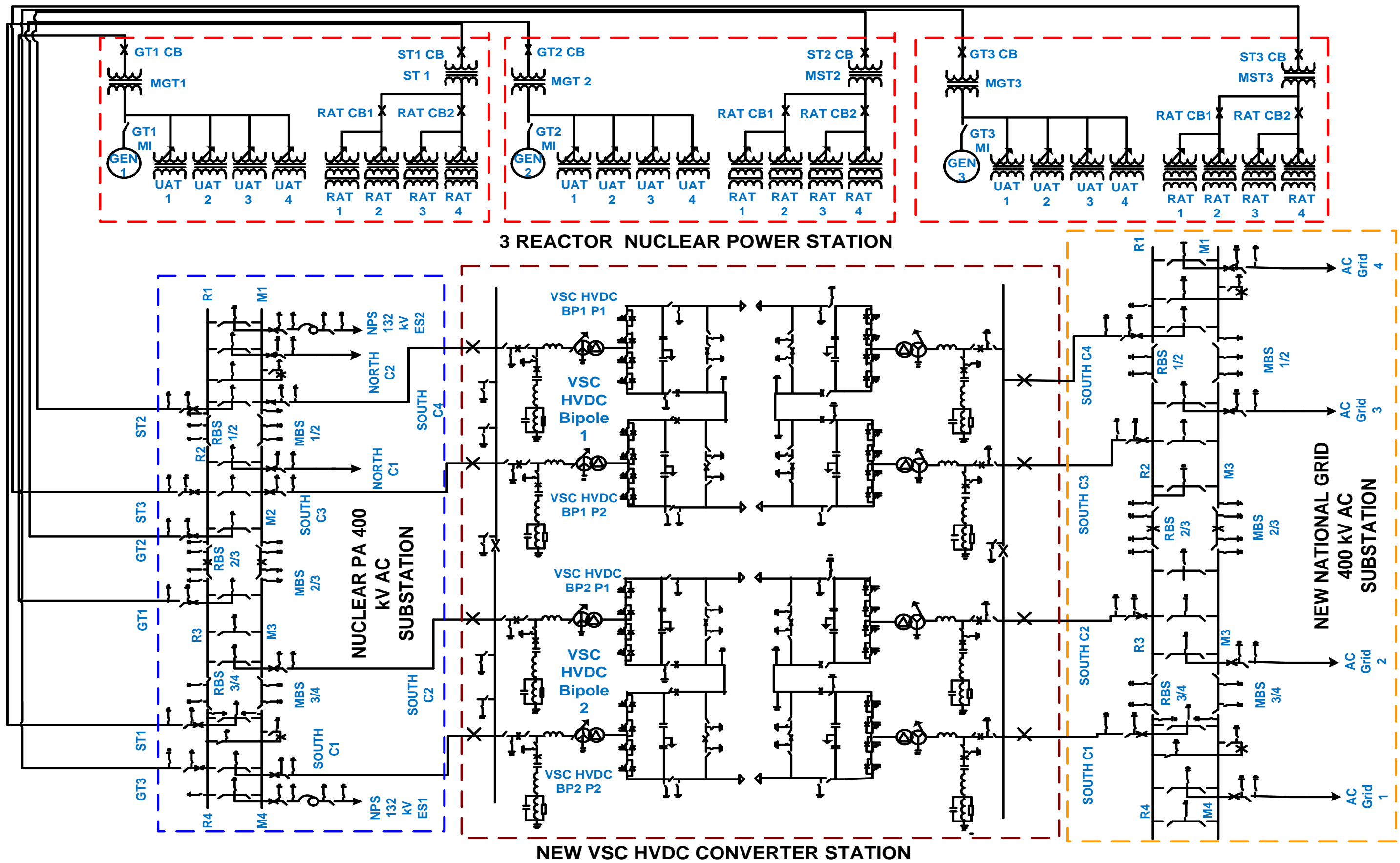


Figure 154: Final design for connecting an NPP by VSC-HVDC technology to an AC grid

6.4 Design of an control system for an HVDC NPP connection

The control system is a vital component in the successful operation of an HVDC link. Without it, power transmission may not be possible and the response can cause undesirable interactions with the AC system [182]. The simulations carried out in chapters 4 and 5 have demonstrated its importance in the operation of both CSC- and VSC-HVDC technology. In particular, the ability of the HVDC control system to maintain the frequency within the NPP when no AC connection is available is important [7].

In the following section, a design of an HVDC control system for an NPP connection is presented. The control system has been incorporated into the previous final VSC-HVDC designs from section 6.3. A desktop study assessing the response required from the HVDC control system with respect to different circuit events within the NPP and AC grid is presented and each of the high-level control functions are described. The aim of the assessment is to determine the response required from the HVDC control system, in order to prevent the thermal ratings of AC circuits from being exceeded.

Finally, an example of a DC controller for maintaining the frequency within the NPP has been designed in Microsoft Office Visio. The controller can be applied in future work and examined in detail via means of simulation or construction of a prototype.

6.4.1 Power system setup

In Figure 155, the VSC NPP connection presented previously has been integrated with an HVDC control system design. A power flow scenario representing that of a real case within National Grid has been selected for the study [1]. The scenario is for maximum summer demand where the primary load flows are from the northern part of the AC grid to the maximum load demand in the south.

With a maximum generation capacity of 4500 MW, the NPP requires 5 –10% house load to supply its own operational and critical safety systems [106]. Assuming 5% is required for house load operation (225 MW) a remaining generation total of 4225 MW is available for supply to the AC grid [106]. A value of 3780 MW of the remaining total flows through the two VSC-HVDC bipole links into the southern part of the AC grid.

A remaining generation of 445 MW flows through the AC feeder circuits 1 and 2 into the northern part of the AC grid, leaving 3780 MW to supply the load demand of the AC system. Each circuit is designated in Table 19.

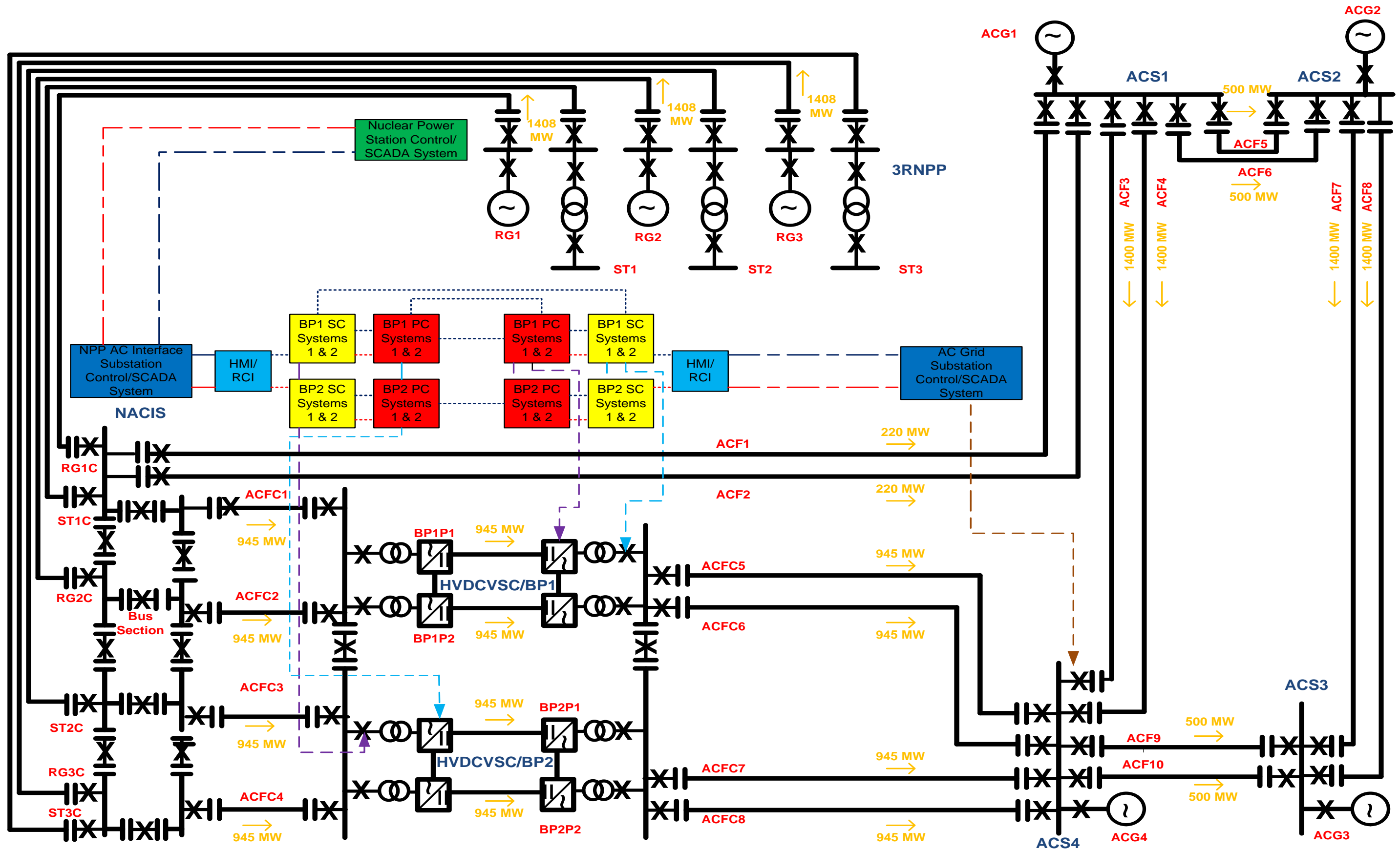


Figure 155: Power system setup for thermal case study

Table 19: Circuit designation and thermal ratings for Figure 152

Key	Definition
ACS1	AC System 1
ACS2	AC System 2
ACS3	AC System 3
ACS4	AC System 4
ACG1	AC Generator 1
ACG2	AC Generator 2
ACG3	AC Generator 3
ACG4	AC Generator 4
3RNPP	3 Reactor Nuclear Power Plant
NACIS	Nuclear AC Interface Substation
HMI/RCI	Human–Machine Interface/Remote Control Interface
BP1SC	Bipole 1 Station Control
BP2SC	Bipole 2 Station Control
BP1PC	Bipole 1 Pole Control
BP2PC	Bipole 2 Pole Control
RG1	Reactor Generator 1
RG2	Reactor Generator 2
RG3	Reactor Generator 3
ST1	Station Transformer 1
ST2	Station Transformer 2
ST3	Station Transformer 2
	Isolator
---	Telecom communication
----	Telecontrol communication
-----	AC telecom communication
-----	AC telecontrol communication
----->	AC plant control communication
----->	Converter control communication
----->	Station Control communication

Each of the two bipolar VSC-HVDC links are rated at 2250 MW and match the HVDC designs already implemented. The 400 kV AC overhead line circuits which connect the NPP to the northern part of the AC grid (AFC1 and AFC2) are shown.

The communication and signalling interfaces between the HVDC and AC control systems are also shown. Both the station- and pole-level control functions are displayed.

The maximum thermal rating of each of the circuits is shown in Table 20. In practice, these circuits would have both nominal and thermal ratings, but this study only considers the maximum thermal ratings as this represents the worst case where any further power transfer above these ratings could result in damage or protection operation [20]. The ratings are expressed in both MVA and MW and have been supplied by National Grid.

Table 20: Circuit designation and thermal ratings for Figure 152

Circuit reference	Designation	Maximum rating (MVA)	Maximum rating (MW)	Circuit Load
ACF1	AC Feeder Circuit 1	2200	2090	220
ACF2	AC Feeder Circuit 2	2200	2090	220
ACF3	AC Feeder Circuit 3	2200	2090	1400
ACF4	AC Feeder Circuit 4	2200	2090	1400
ACF5	AC Feeder Circuit 5	2200	2090	500
ACF6	AC Feeder Circuit 6	2200	2090	500
ACF7	AC Feeder Circuit 7	3100	2945	1400
ACF8	AC Feeder Circuit 8	3100	2945	1400
ACF9	AC Feeder Circuit 9	2200	2090	500
ACF10	AC Feeder Circuit 10	2200	2090	500
ACFC1	AC Cable Feeder Circuit 1	1180	1125	945
ACFC2	AC Cable Feeder Circuit 2	1180	1125	945
ACFC3	AC Cable Feeder Circuit 3	1180	1125	945
ACFC4	AC Cable Feeder Circuit 4	1180	1125	945
ACFC5	AC Cable Feeder Circuit 5	1180	1125	945
ACFC6	AC Cable Feeder Circuit 6	1180	1125	945
ACFC7	AC Cable Feeder Circuit 7	1180	1125	945
ACFC8	AC Cable Feeder Circuit 8	1180	1125	945
BP1P1	Bipole 1 Pole 1	1180	1125	945
B1PP2	Bipole 1 Pole 2	1180	1125	945
BP1	Bipole 1	2370	2250	1890
BP2P1	Bipole 2 Circuit 1	1180	1125	945
BP2P2	Bipole 2 Circuit 2	1180	1125	945
BP2	Bipole 2	2370	2250	1890

6.4.2 HVDC control system design

The HVDC control system is split into separate high-level functions. A description of each of the functions for the design presented in Figure 155 is contained in the following sections, including a description of the Supervisory Control and Data Acquisition (SCADA) systems between the NPP, HVDC converters and AC grid.

6.4.2.1 DC station control

The DC station control is primarily responsible for the monitoring, switching and control of primary switchgear within both the AC and DC switchyards. Such equipment includes circuit breakers, shunt reactors, isolators and filters among others. When the DC link is in bipole mode, the station control is responsible for automatic DC configuration sequences, scheduled bipole power orders, modulation controls, active power runbacks and ramps and data exchange with the remote converter station [22].

In addition to the above, extra functions include the transfer of messages to the local Human–Machine Interface (HMI) and Remote Control Interface (RCI), hardware and software monitoring functions, and the receiving of signals and commands from the system operator. There are usually two station control devices per pole to provide adequate redundancy in case of an outage or fault to the other one. The station control interfaces with the pole control, transmitting power orders and commands for execution purposes.

6.4.2.2 DC pole control

At pole level, the control provides numerous functions and operations which include current order settings, transient control functions such as power oscillation damping, frequency control and ramps and runbacks. At converter level, the pole control contains functions like DC voltage control, SSR damping control, blocking, de-blocking and emergency switch-off (ESOF) sequences. Just like the station control, the pole control is duplicated on a per pole basis, in order to provide sufficient redundancy for possible failures or outages of the other one.

6.4.2.3 HVDC telecontrol/telecom

HVDC telecontrol is a direct communications link from one DC pole control to another with the DC station control. This is used primarily for protection and control functions, and provides fast data exchange with low transmission delays.

HVDC telecom is a direct communication link from one DC station control to the other, which is used to exchange mass data for general SCADA and is much slower than the telecontrol. Data is transferred via the telecom communication channels from the DC station control and is distributed to various receivers at the other station end.

6.4.2.4 Remote control/human–machine interface

The HMI consists of operator personal computers which are used to send commands to the controls and field equipment. Auxiliary systems such as low voltage switchgear and diesel generators can also be controlled from the HMI if desired.

The link between the HVDC protection and control is provided by the RCI. The RCI communicates with the station control and pole control and can also interface with the AC network, so that data can be communicated between the individual systems over fast and secure channels [22].

6.4.2.5 Nuclear power plant SCADA and control system

SCADA is a system for remote monitoring and control that operates with coded signals over different communication channels. The control system can be combined with a data acquisition system by using coded signals over communication channels to obtain information and data about the status of remote equipment.

The NPP control system is responsible for the overall protection and operation of the NPP. Several levels of redundancy may be incorporated into the overall design, which presents a highly complex set of control functions. The interaction of the communications within the NPP and AC system is crucial under dynamic conditions and is well proven in practice. However, when the control system of a HVDC link is also included in the whole system architecture, the coordination between the individual control systems presents an unproven and high level of control complexity. The SCADA allows the NPP controls to be interfaced with the HVDC system for protection and monitoring functions.

6.4.2.6 AC grid substation SCADA and control system

A SCADA system is also required for protection, control and monitoring functions between the AC grid substation and HVDC link. Positions and status of AC switchgear, voltage, power and current measurements are required in case control actions or responses are required from the HVDC link [183]. Signals may also be transferred directly between the AC grid and NPP if needed; an example would include a direct intertrip of one of the nuclear generators due to system instability.

6.4.3 Thermal contingency analysis for NPP HVDC connection

In Table 21, a list of the different contingency events analysed for the power system designed in Figure 152 is presented.

For each of the events, a list of the required control actions from the HVDC and/or AC system to prevent thermal overloading of different circuits is recorded. By using manual calculation, the amount of active power reduction or increase required to maintain system balance without the need for generator intertripping is determined. Following the application of the recommended control actions the final outcome is stated, determining whether generator intertripping is required. In some cases, there may be one or more alternate control actions that can achieve system balance. A total number of 21 individual events have been analysed for the thermal contingency analysis. For most of the events, limited control actions are required due to the level of circuit redundancy incorporated into the overall design but for some events, further actions are required.

During event number 3, an N-2 (loss of a double circuit) is encountered due to the loss of both ACF1 and ACF2 from the NPP to the AC grid via ACF1 and ACF2. A fast active power run-up from both DC links is required, to prevent the need to intertrip generation due to the 440 MW active power bottleneck created by the N-2 situation.

In scenario 8, a trip of one pole results in the whole bipole being tripped as part of conventional HVDC protection and control practice [91]. This results in a full 1890 MW of excess power to be dealt with. A run-up from the other bipole to maximum output, in combination with the automatic redistribution of power through the 400 kV AC feeder circuits (ACF1 and ACF2) is required to maintain equilibrium.

In event number 10, both of the HVDC links have been tripped due to permanent faults in both bipoles. Under this scenario a total 3780 MW of excess power that was originally flowing through both HVDC links create a bottleneck situation. The power will flow through the 400 kV AC double overhead line circuits (ACF1 and ACF2) into the northern part of the grid (ACS1), overloading the circuits by 140 MW requiring a power run back from one NPP generator in order to prevent the need to intertrip.

The extra redundancy in the design presented in Figure 155 provides sufficient capacity to prevent the need for generator intertripping due to circuit thermal ratings being exceeded. Hence, by using large rated HVDC links in combination with high rated AC circuits, a flexible design is produced.

Table 21: Circuit designation and control actions required for Figure 152

Event	Event number	Result	Required action (s)	Final outcome
ACF1 trip	1	220 MW excess	None	Instantaneous flow through ACF2
ACF2 trip	2	220 MW excess	None	Instantaneous flow through ACF1
ACFC1 & ACFC2 trip	3	440 MW excess	BP1 ramped from 1890–2150 MW and bipole 2 from 1890–2070 MW. The NPP may also be able to run back their output power for one bipole ramp	100% power supply to AC grid maintained
BP1P1 trip	4	1890 MW excess	Automatic instantaneous flow through either ACF1 or ACF2 or ramp BP2 from 1890–2150 MW in combination with either AC option	100% power supply to AC grid maintained. Note: BP1P2 will be tripped once BP1P1 is lost as part of conventional HVDC protection strategy
BP1P2 trip	5	1890 MW excess	Automatic instantaneous flow through either ACF1 or ACF2 or ramp BP2 from 1890–2150 MW in combination with either AC option	100% power supply to AC grid maintained. Note: BP1P1 will be tripped once BP1P2 is lost as part of conventional HVDC protection strategy
BP1 trip	6	1890 MW excess	Ramp BP2 from 1890–2150 MW in combination with instantaneous flow through either ACF1 or ACF2	100% power supply to AC grid maintained
BP2 P1 trip	7	1890 MW excess	Automatic instantaneous flow through either ACF1 or ACF2 or ramp BP1 from 1890–2150 MW in combination with either AC option	100% power supply to AC grid maintained. Note: BP2P2 will be tripped once BP2P1 is lost as part of conventional HVDC protection strategy
BP2 P2 trip	8	1890 MW excess	Automatic instantaneous flow through either ACF1 or ACF2 or ramp BP1 from 1890–2150 MW in combination with either AC option	100% power supply to AC grid maintained. Note: BP2P1 will be tripped once BP2P2 is lost as part of conventional HVDC protection strategy
BP2 trip	9	1890 MW excess	Ramp BP1 from 1400–2090 MW in combination with instantaneous flow through either ACF1 or ACF2	100% power supply to AC grid maintained
BP1 & BP2 trip	10	3780 MW excess	Instantaneous flow through either ACF1 or ACF2; however possible overload of these circuits by 140 MW	A runback of 140 MW from one generator would ensure ACF1 and ACF2 are not overloaded
ACF1 & BP1 P1 Trip	11	2110 MW excess	Ramp BP2 from 1890–2150 MW and automatic instantaneous flow through ACF2	100% power supply to AC grid maintained. Note: BP1P2 will be tripped once BP1P1 is lost as part of conventional HVDC protection strategy resulting in total 2110 MW excess
ACF1 & BP1 P2 trip	12	2110 MW excess	Ramp BP2 from 1890–2150 MW and automatic instantaneous flow through ACF2	100% power supply to AC grid maintained. Note: BP1P2 will be tripped once BP1P1 is lost as part of conventional HVDC protection strategy resulting in total 2110 MW excess
ACF1 & BP1 trip	13	2110 MW excess	Ramp BP2 from 1890–2150 MW and automatic instantaneous flow through ACF2	100% power supply to AC grid maintained
ACF1 & BP2 P1 trip	14	2110 MW excess	Ramp BP1 from 1890–2150 MW and automatic instantaneous flow through ACF2	100% power supply to AC grid maintained. Note: BP1P2 will be tripped once BP2P2 is lost as part of conventional HVDC protection strategy resulting in total 2110 MW excess
ACF1 & BP2 P2 trip	15	2110 MW excess	Ramp BP1 from 1890–2150 MW and automatic instantaneous flow through ACF2	100% power supply to AC grid maintained. Note: BP1P2 will be tripped once BP2P2 is lost as part of conventional HVDC protection strategy resulting in total 2110 MW excess
ACF1 & BP2 trip	16	2110 MW excess	Ramp BP1 from 1400–2090 MW in combination with automatic flow through ACF2	100% power supply to AC grid maintained
ACFC1 trip	17	1890 MW excess	Trip BP1. Ramp bipole 2 to maximum 2150 MW rating and automatic flow through ACF1 and ACF2	This action will prevent overloading of ACFC2 but a total of 1890 MW excess is present due to the whole bipole being tripped as part of the HVDC protection strategy
ACFC2 trip	18	1890 MW excess	Trip BP1. Ramp bipole 2 to maximum 2150 MW rating and automatic flow through ACF1 and ACF2	This action will prevent overloading of ACFC2 but a total of 1890 MW excess is present due to the whole bipole being tripped as part of the HVDC protection strategy
ACFC3 trip	19	1890 MW excess	Trip BP2. Ramp bipole 1 to maximum 2150 MW rating and automatic flow through ACF1 and ACF2	This action will prevent overloading of ACFC4 but a total of 1890 MW excess is present due to the whole bipole being tripped as part of the HVDC protection strategy
ACFC4 trip	20	1890 MW excess	Trip BP2. Ramp Bipole 1 to maximum 2150 MW rating and automatic flow through ACF1 and ACF2	This action will prevent overload of ACFC3 but a total of 1890 MW excess is present due to the whole bipole being tripped as part of the HVDC protection strategy
ACFC1 & 2 trip	21	1890 MW excess	Trip BP1. Ramp bipole 2 to maximum 2150 MW rating and automatic flow through ACF1 and ACF2	This action will prevent overload of ACFC3 and ACFC4

6.4.4 HVDC frequency controller design

When an NPP is connected solely by an HVDC link, the frequency within the NPP needs to be maintained by the DC control system; any large deviations in frequency can seriously impact the operation of the NPP safety systems and reactor cooling systems. The design of a suitable controller is paramount for successful operation and security of an NPP connected by HVDC technology [7].

In Figure 156, a design of a frequency controller for application to an NPP connection is presented.

During normal operation, only the left hand side of the frequency controller is active. The aim of this control loop is to maintain the frequency of the NPP within $\pm 1\%$ of nominal (50 Hz). The reference frequency ($F1_{ref}$) is compared to the measured value ($F1$), and any deviation between the two will present an error. This error is then fed into a dead-band limiter which keeps the quantity within system limits before entering a PI controller where the necessary delta change is applied to correct the error, creating an output power reference that is fed to the DC control system, bringing the frequency back within the system operating parameters.

If, during emergency system conditions, the HVDC link is required to provide frequency control to the AC grid, then this can also be enabled. The frequency switchover scheme contact is closed by a command from the DC station control and the right-hand-side control loop of the frequency controller is enabled. Here the measured frequency of both the NPP ($F2$) and AC grid ($F1$) are compared with the reference values ($F1_{ref}$) and ($F2_{ref}$) and if the frequency in either system drifts outside of nominal limits, then an adjustment is made to the DC power reference and a change to active power flow will occur.

Each of the individual components must operate correctly and be coordinated for the system to work. The measurements and signals exchanged between the NPP and HVDC control system must have a high level of accuracy for successful operation – a slight error in control signals or measurements could cause the active power to be over or under modulated. If this happens, then the frequency on both sides of the HVDC link may differ in value and system instability could occur. Rapid changes in frequency will affect the operation and security of the NPP, so stable operation is paramount. The speed and effectiveness of the controller would need to be determined by simulation and by testing of the real protection and control systems during the testing phase of a project.

A description of the key components and their functionality is described in the next section.

Key	
ECV	Extraction control valve
GCS	Governor control system
MSV	Main stop valve
SCV	Steam control valve
EPS	Extraction pressure signal
ETL	Extraction line
BPS	Back pressure signal
GFM	Generator frequency measurement
EL	Exhaust line
SS	Speed signal
GOS	Governor output signal
F1	NPP frequency measurement
F1 REF	NPP frequency reference
F2	AC grid frequency measurement
F2 REF	AC grid frequency reference
PI	Proportional integral controller
dPDC	DC output power order
FSS	Frequency switchover scheme

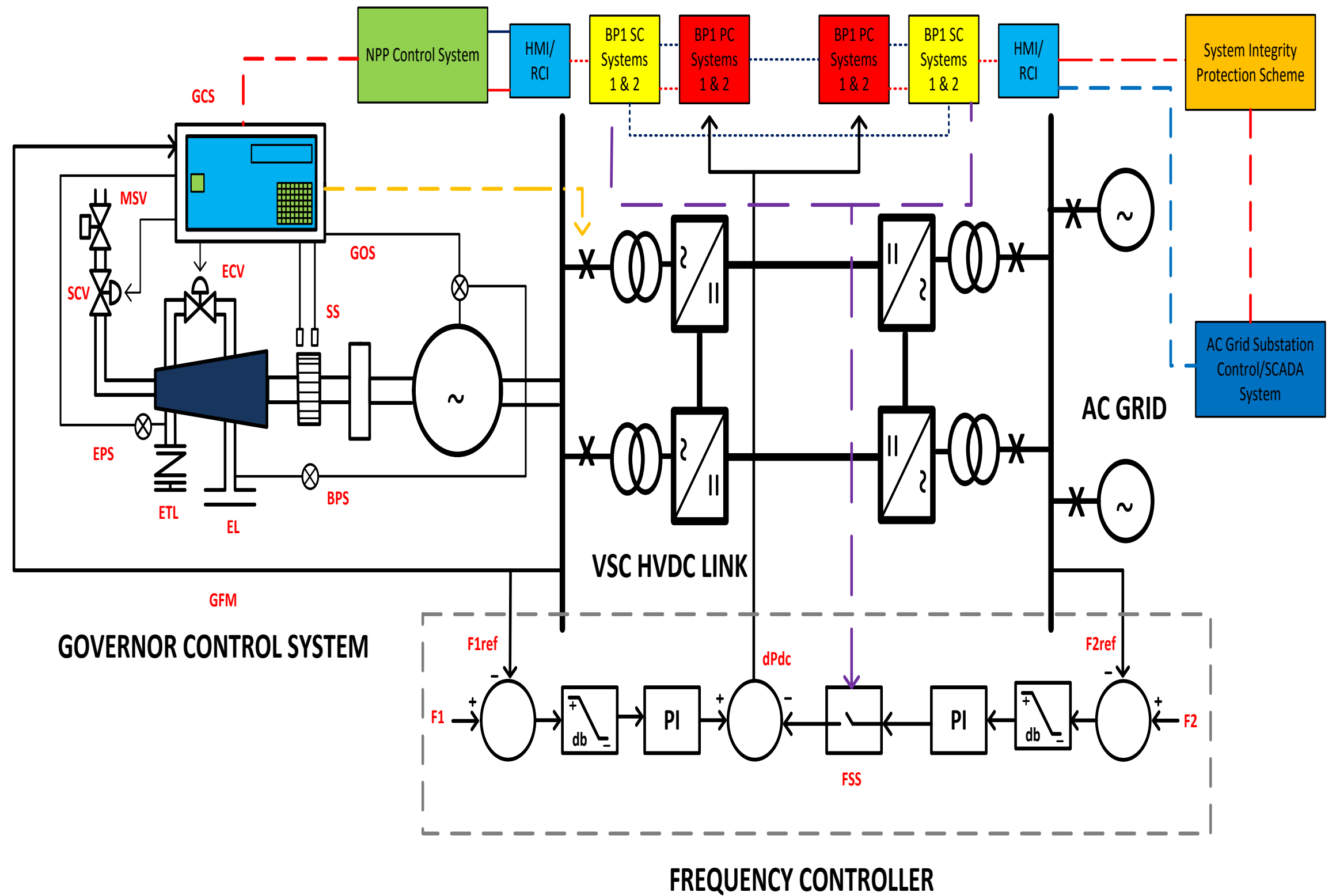


Figure 156: Design of an HVDC frequency controller for NPP operation

6.4.4.1 NPP governor control system

The control system employs a modern mini-computer, which processes information such as measurements and plant statuses and applies control signals or actions to ensure that the governor is operating correctly. The frequency measurement of the NPP is fed back to the controller, and if a deviation occurs, then the speed of the generator is either increased or decreased. During a startup sequence, the controller can initiate actions to close the generator AC circuit breaker once the system voltage and frequency of the NPP are at the target values.

6.4.4.2 Extraction control valve

The extraction control valve can control the feed of steam to meet the power plant's own requirements. The pressure of the steam can also be regulated via feedback signals (extraction pressure signal) to control multiple steam mains, to supply a wide variety of heat exchangers if required. Steam can be released from various stages of the turbine and can be sent to boiler feed-water heaters to improve the overall cycle efficiency. Extraction control valves are very similar to inlet control valves and control the flow of steam to the downstream stages of the turbine [103].

6.4.4.3 Steam control valve

This valve is used to regulate the pressure at which steam enters the turbine; the pressure can either be increased or decreased according to the targeted flow rate of the overall system.

6.4.4.4 Main steam valve

The main steam valve provides the main isolation and control functions of the overall steam flow system. The valve can be automatically or manually shut in case of an emergency that requires the complete shutdown of the turbine system.

6.4.4.5 System integrity protection scheme

A System Integrity Protection Scheme (SIPS) can offer a unified management of system disturbances within the AC grid.

SIPS can monitor and send system information from both local and remote areas to a central processing location where it can initiate actions and counteract the propagation of the system disturbance. With the advancement of communication, measurement and computer devices, equipment can increasingly be used at a local level to improve the response of the power system.

The SIPS is used to send information to the DC station control via the RCI, highlighting events that have occurred within the AC grid. If frequency control is required from the HVDC link, then a signal is sent to the DC station control to initiate this and switch the frequency control scheme into circuit.

6.4.4.6 Startup sequence for successful NPP operation

As discussed previously, the startup sequence for successful NPP operation needs to be coordinated and controlled. Based upon this technical challenge and the work carried out in [103], the following startup sequence has been developed for the design presented in Figure 156:

1. The governor is started in speed (frequency) control and accelerated until the required speed is achieved. No generator excitation occurs at this time.
2. When the generator has reached the rated speed, excitation occurs and the generator AC circuit breaker is closed to energise the system up to the AC interface busbar.
3. The DC station control closes the sending end converter AC circuit breakers and de-blocks the valves.
4. The converter is in DC voltage control and the voltage is ramped up to the target value.
5. Once the DC voltage has reached the required value, the remote end valves are de-blocked and the AC circuit breakers are closed to connect the DC link to the AC grid.
6. An active power ramp is started, and the converter switches from power control to frequency control mode. At the same time, the governor control mode is changed from speed control to power control mode.
7. Power is then provided to the AC grid from the NPP in a coordinated and controlled manner.

The above solution would have to be proven and tested to demonstrate the effectiveness of this suggested startup strategy. For this, a Real Time Digital Simulator (RTDS) and corresponding system protection and control panels would be required due to the complexity of the control signals involved.

6.5 Chapter 6 summary and conclusions

Design solutions incorporating three different technologies for connecting an NPP to an AC grid have been presented. Detailed protection and control systems have been designed which in practice will ensure the prompt removal of internal faults within the affected zones.

From the work carried out, the following findings have been made:

- *For both CSC- and VSC-HVDC technology converter stations, a high number of individual system components are required.*
- *Two 2150 MW bipoles will provide the necessary connection capacity for a maximum 4500 MW rated NPP.*
- *The design of an HVDC control must be robust enough to handle contingencies within the AC grid and NPP. In particular, thermal ratings of circuits must be considered and in-depth studies are needed to determine the speed of response and necessary control actions to ensure system stability is maintained.*
- *A high-level controller within the HVDC control system must be robust and capable of maintaining the frequency within the NPP.*

From the above findings, the following recommendations are made:

- *A higher level of redundancy is to be incorporated into the design to provide greater operational flexibility and enable system contingencies to be handled without the need to intertrip generation.*
- *If HVDC links are used, then the largest circuit ratings available should be adopted to provide a robust design option.*
- *AC overhead line circuits are recommended to provide backup to the HVDC links in case of trip.*

Apart from the technical challenges of an HVDC NPP connection, an economic analysis is required to ascertain the cost, converter station size and technology ratings required for a successful project. Such an analysis is carried out in chapter 7.

Chapter 7: Economic Analysis of NPP HVDC Connections

In this chapter, an economic analysis of connecting an NPP to the National Electricity Transmission System (NETS) is carried out: a cost analysis of both AC and DC technology is carried out by comparing different projects from the UK and around the world, using costs obtained from both completed and active projects; an investigation is undertaken to analyse the footprint size of both AC substations and HVDC converter stations.

Finally, a review is undertaken to establish the industry availability of both AC and DC technology. Voltage and power ratings from current commissioned projects are considered as well as recent technological developments at the current time of writing.

7.1 Costs of AC technology for NPP connections

AC overhead line technology has been applied extensively for NPP projects around the UK. Both 400 kV and 275 kV have now been adopted as the standard transmission voltages of the NETS. The cost of a 400 kV AC overhead line project can vary and is dependent on aspects such as voltage, power rating, number of pylons required, type of overhead line conductor employed, and the number of circuits needed to deliver the power ratings [2].

AC connections have been traditionally used for connecting NPPs to electricity transmission systems around the world. For future planned NPPs in the UK exceeding 3 GW or more in power rating, large capacity power circuits are required for connection into the NETS [2].

National Grid has undertaken significant studies to date on both existing and newly planned NPPs in terms of costs. Examples of these include the newly planned 3400 MW Hinkley Point C nuclear power station in Somerset (south-west England) [2] and the 3400 MW Sizewell C station in south-east England respectively [184]. In the next section, the estimated costs of AC connections for both of these future NPPs are reviewed.

7.1.1 AC technology cost review of Hinkley Point C NPP

As part of the original strategic optioneering process for the connection of the new Hinkley Point C NPP to the NETS, a survey of different onshore routes for AC overhead line connections was undertaken by National Grid.

Two preferred connection options, A and B, were considered and taken forward during the cost review. These are discussed in the following sections below.

7.1.1.1 Hinkley Point AC connection option A

The location of the proposed NPP, together with the existing and planned electricity infrastructure for option A is shown in Figure 175.

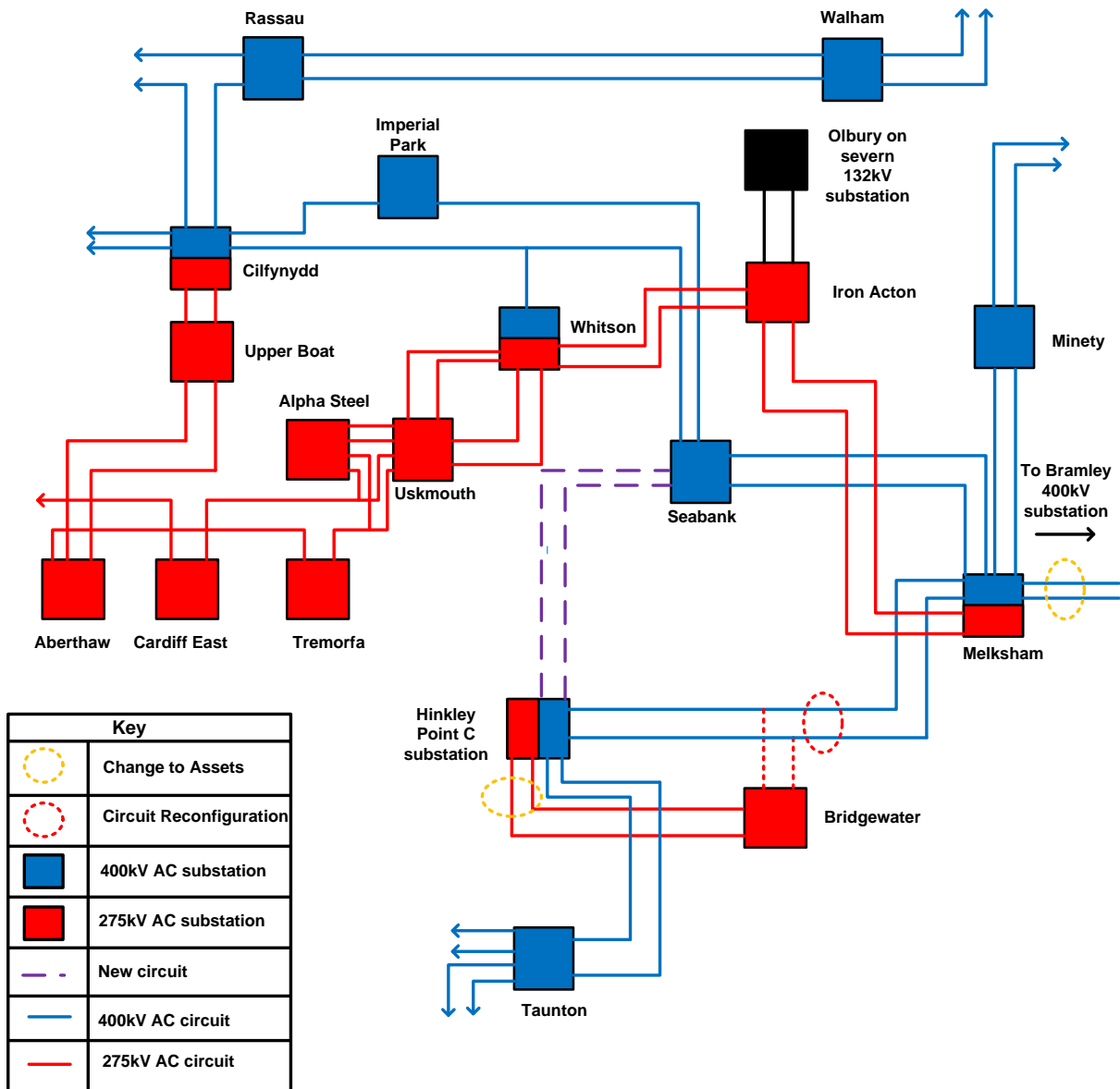


Figure 157: Hinkley Point C NPP AC technology connection option A

A new 400 kV AC overhead line has been considered as part of the required connection package for option A [2]. The route plans to provide a new 400 kV AC overhead line connection to the 400 kV Seabank substation. At first, the connection option and route appears straightforward, however, due to the large 3400 MW capacity of the NPP, additional upgrades are required to the existing AC network.

The additional AC system upgrades required include the following [2]:

- A new 14-bay GIS (Gas Insulated Switchgear) substation at Oldbury on Severn.
- A 4-switch mesh 400 kV GIS substation at Aust.
- An 18-bay 400 kV substation at Hinkley Point.
- An extension to Seabank 400 kV GIS substation of five additional bays.
- Rearranging of line entries at Melksham 400 kV substation.
- Construction of new sections and reconductoring of existing overhead line connections between Oldbury on Severn and Melksham.
- Reconductoring of the Melksham to Bramley overhead line.
- Hotwiring of sections of Seabank to Melksham circuit.
- A two-SGT (Super Grid Transformer) bay 400 kV-teed substation at Bridgewater.
- Construction of Hinkley Point to Seabank AC overhead line.
- Reconductoring of Seabank to Aust AC overhead line.

The total cost of this particular option is approximately £656m.

7.1.1.2 Hinkley Point C connection option B

Connection option B sees the re-routing of the AC overhead line from Hinkley Point to the existing substation located at Melksham shown in Figure 158. Most of the additional works required to facilitate such a connection are very similar to that of option A. The following list of AC system upgrades is required for option B [2]:

- A new 14-bay GIS substation at Oldbury on Severn.
- A 4-switch mesh 400 kV GIS substation at Aust.
- An 18-bay 400 kV substation at Hinkley Point.
- An extension to Seabank 400 kV GIS substation of five additional bays.
- Installation of two 400 kV quadrature boosters at Fawley.
- Rearranging of line entries at Melksham 400 kV substation.
- Construction of new sections and reconductoring of existing overhead line connections between Oldbury on Severn and Melksham.
- Reconductoring of the Melksham to Bramley overhead line.
- Hotwiring of sections of Aust / Seabank to Oldbury on Severn to Melksham overhead line.

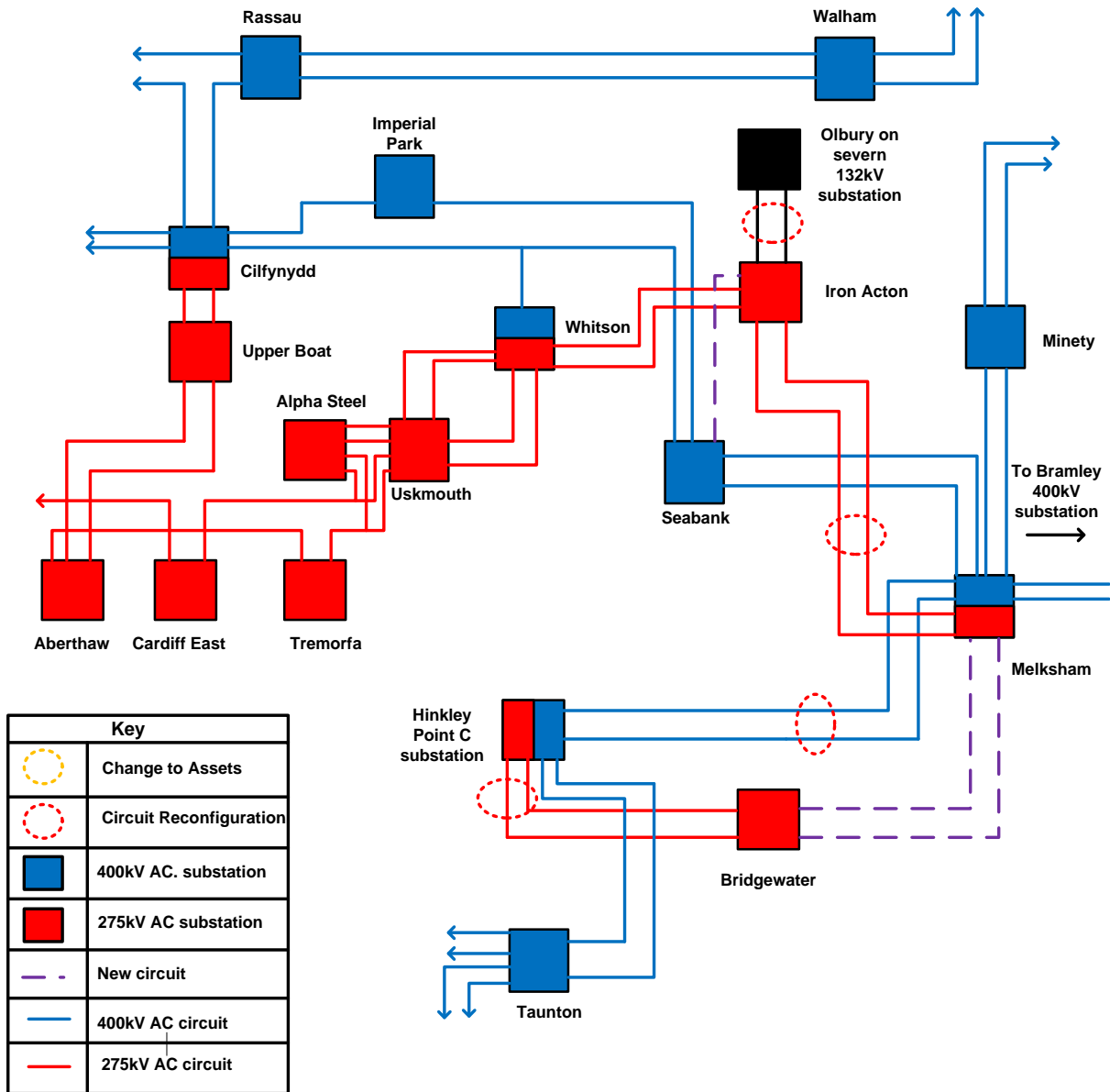


Figure 158: Hinkley Point C NPP AC technology connection option B

Additional infrastructure is required within the existing River Severn crossing area, these include [2]:

- Cross the River Severn west of the M48 river crossing.
- Construct a new 400 kV overhead line between Hinkley Point and Whitson.
- Build a new 400 kV substation at Whitson.
- Replace the existing 400 kV River Severn crossing.

The total cost of this option is approximately £698m.

The main cost difference between the two options is due to the change in route, which includes a longer distance compared to that of option A.

7.1.2 AC technology cost review of Sizewell C NPP

Similar to Hinkley Point C, a brand new NPP, 3400 MW in rating, is planned to be constructed next to the existing Sizewell B station near Suffolk [185]. A new 400 kV AC overhead line will be required as part of the connection options package, similar to that in the Hinkley Point C case. Additional infrastructure is required within the existing network to be able to transport the full output of such a station into the rest of the main transmission system.

As part of the original strategic optioneering process for the connection of Sizewell C NPP into the NETS, a similar survey of different onshore routes for AC overhead line connections was undertaken by National Grid. Two connection options A and B were selected as the preferred options to be taken forward during the cost review [185]. These are discussed in the following sections.

7.1.2.1 Sizewell C connection option A

An additional upgrade of the existing AC transmission system is required to accommodate the extra capacity of Sizewell C NPP. The proposal for option A is shown in Figure 159.

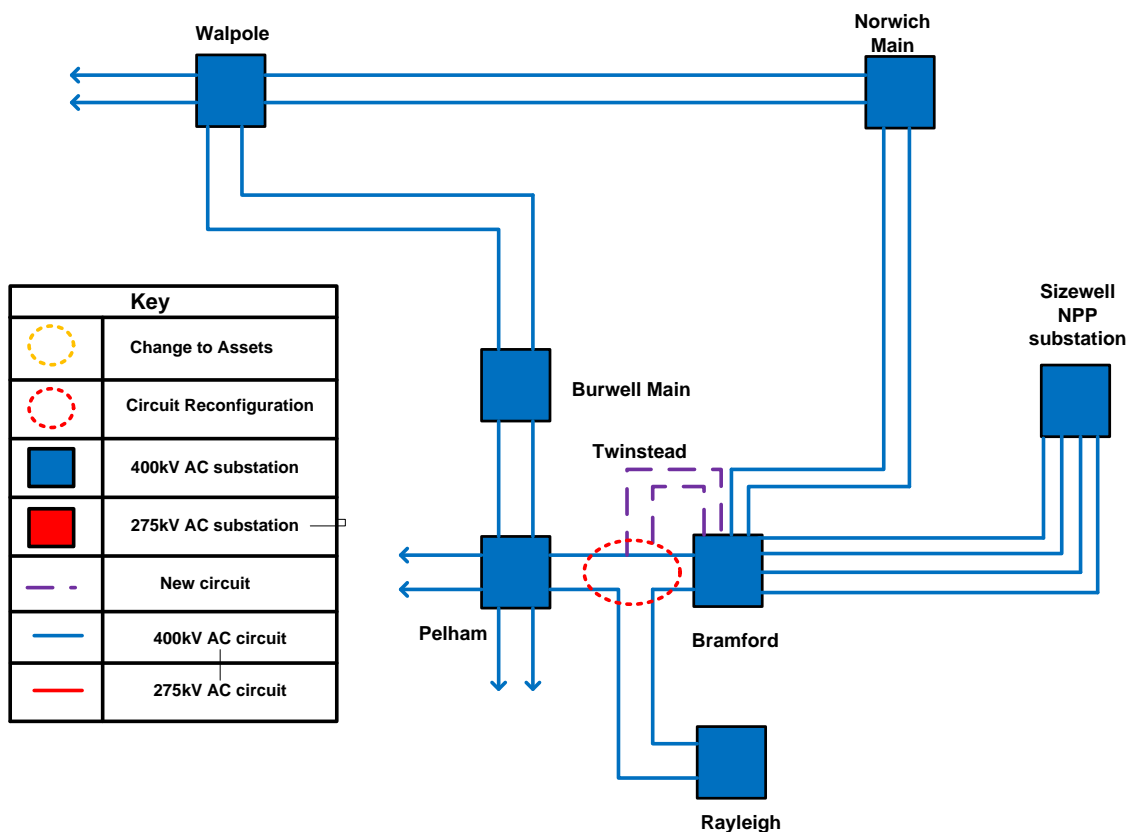


Figure 159: Connection option A for Sizewell C NPP

A list of the required reinforcements for connection option A includes the following [185]:

- A new 20-bay 400 kV GIS substation at Sizewell.
- Two 400 kV 3000 MVA reactors at Sizewell.
- A new 16-bay 400 kV GIS substation at Bramford.
- Modifications at the 400 kV Twinstead tee circuit arrangement.
- Modifications at Tilbury substation.
- 28 km of 400 kV OHL from Bramford to Twinstead substation.
- Reconductoring works.

The total cost for option A is estimated to be £530m.

7.1.2.2 Sizewell C connection option B

For connection option B, a new 400 kV AC substation at Twinstead is required as part of the system upgrades [185]. The required upgrades are shown in Figure 160.

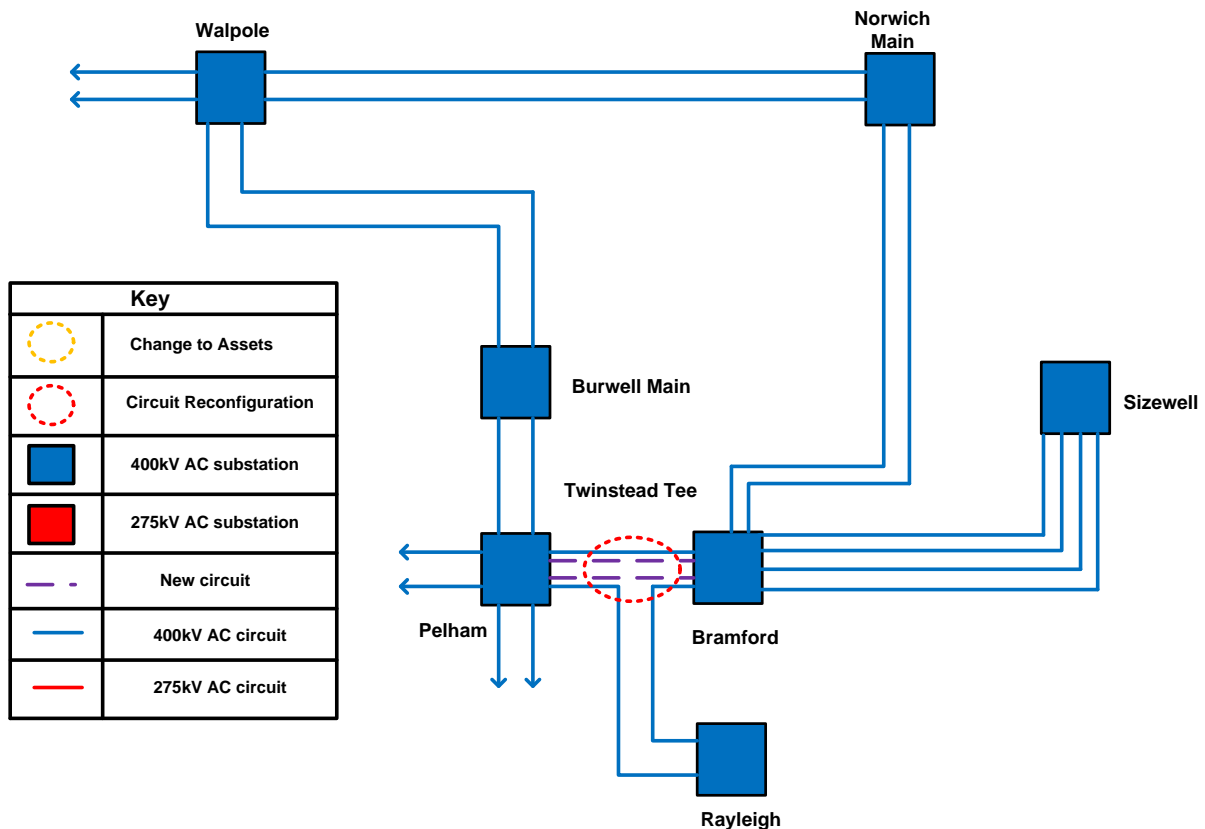


Figure 160: Connection option B for Sizewell C NPP

A list of the required reinforcements for connection option B includes the following:

- A new 20-bay 400 kV GIS substation at Sizewell.

- Two 400 kV 3000 MVA reactors at Sizewell.
- A new 16-bay 400 kV GIS substation at Bramford.
- Modifications at Twinstead tee.
- 28 km of 400 kV OHL from Bramford to Twinstead.
- Reconductoring works.
- Two-SGT Air Insulated Switchgear (AIS) substations between the Twinstead Tee.
- Possible Distribution Network Operator (DNO) requirement for additional 132 kV connections.

The estimated cost for this option is approximately £565m. However, additional costs for DNO and compensation are envisaged. A summary of the four different connection options and connection costs are shown in Figure 161.

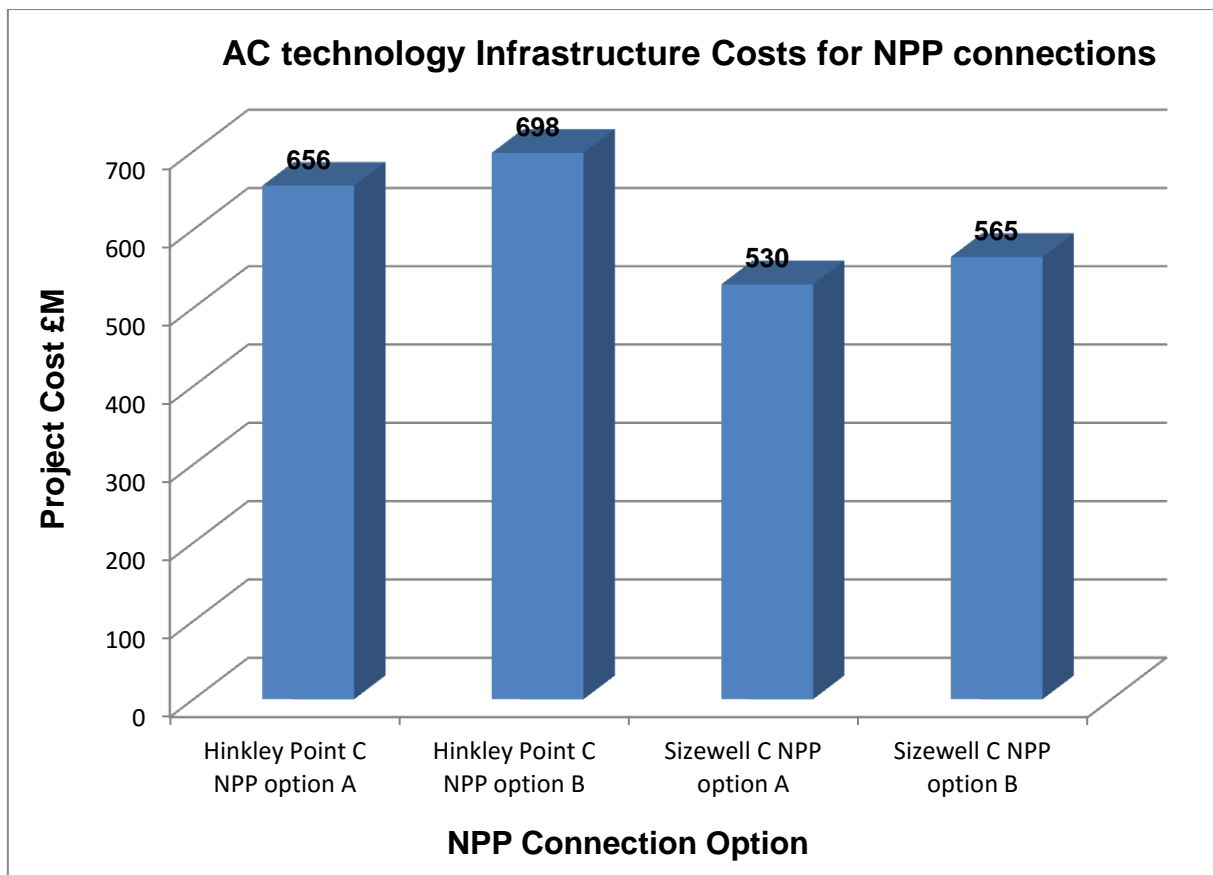


Figure 161: Graph showing the total AC cost versus connection option

In the above graph, the total cost of connection options A and B for Hinkley Point C NPP is significantly higher compared to those of Sizewell. The cost difference is down to the amount of additional infrastructure required to connect the NPP [185].

Hinkley Point C connection option A requires the construction of new AC substations, three in total. Option B requires four new AC substations as well as an extension of the existing Seabank 400 kV GIS substation; this is a large amount of additional infrastructure and adds an incremental amount of cost to this particular connection option.

With two 400 kV AC double circuit overhead lines already constructed, a lot less infrastructure is required for the new Sizewell C NPP. The costs are much lower compared to that of the Hinkley Point C connection options [185] .

Based on the data analysed, a cost range of £400m–£700m is required to provide the connection capacity of the NPPs. Each NPP project will vary in cost depending on the system upgrades required to enable satisfactory connection to the NETS.

7.2 Costs of CSC-HVDC technology for NPP connections

Numerous CSC-HVDC projects have been installed and commissioned around the world. The costs associated with this type of technology can vary and will also depend on factors such as the functional and technical performance requirements from a power system perspective [186], [187]. The following section compares the costs of different CSC-HVDC projects that have been commissioned around the world.

7.2.1 Cost of CSC-HVDC technology

Costs associated with conventional CSC-HVDC links can vary, depending on many different factors associated with the project concerned.

The voltage and power rating of the link can have a large impact on the total costs of the project, especially in terms of the size and number of AC filters required [187]. For example, a 1000 MW link will require approximately 50–60% reactive compensation (approximately 600 Mvar) [41]. A link of 2000 MW rating would require 1200 Mvar, which is double the previous value, and the number of individual components such as resistors and capacitors which make up the filters also increases [41]. The interconnection between converter stations can also have a large impact on the total cost. If an overhead line cost is considered instead of subsea or underground cables, then this can provide a significantly cheaper option. Due to the primary insulation medium of overhead lines being air, the conductors can be smaller, whereas DC cables require more layers, to meet the insulation requirements. Stress control, mechanical protection, size of copper/aluminium conductor may also increase and invoke higher costs [19].

A list of commissioned CSC-HVDC from around the world is displayed in Table 22.

Table 22: Table showing commissioned CSC-HVDC projects around the world

Name	Capacity/Technology	Cost and Distance	Year
North-east Agra multi-terminal project, India	8000 MW CSC overhead line bipole configuration, 3-terminal ± 800 kV DC	Estimated cost \$900m (£636m); 1728 km	First terminal commissioned 2015
Rio Madeira, Brazil	6300 MW CSC overhead line bipole configuration ± 600 kV DC	Estimated cost \$540m (£381m); 2375 km	Commissioned 2013
BritNed (Tennet and National Grid) - interconnector between England and the Netherlands	1000 MW CSC cable bipolar configuration	Estimated cost £600m; 245 km (project cost includes onshore reinforcement works)	Commissioned 2011
Cometa interconnector from Morvedre (Spain) to Santa Ponsa (Majorca)	400 MW CSC cable bipole configuration ± 250 kV DC	Estimated cost 375m Euros (£312m); 247 km	Commissioned 2011
Xiangjiaba–Shanghai HVDC project, China	6400 MW CSC overhead line bipolar configuration	Estimated cost \$440m (£310m); 1980 km	Commissioned 2010
Norned HVDC cable project interconnector between Norway and the Netherlands	700 MW CSC cable ± 450 kV symmetrical monopole configuration	Estimated cost 600m Euros (£500m); 580 km	Commissioned 2008
Neptune RTS interconnector, New Jersey to Long Island	660 MW CSC cable 500 kV monopole configuration	Estimated cost \$600m (£365m); 105 km	Commissioned 2007
Basslink project interconnector between Victoria (Australia) and George Town (Northern Tasmania)	500 MW CSC cable/OHL monopole configuration 400 kV DC voltage level.	Estimated cost \$800m (£436m); 370 km	Commissioned 2005

From the above analysis, the north-east Agra project in north-east India is the most expensive project. The DC voltage (± 800 kV) and power rating (8000 MW) also make this the largest rated project, but the Britned HVDC link between the UK and Netherlands is only £36m less. This project consists of subsea cable compared to that of the overhead line of the north-east Agra project, which highlights the cost that DC cables can add to a project [187].

Another example is the cost comparison between the Xiangjiaba–Shanghai HVDC project (£310m) in China and the Cometa interconnector from Morvedre to Santa Ponsa (£312m) in Spain. Despite the Xiangjiaba–Shanghai project being over nine times the power rating (6400 MW), the difference in cost is just £2m.

Again the cost of the cable contributes significantly to the HVDC project costs. A graph showing the range of costs for each project in Table 22 is shown in Figure 162.

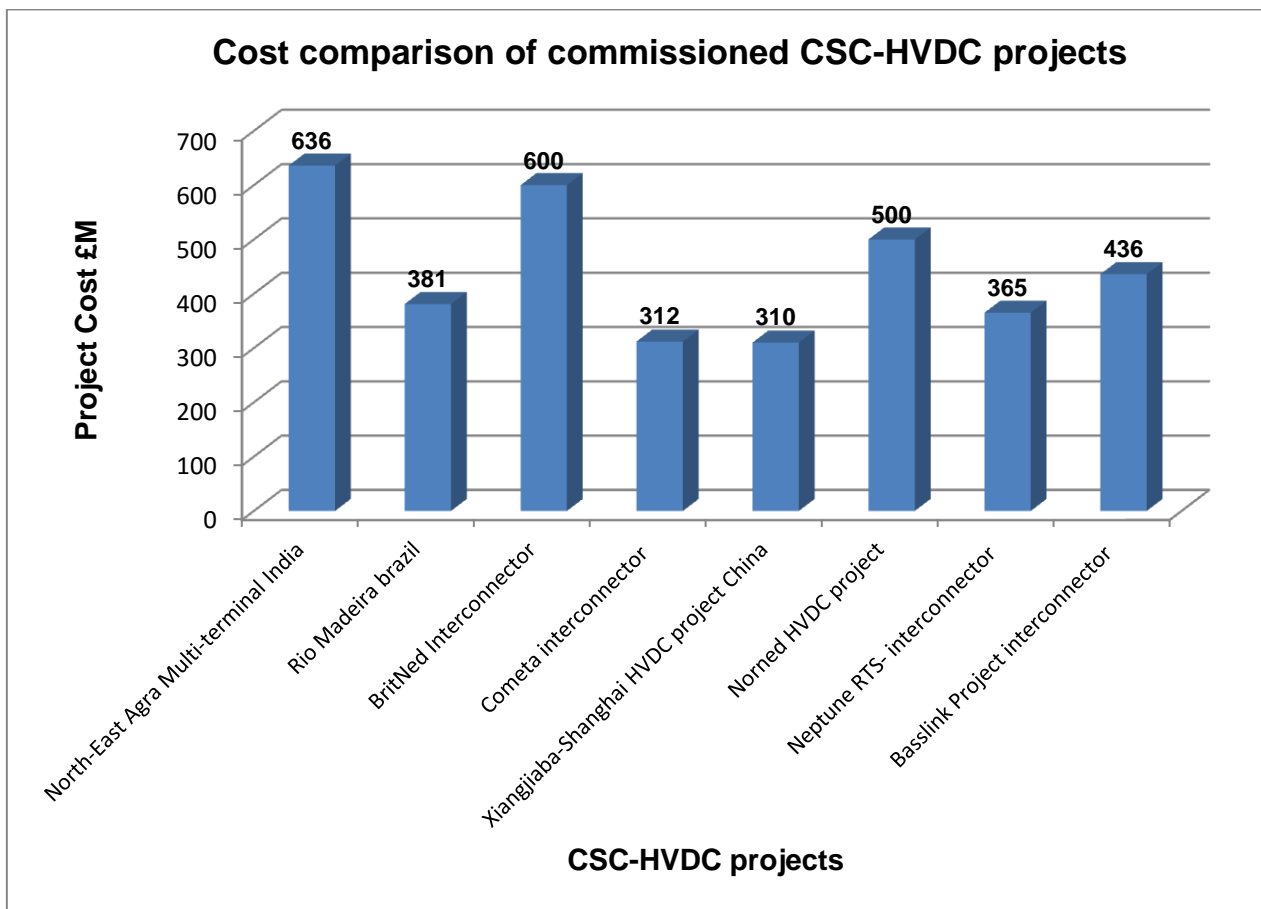


Figure 162: Graph showing number of commissioned CSC-HVDC projects

From the above analysis, as the voltage and power rating of the technology increases the cost might not escalate as one might expect; the DC cable is the most expensive component and will affect the overall cost of an HVDC project. From the above analysis it can be concluded that the costs of different CSC-HVDC projects can vary, and are not just dependent on the power and voltage ratings [187].

7.3 Costs of VSC-HVDC technology for NPP connections

The demand for VSC-HVDC technology is steadily increasing on a year-by-year basis. More VSC-HVDC projects are being installed and commissioned than ever before. The costs of the technology can be similar to CSC-HVDC technology and as discovered previously, are also dependent on the length of DC cables used [187].

In Table 23, VSC-HVDC projects commissioned from around the world are presented.

Table 23: VSC-HVDC projects commissioned around the world

Name	Capacity/Technology	Cost and distance	Year
Nordbalt HVDC interconnector between Sweden and Lithuania	700 MW VSC subsea cable symmetrical monopole configuration ± 300 kV	Estimated cost (£410m); 400 km	Commissioned 2016
Inelfe project HVDC link between Santa Llogaia (Spain) and Baixas (France)	2 x 1000 MW VSC cable symmetrical monopole 2 x ± 320 kV	Estimated cost 700m Euros (£577m); 65 km	Commissioned 2015
Skagerrak 4 HVDC project	700 MW VSC cable asymmetric bipolar ± 500 kV DC	Estimated cost 300m Euros (£248m) or more; 247 km	Commissioned 2015
Eirgrid (EWIC) East-to-West Interconnector between Republic of Ireland and north Wales	500 MW VSC cable ± 250 kV symmetrical monopole	Estimated cost 600m Euros (£495m); 245 km (costs include onshore upgrades)	Commissioned 2013
Caprivi link project, South Africa	300 MW VSC overhead line asymmetrical monopole	Estimated cost (£300m); 950 km	Commissioned 2010
Transbay project HVDC link between San Francisco and Pittsburgh (California)	400 MW VSC cable symmetrical monopole ± 200 kV DC	Estimated cost \$450m; (£274m) 245 km	Commissioned 2011
Estlink VSC project HVDC link between Finland and Estonia	350 MW VSC cable monopole ± 150 kV DC	Estimated cost (£100m); 105 km	Commissioned 2006
Cross Sound HVDC cable project	330 MW VSC cable bipolar configuration ± 150 kV	Estimated cost \$120m (£85m); 40 km	Commissioned 2002

The Inelfe HVDC project involves two separate 1000 MW symmetrical monopole VSC-HVDC links, is the most expensive project in the above table and consists of DC cables [188].

The Caprivi VSC-HVDC link is the world's first VSC-HVDC project to use DC overhead line [189]. At a cost of £300m, this is only slightly more expensive than the Transbay project at £274m, which used DC cables. It is increasingly apparent how much cost DC cables can add to a VSC-HVDC project.

The recent Nordbalt HVDC project is the longest installed VSC subsea cable transmission in the world and at a rating of 700 MW is much higher than the 500 MW rated EWIC interconnector [190]. With a DC voltage rating of ± 300 kV, the Nordbalt project is higher than EWIC but despite this, the EWIC interconnector is still higher in cost than the Nordbalt project. One important factor to notice is the requirement for system upgrades to the onshore networks. From the data in Table 23, it is clear that this can add additional cost to the project [190].

A summary of the costs from Table 22 is displayed in Figure 163.

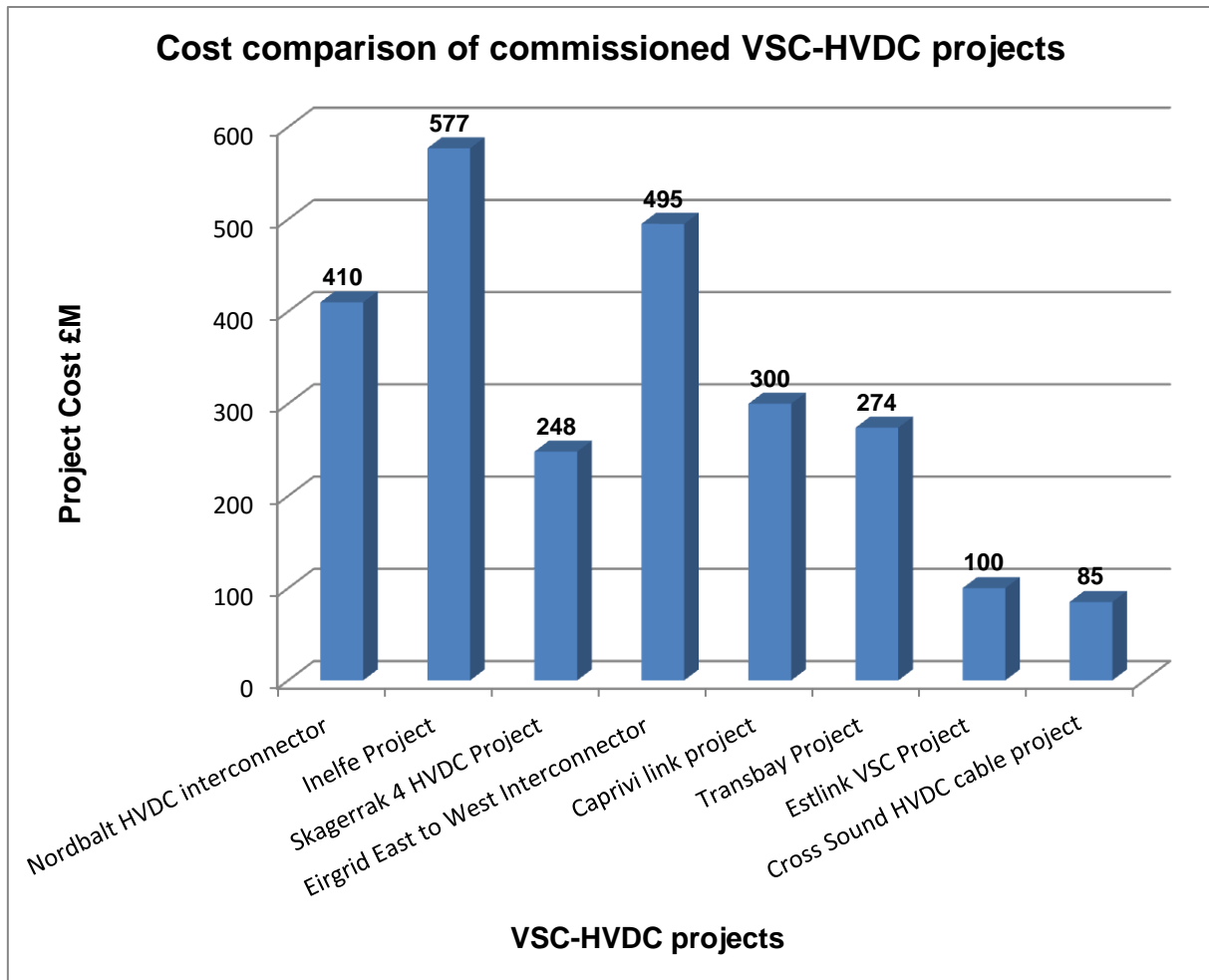


Figure 163: Graph showing the total of commissioned VSC-HVDC projects

The trend shows a gradual increase in project cost as the technology ratings increase. As the technology improves, the requirement for greater distances also increases. The demand for long-distance subsea cabling is growing, and this will add further costs to VSC-HVDC projects over the next decade or so [187]. In order to gain an appreciation of the cost difference between AC and DC technology, a cost comparison for projects where all three options have been considered is required. In the next section such a comparison is carried out for the new Hinkley Point C and Cumbrian NPPs.

7.3.1 Cost comparison between AC and HVDC technology

In this section cost comparisons between both AC and DC technologies for NPP connection projects in the UK are made. AC technologies include overhead line, cables and Gas Insulated Line (GIL). Only VSC-HVDC is considered, due to this being the preferred connection option compared to CSC-HVDC converters due to the superior technical benefits it offers [5].

7.3.1.1 Hinkley Point C NPP technology costs

In Table 24, circuit routes for the connection of Hinkley Point C NPP to the NETS have been gathered from the 2014 National Grid connection options report in [1].

Table 24: Table showing connection options and circuit routes for Hinkley Point C NPP

Connection option	Description
1	30 km offline overhead line rebuild between Iron Acton and Melksham, 6 km of new overhead line between Seabank and Tockington, construction of subsea cables between Hinkley Point and Aberthaw in South Wales (30 km) using AC subsea cables (6380 MW) or 2 x 2 GW VSC-HVDC converters plus AC system upgrades.
2	Upgrading of the existing 275 kV Hinkley Point to Bridgwater circuit to operate at 400 kV, construction of a new transmission connection between Bridgwater and Melksham (80 km), 30 km offline overhead line rebuild between Iron Acton and Melksham, 80 km of subsea circuits between Hinkley and Aberthaw using AC subsea cables (6380 MW) or 2 x 2 GW VSC-HVDC converters plus AC system upgrades.
3	Upgrading of the existing 275 kV Hinkley Point to Bridgwater overhead line to operate at 400 kV, construction of a new transmission connection between Bridgwater and Nursling (110 km) near Southampton, 30 km AC overhead line rebuild between Iron Acton and Melksham, 80 km of subsea circuits between Bridgwater and Nursling, AC subsea cables (6380 MW) or 2 x 2 GW VSC-HVDC converters plus AC system upgrades.
4	Upgrading of the existing Hinkley Point to Bridgwater circuit to operate at 400 kV, construction of a new transmission connection between Bridgwater and Seabank (57 km) in Avonmouth, 57 km of subsea circuits between Hinkley and Aberthaw, using AC subsea cables (6380 MW) or 2 x 2 GW VSC-HVDC converters plus AC system upgrades.
5	Construction of subsea cables between Hinkley Point and Seabank along the Severn Estuary, a distance of approximately 50 km using either AC subsea cables or HVDC subsea cables.

As part of the optioneering, different technologies were considered for providing the required capacity for connection into the NETS.

For each of the options shown in Table 24, two independent VSC-HVDC links, 2000 MW each in rating, provide a total of 4000 MW connection capacity. All VSC-HVDC options utilise subsea cable connections requiring a total of four cables to achieve the 4000 MW connection capacity [1]. As an alternative subsea option, AC subsea cables providing a connection capacity of 6380 MW are also considered.

Each option involves different AC system upgrade works which are not detailed here, but are detailed in [1]. For each connection option, four different technologies were considered: AC overhead line; AC cables; AC GIL; and VSC-HVDC technology. The cost of each technology connection option is shown in Figure 164.

From the costs in Figure 164, AC overhead line technology is the cheapest option. Both AC cable and GIL technology are very similar in price due to the similarities between the conductors except for the Sulpha-hexafluoride (SF6) insulating medium associated with GIL [116].

Connection option number three results in the highest overall cost. For the subsea section, VSC-HVDC technology is significantly cheaper than AC cables where two circuits, each 3190 MVA rating are required. Due to the connection distance of 80 km, shunt compensation is needed for each circuit and will add additional cost to the connection option [1]. The number of AC system upgrades required is higher than any other option and adds further cost.

Option two is the second most expensive option and requires similar AC upgrades to that of option three.

Options one and five consider subsea connection only, as no major AC upgrades are considered (except those listed in Table 24). For option five, due to the shorter length of the subsea cables, the costs are lower [1].

For four out of the five options, VSC-HVDC technology is cheaper than AC cables for the subsea connections. For a connection distance of 50–70 km, shunt compensation is needed to offset the charging current for the AC cables. With DC cables, no such compensation is needed and so DC technology becomes more viable as the cable distance increases [58].

Next, the same analysis is carried out for a newly planned 3600 MW NPP in Cumbria, north-west England [1].

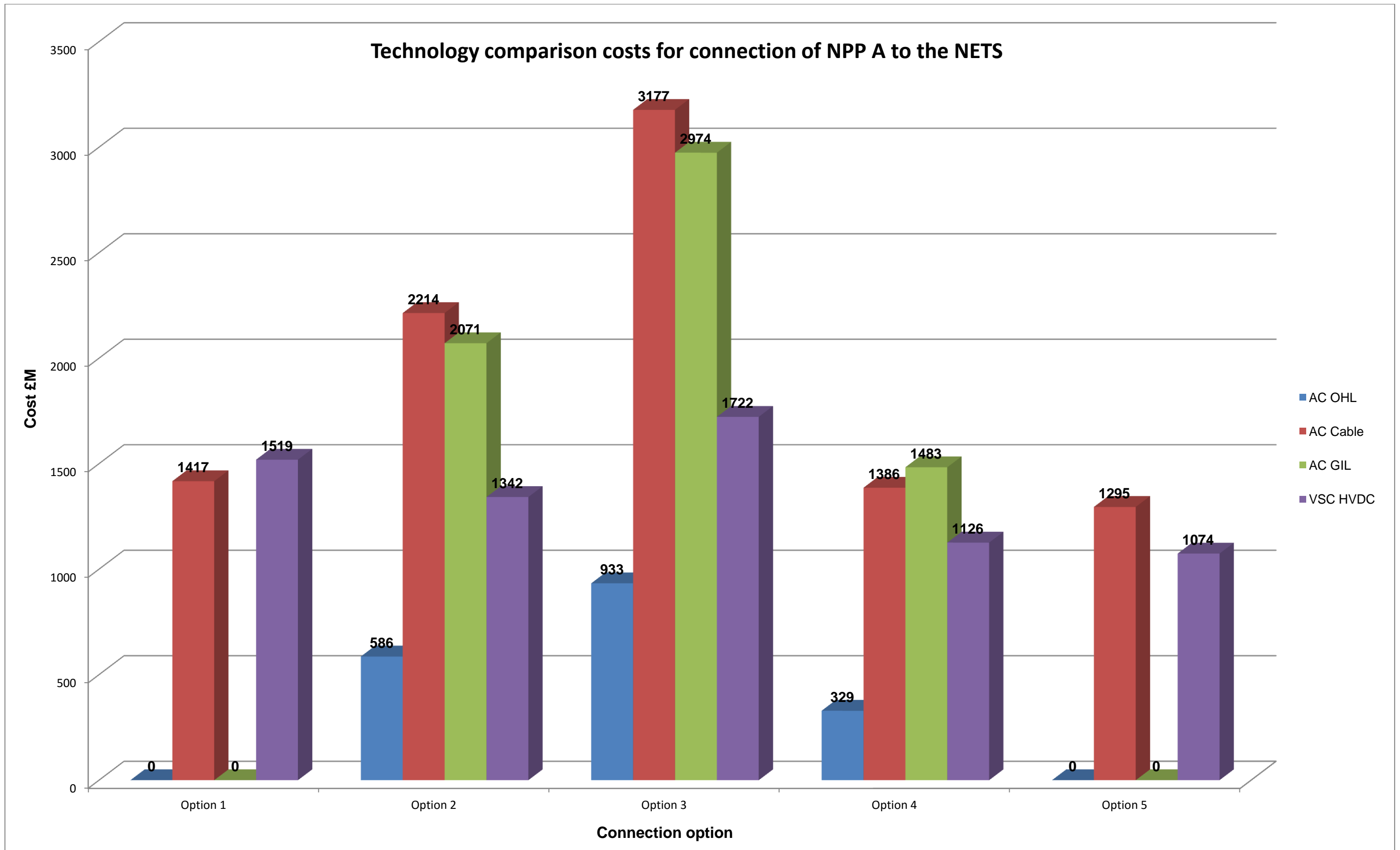


Figure 164: Graph comparing different technology costs for Hinkley Point C connection options

7.3.1.2 Cumbrian NPP technology costs

A 3600 MW NPP is currently under planning for construction on the west coast of Cumbria ready for operation post year 2022 [1]. The nearest connection into the NETS is over 80 km away and new circuits are required to meet the power capacity and to provide the necessary security of supply [1]. In Table 25, circuit routes for the connection of the new NPP in Cumbria have been gathered from a 2014 National Grid connection options report [1].

Table 25: Table showing connection options and circuit routes for Cumbrian NPP

Connection Option	Description
1	Two 75 km onshore double circuits south from NPP
2	Two 75 km offshore circuits south from NPP
3(a)	One onshore double circuit north (70 km) and one onshore double circuit south (75 km) with different AC system upgrades
3(b)	One onshore double circuit north (70 km) and one onshore double circuit south (75 km) with different AC. system upgrades
4(a)	One onshore double circuit north (70 km) and one offshore double circuit south (75 km) with different AC system upgrades
4(b)	One onshore double circuit north (70 km) and one offshore double circuit south (75 km) with different AC system upgrades
5(a)	Two 70 km onshore double circuits north and one additional onshore double circuit south (105 km) as part of AC system upgrade
5(b)	Two 70 km onshore double circuits north and one additional onshore double circuit south (105 km) as part of different AC system upgrades
6(a)	Two 70 km onshore double circuits north and existing 275 kV double circuit south (80 km) upgraded to 400 kV as part of AC system works
6(b)	Two 70 km onshore double circuits north and existing 275 kV double circuit south (80 km) upgraded to 400 kV as part of different AC system works

In the above table, a combination of both onshore and offshore subsea circuits are considered for connection into the NETS. For the offshore element, both VSC-HVDC technology and AC subsea cables are considered. For the onshore routes, the same four technologies considered previously for Hinkley Point C NPP are reviewed. The costs for each connection option are shown in Figure 165.

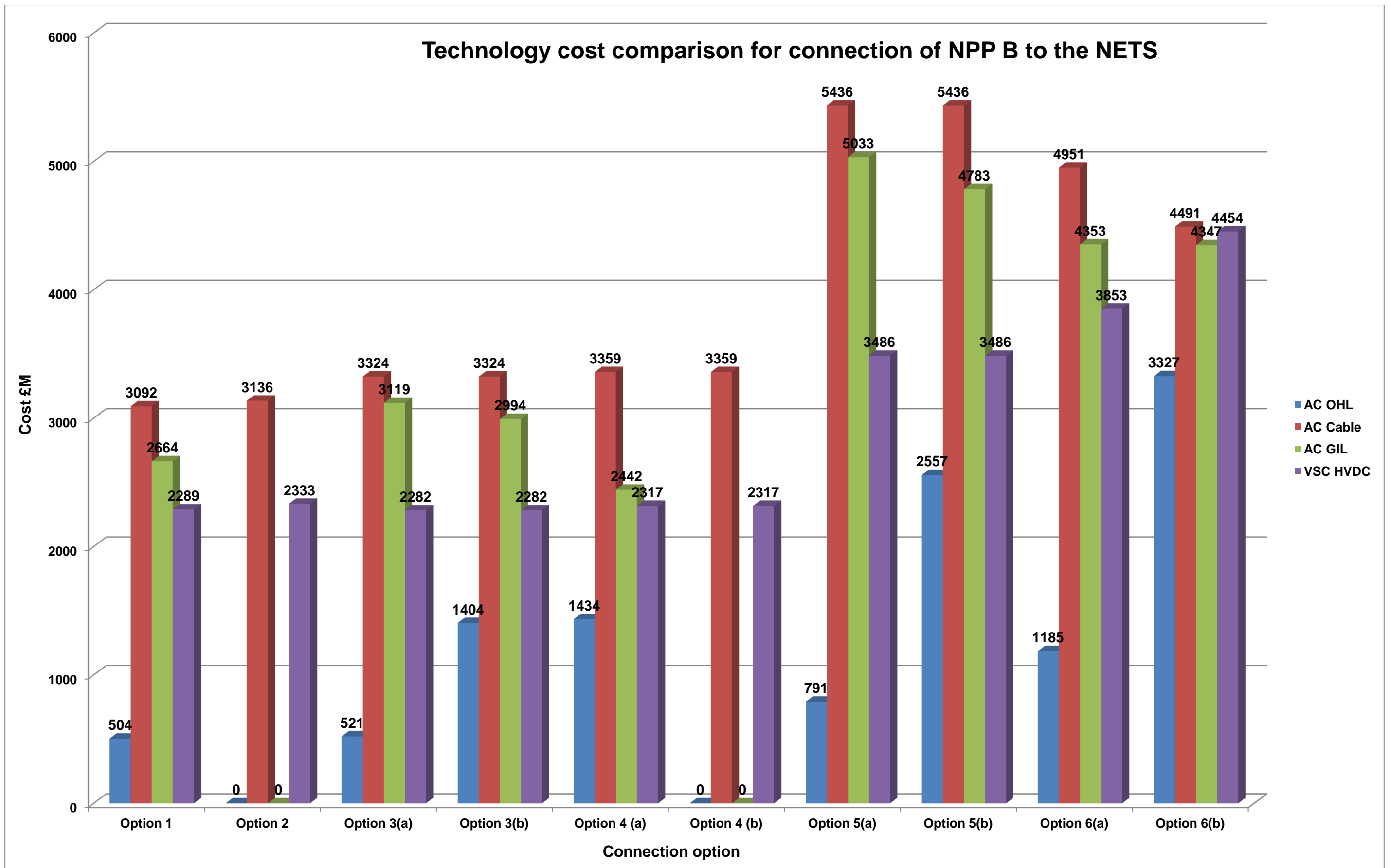


Figure 165: Graph comparing different technology costs for Hinkley Point C connection options

From the data displayed in Figure 165, AC overhead line technology is the cheapest option. AC cables are the most expensive option due to the long distances involved and ratings required (3190 MVA), resulting in six conductors per circuit. With a cable tunnel also considered for the offshore AC cable routes, the cost increases further [1].

The GIL is only slightly cheaper than the AC cable options and would require three tubes (conductors) per circuit. This option results in fewer circuits, but due to the SF6 gas insulation and tubing, the cost is still high [1].

Options 5(a) and 5(b) are the most expensive options. This is due to the large AC grid reinforcements, which include a new onshore double circuit, 105 km in length.

For VSC-HVDC technology, the costs are much greater than that of the Hinkley Point C NPP project [2]. The same circuit ratings are required (2 x 2000 MW), but due to the longer distance, more cable is required, which results in higher amounts of copper conductor. The VSC-HVDC converter stations are large in size when a power rating of 2000 MW and voltage level of ± 500 kV per bipole is considered [161].

In summary, some interesting results for the different technologies considered for NPP connections have been presented. AC overhead lines are by far the cheapest option, while both AC cables and GIL are similar and can prove to be expensive [1]. With costs for VSC-HVDC technology being cheaper than the AC overhead line and GIL this, in combination with AC overhead line circuits, could prove to be cost-effective for an NPP connection. By adopting a hybrid design, AC overhead line circuits provide the cheapest onshore route and VSC-HVDC subsea cables provide the most economical offshore route [1].

7.4 AC technology footprint for NPP connections

When considering a particular technology for an NPP connection, the area of land required is an important project parameter. Gaining land consent to build an AC substation or HVDC converter station can be a timely and costly process [91]. Knowing the exact footprint of an AC substation or HVDC converter station is pivotal to assessing how much land is required for a successful project. In the following section, different sizes of AC substations and HVDC converter stations are assessed from projects commissioned around the world.

7.4.1 AC technology footprint for Hinkley NPP connection

AC substations have dominated the power industry for decades and have formed the backbone of society. The size of an AC substation is dependent on many aspects, power and voltage ratings to name a few [103]. A new 400 kV AC substation is required for the new Hinkley Point C NPP in Somerset, west England [2]. The size of the AC substation is relatively large; an example of a similar footprint is shown in Figure 166.

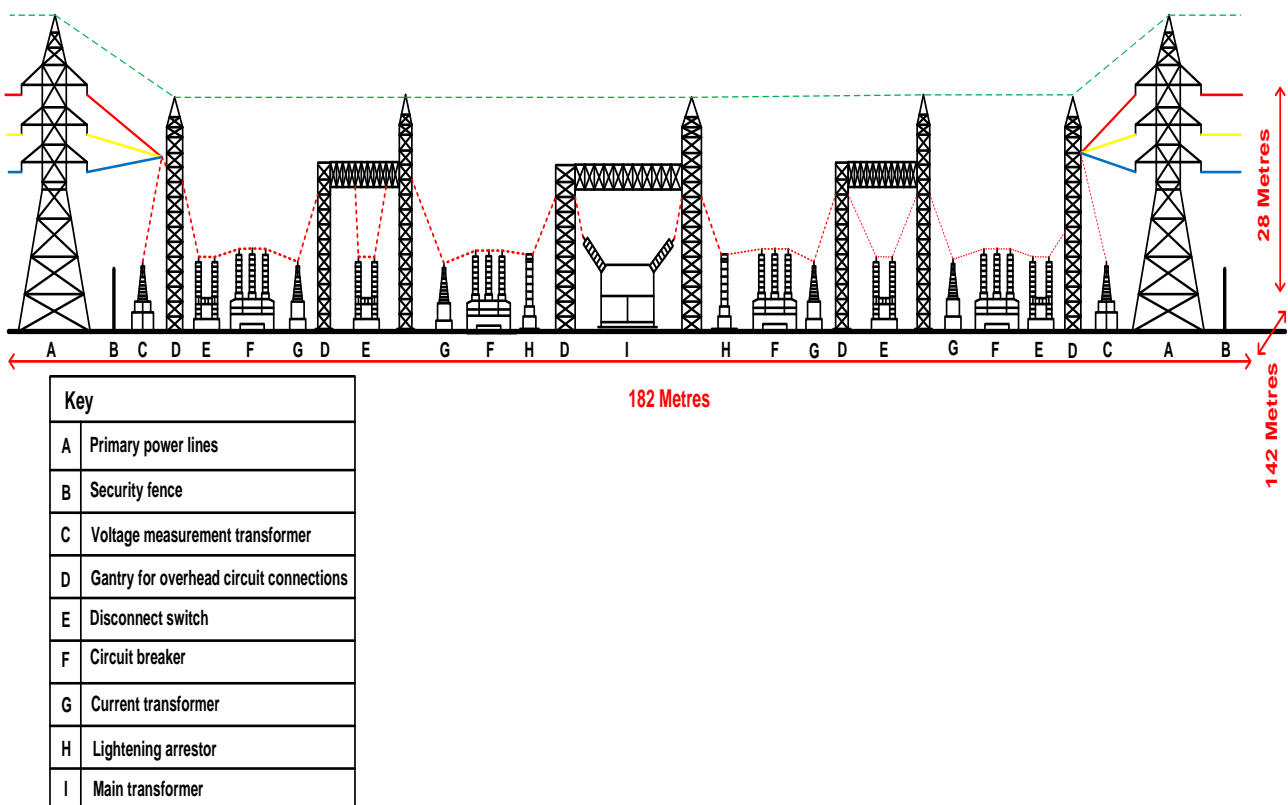


Figure 166: AC substation footprint for NPP connection

Within an AC substation the terminal towers enable the overhead lines to be terminated either into or out of the AC substation. The overhead lines will often be diverted onto a gantry, where they will enter the AC switchyard. The busbars, circuit breakers, disconnectors, power transformers, earth switches and current/voltage transformers make up the majority of the switchyard.

A control room will usually contain the SCADA for the substation, as well as possible offices and mess facilities for staff. Additional rooms could provide provisions for safety and interlocking keys used for isolation and earthing purposes.

A separate AC substation to house all the relevant switchgear and control systems for such connections is normally included but is not shown. The AC substation will be surrounded by a 3.5 m high electrified pulse palisade security fencing [1]. The substation will normally be unmanned and will be controlled remotely from the National Grid Electricity National Control Centre (ENCC). When plant maintenance is required, personnel will be on the site to carry out the necessary duties for the duration of the works.

Underground cables are used to connect the auxiliary unit transformers from the power station to the National Grid GIS substation. Future interconnections via additional AC overhead lines will be required to modify the existing connections to allow adequate power transfer capability and flexibility into the NETS.

7.4.2 AC technology footprint for NPP connection in Cumbria

For the previously mentioned large NPP connection project in Cumbria, new AC substations are required to provide a connection into the NETS; these are likely to be a GIS design due to their coastal locations and will be similar in size to the Hinkley Point C NPP [1].

A 400 kV GIS substation can range from 11–15 m in height, and provides a significant saving on space, with visual and cost benefits compared to the 28 m high AIS shown in Figure 166. A GIS has a gas detection system; the gas inside each compartment is pressure-controlled to have a gas density of 3 kg/cm² [191]. If the pressure drops slightly, the gas is trapped automatically. With new gas leaks, a low pressure alarm is triggered.

The main advantage of GIS over AIS is that its phase-to-phase spacing is significantly smaller. This is more effective in an urban environment where land and size is at a premium. GIS substations are suitable for installation in almost every part of the world, e.g. indoor, outdoor overground or underground [191].

An example of a 400 kV GIS substation design for a 3600 MW NPP connection in Cumbria is shown in Figure 167.

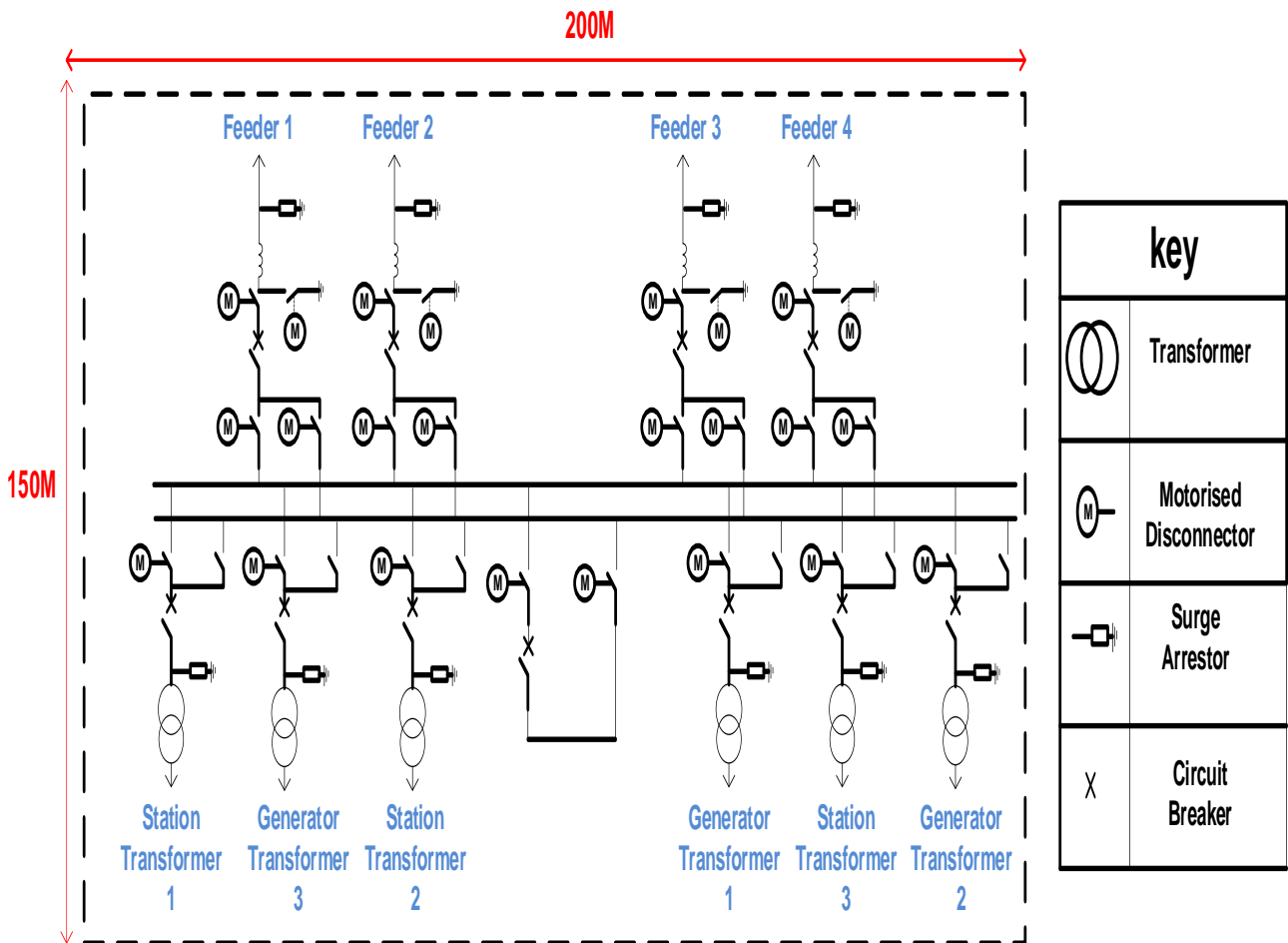


Figure 167: Example of the size of a 400 kV GIS substation for an NPP connection

In GIS substations, all high voltage conductors are enclosed securely in a grounded metal enclosure. Due to the chemical composition of SF₆ gas, it envelops the conductors and insulation and preserves them, enabling long-term trouble-free operation. All these factors lead to an estimated operational life for GIS of 40–50 years, as compared to an asset life of 25–30 years for AIS substations [191].

For most NPPs, due to their coastal locations, GIS designs are likely to be adopted. This offers significant savings on space and reduces the maintenance requirements of the switchgear. If an NPP AC substation needs extending in the future, then an AIS design would provide a more flexible option since the access to the existing busbars and switchgear is easy and does not require de-pressurising, compared to a GIS substation.

7.5 CSC-HVDC technology footprint for NPP connections

HVDC thyristor valve converter stations can vary in both size and height. Aspects such as power and voltage rating, reactive compensation, and harmonic filtering can have a large influence on the overall final design. An example layout of a CSC-HVDC converter station is shown in Figure 168.

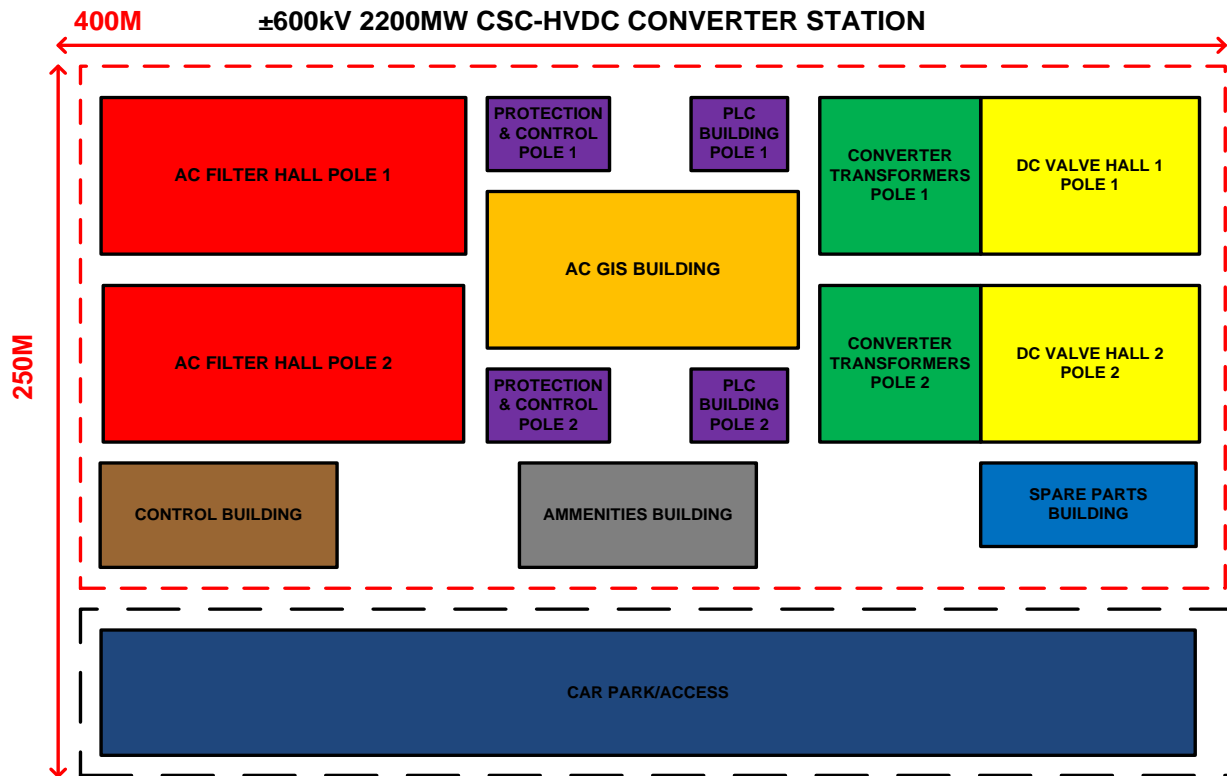


Figure 168: Layout and footprint of a CSC-HVDC converter station for NPP connections

The dimensions are consistent with that of the HVDC converter station in Hunterston, north Scotland, which forms one end of the Western HVDC link project. Hunterston converter station has a DC voltage level of $\pm 600\text{ kV}$ and power rating of 2250 MW [192].

The AC switchyard shown in Figure 168 is the largest part of the converter station, although this can vary from project to project. The GIS solution could help to reduce the size of the footprint and offer sufficient protection against salt and pollution encountered within coastal areas [192].

The shunt capacitors provide the 60% reactive power demand of the CSC-HVDC converter station and the harmonic filters help to mitigate voltage distortion and reduce telephone interference in the connected AC network. The larger the rating of the HVDC link, the more filters that are required [41].

The height and size of the valve hall also depends on the voltage and power rating of the link. In Figure 168 above the valve hall is 30 m in height. The height can vary and depends upon the required power and DC voltage ratings, as well as the space available.

The HVDC converter transformers range in both size and rating, where sometimes single-winding transformers are preferred to three-winding transformers due to transportation and ease of access factors. The DC switchyard can also vary in size and may need additional DC filters if overhead lines are present to help reduce telephone interference with subscriber wires [41].

In Table 26, a list of HVDC projects with details of their dimensions and footprint size is presented. For this section, only the CSC-HVDC projects are considered.

The Western HVDC link project between Scotland and north Wales has a power rating of 2250 MW at a DC voltage level of ± 600 kV. In contrast, the converter station located in Longquan China is rated at 3000 MW with a lower DC voltage level of ± 500 kV [193]. The converter station footprint is a third larger in area compared with Hunterston, and has a 1000 MW higher power rating. Extra space is required for the additional AC filters required to meet the reactive power demand of the converter station. The valve hall in the Longquan project is 3 m smaller than the Western HVDC link project (30 m) due to the lower voltage level. Extra valve modules are needed to obtain the desired voltage level. Hunterston converter station utilises GIS to house both the AC and DC equipment indoors, which decreases the footprint compared to that of the Longquan AIS design.

The Norned HVDC project is, at the time of writing, the longest subsea DC cable installed anywhere in the world [194]. When the converter station is compared to the Grita HVDC project, the voltage and power levels are very similar. The Norned project uses symmetrical monopole converters whereas the Grita project consists of asymmetrical configurations. The larger voltage rating of the Norned project requires extra valve modules, and the height of the converter station increases and is 5 m or more greater than the Grita valve halls. The Norned HVDC project utilises an indoor GIS design for all the switchgear and cables, which helps to save on space in comparison to the Grita HVDC project – where most of the AC connections are AIS – the footprint can be reduced by half.

From the above comparisons, a GIS AC substation design helps to decrease the footprint of a CSC-HVDC converter station by housing the equipment indoors. A higher voltage level requires extra valve modules and the height of the valve hall will increase. In the next section, the footprint of VSC-HVDC converter stations is reviewed.

7.6 VSC-HVDC technology footprint for NPP connections

VSC-HVDC converter stations do not require reactive compensation, compared to CSC-HVDC converter stations. The Nemo HVDC interconnector will connect the UK and Belgian grids. In comparison to the Caithness-Moray-Spittal (CMS) project, the difference in converter station size is minor. The voltage level of the Nemo project is higher but the active power rating of CMS is greater, which results in a higher valve hall for the Nemo project compared to that of the CMS HVDC link.

A bipolar solution is being used for the CMS project, which includes more valves and equipment than the symmetrical monopole configuration of Nemo. A bipolar configuration would normally result in a much larger footprint compared to that of a symmetrical monopolar option. However, because CMS is using a full GIS AC solution, the space requirement is minimal. With Nemo utilising a combination of outdoor and indoor switchgear, the overall footprints are similar.

The East-to-West HVDC interconnector (EWIC) between Ireland and Wales has a very similar footprint to that of the Cross Sound cable project. The higher voltage and power rating of the EWIC HVDC interconnector results in a much higher valve hall than that of the Cross Sound cable project. Because the Cross Sound cable project is located in a built-up area, the design has been made compact, with all HVDC switchgear being located indoors and only minor AC equipment outdoors. This helps to keep the footprint down and enables the converter station to blend in with the surrounding buildings.

For the Inelfe VSC-HVDC project, two identical ± 320 kV 1000 MW, symmetrical monopoles are being used together. The height of the valve halls lies within the 25–30 m range and other dimensions are similar to those of the Nemo project. The overall footprint is larger than the Nemo project, but the addition of a symmetrical monopole only results in a 50% increase in converter station length. This highlights the flexibility of VSC-HVDC converters to be able to be extended vertically, increasing the station height, or horizontally, producing a longer length. The width is almost double that of the Nemo project, but with two symmetrical monopoles side by side, this can be expected. By keeping the modules in VSC-HVDC converter stations at ground level, and employing flexibility to extend these either horizontally or vertically, savings on space can be made.

Table 26: Table of HVDC projects showing converter station footprint

Project	Location	DC voltage/power rating	Configuration	HVDC site footprint (length x width) in metres	Maximum building height in metres	Technology type
Grita HVDC project	Galatina (Italy)–Arachthos (Greece)	400 kV/500 MW	Asymmetrical monopole	225x220	20	CSC
Longquan HVDC project	China	±500 kV/3000 MW	bipole	600x360	27	CSC
Western HVDC Link	Scotland–Wales (Hunterston converter station details)	±600 kV/2250 MW	Bipole	410x210	30	CSC
Norned HVDC project	Norway–Holland	±450 kV/700 MW	Symmetrical monopole	200x100	25–30	CSC
Visakhapatnam back-to-back HVDC project	India	205 kV/500 MW	Back-to-back	90x80	11	CSC
EWIC interconnector	Ireland–Wales	±200 kV/500 MW	Symmetrical monopole	180x115	24	VSC
Nemo interconnector	UK–Belgium	±400 kV/1000 MW	Symmetrical monopole	149x93	30	VSC
CMS HVDC link project	Caithness-Moray-Spittall (North Scotland)	±320 kV/1200 MW	bipolar	151x51	17	VSC
Cross Sound project	Hydro Quebec America	±150 kV/330 MW	bipolar	150x100	11	VSC
Inelfe VSC-HVDC project	France–Spain	±320 kV/1000 MW	2 x symmetrical monopole	225x170	25–30	VSC

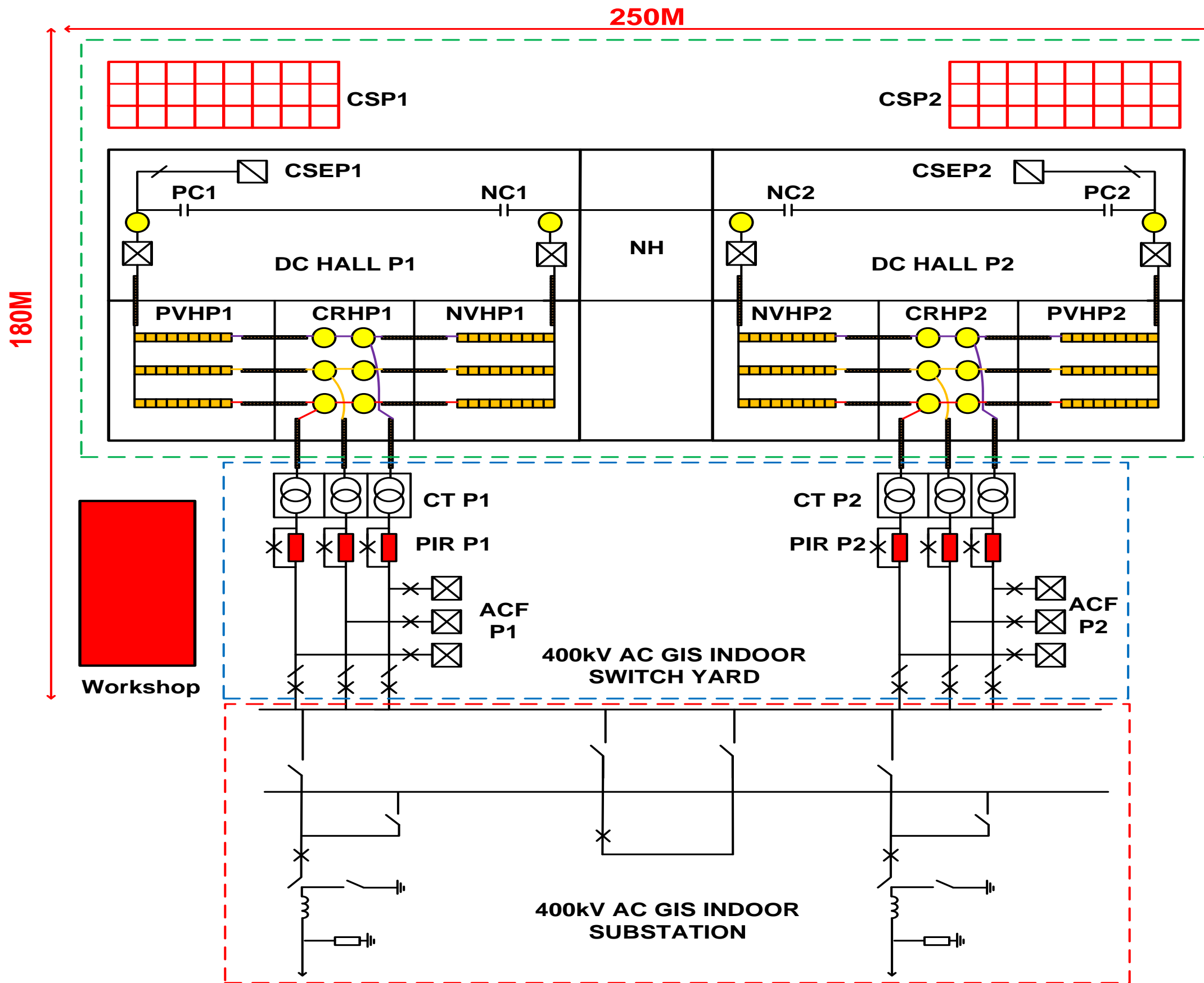
For the ± 600 kV, 2250 MW bipole VSC-HVDC converter station design in chapter 6, the footprint required can be optimised based on the learning from the previous analysis. A design for a single bipole converter station at the above ratings is shown in Figure 169.

A GIS design helps to keep the site compact, helping to reduce the overall footprint. Due to the voltage and power rating being identical to the Western HVDC link project, the maximum height of the valve hall is 30 m. The length of the converter station has been increased from that of the Inelfe project (225 m) to 250 m to allow for the extra IGBTs and valves for the increased 2250 MW power and DC current rating of 1881 A [90].

Due to the valves being extended outwards, the width of the converter station is assumed to be similar to that of the Inelfe project [188], with the GIS AC solution helping to keep the system more compact. Making an allowance for increased safety distances, a width of 180 m is assumed.

Two-bipole converter stations of the dimensions shown in Figure 169 are required for the designs presented in chapter 6. This yields an overall footprint of approximately 500 x 360 m. With the inclusion of car parking and welfare facilities, the overall site footprint increases further.

In summary, the analysis has shown the flexibility of VSC-HVDC module arrangement to achieve the required power and voltage ratings. If a GIS AC substation is incorporated into the design, then the overall footprint can be kept minimal. More valve modules are required to increase the DC voltage level, which results in a higher valve hall. Extra valves will increase the length or width of the building, depending on the design.



KEY	
CSP1	Cooling System Pole1
CSP2	Cooling System Pole 2
CSEP1	Cable Sealing End Pole 1
CSEP2	Cable Sealing End Pole 2
PC1	Pole Capacitor 1
NC1	Neutral Capacitor 1
PC2	Pole Capacitor 2
NC2	Neutral Capacitor 2
NH	Neutral Hall
PVHP1	Positive Valve Hall Pole 1
CRHP1	Converter Reactor Hall Pole 1
NVHP1	Neutral Valve Hall Pole 1
PVHP2	Cooling System Pole 2
CRHP2	Converter Reactor Hall Pole 2
NVHP2	Neutral Valve Hall Pole 2
CT P1	Converter Transformer Pole 1
PIR P1	Pre-Insertion Resistor Pole 1
ACF P1	AC Filter Pole 1
CT P2	Converter Transformer Pole 2
PIR P2	Pre-Insertion Resistor Pole 2
ACF P2	AC Filter Pole 2
	Reactor
	Bushing
	Valve Arm/Cells
	Filter
	Cable Sealing End
	Cooling System
	Isolator
	Circuit Breaker
	Surge Arrestor

Figure 169: Layout design and dimensions for a ±600 kV 2250 MW VSC-HVDC bipole converter station

7.6.1 Comparison of technology footprints for NPP connection

In order to connect the 4500 MW NPP in chapter 6, large capacity circuits are required. In Figure 170 a comparison of the footprints of both AC and DC technology options is presented.

The AC GIS substation in Figure 167 is selected for the AC comparison. The design utilises a voltage level of 400 kV and comprises of four 2200 MW circuits (two double circuit overhead lines). These are based on the same ratings used in [2].

Both the CSC- and VSC-HVDC converter stations are rated at 2250 MW per bipole at a DC voltage level of ± 600 kV. The footprint of the VSC-HVDC design matches that of the design presented in Figure 169. The CSC-HVDC converter station footprint is based on the Western HVDC link project dimensions shown in Figure 168. In Figure 170, the footprint of one bipole converter station for both VSC and CSC-HVDC technology is shown and based upon these sizes, a total of two bipoles are required for the 4500 MW NPP connection, and so the total footprint would be double.

The 400 kV AC GIS substation is much smaller than both HVDC converter stations, and from a space point of view it would be the optimal choice. The VSC-HVDC converter station is more compact than the CSC-HVDC configuration and is the preferred DC connection option.

In summary, after comparing the size and footprint of both AC and DC technology, the AC footprint can be much smaller if GIS is used. VSC-HVDC technology could be more favourable than CSC-HVDC at higher power and voltage ratings due to the reactive compensation requirements of CSC-HVDC in the form of filters. The location of a project can also determine the potential size of the substation or converter station that is required. For example, with most NPPs being based in coastal locations, GIS substations are now being adopted to mitigate the high level of pollution and salt contaminates within the air [102]; this can make a solution more compact and can help keep the cost of a project down. Some substation/converter stations now require additional facilities such as control rooms and additional monitoring facilities which can add to the overall space requirements on top of the primary and secondary systems.

Overall, the size of a particular solution can have a bearing on the outcome of a large project. The size will have an effect on layout, design and potential routing of circuits, which can in turn affect the layout of both the switchgear and switchyard and can change the dimensions considerably.

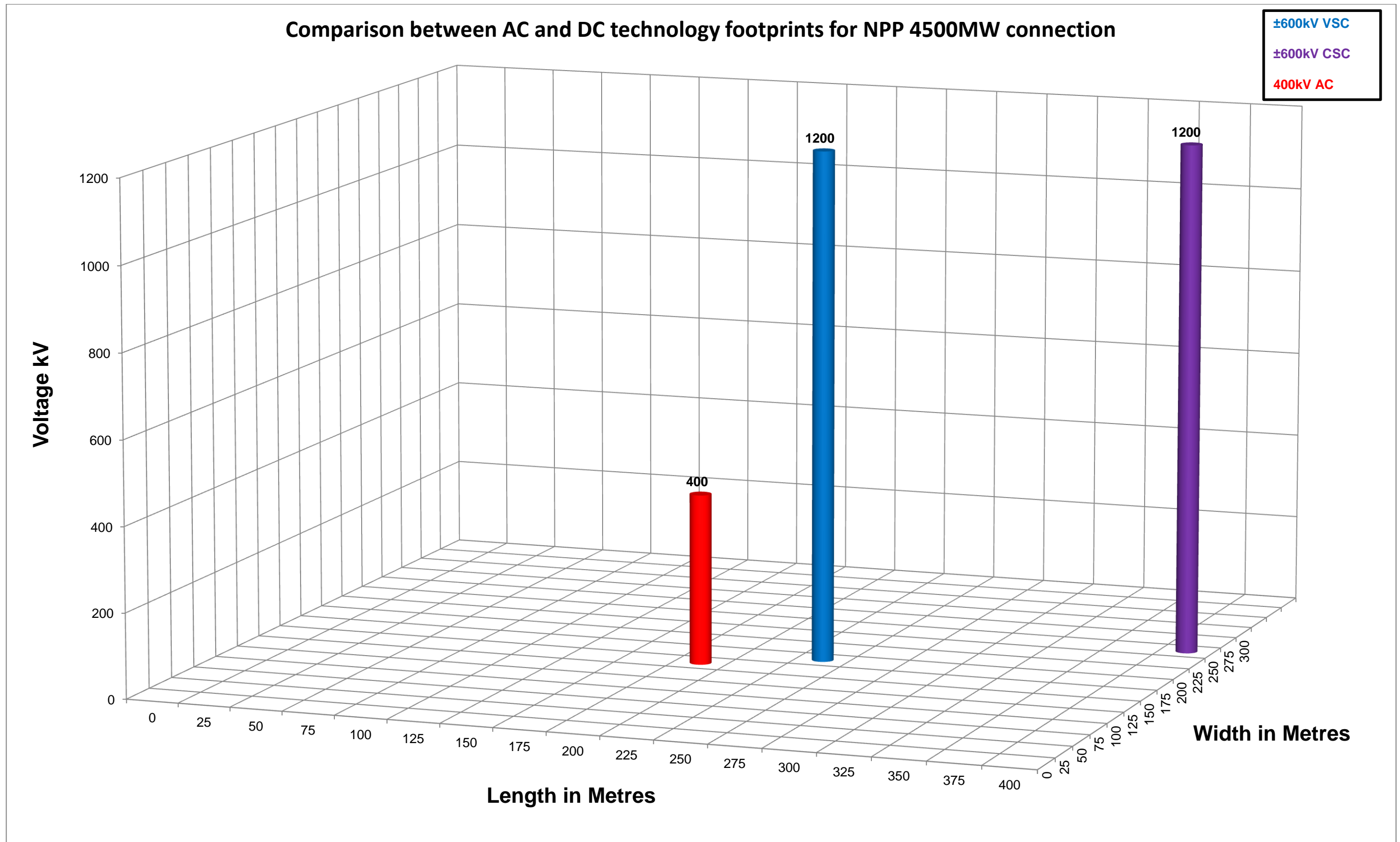


Figure 170: Graph comparing the dimensions between AC and DC technology for a 4500 MW NPP connection

7.7 Transmission technology development for NPP connections

The following section investigates the current development of both AC and DC technology within the supply industry for connecting NPPs to the NETS. Aspects such as power and voltage ratings are reviewed to ascertain the availability of different transmission technologies for NPP connections.

7.7.1 Development of AC technology for NPP connections

AC voltage transformation to very high voltages can be done through high-efficiency power transformers. When voltage is stepped up, the current is reduced which enables the use of smaller conductors and minimises losses. AC generators are much cheaper and simpler than DC for the same power range [102].

For long-distance bulk power transmission, DC is preferred but requires special conversion equipment at each end which can be more expensive. AC induction motors are cheaper, simpler in construction and easier to maintain than their DC equivalent.

AC overhead transmission line circuits have proven to be ideal for connecting power stations to a transmission system for a number of years. Most pylons are constructed at transmission voltage level and are made of steel lattice that can be used to carry large heavy conductors. Different types of pylons such as angle deviation towers can be used to change the direction of a particular route.

The size, voltage and power rating of a particular overhead line can vary and aspects such as distance, cost and consumer demand can all have some bearing on the type adopted. The level of power that can be carried by an AC overhead line will depend on a number of different factors, one of them being distance.

An example of power ratings versus distance is presented in Figure 171.

For distances over 200 km, power levels up to 1000 MW or more per circuit are available with a 400 kV AC overhead line. If the same line is used for a shorter distance, such as 80–100 km for example, then it may be possible to achieve ratings of 2000 MW. For higher voltage levels of 700 kV or more, power can be transferred over longer distances. By using 400 kV AC double circuit overhead lines in the UK for connecting new NPPs, spare capacity is incorporated into the design for future connections.

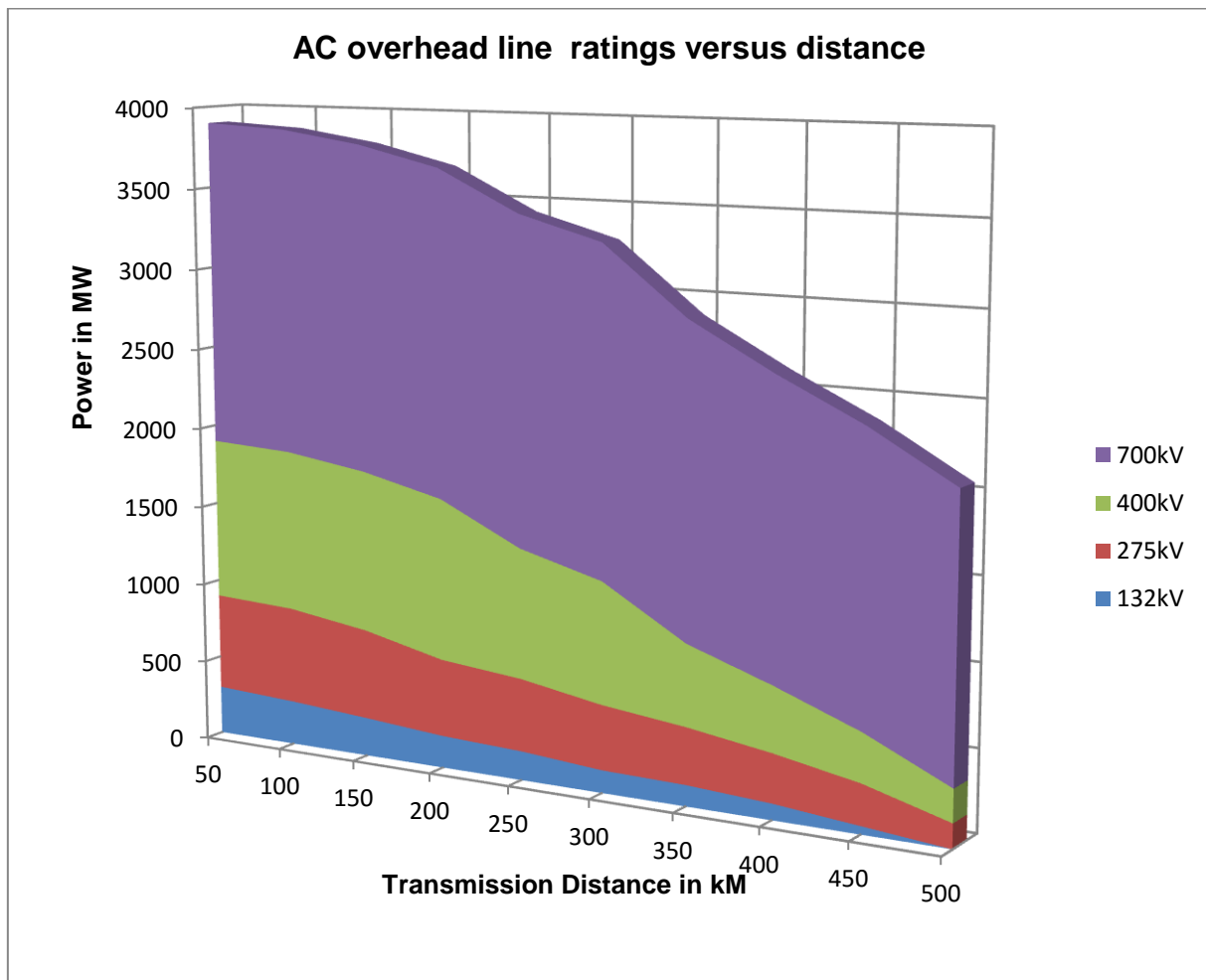


Figure 171: Overhead line power ratings versus distance

The power ratings for different AC technologies can vary forms an important consideration when assessing their suitability for NPP connections. For the new proposed NPP in Cumbria, a range of AC technologies is considered in order to meet the required connection capacity of 3400 MW. These included AC overhead lines, GIL and cable technology [1].

The maximum rating for each technology according to voltage level is shown in Table 27. Both single and double circuit ratings are provided for each technology. For 275 kV transmission voltage level, AC cable technology is limited to the low power range classification. With a maximum power rating of 1000 MVA, at least two 275 kV cables are required to meet the minimum 1595 MVA single circuit rating. For 275 kV overhead line and GIL technology, power levels for the medium and maximum power range are, at the time of writing, unavailable and are not considered [1].

Table 27: Power ratings of different AC technologies for connection of NPP in Cumbria

Power rating classification	Single circuit ratings by voltage		Double circuit ratings by voltage		Technology configuration					
	275 kV	400 kV	275 kV	400 kV	275 kV AC OHL	400 kV AC OHL	275 kV AC cable	400 kV AC cable	275 kV GIL	400 kV GIL
	Total rating for one circuit	Total rating for one circuit	Total rating for two circuits	Total rating for two circuits	No. of conductors on each arm (per circuit)		No. of cables per phase (per circuit)		No. of GIL tubes per phase (per circuit)	
Low	1595 MVA	1595 MVA	3190 MVA (2 x 1595 MVA)	3190 MVA (2 x 1595 MVA)	Two (six)	Two (six)	Four (twelve) (2 x 1000 MVA cables required to meet 1595 MVA single circuit capacity)	One (three)	One (three)	One (three)
Medium	N/A	3190 MVA	N/A	6930 MVA (2 x 3190 MVA)	N/A	Two (six)	N/A	Two (six)	N/A	One (three)
High	N/A	3465 MVA	N/A	6930 MVA (2 x 3465 MVA)	N/A	Three (Nine)	N/A	Three (nine)	N/A	Two (Six standard GIL tubes)

To achieve the required 3400 MW connection capacity with 400 kV AC cables, at least three single-core cables per phase are required for each circuit. A total of nine cables for a single circuit are needed, giving a total requirement of 18 cables for a 400 kV double circuit connection. The situation is very similar for 400 kV GIL technology [1]. The maximum single circuit ratings are shown in Figure 172.

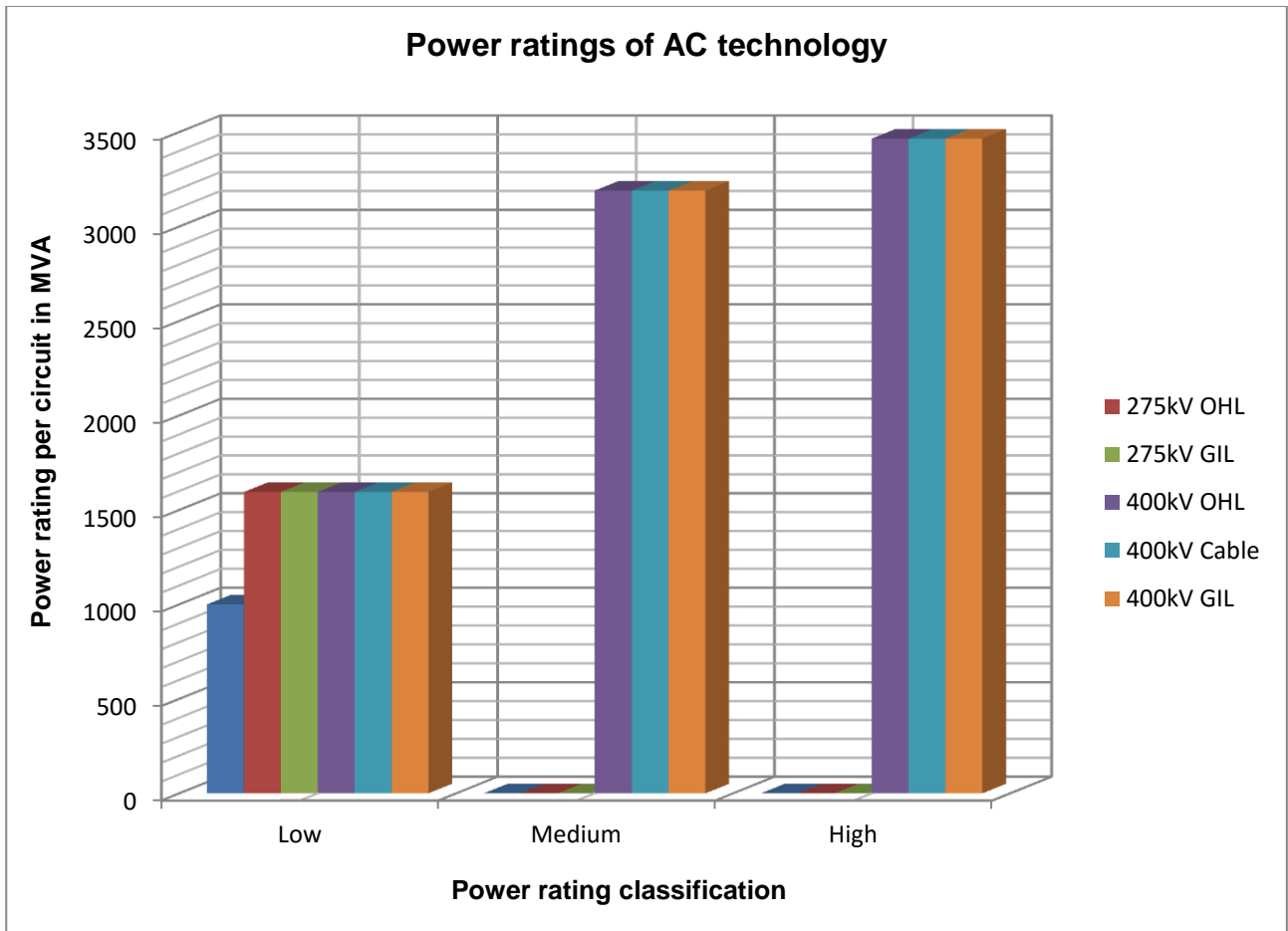


Figure 172: Single circuit power ratings of different AC technologies for NPP connection

From the above graph, 400 kV technology is the preferred option for connecting the NPP in Cumbria to the NETS. A voltage level of 275 kV is considered to be uneconomical due to the limitations in power ratings. AC overhead line technology offers the greatest connection capacity with fewer components required.

Two 400 kV double circuit overhead lines can provide a maximum connection capacity of 6390 MVA. If one double circuit tower is unavailable, then the full output of the 3400 MW NPP can still be supplied via the other tower [1].

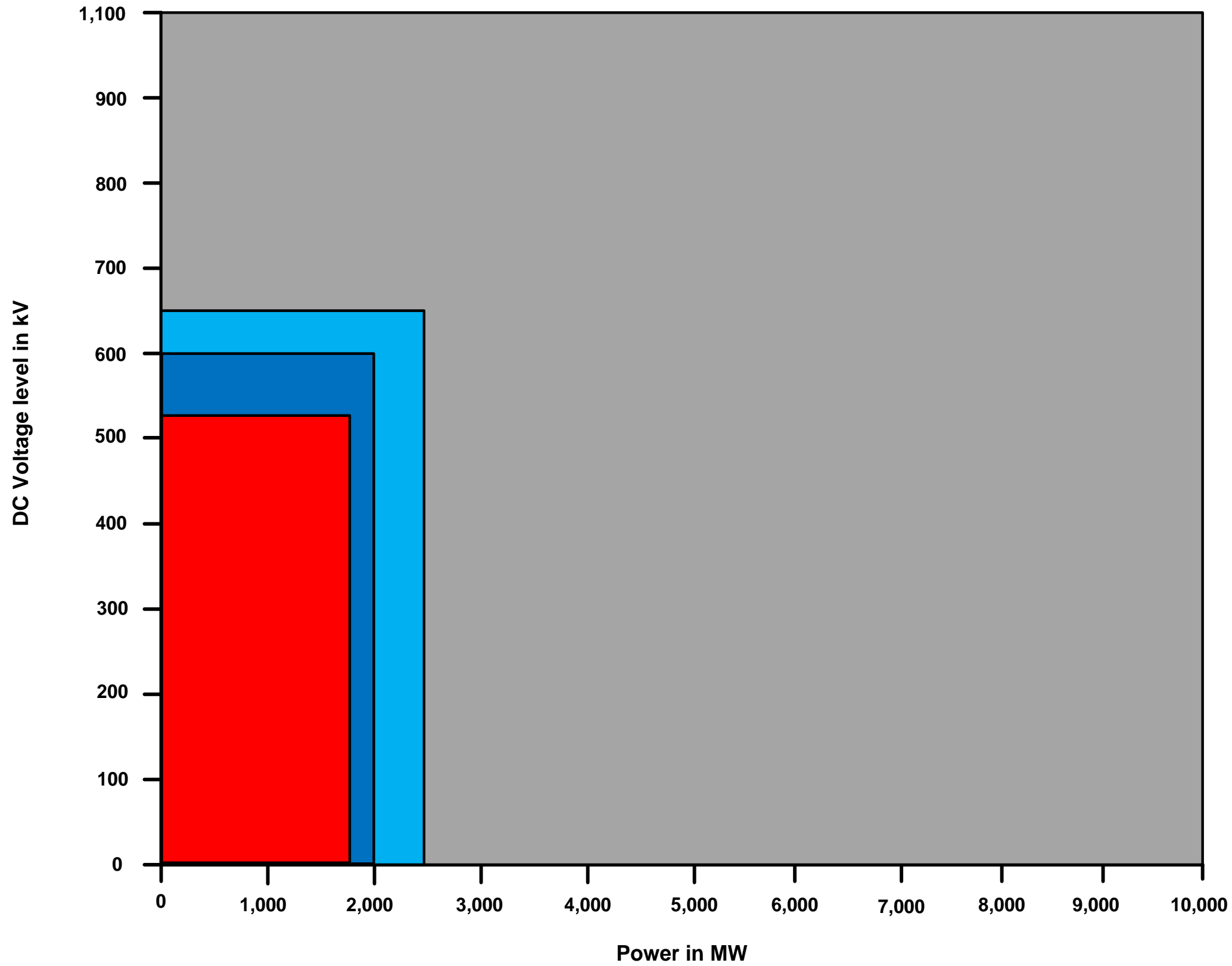
7.7.2 Development of HVDC technology for NPP connections

Conventional thyristor technology has been well established for many decades as a useful method for transmitting energy over long distances with low losses. Since the year 2000, the growth in thyristor technology has been astounding, seeing power ratings reach 8000 MW and DC voltage levels of ± 800 kV have been achieved. The Nelson River hydroelectric scheme, with a power and voltage rating of 1620 MW and 450 kV respectively, was commissioned as far back as 1977. The Yunnan–Guangdong was completed in 2010, achieving power ratings of 5000 MW and DC voltages of ± 800 kV. However, these have all been applied using DC overhead line, where such large power ratings are easily achievable [187].

Due to be commissioned towards the end of 2016, the Western HVDC link project will be the highest DC voltage rated cable anywhere in the world. With a record DC voltage of ± 600 kV being applied to Mass Impregnated Non Draining (MIND) cable, this is a unique project, both in terms of technology rating as well as innovation. With a nominal power rating of 2250 MW, the amount of cross boundary power transfer that can be achieved is a major benefit in helping to boost capacity and relieve bottlenecks between Scotland and England/Wales [178]. The cable technology required to achieve 2 GW circuits for connecting large NPPs is now available. Due to the maturity and proven experience of thyristor based technology around the world, this type of HVDC technology is a potential option for connecting future NPPs to the NETS. However, as with any project, additional aspects also have to be considered as part of the selection process.

VSC-HVDC technology has increased in both DC voltage and power rating over the last few years; the rating of the IGBTs has been the main limitation in achieving the same ratings as those of the conventional thyristor based technology but as more and more projects are commissioned around the world, the confidence in the technology will continue to improve and with it the demand for higher power and voltage ratings will increase. The Skagerrak 4 connection, with a DC voltage of 500 kV, was the largest order in terms of DC voltage rating placed for a VSC-HVDC connection [195]. This has been exceeded by the Nordlink project, with a DC voltage of ± 525 kV and power rating of 1400 MW in bipolar formation [196]. The more VSC-HVDC projects that are successfully commissioned, the greater the confidence and experience gained with the technology. Based upon the above assessment, the power rating and DC voltages achievable with both VSC and CSC-HVDC is shown in Figure 173. The combination of OHL and cable developments results in the maximum ratings obtainable for the different technologies.

Current HVDC Technology Ratings







KEY	
	CSC HVDC technology with OHL
	VSC HVDC technology with OHL
	CSC and VSC HVDC technology with MI cables
	VSC HVDC technology with extruded cables

Figure 173: Available HVDC technology ratings in industry

CSC-HVDC technology with OHL can be applied to very high voltage and power levels. The Western HVDC link project accounts for a maximum power rating of just over 2000 MW when used with MI cable. Despite many publications highlighting the limitations in VSC-HVDC power ratings – and particular restriction to 500 kV extruded or MI cable technology – at least one manufacturer is able to offer higher rating capabilities [90]. When used with OHL, VSC-HVDC technology utilising 640 kV symmetrical base modules, a ± 640 kV bipole solution becomes available. Based upon a maximum IGBT rating of 1886 A, a bipole power rating of 2430 MW is achievable [90]. If the 600 kV MI cable from the Western HVDC link project was combined with a ± 600 kV bipole from the manufacturer concerned [90], a maximum power rating of 2260 MW can be attained. Including losses, 2200 MW of power could be transferred from one end of an HVDC link to the other.

7.7.3 Comparison of AC and DC technology for NPP connections

A review of AC and DC technology ratings has been carried out and based upon the data in Table 27, a maximum power rating of 3465 MVA can be achieved per 400 kV AC overhead line circuit. For a double circuit, this yields a total power rating of 6930 MVA. Assuming a power factor of 0.95, this equates to 6583 MW. If one circuit of a double tower is out of service, the other can carry the full output of a 3600 MW NPP. If a pure AC technology solution is adopted for a 3600 MW NPP connection, then two 6930 MVA 400 kV double circuit overhead lines would provide significant redundancy for future system development.

Two VSC-HVDC bipolar links, each with a DC voltage of ± 500 kV and power rating of 1800 MW, are available from one manufacturer to meet the required connection capacity [90]. If the maximum available ratings of 2260 MW per bipole are used for a 3600 MW NPP, then extra redundancy is also provided. If larger NPP reactor units of up to 1500 MW rating are planned, then the hybrid AC/DC design presented in chapter 5 could offer an optimal solution. If a 400 kV double circuit OHL of 6930 MVA rating is combined with two ± 600 kV, 2260 MW VSC-HVDC bipoles, then a 4500 MW NPP could be connected to the NETS. Such ratings for VSC-HVDC converters and MI cable may present a risk, when each is only available from one manufacturer [90]. Despite this, such a connection is practically possible.

7.8 Chapter 7 review

The costs of AC and DC technology for NPP connections have been investigated and the following findings have been made:

- *AC overhead line technology is significantly cheaper than HVDC converters.*
- *The cost of AC cables is similar to that of HVDC options and a combination of AC overhead line and DC converters can provide an optimal cost-effective solution.*
- *The footprint of CSC-HVDC converter stations is larger than VSC options due to the inclusion of AC filters to meet the reactive power and harmonic requirements.*
- *If a GIS AC substation is combined with a VSC-HVDC converter station, and most of the DC equipment is located indoors, then a design with an optimal footprint can be achieved.*
- *VSC-HVDC bipoles of various voltage and power ratings can be combined with AC overhead lines to provide a future-proof design for NPP connections. By using a hybrid AC/DC design, based upon the maximum technology ratings available, a maximum 4500 MW NPP in rating can be connected to the AC grid.*

From the above findings the author recommends utilising a hybrid AC/DC solution for connecting an NPP to the NETS. AC overhead lines in combination with VSC-HVDC technology can offer a cost-effective solution.

Chapter 8: Conclusions and Future Work

The objective of carrying out a technical and economic analysis of HVDC technology for connecting an NPP to the NETS has been achieved. In the following section, conclusions from the work undertaken are drawn and recommendations for future work in selected key technical areas are made.

8.1 Conclusions

Based upon the work carried out in this thesis into the technical and economic merits of HVDC technology NPP connections, the following conclusions are drawn.

For AC technology:

- AC overhead lines offer the cheapest NPP connection option.
- AC overhead lines for NPP connections are industry proven and the preferred technology connection option.
- AC GIS substations can offer a reduced footprint and are better suited for NPP in coastal locations.

For CSC-HVDC technology:

- The risk of commutation failure in low ESCR scenarios presents a risk to NPP operation and reliability.
- For large power ratings, the physical size of converter stations can result in large project costs.
- At the current time of writing Bipole power ratings of 2250 MW at voltage levels of ± 600 kV are available with MI cable technology for NPP connections.
- For large NPPs, two CSC-HVDC bipoles may be required in order to achieve the required connection capacity.

For VSC-HVDC technology:

- VSC-HVDC technology can offer superior technical benefits for an NPP connection when compared to CSC-HVDC converters. Examples include black-start capability and independent active and reactive power control.
- Converter station designs can be optimised to reduce the footprint and cost.
- At the current time of writing bipole power ratings of 2250 MW at voltage levels of ± 600 kV are available with MI cable technology for NPP connections.
- For large NPPs, two bipoles may be required, in order to achieve the required connection

- capacity.
- VSC-HVDC technology can be combined with AC overhead lines to provide a future-proof NPP hybrid connection option.

In summary, VSC-HVDC technology is the preferred DC option for an NPP connection. When combined with AC technology, a solution that strikes an appropriate balance between the technical and economic aspects can be achieved.

8.2 Further work

Based upon the work carried out there are some key technical issues which merit further work and investigation. These are described in the following sections.

8.2.1 Simulation using larger-rated HVDC models

The impacts of larger NPP connections can be analysed by using detailed Modular Multilevel (MMC) VSC-HVDC converter models of 2000 MW or more in rating. A Real Time Digital Simulator (RTDS) will allow for a larger and more detailed power system – incorporating the NPP, AC grid and DC converters – to be analysed in real time. This will allow a more detailed understanding of the internal performance within the VSC-HVDC converters to be gained. Performance phenomena worthy of investigation would include the distribution of valve arm currents during normal and transient system conditions.

Using larger VSC and NPP ratings enables the wider system impacts such as cross boundary power flows and overvoltage limits to be studied.

8.2.1 Impact of HVDC frequency control on NPP operation

When an NPP is radially connected by an HVDC link, the control system must regulate the frequency. If the frequency within the NPP is not kept constant, then this can have unfavourable effects on operation and safety.

A frequency controller similar to the one presented in this thesis can be designed and its effectiveness on NPP stability can be analysed through simulation. If a sufficiently detailed controller is designed, then the analysis can be performed through the software of choice. The author recommends PSCAD due to the level of detail which can be implemented in HVDC control systems. The response of the controller for different system contingencies can be analysed and specific measurement parameters can be monitored within the NPP model.

8.2.2 HVDC protection and control operating times

The speed and response times of the HVDC protection and control systems need to be ascertained if effective strategies for secure and reliable NPP connections are to be implemented in practice. To obtain the required information, HVDC protection control panels can be interfaced with an RTDS to determine operation and signalling times and emergency control functions such as power reversal and active power ramps and runbacks can be implemented. Power oscillation damping and frequency support functions can also be studied. If access to HVDC protection and control panels is not available, then work could be carried out in collaboration with a manufacturer who does possess such facilities.

8.2.3 Further in-house study

Once accurate operating times of the HVDC technology have been established, the information can be incorporated into further power system studies to determine whether the speed of control and protection response meets the transmission system requirements.

To supplement further in-house studies, the following scenarios are recommended:

- A high-level benchmarking review of synchronous and islanding design and experience associated with existing NPPs.
- In-depth analysis of UK NPP examples, considering specific proposals for the substitution of AC system elements/capabilities and what performance requirements are necessary to put onto the network and the NPP in order to ensure that the generators can satisfactorily operate within the system requirements.
- Investigation of Sub-Synchronous Torsional Interaction (SSTI) between VSC-HVDC technology and the NPP generators.

8.2.4 Industry interaction

Regular interaction with HVDC manufacturers will be required to determine the future state and technical capabilities of both CSC- and VSC-HVDC technology. As VSC-HVDC technology develops and more projects are commissioned, the operational experience gained from different transmission utilities can provide valuable learning opportunities.

Interaction with operators and manufacturers of new NPPs is vital in ascertaining the technical and operational limits/procedures required for secure and successful operation. An understanding of the capability of the new breed of nuclear reactors and their advanced control systems would provide further technical input for future generator connections. By engaging both nuclear and HVDC consultants, a technical specification for NPP HVDC connections can be produced.

Appendix A

Power System Computer Aided Design (PSCAD) for HVDC simulation

PSCAD is a powerful simulation tool which is interfaced to the renowned EMTDC (Electromagnetic Transient simulation programme) and is used by energy utilities and consultants all over the world. The user is able to construct circuits, run simulations, and analyse the results in great detail with a range of different graphical displays. Manual controls, meters and plotting functions enable the user to alter parameters while a simulation is in progress.

A library of models, ranging from generators to power electronic components is readily available to the user and can be used to trial systems or to develop custom models. Some of the models available include transformers, circuit breakers, overhead lines and cables, protection relaying, AC and DC machines, HVDC, SVC and FACTS controllers among many other options.

PSCAD is used by researchers, scientists, utilities, manufacturers, academic institutions and consultants all over the world for planning, design, commissioning, preparing tenders, teaching and research purposes. Routinely conducted investigations carried out on PSCAD include some of the following:

- Relay coordination.
- Lightning strikes, faults or circuit breaker operation.
- Transformer saturation effects.
- Evaluation of filter design and harmonic analysis.
- Control system design and evaluation of HVDC systems, FACTS and SVCs.

A unique advantage of PSCAD is the ability to model HVDC control systems in specific detail. Inner and outer loop controls can be embedded within the HVDC models to save space on the main user screen while ensuring that modelling accuracy is retained. The ability to model control systems in great detail has made this an effective tool for analysing NPP HVDC connections.

Appendix B

MATLAB and Simulink power system software

Engineers use MATLAB to analyse and design systems and products suitable for the real world. MATLAB can be used for signal processing, communications, control design, robotics, image processing and much more.

The operating platform is optimised for solving both engineering and scientific issues. The smart graphics make it simple to visualise and gain insights from data. A vast library of toolboxes enables the user to select essential algorithms for the required domain. These tools and capabilities are rigorously tested and designed to work in tandem. MATLAB code can be integrated with other languages enabling the user to deploy algorithms and applications within enterprise and production systems.

Simulink, developed by MathWorks, is a graphical programming environment for modelling, simulating and analysing multi-domain dynamic systems. Simulink provides a graphical editor, custom block libraries and solvers for modelling and simulating system dynamics. Engineers use Simulink to develop ideas from concept to reality.

Simulink is integrated with MATLAB and enables algorithms to be incorporated into models. Simulation results can then be exported to MATLAB for further analysis.

This functionality makes the software ideal for modelling HVDC control systems. By designing or trialling a particular HVDC model within the MATLAB/Simulink interface, an understanding can be gained before more advanced software, such as PSCAD is utilised. A general control response can be achieved and fine-tuned before being implemented in other software such as PSCAD.

The software has proven useful in the thesis for comparing the dynamic response of a VSC-HVDC model to that of another design in PSCAD.

Appendix C

Power World Simulator power system software

Power World Simulator is a power system simulation package designed to simulate high voltage power systems operation on a time frame ranging from a few minutes to several days. The software contains a power flow package capable of solving systems with thousands of buses.

Tools available within the package include short circuit and contingency analysis, integrated economic despatch, time step simulation, difference flows, as well as generator control.

The software has proved useful for performing a load flow analysis on the designed power system used in the thesis. The results obtained from the load flow enable a comparison to be made with PSCAD to ascertain whether the steady-state limits were acceptable and within the $\pm 1\%$ tolerance requirement.

Appendix D

MATLAB/Simulink rectifier profiles for three-phase fault condition

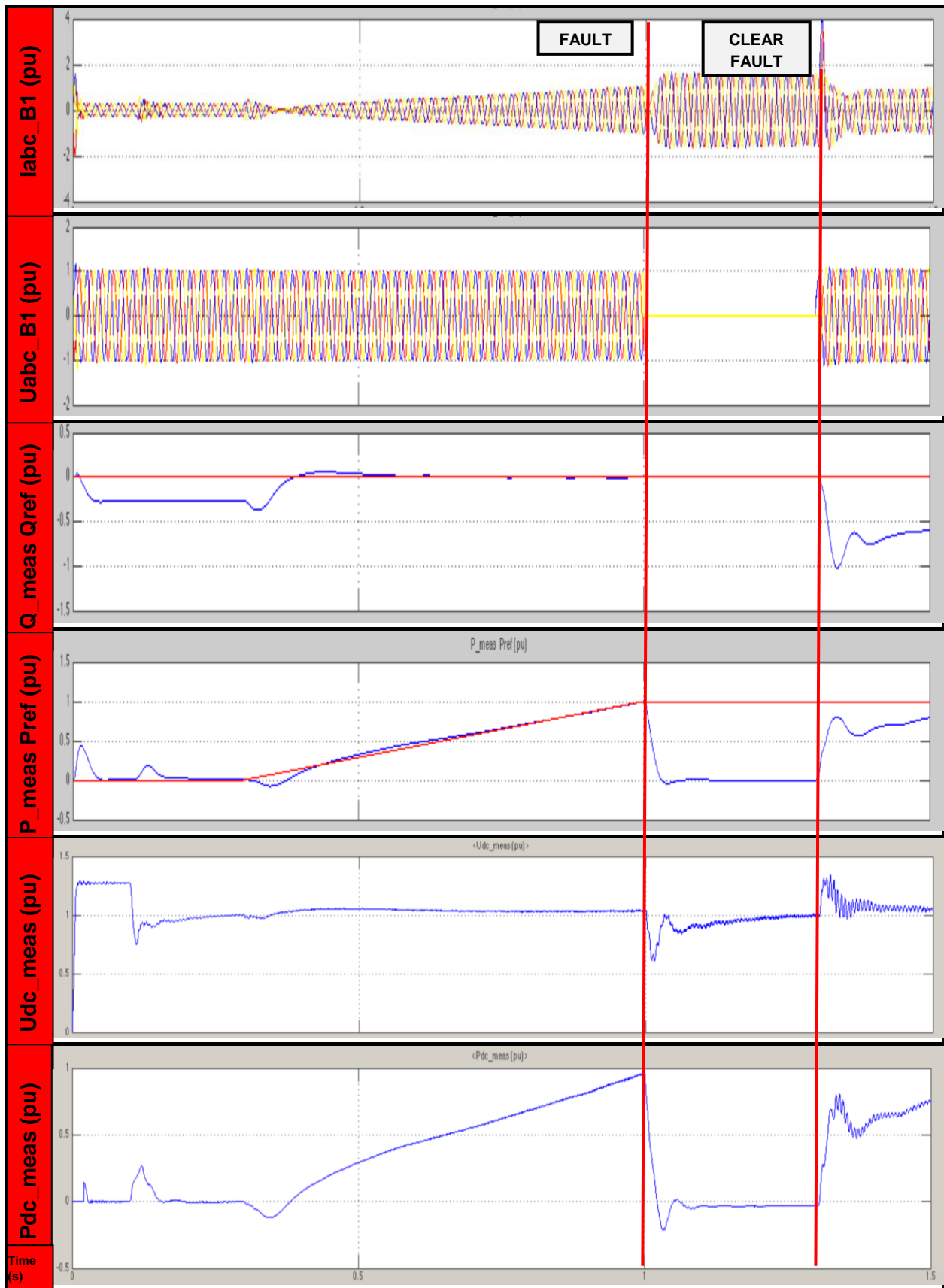


Figure 174: MATLAB/Simulink rectifier profiles for three-phase fault condition

Appendix E

MATLAB/Simulink inverter profiles for three-phase fault condition

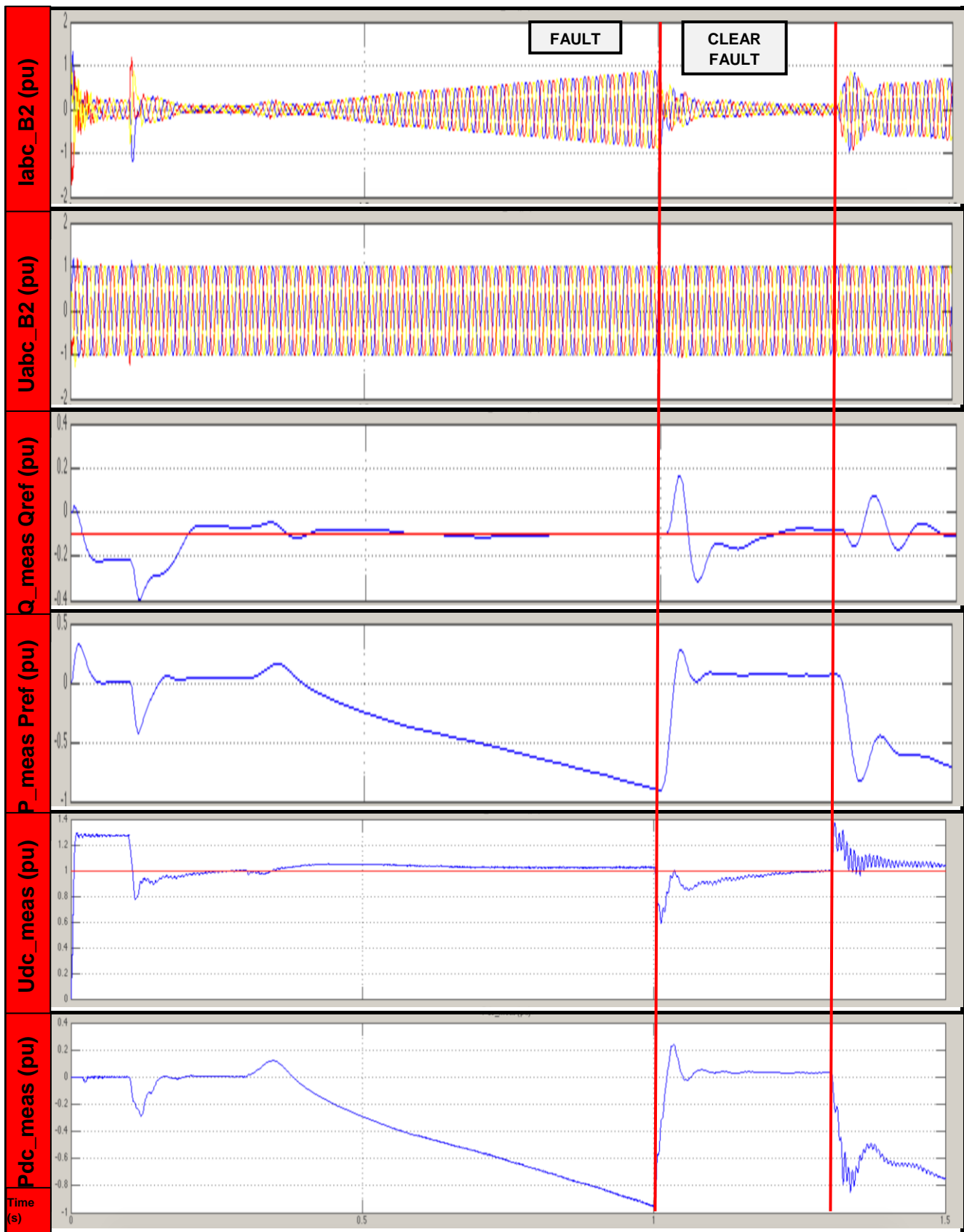


Figure 175: MATLAB/Simulink inverter profiles for three-phase fault condition

Appendix F

PSCAD rectifier profiles for three-phase fault condition

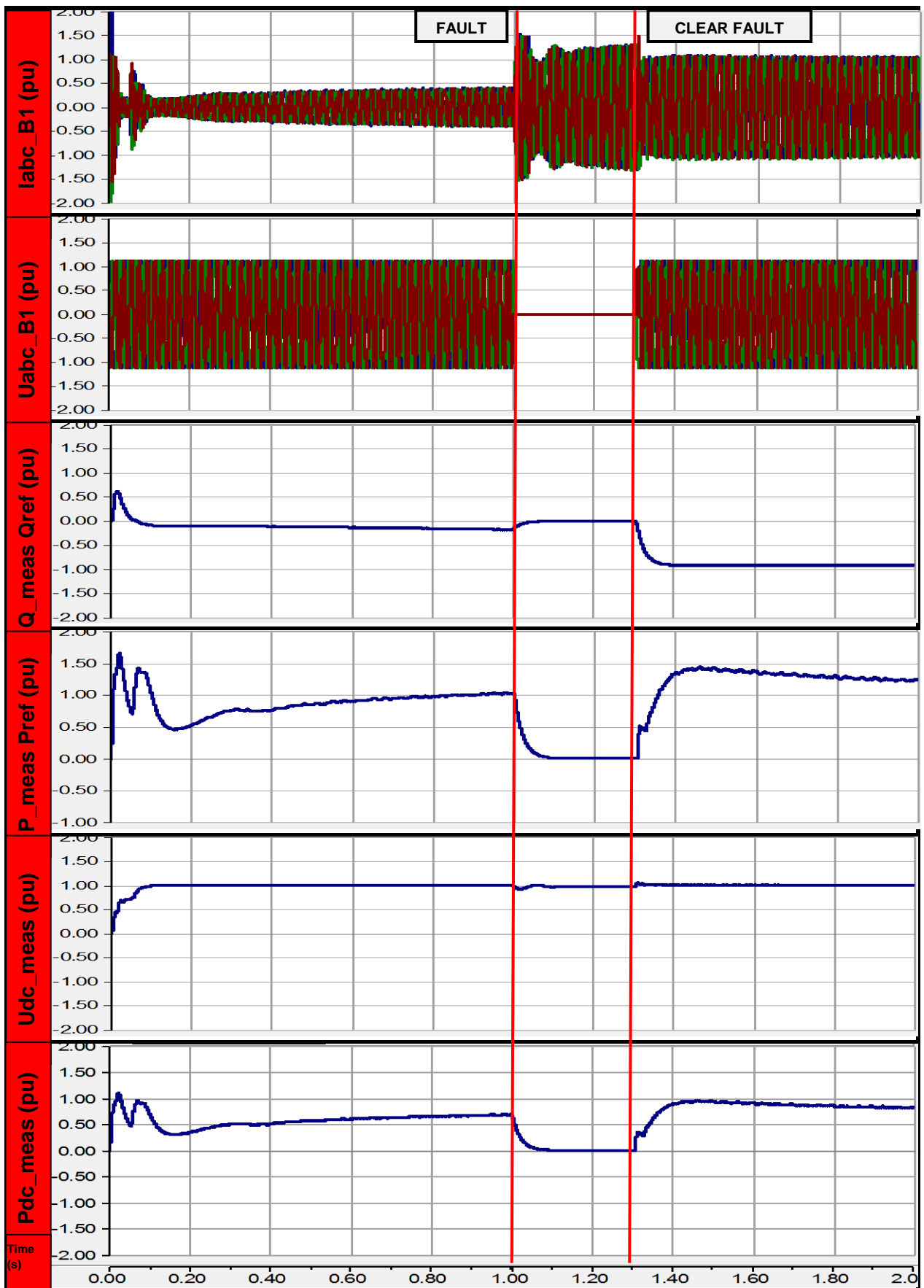


Figure 176: PSCAD rectifier profiles for three-phase fault condition

Appendix G

PSCAD inverter profiles for three-phase fault condition

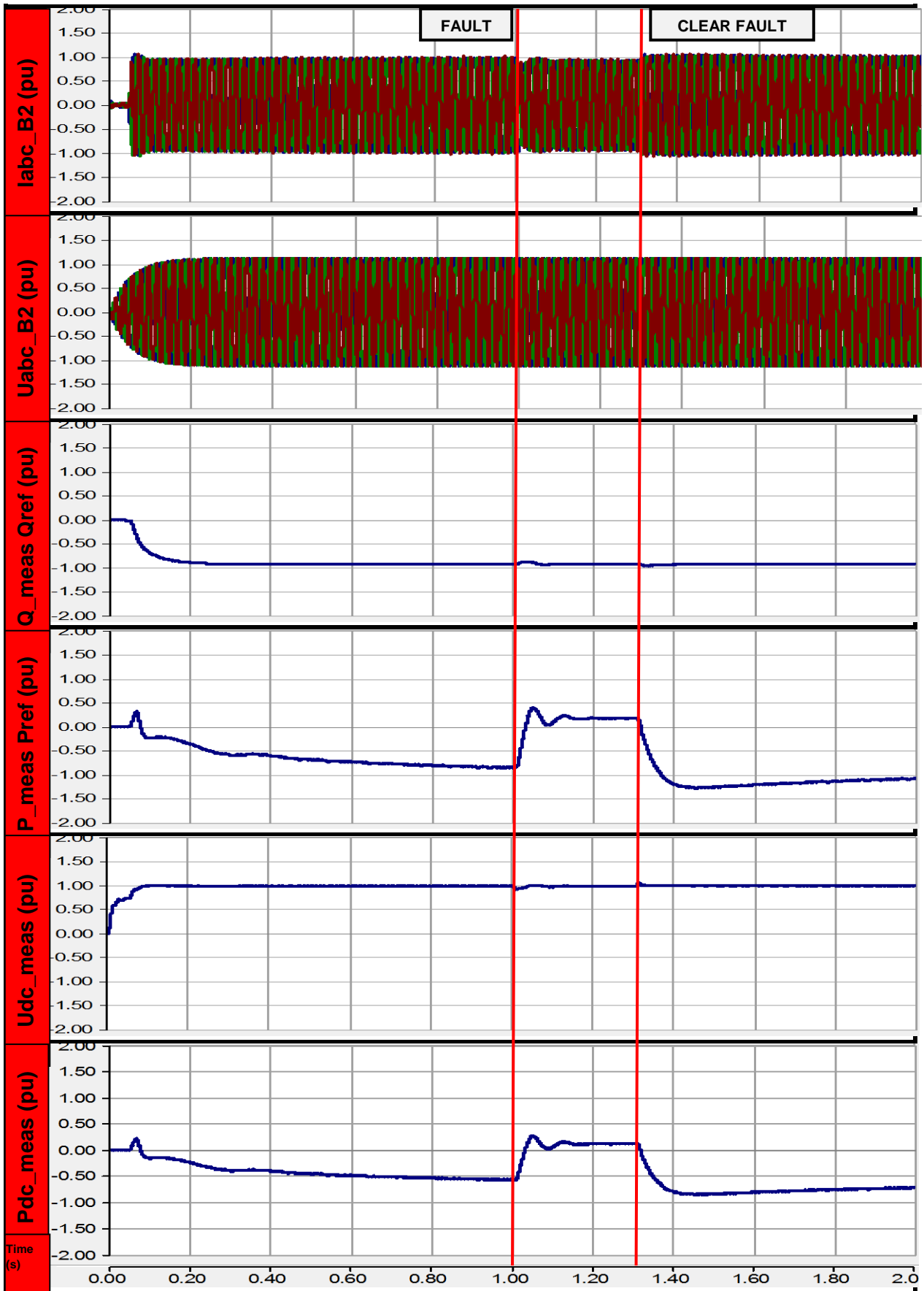


Figure 177: PSCAD inverter profiles for three-phase fault condition

List of References

- [1] National Grid Electricity Transmission, "North West Coast Connections Report Needs Case," 19 October, 2012. [Online]. Available: <http://www.northwestcoastconnections.com/docs/SOR.pdf>. [Accessed 7 June 2014].
- [2] National Grid Electricity Transmission, "Hinkley Point C Connection Project," 4 May 2014. [Online]. Available: <http://infrastructure.planningportal.gov.uk/document/2515308>. [Accessed 6 July 2014].
- [3] Office for Nuclear Regulation, "Nuclear Regulation in the UK," 5 October 2014. [Online]. Available: <http://www.onr.org.uk/documents/a-guide-to-nuclear-regulation-in-the-uk.pdf>. [Accessed 3 June 2015].
- [4] M. dos Santos, J. Jardini, R. Casolari, R. Vasquez-Arnez, G. Saiki, T. Sousa and G. Nicola, "Power Transmission Over Long Distances: Economic Comparison Between HVDC and Half-Wavelength Line," *IEEE Transactions on Power Delivery*, vol. 29, no. 2, pp. 502-509, 2014.
- [5] Chuanyue Li, Xiaobo Hu, J. Guo and J. Liang, "The DC grid reliability and cost evaluation with Zhoushan five-terminal HVDC case study," *Power Engineering Conference (UPEC), 2015 50th International Universities*, Stoke on Trent, 2015, pp. 1-6.
- [6] T. Sakurai, K. Goto, I. Matori, A. Watanabe, T. Kawai and T. Nakao, "Cooperative Control Scheme for an HVDC System Connected to an Isolated BWR Nuclear Power Plant," *IEEE Transactions on Power Apparatus and Systems*, Vols. PAS-102, no. 6, pp. 1894-1902.
- [7] M. Ishikawa, T. Hara, K. Hirayama and K. Sekiya, "Development of a Coordinated Control System for BWR Nuclear Power Plant and HVDC Transmission System," *Power Delivery, IEEE Transactions on*, vol. 1, no. 3, pp. 319 - 325, July 1986 .
- [8] T. Hara, A. Kurita, T. D. Younkins, J. J. Sanchez-Gasca and J. H. Chow, "A Coordinated Multivariable Control System Design for a HVDC Linked Remote ABWR Nuclear Power Park," in *IEEE Power Engineering Review*, vol. PER-7, no. 12, pp. 28-28, Dec. 1987.
- [9] U. Axelsson, A. Holm, C. Liljegren, M. Aberg, K. Eriksson and O. Tollerz, "The gotland hvdc light project experiences from trial and commercial operation," *Electricity Distribution, 2001. Part 1: Contributions. CIREN. 16th International Conference and Exhibition on (IEE Conf. Publ No. 482)*, Amsterdam, Netherlands, 2001, pp. 14-14.
- [10] T. Sakurai, K. Goto, D. B. Klapper and K. Carlsen, "UHV Stability Study Tokyo Electric Power Company," in *IEEE Transactions on Power Apparatus and Systems*, vol. PAS-100, no. 12, pp. 4995-5001, Dec. 1981.
- [11] A. Holzer and Le Anh Tuan, "Effects of nuclear power phase-out in Germany on the Austrian power system," *PowerTech, 2015 IEEE Eindhoven*, Eindhoven, 2015, pp. 1-6.
- [12] D. Tiku, "dc Power Transmission: Mercury-Arc to Thyristor HVDC Valves [History]," in *IEEE Power and Energy Magazine*, vol. 12, no. 2, pp. 76-96, March-April 2014.
- [13] B. E. Danielsson, "HVDC valve with light-triggered thyristors," *AC and DC Power Transmission, 1991, International Conference on*, London, 1991, pp. 159-164.
- [14] H. H. Frey, P. Etter and P. Knapp, "Solid state: Thyristors on the move: New applications are seen in power converters and inverters for trains, industrial motors, and HVDC," in *IEEE Spectrum*, vol. 17, no. 3, pp. 57-62, March 1980.
- [15] T. S. Reynolds and T. Bernstein, "The damnable alternating current," in *Proceedings of the IEEE*, vol. 64, no. 9, pp. 1339-1343, Sept. 1976.
- [16] Daochun Huang, Jiangjun Ruan and Shifeng Yu, "Overview of the recent developments of ultra high voltage AC transmission in China," *Power and Energy Society General Meeting - Conversion and Delivery of Electrical Energy in the 21st Century, 2008 IEEE*, Pittsburgh, PA, 2008, pp. 1-9.

- [17] N. D. Alekseeva, A. V. Bubnova, V. S. Chudny and N. N. Tikhodeev, "Reliability analysis and comparison of long-distance HVAC and HVDC power transmission lines," *Power System Technology, 2002. Proceedings. PowerCon 2002. International Conference on*, 2002, pp. 375-379.
- [18] K. Ferkal, M. Poloujadoff and E. Dorison, "Proximity effect and eddy current losses in insulated cables," in *IEEE Transactions on Power Delivery*, vol. 11, no. 3, pp. 1171-1178, Jul 1996.
- [19] J. Arrillaga, "*High voltage direct current transmission*. London," UK: Institution of Electrical Engineers, 2008.
- [20] M. Deshpande, "*Electrical power system design*," New Delhi: Tata McGraw-Hill, 1984.
- [21] K. Padiyar, "*Power system dynamics*," Hyderabad [India]: BS Publications, 2008.
- [22] J. Arrillaga, Y. Liu and N. Watson, "*Flexible power transmission*," Chichester, England: John Wiley & Sons, 2007.
- [23] Kim., *HVDC Transmission: "Power Conversion Applications in Power Systems"*, John Wiley & Sons, 2009.
- [24] P. C. Sen, M. L. MacDonald and D. J. Clarke, "A novel equidistant pulse control scheme for thyristor converters," in *Canadian Electrical Engineering Journal*, vol. 3, no. 3, pp. 10-14, July 1978.
- [25] R. Agarwal and S. Singh, "Harmonic mitigation in voltage source converters based HVDC system using 12-pulse AC-DC converters," *2014 Annual IEEE India Conference (INDICON)*, Pune, 2014, pp. 1-6.
- [26] P. Kundur, N. Balu and M. Lauby, "*Power system stability and control*," New York: McGraw-Hill, 1994.
- [27] U. Astrom, B. Danielsson and K. Nyberg, "Alternative solutions for thyristor control and gating for HVDC-valves," *Power System Technology, 1998. Proceedings. POWERCON '98. 1998 International Conference on*, Beijing, 1998, pp. 479-482.
- [28] S. Tamai, H. Naitoh, F. Ishiguro, M. Sato, K. Yamaji and N. Honjo, "Fast and predictive HVDC extinction angle control," in *IEEE Transactions on Power Systems*, vol. 12, no. 3, pp. 1268-1275, Aug 1997.
- [29] K. Strunz, "Real time high precision simulation of the HVDC extinction advance angle," *Power System Technology, 2000. Proceedings. PowerCon 2000. International Conference on*, Perth, WA, 2000, pp. 1065-1070 vol.2.
- [30] L. Anzivion, "*HVDC transmission line reference book*," Palo Alto, Calif: EPRI, 1993.
- [31] D. Thukaram, S. Lakpathi, K. Ravishankar and S. Surendra, "Reactive power optimization with different objectives in large power systems including HVDC systems and FACTS devices," *Power Systems, 2009. ICPS '09. International Conference on*, Kharagpur, 2009, pp. 1-6.
- [32] H. Dai, Y. Wang, X. Li, Z. Ming and H. Deng, "Characteristic Analysis of Reactive Power Compensation Device at HVDC Converter Station," *2012 Asia-Pacific Power and Energy Engineering Conference*, Shanghai, 2012, pp. 1-5.
- [33] Haipeng Xie, Zhaohong Bie, Pengfei Dong and Chao Zheng, "The influence of commutation failures on the reliability of HVDC transmission systems," *TENCON 2015 - 2015 IEEE Region 10 Conference*, Macao, 2015, pp. 1-4.
- [34] L. Chen, H. Pan, C. Deng, F. Zheng, Z. Li and F. Guo, "Study on the Application of a Flux-Coupling-Type Superconducting Fault Current Limiter for Decreasing HVdc Commutation Failure," in *Canadian Journal of Electrical and Computer Engineering*, vol. 38, no. 1, pp. 10-19, winter 2015.
- [35] Z. Wei, Y. Yuan, X. Lei, H. Wang, G. Sun and Y. Sun, "Direct-Current Predictive Control Strategy for Inhibiting Commutation Failure in HVDC Converter," in *IEEE Transactions on Power Systems*, vol. 29, no. 5, pp. 2409-2417, Sept. 2014.

- [36] Y. Z. Sun, L. Peng, F. Ma, G. J. Li and P. F. Lv, "Design a Fuzzy Controller to Minimize the Effect of HVDC Commutation Failure on Power System," in *IEEE Transactions on Power Systems*, vol. 23, no. 1, pp. 100-107, Feb. 2008.
- [37] Y. Wang, X. Li, C. Wen and Y. He, "Impact of AC System Strength on Commutation Failure at HVDC Inverter Station," *2012 Asia-Pacific Power and Energy Engineering Conference*, Shanghai, 2012, pp. 1-4.
- [38] Xiaohua Li, Chao Ye, Jiaqi Wu, Lizhu Wu, Longbo Luo and XiaoBing Ding, "Time discreteness of commutation failure in HVDC transmission," *TENCON 2015 - 2015 IEEE Region 10 Conference*, Macao, 2015, pp. 1-6.
- [39] CIGRE Working Group 14.05. "Commutation Failures Causes and Consequences," Technical Brochure 103, 1996.
- [40] G. Bhuvaneswari and B. C. Mahanta, "Analysis of Converter Transformer Failure in HVDC Systems and Possible Solutions," in *IEEE Transactions on Power Delivery*, vol. 24, no. 2, pp. 814-821, April 2009.
- [41] Alstom Grid "Connecting to the Future," Alstom Grid, Levallois-Perret Cedex, France, 2010.
- [42] Lingxue Lin, Yao Zhang, Qing Zhong and Zhigang Wu, "High speed identification and protection for commutation failure in HVDC systems based on wavelet entropy," *Electric Utility Deregulation and Restructuring and Power Technologies, 2008. DRPT 2008. Third International Conference on*, Nanjuing, 2008, pp. 1966-1971.
- [43] B. Qahraman, A. M. Gole and I. T. Fernando, "Hybrid HVDC converters and their impact on power system dynamic performance," *2006 IEEE Power Engineering Society General Meeting*, Montreal, Que., 2006, pp. 6 pp.
- [44] C. Guo, Y. Liu, C. Zhao, X. Wei and W. Xu, "Power Component Fault Detection Method and Improved Current Order Limiter Control for Commutation Failure Mitigation in HVDC," in *IEEE Transactions on Power Delivery*, vol. 30, no. 3, pp. 1585-1593, June 2015.
- [45] S. De Boeck, P. Tielens, W. Leterme and D. Van Hertem, "Configurations and earthing of HVDC grids," *2013 IEEE Power & Energy Society General Meeting*, Vancouver, BC, 2013, pp. 1-5.
- [46] C. K. Kim; V. K. Sood; G. S. Jang; S. J. Lim; S. J. Lee, "Other Converter Configurations for HVDC Transmission," in *HVDC Transmission: Power Conversion Applications in Power Systems*, 1, Wiley-IEEE Press, 2009, pp.352.
- [47] L. Yu, C. Guo, C. Zhao, J. Xu, N. An and X. Hu, "Power Reversal of Hybrid HVDC System," *AC and DC Power Transmission, 11th IET International Conference on*, Birmingham, 2015, pp. 1-6.
- [48] Z. Shao, J. Lu, Y. Lu, Q. Zou and C. Liu, "Research and application of the control and protection strategy for the $\pm 500\text{kV}$ Xiluodu-Guangdong double bipole HVDC project," *Electric Utility Deregulation and Restructuring and Power Technologies (DRPT), 2011 4th International Conference on*, Weihai, Shandong, 2011, pp. 88-93.
- [49] M. Davies, A. Kolz, M. Kuhn, D. Monkhouse and J. Strauss, "Latest control and protection innovations applied to the Basslink HVDC interconnector," *AC and DC Power Transmission, 2006. ACDC 2006. The 8th IEE International Conference on*, London, UK, 2006, pp. 30-35.
- [50] M. Dong, J. He, X. Li and Y. Huang, "Realization of Self-Defined Control System for Constant Extinction Angle Control Using PSCAD/EMTDC," *2009 Asia-Pacific Power and Energy Engineering Conference*, Wuhan, 2009, pp. 1-5.
- [51] Yue Yuan, Liang She, Hang Zhang, Xiaoming Yu and Jia Sun, "A comprehensive pole control unit design for HVDC converter station," *Electric Utility Deregulation and Restructuring and Power Technologies, 2008. DRPT 2008. Third International Conference on*, Nanjuing, 2008, pp. 1821-1825.

- [52] Z. Du, D. Luo, Y. Ruan, F. Zhan, Y. Zhang and C. Xia, "Study on fitting equations of HVDC recovery P-Q characteristics after faults," *2014 IEEE PES Asia-Pacific Power and Energy Engineering Conference (APPEEC)*, Hong Kong, 2014, pp. 1-6.
- [53] B. Zhou, Z. Du, D. Luo, L. Liu and F. Zhan, "VDCOL parameters design of multi-infeed HVDC based on a simplified model of DC P-Q coupling recovery," *2014 IEEE PES Asia-Pacific Power and Energy Engineering Conference (APPEEC)*, Hong Kong, 2014, pp. 1-5.
- [54] A. E. Ariffin, A. A. M. Zin, K. L. Lo and B. C. Kok, "Special HVDC controls for TNB/EGAT HVDC interconnection system," *Power System Technology, 2002. Proceedings. PowerCon 2002. International Conference on*, 2002, pp. 62-66 vol.1.
- [55] C. W. Taylor and S. Lefebvre, "HVDC controls for system dynamic performance," in *IEEE Transactions on Power Systems*, vol. 6, no. 2, pp. 743-752, May 1991.
- [56] W. Guo, "The Principle and Analysis for the Incorrect Pickup of SIEMENS Electrode Bus Differential Protection," *2010 Asia-Pacific Power and Energy Engineering Conference*, Chengdu, 2010, pp. 1-5.
- [57] L. Arioua, B. Marinescu and E. Monmasson, "Control of high voltage direct current links with overall large-scale grid objectives," in *IET Generation, Transmission & Distribution*, vol. 8, no. 5, pp. 945-956, May 2014.
- [58] P. Bahrman and B. K. Johnson, "The ABCs of HVDC transmission technologies," in *IEEE Power and Energy Magazine*, vol. 5, no. 2, pp. 32-44, March-April 2007.
- [59] C. Nguyen Mau, N. T. Trinh, K. Rudion, E. Lerch and Z. A. Styczynski, "Improving ranking of electric power system dynamic behavior in DSA system by applying VSC based HVDC technology," *2012 3rd IEEE PES Innovative Smart Grid Technologies Europe (ISGT Europe)*, Berlin, 2012, pp. 1-7.
- [60] J. Dorn, M. Pohl, D. Retzmann and F. Schettler, "Transformation of the Energy System in Germany ?? Enhancement of System Stability by Integration of innovative Multilevel HVDC in the AC Grid," *Security in Critical Infrastructures Today, Proceedings of International ETG-Congress 2013; Symposium 1:*, Berlin, Germany, 2013, pp. 1-6.
- [61] N. Yousefpoor, A. Narwal and S. Bhattacharya, "Control of DC-Fault-Resilient Voltage Source Converter-Based HVDC Transmission System Under DC Fault Operating Condition," in *IEEE Transactions on Industrial Electronics*, vol. 62, no. 6, pp. 3683-3690, June 2015.
- [62] T. Lüth *et al.*, "Performance of a DC/AC/DC VSC system to interconnect HVDC systems," *AC and DC Power Transmission (ACDC 2012), 10th IET International Conference on*, Birmingham, 2012, pp. 1-6.
- [63] X. Li, Z. Yuan, J. Fu, Y. Wang, T. Liu and Z. Zhu, "Nanao multi-terminal VSC-HVDC project for integrating large-scale wind generation," *2014 IEEE PES General Meeting | Conference & Exposition*, National Harbor, MD, 2014, pp. 1-5.
- [64] Y. Yuefeng, Y. Jie, H. Zhiyuan and W. Haitian, "Research on control and protection system for Shanghai Nanhui MMC VSC-HVDC demonstration project," *AC and DC Power Transmission (ACDC 2012), 10th IET International Conference on*, Birmingham, 2012, pp. 1-6.
- [65] O. Udrea, G. Lazaroiu, G. Ungureanu and V. Violeta, "HVDC transmission corridor — Cost benefit analysis," *Power Engineering Conference (UPEC), 2014 49th International Universities*, Cluj-Napoca, 2014, pp. 1-6.
- [66] S. Li, M. Zhou, Z. Liu, J. Zhang and Y. Li, "A study on VSC-HVDC based black start compared with traditional black start," *2009 International Conference on Sustainable Power Generation and Supply*, Nanjing, 2009, pp. 1-6.
- [67] Ying Jiang-Hafner, H. Duchon, M. Karlsson, L. Ronstrom and B. Abrahamsson, "HVDC with voltage source converters - a powerful standby black start facility," *2008 IEEE/PES Transmission and Distribution Conference and Exposition*, Chicago, IL, 2008, pp. 1-9.

- [68] G. Mazzanti and M. Marzinotto, "Extruded cables for high-voltage direct-current transmission. Piscataway," NJ: IEEE Press, 2013.
- [69] G. P. Adam, O. Anaya-Lara and G. Burt, "Steady-state and transient performance of DC transmission systems based on HVDC technology," *AC and DC Power Transmission, 2010. ACDC. 9th IET International Conference on*, London, 2010, pp. 1-5.
- [70] M. A. Djehaf, S. A. Zidi, Y. I. Djilani Kobibi and S. Hadjeri, "Modeling of a multi-level converter based VSC HVDC supplying a dead load," *Electrical and Information Technologies (ICEIT), 2015 International Conference on*, Marrakech, 2015, pp. 218-223.
- [71] Jiantao Liu, Jianguo Yao, Shengchun Yang and Ke Wang, "Loss analysis of two kinds of flexible HVDC converters," *Power Electronics and Motion Control Conference (IPEMC), 2012 7th International*, Harbin, 2012, pp. 1669-1674.
- [72] P. Geng, W. Wu, M. Huang and F. Blaabjerg, "Efficiency analysis on a two-level three-phase quasi-soft-switching inverter," *Applied Power Electronics Conference and Exposition (APEC), 2013 Twenty-Eighth Annual IEEE*, Long Beach, CA, USA, 2013, pp. 1206-1212.
- [73] J. McNichol, S. T. Ranade, H. Ring and D. Meyl, "Parallel Operation of Nelson River HVDC Bipoles 1 and 2 Control System - Simulator Studies," in *IEEE Transactions on Power Apparatus and Systems*, vol. PAS-101, no. 3, pp. 653-661, March 1982.
- [74] X. Fu, L. A. Dessaint, R. Gagnon, K. Zhou and M. Cheng, "A comparative study of control schemes for VSC-HVDC transmission system," *IECON 2012 - 38th Annual Conference on IEEE Industrial Electronics Society*, Montreal, QC, 2012, pp. 2096-2103.
- [75] R. Adapa, L. Barthold and D. Woodford, "Asymmetrical design of VSC-based HVDC transmission lines," *2012 IEEE Power and Energy Society General Meeting*, San Diego, CA, 2012, pp. 1-6.
- [76] S. Cole, D. Van Hertem and R. Belmans, "VSC HVDC as an alternative grid investment in meshed grids," *Infrastructure Systems and Services: Building Networks for a Brighter Future (INFRA), 2008 First International Conference on*, Rotterdam, 2008, pp. 1-6.
- [77] M. F. M. Arani; Y. A. R. I. Mohamed, "Analysis and Performance Enhancement of Vector-Controlled VSC in HVDC Links Connected to Very Weak Grids," in *IEEE Transactions on Power Systems*, vol. PP, no.99, pp.1-10
- [78] L. Zhang, H. P. Nee and L. Harnefors, "Analysis of Stability Limitations of a VSC-HVDC Link Using Power-Synchronization Control," in *IEEE Transactions on Power Systems*, vol. 26, no. 3, pp. 1326-1337, Aug. 2011.
- [79] L. Zhang, L. Harnefors and H. P. Nee, "Interconnection of Two Very Weak AC Systems by VSC-HVDC Links Using Power-Synchronization Control," in *IEEE Transactions on Power Systems*, vol. 26, no. 1, pp. 344-355, Feb. 2011.
- [80] Minxiao Han, Lingfei Xiong and Lei Wan, "Power-synchronization loop for vector current control of VSC-HVDC connected to weak system," *Power System Technology (POWERCON), 2012 IEEE International Conference on*, Auckland, 2012, pp. 1-5.
- [81] X. Wei and G. Tang, "Analysis and Control VSC-HVDC under Unbalanced AC Conditions," *2006 International Conference on Power System Technology*, Chongqing, 2006, pp. 1-5.
- [82] V. Sood and H. Patel, "Comparison between direct and vector control strategy for VSC-HVDC system in EMTP-RV," *Power Electronics, Drives and Energy Systems (PEDES) & 2010 Power India, 2010 Joint International Conference on*, New Delhi, 2010, pp. 1-6.
- [83] A. Mahjoub and R. Mukerjee, "Modeling of controller for voltage sourced converter based HVDC transmission system," *Power and Energy Conference, 2008. PECon 2008. IEEE 2nd International*, Johor Bahru, 2008, pp. 849-854.

- [84] C. A. H. Mora and N. L. Díaz Aldana, "Vectorial control of a Voltage Source Converter," *Transmission and Distribution Conference and Exposition: Latin America (T&D-LA)*, 2010 IEEE/PES, Sao Paulo, 2010, pp. 689-693.
- [85] C. Han, A. Q. Huang, Y. Liu and B. Chen, "A Generalized Control Strategy of Per-Phase DC Voltage Balancing for Cascaded Multilevel Converter-based STATCOM," *2007 IEEE Power Electronics Specialists Conference*, Orlando, FL, 2007, pp. 1746-1752.
- [86] G. Silva, A. Datta and S. Bhattacharyya, "*PID controllers for time-delay systems*", Boston: Birkhäuser, 2005.
- [87] N. Nayak, S. Mishra, S. Choudhury and P. K. Rout, "Optimal design of VSC based HVDC using Particle Swarm Optimization technique," *Power, Control and Embedded Systems (ICPES)*, 2012 2nd International Conference on, Allahabad, 2012, pp. 1-5.
- [88] Z. Yuan and H. Wang, "The Research on the VSC-HVDC Control System Structure," *2012 Asia-Pacific Power and Energy Engineering Conference*, Shanghai, 2012, pp. 1-4.
- [89] J. Beerten, S. Cole and R. Belmans, "Modeling of Multi-Terminal VSC HVDC Systems With Distributed DC Voltage Control," in *IEEE Transactions on Power Systems*, vol. 29, no. 1, pp. 34-42, Jan. 2014.
- [90] ABB, "HVDC Light® It's time to connect," December 2012. [Online]. Available: <https://library.e.abb.com/public/2742b98db321b5bfc1257b26003e7835/Pow0038%20R7%20LR.pdf>. [Accessed 3 March 2015].
- [91] J. Candelaria and J. D. Park, "VSC-HVDC system protection: A review of current methods," *Power Systems Conference and Exposition (PSCE)*, 2011 IEEE/PES, Phoenix, AZ, 2011, pp. 1-7.
- [92] Hongtao Liu, Zheng Xu and Ying Huang, "Study of protection strategy for VSC based HVDC system," *Transmission and Distribution Conference and Exposition*, 2003 IEEE PES, 2003, pp. 49-54 Vol.1.
- [93] P. Zhao, Q. Chen and L. Xing, "DC fault analysis of VSC-HVDC and DC cable protection principle," *Power and Energy Engineering Conference (APPEEC)*, 2015 IEEE PES Asia-Pacific, Brisbane, QLD, 2015, pp. 1-5.
- [94] A. Patchimpattapong, "Development of Thailand's first nuclear power plant," *Energy and Sustainable Development: Issues and Strategies (ESD)*, 2010 Proceedings of the International Conference on, Chiang Mai, 2010, pp. 1-3.
- [95] N. K. Trehan and R. Saran, "Nuclear power revival," *Nuclear Science Symposium Conference Record*, 2003 IEEE, 2003, pp. 3630-3633 Vol.5.
- [96] Y. Ichihara, "A perspective on nuclear power generation in the future electric power industry-for nonspecialists in the electric power related industries," in *Proceedings of the IEEE*, vol. 89, no. 12, pp. 1793-1807, Dec 2001.
- [97] N. K. Trehan, "Power uprates in nuclear power generating stations," *Nuclear Science Symposium Conference Record*, 2004 IEEE, 2004, pp. 4596-4598 Vol. 7.
- [98] J. Oxstarnd and R. L. Boring, "Human reliability for design applications at a Swedish nuclear power plant," *Resilient Control Systems*, 2009. ISRCS '09. 2nd International Symposium on, Idaho Falls, ID, 2009, pp. 5-10.
- [99] J. T. K. Mao and A. Salvi, "Design Considerations and Features for a Nuclear Power Plant Security System," in *IEEE Transactions on Power Apparatus and Systems*, vol. PAS-100, no. 11, pp. 4493-4501, Nov. 1981.
- [100] G. Kaplan and R. K. Jurgen, "Power/energy: Nuclear power plant safety: A discussion of system design, failure modes, reliability, and human factors with recommendations," in *IEEE Spectrum*, vol. 13, no. 5, pp. 52-69, May 1976.

- [101] G. Antaki and R. Gilada, "Nuclear power plant safety and mechanical integrity," 2014.
- [102] J. Mandula, "Nuclear power plant design characteristics," Vienna: International Atomic Energy Agency, 2007.
- [103] G. I. Maldonado, "The performance of North American nuclear power plants during the electric power blackout of August 14, 2003," *Nuclear Science Symposium Conference Record, 2004 IEEE*, 2004, pp. 4603-4606 Vol. 7.
- [104] T. Schulz, "Westinghouse AP1000 advanced passive plant," *Nuclear Engineering and Design*, vol. 236, no. 14-16, pp. 1547-1557, 2006.
- [105] IEEE Guide for the Definition of Reliability Program Plans for Nuclear Generating Stations and Other Nuclear Facilities - Redline," in *IEEE Std 933-2013 (Revision of IEEE Std 933-1999) - Redline*, vol., no., pp.1-108, Jan. 10 2014.
- [106] G. Petrangeli, "Nuclear safety," Amsterdam: Butterworth-Heinemann, 2006.
- [107] B. Kirby, J. Kueck, H. Leake and M. Muhlheim, "Nuclear Generating Stations and Transmission Grid Reliability," *Power Symposium, 2007. NAPS '07. 39th North American*, Las Cruces, NM, 2007, pp. 279-287.
- [108] S. S. Lee, Y. T. Yoon, S. I. Moon and J. K. Park, "Smart grid based nuclear load-following operation strategies in the South Korean power system," *2013 IEEE Power & Energy Society General Meeting*, Vancouver, BC, 2013, pp. 1-5.
- [109] Sang-Seung Lee, Jong-Keun Park, Seung-Il Moon, Yong-Tae Yoon, Jong-Won Kim and Goon-Cherl Park, "Small nuclear power generation units, and electric power system interconnection," *2006 IEEE Power Engineering Society General Meeting*, Montreal, Que, pp.1-5,2006.
- [110] S. S. Lee, "Northeast Asia power system interconnection and ESS based balance strategies in South Korea," *2014 IEEE PES General Meeting | Conference & Exposition*, National Harbor, MD, 2014, pp. 1-5.
- [111] J. E. Dagle, "Data management issues associated with the August 14, 2003 blackout investigation," *Power Engineering Society General Meeting, 2004. IEEE*, Denver, CO, 2004, pp. 1680-1684 Vol.2.
- [112] H. Clod-Svensson, "Power Failure in Eastern Denmark and Sweden (September 23, 2003)," *e & i Elektrotechnik und Informationstechnik*, vol. 121, no. 10, pp. 367-369, 2004.
- [113] N. K. Trehan, "Power uprates in nuclear power generating stations," *Nuclear Science Symposium Conference Record, 2004 IEEE*, 2004, pp. 4596-4598 Vol. 7.
- [114] T. S. Perry, "Nuclear power gets a second look," in *IEEE Spectrum*, vol. 38, no. 11, pp. 32-33, Nov 2001.
- [115] IEEE Draft Standard Requirements for Reliability Analysis in the Design and Operation of Safety Systems for Nuclear Power Generating Stations," in *IEEE Unapproved Draft Std P577/D3, Feb 2010*, vol., no., pp., 2010.
- [116] M. Raatikainen, T. Männistö, T. Tommila and J. Valkonen, "Challenges of requirements engineering — A case study in nuclear energy domain," *2011 IEEE 19th International Requirements Engineering Conference*, Trento, 2011, pp. 253-258.
- [117] A. K. Vijaya, R. Guptan, S. P. Dharne and S. G. Ghadge, "Risk assessment of operational events methodology for Indian nuclear power plants," *Reliability, Safety and Hazard (ICRESH), 2010 2nd International Conference on*, Mumbai, 2010, pp. 226-229.
- [118] L. Yu-fan, "Simple Analysis about the Environment Protection and Design of Nuclear Power Plant," *2011 Third International Conference on Measuring Technology and Mechatronics Automation*, Shangshai, 2011, pp. 233-235.

- [119] IEEE Standard Criteria for Digital Computers in Safety Systems of Nuclear Power Generating Stations - Redline," in *IEEE Std 7-4.3.2-2010 (Revision of IEEE Std 7-4.3.2-2003) - Redline*, vol., no., pp.1-82, Aug. 2, 2010.
- [120] H. Altomonte, "Japan's Nuclear Disaster: Its Impact on Electric Power Generation Worldwide [In My View]," in *IEEE Power and Energy Magazine*, vol. 10, no. 3, pp. 96-94, May-June 2012.
- [121] G. Srinivas, R. Guptan, S. P. Dhame, S. G. Ghadge and U. Chandra, "Hardware reliability assessment of safety related and safety critical systems in nuclear power plants," *Reliability, Safety and Hazard (ICRESH), 2010 2nd International Conference on*, Mumbai, 2010, pp. 448-454.
- [122] J. J. Kwon, D. Kim, J. J. Park and J. E. Hong, "Collision Analysis of Safety Devices to Prevent Hazards in Safety Critical Systems," *Software Security and Reliability (SERE), 2014 Eighth International Conference on*, San Francisco, CA, 2014, pp. 245-254.
- [123] I. A. S. Teja, A. Jain, L. Yalavarthi and S. Yamujala, "Nuclear power-a potential source to meet future electricity demands in India," *Computation of Power, Energy Information and Commuincation (ICCPEIC), 2015 International Conference on*, Chennai, 2015, pp. 0166-0170.
- [124] R. K. Gajbhiye, P. Kulkarni and S. A. Soman, "Analysis of faulted power systems in three phase coordinates - a generic approach," *2005 International Power Engineering Conference*, Singapore, 2005, pp. 1052-1057 Vol. 2.
- [125] Manitoba Hydro HVDC Reseach Centre, "Power Systems Computer Aided Design User Guide," Winnipeg, 2010.
- [126] Farrokhifar, R. Esmailzadeh, M. Heydari and A. R. Milani, "A study on practical methods to decrease short circuit level in transmission grids," *Industrial Electronics Society, IECON 2013 - 39th Annual Conference of the IEEE*, Vienna, 2013, pp. 1962-1967.
- [127] L. Xu, C. Pan and S. Shao, "A PV Cell Mathematical Model and MPPT Algorithm in PSCAD," *AMR*, vol. 724-725, pp. 10-16, 2013.
- [128] D. Hewings, "West Coast Main Line autotransformer electrification system - test site design & principles," *Power - it's a Quality Thing, IEE Seminar*, London, 2005, pp. 1-2.
- [129] A. Cheldavi and D. Ansari, "Efficient frequency-domain modelling and simulation of nonuniform coupled transmission lines: application in transient analysis of VLSI circuits," in *Canadian Journal of Electrical and Computer Engineering*, vol. 29, no. 3, pp. 167-177, July 2004.
- [130] Nurul Huda Ishak, Iza Sazanita Isa, S. Abdullah, S. Masri and Faizal Mohamad Twon Tawi, "Performance comparison of electric power flow solutions using PSCAD," *Science and Social Research (CSSR), 2010 International Conference on*, Kuala Lumpur, Malaysia, 2010, pp. 542-547.
- [131] H. Gao, C. Wang and W. Pan, "A Detailed Nuclear Power Plant Model for Power System Analysis Based on PSS/E," *2006 IEEE PES Power Systems Conference and Exposition*, Atlanta, GA, 2006, pp. 1582-1586.
- [132] A. Purwadi, N. Heryana, D. Nurafiat, C. Sosityo, A. Setiana and A. Mustaqim, "Testing and diagnostics of power transformer in PT. Indonesia Power Kamojang Geothermal Power Plant unit 1," *Electrical Engineering and Informatics (ICEEI), 2011 International Conference on*, Bandung, 2011, pp. 1-5.
- [133] L. Mendo, "Estimation of a probability with guaranteed normalized mean absolute error," in *IEEE Communications Letters*, vol. 13, no. 11, pp. 817-819, November 2009.
- [134] G. Rabinovich, "Measurement Errors and Uncertainties: Theory and Practice," Springer, 2005.
- [135] National Grid Electricity Transmission, "The Grid Code," 21 August 2014. [Online]. Available: <http://www2.nationalgrid.com/UK/Industry-information/Electricity-codes/Grid-code/The-Grid-code/>. [Accessed 1 October 2014].

- [136] D. S. Crisford, "Introduction to IEC 909 (BS 7639). Short-circuit current calculation in three-phase AC systems," *Fault Level Assessment - Guessing with Greater Precision?*, IEE Colloquium on, London, 1996, pp. 2/1-2/4.
- [137] Hang Wang and K. L. Butler, "Modeling transformers with internal incipient faults," in *IEEE Transactions on Power Delivery*, vol. 17, no. 2, pp. 500-509, Apr 2002.
- [138] S. Zhang, K. R. Pattipati, Z. Hu, X. Wen and C. Sankavaram, "Dynamic Coupled Fault Diagnosis With Propagation and Observation Delays," in *IEEE Transactions on Systems, Man, and Cybernetics: Systems*, vol. 43, no. 6, pp. 1424-1439, Nov. 2013.
- [139] S. E. Arda and K. E. Holbert, "Implementing a pressurized water reactor nuclear power plant model into grid simulations," *2014 IEEE PES General Meeting | Conference & Exposition*, National Harbor, MD, 2014, pp. 1-5.
- [140] A. S. Kullkarni and S. P. Ugale, "Advanced thermal overload protection for high tension motors using digital protection relays," *Computer, Communication and Control (IC4), 2015 International Conference on*, Indore, 2015, pp. 1-7.
- [141] L. Y. Taylor, R. A. Jones and S. M. Halpin, "Development of load models for fault induced delayed voltage recovery dynamic studies," *Power and Energy Society General Meeting - Conversion and Delivery of Electrical Energy in the 21st Century, 2008 IEEE*, Pittsburgh, PA, 2008, pp. 1-7.
- [142] K. Raja and N. Theivarajan, "Emergency power supply system of a Nuclear Power Plant-modelling and simulation studies of Diesel generators and load pickup on emergency transfer," *Electrical Energy Systems (ICEES), 2011 1st International Conference on*, Newport Beach, CA, 2011, pp. 302-307.
- [143] A. Plaisant and J. Reeve, "An active filter for AC harmonics from HVDC converters. Basic concepts and design principles," *Power Engineering Society Summer Meeting, 1999. IEEE*, Edmonton, Alta., 1999, pp. 395-400 vol.1.
- [144] C. Zhan, "AC harmonic filters for Konti-Skan 1 Refurbishment HVDC project," *AC and DC Power Transmission, 2006. ACDC 2006. The 8th IEE International Conference on*, London, UK, 2006, pp. 36-40.
- [145] R. Mardiana, "Parameters affecting the ampacity of HVDC submarine power cables," *Electric Power and Energy Conversion Systems (EPECS), 2011 2nd International Conference on*, Sharjah, 2011, pp. 1-6.
- [146] D. H. Kwon, H. J. Moon, R. G. Kim, C. G. Kim and S. I. Moon, "Modeling of CIGRE benchmark HVDC system using PSS/E compared with PSCAD," *Energy (IYCE), 2015 5th International Youth Conference on*, Pisa, 2015, pp. 1-8.
- [147] M. O. Faruque, Yuyan Zhang and V. Dinavahi, "Detailed modeling of CIGRE HVDC benchmark system using PSCAD/EMTDC and PSB/SIMULINK," in *IEEE Transactions on Power Delivery*, vol. 21, no. 1, pp. 378-387, Jan. 2006.
- [148] P. Wang, Y. Zhang, H. Chen, X. Li, S. Song and J. Bai, "Analysis on the Interaction of AC/DC Systems Based on Multi-Infeed Q Effective Short Circuit Ratio," *2012 Asia-Pacific Power and Energy Engineering Conference*, Shanghai, 2012, pp. 1-4.
- [149] A. ElMehdi, A. Momen and B. K. Johnson, "Dynamic reactive compensation requirements at the rectifier end of an LCC HVDC link connected to a weak AC system," *North American Power Symposium (NAPS), 2014*, Pullman, WA, 2014, pp. 1-6.
- [150] R. Devarapalli and R. K. Pandey, "Performance evaluation of HVDC system with ESCR variation," *Engineering and Systems (SCES), 2012 Students Conference on*, Allahabad, Uttar Pradesh, 2012, pp. 1-6.

- [151] C. L. Chen and T. Y. Lee, "Impact Analysis of Transmission Capacity Constraints on Wind Power Penetration and Production Cost in Generation Dispatch," *Intelligent Systems Applications to Power Systems, 2007. ISAP 2007. International Conference on*, Toki Messe, Niigata, 2007, pp. 1-6.
- [152] Y. Zhang and A. M. Gole, "Comparison of the transient performance of STATCOM and Synchronous condenser at HVDC converter stations," *AC and DC Power Transmission, 11th IET International Conference on*, Birmingham, 2015, pp. 1-8.
- [153] S. Hwang, M. Yoon and G. Jang, "Evaluation of STATCOM capacity on transient stability in Jeju-island system with HVDC and wind farms," *2015 9th International Conference on Power Electronics and ECCE Asia (ICPE-ECCE Asia)*, Seoul, 2015, pp. 367-372.
- [154] J. Burr, S. Finney and C. Booth, "Comparison of Different Technologies for Improving Commutation Failure Immunity Index for LCC HVDC in Weak AC Systems," *AC and DC Power Transmission, 11th IET International Conference on*, Birmingham, 2015, pp. 1-7.
- [155] Z. Siyu, W. Jun, C. Wenjia, L. Sizhuo and Y. Wei-yang, "Study on transient characteristics of CCC-HVDC transmission systems," *Sustainable Power Generation and Supply (SUPERGEN 2012), International Conference on*, Hangzhou, 2012, pp. 1-5.
- [156] R. Faizal, M. Nurdin, N. Hariyanto, R. Faizal, S. Pack and J. Plesch, "Sumatra-Java HVDC transmission system modelling and system impact analysis," *PowerTech, 2015 IEEE Eindhoven*, Eindhoven, 2015, pp. 1-6.
- [157] Haifeng Sun, Xiang Cui, Lei Qi and Qi Wang, "Calculation of overvoltage distribution in HVDC thyristor valves," *2010 Asia-Pacific International Symposium on Electromagnetic Compatibility*, Beijing, 2010, pp. 540-543.
- [158] Y. Liu and Z. Chen, "Short Circuit Ratio analysis of multi-infeed HVDC system with a VSC-HVDC link," *IECON 2011 - 37th Annual Conference on IEEE Industrial Electronics Society*, Melbourne, VIC, 2011, pp. 949-954.
- [159] J. Yang, J. Zheng, G. Tang and Z. He, "Characteristics and Recovery Performance of VSC-HVDC DC Transmission Line Fault," *2010 Asia-Pacific Power and Energy Engineering Conference*, Chengdu, 2010, pp. 1-4.
- [160] Y. Jiang-Hafner, M. Hyttinen and B. Paajarvi, "On the short circuit current contribution of HVDC Light," *Transmission and Distribution Conference and Exhibition 2002: Asia Pacific. IEEE/PES*, 2002, pp. 1926-1932 vol.3.
- [161] A. Egea-Alvarez, S. Fekriasl, F. Hassan and O. Gomis-Bellmunt, "Advanced Vector Control for Voltage Source Converters Connected to Weak Grids," in *IEEE Transactions on Power Systems*, vol. 30, no. 6, pp. 3072-3081, Nov. 2015.
- [162] Y. Wang, S. Z. Zhao, C. Huangfu and J. J. Ruan, "Dynamic Model and Control of Voltage Source Converter Based HVDC," *2009 Asia-Pacific Power and Energy Engineering Conference*, Wuhan, 2009, pp. 1-5.
- [163] F. Zichao, L. Wenhua and S. Qiang, "A Unified Switching Model for VSC Validated by IGCTs and IGBTs," *APEC 07 - Twenty-Second Annual IEEE Applied Power Electronics Conference and Exposition*, Anaheim, CA, USA, 2007, pp. 1485-1488.
- [164] MathWorks, "VSC-Based HVDC Transmission System (Detailed Model)," Simulink, 2015.
- [165] J. Z. Zhou, H. Ding, S. Fan, Y. Zhang and A. M. Gole, "Impact of Short-Circuit Ratio and Phase-Locked-Loop Parameters on the Small-Signal Behavior of a VSC-HVDC Converter," in *IEEE Transactions on Power Delivery*, vol. 29, no. 5, pp. 2287-2296, Oct. 2014.

- [166] J. Z. Zhou and A. M. Gole, "VSC transmission limitations imposed by AC system strength and AC impedance characteristics," *AC and DC Power Transmission (ACDC 2012), 10th IET International Conference on*, Birmingham, 2012, pp. 1-6.
- [167] M. Janaki, R. Thirumalaivasan and N. Prabhu, "Design of robust controller for VSC based HVDC using Genetic Algorithm," *Advances in Electrical Engineering (ICAEE), 2014 International Conference on*, Vellore, 2014, pp. 1-6.
- [168] B. Kasztenny and J. Cardenas, "New phase-segregated digital busbar protection solutions," *Protective Relay Engineers, 2004 57th Annual Conference for*, College Station, TX, USA, 2004, pp. 308-338.
- [169] F. Yang, A. P. S. Meliopoulos, G. J. Cokkinides and Q. B. Dam, "Effects of Protection System Hidden Failures on Bulk Power System Reliability," *2006 38th North American Power Symposium*, Carbondale, IL, 2006, pp. 517-523.
- [170] S. Chowdhury, P. A. Crossley, J. Fitch and S. P. Chowdhury, "A survey on performance evaluation of low impedance numeric and high impedance busbar protection schemes," *Electricity Distribution - Part 1, 2009. CIRED 2009. 20th International Conference and Exhibition on*, Prague, Czech Republic, 2009, pp. 1-6.
- [171] IEEE Draft Guide for Breaker Failure Protection of Power Circuit Breakers," in *PC37.119/D2, July 2015*, vol., no., pp.1-71, Sept. 12 2015.
- [172] W. An, N. Tart, D. Barron, M. Bingham and A. Hackett, "A transmission utility's experience to date with feeder unit protection systems," *Developments in Power Systems Protection, 2012. DPSP 2012. 11th International Conference on*, Birmingham, UK, 2012, pp. 1-6.
- [173] Q. Cheng and B. Yun, "The Implementation Scheme of Distance Protection Based on Parameter Identification," *Computer, Consumer and Control (IS3C), 2014 International Symposium on*, Taichung, 2014, pp. 646-649.
- [174] H. Wang, G. Song, J. Ding and L. Yang, "Long line distance protection based on fast phasor calculation algorithm," *Developments in Power System Protection (DPSP 2014), 12th IET International Conference on*, Copenhagen, 2014, pp. 1-5.
- [175] I. Gordiyenko, A. Gusev and A. Sulaimanov, "Distance protection simulation by considering hardware and measuring transformers realization," *Strategic Technology (IFOST), 2012 7th International Forum on*, Tomsk, 2012, pp. 1-5.
- [176] J. Kosev and G. L. Arsov, "A simple inductorless AC-line voltage autotransformer," *Industrial Electronics, 1999. ISIE '99. Proceedings of the IEEE International Symposium on*, Bled, 1999, pp. 584-589 vol.2.
- [177] K. Harker, "Power System Commissioning and Maintenance Practice," (Energy Engineering, Institution of Engineering and Technology, 1997.
- [178] S. Achenbach, V. Barry, C. H. Bayfield and P. F. Coventry, "Increasing the GB electricity transmission networks' power transfer capability between North and South — The Western HVDC Link," *AC and DC Power Transmission (ACDC 2012), 10th IET International Conference on*, Birmingham, 2012, pp. 1-4.
- [179] Y. P. Li, D. G. Wang, A. P. Hu, W. Wang and Z. Q. Yao, "Real-time simulation study on HVDC control and protection," *Power System Technology (POWERCON), 2010 International Conference on*, Hangzhou, 2010, pp. 1-6.
- [180] W. Leterme, J. Beerten and D. Van Hertem, "Nonunit Protection of HVDC Grids With Inductive DC Cable Termination," in *IEEE Transactions on Power Delivery*, vol. 31, no. 2, pp. 820-828, April 2016.
- [181] L. Qing, W. Zengping and W. Liying, "Optimization of HVDC Converter Transformer Back-up Protection," *2006 International Conference on Power System Technology*, Chongqing, 2006, pp. 1-4.

- [182] CIGRE Joint Working Group C4/B4/C1.604, "Influence of Embedded HVDC Transmission on System Security and Network Performance," Technical Brochure 536, 2013.
- [183] M. B. Mollah and S. S. Islam, "Towards IEEE 802.22 based SCADA system for future distributed system," *Informatics, Electronics & Vision (ICIEV), 2012 International Conference on*, Dhaka, 2012, pp. 1075-1080.
- [184] EDF. Energy, "Sizewell C Stage 1: Pre-Application Consultation," London, 2012.
- [185] National Grid Electricity Transmission, "Bramford to Twinstead Tee Connection Project," 1 October 2012. [Online]. Available:<http://www.bramfordtwinstead.co.uk/assets/downloads/consultationFeedbackReport.pdf>. [Accessed 4 June 2013].
- [186] F. M. Kasangala and G. Atkinson-Hope, "Electrical energy losses and costs evaluation of HVDC and UHVDC transmission lines," *Industrial and Commercial Use of Energy Conference (ICUE), 2013 Proceedings of the 10th*, Cape Town, 2013, pp. 1-7.
- [187] CIGRE Working Group 14.20 "Economic assessment of HVDC links" Technical Brochure 186, 2001.
- [188] P. L. Francos, S. S. Verdugo, H. F. Álvarez, S. Guyomarch and J. Loncle, "INELFE — Europe's first integrated onshore HVDC interconnection," *2012 IEEE Power and Energy Society General Meeting*, San Diego, CA, 2012, pp. 1-8.
- [189] T. Magg, M. Manchen, E. Krige, J. Wasborg and J. Sundin, "Connecting networks with VSC HVDC in Africa: Caprivi Link interconnector," *Power Engineering Society Conference and Exposition in Africa (PowerAfrica), 2012 IEEE*, Johannesburg, 2012, pp. 1-6.
- [190] A. Ltd, "Nordbalt VSC HVDC project," ABB AB HVDC, Ludvika, 2015.
- [191] Tik Son Wong, J. Lopez-Roldan and T. Saha, "Development of a life cycle cost estimating tool to compare GIS and AIS substation projects," *2015 IEEE Power & Energy Society General Meeting*, Denver, CO, 2015, pp. 1-5.
- [192] Western HVDC link, "Western Link Project," 4 October 2011. [Online]. Available: <http://www.westernhvdclink.co.uk/hunterston-converter-station.aspx>. [Accessed 20 June 2015].
- [193] Zehong Liu, "Design features of Three Gorges-Changzhou ± 500 kV HVDC Project," *Power Engineering Society Winter Meeting, 2000. IEEE*, 2000, pp. 12-16 vol.1.
- [194] ABB Ltd, "The NorNed HVDC project," ABB HVDC, Ludvika, 2008.
- [195] ABB.Ltd, "Skagerrak 4: An excellent example of the benefits can be achieved through interconnections," ABB HVDC, Ludvika, 2015.
- [196] ABB. Ltd, "The North Sea Link HVDC Project," ABB HVDC, Ludvika, 2015.

List of Publications

- [1] R. Poole, "Technical Issues Associated with the connection of Nuclear Power Plants to the National Electricity Transmission System," *Engineering and Technology Reference (IET)*, pp. 1-12, 2015.
- [2] R. Poole, "A Review of Nuclear Power within the United Kingdom," *Engineering and Technology Reference (IET)*, pp. 1-8, 2016.